Coastal Research Library 7

Christoph Wetzelhuetter *Editor*

Groundwater in the Coastal Zones of Asia-Pacific

Springer

Groundwater in the Coastal Zones of Asia-Pacific

Coastal Research Library

VOLUME 7

Series Editor:

Charles W. Finkl
Department of Geosciences
Florida Atlantic University
Boca Raton, FL 33431
USA

The aim of this book series is to disseminate information to the coastal research community. The Series covers all aspects of coastal research including but not limited to relevant aspects of geological sciences, biology (incl. ecology and coastal marine ecosystems), geomorphology (physical geography), climate, littoral oceanography, coastal hydraulics, environmental (resource) management, engineering, and remote sensing. Policy, coastal law, and relevant issues such as conflict resolution and risk management would also be covered by the Series. The scope of the Series is broad and with a unique crossdisciplinary nature. The Series would tend to focus on topics that are of current interest and which carry some import as opposed to traditional titles that are esoteric and non-controversial. Monographs as well as contributed volumes are welcomed.

For further volumes:
http://www.springer.com/series/8795

Christoph Wetzelhuetter
Editor

Groundwater in the Coastal Zones of Asia-Pacific

Springer

Editor
Christoph Wetzelhuetter
The Coastal Education and Research
Foundation Inc. (CERF)
Perth, WA, Australia

ISSN 2211-0577 ISSN 2211-0585 (electronic)
ISBN 978-94-007-5647-2 ISBN 978-94-007-5648-9 (eBook)
DOI 10.1007/978-94-007-5648-9
Springer Dordrecht Heidelberg New York London

Library of Congress Control Number: 2013939191

Printed on acid-free paper

Springer is part of Springer Science+Business Media (www.springer.com)

Foreword

Humankind has an overwhelming desire to live, work, and vacation near the ocean. More than 1.2 billion people live within 100 km of shoreline and 100 m of sea level; this coastal zone has an average population density nearly three times higher than the global average. Each year more than 50 million people move to the coastal zone worldwide. The coastal populations swell seasonally by hundreds of millions of tourists that flock to local beaches. Coastal zones also have some of the largest and most industrialized cities, many of which have grown from historic ports and centers of shipping and trade.

This strong and growing human footprint in coastal zones has put an enormous pressure on many sensitive ecosystems and limited natural resources. Among the most vulnerable are coastal freshwater resources, including the critically important water resource beneath land surface – groundwater.

Groundwater is an essential part of the global hydrologic cycle and the largest distributed store of freshwater. Groundwater supplies fresh drinking water to almost half the world's population and supports and sustains many streams, lakes, wetlands, aquatic communities and ecosystems, economic development and growth, irrigated agriculture, and food production worldwide. The demand for groundwater has threatened its sustainability. Coupled socioeconomic and climate stresses have led to groundwater depletion and reduced water quality in many aquifers around the world.

Aquifers in coastal zones are particularly vulnerable because of the additional threat of seawater intrusion from over-pumping and abstraction, sea-level rise, and storm surges. The mitigation and remediation of seawater intrusion within coastal aquifers is prohibitively expensive, necessitating the prevention of seawater intrusion to become a primary goal for many coastal groundwater managers. Because of competing stakeholder needs and uncertain scientific findings and recommendations, particularly regarding climate change and the timing and magnitude of sea-level rise, coastal managers and policy makers must often make complex and controversial

decisions to best use local groundwater while protecting against seawater intrusion. However, many coastal management decisions are made without clear groundwater sustainability goals or development plans.

Such coastal groundwater issues are becoming increasingly important in the Asia-Pacific region of the western Pacific Ocean. The Asia-Pacific region has many islands and continental, low-lying shorelines that support major population centers, but are susceptible to wave erosion, seawater inundation, and storm surge. The projected global sea levels will likely exacerbate these hazards and have a wide ranging socioeconomic consequence for the region, especially for coastal groundwater resources.

Groundwater resources support a tremendous range of development across the Asia-Pacific region, from densely populated megacities to sparsely populated, rural and developing areas. For example, the North China Plain aquifer and many other coastal aquifers help support nearly 60 % of China's more than 1.3 billon people that live in the 12 coastal provinces along the western Pacific Ocean. The Asia-Pacific megacities, defined as metropolitan areas with populations in excess of ten million, include Karachi, Calcutta, Bangkok, Jakarta, Hong Kong, Manilla, Osaka, and Tokyo. Groundwater beneath these megacities is often contaminated and over-abstracted, which led to land subsidence in Tokyo and Osaka during the mid-1900s. Subsequent groundwater-pumping regulation led to groundwater levels that recovered to historical levels, but created new problems with the rising groundwater levels causing buoyancy of underground structures such as subway stations. Along the eastern Pacific Ocean, approximately 80 % of California's more than 35 million residents live within 50 km of the coast – a region that has localized seawater intrusion from over-pumping of groundwater to meet strong economic demands for groundwater-fed irrigated agriculture and drinking-water supply.

The Asia-Pacific region also has nearly 1,000 populated, small tropical and subtropical islands, many of which are underdeveloped or developing countries. Many of these small island developing states (SIDS) face severe constraints in terms of freshwater resources. Many SIDS lack any substantial surface storage for water and thus are highly reliant on groundwater. Groundwater beneath low-lying atolls and coral islands is often present as thin lenses of freshwater floating on seawater. Groundwater lens beneath small islands are particularly vulnerable to seawater intrusion from natural tidal fluctuations, climate variability and change, storm surges, over-pumping, and point and non-point source contamination from human activities and livestock. Conflicts surrounding land ownership, inadequate governance, and inadequate knowledge, including a lack of well-trained hydrogeologists, groundwater engineers, and managers are central problems that enhance the vulnerability of groundwater lens to seawater intrusion across the Asia-Pacific region.

To address these important questions in the Asia-Pacific region, this volume provides a valuable overview and collection of case studies about the current state of research to better understand seawater intrusion and other important processes

that affect groundwater resources in aquifers of the continental shoreline and island settings. Results and findings from this volume will help groundwater scientists, engineers, managers, and policy makers develop strategies toward sustainable groundwater resources under continued population growth and uncertain consequences of climate variability and change.

Department of Geosciences
San Francisco State University
San Francisco, California, USA

Jason J. Gurdak

Contents

Part I
Understanding the Movement of Groundwater in the Coastal Zone

Chapter 1
Groundwater in the Coastal Zones of the Asia–Pacific Region—A Threatened Resource Needing Integrated Management

Chris Wetzelhuetter

Abstract Groundwater management and conservation are becoming an increasingly important issue in the heavily urbanized coastal zones of the Asia–Pacific region. This volume of papers is intended to support groundwater managers in their planning, and offer potential solutions for decision makers.

This chapter provides a comprehensive overview of the general concept of this volume. It describes the composition, content and objectives of the different chapter contributions. Furthermore, it also, outlines how the status of coastal groundwater research is presented and illustrates how this volume offers an integrated view of groundwater processes in coastal aquifers in the Asia–Pacific region. It includes a discussion of the methodologies and technologies used to assess processes associated with coastal groundwater development. A summary of the case studies and local examples aims to provide the reader with a broader understanding of the diversity of costal aquifers and their groundwater resources.

1.1 Introduction

The coastal zone is marked by significant biological diversity, and of great importance for fisheries and urban populations. In the Asia–Pacific Region it is under ever increasing pressure due to population growth and activities related to industry and tourism.

The groundwater in coastal zones faces many new threats. For example, wells can be destroyed when being overrun by waves. They can also become contaminated with saline water or other pollutants during flood events or by leaching from saline ponds or the soil after flooding. Groundwater pollution is caused by the spreading of waste, sewerage, and/or chemicals, and the inland

C. Wetzelhuetter (✉)
CERF (Coastal Education and Research Foundation), Perth, WA, Australia
e-mail: cwetzelhuetter@gmx.com

C. Wetzelhuetter (ed.), *Groundwater in the Coastal Zones of Asia-Pacific*,
Coastal Research Library 7, DOI 10.1007/978-94-007-5648-9_1,

migration of the fresh water–saline water interface. The volume of freshwater on small islands can be reduced by 'natural' marine incursion, e.g. during storms, and/or as the result of over-exploitation. Last but not least, the movement of a fresh water–saline water interface upriver, either in response to sea-level rise or surface water abstraction, might have significant impacts on the ecosystem.

Groundwater is an important freshwater resource. In order to deal with potential threats to this resource it is therefore important to gain an understanding of the fresh water–saline water interface between marine levels that vary due to tidal effects and fresh groundwater moving along the coastal zone. The hydrogeochemical changes resulting from the movement of the interface are complex and must also be understood to enable preservation/conservation of the limited freshwater resource. It will also allow integration and the development of innovative management solutions for the sustainable management of coastal zone groundwaters.

The purpose of this chapter is to provide an overview of topics related to coastal groundwater with a focus on the Asian–Pacific Region. The chapter content closely follows the same order as the book content. It summaries and discusses the results of the different approaches and concepts by the contributing authors. The aim of this book is to lead to disseminate the concepts applied in coastal groundwater research, and allow researchers and managers to choose methods and find solutions to meet specific project requirements. The reader will acquire the knowledge needed to develop specific project plans for a sustainable management of coastal aquifers and the near-shore marine environment.

1.2 The Structure of the Book

The book consists of four parts.

Part 1 (Chaps. 1, 2, 3) deals with the fundamentals and principal concepts of hydrogeology in the coastal zone. It provides the basis of an understanding of groundwater flow, the hydrochemistry of ground- and seawater, and aquifer properties in coastal zones.

Part 2, is a seven part series (Chaps. 4, 5, 6, 7, 8, 9, 10) dedicated to descriptions of typical methodologies and applications for groundwater investigations in coastal zones. These include geophysical methods and numerical modeling, and provide the reader with an overview of well-established methods and the latest technologies developed and applied in case studies.

Part 3 (Chaps. 11, 12, 13, 14) is about various projects and cases studies that focus on impacts on groundwater in the coastal zone. These chapters are examples of assessments undertaken to investigate threats to groundwater, including sea-level rise, pollution resulting from flooding and/or over-exploitation of groundwater resources.

Part 4 is a series of three chapters (15, 16, 17 inclusive) dealing with water management issues and gives a general overview of the situation in the region. It includes examples of the different ways of groundwater management.

Of the 17 chapters:

- The majority was written by researchers summarizing the latest results of their work in coastal research. Some include descriptions of methodologies that are commonly used for research or assessments, or describe a new technology or unique approach. They address readers who are not experts in these disciplines, and provide the principles and information required for further understanding. Students of marine and environmental studies, geology and/or hydrology, or related topics, will find these details helpful.
- Some chapters provide an overview of an actual topic such as sea-level rise, climate change or saltwater intrusion, or a more general discussion on the current state of groundwater research in coastal zones in the Asia–Pacific Region. The region is large area and almost every country in it has a different potential and issues for groundwater research and coastal management. Hence, these chapters reflect specific local requirements.
- The principal features of the chapters are: being structured like a scientific report, including abstract, introduction, methodology, discussion of results, and summary. All of the chapters are related to the region and include a case study—except for Chaps. 1 and 15—where the discussion in general relates to groundwater management in the Asia–Pacific Region.
- The Asia–Pacific Region, as referred to in or by all of the chapters, covers an area from the Indian Ocean in the west to the Pacific Ocean in the east. The region incorporates the smaller adjacent seas and bays along the shores of Iran, India, Indonesia, Papua New Guinea and China, such as the Arabian Sea, the Bay of Bengal, and the South and East China Seas (Fig. 1.1).

1.3 Locations of Case Studies

The case studies dealt with in this book cover this vast area from as far west as the coast of Africa to the islands of Hawaii in the central Pacific in the east. Authors from Australia contributed five case studies, two are from by India, and one each from China, USA (Hawaii), Malaysia, France (Mayotte), Thailand, UAE and Indonesia. The locations pertaining to these case studies relate cover a wide range of different climates and geomorphological settings, including tropical islands, high-density populated urban areas, river banks and estuaries, agricultural plains, deserts, and temperate woodlands and swamps in the coastal zone (Fig. 1.2).

1.4 Content and Objectives

Chapter 2 (by H. Li et al.) deals with mud beaches and mangrove swamps in the Dongzhaigang National Nature Reserve. This is the largest mangrove forest nature reserve in China. The author explains how changes in the hydrogeology and

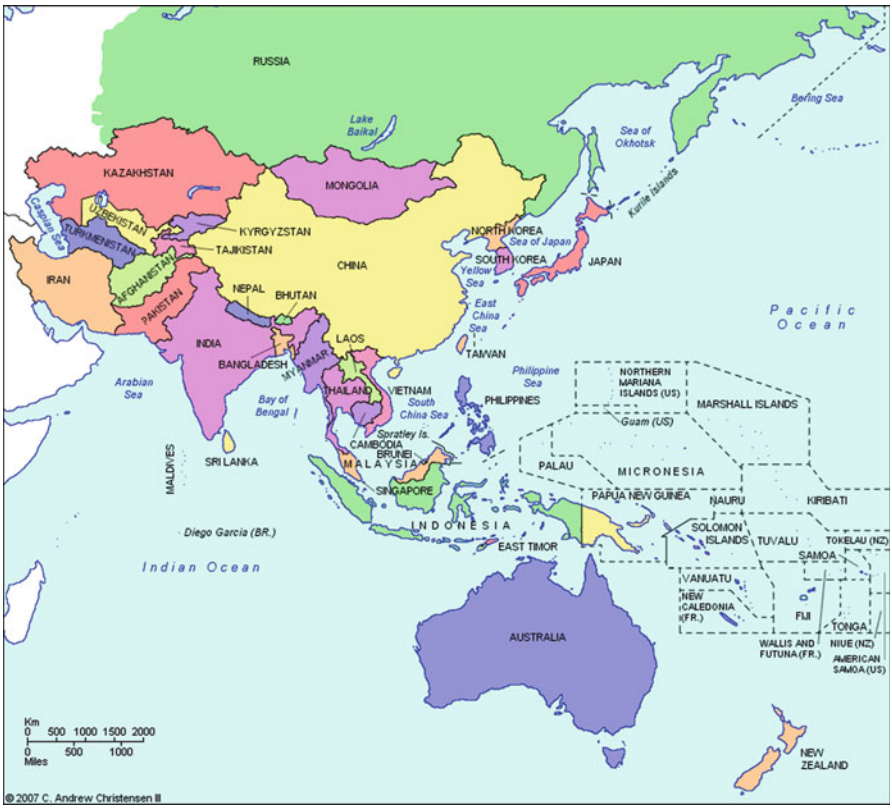

Fig. 1.1 The Asia–Pacific region (from C. Andrew Christensen III, www.worldmonitor.info, Regions, Asiapacific, March 2006)

hydrochemistry along the two transects could have ecological implications for the restoration, protection and management of mangrove ecosystems. The intertidal zones of a mangrove transect and a 'bald beach' transect with similar topography and tidal actions were selected for a comparative study. The chemistry of water sampled along the transects was compared and variations in the water table investigated.

Chapter 3 (by P. Swarzenski et al.) is an examination of coastal groundwater discharges and associated nutrient loadings at selected coastal sites in Hawaii (USA). The suite of tools used to evaluate groundwater discharge included selected U/Th-series radionuclides, a broad spectrum of geochemical analytes, multi-channel electrical resistivity, and *in situ* oceanographic observations. The data derived from this investigation will extend our basic understanding of the physical controls on coastal groundwater discharge, and provide an estimate of the magnitude and physical embodiments of submarine groundwater discharges and the associated trace metal and nutrient loads conveyed by this submarine route.

Fig. 1.2 Locality map: Case studies reported in relation to research in groundwater in the coastal zones of the Asia Pacific Region (Modified from Google Earth)

Chapter 4 (by L. Surinaidu et al.) demonstrates how geophysical and hydrochemical tools were applied to identify the source of salinity in an aquifer and to assess the extent of saline water intrusion in the Godavari Delta in the Bay of Bengal (India). The author shows how hydrogeologists carry out site characterization and present the results in maps and provides an overview of the benefits of using a combination of electrical resistivity tomography and hydrochemistry.

Chapter 5 (author S.C. Singh) is a discussion of some geophysical techniques and refers to the Kasai–Subarnarekha River Basin, West Bengal (India). Downhole geophysical logging and different types of surface electrical resistivity surveys were employed to investigate complex hydrogeological settings. The study demonstrates the way in which sound hydrogeological investigations can support the development of a groundwater resource.

Chapter 6 (by A. Davis et al.) presents relevant research used to characterize a coastal aquifer system on the Eyre Peninsula, South Australia, using surface-based nuclear magnetic resonance (NMR). This technique enables direct detection of groundwater in the subsurface. The chapter will give a better understanding of the potential level of connectivity between the Uley Basin and the Southern Ocean, and enable consideration of whether new groundwater resources could be tapped in this coastal aquifer.

Chapter 7 (by C. Schamper et al.) provides a detailed description of the airborne electromagnetic method. It includes a discussion of the processing and inversion of the data produced, giving the reader an excellent introduction of the method. The

results from an investigation are demonstrated by a case study from the volcanic island of Mayotte, where key geological structures and saline intrusion were mapped successfully. While the location of this case study is closer to Africa than Asia, it is relevant as an example for many island settings in the Asia–Pacific Region that have similar environments, geology and hydrogeology.

Chapter 8 (by H. Duerrast and J. Srattakal) deals with an investigation of salt water intrusions in the coastal aquifer of Songkhla in Southern Thailand. Seismic reflection and refraction, and vertical electrical sounding (VES) were employed to investigate the deeper aquifers, and contribute to the understanding of the aquifer and groundwater conditions for groundwater management

Chapter 9 (by A.D. Werner and L. Dung Dang) deals with the development of a three-dimensional seawater intrusion model of the Uley South Basin, South Australia, using a numerical model with code derived from MODHMS. The modelling enables simulation, for the first time, of the current extent of seawater intrusion in the aquifer, the temporal salinity variability, and the susceptibility of the aquifer to seawater intrusion. As such, the model is a significant step beyond results of modelling attempts, and provides important insights into salinity distribution and mobility.

Chapter 10 (by L.K. Morgan et al.) presents the application of a rapid-assessment method for seawater intrusion vulnerability via a case study in the Willunga Basin, South Australia. This study provides guidance for both well installation and future data collection, and will be of significant interest and value to groundwater managers.

Chapter 11 (by A. Zaharin et al.) deals with the impacts of ecotourism on groundwater on small tropical islands in Malaysia. The author demonstrates how hydrochemical investigations can provide information for sustainable groundwater development and management, and how groundwater must be considered in order to avoid the effects of its over-exploitation hindering the growth and development of ecotourism.

Chapter 12 (by J.P. Terry et al.) investigates into the groundwater resources of atolls that are at risk of storm-generated marine flooding. The chapter includes a case study on the Pacific island of Pukapuka with a summary of the findings of an investigation of the effects on freshwater lens profiles of storm waves washing over and across atoll islets, and the subsequent patterns of recovery over time. Both field and modelling approaches are used.

Chapter 13 (by M. Sherif et al.) discusses the employment of MODFLOW and MT3D to simulate groundwater flow and assess the saline intrusion problem in Wadi Ham, UAE, and possible mitigation measures. The study provides important information about management of the local coastal aquifer. The impacts of excessive pumping and artificial recharge are investigated.

Chapter 14 (by T. Laattoe et al.) is about the impacts of sea-level rise (SLR) and any associated saline (salt water) intrusion (SWI). Variable-density numerical modelling is used to examine the implications of transgression for a range of SWI scenarios, based on simplified coastal aquifer settings. The findings of this study suggest that modelling analyses that neglect the effects of transgression in SLR–SWI investigations may underestimate the rates and extent of SWI significantly.

Chapter 15 (author K. Villholth) deals with the current level of knowledge of coastal groundwater systems in continental and island settings in the Asia–Pacific region, their utilization and vulnerabilities, and the hazards arising from various sources. It is proposed that an integrated framework approach could be used to show how sustainable and resilient groundwater management can be promoted and enhanced. The work described is partially based on the tsunami event of December 26, 2004 in eastern Sri Lanka and the immense challenges generated by that. The opportunities for local and higher level groundwater management are also noted.

Chapter 16 (author S.B. Kusumayudha) demonstrates the way in which hydrogeological investigations can be used to support the development of a Geopark. Discharges of groundwater from springs along a coastal stretch in Indonesia are evaluated as resources for drinking water supply and tourist attractions.

Chapter 17 (author L. Leonhard et al.) exemplifies the use of groundwater models as tools for groundwater management. The study demonstrates that it is essential to ensure that the required quantity and quality of groundwater can be sustained through extensive periods of zero recharge for alluvial aquifer systems. The modelling outputs are combined with the results of regular measurement of both groundwater level and salinity obtained from a network of observation bores, to ensure the sustainability of the water supply.

1.5 Conclusions

With its discussions of a broad range of studies related to groundwater in coastal zones of the Asia–Pacific Region, this volume offers a critical tool for coastal researchers, geoscientists in related fields, water engineers, groundwater managers and decision makers. It illustrates human and environmental impacts on coastal groundwater resources, their relationship to coastal zone management strategies, and the development of sustainable management approaches.

Acknowledgments The Editor gratefully acknowledges all contributors to this book, especially Charles W. Finkl and the Coastal Education & Research Foundation for their promotion. Many thanks go to all the supporters and reviewers who made publication possible and offered their help in editing, Bernd Striewski and Jeremy Joseph.

Reference

C. Andrew Christensen III, www.worldmonitor.info, Regions,Asiapacific, March 2006

Chapter 2
Hydrogeology and Hydrochemistry Along Two Transects in Mangrove Tidal Marshes at Dongzhaigang National Nature Reserve, Hainan, China

Hailong Li, Yuqiang Xia, and Xiaolong Geng

Abstract Dongzhaigang National Nature Reserve is the largest mangrove forest nature reserve in China, holds the most abundant mangrove species, and has been giving the best preservation. However, bald mud beaches were found among the mangrove marshes in the reserve. In order to investigate the environmental characteristics behind this phenomenon, the intertidal zones of a mangrove transect and a bald beach transect with similar topography and tidal actions were selected for comparison study. Several monitoring wells were installed along the two transects for in-situ measurements of pH, ORP, salinity and temperature of groundwater. Groundwater samples were collected for lab analysis as well. The results showed that pH values of the mangrove transect were higher than that of the bald beach transect, ORP measurements indicated that the mangrove transect had an oxidizing environment and the bald beach transect has a reducing environment. Lab analysis showed that the concentrations of anions (Cl^-, SO_4^{2-}, Br^-) and cations (K^+, Na^+, Ca^{2+}, Mg^{2+}) of water sampled from the bald each transect were much higher than that of the mangrove beach transect. Along both transects, observed water table variations were significant in the high and low intertidal zones and negligible in the middle intertidal zones. The observed groundwater salinity was significantly smaller along the mangrove transect than along the bald beach

H. Li (✉)
State Key Laboratory of Biogeology and Environmental Geology, China University of Geosciences-Beijing, Beijing 100083, China
e-mail: hailongli@cugb.edu.cn

Y. Xia
Changjiang River Scientific Research Institute (CRSRI), Changjiang Water Resources Commission of the Ministry of Water Resources, Wuhan 430010, China
e-mail: xiayqcug@gmail.com

X. Geng
Department of Civil and Environmental Engineering, Newark College of Engineering, The New Jersey Institute of Technology, 323 MLK Blvd, Newark, NJ 07102, USA
e-mail: gengxiaolong@gmail.com

C. Wetzelhuetter (ed.), *Groundwater in the Coastal Zones of Asia-Pacific*,
Coastal Research Library 7, DOI 10.1007/978-94-007-5648-9_2,

transect. Previously published analysis concluded that the two transects have a mud-sand two-layered structure: a surface zone of low-permeability mud and an underlying high-permeability zone that outcrops at the high and low tide lines. The freshwater recharge from inland is considerable along the mangrove transect but negligible along the bald beach transect, this may explain the lower concentrations of salt and regular ions along the mangrove transect than along the bald beach transect. This comparative study of hydrogeology and hydrochemistry along the two transects would provide ecological implications on the restoration, protection and management of mangrove ecosystems.

2.1 Introduction

As one of the most important salt marsh ecosystems, mangrove marshes typically occur along tidal estuaries and coastlines in tropical and subtropical regions (Chapman 1977; Kjerfve et al. 1990; Spalding et al. 1997). They are important for coastal ecology and play an important and irreplaceable role in the maintenance of coastal biodiversity (Field et al. 1998; Bosire et al. 2008). However, mangrove forests are also one of the world's most threatened tropical ecosystems with an obvious global degradation (Valiela et al. 2001; Duke et al. 2007; Gilman et al. 2008).

Dongzhaigang National Nature Reserve is the largest mangrove forest nature reserve in China, holds the most abundant mangrove species, and has been giving the best preservation. Most mangroves are distributed along the broad shallow beach such as Sanjiang plain and the coastal area of Tashi, other mangrove forests are situated along rivers (e.g., Yanfeng River, Fig. 2.1). However, bald beaches without any vegetation were found among mangrove marshes. In order to investigate the hydrogeological and hydrochemical characteristics critical to mangrove development, a mangrove transect and a bald beach transect were selected to conduct a comparison study (Fig. 2.1). The mangrove transect is located in the Changningtou tidal marsh, and adjacent to the estuary of Yanfeng River. The bald beach transect is situated in a tidal beach without any vegetation and abuts the Shanweitou Village and Dongzhaigang Bay. Along each transect, eight or nine observation wells were installed (Fig. 2.2), and the water level, salinity, pH, ORP and temperature in the wells were measured for 3 days with intervals of 1–3 h. Water samples were also collected for lab analysis of water quality.

2.2 Study Sites

The Dongzhaigang National Nature Reserve is the first mangrove forest reserve in China founded in 1980. It is located in Dongzhaigang Bay bordering the administrative regions of Qiongshan City and Wenchang City, in north eastern Hainan

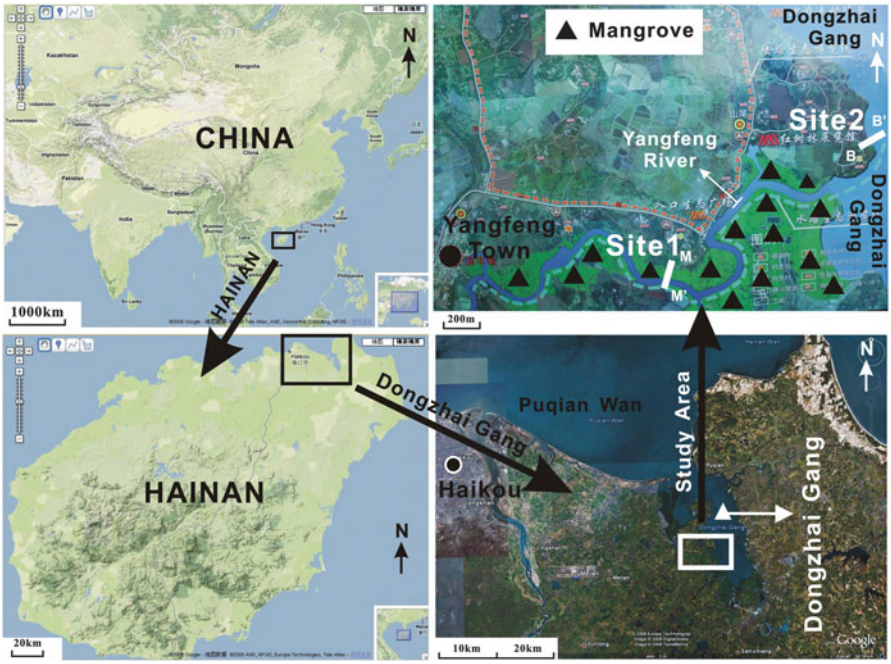

Fig. 2.1 Location maps of Dongzhaigang National Nature Reserve, China and the mangrove transect M–M′ and the bald beach transect B–B′

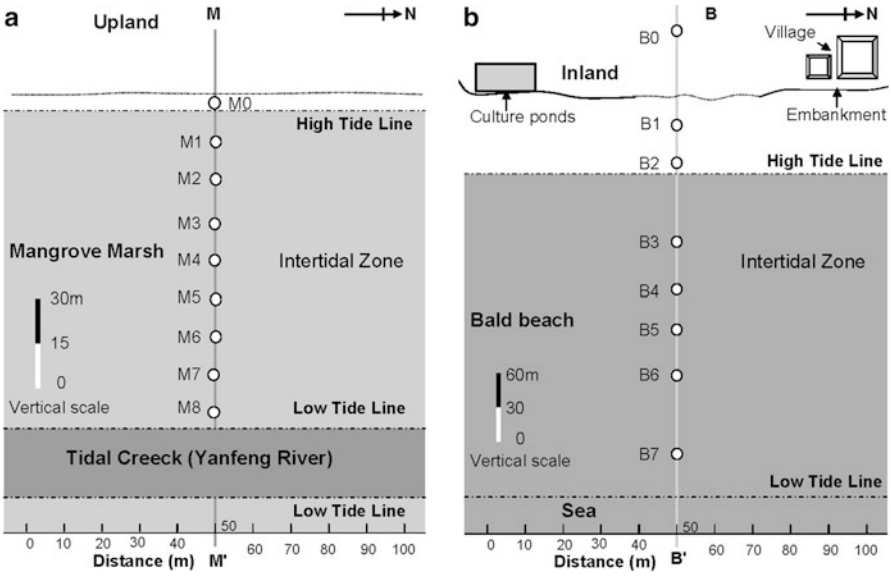

Fig. 2.2 The bird-eye's view of the two transects

Province. Its geographical coordinates are 19°57′–20°01′N, 110°32′–110°37′E (Fig. 2.1). The area trans-bounds the tropical and sub-tropical zones of southern China and has a correspondingly diverse transitional fauna and flora with the southern sub-tropical species dominant. The transitional climatic and hydrological conditions, specific topographic features (estuarine ecosystems) and its rich biodiversity ensure its global significance as a wetland of international importance. Its relatively large area of mangrove forests and wide inter-tidal sands and mudflats provide migratory water birds and fish with rich feeding grounds and breeding habitats (Chen et al. 1999).

The Dongzhaigang estuary has an irregular rectangle shape with a south–north orientation. It is the largest bay in Hainan Province with a total area of nearly 100 km^2. The estuary is a shallow water bay formed by continental sink during the 1605 Great Qiongzhou Earthquake, and has a typical subtropical monsoon marine climate (Xia and Li 2012). The estuary forms a nearly closed lagoon having only two narrow channels connected it to the South China Sea in the north. Beigang Island, situated at the mouth between the two channels, is large enough to block the effects of strong storms from the South China Sea. The eastern side of the estuary consists of an alluvial plain and the western side is bordered by low hills. The base rocks in this area are mainly basalt and olive basalt and these are the origin of overlying soils. Typical acid red soils have been developed under the sub-tropical and tropical climate. The soil layer is generally between 1 and 1.5 m thick and the acidity is pH 5–6. The soils under the mangroves are mainly saline marsh soils (Chen et al. 1999).

The Dongzhaigang National Nature Reserve has a tropical monsoon marine climate with an average rainfall range of 1,700–1,933 mm (data during 1973–1986) with 80 % of the precipitation occurring during May to October and a mean annual temperature of 23.3–23.8 °C. The region is usually affected by typhoons during the summer months (Fu 1995; Xia and Li 2012).

Four rivers enter into the Dongzhaigang Bay, they are Yanzhou River, Sanjiang River, Yanfeng River and Xi River. During the rainy season, the four rivers carry large amount of silts which are largely deposited within the bay to create the extensive inter-tidal mudflats. It is the mudflats that provide a suitable environment for mangrove growth in this area. The annual average temperature of the surface sea water is 24.5 °C within the estuary, while the highest mean water temperature from May to July is 31.5 °C and the lowest is 17.7 °C in January (Chen et al. 1999). Tides in this area are mixture of diurnal and semidiurnal components. The tidal range is about 1.92 m during spring tides and 0.38 m during neap tides (NMDIS 2008).

With 2,065 km^2 of mangrove forests distributed in the shoals of the tidal zone, Dongzhaigang National Nature Reserve accounts for 44.51 % of mangrove forests of Hainan Island and is the largest mangrove forest nature reserve in China, holds the most abundant mangrove species, and has been giving the best preservation (Xia and Li 2012). Dongzhaigang mangrove forest has 26 “true” mangrove species belonging to 12 families, and 40 semi-mangrove and mangrove-associated species belonging to 22 families (Chen et al. 1999). The mangrove marshes in

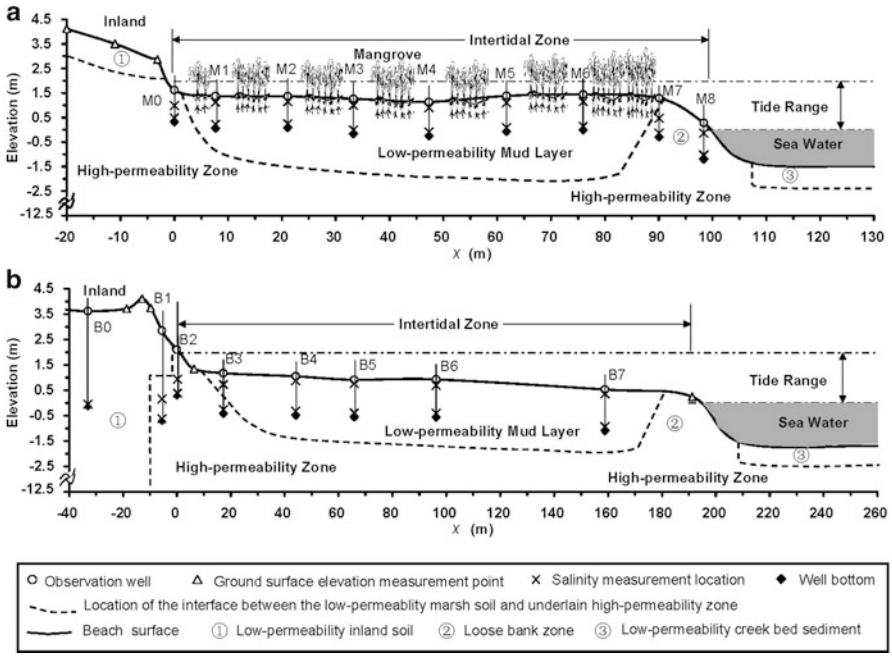

Fig. 2.3 The cross-section of (**a**) the mangrove transect M–M′ and (**b**) the bald beach transect B–B′. The intertidal zone is located within 0 m $\leq x \leq$ 100 m for the mangrove transect and 0 m $\leq x \leq$ 190 m for the bald beach transect, where x is the seaward distance from the high tide mark. The detailed information about monitoring wells is presented in Tables 2.1 and 2.2

Dongzhaigang National Nature Reserve mainly distribute in three coastal areas: Tashi, Yanfeng and Sanjiang Plain (Fig. 2.1).

Two transects were selected for field investigations in Yanfeng and their distance is about 1.8 km (Fig. 2.1b). The first (mangrove transect) is located in Changningtou mangrove tidal marsh, and adjacent to the estuary of Yanfeng River. Mangrove plant species in this site mainly include *Aegiceras corniculatum*, *Bruguiera sexangula*, *Bruguiera gymnorrhiza*, *Kadelia candel*, *Ceriops tagal* and *Acanthus ilicifolius* (Ye and Lu 2001). Nine monitoring wells (M0–M8) were installed along the mangrove transect (M–M′ in Figs. 2.1b, 2.2a, 2.3a) perpendicular to the high tide mark. Well M0 is located at the intersection of mangrove marsh and inland hill. The width of intertidal zone is about 100 m. The second (bald beach transect) is situated in a tidal beach without any vegetation. It abuts the Shanweitou Village and Dongzhaigang Bay. The beach sediment is mainly mud. Eight monitoring wells (B0-B7) were set up in the bald beach transect perpendicular to the high tide mark (B–B′ in Figs. 2.2b, 2.3b). The width of the intertidal zone is about 190 m. More information about the selection of transects can be found in Xia and Li (2012).

2.3 Methods

2.3.1 Field Measurements

Boreholes were drilled with Hand Auger (AMS Inc., USA) to install observation wells. Each well was made up of inner and outer PVC pipes, the inner pipe was put inside the outer one, the outer and inner pipes were wrapped by fine plastic screen, and the space between the two pipes was filled with coarse sands. All these measures were taken in order to prevent the fine beach sediments from entering wells and to guarantee good hydraulic connection between the beach groundwater and the water inside the well. Installation details of the observation wells were described in Xia and Li (2012).

Wells were installed during 12–17 December 2007, which provided 7–13 days for the disturbed groundwater level, salinity profiles and other characteristics to recover to natural status. The elevations of wells and the topography of study profiles were geometrically leveled using an Electronic Total Station (TOPCON, Japan) which has a measurement accuracy of ±2 mm. The data are summarized in Tables 2.1 and 2.2. The sediments around B0–B3 are dominated by sandy loam with gravel, and mud sediments are extensively distributed on the tidal platform (B4–B7). The sediments in the intertidal zone of the mangrove transect are almost uniform (mainly mud). The soil properties along the mangrove transect is much simpler than those along the bald beach transect (Xia and Li 2012).

Water level and salinity in each well were measured by using an electronic dipper system and the Salinity Handheld meter (JENCO Inc., USA), respectively. The values of pH, ORP, and temperature of water samples in the wells were detected by the pH/ORP/Temperature Handheld meter (JENCO Inc., USA). The observation period was from 25 December 2007, 08:00 to 28 December 2007, 08:00. There was no rainfall during the 3 days. Water samples were collected at

Table 2.1 Locations and depths of wells at the mangrove transect M–M′

Locations	Distance (m)	Elevation (m)	Well length above surface (m)	Well length below surface (m)	Elevations of salinity measurement (m)		Thickness of mud layer (m)
					Shallow	Deep	
M0	0.000	1.615	0.67	1.33	0.985	0.485	0.8
M1	7.679	1.367	0.65	1.35	1.117	0.217	2.5
M2	21.081	1.366	0.68	1.32	1.146	0.246	2.5
M3	33.291	1.259	0.53	1.47	0.989	−0.011	2.6
M4	47.331	1.133	0.57	1.43	0.903	−0.097	3.0
M5	61.719	1.375	0.52	1.48	1.095	0.095	3.5
M6	75.985	1.435	0.51	1.49	1.145	0.145	3.7
M7	90.096	1.284	0.38	1.62	0.464	−0.136	0.4
M8	98.378	0.273	0.49	1.51	−0.137	−1.037	0.0

Table 2.2 Locations and depths of wells at the bald beach transect B–B′

Locations	Distance (m)	Elevation (m)	Well length above surface (m)	Well length below surface (m)	Elevations of salinity measurement (m)		Thickness of mud layer (m)
					Shallow	Deep	
B0	−33.000	3.611	0.23	3.77	/[a]	−0.059	/
B1	−5.568	2.839	0.44	3.56	0.149	−0.621	2.0
B2	0.000	2.094	0.19	1.81	1.112	0.562	0.0
B3	17.284	1.166	0.38	1.62	0.726	−0.254	0.9
B4	44.078	1.048	0.43	1.57	0.878	−0.322	2.5
B5	65.835	0.907	0.50	1.50	0.757	−0.393	2.5
B6	96.196	0.921	0.47	1.53	0.691	−0.409	2.5
B7	158.884	0.527	0.33	1.67	0.357	−0.943	2.5

[a]/ means not available

shallow and deep depths in each well using a sterile syringe and then filtered through 0.45 μm (or smaller) filters. The collection vial was rinsed three times with filtrate before being filled brimful of sample filtrate. Samples were stored cold until they could be processed. Samples collected in well M7 were broken.

2.3.2 Laboratory Analysis

Water samples were analyzed by ICP-AES (Inductively Coupled Plasma-Atomic Emission Spectroscopy) for cation elements like Ca, Mg, Mn, Fe, Zn, Na, K. ICP-AES systems consist of several components such as the sample introduction system, the torch assembly, and the spectrometer. The sample introduction system on the ICP-AES consists of a peristaltic pump, Teflon tubing, a nebulizer, and a spray chamber. The fluid sample is pumped into the nebulizer via the peristaltic pump. The nebulizer generates an aerosol mist and injects humidified Ar gas into the chamber along with the sample. This mist accumulates in the spray chamber, where the largest mist particles settle out as waste and the finest particles are subsequently swept into the torch assembly. Approximately 1 % of the total solution eventually enters the torch as a mist, whereas the remainder is pumped away as waste. In the ICP-AES a plasma source is used to make specific elements emit light, after which a spectrometer separates this light in the characteristic wavelengths. Sequential (monochromator) spectrometers were used in ICP-AES analysis for this study. Generally 10 mL of solution was used for estimation of basic elements, and blank solution for each batch of samples was also provided.

The ion chromatography was used for analysis of water samples for common anions such as Cl^-, SO_4^{2-}, and Br^-. Ion chromatography is a form of liquid chromatography that uses ion-exchange resins to separate atomic or molecular ions based on their interaction with the resin (Weiss and Weiss 2005). Water samples were filtered prior to evaluation with an ion chromatograph to remove sediment and other particulate matter as well as to limit the potential for microbial alteration before the sample is run. The minimum sample required for analysis is approximately 5 mL, with no maximum limits.

2.4 Results and Discussions

2.4.1 Variations of Salinity, pH, ORP and Temperature

Figure 2.4 depicts the observed salinity, pH, ORP and temperature of groundwater in shallow and deep depths of monitoring wells along the mangrove and bald beach transects. It is obvious that the shallow water and depth water show a considerable difference along the mangrove transect, while they are close to each other along the

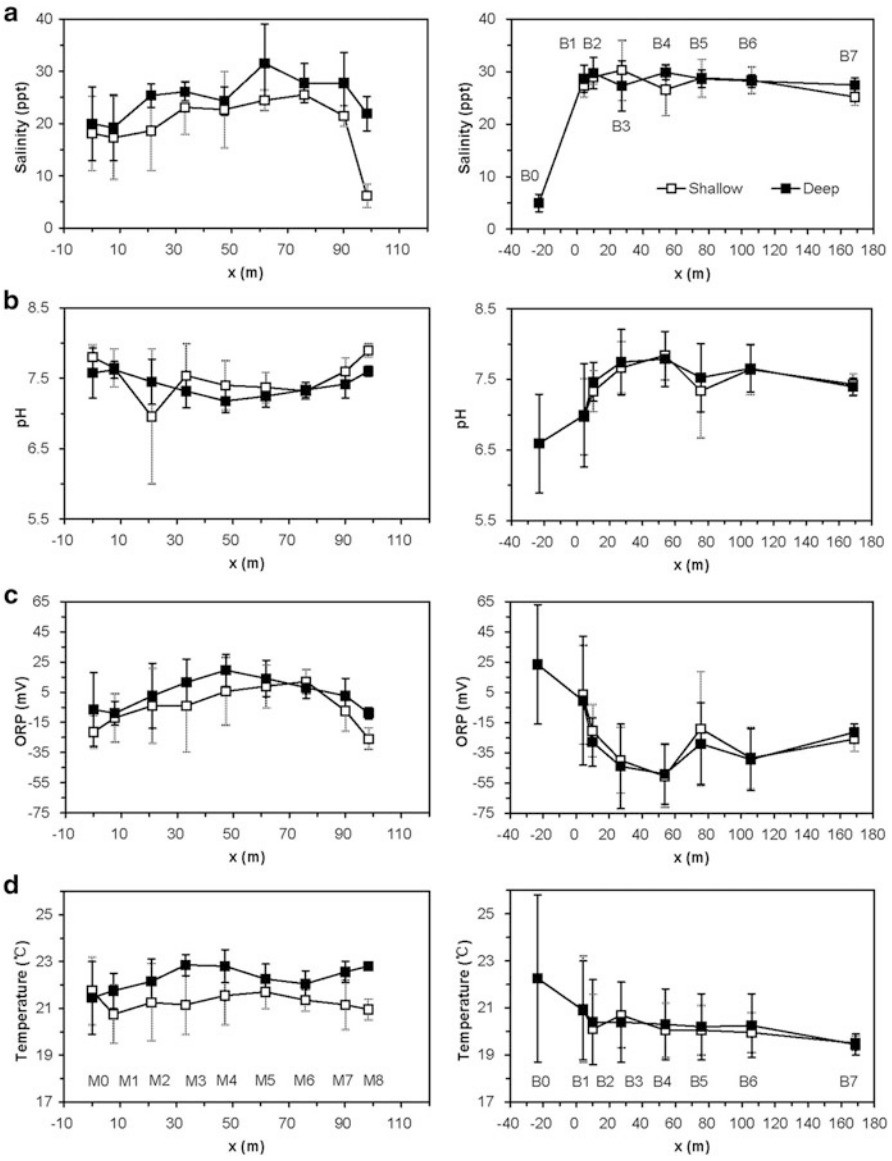

Fig. 2.4 Observed pH, salinity, ORP and temperature of the mangrove (*left panel*) and bald beach (*right panel*) transects. The average is indicated by *symbols*, and the maximum and minimum are indicated by the upper and lower ends of the *vertical bars*, respectively. The shallow and deep locations for each well were indicated in Fig. 2.3 and given in Tables 2.1 and 2.2

bald beach transect, indicating a different subsurface environment between them (Xia and Li 2010).

Figure 2.4a reports the groundwater salinity over the 3-day observation period at two depths of each well in the intertidal zones of the mangrove and bald beach transects. The salinity distribution along the two transects shows a significant difference. The averaged salinity in each well along the mangrove transect is significantly lower than that along the bald beach transect, particularly in the high intertidal zones and near the low tide lines of the two transects. Further calculations showed that the average salinity of all the wells is 23.0 ppt for the mangrove transect and 28.5 ppt for the bald beach transect. The salinity varies significantly along the mangrove transect implies a strong saltwater and freshwater exchange there. In addition, in each well of the mangrove transect, salinity at shallow location is always lower than that at deep location. As documented by the observations of both water table and salinity and numerical simulations of the water table that were conducted by Xia and Li (2012), the salinity discrepancy between the two transects was most probably caused by the difference of freshwater recharge conditions between them.

Figure 2.4b shows that in the mangrove transect, pH values of the high intertidal zones and near the low tide lines were higher than that of the middle intertidal zone, indicating that the vegetation has an effect of decreasing the pH value of groundwater in the rhizosphere. On the contrary, in the bald beach transect, pH values of the high intertidal zones and near the low tide lines were lower than that of middle intertidal zone, indicating that the biogeochemistry dominated by the fauna in the intertidal zone has an effect of increasing the pH value of groundwater.

The ORP in the intertidal zone of the mangrove transect is significantly higher than that of the bald beach transect as depicted in Fig. 2.4c. Along the mangrove transect, the averaged ORP values in almost all the wells were positive. Along the bald beach transect, most of the averaged ORP values were negative. The above observations indicate that the mangrove transect has an oxidizing environment (particularly between M2 and M7 of the mangrove transect where the rhizosphere of the mangroves is located) and the bald beach transect has a reducing environment.

The temperatures of groundwater demonstrated in Fig. 2.4d further indicate a different subsurface environment along the two transects. The temperature along the mangrove transect shows a significant variation with depths (increasing of temperature with depth). The temperature along the bald beach transect is almost constant with depths. These phenomena may be explained by the fact that in winter the temperature of surface water is lower than that of the groundwater.

2.4.2 Water Quality

In order to identify the difference of hydrochemistry characteristics between the mangrove and bald beach transects, we compared the concentrations of common anions and cations of groundwater sampled approximately at the same time from

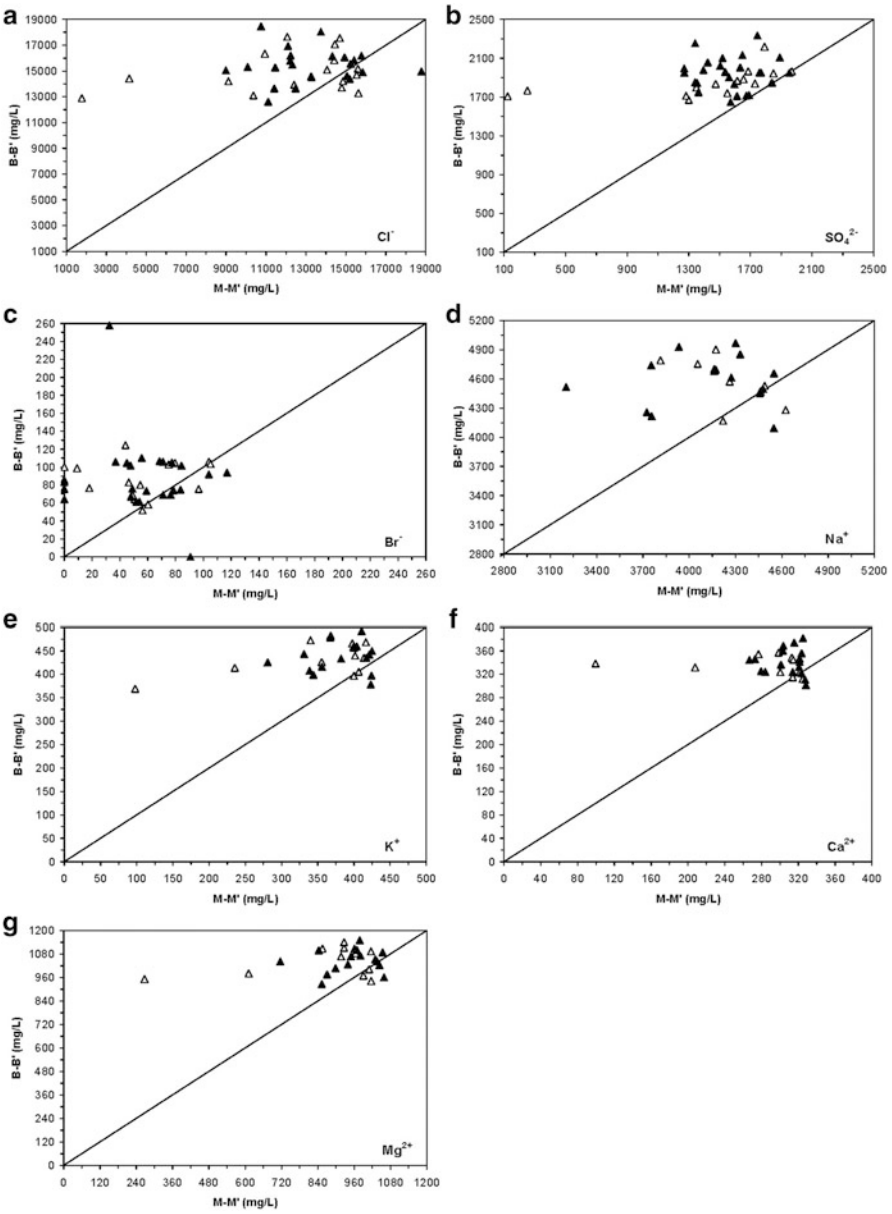

Fig. 2.5 Comparison of the concentrations of common anions (**a**) Cl^-, (**b**) SO_4^{2-}, (**c**) Br^- and cations (**d**) K^+, (**e**) Na^+, (**f**) Ca^{2+}, and (**g**) Mg^{2+} of groundwater sampled approximately at the same time from the seven pair of geomorphologically similar wells (M0, B1), (M1, B2), (M2, B3), (M3, B4), (M4, B5), (M6, B6), and (M8, B7) of the bald beach and the mangrove transects. For example, the concentration of the anion Cl^- of a sample from the shallow location of the well M0 and that of the shallow location of the well B1 at approximately the same time may produce a point in (**a**). The *hollow triangles* represent samples from the shallow locations, and the *black triangles*, from the deep locations. The shallow and deep locations for each well were indicated in Fig. 2.3 and given in Tables 2.1 and 2.2

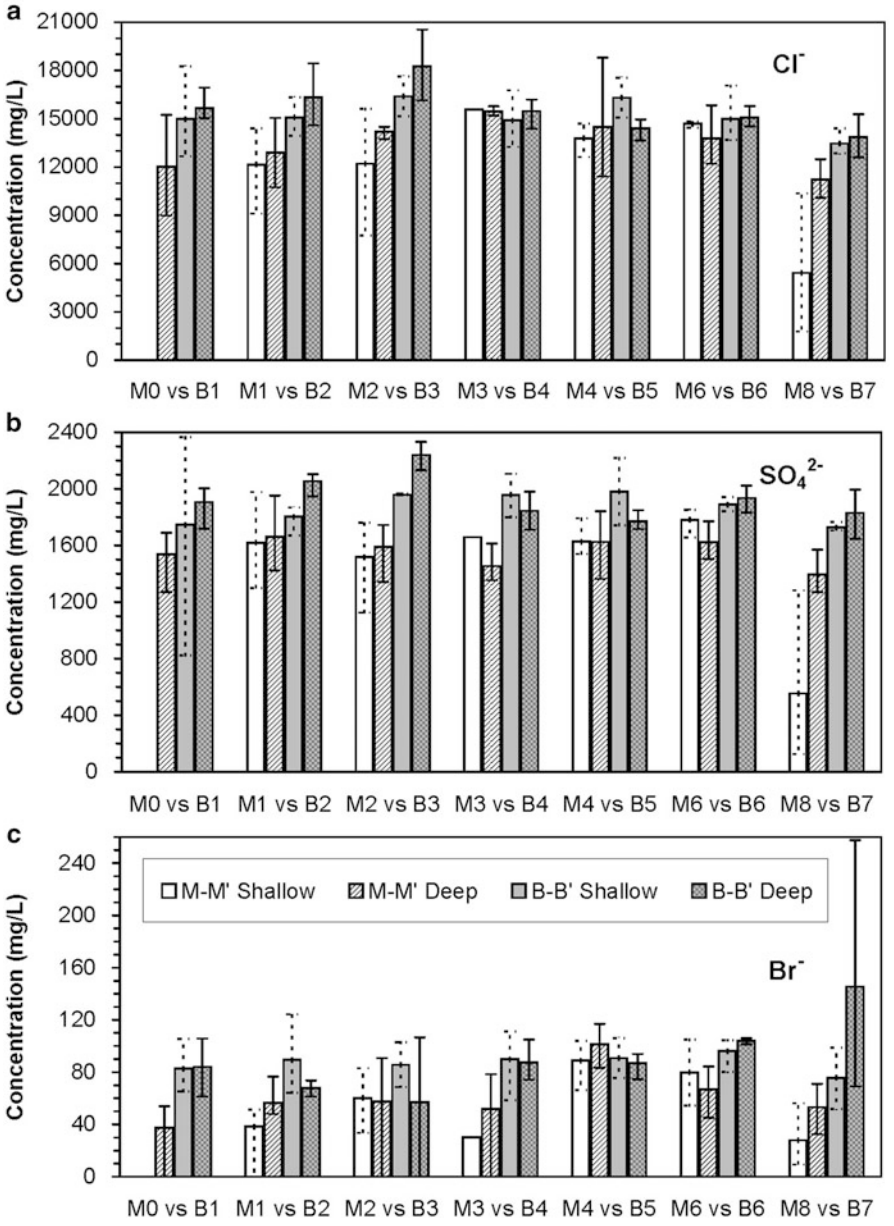

Fig. 2.6 Averaged concentrations of common anions of groundwater sampled at different times from shallow and deep depths in each pair of geomorphological similar wells (M0, B1), (M1, B2), (M2, B3), (M3, B4), (M4, B5), (M6, B6), and (M8, B7) of the bald beach and the mangrove transects. The maximum and minimum with respect to the time are indicated by the upper and lower ends of the *vertical bars*, respectively

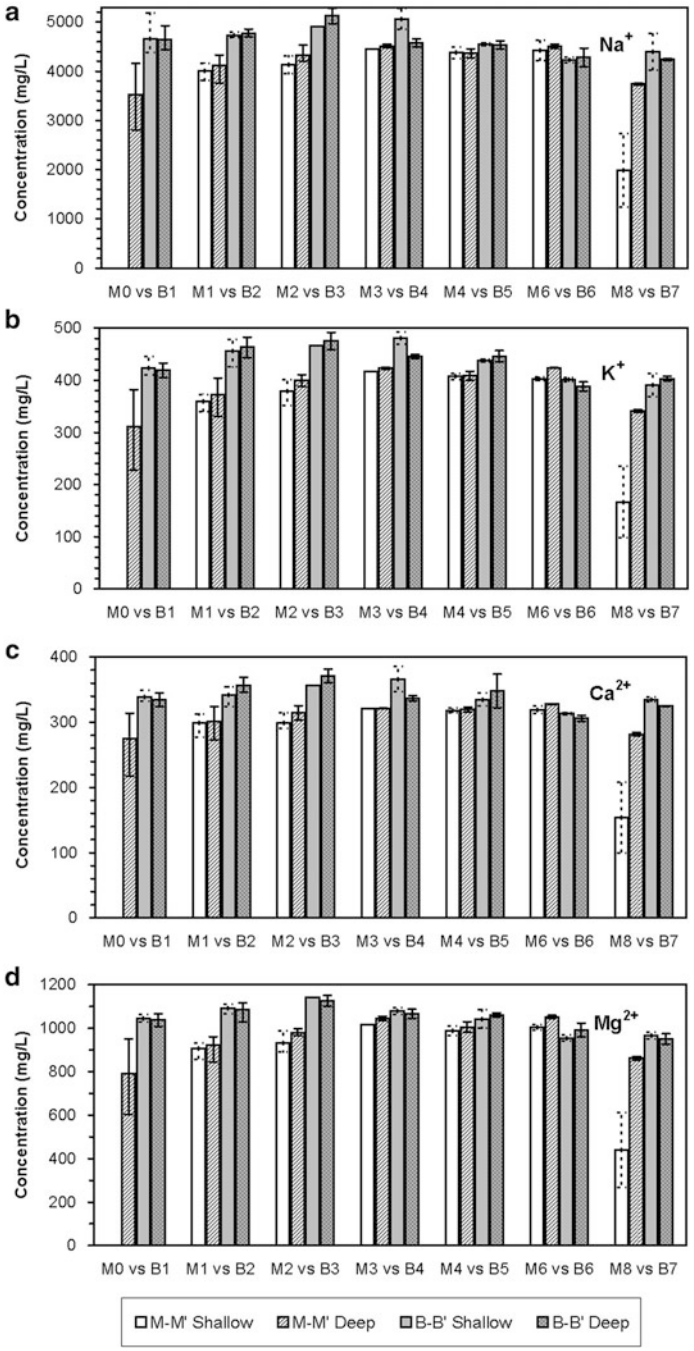

Fig. 2.7 Averaged concentrations of common cations of groundwater sampled at different times from shallow and deep depths in each well along the bald beach and mangrove transects. The maximum and minimum with respect to the time are indicated by the upper and lower ends of the *vertical bars*, respectively

the seven pair wells (M0, B1), (M1, B2), (M2, B3), (M3, B4), (M4, B5), (M6, B6), and (M8, B7) of the bald beach and the mangrove transects. Each pair of wells were matched according to the geomorphological similarity in the intertidal zone of the two transects. For example, both of the well M0 of the mangrove transect and the well B1 of the bald beach transect are located at the high tide mark, so they comprise a pair of wells for comparison. The other six pair of wells were also submerged by the tides at approximately the same time.

As depicted in Fig. 2.5, Lab analysis showed that the concentrations of common anions (Cl^-, SO_4^{2-}, Br^-) and cations (K^+, Na^+, Ca^{2+}, Mg^{2+}) of water sampled from the bald each transect were significantly higher than those of the mangrove beach transect, which is consistent with the observed salinity. The reasons for these include the following. (1) There is a significant fresh groundwater recharge from inland along the mangrove transect but no inland freshwater recharge along the bald beach transect (Xia and Li 2012). (2) The bald beach transect is nearer to the open seawater than the mangrove transect.

Figures 2.6 and 2.7 further show the concentrations of common anions and cations, respectively, at shallow and deep depths in each well along the two transects. The anions and cations in the most seaward well M8 along the mangrove transect show the lowest concentrations (Fig. 2.6), which could be due to the dilution effect of freshwater runoff from the upper stream. In addition, the large concentration difference between the shallow and deep locations at M8 indicated that inland freshwater discharge might dilute the shallow pore water at M8. Along the bald beach transect, the concentrations of anions and cations in well B0 were much lower than that in other wells where the concentrations are close to each other (Fig. 2.7), indicating well B0 has a very poor connection with other wells and the tidal water (Guo et al. 2010; Xia and Li 2012).

2.5 Summary and Conclusions

This paper reported a comparison study of hydrogeology and hydrochemistry along two transects in mangrove tidal marsh at Dongzhaigang National Nature Reserve, Hainan, China. The results indicated that the mangrove transect had an oxidizing environment and the bald beach transect has a reducing environment. Lab analysis of water samples showed that the concentrations of anions and cations along the bald each transect were much higher than that of the mangrove beach transect. The freshwater recharge from inland is considerable along the mangrove transect but negligible along the bald beach transect, this may be one of the main reasons for that the concentrations of salt and regular ions were lower along the mangrove transect than along the bald beach transect.

Acknowledgments This research is supported by the National Science Fund for Distinguished Young Scholars (No. 41025009), the Scientific Research Foundation for the Returned Overseas Chinese Scholars, and the Fundamental Research Funds for Central Public Welfare Research Institutes.

References

Bosire JO, Dahdouh-Guebas F, Walton M, Crona BI, Lewis RR, Field C, Kairo JG, Koedam N (2008) Functionality of restored mangroves: a review. Aquat Bot 89:251–259

Chapman VJ (1977) Wet coastal ecosystem. Elsevier, Amsterdam

Chen KL, Chen GZ, Huang ZQ, Howes J, Li ZW, Mo YN, Wu HS, Wu TJ, Yan CG, Yuan DX, Zheng XR (1999) Management plan of Dongzhaigang National Nature Reserve. Ramsar Site Management Plans, Hainan

Duke NC, Meynecke JO, Dittmann S, Ellison AM, Anger K, Berger U, Cannicci S, Diele K, Ewel KC, Field CD, Koedam N, Lee SY, Marchand C, Nordhaus I, Dahdouh-Guebas F (2007) A world without mangroves. Science 317:41–42

Field CB, Osborn JG, Hoffman LL, Polsenberg JF, Ackerly DD, Berry JA, Bjorkman O, Held A, Matson PA, Mooney HA (1998) Mangrove biodiversity and ecosystem function. Glob Ecol Biogeogr Lett 7:3–14

Fu GA (1995) The mangroves of Dongzhai Gang Natural Reserve, Hainan. Guihaia 15:340–346 (in Chinese)

Gilman EL, Ellison J, Duke NC, Field C (2008) Threats to mangroves from climate change and adaptation options: a review. Aquat Bot 89:237–250

Guo HP, Jiao JJ, Li HL (2010) Groundwater response to tidal fluctuation in a two-zone aquifer. J Hydrol 381:364–371

Kjerfve B (1990) Manual for investigation of hydrological processes in mangrove ecosystems, UNESCO/UNDP Project, Research and its Application to the Management of the Mangroves of Asia and the Pacific (RAS/86/120). UNESCO, Paris

NMDIS (2008) Tide table. National Marine Data & Information Service, China

Spalding M, Blasco F, Field C (1997) World mangrove atlas. International Society for Mangrove Ecosystems, Okinawa, 178 pp

Valiela I, Bowen JL, York JK (2001) Mangrove forests: one of the world's threatened major tropical environments. Bioscience 51:807–815

Weiss J, Weiss T (2005) Handbook of ion chromatography. 3rd, completely revised and enlarged edn. Wiley, Weinheim, 931p

Xia YQ, Li HL (2010) Environmental & hydrogeological factors of tidal marsh: a case study in Dongzhaigang Mangrove Reserve. J Yangtze River Sci Res Inst 27:35–38 (in Chinese with English abstract)

Xia YQ, Li HL (2012) A combined field and modeling study of groundwater flow in a tidal marsh. Hydrol Earth Syst Sci 16:741–759

Ye Y, Lu C (2001) Dynamics of CH4 in soil under *Aegiceras Corniculatum* mangrove at Changning estuary of Hainan Island. J Trop Oceanogr 20:35–42 (in Chinese)

Chapter 3
A Geochemical and Geophysical Assessment of Coastal Groundwater Discharge at Select Sites in Maui and O'ahu, Hawai'i

P.W. Swarzenski, H. Dulaiova, M.L. Dailer, C.R. Glenn, C.G. Smith, and C.D. Storlazzi

Abstract This chapter summarizes fieldwork conducted to derive new estimates of coastal groundwater discharge and associated nutrient loadings at select coastal sites in Hawai'i, USA. Locations for this work were typically identified based on pronounced, recent ecosystem degradation that may at least partially be attributable to sustained coastal groundwater discharge. Our suite of tools used to evaluate groundwater discharge included select U/Th series radionuclides, a broad spectrum of geochemical analytes, multi-channel electrical resistivity, and *in situ* oceanographic observations.

Based on the submarine groundwater discharge tracer ^{222}Rn, coastal groundwater discharge rates ranged from about 22–50 cm per day at Kahekili, a site in the Ka'anapali region north of Lahaina in west Maui, while at Black Point in Maunalua Bay along southern O'ahu, coastal groundwater discharge rates ranged up to 700 cm per day, although the mean discharge rate at this site was 60 cm per day. The water chemistry of the discharging groundwater can be dramatically different than ambient seawater at both coastal sites. For example, at Kahekili the average concentrations of dissolved inorganic nitrogen (DIN), dissolved silicate (DSi) and total dissolved phosphorus (TDP) were roughly 188-, 36-, and 106-times higher in the discharging groundwater relative to ambient seawater, respectively. Such data extend our basic understanding of the physical controls on coastal groundwater discharge and provide an estimate of the magnitude and physical forcings of

P.W. Swarzenski (✉) • C.D. Storlazzi
U.S. Geological Survey, 400 Natural Bridges Dr., Santa Cruz, CA 95060, USA
e-mail: pswarzen@usgs.gov

H. Dulaiova • C.R. Glenn
Department of Geology and Geophysics, School of Ocean and Earth Science and Technology, University of Hawaii, Honolulu, HI 96822, USA

M.L. Dailer
Department of Botany, University of Hawaii, Manoa, 3190 Maile Way, Honolulu, HI 96822, USA

C.G. Smith
U.S. Geological Survey, 600 4th Street South, St. Petersburg, FL 33701, USA

C. Wetzelhuetter (ed.), *Groundwater in the Coastal Zones of Asia-Pacific*,
Coastal Research Library 7, DOI 10.1007/978-94-007-5648-9_3,

submarine groundwater discharge and associated trace metal and nutrient loads conveyed by this submarine route.

3.1 Introduction

While one can only guess what the population of Hawai'i might have been when Captain James Cook first stepped ashore on these islands in early 1778, today many of the Hawaiian Islands are experiencing an unprecedented and sustained population growth. The Ka'anapali region north of Lahaina in west Maui is one good example of such growth, as it has become a highly desirable tourist destination. Not surprisingly, this shoreline is now rapidly being developed with newly-constructed resorts, hotels, and associated infrastructure (Dailer et al. 2010). Such development places new and challenging demands on scarce island resources that are already particularly vulnerable to external stressors. As surface water and groundwater resources become compromised by overuse and contamination, fragile nearshore ecosystems (e.g., coral reef systems) are often the most visibly affected by persistent anthropogenic burdens and can eventually sustain temporary or even permanent damage.

This chapter presents work that was conducted off the islands of O'ahu and Maui, Hawai'i, USA, to examine land-sea exchange processes in areas that have recently experienced dramatic ecosystem degradation (Fig. 3.1). One site is located in west Maui just north of Kahekili Beach Park in the Ka'anapali region (Fig. 3.2). This site is directly adjacent to widespread construction activities and tangentially down-gradient from a wastewater treatment plant that is located just a half a kilometer from the beach. This site has also recently been established as a U.S. Coral Reef Task Force priority study area as well as the Hawai'i Department of Land and Natural Resource's Division of Aquatic Resources' Kahekili Herbivore Fisheries Management Area (HFMA).

Areas of the seabed at Kahekili that were once dominated by substantial coral coverage are now coated mostly by turf- or macro-algae. At this site there are multiple active groundwater springs located just offshore, in 2 m of water and within 50 m of shore, where low salinity water can readily be seen discharging into nearshore bottom waters. These vents are obvious conduits that connect watershed activities directly to the coastal environment.

Previous scientific efforts at this site have been plentiful and have utilized, for example, dissolved nitrate – $\delta^{15}N$ records (Dailer et al. 2012), as well as a suite of tell-tale organic pollutants (e.g., Hunt and Rosa 2009) to infer focused wastewater discharges. In 2010, the US Coral Reef Task Force (USCRTF) designated the Ka'anapali linked watershed-reef system (ahupua'a) a USCRTF Hawaiian Local Action Strategy to address Land-Based Pollution (HI-LBP/LAS) priority study site to focus research and restoration efforts. At the same time, the Hawai'i Department of Land and Natural Resource's Division of Aquatic Resources' (DLNR/DAR) established the Kahekili HFMA in an effort to increase the number of herbivores to help reduce the turf- or macro-algae that have overgrown the corals at the site.

Coastal groundwater discharge was also studied at Maunalua Bay, located on the southern shores of O'ahu and close to Honolulu and Waikiki (Fig. 3.3). Sustained

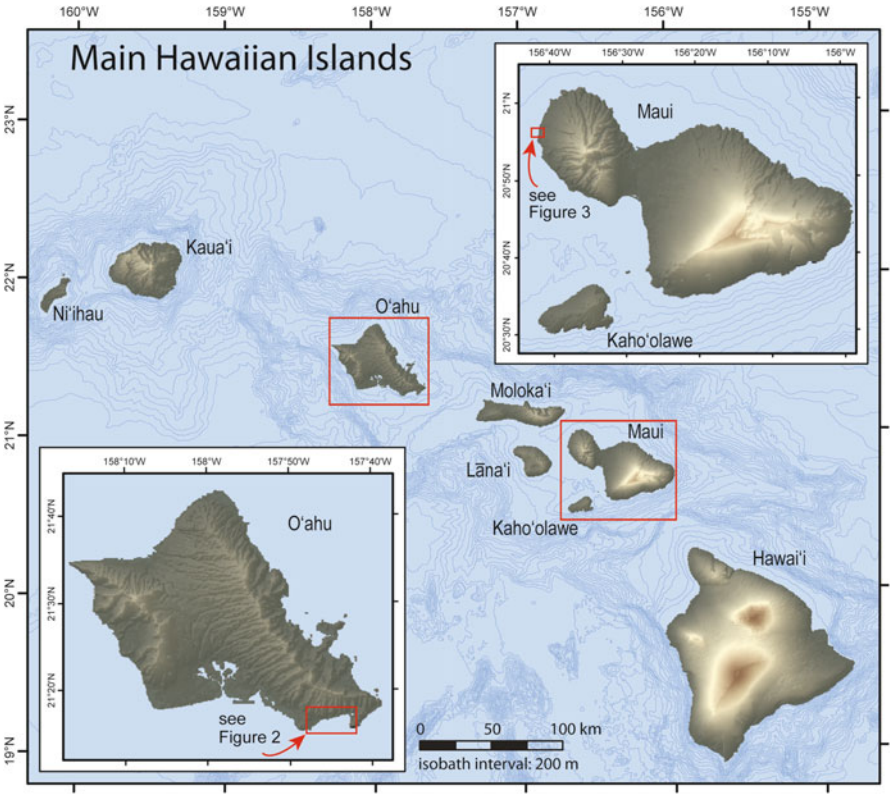

Fig. 3.1 General location map depicting the Hawaiian Islands. Field sites on west Maui (Kahekili) and south O'ahu (Maunalua Bay) are *highlighted*

anthropogenic perturbations (e.g., widespread urbanization, increased sediment erosion and downstream transport, increased nutrients and downgradient transport, shoreline armoring, dredging) in the watersheds of the nine smaller streams that enter Maunalua Bay have dramatically degraded the nearshore coral reef ecosystems, including the local fisheries (Wolanski et al. 2009). At the turn of the century, there were large, permanent, coastal freshwater springs (Hitchcock 1905) observed in Maunalua Bay. Today it is still possible to see surface-water expressions of a few active spring discharges, although the hydrology of the bay has been considerably impacted by onshore activities (Swarzenski et al. 2009). Varied restoration and resource management projects underwater today in Maunalua Bay are attempting to halt or reverse some of the causes of this ecological degradation (c.f. malamamaunalua.org).

Our study presents an interdisciplinary investigation where geochemical, geophysical, and oceanographic observations were utilized together to assess scales, rates, and constituent loadings associated with sustained, focused coastal groundwater discharges (Swarzenski 2007). These data extend our basic understanding of

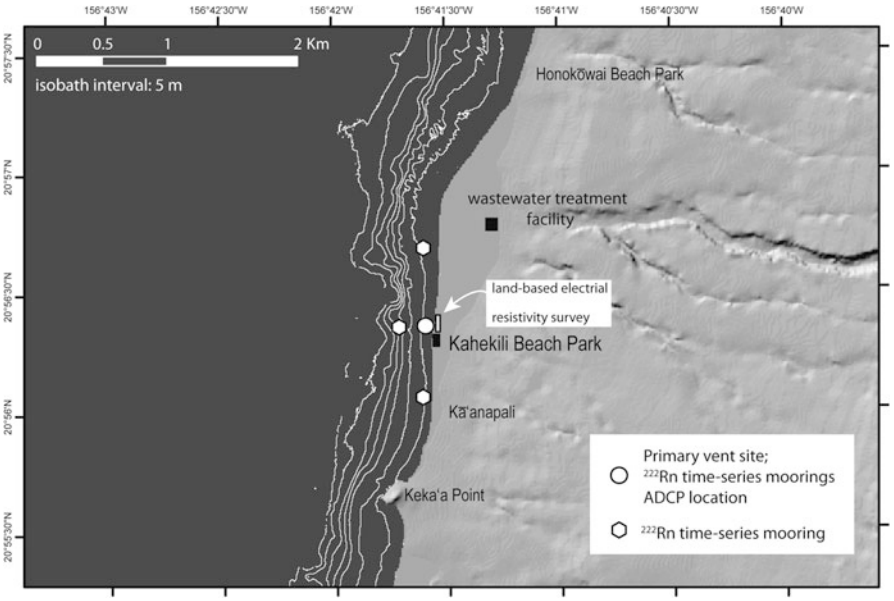

Fig. 3.2 Map depicting the Ka'anapali region of west Maui. Our field site at the primary vent site was located just north of Kahekili Beach Park. The surface water ^{222}Rn time-series mooring sites, the location of the land-based resistivity survey, and the wastewater treatment plant are also identified

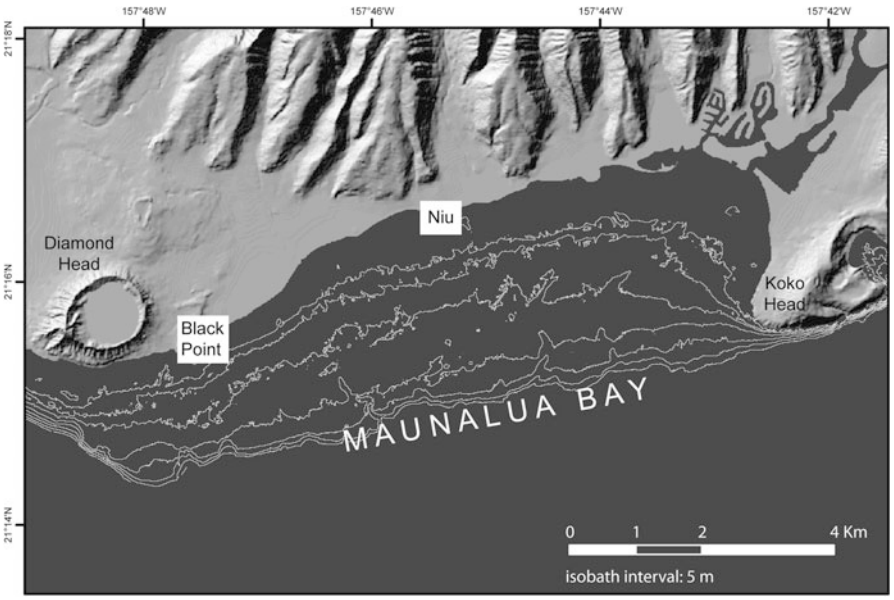

Fig. 3.3 Map depicting Maunalua Bay, O'ahu. Field efforts in Maunalua Bay were focused at Black Point and at Niu. Surface water and groundwater samples were collected at Black Point and the shore-perpendicular land-based resistivity survey was conducted at mid-bay at Niu. At both sites in Maunalua Bay there are surface water expressions of buoyant spring discharges

land/sea exchange at these locations (c.f. Bratton 2010), and provide observations of the magnitude and physical forcings of submarine groundwater discharge (SGD) and associated trace metals and nutrient loads conveyed by this submarine route (Swarzenski 2007). Based on multi-day, surface water ^{222}Rn time-series deployments at several sites in west Maui (Kahekili) and southern O'ahu (Maunalua Bay), coastal groundwater discharge rates were derived using a simple box model that accounted for loss and input terms. These flux estimates were quantified in terms of upward water movement (in cm per day) and used to derive associated constituent loadings for a suite of trace elements and nutrients. Loading estimates were then also compared to similarly-derived constituent loads for other select Hawaiian coastal waters.

3.2 Methods

3.2.1 Submarine Groundwater Discharge – Field Methods

Results for this work stem from two field efforts to the Hawaiian Islands. Maunalua Bay, on the southern shore of O'ahu was sampled during November 2008, while the site off west Maui just north of Kahekili Beach Park was sampled during July 2010. Further details on coastal groundwater discharge at Kahekili can be found in Swarzenski et al. (2012).

Continuous, *in situ* oceanographic information of the tides, waves, currents, and water temperature were typically collected at these sites during our field efforts (Fig. 3.4) using a 2-MHz Nortek Aquadopp acoustic Doppler current profiler (ADCP). This upward-looking profiler was attached to a seabed-mounted frame that was placed at a strategic site into shallow (~2 m) water. These physical oceanographic measurements provided information on the oceanographic forcings of the discharging vent plume and were used to place SGD results into a coastal oceanographic context.

To capture discharging vent water, a CTD-instrumented stainless-steel piezometer was carefully inserted into a prominent spring vent by SCUBA and monitored to assure that the groundwater discharge stream was not contaminated by ambient seawater. Subsequent time-series measurements of ^{222}Rn, as well as nutrients and select trace elements, were conducted from this piezometer and complimented with concurrent surface water samples that were collected from a small, moored boat. Water-quality parameters were continuously monitored using a calibrated YSI multi probe. In all instances at Kahekili, the dissolved oxygen concentrations in discharging groundwater samples were close to 1 mg/L (strongly sub-oxic), indicating that the groundwater samples were indeed not compromised by intruding seawater.

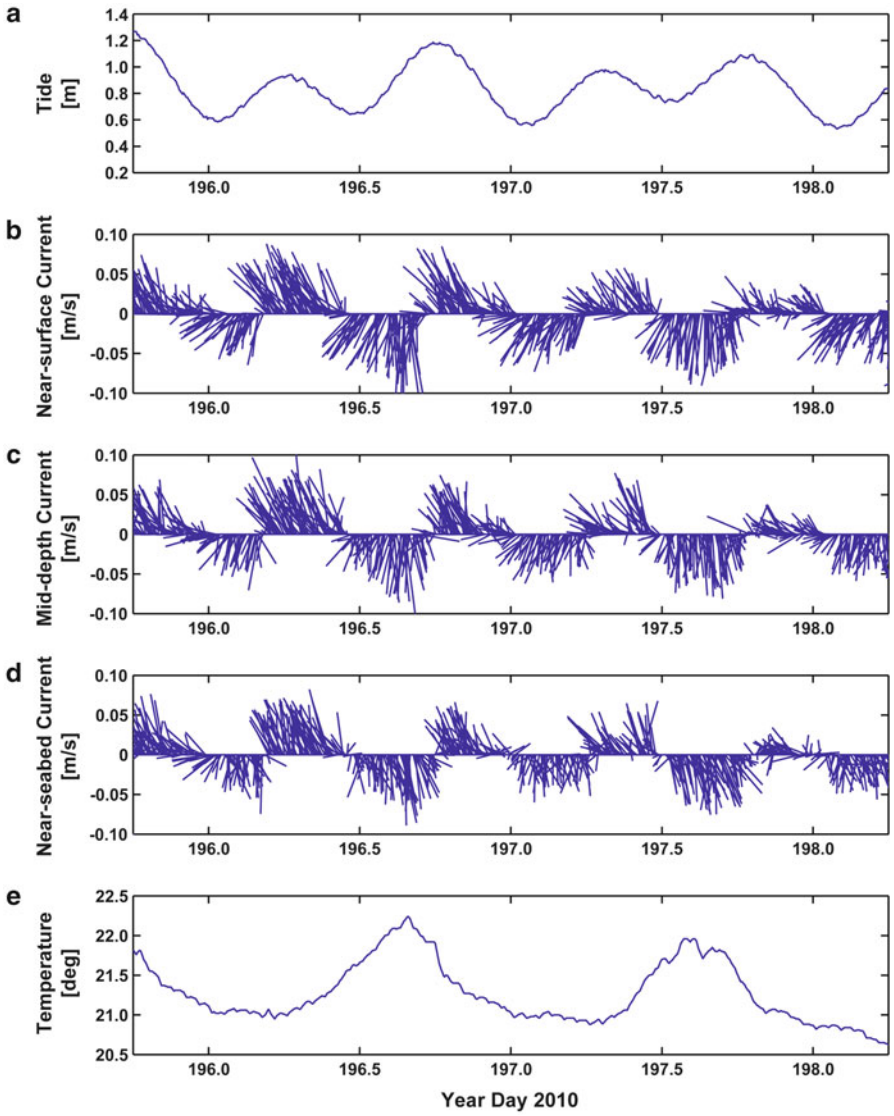

Fig. 3.4 Time-series plots of tide, current, and water temperature data from the ADCP at the primary vent site at Kahekili, Maui. (**a**) Tidal height, in meters. (**b**) Near-surface current speeds and directions, in meters per second from true north. (**c**) Mid-depth current speeds and directions, in meters per second from true north. (**d**) Near-bed current speeds and directions, in meters per second from true north. (**e**) Temperature, in degrees Celsius. The 2-day time series-shows the currents were fairly uniform throughout the water column and were modulated by the tide

3.2.2 Submarine Groundwater Discharge – Geochemical Tracers

The well-known ^{238}U-series decay-chain product radon (^{222}Rn) is a versatile and useful tracer for groundwater water transport and exchange, including SGD. The utility of ^{222}Rn as a water mass tracer is due to its very short half-life of 3.8 days, its existence as a noble gas (i.e., chemically inert), and because most often ^{222}Rn is many-times enriched in groundwater relative to surface water (Swarzenski 2007). As a side note, radium (^{226}Ra is a direct radiogenic parent of ^{222}Rn) is typically present in Hawaiian coastal waters in such low activities that this tracer's proven ability to track coastal groundwater discharge in many other coastal settings remains challenging in these waters.

Recent advances in the determination of ^{222}Rn have been simplified by the use of a commercially available Rn-in-air monitor and a simple water/air exchanger. Such a setup allows for the almost real-time calculation of the aqueous Rn concentration by measuring the air ^{222}Rn concentration and by knowing the temperature dependent ^{222}Rn partitioning coefficient (Burnett and Dulaiova 2003; Burnett et al. 2003, 2006, 2007; Dulaiova et al. 2006; Swarzenski et al. 2006). A peristaltic or submersible pump was used to convey a continuous stream of either vent-, bottom-, or surface-water into the water/air exchanger. Air from the exchanger is then continuously pumped into the radon monitor where a solid-state, planar, Si alpha (PIPS) detector converts alpha radiation into usable electronic signals that can discriminate various short-lived daughter products (e.g., ^{218}Po, ^{214}Po) from ^{222}Rn.

Time-series measurements of surface water ^{222}Rn were typically obtained using a single RAD7 radon monitor setup for 30-min counting intervals. For each ^{222}Rn time-series, the surface- and bottom-waters were instrumented with Solinst LTC Leveloggers that continuously measured pressure, conductivity, and temperature on ambient seawater. The radon and pressure data were then modeled using a simple box model to derive total (fresh + brackish) submarine groundwater discharge (SGD) rates following methods developed by Burnett and Dulaiova (2003) and Burnett et al. (2001, 2006). Site locations for these surface water time-series deployments were strategically placed based on perceived gradients in oceanographic-, geologic-, and hydrologic-controls, as well as the level of anthropogenic perturbations. At the primary vent site at Kahekili, three additional time series mooring sites were spaced roughly equidistant from the primary vent site (Swarzenski et al. 2012). The purpose of these additional deployments was to observe how SGD rates may vary spatially and within different bottom types.

In general, a suite of time-series surface- and ground-water samples were analyzed at each site for ammonium (NH_4^+), dissolved silicate (DSi), soluble reactive phosphorus (SRP), nitrate-nitrite (NO_3^- + NO_2^-), dissolved inorganic nitrogen, (DIN), dissolved organic nitrogen (DON), total dissolved nitrogen (TDN), total dissolved phosphorus (TDP), molybdenum (Mo), barium (Ba), rhenium (Re), vanadium (V), iron (Fe), cesium (Cs), uranium (U), chromium (Cr), and manganese (Mn). As per methods summarized in Swarzenski et al. (2007a), the suite of nutrients was determined on a Lachat Instruments QuickChem 8000 at Woods

Table 3.1 Mean trace element concentrations (nM) in surface water and discharging groundwater at the primary vent site at Kahekili Beach Park, Maui

	Mo	Ba	V	Fe	U	Cr	Mn
	(nM)						
Surface water							
Mean	106.0	30.2	39.2	1,492.9	11.0	59.6	112.4
+/−	2.9	0.3	5.8	1,362.9	0.3	60.8	98.0
Min	98	29	32	66	10	3	7
Max	110	30	51	3,859	11	178	320
Groundwater							
Mean	45.3	17.2	291.0	2,304.8	0.8	82.8	12,228.5
+/−	7.5	3.5	44.4	2,064.1	0.2	64.3	1,990.2
Min	30	11	200	44	1	1	8,355
max	54	22	348	6,976	1	204	14,500

Table 3.2 Mean nutrient concentrations (μM) in surface water and discharging groundwater at the primary vent site at Kahekili Beach Park, Maui

	NH_4	DSi	PO_4	$[NO_2 + NO_3]$	DIN	DON	TDN
	(μM)						
Surface water							
Mean	0.07	15.97	0.11	0.20	0.19	6.69	6.88
+/−	–	5.93	0.06	0.15	0.14	1.20	1.22
Min	0.07	9.48	0.05	0.03	0.03	5.65	5.68
Max	0.07	25.38	0.23	0.40	0.40	9.30	9.48
Groundwater							
Mean	0.09	629.42	12.14	41.33	41.42	10.47	51.88
+/−	0.04	139.27	0.60	1.24	1.25	1.21	1.78
Min	0.03	431.91	10.97	38.36	38.41	8.81	48.87
Max	0.17	813.87	13.05	42.18	42.28	12.81	54.65

All samples unacidified unless denoted
DSi dissolved silicate, *DIN* dissolved inorganic nitrogen, *DON* dissolved organic nitrogen, *TDN* total dissolved nitrogen, *TDP* total dissolved phosphorus

Hole Oceanographic Institution (WHOI), while the suite of trace elements was analyzed on a HR-ICPMS at the University of Southern Mississippi. Mean trace element concentrations (in nM) from the Kahekili primary vent site are presented in Table 3.1, while mean nutrient concentrations are presented in Table 3.2.

3.2.3 Multi-channel Electrical Resistivity

Land-based electrical resistivity (ER) techniques, including newer multi-channel systems and custom streamer arrays, can provide useful information on the dynamics of the freshwater/saltwater interface (Manheim et al. 2004; Swarzenski et al. 2004,

2006; Dimova et al. 2012). Depending on the electrode streamer configuration (i.e., cable length and electrode spacing), this interface can be readily examined to depths that approach 20–30 m below the surface of the earth. The electrical resistivity of underlying beach sediment at study sites was surveyed using an Advanced Geosciences Inc. (AGI) eight channel Marine SuperSting R8 system connected to an external switch box that controlled the flow of current along the 56-electrode cable. This system was programmed to measure current potentials in a distributed array so that resolution and signal-to-noise ratio can be maximized.

For each resistivity measurement, the receiver injects an optimized current, reverses the polarity and then re-injects the current again to cancel any potential spontaneous voltages. This process is typically repeated until the error falls below a prescribed threshold value. Land-based electrical resistivity surveys were conducted along the beach face adjacent to the primary vent site at Kahekili, as well as at other beach sites adjacent to the two more distal ^{222}Rn mooring sites. For this work, the streamer was oriented shore-parallel and placed just landward of the high-tide line. Current flow was routed down-cable from a user-defined command file using a dipole-dipole configuration. These settings enabled the collection of more than 760 discrete resistivity readings in less than 25 min. This is usually fast enough to capture tidal forcings on the freshwater/saltwater interface.

3.3 Results and Discussion

During fieldwork conducted in July 2010 at Kahekili in west Maui, the maximum tidal range was 0.74 m, the mean wave heights were 0.50 m, and the wave periods and directions ranged from 4.2 to 11.0 s and from 225.9 to 263.6°, respectively. Nearshore currents appear to be forced by the tide, and near-surface and near-seabed current speeds ranged up to 0.11 and 0.09 m/s, respectively. In general, while the primary orientation of near-shore flow was alongshore, the mean current direction throughout most of the water column at the deployment site was directed offshore in a west-southwest direction (Fig. 3.4).

3.3.1 Submarine Groundwater Discharge – Nutrient Loadings

At Kahekili, the salinity of the discharging vent water was surprisingly fresh and fluctuated (salinity ranged from under 2 to more than 12) depending on the tide (Fig. 3.5). Ambient seawater salinities above the primary vents were consistently between 34 and 36, indicating only slight freshening relative to true open-ocean salinities. Nonetheless, the surface water salinity was noticeably lower than the bottom water salinity during much of the time-series, indicating the presence of a buoyant spring plume.

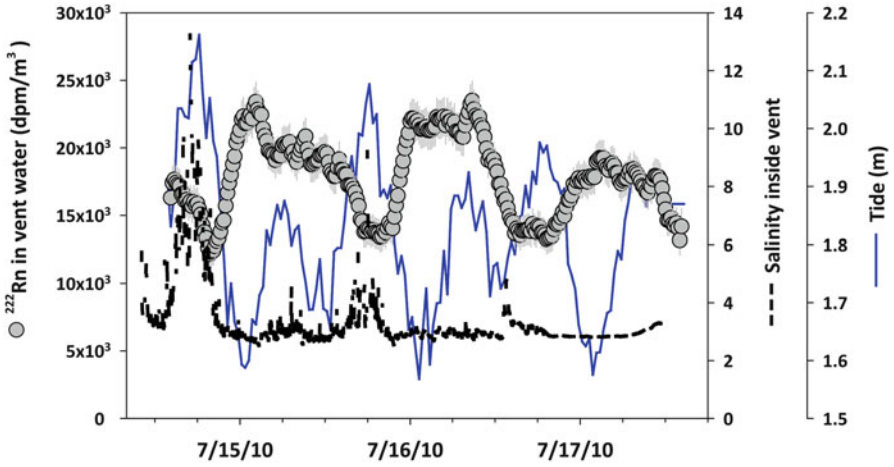

Fig. 3.5 Surface water, time-series plot of ^{222}Rn activities (in disintegrations per minute per cubic meter, dpm m^{-3}), salinity, and water levels at the primary vent site at Kahekili. This discharging groundwater was captured using a piezometer that was inserted into the throat of an active spring vent using SCUBA. A representative groundwater endmember ^{222}Rn value (27,045 dpm m^{-3}) used in the radon mass balance was extracted from this groundwater ^{222}Rn time series

The mean ^{222}Rn activity in the discharging vent water at Kahekili varied inversely as a function of the tide (Fig. 3.5). From this groundwater ^{222}Rn time-series, a representative mean value of the discharging vent water ^{222}Rn activity (27,045 dpm m^{-3}) was used to calculate submarine groundwater discharge rates at all four surface water mooring sites. Acknowledging the various assumptions that are inherent in the application of a ^{222}Rn box model (Burnett and Dulaiova 2003; Burnett et al. 2001, 2003, 2006, 2007; Dulaiova et al. 2006; Swarzenski et al. 2006, 2007a,b, 2009; Smith and Swarzenski 2012) to derive a rate of submarine groundwater discharge, the calculated SGD rate was highest (mean = 55 ± 56 cm per day; max = 277 cm per day) at the primary vent site and consistently lower (20–30 cm per day) at the three surrounding sites. The three more distal ^{222}Rn mooring sites were chosen based on bottom sediment/bedrock type as well as distance from the main vent site (Swarzenski et al. 2012). Based on these radon data, it appears that groundwater discharge was most pronounced at the shallow primary vent site but was still enhanced at each of the more distal Rn-mooring sites. This implies that groundwater discharge at Kahekili may not be confined to just an area within the shallow vent sites, but is likely more regional in scale.

Similarly, at Maunalua Bay on O'ahu, ^{222}Rn time-series data show a dramatic response to tidal forcing. Figure 3.6a illustrates a multi-day, surface water ^{222}Rn time series conducted at Black Point in Maunalua Bay, O'ahu during November 2008. Radon activities sharply spiked during the primary and even the secondary low tide events, attaining levels above 70,000 dpm m^{-3} at the lowest tides. Radon activities rapidly fell back to background values at all but these low tide events. Spanning several tidal cycles, the shallow groundwater at a beach at Black Point

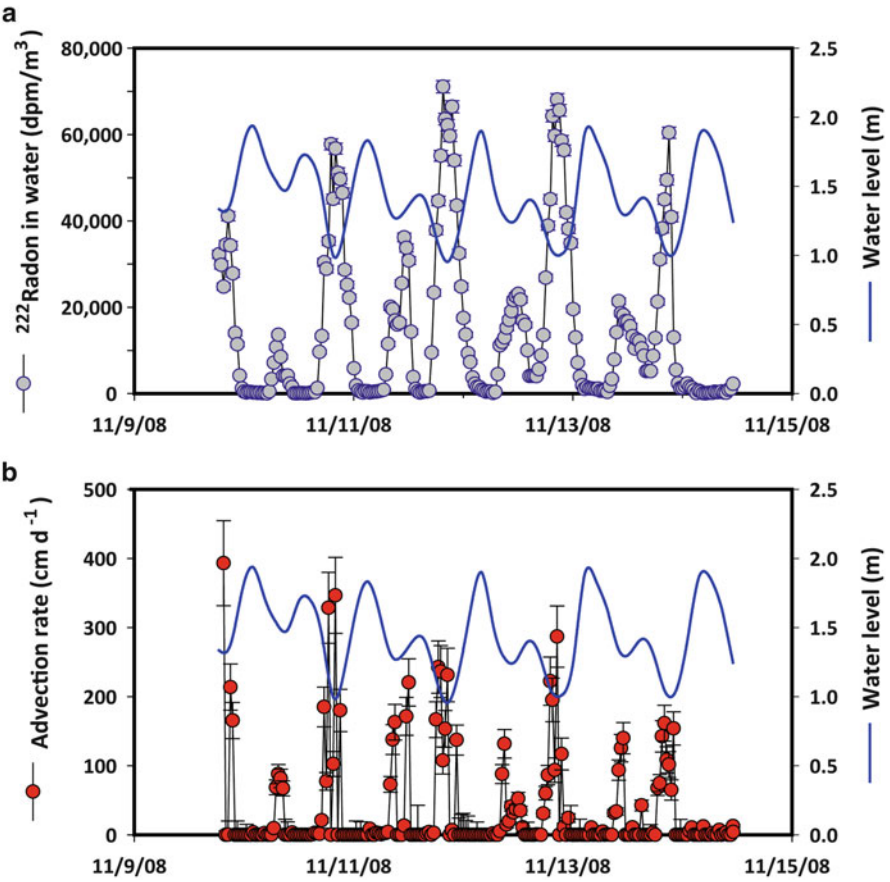

Fig. 3.6 (**a**) Multi-day, time-series plot of surface water ^{222}Rn activities (in disintegrations per minute per cubic meter, dpm m^{-3}) as a function of the tide at Black Point, Maunalua Bay, O'ahu. (**b**) Model results of radon-derived advective rates (in cm per day). The mean advective discharge rate for the duration of the time-series was 60 cm per day

was also sampled continuously for a suite of analytes, including ^{222}Rn. In these samples, the mean groundwater ^{222}Rn activity approached 400,000 dpm m^{-3}. This discharging groundwater endmember activity was used to calculate advection rates (Fig. 3.6b) for this site, following methods previously outlined. A more thorough discussion on the development of this simple box model to calculate SGD rates from radon time-series data is presented in Smith and Swarzenski (2012). Advection rates at Black Point ranged to just over 700 cm per day, while the mean advective discharge rate for the duration of the time-series was 60 cm per day.

Using the ^{222}Rn time-series distribution, a first estimate of the distance and direction of the submarine groundwater discharge plume can be derived from the *in situ* oceanographic observations. At the primary vent site, 3-h progressive vector diagrams of projected cumulative flow starting from the vent site at low tide were

computed following methods described by Siegel et al. (2003) (Fig. 3.7). These calculations assume uniform alongshore and across-shore flow which may not always be the case (Storlazzi and Jaffe 2003, 2008; Storlazzi et al. 2003, 2004, 2006; Storlazzi and Field 2008). These projections do, however, provide information on the relative direction and magnitude of transport of nutrient-laden submarine groundwater discharged from the vent during the projected time period if the forcing mechanisms (wind and tides) remain uniform over the projected travel path. Our measurements off Kahekili showed that there was net alongshore flow, and, therefore net transport of nutrient-laden water, to the south from the vent site towards Keka'a Point during the 3 h following low tides when the submarine groundwater discharge rate was greatest.

In addition to the surface water and groundwater ^{222}Rn time-series data, discrete water samples were also collected at the primary vent site. Table 3.1 summarizes the mean trace element concentrations (in nM) obtained during this sampling at Kahekili. The discharging vent water was strongly depleted in dissolved oxygen (as measured with a YSI multi-probe; data not shown), which was also manifested in some of the observed redox-sensitive trace element concentrations (i.e., Mn, U, V, and Mo). For example, mean vanadium and manganese concentrations were about 7- and 108-times more enriched in the discharging groundwater than in ambient seawater, respectively. In contrast, Fe is only enriched roughly 1.5-times in the reduced groundwater relative to seawater. Some trace element concentrations (e.g., Fe, Cr, and Mn) increased systematically after the 10:00 low tide event, verifying that the tide modulates groundwater discharge rates and associated constituent concentrations.

Mean nutrient (NH_4, DSi, PO_4^{-3}, DIN, DON, and TDN) concentrations (μM) in surface water and discharging vent water at Kahekili are summarized in Table 3.2. Very little ammonia was present either in the surface water (mean concentration = 0.07 μM) or the discharging groundwater (mean concentration = 0.09 μM). Mean silica concentrations were roughly 36-fold greater in discharging groundwater (mean = 629.4 μM) than ambient surface seawater (mean = 15.97 μM). Dissolved inorganic nitrogen (DIN) concentrations were also much higher in discharging groundwater (mean = 41.4 μM) than in ambient surface seawater over the vents (mean = 0.2 μM). The mean N:P (DIN/PO_4^{-3}) molar ratio for discharging groundwater at this site was 3.4.

One can use mean coastal groundwater nutrient concentrations (Table 3.3) and calculated SGD rates to derive submarine groundwater discharge-associated nutrient loading estimates into nearshore waters (Garrison et al. 2003; Swarzenski and Izbicki 2009; Johnson et al. 2008; Peterson et al. 2009; Knee et al. 2010; Smith and Swarzenski 2012). The calculated mean submarine groundwater discharge rate for the primary vent site at Kahekili Beach Park (55 cm per day; or 55 m^3 per day per m of shoreline if we assume that the SGD occurs within a 100-m wide zone) is on the same order of magnitude as the mean Rn-derived submarine groundwater discharge rates obtained recently for two sites in Maunalua Bay, O'ahu (Black Point = 60 cm per day, Swarzenski et al. 2009) as well as two additional SGD rate estimates reported in Johnson et al. (2008) and Peterson et al. (2009) for the Kona coast of Hawai'i. Using these Rn-derived mean SGD rates, the following nutrient loading estimates are

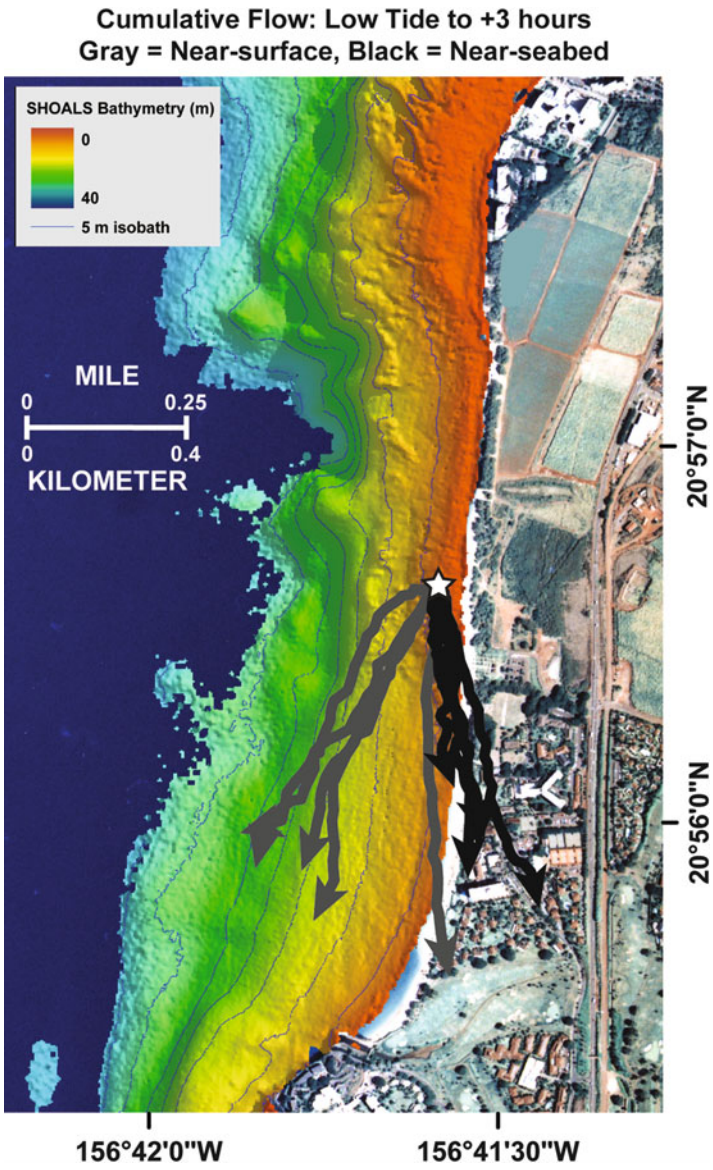

Fig. 3.7 Map showing modeled cumulative flow distance for 3 h following low tide at the near surface (*gray* vectors) and near bed (*black* vectors) starting at the primary vent site at Kahekili. Submarine groundwater discharge volumes were highest in the 3 h following low tide, so these data provide insight into the dominant direction and distance of submarine groundwater transport. The flow at the near surface was slightly faster and more to the southwest than the flow near the seabed

Table 3.3 Mean discharging groundwater nutrient concentrations (μM) at two sites in Maunalua Bay, Hawai'i

	NH_4	DSi	PO_4	$[NO_2 + NO_3]$	DIN	DON	TDN
	(μM)						
Black Point	1.2	210.8	2.6	141.9	143.1	10.3	153.4
Niu	0.3	234.4	1.2	47.1	47.4	4.2	51.6

DSi dissolved silicate, *DIN* dissolved inorganic nitrogen, *DON* dissolved organic nitrogen, *TDN* total dissolved nitrogen, *TDP* total dissolved phosphorus

Table 3.4 Mean SGD-associated nutrient loading estimates (moles per day per meter of shoreline) at select nearshore sites in Kahekili (Maui) and Black Point and Niu, Maunalua Bay (O'ahu)

	NH_4	Silicate	PO_4^{3-}	$[NO_2 + NO_3]$	DIN	DON	TDN
Site	(mol/d/m)						
Kahekili, Maui	0.0	34.6	0.7	2.3	2.3	0.6	2.9
Black Point, O'ahu	0.08	12.65	0.16	8.24	8.32	0.53	8.85
Niu, O'ahu	0.01	7.61	0.04	1.49	1.50	0.14	1.65

DSi dissolved silicate, *DIN* dissolved inorganic nitrogen, *DON* dissolved organic nitrogen, *TDN* total dissolved nitrogen, *TDP* total dissolved phosphorus

calculated for the primary vent site at Kahekili (moles per day per meter of shoreline): NH_4^+: 0.01 mol/day/m, DSi: 34.6 mol/day/m, PO_4^{-3}: 0.70 mol/day/m, $[NO_2^- + NO_3^-]$: 2.3 mol/day/m, DIN: 2.3 mol/day/m, DON: 0.6 mol/day/m, and TDN: 2.9 mol/day/m.

Table 3.4 summarizes these results from the primary vent site at Kahekili and compares them to similarly obtained SGD-derived nutrient fluxes at Niu and Black Point in Maunalua Bay, O'ahu. It is interesting to note that the mean $[NO_2^- + NO_3^-]$ concentrations were comparable for the Niu (Maunalua Bay, O'ahu) and Kahekili (Maui) sites, while at Black Point (Maunalua Bay, O'ahu) these nutrients were about 3.5-times higher. Figure 3.8 illustrates select groundwater nutrient concentrations collected during a 10-h time-series at a beach at Black Point, Maunalua Bay, O'ahu. This time-series sampling was started at low tide and extended through high tide. Dissolved silicate (DSi) and ammonia (NH_4^+) concentrations generally increased with the tide, while $[NO_2^- + NO_3^-]$ concentrations dropped as the tide and salinity rose. Our groundwater piezometer at this site was installed close to a large upgradient residential community and elevated nutrients observed here may reflect associated enhanced nutrient loads. In developing realistic bay-wide SGD-related nutrient loading estimates, establishing a representative groundwater nutrient or radionuclide endmember is obviously critical.

3.3.2 Multi-channel Electrical Resistivity Surveys

Beneath many of Hawai'i's beaches, focused submarine groundwater discharge provides a direct conduit of exchange between the watershed, the coastal aquifer,

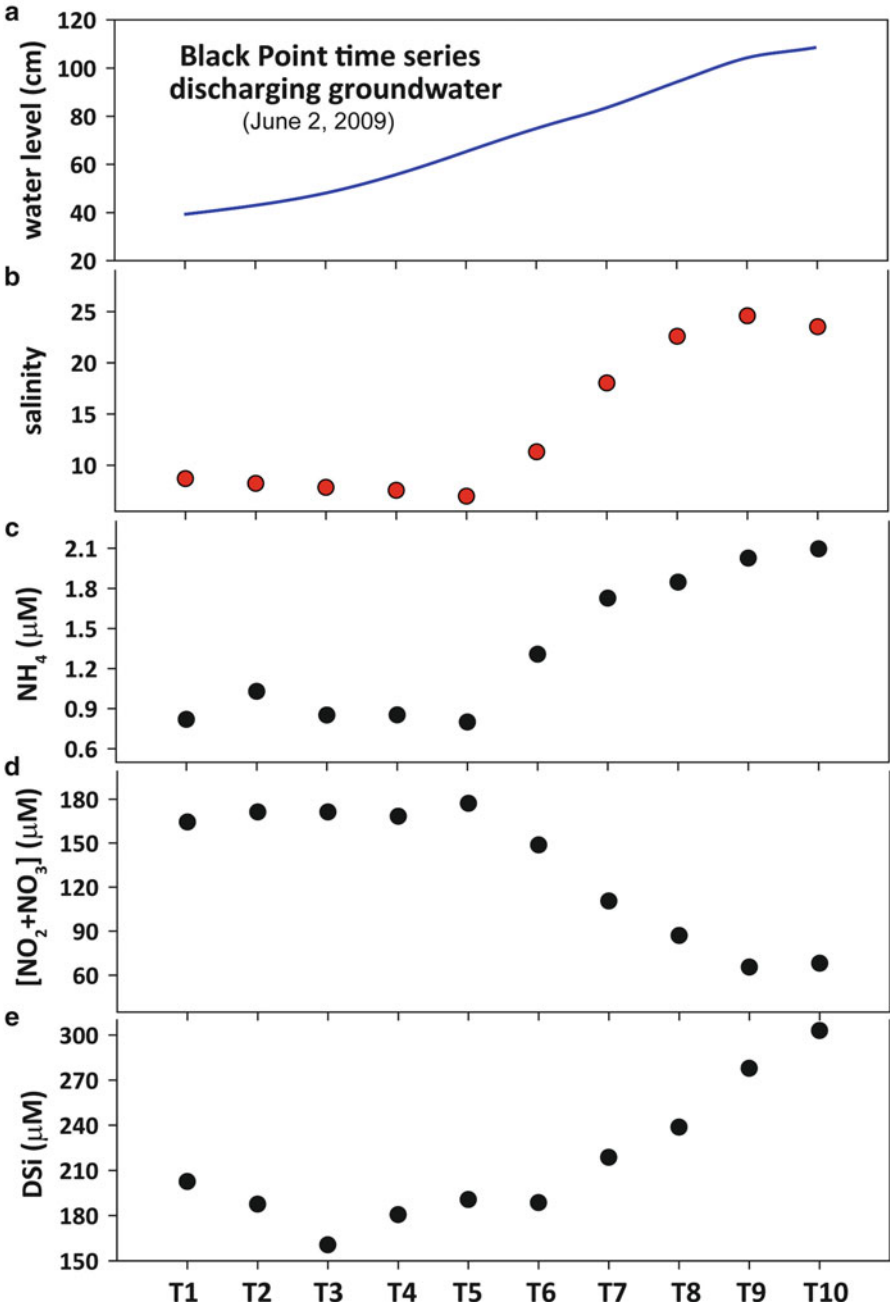

Fig. 3.8 A 10-h time-series surface- and ground-water sampling conducted at a beach face at Black Point, Maunalua Bay, O'ahu. This time-series was initiated at low tide and lasted past high tide. (**a**) water level (tide, in cm); (**b**) salinity; (**c**) NH_4^+ concentrations (in μM); (**d**) $[NO_2^- + NO_3^-]$ concentrations (in μM); and (**e**) dissolved silicate (DSi) concentrations (in μM)

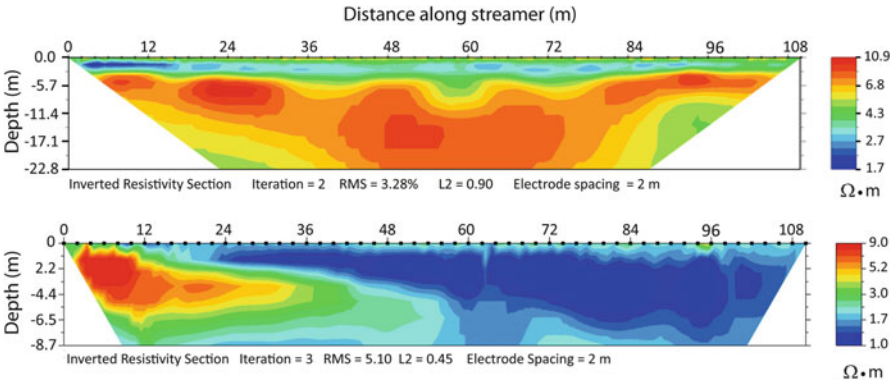

Fig. 3.9 (**a**) Shore-parallel, electrical resistivity survey conducted along the beach face at Kahekili in west Maui adjacent to the primary vent site (*y*-axis is meters below the surface of the earth). Although resistivity values are influenced both by geologic and hydraulic parameters (Swarzenski et al. 2007a, b), it is likely that the higher resistive layers observed in this model define zones of enhanced hydrologic permeability. (**b**) Shore-perpendicular electrical resisitivty survey conducted at low tide at Niu, Maunalua Bay, O'ahu. The dynamic mixing of different salinity groundwater enroute to the sea can be readily identified. (Redrawn from Dimova et al. 2012)

and the nearshore water column. Changes in groundwater (i.e., pore water) conductivity (conductivity = resistivity^{-1}) cause a large increase in resistivity according to well-known empirical laws governing the resistivity in porous matrices (Day-Lewis et al. 2006). For example, Archie's Law relates bulk resistivity (Ω-m) of a porous rock to a formation factor (Manheim et al. 2004; Swarzenski et al. 2006):

$$\rho_T = \rho_f F;\ F = \Phi^{-m}$$

where

ρ_T = the bulk resistivity (Ω-m) of the saturated material;
ρ_f = the resistivity (Ω-m) of the pore fluid;
F = Formation Factor (unitless);
Φ = fractional porosity (unitless) of the matrix material; and
m = an empirical exponent (unitless) based on the lithology.

Applying Archie' Law, one can, for example, estimate that the bulk resistivity of an unconsolidated sand layer ($m \sim 2$) may be roughly four times the resistivity of seawater, which is about 0.3 Ω-m). Deviations from this may be interpreted in terms of a hydrologic control, i.e., the presence of a more resistive (freshened) groundwater parcel.

At Kahekili in west Maui and at Niu in Maunalua Bay, O'ahu, land-based resistivity surveys were conducted to examine: (i) the tidal modulation of fresh water/salt water interface, (ii) the hydrogeologic controls on submarine springs, and (iii) the scales of submarine groundwater discharge. One representative, processed land-based electrical resistivity image is shown for each study site in Figs. 3.9a and b.

At Kahekili (Fig. 3.9a), where the streamer array was positioned shore-parallel, a sharp contact was observed along the entire line roughly 2–5 m below the beach face. It is likely that this contact represents a transition between surficial beach sands and deeper geologic deposits. These deeper layers likely represent limestone, caprock, and gravel alluvium that is situated above older volcanic-rock aquifers. Groundwater would be preferentially conveyed in these deposits towards the coast where they can rise to the surface due their density contrast with seawater (Manheim et al. 2004; Swarzenski et al. 2006, 2007a, b).

Figure 3.9b illustrates a shore-perpendicular resistivity image collected at Niu, which is located about midway along the shoreline of Maunalua Bay, O'ahu. At this site, there also exist several submarine springs that continuously discharge less saline groundwater into surrounding seawater. The resistivity image appears to capture these spring vents that occur within a few meters of the shore and provides a visual perspective of the dynamic mixing that occurs within a coastal aquifer that discharges to the sea.

3.4 Conclusions

Any beach is a tremendously dynamic and rewarding environment in which to study the interplay between terrestrial and marine forcings. There may be no better place to study these geologic, hydrologic, and oceanographic processes than on Hawai'i's beaches. By their island nature, many coastal aquifers in Hawai'i are particularly vulnerable to overuse, contamination, and global climate change. Often, the hydrology of the islands can be vastly different depending on orographic and climatic controls (c.f. Knee et al. 2010). For example, on the relatively dry, western ('Kona') side of the Big Island of Hawai'i, nearly all rainfall rapidly infiltrates into porous basalts, and thus most material flow towards the coast is conveyed via groundwater. In contrast, on the eastern side of Hawai'i, precipitation rates can be very high and abundant streams contribute significantly to the seaward transport of terrestrial materials. Yet, the persistent discharge of a coastal aquifer to the ocean – be it through diffuse seepage or focused springs – provides a direct window into the environmental well-being of the upland watershed. Global climate change induced impacts on local hydrology (Vecchi et al. 2006) and focused anthropogenic stressors along coastal margins will thus be expressed quite differently whether one resides on the leeward- versus the windward-side of an island. These short- and long-term impacts are just now beginning to be better understood and assessed.

This paper summarizes recent field efforts to two islands in Hawai'i, USA to quantify coastal groundwater discharge rates and scales, and estimate associated nutrient loadings. Such work has relevance to coastal resource managers and scientists alike, who need comprehensive information to develop accurate nutrient budgets to best oversee and study real and perceived threats to an ecosystem.

Our study sites in west Maui (Kahekili) and in south O'ahu (Maunalua Bay) have many similarities. For example, both unfortunately suffer from advanced, chronic ecosystem degradation. Luckily both are also targets of directed restoration efforts that hope to attenuate or even reverse some of the principal contributors to this ecosystem degradation. Both systems lie downstream either of widespread urbanization (Maunalua Bay) or construction (Kahekili). Both also have active submarine springs that discharge lower salinity groundwater directly into ambient seawater. How this groundwater is conveyed to the coast and the general groundwater quality relative to ambient seawater are, however, quite different in these two settings and interesting to study.

The discharging groundwater at the primary vent site north of Kahekili Beach Park in west Maui had a salinity of about 2. In contrast, the salinity of discharging groundwater was roughly 7 at the Black Point site in Maunalua Bay, O'ahu. While advection peaked close to 700 cm per day at Black Point, the mean advection rate of 60 cm per day is on the same order of magnitude as the mean advection rate computed for the primary vent site at Kahekili (55 cm per day). Discharging groundwater nutrient concentrations, collected from temporary piezometers placed close to the respective high-tide lines at either site showed stark local differences. For example, dissolved silicate was much higher at Kahekili than at Black Point, while $[NO_2^- + NO_3^-]$ concentrations were about 3.5 times higher at Black Point than at Kahekili. Radon-derived advection rates multiplied by groundwater nutrient concentrations can yield first- order estimates of SGD-associated nutrient loadings to respective coastal waters. During the studies, most of the total dissolved nitrogen (TDN) conveyed to the sea occurs in the form of dissolved inorganic nitrogen (DIN). Ammonia concentrations are systematically low at all study sites and so contribute only minimally to this DIN pool. Dissolved silicate and PO_4^{-3} loadings were highest at Kahekili relative to the two sites in Maunalua Bay, O'ahu.

Such observations provide new information as to the scales, magnitudes, and constituent loadings of submarine groundwater discharge into nearshore coastal waters, and can be used to refine constituent mass balances and to help develop best management strategies.

Acknowledgements PWS gratefully acknowledges continued support for this work from the USGS Coastal Aquifer Project and the USGS Pacific Coral Reef Project, both of which are funded by the USGS Coastal and Marine Geology Program (CMGP). We would also like to thank Russell Sparks and Darla White (HI-DLNR/Division of Aquatic Resources) for invaluable logistical support, Chip Hunt (USGS-Honolulu) for early discussions that helped define original project objectives, and Susie Cochran (USGS-Santa Cruz) for expert GIS contributions. Technical reviews by Jessie Lacy and Nancy Prouty made substantial improvements to this paper.

CRG acknowledges support by a grant/cooperative agreement from the National Oceanic and Atmospheric Administration, Projects R/HE-2 and R/HE-17, which are sponsored by the University of Hawaii Sea Grant College Program, SOEST, under Institutional Grant No. NA09OAR4170060 from NOAA Office of Sea Grant, Department of Commerce. The views expressed herein are those of the author(s) and do not necessarily reflect the views of NOAA or any of its subagencies. UNIHI-SEAGRANT-BC-12-01. The use of trade names is for descriptive purposes only and does not imply endorsement by the U.S. Government.

References

Bratton JF (2010) Three scales of submarine groundwater flow and discharge across passive continental margins. J Geol 118:565–575

Burnett WC, Dulaiova H (2003) Estimating the dynamics of groundwater input into the coastal zone via continuous radon-222 measurements. J Environ Radioact 69:21–35

Burnett WC, Kim G, Lane-Smith D (2001) A continuous radon monitor for assessment of radon in coastal ocean waters. J Radioanal Nucl Chem 249:167–172

Burnett WC, Cable JE, Corbett DR (2003) Radon tracing of submarine groundwater discharge in coastal environments. In: Taniguchi M, Wang K, Gamo T (eds) Land and marine hydrogeology. Elsevier, Amsterdam, pp 25–43

Burnett WC, Aggarwal PK et al (2006) Quantifying submarine groundwater discharge in the coastal zone via multiple methods. Sci Total Environ 367:498–543

Burnett WC, Santos I, Weinstein Y, Swarzenski PW, Herut B (2007) Remaining uncertainties in the use of Rn-222 as a quantitative tracer of submarine groundwater discharge. In: Sanford W, Langevin C, Polemio M, Povinec P (eds) A new focus on groundwater–seawater interactions, vol 312. IAHS, Wallingford, pp 109–118

Dailer ML, Knox RS, Smith JE, Napier M, Smith CE (2010) Using $\delta^{15}N$ values in algal tissue to map locations and potential sources of anthropogenic nutrient inputs on the island of Maui, Hawai'i, USA. Mar Pollut Bull 60:655–671. ISSN 0025-326X, doi: 10.1016/j.marpolbul.2009.12.021

Dailer ML, Ramey HL, Saephan S, Smith CM (2012) Algal $\delta^{15}N$ values detect a wastewater effluent plume in nearshore and offshore surface waters and three-dimensionally model the plume across a coral reef on Maui, Hawai'i, USA. Mar Pollut Bull 64:207–213

Day-Lewis FD, White EA, Johnson CD, Lane JW Jr (2006) Continuous resistivity profiling to delineate submarine groundwater discharge – examples and limitations. The Lead Edge 25:724–728

Dimova NT, Swarzenski PW, Dulaiova H, Glenn C (2012) Utilizing multi-channel electrical resistivity methods to examine the dynamics of the freshwater – saltwater interface in two Hawaiian groundwater systems. J Geophys Res 117. doi: 10.1029/2011JC007509

Dulaiova H, Burnett WC, Chanton JP, Moore WS, Bokuniewicz HJ, Charette MA, Sholkovitz E (2006) Assessment of groundwater discharges into West Neck Bay, New York, via natural tracers. Cont Shelf Res 26:1971–1983

Garrison GH, Glenn CR, McMurtry GM (2003) Measurement of submarine groundwater discharge in Kahana Bay, O'ahu, Hawai'i. Limnol Oceanogr 48:920–928

Hitchcock CH (1905) Freshwater springs in the ocean. Pop Sci Mon 67:673–683

Hunt CD Jr, Rosa SN (2009) A multi-tracer approach to detecting wastewater plumes from municipal injection wells in nearshore marine waters at Kihei and Lahaina, Maui, Hawaii. U.S. Geological Survey Scientific Investigations Report 2009-5253, 166p

Johnson AG, Glenn CR, Burnett WC, Peterson RN, Lucey PG (2008) Aerial infrared imaging reveals large nutrient-rich groundwater inputs to the ocean. Geophys Res Lett 35:L15606. doi: 10.1029/2008GL034574

Knee KL, Street JH, Grossman EE, Boehm AB, Paytan A (2010) Nutrient inputs to the coastal ocean from submarine groundwater discharge in a groundwater-dominated system: relation to land use (Kona coast, Hawai'i, USA). Limnol Oceanogr 55(3):1105–1122

Manheim FT, Krantz DE, Bratton JF (2004) Studying groundwater under DELMARVA coastal bays using electrical resistivity. Groundwater 42:1052–1068

Peterson RN, Burnett WC, Glenn CR, Johnson AG (2009) Quantification of point-source groundwater discharges to the ocean from the shoreline of the Big Island, Hawai'i. Limnol Oceanogr 54:890–904

Siegel DA, Kinlan BP, Gaines SD (2003) Lagrangian descriptions of marine larval dispersion. Mar Ecol Prog Ser 260:83–96

Smith CG, Swarzenski PW (2012) An Investigation of submarine-groundwater-borne nutrient fluxes to the west Florida Shelf and recurrent harmful algal blooms. Limnol Oceanogr 57:471–485. doi: 10.4319/lo.2012.57.2.000

Storlazzi CD, Field ME (2008) Winds, waves, tides, and the resulting flow patterns and fluxes of water, sediment, and coral larvae off West Maui, Hawaii. U.S. Geological Survey Open-File Report 2008-1215. U.S. Geological Survey, Reston, 13p. http://pubs.usgs.gov/of/2008/1215/

Storlazzi CD, Jaffe BE (2003) Coastal circulation and sediment dynamics along West Maui, Hawai'i, PART I: long-term measurements of currents, temperature, salinity and turbidity off Kahana, West Maui: 2001-2003. U.S. Geological Survey Open-File Report 03-482, 28p. http://pubs.usgs.gov/of/2003/of03-482/

Storlazzi CD, Jaffe BE (2008) The relative contribution of processes driving variability in flow, shear, and turbidity over a fringing coral reef: West Maui, Hawai'i. Estuar Coast Shelf Sci 77(4):549–564

Storlazzi CD, Logan JB, McManus MA, McLaughlin BE (2003) Coastal circulation and sediment dynamics along West Maui, Hawai'i, PART II: hydrographic survey cruises A-3-03-HW and A-4-03-HW Report on the spatial structure of currents, temperature, salinity and turbidity along Western Maui. U.S. Geological Survey Open-File Report 03-430, 50p. http://pubs.usgs.gov/of/2003/of03-430/

Storlazzi CD, Field ME, Ogston AS, Logan JB, Presto MK, Gonzales DG (2004) Coastal circulation and sediment dynamics along West Maui, Hawai'i, PART III: flow and particulate dynamics during the 2003 summer coral spawning season. U.S. Geological Survey Open-File Report 2004-1287, 36p. http://pubs.usgs.gov/of/2004/1287/

Storlazzi CD, McManus MA, Logan JB, McLaughlin BE (2006) Cross-shore velocity shear, eddies, and heterogeneity in water column properties over fringing coral reefs: West Maui, Hawai'i. Cont Shelf Res 26:401–421

Swarzenski PW, Burnett B, Reich C, Dulaiova H, Peterson R, Meunier J (2004) Novel geophysical and geochemical techniques to study submarine groundwater discharge in Biscayne Bay, Fl. U.S. Geological Survey FS-2004-3117

Swarzenski PW (2007) U/Th series radionuclides as tracers of coastal groundwater. Chem Rev 107(2):663–674. doi: 10.1021/cr0503761

Swarzenski PW, Izbicki JA (2009) Examining coastal exchange processes within a sandy beach using geochemical tracers, seepage meters and electrical resistivity. Estuar Coast Shelf Sci 83:77–89. doi: 10.1016/j.ecss.2009.03.027

Swarzenski PW, Burnett WC, Weinstein Y, Greenwood WJ, Herut B, Peterson R, Dimova N (2006) Combined time-series resistivity and geochemical tracer techniques to examine submarine groundwater discharge at Dor Beach, Israel. Geophys Res Lett 33:L24405. doi: 10.1029/2006GL028282

Swarzenski PW, Simonds FW, Paulson T, Kruse S, Reich C (2007a) A geochemical and geophysical examination of submarine groundwater discharge and associated nutrient loading estimates into Lynch Cove, Hood Canal, WA. Environ Sci Technol 41:7022–7029

Swarzenski PW, Kruse S, Reich C, Swarzenski WV (2007b) Multi-channel resistivity investigations of the fresh water/saltwater interface: a new tool to study an old problem. In: Sanford W, Langevin C, Polemio M, Povinec P (eds) A new focus on groundwater–seawater interactions, vol 312. IAHS, Wallingford, pp 100–108

Swarzenski PW, Izbicki JA, Grossman EE, Glenn CR, Plath CA, Kelly JL (2009) A multiproxy tracer approach to submarine groundwater discharge studies: examples from Santa Barbara, CA and Maunalua Bay, Oah'u, HI. Geochim Cosmochim Acta 73:A1299–A1299

Swarzenski PW, Storlazzi CD, Presto MK, Gibbs AE, Smith CG, Dimova NT, Dailer ML, Logan JB (2012) Nearshore morphology, benthic structure, hydrodynamics, and coastal groundwater discharge near Kahekili Beach Park, Maui, Hawaii. U.S. Geological Survey Open-File Report 2012-1166, 34p. http://pubs.usgs.gov/of/2012/1166/

Vecchi GA, Soden BJ, Wittenberg AT, Held IM, Leetmaa A, Harrison MJ (2006) Weakening of tropical Pacific atmospheric circulation due to anthropogenic forcing. Nature 441. doi: 10.1038/nature04744

Wolanski E, Martinez JA, Richmond RH (2009) Quantifying the impact of watershed urbanization on a coral reef: Maunalua Bay, Hawai'i. Estuar Coast Shelf Sci 84:259–268. doi: 10.1016/j.ecss.2009.06.029

Part II
Methods in Coastal Groundwater Investigation and Assessment Tools

Chapter 4
Use of Geophysical and Hydrochemical Tools to Investigate Seawater Intrusion in Coastal Alluvial Aquifer, Andhra Pradesh, India

Surinaidu Lagudu, V.V.S. Gurunadha Rao, P. Rajendra Prasad, and V.S. Sarma

Abstract India has a very long coastline and 25 % of the country's population live in the coastal zone. Urban centers are located along the coast and three out of four metro cities are located on the coast. The high population density along the banks of major rives and coast Increasing population and demand for water putting the coastal aquifers under stress and causing sea water inrush and salinity upcoming in the coastal aquifers. Apart from sea water contamination, urban waste releases and agriculture inputs threatening the coastal groundwater aquifer systems. Generally coastal areas receive more pollutant loads from different sources including geogenic and anthropogenic sources. Central Godavari delta is located adjacent to the Bay of Bengal Coast, Andhra Pradesh, India and is drained by Pikaleru, Kunavaram and Vasalatippa drains. The area is occupied by recent Quaternary alluvium and gone through a series of marine transgression and regression. The entire study area comes under Godavari central canal command area, water is available throughout year except first week of June and last week of April in the canals. Water requirements for irrigation met from surface water in the delta. There is no groundwater pumping for agriculture as wells as for domestic purpose due to brackish nature of the groundwater at shallow depths. The groundwater depths varying from 0.8 to 3.4 m dug wells and in bore wells located near the coast 4.5–13.3 m. The established groundwater flow direction is to be towards Bay of Bengal from Amalapuram. Geophysical and hydrochemical tools were applied to

S. Lagudu (✉)
International Water Management Institute (IWMI), C/O ICRISAT,
Hyderabad 502 234, India

Groundwater Department, National Geophysical Research Institute (NGRI), Hyderabad, India
e-mail: L.Surinaidu@cgiar.org

V.V.S.G. Rao • V.S. Sarma
Groundwater Department, National Geophysical Research Institute (NGRI), Hyderabad, India

P.R. Prasad
Department of Geophysics, Andhra University, Vishakhapatnam, India

C. Wetzelhuetter (ed.), *Groundwater in the Coastal Zones of Asia-Pacific*,
Coastal Research Library 7, DOI 10.1007/978-94-007-5648-9_4,

identify the source of the salinity and to assess the saline water intrusion in the Godavari delta. Electrical Resistivity Tomography (ERT) surveys were carried out at several locations in the deltaic region to delineate the aquifer geometry and to identify saline water aquifer zones. The results inferred from ERT indicate 12–15 m thick loamy sands were existed from surface to subsurface and it is followed by 18–25 m thick clay layers. The thickness of clay is being increased toward Sea from inland. The low resistivity values in the delta are attributed to existence of the thick marine clays in the subsurface and relative high resistivities are attributed to existence of fresh water. The resistivity values similar to saline water <0.01 Ωm is attributed to the mixing of the saline water along surface water drains. In the Ravva Onshore Terminal low resistivity values indicated up coning of brines and mixing of saline water from Pikaleru drain. Groundwater samples were collected and analyzed for major ions (pH, EC, Ca^{2+}, $Mg^{2+,}$ Na^{+}, F^{-}, $HCO_3{}^{2-}$, Cl^{-}, $SO_4{}^{2-}$, $NO_3{}^{-}$). The elevated TDS, Na^{+} and Cl is due to dilution of clay minerals upstream and in the downstream mixing of sea water along the drains in the pre monsoon. The quality is being increase in the post monsoon season. The molar ratios of Na^{+2}/Cl (>0.86) and $SO_4{}^{-2}/Cl^{-}$ (<0.05) in the pre monsoon indicated strong influence of sea water and in the post monsoon increased Na^{+2}/Cl^{-} and $SO_4{}^{-2}/Cl^{-}$ (>0.05) indicated marine palaeo salinity, dilution of marine clays and dissolution of evaporites. The high $SO_4{}^{-2}/Cl$ in the post monsoon is attributed to dilution groundwater salinity due to rainfall infiltration and irrigation return flows in the delta. The low Na^{+2}/Cl^{-} ratios in upstream of the delta are due to sand exposures and isolated fresh water lances in the perched aquifers.

4.1 Introduction

Increased urbanization and land use pattern for irrigated agriculture has placed a high demand on groundwater resources in coastal areas worldwide and has also placed these resources at great risk to contamination of seawater (Kremer and Crossland 2002). The semi consolidated and unconsolidated sediments along the coastline helped mankind to go in for deeper groundwater exploration during the first half of the last century. As the exploration advanced towards deeper horizons, problems like salinity hazard, salt water intrusion, land subsidence etc. were faced, which made the situation quite complex. Most of the coastal aquifers are sedimentary in nature, with a few out crops of hard rocks along the coast. One of the important features of the coastal deposits is the occurrence of ground water in multilayered alluvial and marine sands, silts, clays and carbonate rocks deposited under beach, lagoonal, estuarine and marine environments. All these factors have a control on the quality of the formation of water. The coastal configuration and land forms vary widely depending upon the intensity of wave action, tides, other currents, sediment load, stage of the rivers, wind action and the ever changing riverine regime. The distribution of fresh water aquifers is controlled by the dynamic equilibrium between hydrostatic heads in the fresh and saline water

zones, influx of sea water into the streams and lagoons and the relative mound of sea with respect to the land mass. Hence, the coastal aquifers are highly vulnerable to seawater intrusion and the shallow aquifers are easily depleted due to overexploitation of groundwater in many parts of India and worldwide (Lambrakis 2006; Sarwade et al. 2007; Chidambaram et al. 2008; Alpar 2009; Carreira et al. 2010; Mondal et al. 2011). It causes potential salinization of groundwater and their sources are diverse including natural saline groundwater (Vengosh et al. 1999; Trefry et al. 2007; Falgas et al. 2009); halite dissolution (Hidalgo and Cruz-Sanjulian 2001); presence of palaeo-brackish water (Lozano-García and Ortega-Guerrero 1998) seawater intrusion (Kouzana et al. 2010; Sanford and Pope 2010); domestic, agricultural, and industrial effluents (Danielopol et al. 2003; Custodio 2010; Mondal et al. 2011), etc. Among these sources, seawater intrusion is the most common and widespread in coastal areas, and forces the abandonment of water wells in many instances (Giordana and Montginoul 2006).

Geophysical techniques combined with geochemical methods are effective tools to investigate the saline water intrusion and salinity source. The resistivity tomography tool has been successfully used to demarcate the saltwater–freshwater interface in different coastal settings worldwide (Bugg and Lloyd 1976; Urish and Frohlich 1990; Van Dam and Meulenkamp 1967; Zohdy 1969; Frohlich et al. 1994; Nowroozi et al. 1999; Choudhury et al. 2001). The chemistry of groundwater is largely a function of the mineral composition of the aquifer through which it flows. The hydrochemical processes and hydrogeochemistry of the groundwater vary spatially and temporally, depending on the geology and chemical characteristics of the aquifer. Apodaca et al. 2002; Martinez and Bocanegra 2002, have inferred that hydrogeochemical processes such as dissolution, precipitation, ion-exchange processes and the residence time along the flow path control the chemical composition of groundwater. Abimbola et al. 2002; Olatunji et al. 2001, also established that geology plays a significant role in the chemistry of subsurface water. The use of geochemical evolution of groundwater has been elucidated by (Wicks et al. 1995; Plummer 1977; Bredehoeft et al. 1983; Hendry and Schwartz 1990).

The present study illustrated the applications of geophysical techniques in the form of Electrical Resistivity Tomography (ERT) along with major ion chemistry of groundwater to assess the saline water intrusion and to identify the source of the salinity in the central Godavari delta region, Andhra Pradesh, India.

4.2 Description of the Study Area

The present study is Central Godavari delta located adjacent to Bay of Bengal coast, East Godavari district, Andhra Pradesh and covers 295 km^2 area (Fig. 4.1). The average annual rainfall in the study area is about 1,137 mm distributed unevenly over 57 rainy days, 72 % rainfall occurs during the southwest monsoon season (June–September) (Gurunadha Rao et al. 2011). Three crops are grown successively in a year and the use of fertilizers and pesticides is also very high in this

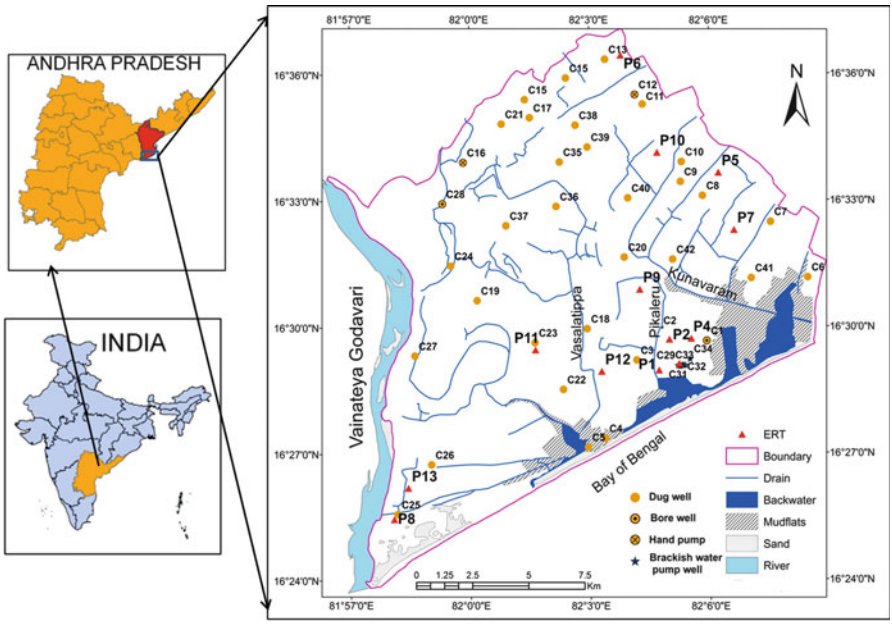

Fig. 4.1 Location of the Central Godavari delta, East Godavari district, A.P., India

region. As ample surface water is made available to irrigate the delta, there has been little or no effort to use groundwater in the deltaic region. The area is experiences seasonal floods in every alternate year resulted floods through Godavari River. Godavari irrigation canal network is well spread out in the area and provides perennial source of irrigation in all seasons. Irrigation Canals in the area flows towards the Bay of Bengal through three important drains, viz., Vasalastippa, Kunavaram and Pikaleru drains. Large network of Godavari canals are providing perennial irrigation as well as drinking water needs in the delta. These canals significantly help in reducing the native salinity of underlying marine clays due to recession of sea from inland to shore. The canals are in operation during last century and had been contributing for groundwater recharge, which impacted the improvement of groundwater quality in the area (Chachadi and Leitao 2002).

4.3 Geology and Hydrogeology

The area has rich in Quaternary alluvial formed by river Godavari and topography is having a gentle slope towards the coast with a value of 0.001 km^{-1} (Bobba 2002; Rao 1993). Major part of the area consists of sandy loams and sandy clay loams. The quaternary sediments occupying along the coastal tract and inland river valleys include thick blankets of alluvium, gravel and colluvial deposits, beach sand,

kankar, soils of various types. The upper deltaic sediments are essentially fluvial while those in the lower delta region are fluvio-marine sediments (GSI 2006). Silts and gravel beds are mixed with clay in varying proportions in the Godavari delta region. The thickness of alluvium varies from a few meters to more than 300 m and it overlies Rajahmundry sandstones. The thickness of granular zones in the alluvium ranges from 18 to 258 m within the explored depths (CGWB 1999; Bobba 2000). The delta region is occupied by loamy sandy soils and are underlined by thick clay beds of about 18–25 m and followed by coarse sands with saline water (Gurunadha Rao et al. 2011; Naidu et al. 2012).

4.4 Materials and Methodologies

4.4.1 Major Ions

For the assessment of groundwater quality, 42 groundwater samples were collected in the summer (June) and winter (November) seasons in the year 2006 from the represented dug wells, bore wells and hand pumps distributed throughout the study area. Samples were analyzed for major and minor ions (pH, EC, Ca^{+2}, Mg^{+2}, Na^{+}, HCO_3^{-}, Cl^{-}, SO_4^{-2}, NO_3^{-} and Br) by following standard methods suggest by APHA (2005). These samples were collected in 1 L polythene bottles. Prior to collection the bottles were thoroughly washed with diluted HNO_3 acid, and then with distilled water in the laboratory before filling the bottle with the sample. The bottle is rinsed to avoid any possible contamination in bottling and every other precautionary measure has been taken. The chemical parameters analyzed include Ca^{2+}, Mg^{2+}, HCO^{3-}, CO^{3-} and Cl^{-} by volumetric method, Na and K were analyzed by flame photometer; F was analyzed by ion metric methods, NO_3^{-} by double beam spectro photometer, SO_4^{-2} by turbidity, pH by a pH meter, total dissolved salt by gravimetric method and conductivity by conductivity meter.

4.4.2 Electrical Resistivity Tomography (ERT)

The resistivity data was collected using SYSCAL PRO-96, IRIS-make instrument. It is a ten-channel multi-electrode automatic resistivity meter with high accuracy. Multi-core cable used with this equipment supports with 5 m maximum inter-electrode spacing physically. The measured apparent resistivity is converted in to true resistivity using RES2D.INV inversion program in order to produce the 2D resistivity cross-section image. The data inversion was calculated with the least squares inversion method (Dahlin 1996). The output from the RES2DINV displays three sections, i.e., measured and calculated apparent resistivity pseudo-sections and the inverse model resistivity section. The pseudo-sections are a qualitative way

of presenting spatial variation of the measured or calculated apparent resistivity along cross-section and do not reflect the true depth and true formation resistivity. In the present study 2D Wenner-Schlumberger array was used to investigate subsurface of aquifer system. To tackle the 2D and 3D problems, we need more intensive data which is possible with multi-electrode systems (Griffiths and Barker 1993) and resistivity surveying instruments (Griffths et al. 1990) and fast computer inversion software (Loke 1994). This entire measurement carried out by the system and the data is stored in the system itself. 2D resistivity/IP data is interpreted using 2D-Forward modeling software. Apparent resistivity values are calculated using finite-difference (Dey and Morrison 1979) method.

4.5 Results and Discussion

4.5.1 Electrical Resistivity Tomography (ERT)

The electrical resistivity of a geological formation is physical characteristic, determines the flow of electric current in the formation. Resistivity varies with texture of the rock, nature of mineralization and conductivity of electrolyte contained within the rock (Parkomenko et al. 1967). Resistivity not only changes from formation to formation but even within a particular formation (Sharma 1997). Resistivity increases with grain size and tends to maximum when the grains are coarse (Sharma and Rao 1962), also when the rock is fine grained and compact. The resistivity drastically reduces with increase in clay content and which are commonly dispersed throughout as coatings on grains or disseminated masses or as thin layers or lenses. In saturated rocks low resistivity can be due to increased clay content or salinity. Hence the resistivity surveys are the best suited for delineation of clay or saline zone. In the present study area geophysical investigations using Electrical Resistivity Tomography (ERT) surveys have been carried out at 13 locations in the Godavari delta and the locations were shown in Fig. 4.2. Wenner-Schluberger array with 5 m electrode spacing was used to collect resistivity data as the array can adequately represents signal/noise ratio and also provides adequate resolution, which is an important parameter in low resistivity. The depth of investigation of about 45 m and various subsurface geological formations like marine clays and saline water mixing areas were inferred from the resistivity contrast up to a depth of 45 m only. In the coastal areas, the principal aquifers were formed in the unconsolidated alluvial formations, deposited under various sedimentary environments. The geo-electrical profiles shown resistivity values that varied laterally with depth and also in the vertical aspect, two levels could be distinguished in accordance with the resistivity signatures obtained from ERT sections. The aquifer geometry and in situ salinity of marine clays in the area was ascertained from the electrical resistivity profile/images (P3, P4, P5, P11 (Figs. 4.2 and 4.3)).

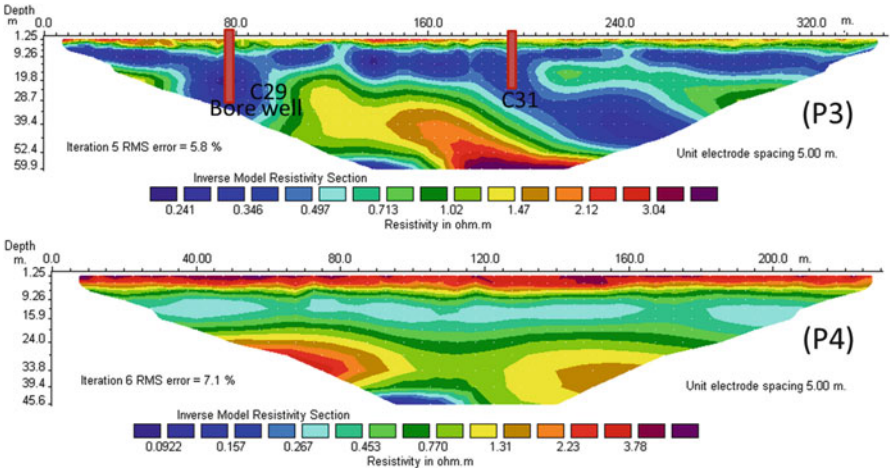

Fig. 4.2 Electrical Resistivity Tomography (ERT) profiles, near Rave Terminal, East Godavari district, A.P., India

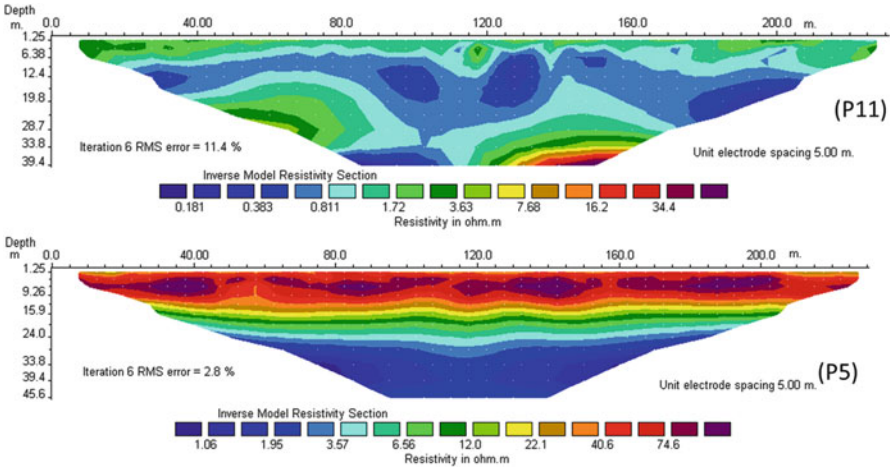

Fig. 4.3 Electrical Resistivity Tomography (ERT) profiles, near Uppalaguptham (P5) and Devaguptam (P11), East Godavari district, A.P., India

The profile P3 (W-E oriented) was carried in the Ravva Onshore Terminal with a spread of 340 m. The image depicts that upper layer as a very low resistivity formation with resistivity of <1 Ωm up to a depth of 19 m in the subsurface, it is due to existence of clay with saturated saline water or mixing of saline water in ground water from back waters. The low resistivity values at 80 and 200 m profile up to 39 m in the subsurface is due to upcoming of saline water due to large scale groundwater pumping at point location in the Ravva Terminal. The relative high

resistivity value >3 Ωm between 80 and 240 m profile is due to the presence of coarse grained sands from 19 to 60 m in the subsurface.

The profile P4 (N-S orientated) has been carried out near Ravva Onshore Terminal in Surasana Yanam village. The image deciphers that existence of three subsurface conditions. Top layer exhibits very low resistivity value of >3 Ωm and extended up to 6 m depth from the surface, it is due to coarse grained sand with top soil. Second layer represent the low resistivity formation with <1 Ωm 9 to 15 m depth, it may be because of clay formation. Third layer having higher resistivity with 1–2 Ωm up to a depth of 44 m, indicate coarse grained sand with clay. It is also depicts that extension of clay formation from 45 m depth in the subsurface with low resistivity <1 Ωm.

The profile P5 was carried out in upstream of Uppalaguptham Village and laid on the NE-SW direction. The top layer exhibits high resistivity >7 Ωm from the surface and extended up to 15 m depth, it would be due to the presence of consolidated material mostly with coarse sand and clay. Further underlain by low resistivity formation with resistivity of <4–22 Ωm from 15 to 24 m depth in the subsurface is due to clay with coarse grained sands. Further, the imaged indicted from 22 to 45 m in the subsurface with low resistivity value is due to clay deposition in the area.

The profile P11 was carried out in the Devaguptam Village, laid in the direction of N-S. The resistivity of the area indicates the existence of coarse grained material at the surface up to 1 m thick. The low resistivity value 3–19 m depth in the subsurface is due to clay with saline water. The downstream of the delta is affected by saline water mixing during the high tides, saline water mixing with groundwater tends to decrease the resistivity of the formation. The high resistivity value at the depth of 39 m indicates coarse grained material.

4.5.2 Major Ion Chemistry

Groundwater occurs at shallow depths in the Godavari delta, groundwater levels in the dug wells are varying from 0.8 to 3.4 m in the delta. In the Ravva Onshore Terminal wells it is varying from 4.5 to 13.2 m. The total depth of dug wells varying from 1.2 to 4.5 m and in bore wells located in the Ravva Terminal is varying from 18 to 160 m. The established groundwater flow direction is to be towards Bay of Bengal from Amalapuram (Fig. 4.4). Groundwater samples were analyzed for major ions in the Godavari delta region in the pre (June) and post monsoon (October) periods of 2006. The descriptive statistics for major ions and TDS pH were presented in Tables 4.1 and 4.2. In the pre monsoon groundwater TDS exceeded TDS 11,550 mg L^{-1} in 25 % of samples (Q75), where as in the post monsoon ground water samples exceeded 6,000 mg L^{-1} in 25 % samples (Q75). The average groundwater salinity (TDS) is varying from 8,266 to 6,307 mg L^{-1} from pre monsoon to post monsoon, indicate in the post monsoon the groundwater salinity is decreased due to groundwater dilution with rain water infiltration in the

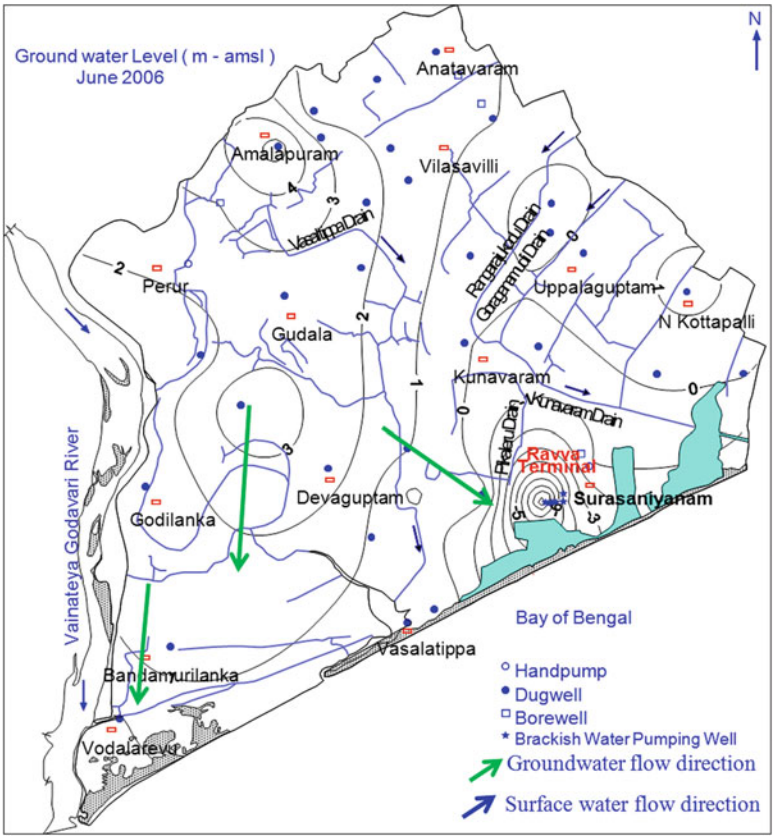

Fig. 4.4 Groundwater flow direction in the Central Godavari district, A.P., India

Table 4.1 Statistical analysis of groundwater samples, in the central Godavari delta, East Godavari District, A.P., India, June 2006

Parameter	Min	Max	Average	St. Dev.	Q25	Q50	Q75
pH	7.3	8.9	7.9	8.0			
TDS	274	27,856	8,266	8,120	1,635	4,813	11,510
HCO_3^-	37	220	109	47	73	98	122
Cl^-	57	6,308	1,606	1,810	355	956	1,585
SO_4^{2-}	20	285	88.6	87.0	30	50	78
NO_3^-–NO_3^-	2.2	79.2	11.5	14.3	4.8	7.9	9.3
F^-	0.25	0.95	0.7	0.2	0.44	0.75	0.85
Na^+	24	14,260	3,753	3,814	736	2,093	5,152
K^+	2	803	247.2	186.1	105	191	341
Ca^{2+}	12	952	156.3	258.3	32	40	128
Mg^{2+}	10	596	136.0	151.2	32	66	165

Table 4.2 Statistical analysis of groundwater samples, in the central Godavari delta, East Godavari District, A.P., India, November 2006

Parameter	Min	Max	Average	St. Dev.	Q25	Q50	Q75
pH	7.4	8.8	7.9	8.1			
TDS	248	27,771	6,307	7,819	1,035	3,545	6,025
HCO_3^-	61	1,037	238	151	162	213.5	268
Cl^-	64	6,996	1,665	1,998	263	839	1,769
SO_4^{2-}	30	350	97.4	90.0	45	60	95
NO_3^-–NO_3^-	1.1	22	3.1	3.8	1.8	2.05	3.4375
F^-	0.32	1.02	0.7	0.2	0.56	0.7	0.88
Na^+	32	12,906	2,164	3,604	140	627	1,463.75
K^+	2	789	163.0	220.1	23.25	67.5	192.5
Ca^{2+}	24	1,864	210.8	416.0	36	52	92
Mg^{2+}	5	803	93.4	154.8	24.75	39	74.5

post monsoon. The maximum TDS was observed in the Ravva Onshore Terminal well in both seasons (>27,000 mg L^{-1}) and minimum was in Vannechinthalapudi village (<274 mg L^{-1}). The TDS variations in ground water quality from pre to post monsoon is mainly due to aquifer recharge by rainfall infiltration and irrigation return flows and it is indicated by increase in HCO_3^- and SO_4^{2-} in the post monsoon. In the post monsoon increase in Mg^{2+}, Ca^{2+} and decrease in Na^+ indicate ion exchange process accelerating the ground water salinity in the delta. In the delta use of fertilizers and pesticides are very high and it reflected in the ground water quality by increased NO_3^- and SO_4^{2-} in the post monsoon.

4.5.2.1 Ionic Ratios

Ionic ratios are good hydrochemical markers to identify the salinity source, Na^{+2}/Cl^- ratio, 0.85–1 and SO_4^{-2}/Cl^- <0.05 indicate seawater intrusion (Vengosh and Ben-Zvi 1994; Vengosh et al. 1999; Howard and Mullings 1996). The spatial distribution of Na^{+2}/Cl^- and SO_4^{-2}/Cl^- for both pre and post monsoon seasons of 2006 was presented in Figs. 4.5, 4.6, 4.7, and 4.8. The molar ratios of Na^{+2}/Cl^- (>0.86) and SO_4^{-2}/Cl^- (<0.05) in the pre monsoon indicated strong influence of sea water. In the post monsoon increased Na^{+2}/Cl^- and SO_4^{-2}/Cl^- (>0.05) indicated marine palaeo salinity, dilution of marine clays and dissolution of evaporites. The high SO_4^{-2}/Cl in the post monsoon is attributed to dilution groundwater salinity due to rainfall infiltration and irrigation return flows in the delta. The low Na^{+2}/Cl^- ratios in upstream and some isolated pockets in delta are due to sand exposures and isolated fresh water lances in the perched aquifers.

4.5.3 ERT Versus Quality

The use of resistivity data with hydrochemical data (dissolved solids (TDS) or electrical conductivity measurements (EC)) in groundwater wells can help to identify the contaminated zones. The combination of hydrogeological, geochemical

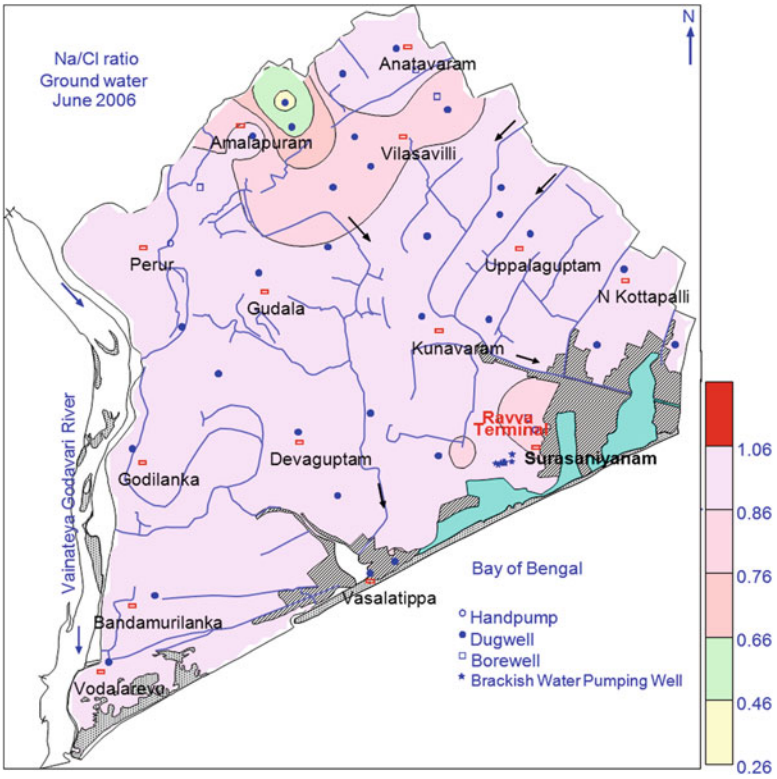

Fig. 4.5 Spatial distribution of Na/Cl ratios in June 2006 (meq L^{-1}) > 0.86 may represent presence of seawater

and geophysical investigations can be very effective tools to detect the contaminant migration in groundwater due to waste disposals, to investigate the seawater intrusion, to identify the oil field leakage and mine seepage (Warner 1969; Abu-Zeid et al. 2004; Bernstone and Dahlin 1997; Bisdorf and Lucius 1999; Barker and Moore 1998). Comparison of resistivity data with hydrochemical data increase the reliability, and reduces the uncertainty of the ERT data interpretation. Such a study enabled estimation of resistivity of two primary composite zones, the freshwater zone and the saline water zone. In the present study, the sampling depth of dug wells and hand pumps (C1 to C28 and C35 to C42) is <3.5 m and bore wells (C29 to C34) located near in Ravva Terminal is 10–13.5 m. The sampling depth of all samples are confined to first layer in ERT images discussed in above section and the groundwater quality is varied depends on mixing of saline water and other depositional conditions, the resistivity values varied from Bay of Bengal to Amalapuram based on combined effect of depositional conditions and saline water mixing. The resistivity values show very low values in alluvial aquifers rich in sands, clay and fine grained than compared to other aquifers materials in the subsurface. Indeed,

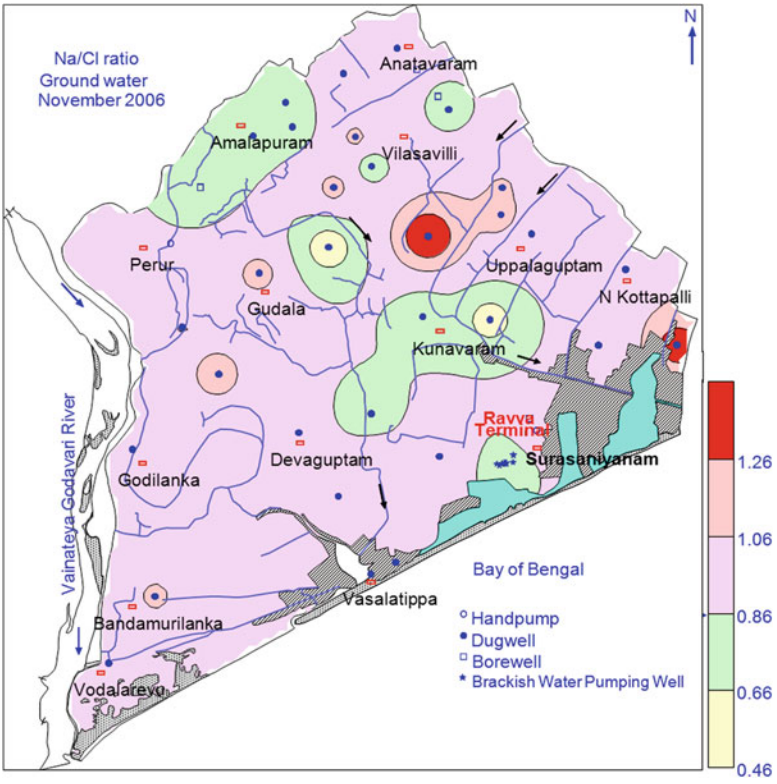

Fig. 4.6 Spatial distribution of Na/Cl ratios in November 2006 (meq L^{-1}) > 0.86 may represent presence of seawater

fine-grained sand formation contain high TDS (>1,000 mg L^{-1}) in ground water may be responsible for low resistivity value of the aquifer in the area, and any formation having less than this optimum resistivity value may represent either clay or sand formation. The elevated TDS (>4,000 mg L^{-1}) and sulphate (60 mg L^{-1}) concentrations are reported at Surasaniyanam and Devaguptam is due to mixing of sea water and upcoming of paleao salinity from deeper part of the aquifer (Table 4.3). The same thing was reflected in ERT images in those corresponding images with low resistivity <0.5 Ωm (P3, P4 and P11). The higher concentrations and low resistivity may be due to infiltration of sea water during high tides. The lowering of resistivity resulted may be due to the infiltration of seawater into the freshwater zones in the area. ERT profiles and elevated chloride concentrations confirm brackish condition of the groundwater. The elevated TDS, sulphate, chloride, and sodium concentrations reported in the delta may be due to in situ salinity from the overlying clay formations. The interpretation of ERT images indicated sand and saline water-saturated sand are mostly found near surface up to 10–15 m, coarse grained sand with clay is followed by saline water-saturated clay layer are

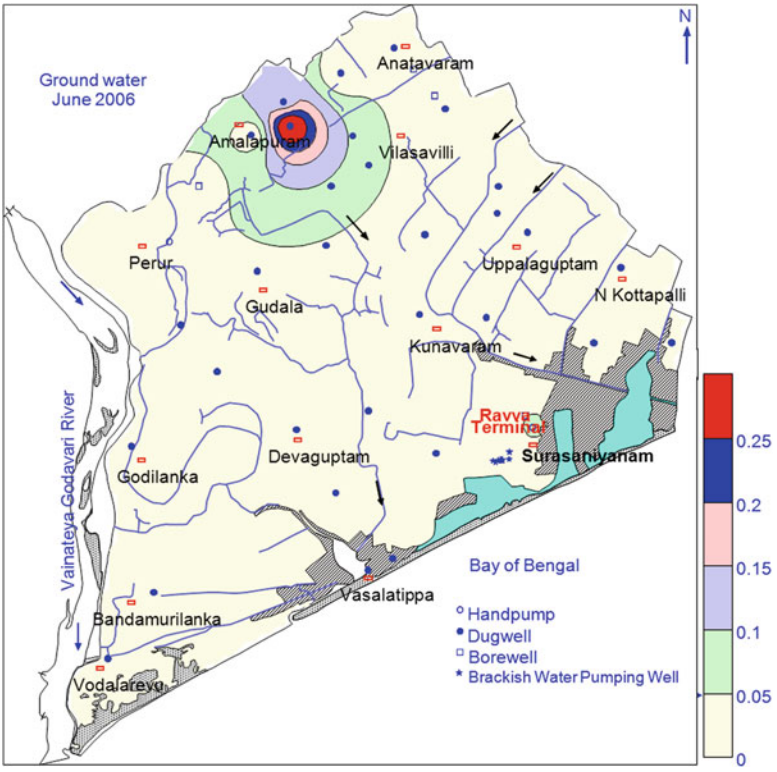

Fig. 4.7 Spatial distribution of SO_4^{-2}/Cl^- ratio in June 2006 (meq L^{-1}) < 0.05 may represent presence of seawater

present with a thickness of 30–35 m. The high resistivity values (>70 Ωm) and low TDS values in the Uppalaguptam village is due to existence of coarse grained sand material with relative fresh water in the delta (P5). Profile P3 is highly correlated with groundwater quality of C29 and C31 wells, these wells having very high TDS, Cl^- and SO_4^{2-} indicated mixing of saline water or upcoming brines from deeper part of the aquifer which is represented in the ERT image with very low resistivity value <0.5 Ωm.

4.6 Conclusions

Geophysical and hydrochemical analysis were carried out to identify the saline water intrusion and salinity origin in the Central Godavari delta, Bay of Bengal Coast in Andhra Pradesh, India. The consistent groundwater flow direction is towards Bay of Bengal coast from Amalapuram area. Geophysical investigations indicated that thick marine clays are present on the surface and extended up to a

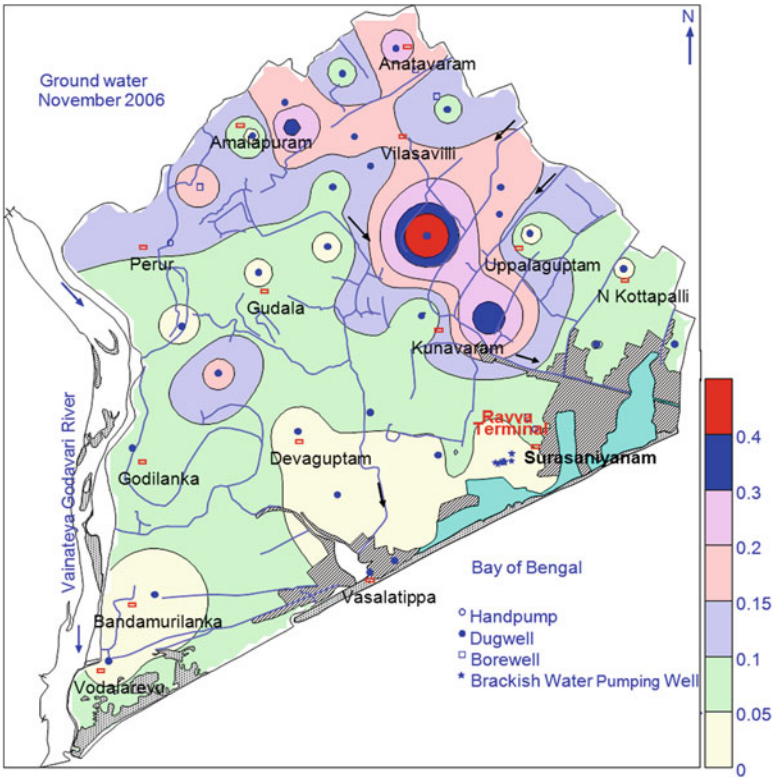

Fig. 4.8 Spatial distribution of SO_4^{-2}/Cl^- ratios in November 2006 (meq L^{-1}) < 0.05 may represent presence of seawater

Table 4.3 Comparison of ERT results with water quality in the central Godavari delta, A.P., India

Village	Profile no.	Well no.	TDS	Na^+	Cl^-	SO_4^{2-}
S.Yanam	P4	C01	4,813	338	362	60
Devaguptam	P11	C23	4,595	1,702	1,334	50
Uppalaguptam	P5	C08	2,001	1,288	204	30
Ravva Terminal	P3	C29	21,307	9,143	5,320	220
		C31	26,797	10,580	6,308	285

thickness of about 12–15 m in the subsurface. The low resistivity in S. Yanam and Devaguptam villages was due to the mixing and infiltration of saline water into the freshwater zones during the high tides from the surface water drains. Hydrochemical analysis results indicated effects of the seawater mixing and particularly TDS and Chloride concentrations are the simplest indicators for assessment of mixing process. The large thicknesses of clay formations are responsible for groundwater salinity in the Godavari delta. The marine clays possess the palaeo

salinity due to the recession of the sea level. The depositional history and the elevated values of TDS, Na^+, SO_4^{2-}, Cl^- chloride concentrations are indicating that salinity is due to in-situ salinity of groundwater in the marine clays rather than lateral movement of sea water from Bay of Bengal. The elevated ionic ratios of SO_4^{2-}/Cl^- and Na^{2+}/Cl^- indicated that salinity in the delta region is not due to sea water intrusion, it is due to dissolution of evaporites and dilution of marine clays rich in sodium as the groundwater flow direction is towards Bay of Bengal.

Acknowledgments Authors are thankful to Director, NGRI, Hyderabad, for his encouragement to publish this work. Authors are expressing their sincere thanks to the Cairn India Ltd for sponsoring the project to the NGRI for the present research work.

References

Abimbola AF, Odukoya AM, Olatunji AS (2002) Influence of bedrock on the hydrogeochemical characteristics of groundwater in Northern part of Ibadan metropolis, SW Nigeria. Water Resour J 9:1–6

Abu-Zeid N, Bianchini G, Santarato G, Vaccaro C (2004) Geochemical characterization and geophysical mapping of landfill leachates: the Marozzo canal case study (NE Italy). Environ Geol 45(4):439–447

Alpar B (2009) Vulnerability of Turkish coasts to accelerated sea-level rise. Geomorphology 107 (1–2):58–63

APHA (2005) Standard methods for the examination of water and wastewater, 21st edn. American Public Health Association, Washington, DC

Apodaca LE, Jeffrey BB, Michelle CS (2002) Water quality in shallow alluvial aquifers, Upper Colorado River Basin, Colorado. J Am Water Res Assoc 38:133–149

Barker R, Moore J (1998) The application of time-lapse electrical tomography in groundwater studies. The Lead Edge 17:1454–1458

Bernstone C, Dahlin T (1997) DC resistivity mapping of old landfills: two case studies. Eur J Environ Eng Geophys 2:121–136

Bisdorf RJ, Lucius JE (1999) Mapping the Norman, Oklahoma, landfill contaminant plume using electrical geophysics. Water-Resources Investigations Report 99-4018C. U.S. Geological Survey, Reston

Bobba AG (2000) Numerical simulation of saltwater intrusion into east coastal basin of Indian sub-continent due to anthropogenic effects. In: ICIWRM 2000 (Proceedings of the international conference on integrated water resources management for sustainable development), New Delhi, 19–21 Dec 2000, pp 323–340. National Institute of Hydrology

Bobba AG (2002) Numerical modeling of salt-water intrusion due to human activities and sea-level change in the Godavari Delta, India. Hydrol Sci J 47:S67–S80

Bredehoeft JD, Neuzil CE, Milly PCD (1983) Regional flow in the Dakota aquifer: a study of the role of confining layers. US Geol Surv Water Suppl Pap 2237:45p

Bugg SF, Lloyd JW (1976) A study of freshwater lens configuration in the Cayman Islands using resistivity methods. Q J Eng Geol 9:291–302. doi:10.1144/GSL.QJEG.1976.009.04.02

Carreira PM, Marques JM, Pina A, Gomes AM, Galego Fernandes PA, Santos FM (2010) Groundwater assessment at Santiago Island (Cabo Verde): a multidisciplinary approach to a recurring source of water supply. Water Resour Manage 24(6):1139–1159

CGWB (1999) Groundwater resources and development prospects in East Godavari District, Andhra Pradesh. Unpublished Report, Ministry of Water Resources, Government of India. 210 pp

Chachadi AG, Leitao T (2002) Health of groundwater regime in coastal delta of East Godavari, Andhra Pradesh in Coastin. Coastal Research Newsletter 6:S.5–8
Chidambaram S, Kumar GS, Prasanna MV, Peter AJ, Ramanthan AL, Srinivasamoorthy K (2008) A study on the hydrogeology and hydrogeochemistry of groundwater from different depths in a coastal aquifer: Annamalai Nagar, Tamil Nadu, India. Environ Geol 57(1):59–73
Choudhury K, Saha DK, Chakraborty P (2001) Geophysical study for saline water intrusion in a coastal alluvial terrain. J Geophys 46:189–200. doi:10.1016/S0926-9851(01)00038-6
Custodio E (2010) Coastal aquifers of Europe: an overview. Hydrogeol J 18(1):269–280
Dahlin T (1996) 2D resistivity surveying for environmental and engineering applications. First Break 14:275–284
Danielopol DL, Griebler C, Gunatilaka A, Notenboom J (2003) Present state and future prospects for groundwater ecosystems. Environ Conserv 30(2):104–130
Dey A, Morrison HF (1979) Resistivity modelling for arbitrary shaped two-dimensional structures. Geophys Prospect 27:1020–1036
Falgas E, Ledo J, Marcuello A, Queralt P (2009) Monitoring freshwater-seawater interface dynamics with audiomagnetotelluric data. Near Surf Geophys 7(5–6):391–399
Frohlich RK, Urish DW, Fuller J, Reilly MO (1994) Use of geoelectrical method in groundwater pollution surveys in a coastal environment. J Appl Geophys 32:139–154
Geological Society of India (GSI) (2006) Miscellaneous Publication No. 30 Part VII 2nd revised ed. Geology and Mineral Resources of Andhra Pradesh, p 91
Giordana G, Montginoul M (2006) Policy instruments to fight against seawater intrusion in coastal aquifers: an overview. Vie Et Milieu – Life Environ 56(4):287–294
Griffiths D, Barker R (1993) Two dimensional imaging modeling in areas of complex geology. J Appl Geophys 20:211–226
Griffths DH, Turnbull J, Olayinka AI (1990) Two dimensional resistivity mapping with a computer controlled array. First Break 8:121–129
Gurunadha Rao VVS, Thamma Rao G, Surinaidu L, Rajesh R, Mahesh J (2011) Geophysical and geochemical approach for seawater intrusion assessment in the Godavari Delta Basin, A.P., India. Water Air Soil Pollut 217:503–514
Hendry MI, Schwartz FW (1990) The chemical evolution of groundwater in the Milk River Aquifer, Canada. Groundwater 28:253–261
Hidalgo MC, Cruz-Sanjulian J (2001) Groundwater composition, hydrochemical evolution and mass transfer in a regional detrital aquifer (Baza Basin, southern Spain). Appl Geochem 16 (7–8):745–758
Howard KWF, Mullings E (1996) Hydrochemical analysis of groundwater-flow and saline incursion in the Clarendon Basin, Jamaica. Groundwater 34(5):801–810
Kouzana L, Benassi R, Ben Mammou A, Felfoul MS (2010) Geophysical and hydrochemical study of the seawater intrusion in Mediterranean semi arid zones. Case of the Korba coastal aquifer (Cap-Bon, Tunisia). J Afr Earth Sci 58(2):242–254
Kremer H, Crossland C (2002) Coastal change and the "anthropocene": past and future perspectives of the IGBPLOICZ project. In: Proceedings of the international symposium on low-lying coastal areas, Bremerhaven, 9–12 Sept 2002
Lambrakis N (2006) Multicomponent heterovalent chromatography in aquifers. Modelling salinization and freshening phenomena in field conditions. J Hydrol 323(1–4):230–243
Loke MH (1994) The inversion of two dimensional resistivity data. Unpublished Ph.D. thesis, University of Birmingham, Birmingham
Lozano-García MS, Ortega-Guerrero B (1998) Late quarternary environmental changes of the central part of the Basin of Mexico: correlation between Texcoco and Chalco basins. Rev Palaeobot Palynol 99:77–93
Martinez DE, Bocanegra EM (2002) Hydrogeochemistry and cation exchange processes in the coastal aquifers of Mar Del Plata, Argentina. Hydrogeol J 10:393–408
Mercado A (1985) The use of hydrogeochemical patterns in carbonate sand and sandstone aquifers to identify intrusion and flushing of saline water. Groundwater 23(1985):635–645

Mondal NC, Singh VP, Singh S, Singh VS (2011) Hydrochemical characteristic of coastal aquifer from Tuticorin, Tamil Nadu, India. Environ Monit Assess 175(1–4):531–550

Naidu LS, G. Rao VVS, T. Rao G, Mahesh J, Padalu G, Sarma VS, Prasad PR, Rao SM, R. Rao BM (2012) An integrated approach to investigate saline water intrusion and to identify the salinity sources in the Central Godavari delta, Andhra Pradesh, India. Arab J Geosci. doi:10.1007/s12517-012-0634-2

Nowroozi AA, Stephen BH, Henderson P (1999) Saltwater intrusion into the freshwater aquifer in the eastern shore of Virginia: a reconnaissance electrical resistivity survey. J Appl Geophys 42:1–22. doi:10.1016/s0926-9851(99)00004-x

Olatunji AS, Tijani MN, Abimbola AF, Oteri AU (2001) Hydrogeochemical evaluation of water resources of Oke-Agbe Akoko, SW Nigeria. Water Resour J 12:81–87

Parkhomenko EI (1967) Electrical properties of rocks. Translated from Russian and edited by George V. Keller. Plenum Press, New York

Plummer LN (1977) Defining reactions and mass transfer in part of the Floridan aquifer. Water Resour Res 13:801–812

Rao GN (1993) Geology and hydrocarbon prospects sea coast sedimentary basins of India with special reference to Krishna Godavari Basin. J Geol Soc India 41(2):444–445

Sanford WE, Pope JP (2010) Current challenges using models to forecast seawater intrusion: lessons from the Eastern Shore of Virginia, USA. Hydrogeol J 18(1):73–93

Sarwade DV, Nandakumar MV, Kesari MP, Mondal NC, Singh VS, Singh B (2007) Evaluation of seawater ingress into an Indian atoll. Environ Geol 52(2):1475–1483

Sharma PV (1997) Environmental and engineering geophysics. Cambridge University Press, Cambridge, 475 p

Sharma VVJ, Rao B (1962) Variation of electrical resistivity of river sands, Calcite and Quartz powders with water content. Geophysics 17(4):470–479

Trefry MG, Svensson TJA, Davis GB (2007) Hypoaigic influences on groundwater flux to a seasonally saline river. J Hydrol 335(3–4):330–353

Urish DW, Frohlich RK (1990) Surface electrical resistivity in coastal groundwater exploration. Geoexploration 26:267–289

Van Dam JC, Meulenkamp JJ (1967) Some results of the geo-electrical resistivity method in groundwater investigations in The Netherlands. Geophys Prospect 15(1):92–115

Vengosh A, Ben-Zvi A (1994) Formation of a salt plume in the coastal plain aquifer of Israel: the Be'er Toviyya region. J Hydrol 160:21–52

Vengosh A, Spivack AJ, Artzi Y, Ayalon A (1999) Geochemical and boron, strontium, and oxygen isotopic constraints on the origin of the salinity in groundwater from the Mediterranean coast of Israel. Water Resour Res 35(6):1877–1894

Warner DL (1969) Preliminary field studies using earth resistivity measurements for delineating zones of contaminated groundwater. Groundwater 7:9–16

Wicks CM, Herman JS, Randazzo AF, Joe JL (1995) Water-rock interactions in a modern coastal mixing zone. Geol Soc Am Bull 107:1023–1032

Zohdy AAR (1969) The use of Schlumberger and equatorial soundings on ground water investigations near El Paso, TX. Geophysics 34:713–728

Chapter 5
Geophysical Viewpoints for Groundwater Resource Development and Management in Coastal Tracts

Subhash C. Singh

Abstract Ever since the beginning of human civilization, people have settled along riverbanks and coasts. Throughout the world, the extent of coastal regions that have sustainable groundwater bodies is shrinking by the day. The problems that dominate in the use of such groundwater are depletion due to overdraft, and salinisation arising from pollution and/or sea water (saline) intrusion. Around the world, especially in regions with high population density, dynamic tube-well-irrigated agriculture and insufficient surface water, many consequences of the overdevelopment of groundwater are increasingly evident. The most common symptom is decline in water tables. In coastal areas, the most serious consequence of intensified pumping of groundwater for irrigation is saline ingress into coastal aquifers. All these problems will impair the region's water supply capacity and its ability to meet the demand from its growing population. One of the most serious side-effects caused by groundwater depletion is saline intrusion in coastal aquifers like those in Egypt, Turkey, China and India. Thus the need for sustainable groundwater development warrants detailed mapping of the saline-fresh groundwater interface and monitoring of salt water ingress. In this respect, geophysical investigations can help in the assessment of sub-surface hydrogeological conditions and optimization of the number and location of boreholes to be drilled for sustainable water resource development in any particular coastal area. Use of such techniques is quite economical. The purpose of applying geophysics is to enable development of a picture of the variations in physical properties of the sub-surface horizons and translate them subjectively into a profile of the hydrogeological situation. While surface geophysical techniques help to define the negative and positive areas before taking up the drilling programme, post-drilling down-hole geophysical logging enables identification of the depth zones minutely, confirmation of the hydrogeological characterization and specific emplacement of the

S.C. Singh (✉)
Rajiv Gandhi National Ground Water Training and Research Institute, Central Ground Water Board, Ministry of Water Resources, Government of India, Raipur, Chhattisgarh, India
e-mail: singh_subhash_ch@hotmail.com

C. Wetzelhuetter (ed.), *Groundwater in the Coastal Zones of Asia-Pacific*,
Coastal Research Library 7, DOI 10.1007/978-94-007-5648-9_5,

cement seals in the boreholes to avoid mixing of groundwaters of different qualities by vertical flow. Geophysical logging techniques also help in deciphering the regional as well as local geometry of the aquifers and the direction of groundwater flow in them, as well as in monitoring variations in water quality. No single geophysical discipline or technique seems to be able to provide the wide range of data required to unravel enigmatic sub-surface hydrogeological conditions. When such unravelling is needed, subjective integration of the results from different techniques becomes essential to minimize ambiguity and make the exploration relatively foolproof. It should also be noted that geophysical exploration in coastal, areas demands a greater level of accuracy in data acquisition and interpretation than similar exploratory work inland. In such areas, resistivity methods face limitations such as the development of very low potential, transition in resistivity with depth, suppression of thin layers with intermediate resistivity values and severe ambiguity in layer parameters, because of the equivalence. In spite of this, the resistivity method has found wide application in coastal areas, mainly in the assessment groundwater quality. Reliability in estimating layer parameters is enhanced if the resistivity method is supplemented with seismic, induced polarization, electromagnetic and/or other geophysical techniques. A detailed geophysical case study from West Bengal in India is presented below. The geophysical inferences concerning coastal hydrogeological conditions, their scope in defining the zones prone to sea water encroachment and the potential areas of groundwater development are highlighted in the text.

5.1 Introduction

In coastal areas, the management of water resources is considered to be the management of both surface- and ground- water in terms of quality and quantity. The process is complex and involves a number of socio-economic and technical considerations. As far as groundwater is concerned, the movement of groundwater in coastal areas is such that, while there might be saline intrusion in one zone, there could be a significant discharge of fresh groundwater to the sea elsewhere. In coastal areas, where groundwater is often brackish and becoming increasingly contaminated by the sea water ingress, sustained development and effective management is essential for resources going to the sea as waste. This requires an adequate understanding of groundwater movement and sub-surface hydrochemical conditions to enable identification of the potential areas for groundwater development. The areas prone to saline intrusion or with the potential to be used for artificial recharge to groundwater must be identified and defined, to enable the management of groundwater quality. Adequate information on aquifer disposition and water quality should be prerequisites prior to any groundwater development activity in coastal areas. The sinking of test boreholes alone, in order to assess the sub-surface hydrogeology or trace the water quality interface, is not economic but is

time consuming. It is, therefore, important to look for an alternative approach that can yield adequate sub-surface information prior to drilling any supply wells.

Geophysical investigations help in the assessment of sub-surface hydrogeological conditions and in optimizing the number of boreholes to be drilled for sustainable water resource development in coastal areas, and are quite economical to use. The purpose of applying geophysics is to bring out a picture of the variations in physical properties of sub-surface horizons and translate them subjectively into a representation of the hydrogeological situation. While surface geophysical techniques can help to delineate the negative and positive areas before the drilling programme starts, the post-drilling, downhole geophysical techniques are used to identify the depth zones minutely, ascertain the hydrogeological characterization and help in placement of the cement seals in the boreholes to avoid uncontrolled, vertical groundwater movement. Downhole geophysical logging techniques can also help in deciphering both the regional and local geometry of the aquifers, and the direction of groundwater flow in them, as well as enabling monitoring of water quality variations in them. No single discipline or technique appears versatile enough, however, to enable the unraveling of enigmatic sub-surface hydrogeological conditions, and the subjective integration of the results from various techniques becomes essential to minimize the extent of ambiguity and make the results of exploration relatively foolproof.

The application of surface electrical resistivity and its integration with electromagnetic and/or other techniques is quite old. It has been found effective in exploration for groundwater development and management in coastal areas. The geophysical method of investigation is based on the principle of estimating physical parameters in the earth's horizons in the area or location. The physical properties of the sub-surface material are determined from measurements made on the ground or within boreholes. Interpretation of the observed variations of these physical properties, laterally and with depth, is correlated in terms of geology, lithology and hydrogeology, as well as geological structures. Measurement of electrical resistivity is quite common in groundwater studies. The resistivity of sub-surface materials depends on the type of soil, rock formation, degree of weathering, presence of fractures and fissures, etc. Because of this dependence on the rock formation its simplicity of operation and the ready availability of the equipment, the resistivity method is considered the most suitable technique for investigating and determining the sub-surface hydrogeological characteristics in coastal areas.

5.2 Geophysical Methods

Geophysical methods are non-destructive. They can provide sub-surface hydrogeological information from beneath the surface to enable delineation of an aquifer system or systems. Geophysics is the science applying the principles of physics to the investigation of the physical properties of the earth and explaining it in terms of the sub-surface lithological layers in the system. Geophysical anomalies are

responses to the contrast in physical properties of existing materials beneath the earth's surface. Geophysical investigations are conducted on the ground, within boreholes (downhole) and from air, in order to achieve a wide range of hydrogeological objectives. They are focused on targets within the earth to find hidden geological structures forming aquifer systems at depth as well as the lithological characteristic of near surface geological features – i.e., those within a few metres of the surface. Geophysical methods continue to evolve, involving the adoption of different techniques, as well as newer approaches and interpretational procedures for aquifer mapping in coastal areas.

As new geophysical methods and variations become available, it is fundamentally important to understand the outcomes to be expected outcomes from the geophysical investigations before they are applied. For aquifer mapping the type of hydrogeological problem, objectives, target depths and time for investigation should all be defined beforehand. Prior hydro-geophysical information available for the area should be studied and the additional supportive information to be obtained through the use of geophysics must be determined and understood. On the basis of the above, assessing the scope of any geophysical coverage must be seen and treated as a significant issue. Such an assessment must lead to the selection of the individual and/or combinations of geophysical techniques needed to obtain the optimum results for aquifer mapping. The process of data acquisition, interpretation and presentation must also be defined.

Since, the basis of any geophysical application is the contrast between the physical properties of the target and the surrounding environs, the greater the contrast or anomaly, the better the geophysical response and hence the quality of identification. The efficacy of a geophysical technique rests upon its ability to sense and resolve hidden sub-surface conditions accurately. Some geophysical techniques are more responsive to certain types of heterogeneity or variation than others, which might or might not be at all responsive. In other words, a judicious application of techniques is essential if the outcomes/results are to be useful in aquifer mapping, technologically as well as economically.

It is well known, as noted above, that sub-surface aquifer systems cannot be deciphered independently by any single geophysical method used on its own. Because of this, any interpretation must be contextual, and a broad understanding of sub-surface variations and conditions is a prerequisite. While the need to unravel sub-surface features as realistically as possible has brought about a remarkable level of advance in the techniques available, in terms of innovative approaches, data acquisition, processing and interpretation, as well as in geophysical instrumentation, there continues to be much further scope to improve the predictive aspect with respect to aquifer systems. The future lies in accuracy of data acquisition and manipulation, fast and continuous coverage, and deeper investigation with the least possible spread of equipment at the surface.

Various different surface geophysical techniques are available for use in aquifer mapping in coastal environment that depend on measuring the earth's physical properties. Electrical resistivity techniques are most commonly used, because of their relatively simple response to the quantity and chemical quality of

groundwater. Other methods that can be used for coastal aquifer mapping include the induced polarization and electromagnetic methods. The basis of the approach in surface geophysical surveys is sensing the sub-surface remotely, and so the inherent limitations on uniqueness and resolution remain because the distance (depth), shape and size combine to determine the response. Because of this it is pretty well essential to combine at least one other geophysical technique with the conventional resistivity methods and, if possible, to integrate the information from other disciplines, to reach the desired common solution – i.e., the best one – with the lowest level of ambiguity.

5.2.1 Electrical Resistivity Method

The electrical resistivity method is used in groundwater development and management in coastal tracts because of its efficacy. This arises mainly from electrolytic conduction, attributable to the presence of interstitial waters in the pores and their chemical quality. In other words, the method can be used to differentiate between unsaturated and saturated aquifer systems, and between fresh, brackish and saline formation waters. It can be used to identify lithologies, and to determine the depth and thickness of detectable geoelectric layers that might form the aquifer system. The main purpose of use of the method in coastal areas is to identify groundwater yielding zones, and to determine zone geometry and variations in the chemical quality of groundwater.

The electrical resistivity of any material is defined as being equal numerically to the resistance (in Ohms) between the opposite faces of a unit cube of the material. The conventional unit of resistivity is ohm-meter (Ωm). The bulk resistivity of water bearing geological formations depends on their ability to conduct electric currents through interstitial waters present in the pore spaces and through matrix. Thus, the bulk resistivity varies with the amount, distribution and salinity of interstitial waters as well as with lithology. The variations in resistivity of any water bearing formation manifest the combined variations in lithology and in the characteristics of any groundwater present. There is a significant contrast in resistivity between dry and water saturated formations, and formations with fresh and brackish/saline water. In general, there are defined ranges of resistivity that occur in different formations, e.g., sands of various grain sizes, clays, etc. As a result of the combined effects of the quality of the formation waters and the formation matrix, there are overlaps in the resistivity ranges that are found. Using Ohm's law, the electrical resistivity of sub-surface geological formation is determined by energizing the sub-surface horizons artificially and determining the measurements on the ground surface. It is the contrast in resistivity of a layer with those surrounding it or its effective presence (which depends upon its relative resistivity and thickness) that makes it detectable.

In the simplest form of the resistivity method, a known electrical current is sent into the ground through a pair of electrodes and the potentials that develop in the

ground are measured across another pair of ground electrodes. Multiplication of the ratio of the potential difference that develops by the 'geometric factor' of the electrode configuration gives the 'apparent' resistivity of the 'inhomogeneous' ground. This is reported as $\rho a = K\partial V/I$, where ρa is the apparent resistivity in ohm-m, K is the geometric factor (m), ∂V is the potential developed (v) and I is the current input (a). To study the variation with depth, i.e. acquiring information deeper and deeper below the surface, the separation between the current electrodes is increased successively. The set of successive measurements made, keeping the central point of the electrode configuration fixed with increasing separation between the current electrodes in steps, is referred to as Vertical Electrical Sounding (VES). A graphical plot of apparent resistivity with increasing current electrode separation yields the apparent resistivity curve or field curve at the point of observation. Since the depth of penetration of the current is increased by increasing the electrode separation (specifically the distance between the potential and current electrodes), the curve reveals any depth-related variation in resistivity. Matching of the field curve with the theoretical curve for a known vertical distribution of resistivity and thickness gives the geoelectric layer sequence at the point of measurement, within the zone extending down to the maximum depth investigated.

In depth-related resistivity measurements – i.e., when VES are conducted, important assumptions must be made in order to validate the data interpretation. The detectable sub-surface layers, termed the geoelectric layers, are assumed to lie parallel to the surface of measurement and to be extensive laterally. In reality, it is sufficient if the dip is within 15° of the surface slope, and the layers extend radially at least within a circle of radius equal to the maximum separation between the end electrodes, with respect to the locus of measurement, so that lateral inhomogeneities are obviated. The individual geoelectric layers must be sufficiently homogeneous and anisotropic that the electrical resistivity of any layer does not change laterally and/or vertically, except at the interfaces above and below it. The lowest (bottom) layer is assumed to be of infinite thickness. The resistivity of each layer should be distinct.

A variety of configurations exists according to which the current and potential electrodes can be placed. The best known of these include the Schlumberger, Wenner, and dipole-dipole configurations, etc. The most commonly used electrode configurations for soundings are the 'Schlumberger' set.

5.2.2 Geophysical Logging

Downhole geophysical logging is used to determine the physical and chemical characteristics of aquifer systems as well as of the pore fluids within them. The geophysical logs are important for the correlation and validation of the surface geophysical results. Downhole logging includes all the techniques in which sensing devices are lowered into a borehole so that physical parameters can be recorded. The results are interpreted in terms of rock characteristics and the contained fluids. The techniques allow rapid characterization of rock types occurring at different

depths on the basis of their physical properties and help to delineate different units into zones according to the probable occurrence of groundwater and water quality. The methods are useful in the characterization of lithology, the estimation of aquifer parameters, and the delineation of any saline water zone(s), as well as in contaminant monitoring, etc.

Downhole geophysical logging is the depth-related recording of various physical properties of the formations by lowering a sensor down a borehole. This type of logging is a dependable technique for obtaining data to enable understanding the sub-surface environment. It has led to the correct identification of aquifers for the construction of water wells. Prior to logging a borehole it is necessary to know the environment that the borehole passes, which includes broadly the set of hydrogeological and borehole conditions. The former includes the types of formations encountered in the borehole, the extent of any clay zones, the presence of any open zones, and the fractures and bed thickness, etc., while the latter includes the diameter of the hole vis-a-vis tool or probe geometry, the extent of invasion by drilling fluid or mud, the logging speed and presence (or not) of any hostile environment(s).

There are basically two types of downhole logging technique. In the first, natural sources and resources are used, as in the cases of self potential, temperature, and natural gamma-ray logging. In the second, including all resistivity techniques – both focused and unfocussed – neutron, gamma-gamma, sonic, etc., simulated controlled sources are used. The former are obviously economic in use, offering ease of operation and analysis. On the flip side, however, the volume of measurement cannot be controlled. The logging devices used in the second category are costlier and the analysis is complicated, but they offer good control over the volume of measurement with respect to lateral penetration.

5.3 Case Study: Digha Area, East Medinipur, West Bengal, India

Geophysical surveys were initiated as early as 1960 for delineating fresh water aquifers in the coastal tracts of West Bengal, India. These studies were confined to the extreme southwestern coastal tract of the East Medinipur district. They indicated the presence of very low resistivity (1–2 Ωm) layers within 25–30 m of the surface and identified these layers with plastic clays and not the brackishness of groundwater. The resistivities of less than 1 Ωm for the near surface coastal sand, on the other hand, were attributed to the presence of brackish groundwater. These studies showed that there was no occurrence of brackish groundwater in the Digha area. Subsequently, the East Medinipur district coastal tract, from the western boundary of the State near The Subarnarekha River west of Digha to Kolaghat on the right bank of the River Haldi –a stretch of 90 km – was surveyed in detail geophysically through the Kasai-Subarnarekha UNDP Project of the Central

Ground Water Board (CGWB) of the Government of India. Under this programme geophysical investigations comprising eighty two, deep VESs and the downhole logging of sixteen boreholes were conducted in the coastal sedimentary terrain of Kasai-Subernerekha Basin. The parametric standardization attributes very low resistivity values to the brackishness of the formation waters.

Schlumberger VESs with a current electrode separation of 1,400–2,400 m were conducted at an average interval of 4–5 km along selected sections. The resistivity ranges for the sub-surface lithology, were established by observing set out VESs near known hydrogeological points – i.e., existing wells. The VES results were calibrated using the results from boreholes that were drilled subsequently. Continuous, wire line, analog, geophysical logging of the boreholes was conducted to obtain measurements of electrical and natural gamma radioactivity parameters. In the electrical logging set, self potential (SP) and apparent resistivity were recorded with 16 and 64″ normal electrode spacing. For natural radioactivity, the natural gamma emissions of the formations were measured in terms of relative radioactivity counts per second. The resistivity of the drilling mud and that of the source water for the mud fluid were also measured.

The electrical potentials that developed during the VESs were very low, because of the presence of highly conductive and thick overburden, causing measurement error. The potentials were enhanced as far as possible by moving the potential electrodes (MN) outwards within the Schlumberger array (MN $<1/5$ AB) that was used. The resulting measurements were quite accurate because a microprocessor based stacking and averaging facility was available with the equipment. The Schlumberger VES field data were plotted on double logarithmic graph sheets. The VES curves are of H, A, K and Q types, and include a number of multi-layer types such as HA, KH and AA. The breaks in the VES curves caused by changing the potential electrode position were smoothed out.

Preliminary interpretation of the VES curves was attempted using conventional curve matching techniques involving two- and three- layer master curves, and an auxiliary point chart. In applying this type of technique the basic principle is to assume an appropriate sub-surface geoelectric layer model defining a theoretical VES curves (the master curve) and to compare it visually with the field VES curve. If the field curve matches the theoretical curve satisfactorily, the layer parameters for the field curve are assumed to be identical with those of the theoretical curve. Two- and three- layer field VES curves can be matched fully with the theoretical curves. If the field curve shows more than three layers, it is matched in steps with the two- and three- layer theoretical curves. The layer parameters obtained through such partial curve matching are modeled with a computer-aided, iterative interpretation process, and the layer parameters modified in accordance with the sub-surface depth-lithology information available. Since downhole geophysical logs were available for the area, the layer resistivity and thickness obtained from VES curve computations were calibrated and standardized using them. Apart from some reasonable variations in the geoelectric layer parameters derived from the VESs, some geoelectric cross-sections (Figs. 5.1, 5.2 and 5.3) were drawn for coastal area in order to understand the characteristics of the sub-surface aquifer system. The

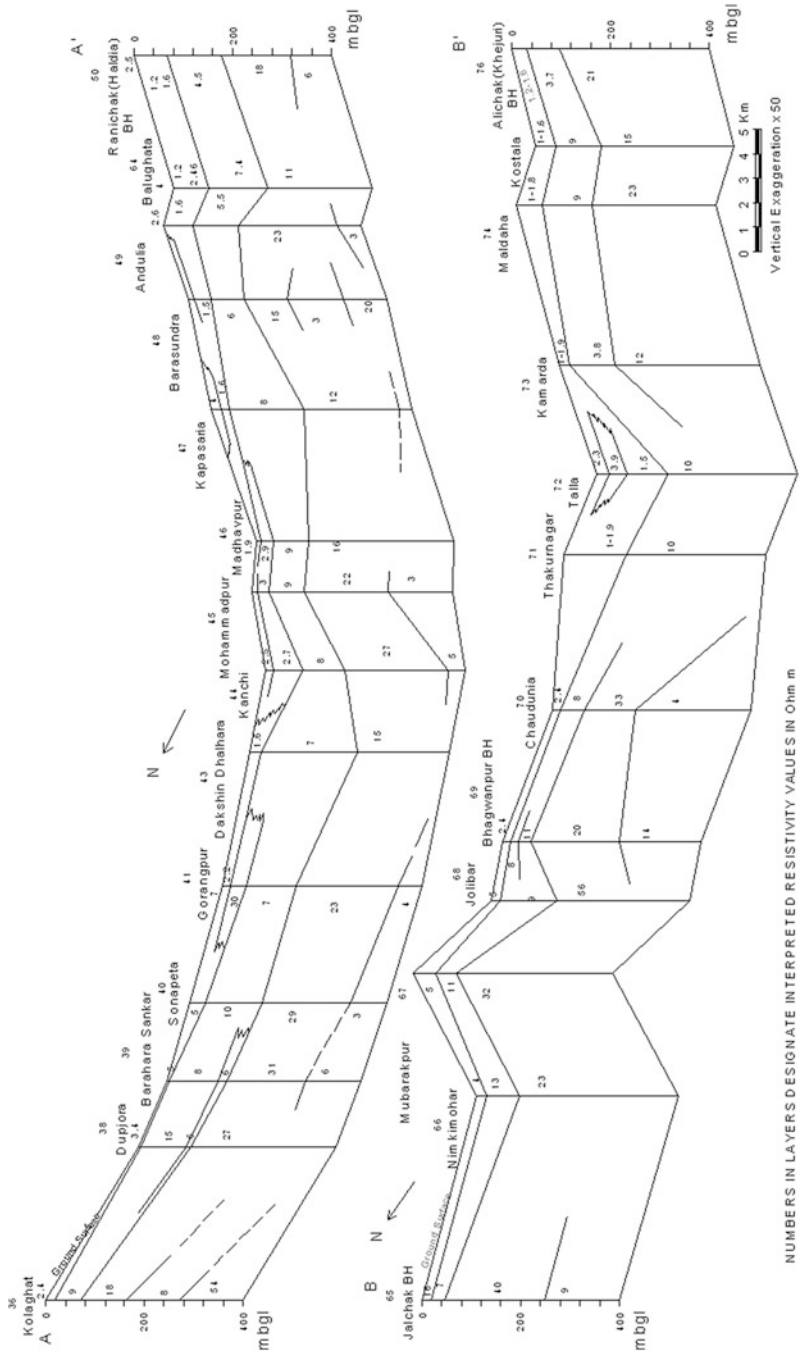

Fig. 5.1 Geoelectric cross-sections, East Medinipur District, West Bengal, India (Singh 1993 modified after Chandra et al. 1989)

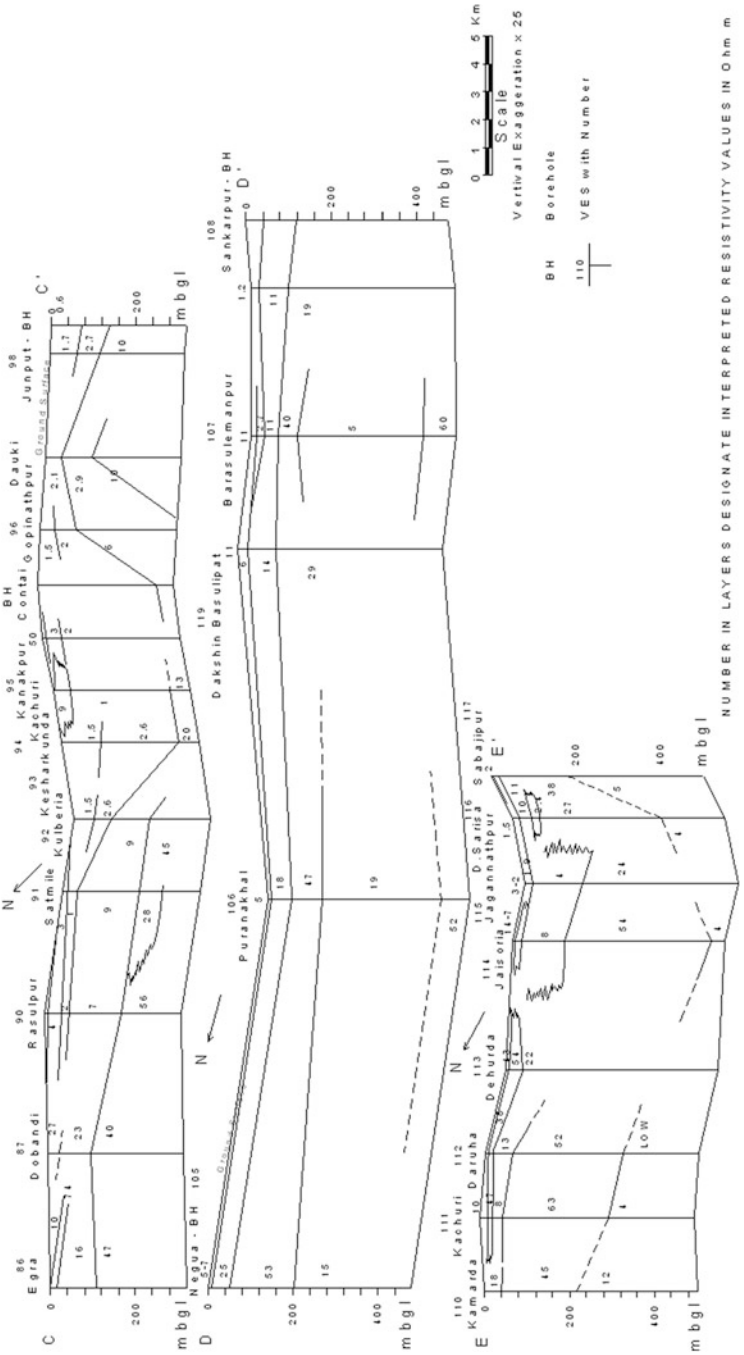

Fig. 5.2 Geoelectric cross-sections, East Medinipur District, West Bengal, India (Singh 1993 modified after Chandra et al. 1989)

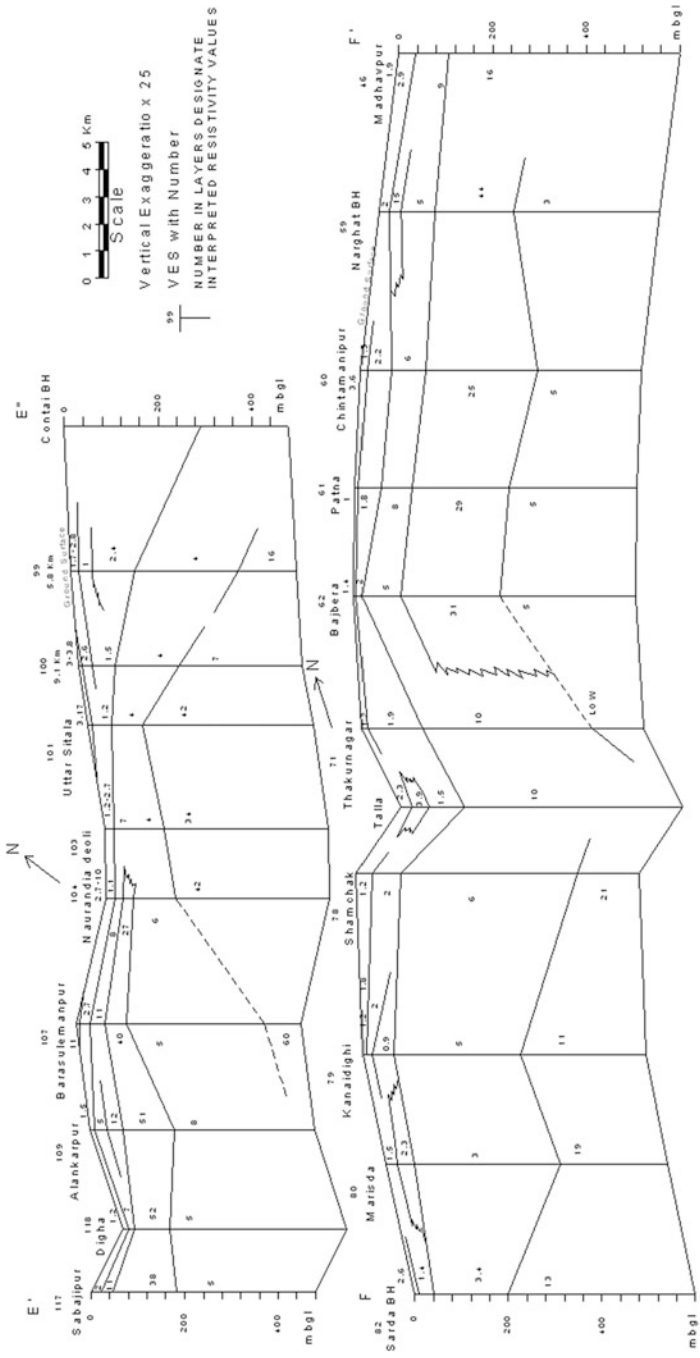

Fig. 5.3 Geoelectric cross-sections, East Medinipur District, West Bengal, India (Singh 1993 modified after Chandra et al. 1989)

inherent limitations of the resistivity method meant that many reasonable assumptions had to be adopted in preparing the geoelectric cross-section(s).

The general sub-surface sequence of geoelectric layers in the area, within 400 m of the surface, is a thin surface layer with varied resistivity, followed by a layer 20–135 m thick of very low resistivity (1–2.5 Ωm) and then a layer of comparatively higher resistivity (4–15 Ωm) and thickness (25–350 m). These are further underlain by a thick (40–350 m) layer associated with resistivity in the range 25 to 60 Ωm. This is the last layer delineated at many locations, although at others it is again underlain by a comparatively less resistive layer (5–10 Ωm) reported as between about 60–300 m in thickness. At a few sites, this in turn lies above a moderately resistive (50–60 Ωm) substratum. As noted, these layer combination sequences are all observed within about 400 m of the surface.

This set of geoelectric layers is identified as the sequence of surface soil, brackish water saturated sands and clays, and, below that, thick and alternating layers of clays and sands containing fresh groundwater (Figs. 5.1, 5.2, 5.3). The resistivity of brackish water saturated sands differs only a little from that of clays saturated similarly, and so they could not be differentiated.

The bottom of the very low resistivity layer forms the brackish/fresh groundwater interface at depth. It was delineated over an area of 2,400 sq km covering the 90 km stretch along the coast. The lateral variation of resistivity at different depths and the inferred depth to the saline/fresh groundwater interface are shown in Fig. 5.4. The sub-surface disposition of the aquifers and the salinity interface is depicted through a panel diagram of the coastal area (Fig. 5.4).

Iso-resistivity maps of the area have been drawn for different depth levels on the basis of interpretations of the layer parameters of the VESs. The different maps showing variation in resistivity from the surface to depths of 300 m bgl are shown in Fig. 5.5. The maps give clear depictions of the changes in formation water quality at different depths. The lower range of resistivity is indicative of the occurrence of poor quality groundwater.

At some locations VES measurements have been repeated in different seasons. The plots from these are shown in Fig. 5.6. The changes in water quality through the different seasons are readily apparent.

There is generally a near surface, low resistivity, brackish/saline water saturated zone in the Quaternary coastal sediments of the East Medinipur District. Its thickness varies from 20 m in the upland areas to a maximum of 130 m near the coast line, except at Kanthi where it is more than 250 m thick and extends to about 300 m bgl. The aquifers in the sediments underlying the near surface brackish/saline water zone contain fresh groundwater. The saline/fresh water interface and fresh groundwater zones are shown in Fig. 5.4. Geophysical surveys have also been used to delineate a group of fresh water aquifers occurring between of 150 and 360 m bgl, sandwiched between saline water zones. No sea water intrusion was identified in this area. A significant geophysical outcome was delineation of the brackish/saline ground water zone to about 300 m bgl around Kanthi, which is 10 km inland. Towards the coast the brackish water zone is about 40 m thick some 4 km inland and about 135 m on the coast. Around Digha, in the extreme southwest

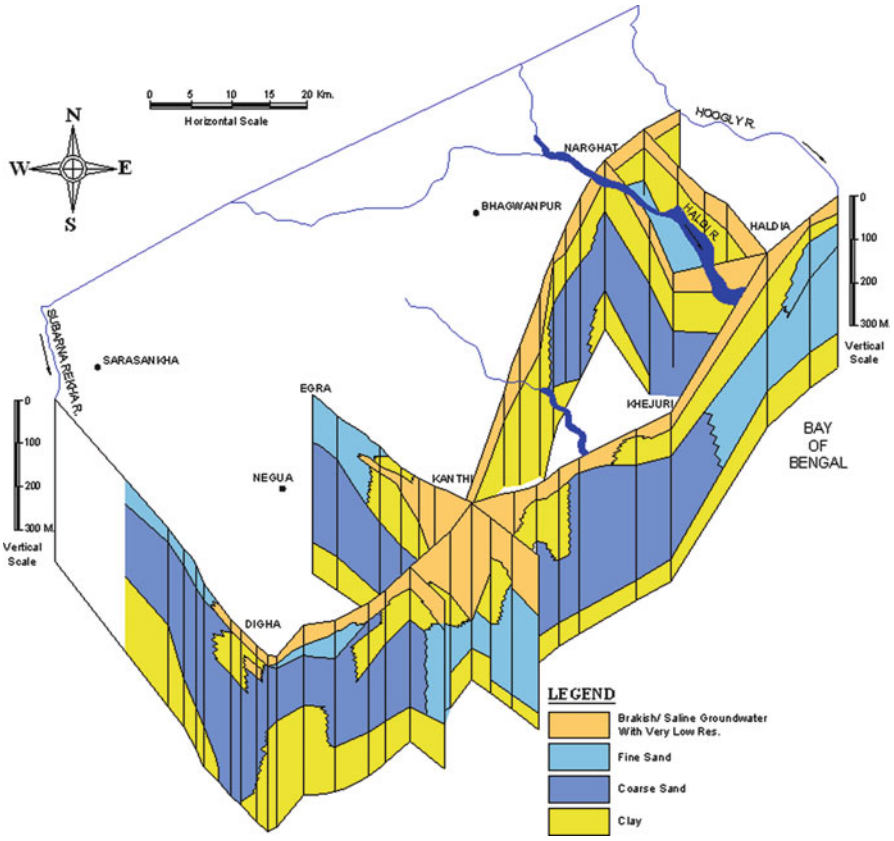

Fig. 5.4 Panel diagram showing general lithological and groundwater salinity variations along the Haldia-Digha coast, East Medinipur District, West Bengal, India (Singh 1993 modified after Chandra et al. 1989)

coastal part of East Medinipur District, the topmost saline water zone is confined to a maximum depth of 20 m and is separated from the deeper, thicker fresh water zone by a layer that consists predominantly of clay.

The SP, resistivity and natural-gamma logs collected from the coastal belt have been analyzed qualitatively as well as quantitatively. The quality of formation waters was estimated through the SP and resistivity values of the mud fluid. Confirmation of groundwater quality was obtained from the 64″ normal log resistivity values, as well as chemical analysis of water samples. The promising aquifers were identified on the basis of their 'low' gamma radioactivity counts and the higher resistivity values seen on the downhole geophysical logs. Low gamma counts and low resistivity indicated the presence of brackish/saline water in the granular formations. Correlation of the downhole geophysical logs revealed the sub-surface disposition of the aquifers (Figs. 5.7 and 5.8).

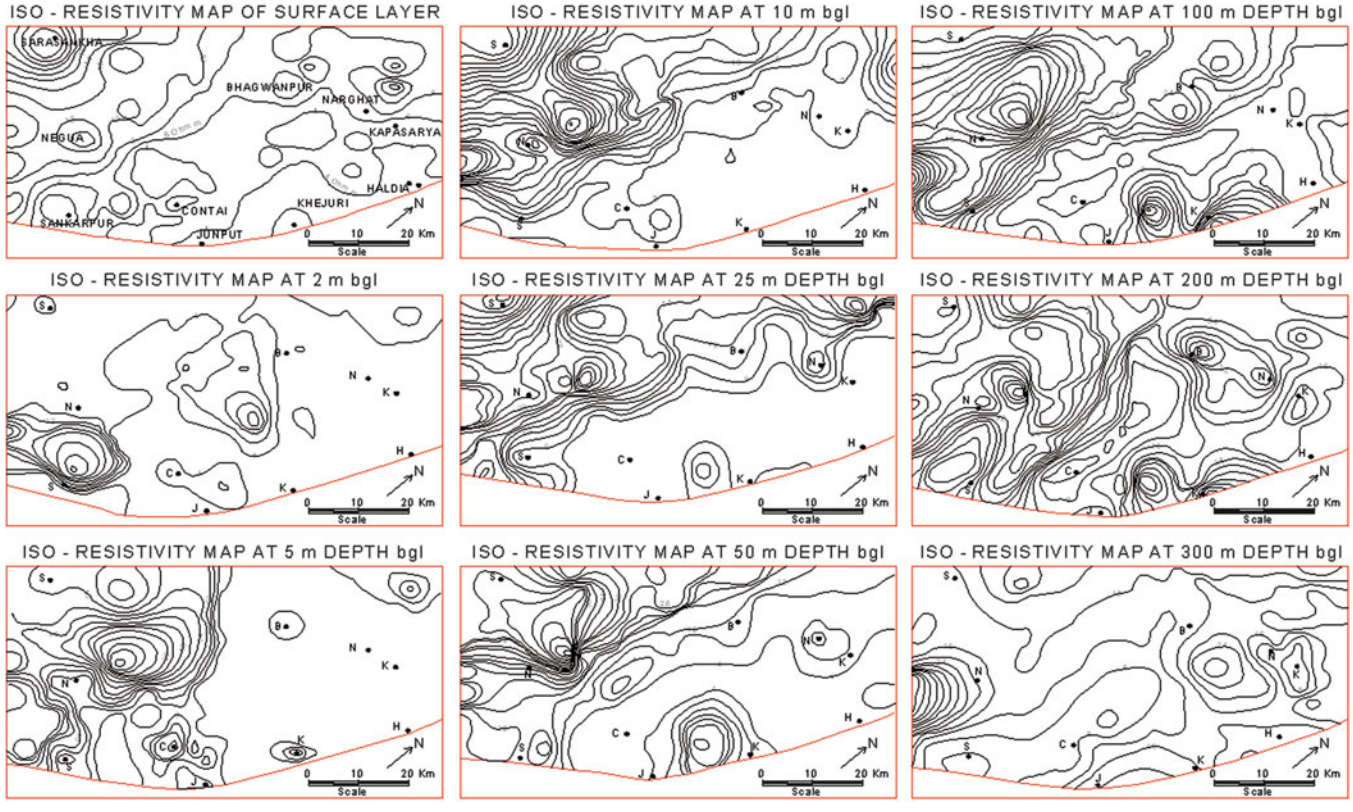

Fig. 5.5 Iso-resistivity depth slicing, coastal area, East Medinipur District, West Bengal, India (Singh 1993 modified after Chandra et al. 1989)

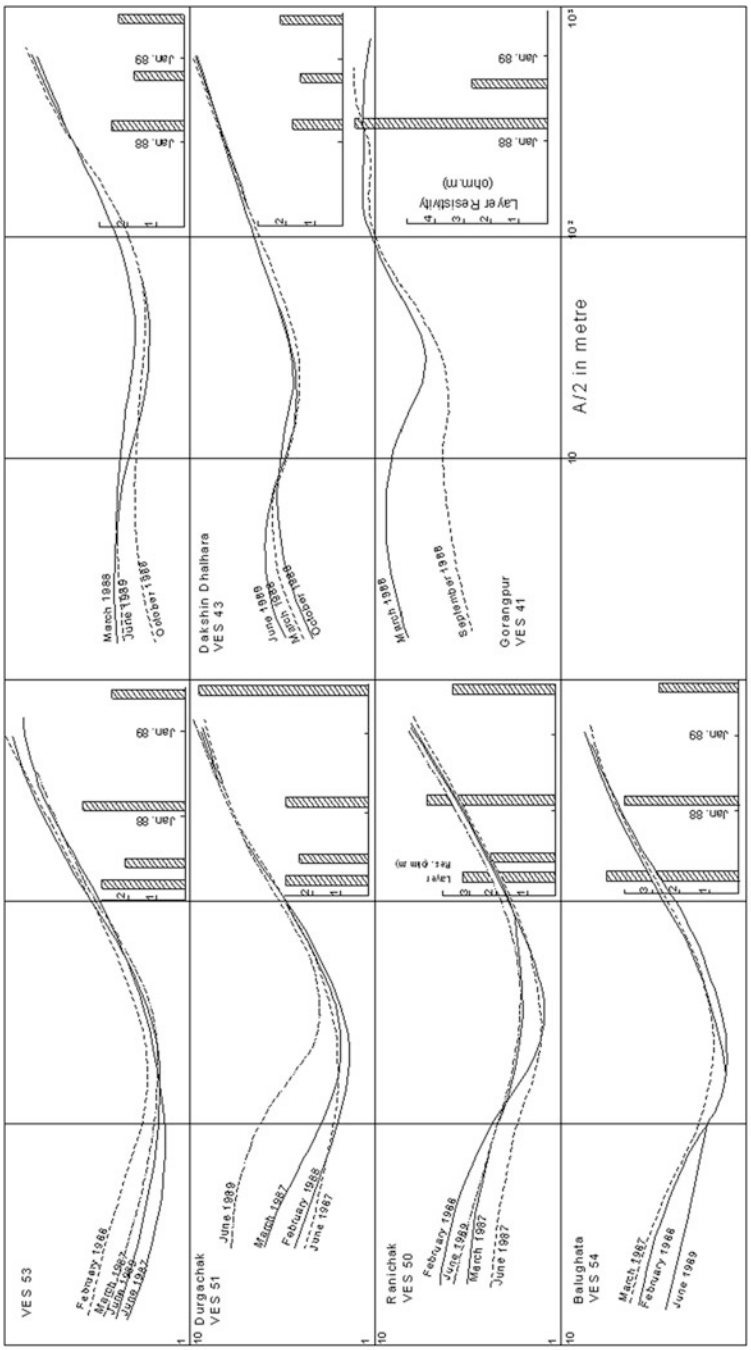

Fig. 5.6 Plots of repeated VES measurements used to monitor the quality of groundwater below the coastal plains of East Medinipur District, West Bengal, India (Singh 1993 modified after Chandra et al. 1989)

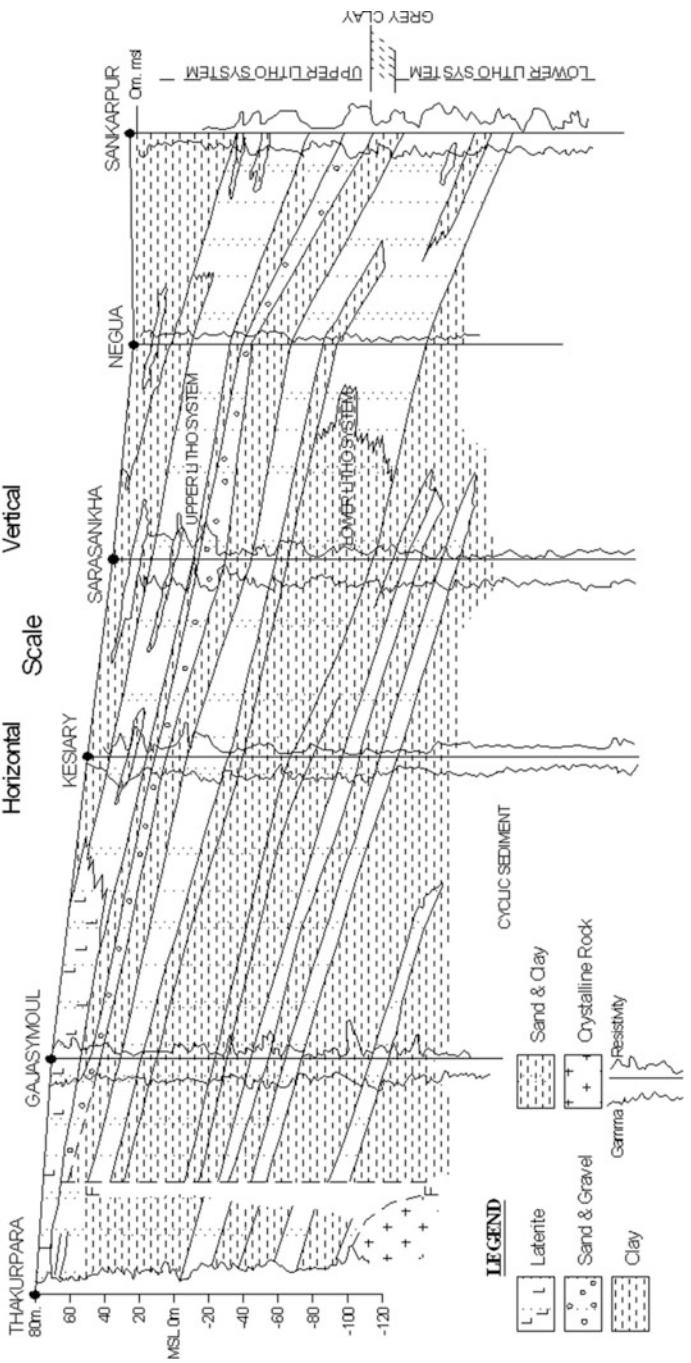

Fig. 5.7 Correlation along the Thakurpara-Sankarpur section, East Medinipur District, West Bengal, India (Singh 1993 modified after Chandra et al. 1989)

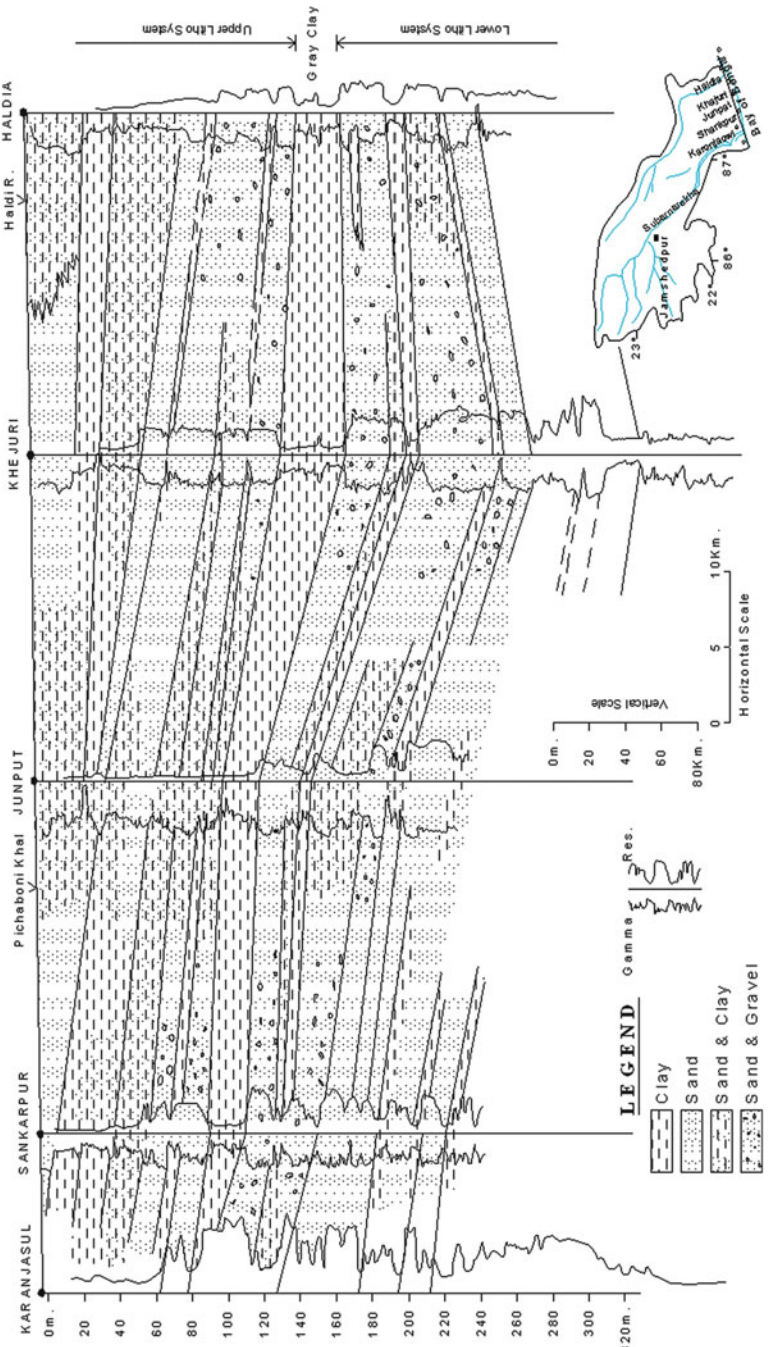

Fig. 5.8 Correlation along the Karanjasul-Haldia section, East Medinipur District, West Bengal, India (Singh 1993 modified after Chandra et al. 1989)

5.4 Discussion and Conclusions

The coastal tract of the Kasai-Subarnarekha Basin, West Bengal, India poses a typical geophysical exploration problem, wherein the overburden is highly conductive (typically 1–3 Ωm), because it is saturated with saline/brackish groundwater. The thickness of this highly conductive, near surface, geoelectric layer is about 120–140 m on the coast and 20–30 m inland. The layer that underlies it immediately consists predominantly of clay. It is saturated with better quality groundwater and has a comparatively higher resistivity varying within the range 5–12 Ωm. This geoelectric layer sequence in which the resistivity increases with depth is succeeded by a layer in which sand predominates and which has still higher levels of resistivity. While this lower layer in which sand predominates – the fresh aquifer – is easy to distinguish because of its resistivity in the upland areas, but this is not true in the coastal strip.

Geoelectrical exploration demands greater accuracy in data acquisition in coastal areas than it does inland. In coastal areas, resistivity methods face limitations like the development of very low potentials, transition in resistivity with depth, suppression of thin layers with intermediate resistivity values, and severe ambiguity in layer parameters because of equivalence. In spite of these limitations, the resistivity method has found wide application in coastal areas, mainly in assessing groundwater quality. The reliability of estimation of layer parameters is enhanced if resistivity techniques are supplemented by seismic, induced polarization and/or electromagnetic methods.

The coastal study area incorporates a near surface, brackish/saline groundwater zone. A serious attempt was made to obtain results from deep resistivity sounding in the area and thus to delineate the deeper zones. The resistivity results and subsurface information obtained from this work have been found to be accurate. A typical area of data acquisition was around Contai, where the information available prior to exploration also revealed the occurrence of a deeper, highly conductive horizon. Its exact depth of occurrence was not ascertained from these data, however. On the other hand, a typical case for the interpretation of resistivity data existed in the area around Kesiari and Negua, where prior information from lithologic logs and groundwater quality was not available. The VES at Contai could not be extended beyond 500 m (AB\2) the space available was limited. Apparent resistivity values between 1 and 2 Ωm for AB\2 were recorded at 250–300 m. Apparent resistivity values of the order of 4 Ωm were recorded up to AB\2 of 100 m. In fact, there are a number of VESs in which the apparent resistivity values for electrode separations of up to 100 m AB\2 vary from 1 to 2 Ωm. It was observed that in all such cases resistivity equipment with stacking facilities was effective in obtaining data of sufficient reliability.

As far as the interpretation of VESs is concerned, the depth ranges were determined by the application of equivalence and, in some cases, the layer resistivity was standardized on the basis of corrected, 64″ normal resistivity values obtained from the logs from boreholes drilled nearby.

The role of electrical logging as well as natural gamma logging of borehole was found significant, in confirming the surface resistivity results, particularly in

separating the saline zones from low resistivity clay zones, as inferred from the VES results. The results interpreted from the VES could elucidate the sub-surface configuration of the saline\fresh groundwater interface as well as those of the deeper fresh water aquifers. For this area, layer(s) with resistivity/ies of up to 3 Ωm could be taken as containing brackish groundwater. This resistivity range is confirmed by the results from the boreholes that were drilled. The saline\fresh groundwater interface was delineated to depths of 300 m bgl.

Spatial correlation of the logs to determine the regional sub-surface hydro-geological conditions in the dip and strike directions brought out the geometry of the aquifers in both the Tertiary and Quaternary sediments. The 'grey clay' bed separating the Tertiary horizons from the overlying Quaternary alluvium was taken as the marker horizon for the correlation. It was observed that the aquifers in the upland area have higher resistivity than those in the coastal area. For example, the resistivity of the aquifer at Bhagwanpur, where it is between 190 and 220 m bgl, is about 40 Ωm but is only 20 Ωm at Khejuri. This change in resistivity is not due to lithofacies changes – the sediments becoming finer towards the coast – and they are not, in any case, uniform across the coastal strip. Unlike the area around Bhagwanpur, Khejuri and Haldia, there is little change in the southwestern part around Negua and Digha, where layers with resistivities of the order of 30–50 Ωm were delineated even near to the coast. The industrial area of Haldia depends totally on groundwater with daily abstraction of the order of 20 M gallons from the clayey-sand aquifers in the Tertiary formations. The depleted piezometric surface is at −7 m msl. Had it been in the predominantly sand aquifer around Digha, the condition would have been even worse. There is no thick, protective layer of clay between the deeper fresh aquifers and the overlying saline water zone in the Digha area, like that which exists in the Haldia area. Under the prevailing, sub-surface hydrogeological conditions, excessive abstraction in the Digha area would allow lateral ingress of the deeper interface, which is currently located offshore. It would also allow vertical leakage to occur from the shallow, saline-water zones. On the basis of the geoelectric study it was possible to identify the areas where future groundwater development could be carried out safely. Regionally, the deeper aquifers in the southwestern part between Digha and Purana Khal could be developed. Excessive abstraction of groundwater from the coastal aquifer may trigger the lateral ingress of sea water and/or the up-coning of salt water from the deeper zones. This would lead to the deterioration of groundwater quality and hence degradation of the environment.

Bibliography

Abdul Nassir SS, Loke MH, Nawawi MN (2000) Salt-water intrusion mapping by geoelectrical imaging surveys. Geophys Prospect 48:647–661

Al-Sayed EA, El-Quady G (2007) Evaluation of sea water intrusion using the electrical resistivity and transient electromagnetic survey: case study at Fan of Wadi Feiran, Sinai, Egypt. In: EGM 2007 international workshop, Capri, 15–18 Apr 2007

Archie GE (1942) The electrical resistivity log as an aid in determining some reservoir characteristics. Am Inst Min Metall Eng Trans 146:54–62
Balia R, Gavaudo E, Ardau F, Ghiglieri G (2003) Geophysical approach to the environmental study of a coastal plain. Geophysics 68(5):1446–1459
Bhattacharya PK, Patra HP (1966) Geoelectric sounding. Dept. Geol. Geophysics; Indian Inst. Technology, Kharagpur, 174 pp
Bichara M, Lakshmanan J (1976) Fast automatic processing of resistivity sounding. Geophys Prospect 24:354–370
Chandra PC (1993) Role of geophysical techniques in pinpointing artificial recharge sites in coastal area. Work. art. Recharge in coastal areas; Bhubaneswar, 27–28 Mar 1993
Chandra PC, Reddy PHP, Singh SC (1989) Geophysical studies in Kasai-Subarnarekha river basin, UNDP/CGWB Project report
Chitea F, Georgescu P, Ioane D (2011) Geophysical detection of marine intrusions in Black Sea coastal areas (Romania) using VES and ERT data. Geo-Eco-Marina 17:95–102
Choudhury K, Saha DK, Chakraborty P (2001) Geophysical study for saline water intrusion in a coastal alluvial terrain. J Appl Geophys 46(3):189–200
Compagnie Generale De Geophysique (1963) Master curves for electrical soundings, 2nd edn. European Assoc. Exploration Geophysicist, The Hague, 49 pp
Deb S (1960) Groundwater resources of West Bengal with particular reference to coastal areas. Bull Natl Inst Sci India, 16 pp
Gema il K, Sam ir A, Oelsner C, Mousa SE, Ibrahim S (2004) Study of saltwater intrusion using 1D, 2D and 3D resistivity surveys in the coastal depressions at the eastern part of Matruh area, Egypt. Near Surf Geophys 2:103–109
Georgescu P, Dinu C, Niculescu V, Ion D (1993) Some applications of VES to groundwater exploration in the vicinity of Romanian coast of the Black Sea. Rev Roum Geophys 37:113–121
Georgescu P, Ioa ne D, Niculescu BM, Chitea F (2009) Long-time geoelectrical monitoring of groundwater contamination. Case studies from Romania. In: EAGE 15th European meeting of environmental and engineering geophysics, Abstracts volume, Dublin, 2009
Georgescu P, Ioa Ne D, Niculescu BM, Chitea F (2010) Geoelectrical investigations of marine intrusions on the Romanian Black Sea shore. Geo-Eco-Marina 16:85–92
Ghosh DP (1971) The application of linear filter theory to the direct interpretation of geoelectrical sounding measurement. Geophys Prospect 19:192–217
Gnanasundar D, Elango L (1999) Groundwater quality assessment of a coastal aquifer using geoelectrical techniques. J Environ Hydrol 7(17):3411–3419
Heigold PC et al (1979) Aquifer transmissivity from surficial electrical methods. Groundwater 17(4):338–345
Henriet JP (1976) Direct application of the Dar Zarrouk parameters in groundwater surveys. Geophys Prospect 24:344–353
Heslop A (1974) Gamma ray log response of shaly sandstones. Paper presented at the fifteenth annual logging symposium of SPWLA, Mcfdlen, 2–5 June 1974
Himi M, Stitou J, Rivero L, Salhi A, Tapias JC, Casas A (2010) Geophysical surveys for delineating salt water intrusion and fresh water resources in the Oued Laou coastal aquifer. In: Near surface – 16th European meeting of environmental and engineering geophysics, Abstracts volume, Zurich, 2010
Johansen KK (1975) An interactive computer/graphic-display-terminal system for interpretation of resistivity sounding. Geophys Prospect 23:449–458
Jorreto S, Pulido-Bosch A (2009) Characterization of seawater intrusion using 2D electrical imaging. Near Surf Geophys 7:377–390
Kasai-Subernrekha Project (1989) Final report on groundwater studies in Kasai and Subernrekha river basin, (UNDP Project IND/84/011, India). Unpublished CGWB report
Kelly WE (1977) Geoelectrical sounding for estimating aquifer electrical and hydraulic properties. Groundwater 23(2):182–188

Koefoed O (1969) An analysis of equivalence in resistivity sounding. Geophys Prospect 17:327–355
Koefoed O (1976) Progress in the direct interpretation of resistivity sounding. Geophys Prospect 24:233–240
Koefoed O (1979) Geosounding principles, vol 1, Resistivity sounding measurements. Elsevier, Amsterdam, pp 11–15
Manoutsoglou E, Vafidis A (2010) Integrated geophysical methods for imaging saline karst aquifers: a case study of Stylos, Chania, Greece. J Balk Geophys Soc 13(1):1–8
Murthy KSR (2011) Marine geophysical studies for mapping seismic hazards in coastal areas. Int J Earth Sci Eng 4(6):173–177 (Special issue)
Orellana E, Mooney HM (1966) Master tables and curves for VES over layered structure. Interciencia, Madrid, 193 pp
Overmeeren RAV (1989) Aquifer boundaries explored by geoelectrical measurement in the coastal plain of Yemen: a case of equivalence. Geophysics 54(1):38–48
Page LM (1968) Use of geoelectrical investigation for geologic and hydrogeological condition in Santa Clara Valley California. J Hydrol 7(2):167–177
Patra HP (1967) A note on the possibility of saline water invasion around the Jhalda coast, West Bengal (India). Geoexploration 5(1957):95–101
Patra HP, Bhattacharya PK (1966) Geophysical exploration for groundwater around Digha in the coastal region of West Bengal, India. Geoexploration 4:209–218
Ponzini G, Ostroman A et al (1984) Empirical relation between electrical transverse resistance and hydraulic transmissivity. Geoexploration 22:1–15
Prasad PR, Pekdeger A, Ohse W (1983) Geochemical and geophysical studies of salt water intrusion in coastal regions. In: Proceedings of the Hamburg symposium, Hamburg, 1983, IAHS Publication No. 146
Rijkswaterstaat (1969) Standard graphs for resistivity prospecting. European Association of Exploration Geophysicist, Zeist
Sengupta S (1966) Geological and geophysical studies in the western part of The Bengal Basin, India. Bull Am Assoc Pet Geol 50:1001–1017
Singh SC (1993) Integrated geophysical approach to groundwater resources development and management in Kasai-Subarnarekha River Basin. Ph.D. thesis, Banaras Hindu University, Varanasi
Singh UK, Das RK, Hodlur GK (2004) Significance of Dar-Zarrouk parameters in the exploration of quality affected coastal aquifer systems. Environ Geol 45(5):697–702
Singhal BBS (1963) Occurrence and geochemistry of groundwater in the coastal region of Midnapur, West Bengal, India. Econ Geol 58:419–433
Stewart MT (1988) Electromagnetic mapping of fresh-water lenses on small oceanic islands. Groundwater 26(2):187–191
Stewart MT et al (1983) Application of resistivity surveys to regional hydrogeologic reconnaissance. Groundwater 21(1):42–46
Worthington PF (1975) Quantitative geophysical investigation of granular aquifers. Geophys Surv 2:313–366
Zohdy AAR (1965) The auxiliary point method of electrical sounding interpretation, and its relationship to the Dar Zarrouk parameters. Geophysics 30:644–660
Zohdy AAR (1974) Automatic interpretation of Schlumberger sounding curves, Geol Surv Bull 1313-E, U.S. Government Printing Office, Washington, DC
Zohdy AAR (1989) A new method for automatic interpretation for Schlumberger and Wenner curves. Geophysics 54:245–253
Zohdy AAR, Jackson DB (1969) Application of deep electrical sounding for groundwater in Hawai. Geophysics 34:584–600

Chapter 6
Characterisation of a Coastal Aquifer System in the Eyre Peninsula, South Australia, Using Nuclear Magnetic Resonance Methods

Aaron Davis, Tim Munday, and Nara Somaratne

Abstract The coastal aquifers of the Uley Basin, which are the most important source of potable groundwater for the Eyre Peninsula, consist of unconfined Quaternary limestone overlying Tertiary clays and sandstones. Despite its importance, elements of the connectivity and total water resource basin remain relatively poorly understood. To address this, hydrogeophysical methods have been employed to better characterise the aquifer systems present. Interpretation of airborne electromagnetic data provided evidence for the delineation of the base of the Quaternary (limestone) aquifer and a basement low in the southwest corner of the South Uley Groundwater Lens, where there is a limited number of lithological bores or groundwater wells. The basement low, adjacent to the coast, suggests a preferential groundwater flow path and a possible connection between the Basin aquifers and the Southern Ocean.

Geophysical methods are routinely employed for groundwater exploration, assessment, and aquifer characterisation, particularly where access to land is limited and where other investigation techniques such as drilling may be limited or prohibited. In areas of environmental significance, or where access is generally difficult, non-invasive hydrogeophysical methods offer an alternative to exploratory drilling, by targeting areas of interest and better defining groundwater and aquifer characteristics in advance. We discuss the application of the hydrogeophysical technique of surface nuclear magnetic resonance (sNMR) for groundwater assessment. Presently, sNMR is the only hydrogeophysical technique that allows for direct detection of groundwater in the subsurface.

To better understand the possible inter-connectivity between the Uley Basin and the Southern Ocean; and as a precursor to considering whether new groundwater resources could be tapped, we investigate a series of (sNMR) soundings along a

A. Davis (✉) • T. Munday
Earth Science and Resource Engineering, CSIRO, 26 Dick Perry Ave,
Kensington, WA 6151, Australia
e-mail: aaron.davis@csiro.au

N. Somaratne
SA Water, 250 Victoria Square/Tarndanyangga, Adelaide, SA 5000, Australia

C. Wetzelhuetter (ed.), *Groundwater in the Coastal Zones of Asia-Pacific*,
Coastal Research Library 7, DOI 10.1007/978-94-007-5648-9_6,

transect and also at locations where information about the aquifer is better known. We confirm the presence of a Quaternary limestone aquifer containing potable water, extending 1–2 km across the south western corner of the Uley South Basin. The aquifer is defined to be about 15–20 m in thickness and possesses an effective porosity of around 20 %; it overlies clay layers that separate the limestone from a brackish Tertiary sandstone aquifer beneath. In conjunction with conductivity-depth sections derived from AEM data, our sNMR results deliver completely new knowledge and extend the hydrogeological understanding of this corner of the Uley Basin at a relatively low cost and minimal environmental impact.

6.1 Introduction

Geophysical techniques have been used extensively in the study and characterisation of coastal aquifer systems. Combinations of ground and airborne methods have been deployed to map and monitor the extent of saltwater intrusion (see for example Fitterman and Deszcz-Pan 1998), or to define groundwater quality (Kirkegaard et al. 2011). Often, this work is undertaken to manage the potential threat of groundwater contamination from saltwater intrusion resulting from over extraction. In many areas, geophysical investigations are followed up by exploratory drilling to further determine aquifer characteristics, water availability and quality. In this chapter we discuss the application of two different geophysical techniques for the characterisation of a coastal aquifer system in the Eyre Peninsula of Southern Australia. The first technique, airborne electromagnetics (AEM), is a proven method for rapidly characterising groundwater condition and for determining aquifer bounds (see, for example, Paine and Minty 2005; Siemon et al. 2008). The second, surface nuclear magnetic resonance (sNMR), is a relatively new technology now being employed more widely for groundwater assessment and aquifer characterisation.

In the Eyre Peninsula of South Australia a series of freshwater lens systems developed in unconfined Quaternary coastal aquifers, are a key source of potable water for the local communities. Of these, the Uley South Basin and its associated lens systems are among the most important aquifers in the region (Fig. 6.1). Since pumping of the Uley South aquifer first began, the groundwater level has been experiencing long-term decline due both to extraction and significant dry periods of lower recharge. Given its importance as a water supply, this coastal aquifer has been subject to numerous investigations in the last decade. As a result, the Basin and its lens systems are now better understood.

Recent studies, including an isotopic survey, have shown that there is connection between the unconfined Quaternary Bridgewater Limestone aquifers that produce the greatest amount of fresh water and the underlying sandstones of the Uley and Wanilla Formations which contain more brackish water (Evans 1997). Groundwater modelling studies have determined that the primary discharge of Quaternary aquifers (other than through pumping) is to the southwest into the Southern Ocean (Harrington et al. 2006; Zulfic et al. 2007). A recently completed AEM survey over the Coffin Bay and Uley South Lens systems (outlined in purple in Fig. 6.1)

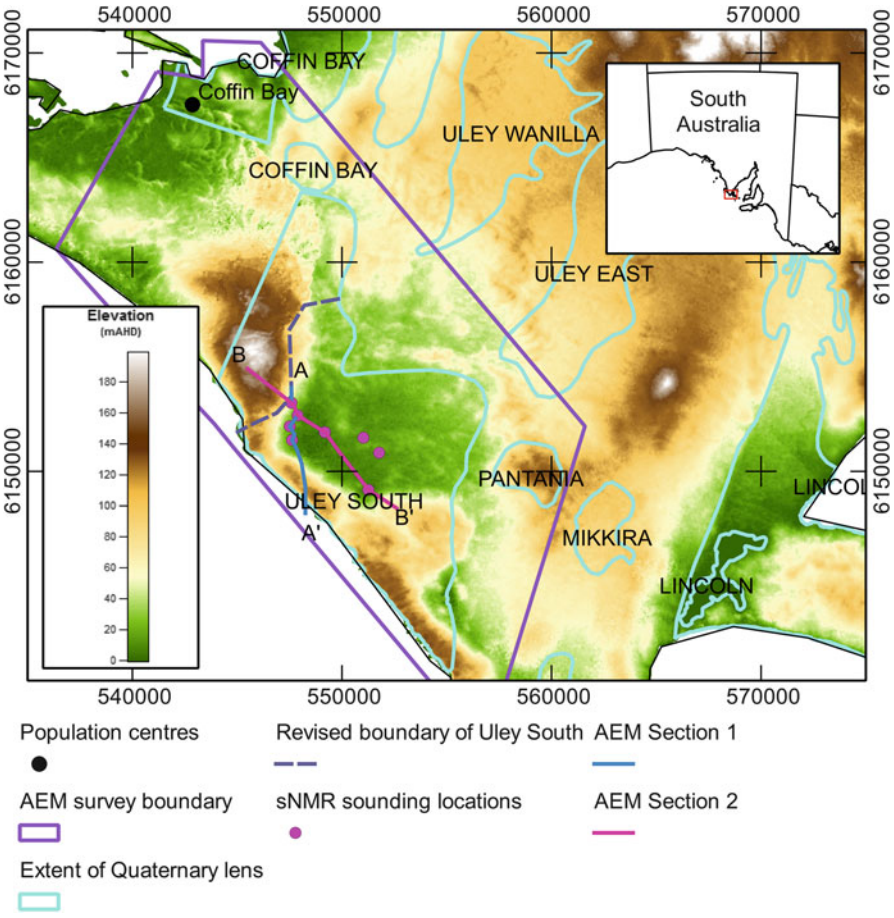

Fig. 6.1 Groundwater aquifers in the Uley Basin at the southern end of the Eyre Peninsula, South Australia. *Cyan lines* mark the outlines of the groundwater lenses in the Uley system, *magenta line* shows the outline of the 2006 Tempest AEM survey. *Blue line* indicates a 2006 revision in the western border of the Uley South groundwater lens (Harrington et al. 2006)

suggested a complex interconnection between the coastal Lens systems, specifically the Coffin Bay 'A' and Uley South Lenses underneath the Coffin Bay National Park (Fitzpatrick et al. 2009).

The Uley South Lens system is located in the Prescribed Wells area of the Uley Basin. Access to the area for exploratory drilling is restricted without special environmental approvals. These conditions make further hydrogeological assessments both time-consuming and expensive. In areas of environmental significance, or where access is generally difficult, non-invasive hydrogeophysical methods offer an alternative to exploratory drilling, by targeting areas of interest and better defining groundwater and aquifer characteristics, including their hydraulic properties in advance. Here we discuss the potential application of surface nuclear magnetic resonance (sNMR) as an innovative alternative to further explore the potential of groundwater resources in

the Uley South aquifer. We also consider its value as a means of supplementing information available to water resource managers thereby assisting them in decisions relating to groundwater resource allocation and supply.

NMR is the only non-invasive hydrogeophysical technique that allows for direct detection of groundwater in the subsurface. It also provides information on the aquifer and its hydraulic properties. In this study, we have conducted a series of surface nuclear magnetic resonance soundings in the southwest corner of the Uley South Basin, and compare the results of our sNMR soundings to bore data in the vicinity of production bores located near the centre of the Uley South lens where the hydraulic properties of the Quaternary Bridgewater Limestone aquifers are better known. To aid the reader, we also explain the principle of the nuclear magnetic resonance effect and how it relates to the geophysical application of surface NMR soundings for groundwater exploration. The results from a selection of sNMR soundings in the region are examined against information obtained from the AEM survey covering the Basin, and from coincident time domain EM soundings and comment is made on how these data supplement the conceptual hydrogeological model of the area.

6.2 Methodology

6.2.1 Use of NMR in Groundwater Studies

Nuclear magnetic resonance (NMR) has been used as a geophysical tool for many years. Shortly after the discovery of the NMR effect, geophysicists began to apply it in studying the properties of water and oil in saturated rock (Dunn et al. 2002). Soon after that, NMR tools were constructed for use in down-hole measurements linked to petroleum exploration (eg, Wyman 1962), and the technology is routinely used in the petroleum industry as a reservoir characterisation tool (Coates et al. 2001; Dunn et al. 2002). It was not until the 1980s that NMR was used in an application for groundwater assessment from the surface. The Hydroscope surface NMR instrument was the first of its kind, and began to be used in the hydrogeophysical community (Legchenko et al. 2002). Surface NMR was introduced to Australia (Schirov et al. 1991), but it was not widely adopted in this country. For the next decade surface NMR was a marginal tool in geophysical usage for groundwater exploration, detection and characterisation compared to other more traditional geophysical techniques such as resistivity and electromagnetics, despite its obvious advantages over them for groundwater assessment. The field has experienced an increase in interest and usage in the last 10 years, primarily due to increased power output in the transmission of the NMR pulse, faster switching in the power-electronics, improved techniques for noise reduction of the NMR signal, and the general increase in awareness that water is a precious commodity. Presently, surface and borehole NMR for near-surface applications are experiencing a surge of attention from the academic, research, government, and consulting communities

providing a thriving forum for the continuing development of a potentially valuable geophysical technique. More recently NMR has been applied to research in the near-surface for groundwater characterisation (Davis et al. 2012; Knight et al. 2012; Vouillamoz et al. 2012).

6.2.2 Physical Principles of NMR

Nuclear magnetic resonance (NMR) is a technique that exploits some of the fundamental quantum mechanical properties of atomic nuclei. From quantum mechanics, we know that all matter possesses the property of angular momentum. For subatomic particles such as electrons and protons, there are two types of angular momentum: orbital and intrinsic. The intrinsic angular momentum, which is inherent to the particle, is commonly referred to as 'spin'. In the same way as mass and charge are fundamental to matter; spin is used to describe the quantum state of the angular momentum of a particle such as an electron or a proton. The simplest way of imagining particle spin is to picture a mass rotating about its axis: the direction of the rotation also determines the spin direction. This classical analogy can be taken too far since, unlike orbital angular momentum, the spin of a particle cannot be sped up or slowed down; and only its direction may be changed. Since spin is a quantum property, it can be described with a quantum number; and spin values for electrons and protons can only be half-integer (i.e. $s = ½$). Since we are interested in the nuclear magnetic resonance effect in water, this paper will focus only on the properties of the protons of hydrogen atoms. When we look specifically at the hydrogen atom, the spin of the proton is limited to $s = ½$ or $s = -½$, and therefore its direction can be only 'up' or 'down', in association with the half-integer allowable quantum states (Bransden and Joachain 1994).

As stated earlier, protons also possess the fundamental properties of mass and charge. Since the proton has non-zero spin and a positive charge, we naturally expect it to also have an intrinsic net magnetic dipole moment that is parallel to the direction of its spin. Because the spin of the proton is quantised, we also expect the dipole magnetic moment of the proton to be quantised with quantum numbers of $j = ½$ and $j = -½$. The ratio of the observed magnetic moment (of the proton) to its spin is the gyromagnetic ratio, γ (for a hydrogen proton, $\gamma_H = 2.64 \times 10^8$ rad/T/s); and it is the concept of spin and nuclear magnetic dipole moment, coupled through the gyromagnetic ratio, that is most important when we consider the phenomenon of nuclear magnetic resonance (Abragam 1961).

Let us consider a single hydrogen proton with nuclear magnetic dipole moment $\boldsymbol{\mu}$ in the presence of an external static and uniform magnetic field $\mathbf{B}_0$. Before the field $\mathbf{B_0}$ is present, the magnetic moment of the hydrogen atom can point in any direction; however, once $\mathbf{B_0}$ is turned on, the moment will be affected by the external field. Since magnetic dipole moment is quantised, there are two allowable directions for the magnetic moment vector to align. The difference in the direction

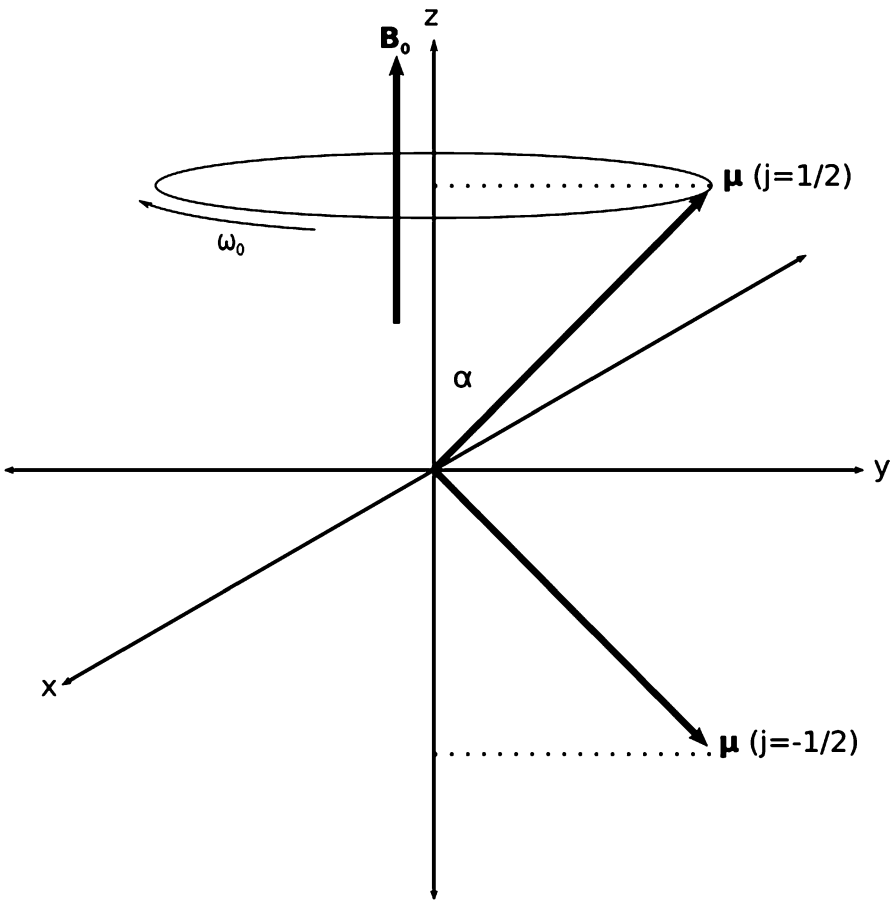

Fig. 6.2 Schematic of the effect on a nuclear magnetic moment dipole (μ) with allowable dipole numbers of s, j = ½ and −½ in an external magnetic field B_0. The dipole will either align in the direction of B_0, or align counter to its direction, corresponding to 2 distinct energy states. The energy state whereby the dipole aligns with B_0 is lower energy and hence, favoured. The dipole will precess about the axis of B_0 due to the spin angular momentum

of alignment is given by the interaction energy of the magnetic dipole moment with the external magnetic field:

$$\begin{aligned} E &= -\boldsymbol{\mu} \cdot \mathbf{B_0} \\ &= -\gamma_H \hbar B_0 j, \text{where j} = 1/2,\ 1/2 \\ &= \cos\alpha, \end{aligned}$$

where $\hbar$ is Planck's constant divided by 2π, $\mathbf{B_0}$ is the magnitude of the external field, j is the quantum number of the nuclear magnetic dipole moment and α is the angle made between the external magnetic field and the dipole moment. A schematic of this is shown in Fig. 6.2. We see that the particle has a lower energy when it aligns in

the direction of the external magnetic field (Ames 1967). If a collection of hydrogen atoms is subject to the external field, we will see slightly more than half of the atoms aligned with the field than against it, since the atoms will obey Boltzmann statistics. Thus, for a collection of hydrogen atoms in an external magnetic field (such as the earth's) there is a net macroscopic magnetisation, **M**, that aligns with it. It is this field which is used for the nuclear magnetic moment effect.

From classical theory, we know that when a magnetic dipole is subjected to an external magnetic field ($\mathbf{B_0}$), the magnetic dipole experiences a torque that tends to align it in the direction of the field. However, since the hydrogen atom is a quantum particle, it also possesses angular momentum; the application of the external magnetic field forces the magnetic dipole moment to precess about the axis of $\mathbf{B_0}$ in a plane that is perpendicular to its direction. The rate of precession of the magnetic moment is given by the Larmor frequency of the proton

$$f_{Larmor} = \gamma_H B_0 / 2\pi,$$

and this describes the rate at which the magnetic moments of all hydrogen atoms in the external magnetic field spin about it.

We achieve the effect of nuclear magnetic resonance by applying a secondary magnetic field $\mathbf{B_T}$ at right angles to the external magnetic field $\mathbf{B_0}$. This creates an effective magnetic field that forces the net nuclear magnetisation vector **M** to rotate away from the direction of $\mathbf{B_0}$ and towards $-\mathbf{B_0}$ while also precessing with frequency f_{Larmor}. This is shown schematically in panel (a) of Fig. 6.3. By applying the secondary field pulse for a short period of time τ_p, we tip the net magnetisation vector by angle $\theta(\tau_p) = \gamma_H t |B_T|$ away from $\mathbf{B_0}$. After the pulse has been turned off, the magnetisation vector re-aligns back to the external magnetic field (see panel (b) of Fig. 6.3), and it is this change in magnetisation that we record for the NMR signal.

The change of the net magnetisation vector, **M**, to realign back to the external magnetic field, $\mathbf{B_0}$, tells us information about the material being studied in the NMR experiment. In the application described in this paper, namely, the use of nuclear magnetic resonance for groundwater detection, the change in **M** gives us information on water content and water mobility (eg, Coates et al. 2001). The relaxation of **M** has been described by Bloch (1946) by the introduction of two phenomenological characteristic times, T_1 and T_2. The time T_1 describes the increase of **M** in the direction of $\mathbf{B_0}$ and is related to the interactions of the hydrogen protons with the surrounding lattice (hence the names longitudinal and spin–lattice relaxation time); while T_2 describes the decrease of **M** from the plane perpendicular to $\mathbf{B_0}$ and is related to the interactions of the protons with each other (this time is also called the transverse and spin-spin relaxation time). In normal NMR experiments, T_2 gets further complicated by de-phasing effects of the spins in the ensemble and inhomogeneity effects due to spatial variations in the magnitude of resonant pulse field $\mathbf{B_T}$. Typically, a coil is used to detect changes in **M** by using Faraday's Law of induction, which states that a time-varying change in magnetic field through a closed loop will generate an electric current in the loop itself. A device recording the rate of change of **M** with respect to time after a single pulse of the transverse

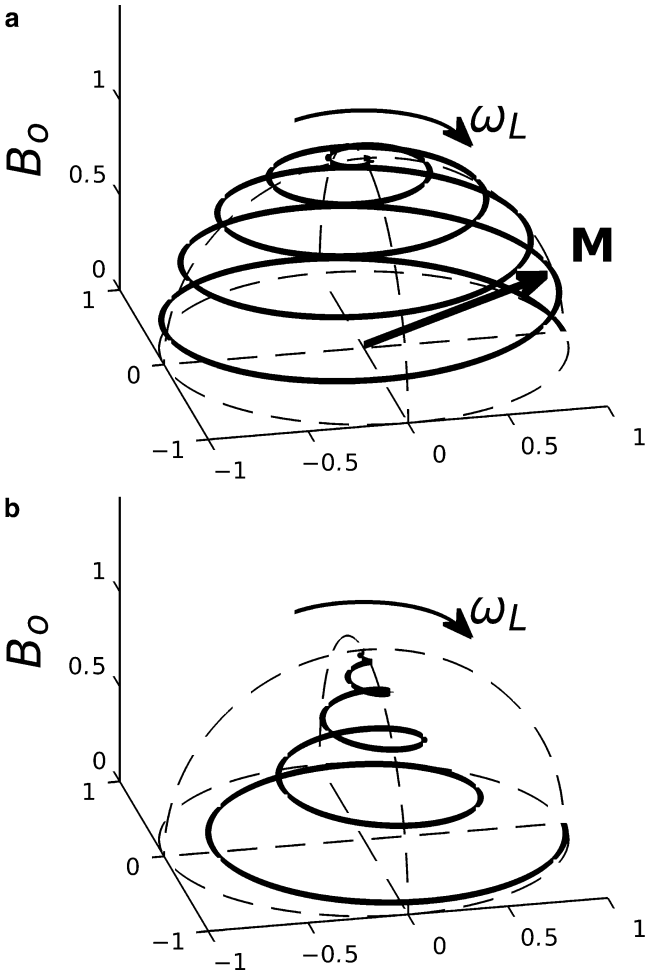

Fig. 6.3 A schematic of the macroscopic nuclear magnetisation vector: (**a**) precessing to rotate in the plane perpendicular to B_0 during the resonant pulse magnetic field; (**b**) returning to realign with B_0 after the resonant pulse has been turned off (where $T_1 = 2\ T_2$)

resonant field $\mathbf{B_T}$ will often measure a combination of T_1, T_2 and the other effects: these can be combined into a new time constant, T_2^*. The signal measured is thus called the free induction decay, and it is this which is recorded in the surface NMR experiment.

6.2.3 Surface NMR Soundings

Surface nuclear magnetic resonance sounding (sNMR) is presently the only non-invasive geophysical technique that is capable of directly detecting the presence of

subsurface water at a specific site (Legchenko and Valla 2002). Using the phenomenon of nuclear magnetic resonance, we excite the protons of hydrogen atoms of water in the ground with a resonant magnetic field that is tuned to the Larmor frequency at the sounding location. In this case, the static external magnetic field is that due to the intrinsic magnetic field of the earth. The resonant frequency value depends on the local intensity of the magnetic field of the earth, so a measure of the total magnetic field strength at the sounding location must be taken. Typical values of magnetic field intensity of the earth are 23,000–66,000 nT, which corresponds to a Larmor frequency of ~1,000–2,800 Hz. The governing equation to calculate the resonant frequency of the hydrogen atoms is

$$f_{Larmor} = B_o \gamma_H.$$

For an sNMR sounding, the transverse resonant magnetic field is produced using an electrical current pulse that is forced around a surface loop laid out in a geometry suitable to the sounding that is required (Weichman et al. 2000). The current forced around the surface-loop produces a magnetic field in the surroundings that travels out and downward through the earth. The electromagnetic pulses, which oscillate at the Larmor frequency, force the hydrogen atoms in the ground away from the magnetic field of the earth and into a plane at right angles to it. Once the pulse is shut off, the nuclei return to the direction of the earth's magnetic field. The resulting change in nuclear resonant magnetisation is measured as a voltage induced in the surface-loop due to the time-varying secondary magnetic field. Hence, we see that the surface loop operates as both a transmitter and receiver. The duration of the pulses, and their strength, determines the depth of investigation at the sounding site. The measure of pulse duration time, t, multiplied by peak pulse current, I, is called the pulse moment, $q = tI$, and this variable determines how deeply and how clearly we can resolve water in the subsurface.

Following Weichman et al. (2000), the net nuclear magnetisation vector $\mathbf{M}_N(\mathbf{r}, t)$ evolves in time as

$$\mathbf{M}_N(\mathbf{r}, t) = \chi_N(\mathbf{r})\mathbf{B}_0 \cos(\theta_T(\mathbf{r}, t)) + (\chi_N(\mathbf{r})\mathbf{B}_0 \times \hat{\mathbf{B}}_T^+(\mathbf{r}, t)) \sin(\theta_T(\mathbf{r}, t)),$$

where $\chi_N(\mathbf{r})$ is the equilibrium nuclear magnetisation density, $\theta_T(\mathbf{r}, t)$ is the spatial and time-dependent tipping angle of the magnetisation vector, and $\hat{\mathbf{B}}_T^+(\mathbf{r}, t)$ is a unit vector of one axis of a co-rotating frame of reference which is at right angles to the static magnetic field due to the earth, $\mathbf{B_0}$, and rotating at the Larmor frequency, ω_L. From the equation above, we see that the magnetisation in the subsurface, as a function of time and space, can be divided into components that are parallel to the stationary (earth) magnetic field (first term) and at right angles to it (second term in equation above). In the surface NMR sounding, the greatest proportion of the signal comes from the second (perpendicular) term in the equation. The portion of the magnetisation field that we measure with the receiver loop is proportional to the amount of flux that is cut by the receiver loop. Since the receiver loop is the same as the transmitter loop, the

calculation simplifies greatly, and the time-varying nuclear magnetic field can be directly expressed as a single volumetric integral equation. The voltage induced in the receiving loop due to the NMR pulse sequence can then be expressed as:

$$V(q, \mathbf{x}_0) = -\int d^3\mathbf{r}\, K(q, \mathbf{r}) \cdot n_N(\mathbf{r}),$$

where $K(q, \mathbf{r})$ is the kernel that explains the physical interaction of the magnetic fields as a function of pulse moment and space, and $n_N(\mathbf{r})$, which is the spatial distribution of groundwater in the subsurface. The initial voltage measured in the receiver for a pulse moment q is given by the volume integral over all space multiplied by the water distribution; and it is directly sensitive to water in the subsurface. Starting from the initial amplitude E_0, the signal will decay to zero after a certain amount of time has passed. The free induction decay signal is governed by the distribution of water in the subsurface, and how it is contained in the pore spaces of the earth. From the equation above, we see that the voltage induced in the measurement loop is directly proportional to water content: this means that, by estimating E_0, the initial amplitude of the decaying envelope of the Larmor frequency oscillation, we can estimate the porosity of the water-bearing soils in the subsurface. By adjusting the pulse moment parameter q, which focuses the magnetic field pulse of the transmitter loop to certain depths, we can obtain estimates of water content with depth in the subsurface. An example of the free induction decay for a 0.82 As pulse taken from a sNMR sounding in Uley South is shown in panel (a) of Fig. 6.4. In this figure, we see the free induction decay of the sNMR response start from approximately 600 nV and decay to noise levels after about 400 ms. With proper calibration of the sNMR equipment, this corresponds to water content in the subsurface. The second part of the sNMR signal to be analysed is the characteristic time T_2^*. We know that this time constant is composed of field inhomogeniety effects, but it also reflects properties of the subsurface. Importantly, T_2^* yields information about the pore spaces that the water is contained in. In general small pores will produce more interactions of the hydrogen protons with the surrounding soil material than larger pores, since the ratio of surface area to volume of the pore space increases with decreasing radius. For every free induction decay from a given pulse moment in a sounding, or for every layer of water content that is calculated in the inversion, we can estimate a distribution of T_2^* that creates the total sum of responses for a sounding signal or layer. The distribution of T_2^* tells us information about the size of the pores containing the water. An example of this is shown in panel (b) of Fig. 6.4, which shows the T_2^* distribution for the 20th layer in the inversion for water content at Site 3 in the Uley South aquifers (cf Fig. 6.9). From experience, we choose a cut-off of 33 ms in the T_2^* distribution that marks the difference between 'free' and 'bound' water in the subsurface. We expect free water to be that which is productive if we were to place a bore in the aquifer at the sounding site and screen it at the appropriate interval; while we would not be able to produce water from an aquifer that contained only bound water: the pore spaces

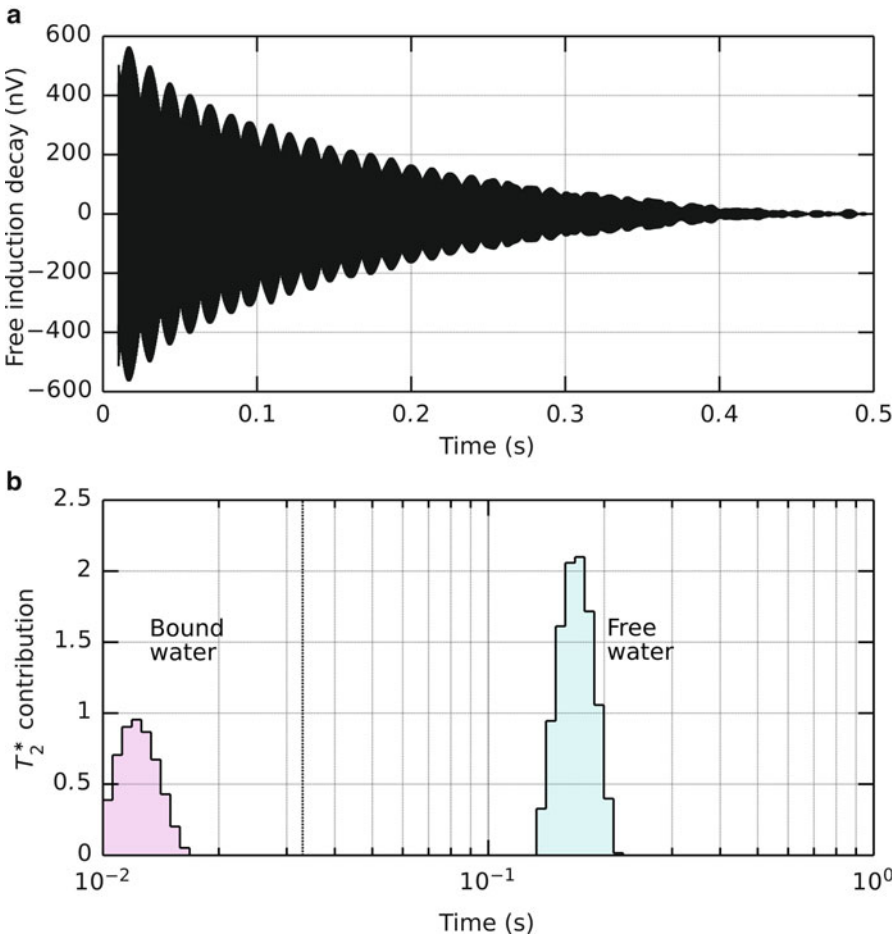

Fig. 6.4 (**a**) Free induction decay from a 0.82 As pulse at Site 3 in the Uley South aquifer. Loop size was 75 m, pulse width was 40 ms, and the Larmor frequency was 2,519.7 Hz. (**b**) T_2^* distribution for the 20th layer of the water content-depth inversion for Site 3 (cf Fig. 6.9). *Pink shape* represents water content that is below 33 ms and therefore bound; *cyan* is water content that is above 33 ms and therefore free. 33 ms boundary is marked with *vertical dotted line*

would not permit water to travel through them in any appreciable amount. We see, then, that not only can we estimate water quantities; we can also provide estimates of water mobility. Finally, a surface NMR sounding can provide us with an estimate of the permeability of the subsurface at a sounding location with respect to depth. By taking the sum of the square of each of the T_2^* values in the distribution for a given layer, we arrive at an estimate of the mobility of groundwater at that depth for that site. Using the same sounding setup at different sites will allow us to gain an idea of the mobility of water in one location relative to that of another. We call this value the relative permeability (K_{rel}), and use it as a comparison of water

availability in our sounding work in the Uley South aquifers. An example of the relative permeability of the subsurface with depth is shown with the red curve of the right-hand panel of Fig. 6.9: in this figure, values of K_{rel} are scaled logarithmically.

For more information on the derivation of the voltage induced in the receiver loop from the sNMR signal, (Hertrich 2008; Legchenko and Valla 2002; Weichman et al. 2000) offer clear expositions on the subject.

The process of sNMR data acquisition is as follows:

1. A site is selected for the sounding and a loop is laid out at the site. Typical loop side lengths are on the order of tens of metres to about 150 m, depending on the type of measurement wanted, the maximum depth of investigation desired, and the noise characteristics of the location.
2. A transmitter is attached to the loop, and the circuit is tuned to resonate at the Larmor frequency of the hydrogen protons at the site.
3. A series of measurements are taken at the site with several different pulse moments (ie length and magnitude of the pulse current). For every pulse moment, the voltage induced in the receiver loop is recorded. Typically, about 20–30 different pulse moments are used at a single sounding, and each pulse moment is repeated several times, depending on noise levels present in the data.

Once the survey soundings are complete and the data has been processed for sample stacking and noise reduction, the sNMR data must be inverted for water content with depth. There are many inversion schemes that are available, including: linear pseudo-inverse techniques (Walsh 2008); Tikhonov regularisation (Legchenko and Shushakov 1998); linear programming (Guillen and Legchenko 2002); and QT inversion using the entire dataset (Mueller-Petke and Yaramanci 2010). Each inversion scheme has separate advantages and levels of sophistication; and some include the electrical conductivity structure of the earth. In this paper we use the linear pseudo-inverse of Walsh (2008), mainly due to the fact that software for the inversion of NMR data is limited in availability (at time of publication), and that the survey areas were electrically resistive justifying the use of an inversion process that does not consider electrical conductivity in the ground.

6.3 An Introduction to the Case Study: Uley South Aquifer System

The Uley Basin consists of a system of aquifers located in the southernmost part of the Eyre Peninsula, South Australia (cf Fig. 6.1). The major aquifer systems that are used for groundwater production in the Uley Basin are the Coffin Bay lens, the Uley East lens, the Uley-Wanilla Lens, and the Uley South lens. The Uley South lens, which is the greatest resource, is a topologically closed basin located in the southern part of the Uley Basin, bordering on the Southern Ocean. It is the principal source of groundwater for the Eyre Peninsula water supply, with a current allocation of

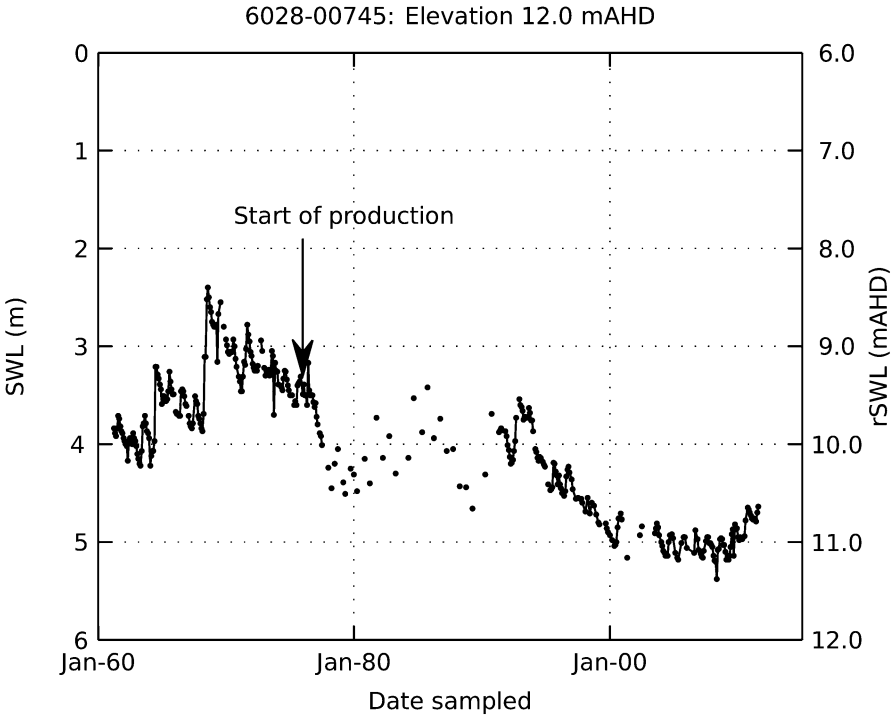

Fig. 6.5 Fifty-year history of standing water level (SWL) in the Quaternary aquifer of bore 6028–00745 in the Uley South freshwater lens. Water production from the Uley South Quaternary aquifer began in 1976, with relatively constant rates of production

approximately 6–7 GL/a (Martin and Clarke 2000). Since initial pumping began out of the Uley-Wanilla lens in 1948 (Segnit 1942), increased water demand in the area prompted drilling investigations in the Coffin Bay area and southward to Uley Homestead (Shepherd 1962, 1963, 1965). Drilling in the Uley South aquifer began in 1959 and continued on through the 1960s, and Uley South was quickly found to be extremely productive over at least two different aquifers (Morton and Steel 1966, 1968, 1970; Painter 1970). Extraction of groundwater from the Uley South lens began in 1976 through eight production wells (Sibenaler 1976; Barnett 1978). A computer model on groundwater flow was conducted in 1980 by (Shepherd 1980), and the recommendation from the report was that groundwater extraction of the Uley South Lens could safely expand by 50 %. Subsequently, the groundwater extraction was later expanded to 17 production wells by 1999, with decreasing production from the Uley-Wanilla lens over the same period (Evans et al. 2009). In 2000, Martin and Clarke explored the long-term trending of water levels due to pumping and recharge, raising awareness about possible stressing of the Uley South lens due to extraction of groundwater (see, e.g. Fig. 6.5). Consequently, there has been an increase in public awareness of the Uley Basin region and a definite need to

increase the hydrogeological knowledge of the Uley Basin had been identified (Government of South Australia 2001).

The geology of the Uley Basin system has been studied since the 1930s (Segnit 1935). Since then, both the geological and hydrogeological understanding of the area has increased. Segnit (1942), and (Johns 1961) conducted the first geological studies of the area, with hydrogeological information provided by many authors (e.g. Shepherd 1965; Morton and Steel 1966; Sibenaler 1976; Barnett 1978). This included geological models from boreholes, geological surface mapping, pump tests and meteorological data, with attention focussed primarily in the Uley-Wanilla aquifer, shifting to Uley East, and then, increasingly to the Uley South lens. Evans (1997) addressed recharge rates and residence of water in the Quaternary and Tertiary aquifers of the Uley Basin: information which was extended into the 2006 Department of Water, Land and Biodiversity Conservation report (Harrington et al. 2006). James-Smith and Brown (2002) conducted a numerical study of groundwater recharge and flow for the Uley South groundwater lens, and were able to reproduce general trends in the steady-state and transient periods of groundwater flow in the aquifer. As an additional investigation into the stresses acting on the Uley South lens, Clarke et al. (2003) conducted a review of the state of health of the existing network of monitoring bores in the production zone, and a brief geophysical survey of the saltwater interface of this coastal aquifer. More recently, the reports of Harrington et al. (2006) and Zulfic et al. (2007) have greatly increased the geological, hydrogeological, chemical, and hydrodynamic understanding of the Uley South Basin, investigating residence, rates of recharge, water balance and connectivity between aquifers in the Quaternary and Tertiary layers.

There are three major groundwater systems in the Uley Basin. The uppermost aquifers are in the Bridgewater Formation, which consists of Quaternary Limestone. These aquifers are generally unconfined, with high yield and low salinity. In the Uley Basin, the Bridgewater Formation forms a thin veneer over the deeper structures in the east and north-west of the Uley South basin, but can range up to $>$100 m thick (Harrington et al. 2006). It consists of Aeolian sediments and fine shell fragments. The Bridgewater Formation is generally either unconsolidated or loosely aggregated; however, there are also regions of secondary cementation in the form of calcrete horizons (limiting porosity), and hard and cavernous zones as well. Groundwater in this formation is contained in unconfined aquifers that form lenses in the saturated zones of the Quaternary Limestone. The main freshwater lenses in the Quaternary Limestone are the Uley-Wanilla, the Uley East, Coffin Bay and Uley South. These aquifers have been the focus of many studies and have received most attention since they have traditionally been the main water supply source for the Southern Eyre peninsula.

For the Bridgewater Formation in the Uley South Basin, rainwater is the primary source of recharge (Harrington et al. 2006; Zulfic et al. 2007). Water production is moderate to high, and water quality is very good. There is some evidence of recharge of the Uley South lens from the underlying Tertiary aquifer, but this is still uncertain. Groundwater outflows from the Bridgewater Formation lenses trend to the southwest, with eventual discharge to the Southern Ocean. It is believed that

groundwater is also lost due to evapotranspiration, although this has not been completely studied.

The Uley Formation is a Tertiary Clay that forms a lateritic aquitard separating the Quaternary Bridgewater Formation from the underlying Tertiary Sand (Wanilla Formation) aquifer. Typically, the Uley formation consists of clays and silty clays, is expected to be laterally varying, and does not entirely prevent movement of groundwater between the Bridgewater Formation and the underlying Tertiary Sands. It is expected that there is some recharge of the Bridgewater Formation through the Uley clays from the Wanilla sandstone (Morton and Steel 1968).

The Wanilla Formation is the secondary aquifer in the Uley Basin system. It consists of fluvial sands and gravels, clays and lignitic lenses. In some areas, the Wanilla Formation is silty and carbonaceous. Production from this aquifer is poor to moderate, and groundwater tends to be more saline than the Bridgewater Formation. This aquifer tends to lie mostly below sea level and is of largely unknown extent in the Uley Basin (Harrington et al. 2006). Recharge of the Wanilla sandstones is expected to be from direct recharge where the Quaternary Limestone connects directly with the Tertiary Sands (particularly in the Uley-Wanilla and Uley East lenses), through the Uley Formation Clays, and laterally throughout the study area. Groundwater in the Wanilla Formation discharges to the Southern Ocean at the south-western edges of the boundary and, potentially, upwards through the Uley Clays to the Bridgewater Formation above (Zulfic et al. 2007).

The Basement Units of the Uley Basin system are the third groundwater aquifer in the area. Weathered and un-weathered Archaean gneiss, quartz and feldspar create a poorly-defined aquifer system that is not believed to interact greatly with the overlying Tertiary and Quaternary units. In general, the basement structures determine the geometric expression of the Wanilla, Uley and Bridgewater Formations. Basement ridges in the Uley Basin trend north–south, with elevation changes of 50–200 m, and ridges tend to be 5,000–7,000 m apart (Evans 1997). Troughs in the basement form the structure of the Wanilla Formation in the Uley South aquifer system, but have less control over the eastern and northern margins of the Quaternary Bridgewater Formation. A conceptual model of the geology of the Uley East and Uley South Basin is shown in Fig. 6.6.

The reports of (Zulfic et al. 2007; Harrington et al. 2006) were instrumental in increasing the understanding of the hydraulic characteristics of the Uley Basin. They also identified further steps that were necessary for improving the groundwater model calibrations for the Uley South lens, such as thickness and extent of the Bridgewater Formation, thickness and extent of the Uley and Wanilla Formations, lateral extent and assessment of risk of saltwater intrusion into the Uley South aquifer, and possible connections between aquifers in the Uley Basin. In 2006, a multi-client airborne electromagnetic (AEM) survey was flown over the southern portion of the Uley Basin (Fitzpatrick et al. 2009) to address these issues. Based on the preliminary findings of (Clarke et al. 2003), electromagnetic methods were believed to provide an efficient and inexpensive method to explore the subsurface of the Coffin Bay and Uley South groundwater lenses. The Tempest system of Fugro Airborne Surveys Pty Ltd was used to acquire 1,016 line-km of AEM data in

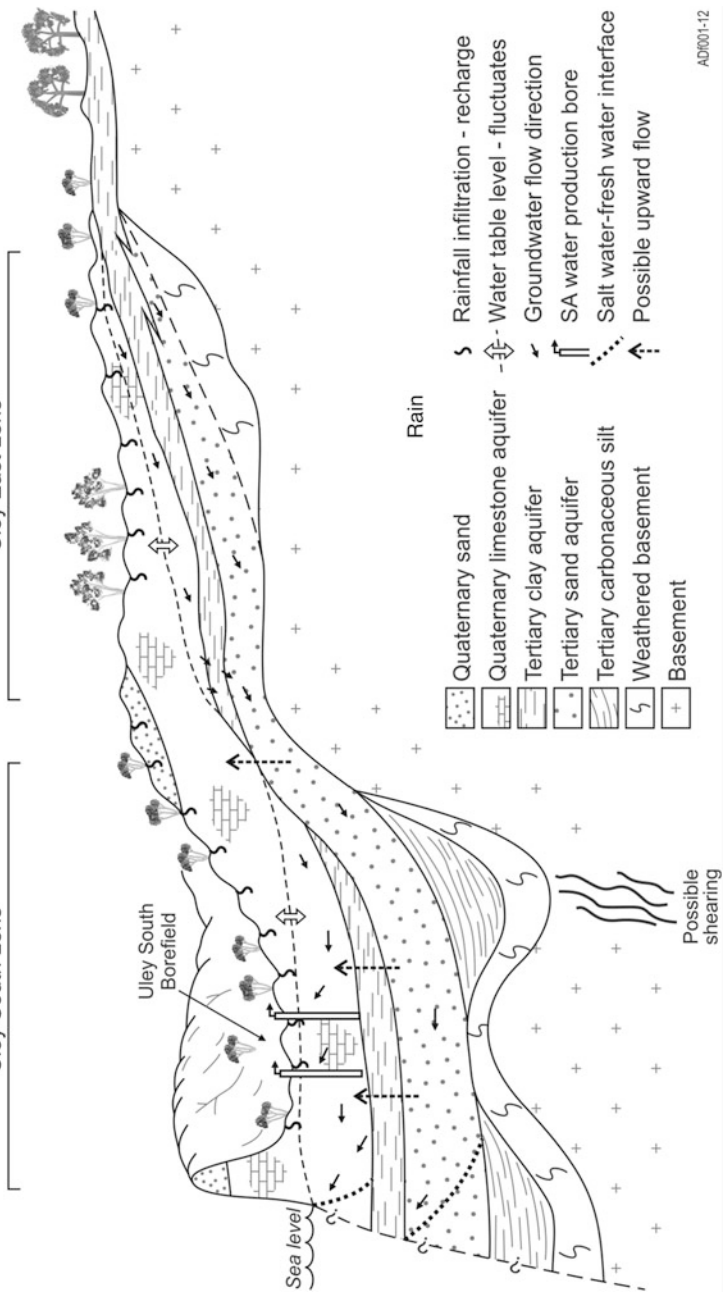

Fig. 6.6 Conceptual model of the stratigraphy and hydrology of the Uley Basin system of aquifers. Modified from (Evans 2002)

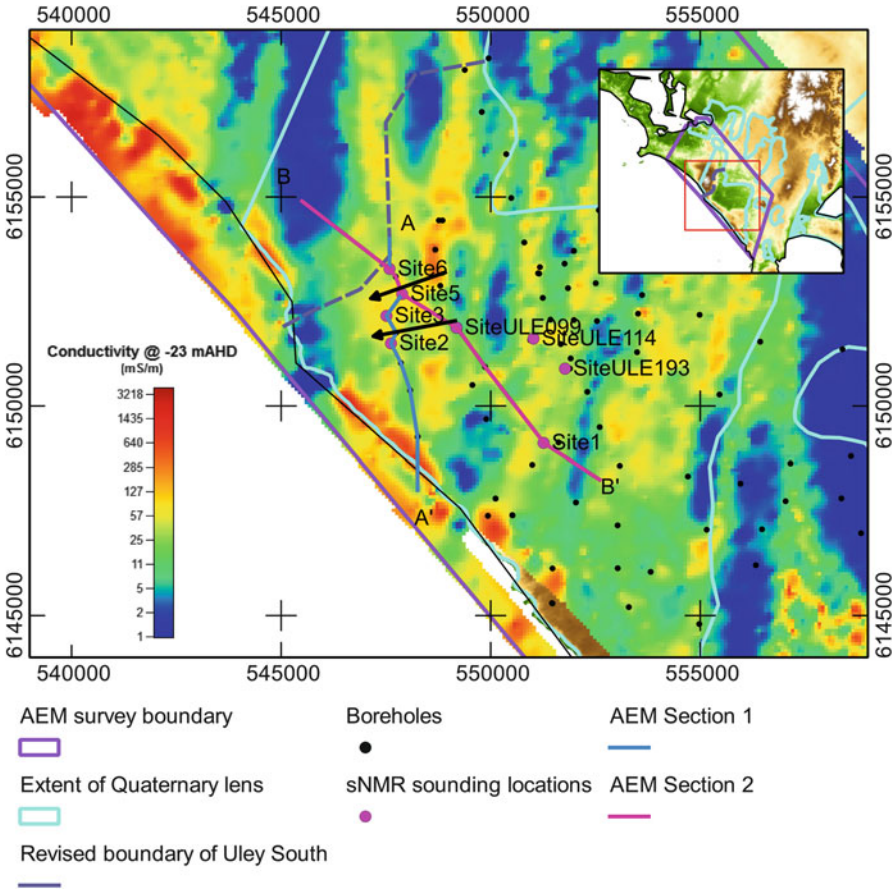

Fig. 6.7 Gridded conductivity slice at −23 mAHD from the Tempest AEM survey. *Black arrows* show surmised direction of groundwater flow in the Quaternary aquifer. *Black dots* show the location of boreholes in and around the Uley South aquifer, and *magenta dots* show the location of sNMR soundings

September 2006 (cf magenta outline in Fig. 6.1). The results of the AEM survey have been summarised by (Fitzpatrick et al. 2009), who used a laterally constrained inversion to derive conductivity-depths values of the sub-surface (Brodie 2010). In addition to providing estimates of the thickness and extent of the Bridgewater, Uley and Wanilla Formations, Fitzpatrick et al. delineated the frontline of a saltwater intrusion in the southeast of the Uley South Basin, and an apparent groundwater connection between the Coffin Bay 'A' and Uley South lenses. Subsequent analysis by SA Water indicates that there is a basement low in the southwest corner of the Uley South groundwater lens. Further support for this is the suggestion by (Zulfic et al. 2007) that groundwater probably flows through the southwest boundary of the Uley South lens. Surmised groundwater flow is shown with black arrows in Fig. 6.7,

which displays a grid of the inverted AEM conductivity values at −23 mAHD (metres referenced to the Australian Height Datum, which is approximately mean sea level). The blue feature that trends north–south at 545,000 mE is interpreted as a basement high. The basement is not as obvious at 6,152,000 mN, but it is known to outcrop to the surface at the shoreline of the Uley South Basin immediately to the south (Shoal Point). In order to test the hypothesis that there is a preferential pathway of groundwater to the southwest of the Uley South boundary, to incorporate the results of the AEM findings, and to assist in the development of a new conceptual model for the southwest of the Uley South Basin, a series of surface nuclear magnetic resonance soundings were conducted in the western margin of the Uley South Basin. In this study, sNMR soundings were used to determine the depth and extent of the saturated and unsaturated Quaternary Bridgewater Formation, and to determine depth to Uley and Wanilla Formations along a north–south transect (shown with magenta dots in Fig. 6.7). We conducted four more soundings in other portions of the Uley South Basin in order to calibrate the sNMR soundings against known hydrological data.

6.4 Results of NMR Study

In Fig. 6.4, we show the free induction decay (FID) of a single 0.82 As sNMR at Site 3 in the Uley South aquifer (cf Fig. 6.7). The pulse time used in this sounding was 40 ms, the loop was 75 × 75 m, and the Larmor frequency was 2,519.7 Hz. The data quality in this figure is representative of the low-noise data that we recorded during the sNMR survey in Uley South. With peak FID voltages on the order of ½ a microvolt, we did not find it necessary to use signal processing to remove remote anthropogenic and sferic noise (Walsh 2008). For this sounding location, we used 36 different pulse moments for the sounding, ranging logarithmically from 0.11 to 12 As. The free induction decay and phase shift for all soundings is shown in Fig. 6.8. We see that the peak free induction decay occurs between 1 and 3 As, and that there is useable signal to about 400 ms. This implies that there is greater water content at the depths that are scanned by the 1–3 As pulse moments. Panel (b) shows the phase shift between the transmitted pulse and the received signal over time for a given pulse moment. We see very little phase shift between 1 and 3 As, indicating that there is not very much variation in conductivity over that pulse moment range; however there is a phase change at late time in the 5–10 As range, indicating that the receiver signal is shifted in phase from the transmitted pulse. This indicates that there is a conductive layer at the depths being investigated by the larger energy pulses.

Using the procedure of (Walsh 2008), we inverted the data at Site 3 for water content with depth. The results are shown in Fig. 6.9. Magenta shows the water content that is bound: water that is contained in pore spaces that would not produced water if they were pumped. Cyan shows free water: water that would potentially be available for production from the aquifer. The summation of free and bound water

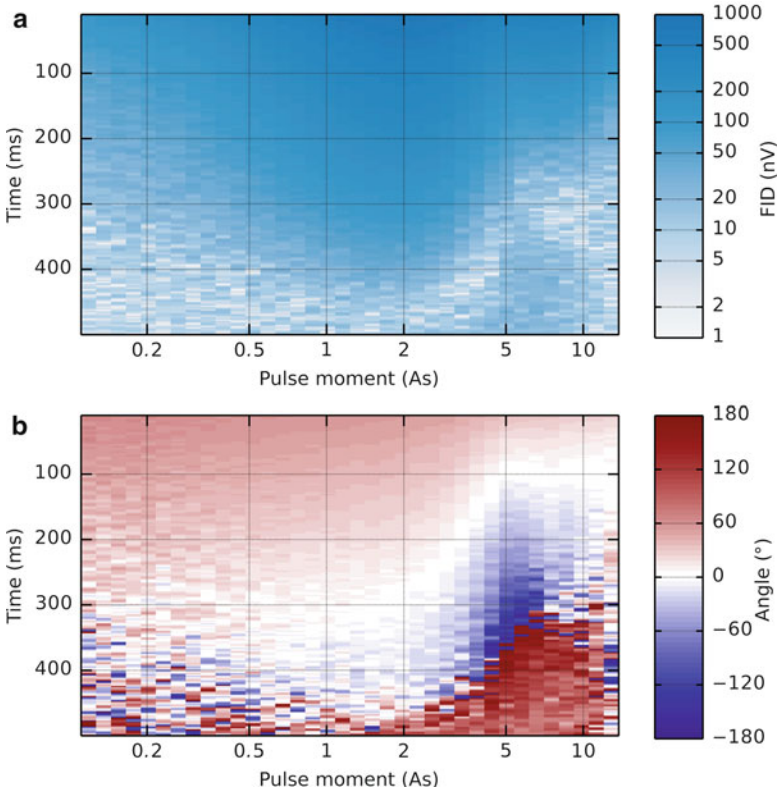

Fig. 6.8 (**a**) Complete pulse moment and free induction decay sequence for the sNMR sounding at Site 3 (cf Fig. 6.7). Most signal comes from pulse moments between 1 and 5 As, with measurable decays to 400 ms. (**b**) Demodulated signal phase shift between the transmitted and measured signals in the free induction decay from the sNMR pulses. We can see a phase shift occurring at large pulse moments and late times. This can be an interpreted as the influence of a conductive layer deeper in the subsurface

is an estimate of the total water content at a given depth (x-axis on the RHS panel). The red curve shows an estimate of the relative permeability of the aquifers detected in the sounding, while the black curve shows the conductivity-depth inversion from a NanoTEM sounding at the same location. The two leftmost panels of Fig. 6.9 show the lithology and stratigraphical classification of the Uley South observation bore ULE098, located about 460 m SSE of Site 3. Because the sounding location is about 460 m away from the borehole, it is reasonable to expect some differences in the elevation of the Formations; however there is an excellent correlation between the stratigraphical units and the water content with depth in this figure: the sand layer of the Bridgewater Formation, which ranges from ~7 to −3 mAHD is consistent with the saturated layer of free water in the right panel (4 to −6 mAHD) and is also the layer that has the largest value of relative permeability; the marl and limestone bands of the Uley Formation may be seen in

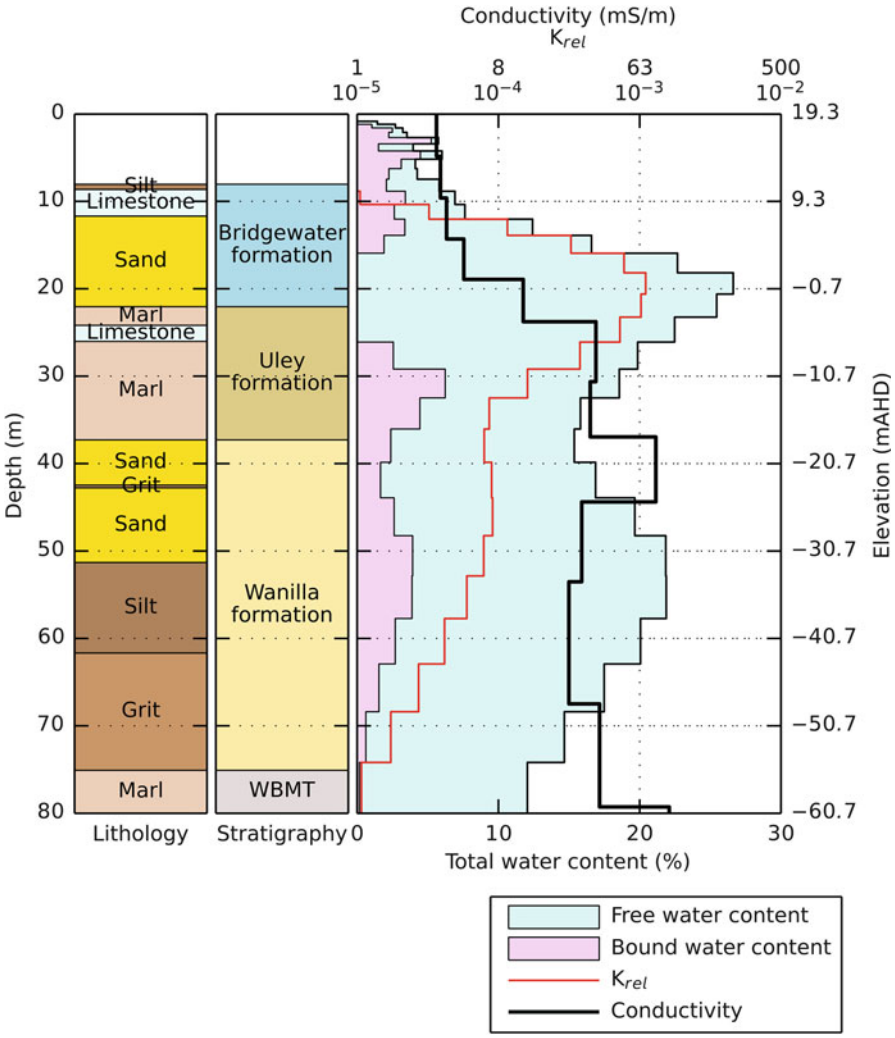

Fig. 6.9 Inversion of water content with depth from the sNMR sounding at Site 3. *Magenta* shows the content of water that is considered to be bound; *cyan* shows the free water content. *Red line* is an estimate of the relative permeability of the subsurface. *Black line* shows a 13-layer conductivity-depth inversion from a NanoTEM sounding taken at the same location. Panels on the left-hand side display the lithology and stratigraphical classification of observation bore ULE098 located about 460 m SSE of sNMR sounding Site 3

the water-content inversion from −6 to −16 mAHD, followed by the sandy Wanilla Formation from −16 to −26 mAHD. Beneath these layers, the sNMR inversion begins to lose resolution, but we can see an increase in bound water content and a decrease in the relative permeability over these layers.

We can conjecture that the upper layer of the sNMR site is composed of unsaturated limestone, as there is little change in the conductivity-depth profile

until about 4 mAHD (TEM conductivity-depth inversion is shown in black in the RHS panel). Below this, we see an increase of conductivity with depth, with a sudden jump by a factor of about 3 at −20 mAHD. This is consistent with the first sand layer of the Wanilla Formation, which is known to contain water of poorer quality than that found in the Bridgewater Formation. We see another increase of electrical conductivity at −60 mAHD in the final panel of Fig. 6.9: this is the weathered basement interface, and marks the end of the Wanilla Formation at this site. We see that, while there is still free water content at this elevation, the relative permeability is much lower than any of the other Formations.

We next examine Site 6, which is at the northern end of the sNMR transect, located about 1 km North of Site 3 (cf Fig. 6.7). The inverted water content and conductivity with depth is shown in the right-hand panel of Fig. 6.10, while the stratigraphical classification and lithology of the nearby borehole ULE208 is displayed in the left two panels. At this site, the drilling logs record a loss of returns and very hard drilling after 25 m drilling. The logs suggest that the drillers suspected the interception of bedrock, since they knew there were some outcrops at Shoal Point. However, the sNMR and TEM inversions suggest a different possibility: namely that saturated Bridgewater Formation persists to −20 mAHD, and it overlies the saturated Wanilla Formation. Due to the lack of bound water below 0 mAHD, and no indication from the drill log of ULE208, we do not have evidence for the clay-rich Uley Formation at this site. Lateral consistency of a conductive layer at −23 mAHD (Fig. 6.7) further suggests that this layer is Wanilla Formation. Water content and relative permeability in the upper layers suggest 15 % free water, but of lower permeability than the saturated Bridgewater Formation of Site 3. We see that the upper layers of clay and sand of Site 6 are relatively unsaturated, suggesting either direct run-off of rainwater down into the Uley South Basin or percolation of water to the underlying Quaternary Limestone.

6.5 Discussion

We have seen examples of the free-induction decay, T_2^* distribution, and inversions of water content versus depth for two specific sites on the southwest edge of the Uley South freshwater lens for the purpose of groundwater detection in that region. Both examples showed the powerful ability of nuclear magnetic resonance to detect and quantify water in the subsurface of the earth without the need for exploration drilling. At each site, the saturated and unsaturated zones of the ground were delineated, with total water content in the saturated zone approaching 27 % in the Quaternary Bridgewater Formation at Site 3 and 20 % at Site 6. Results from Sites 2 and 5 showed similar patterns of free and bound water content with depth. By using the sNMR results with the conductivity-depth inversion from the electromagnetic results taken at the same locations, we see excellent correlation between water content, electrical conductivity and stratigraphical classification at these locations.

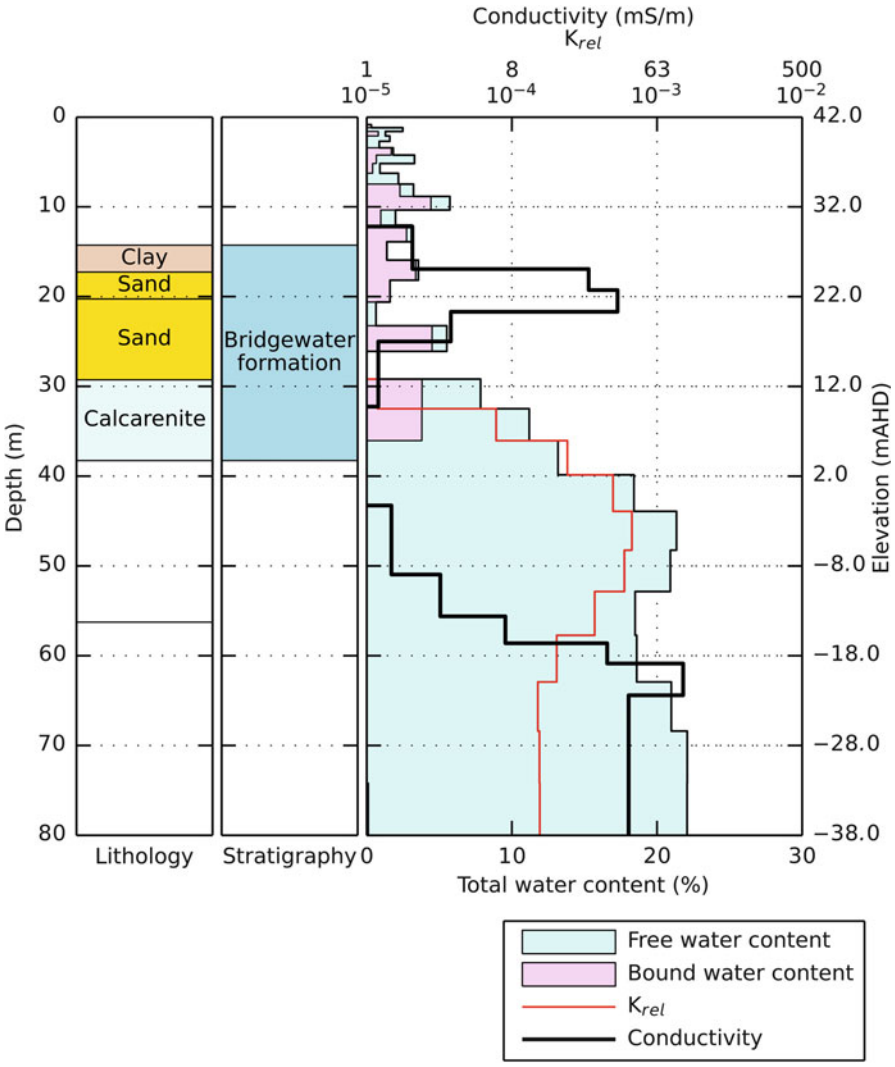

Fig. 6.10 Inversion of water content with depth from the sNMR sounding at site 6. *Magenta* shows bound water content: *cyan* is free water content. *Red line* shows an estimate of the relative permeability of the subsurface. *Black line* is the conductivity-depth inversion from a NanoTEM sounding at the location. Water table is encountered at about 30 m depth. *Left panels* display lithology and stratigraphical classification from observation bore ULE208, located about 240 m SE of the sounding location

Surface NMR also provides an estimate of the relative permeability of saturated water in the detection zones and, while these numbers are not correct in an absolute sense without some sort of calibration, we can use the values to provide information about mobility of water from areas where we do have more information. As an

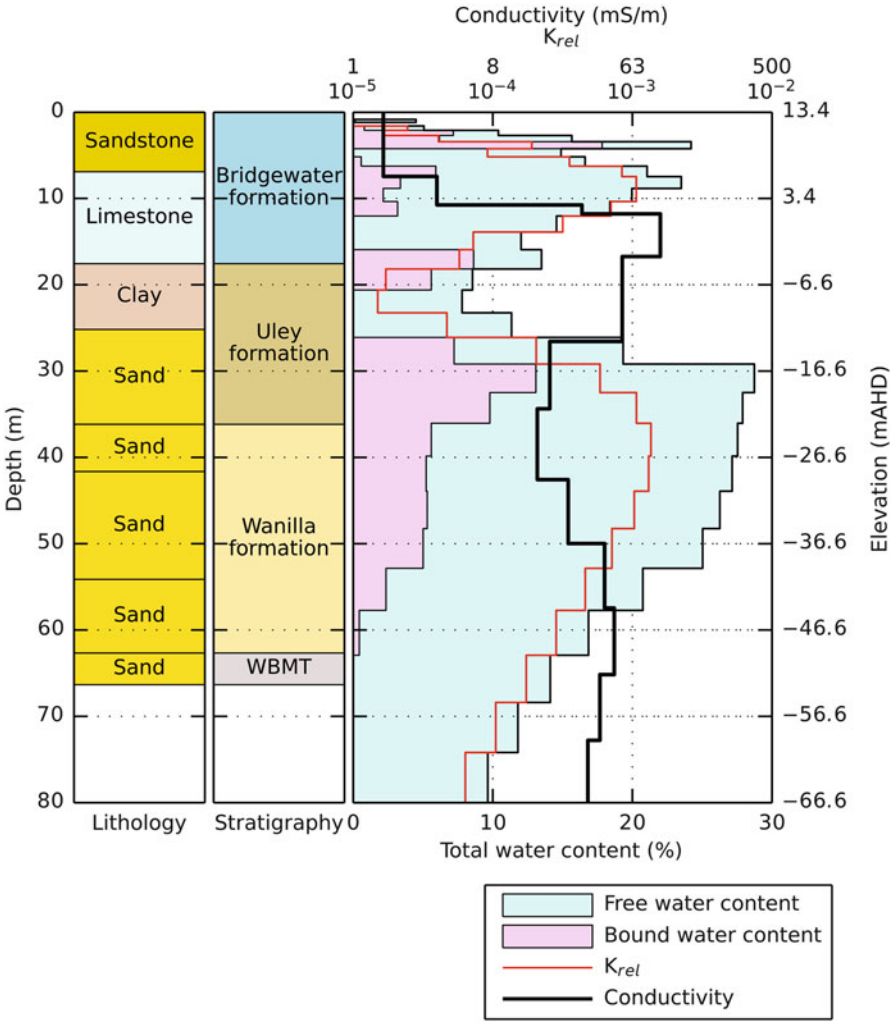

Fig. 6.11 Inversion of water content with depth from the sNMR sounding at site ULE193. *Magenta* shows bound water content: *cyan* is free water content. *Red line* shows an estimate of the relative permeability of the subsurface. *Black line* is the conductivity-depth inversion from a NanoTEM sounding at the location. *Left panels* display lithology and stratigraphical classification from observation bore ULE116, located about 280 mN of the sounding location

example of this, Fig. 6.11 shows the stratigraphy and lithology of observation bore ULE116, located 280 m north of sounding location ULE193. As in earlier figures, we clearly see the major Formations of the Uley South aquifers; however ULE 193 is located close to some of the major production wells of the Uley South freshwater lens. Production rates in this area are regularly 35 L/s, with estimated hydraulic conductivities of 400–1,000 m/day. Looking at the estimated K_{rel} values in

Figs. 6.11 and 6.9, we see that they are similar. It is therefore reasonable to expect similar hydraulic conductivity values in the vicinity of Sites 2, 3 and 5 in the western side of the basin.

As a means of using the sNMR inversion data obtained at specific sites and applying it to a broader scale in the Uley South aquifers, we have combined the sNMR data with the conductivity-depth inversions obtained from the Tempest AEM data flown in 2006. The first section that we show is the north to south section drawn in blue in Fig. 6.1 and labelled A–A′. This is displayed in Fig. 6.12 with a logarithmic colour stretch of 1–200 mS/m for the AEM data, and the water content inversions from Sites 6, 5 and 2 overlain. Also included are the stratigraphy layers from observation bores ULE208, ULE098, ULE194, ULE207 and ULE212. In this figure, we can clearly see the lateral extent of each of the major Formations of the Uley South aquifers. The Bridgewater Formation of Site 6 extends south through Site 5 and Site 3, thinning out near Site 2, only to increase again in thickness by ULE207 and ULE212. The Uley Formation, detected in Site 3 as a mixture of free and bound water content, together with an increase in conductivity, is clearly seen lateral extent from ULE212 all the way to Site 5. We can also detect the Wanilla Formation, with its greater conductivity and water content it is perhaps most clearly seen at Site 5, which also shows the vertical extent of the Wanilla Formation at that site and the weathered basement beneath (at −40 mAHD). The bright red feature in the south of the figure (A′) is the Southern Ocean, and we can see an interface of seawater intrusion that stretches to the north of it (the breaks in the saltwater intrusion zone are due to 1D inversion of the AEM data and gridding artefacts). We reproduce Fig. 6.12 with stratigraphical interpretation in Fig. 6.13, with the different units coloured in the same shadings as found in the earlier figures. More interesting features are shown if we examine a section that more closely parallels the coast of the Southern Ocean. Section 2, shown in magenta in Fig. 6.1 and marked with B–B′, is displayed in Fig. 6.14. In this, we again see the sounding locations of Site 6 and 5, but we also extend to the southeast to Site ULE099 and Site 1. In this figure, we again see the lateral extent of the Bridgewater Formation across the Uley South Basin, and the variations in thickness and expression of the Uley Formation. Along this section, the drillers' logs suggest that the Wanilla Formation is not present at ULE099 (hidden behind the water content inversion of Site ULE099), but is present at both ULE105 and ULE135 (beside Site 1, but not shown in this figure). There is a similar expression in the Uley Formation as well, with drillers' logs indicating clay-like formations at ULE105, but not ULE135. The deep blue areas at 9,200 m and 0–600 m are bedrock, an expression of which is also seen in the driller log at Site ULE099. Along most of the transect we see a band of more conductive material between 0 and −30 mAHD. We interpret this as a blend of Wanilla and Uley Formations overlying the weathered basement. We see that the Wanilla Formation tends to dip down to the west at Site 6, indicating that there is a deep basement valley at about 1,500 m distance along the section. This area is expected to be overlain by saturated Bridgewater formation, and examining Fig. 6.7, it should extend well north of Site 6 toward the top end of the Quaternary lens extent borders (the cyan lines in Fig. 6.7). We have redrawn Fig. 6.14 with a stratigraphical interpretation in Fig. 6.15 which reflects these findings, and shows

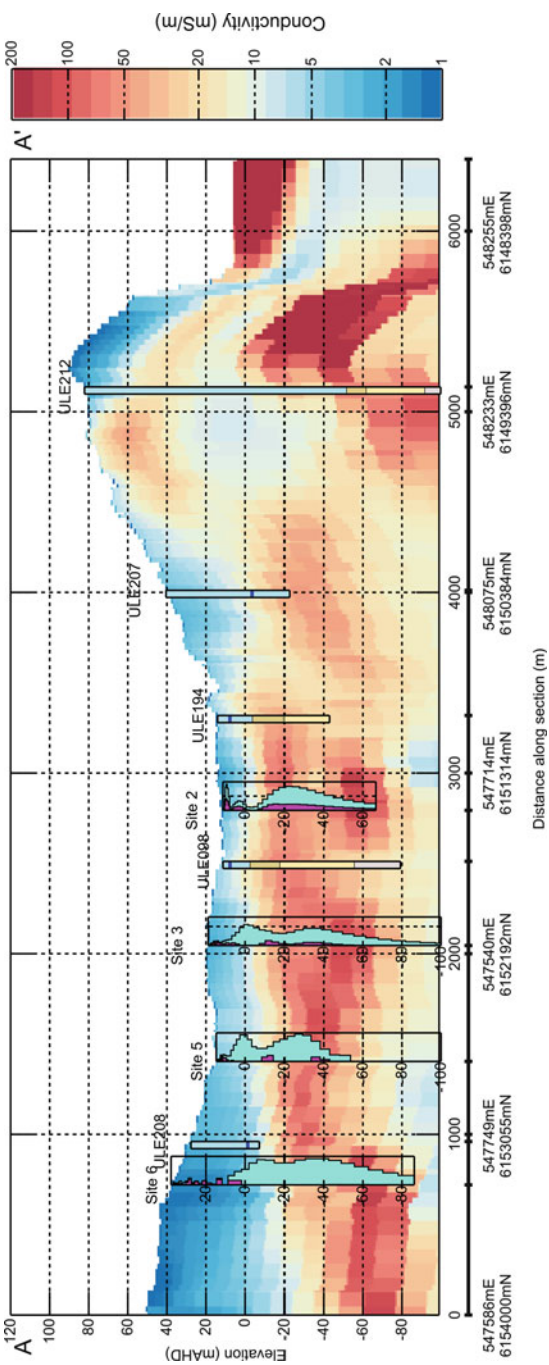

Fig. 6.12 Conductivity-depth profile of AEM section 1 (cf Figs. 6.1, 6.7) with sNMR sounding inversions from sites 6, 5, 2 and 3 overlaid. Also included is stratigraphical classification from monitoring boreholes

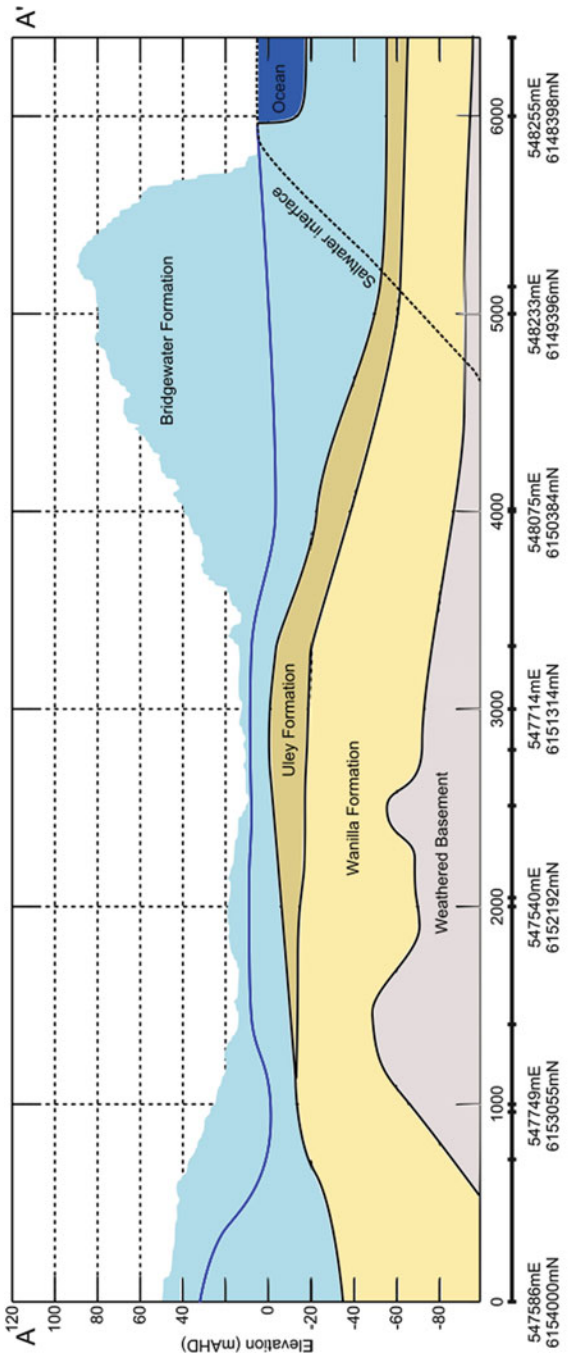

Fig. 6.13 Geological interpretation of AEM section 1 (cf Figs. 6.1, 6.7) made from sNMR and AEM data

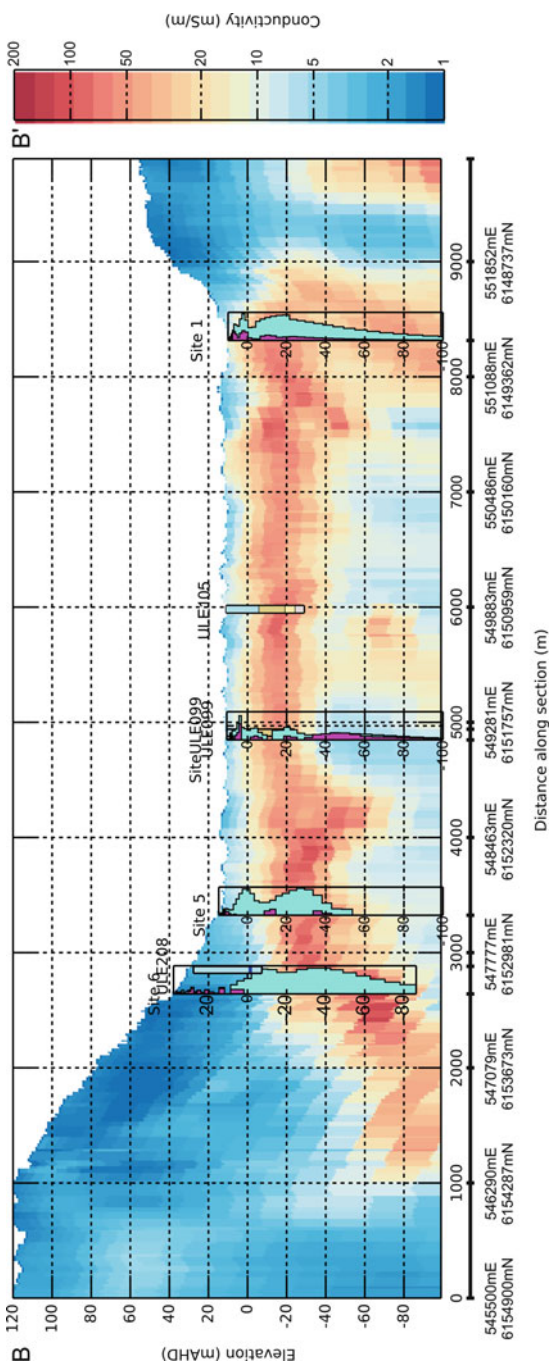

Fig. 6.14 Conductivity-depth profile of AEM section 2 (cf Figs. 6.1, 6.7) with sNMR sounding inversions from sites 6, 5, ULE099 and Site 1 overlaid. Also included is stratigraphical classification from monitoring boreholes

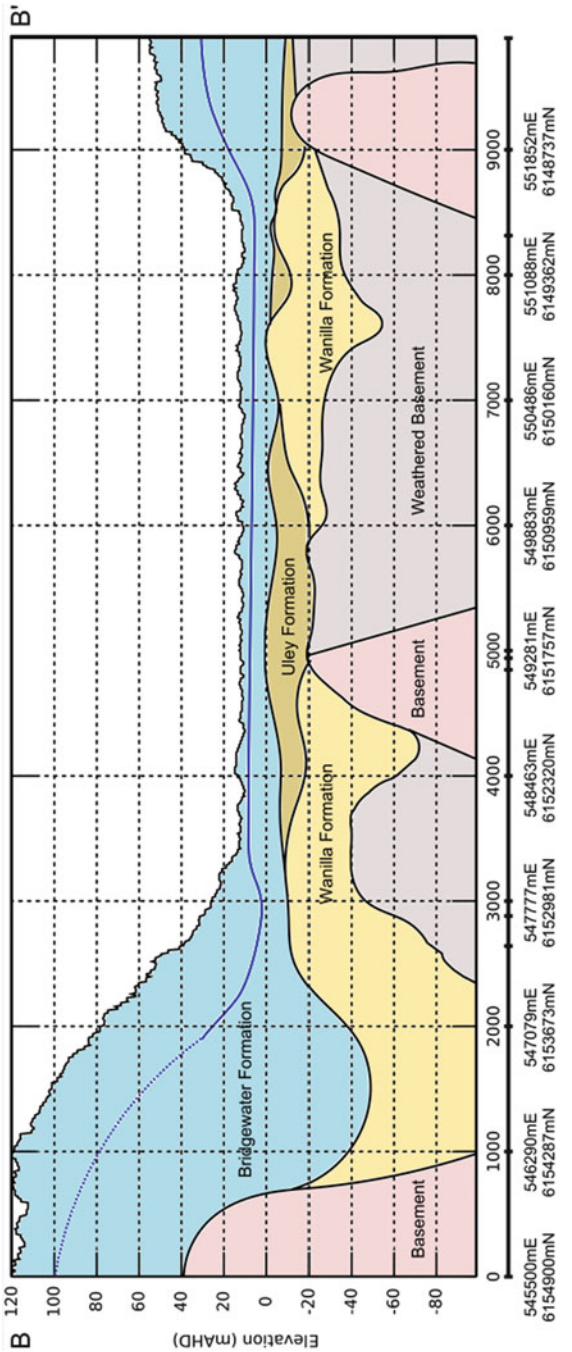

Fig. 6.15 Geological interpretation of AEM section 2 (cf Figs. 6.1, 6.7) made from sNMR and AEM data

the potential uncharacterised aquifer to the west of Sites 2–6. Examination of Figs. 6.9 and 6.10 shows productive water contents of up to 20 % at 0 mAHD in the Bridgewater Formation in this area of Uley South, so it is possible that the interpreted valley of Bridgewater Formation to the west of these sites contains similar water quantities over greater thicknesses of saturated limestone. We see from Fig. 6.11 that the relative permeability of the saturated zones at Sites 2–6 should yield similar production values as those enjoyed near ULE193.

6.6 Conclusion

The aquifer systems of the Uley South Basin are the most important sources of groundwater in the Eyre Peninsula of South Australia, providing approximately 7,500 GL/a to the reticulated network of the area. Further development of the aquifer has been proposed to meet increased demand for potable water in the region. This has required further investigation to better understand the true extent of the Basin, a more complete assessment of the available resource and its sustainability. Available evidence suggests the available resource in the Basin is currently underestimated and that there are additional resources available in the southwest corner of the Basin where borehole information is scarce. The interpretation of a series of surface nuclear magnetic resonance soundings conducted in this area, coupled with a reinterpretation of the existing AEM data suggests that the unconfined Quaternary Bridgewater aquifer is more extensive than originally thought and that available resources might be supplemented as a result.

Specifically, we have identified the existence of a deep valley to the southwest of the basin which contains saturated Quaternary limestone beds, ranging from 10 to 20 m in thickness with an effective porosity of 15–25 %. From the sNMR soundings taken in the centre of the Uley South basin, we predict that the Quaternary limestone in the southwest corner should have groundwater production rates similar to the main production area of Uley South. This unconfined aquifer overlies a sandy Tertiary clay layer that has an effective porosity of about 12 %, most of which is filled with immobile or trapped water. This gently undulating layer varies from 5 to 10 m in thickness.

In addition to the saturated limestone aquifer, we are relatively confident that we have detected the top of the Tertiary sandstone aquifer in the region. The effective porosity of this unit is about 20 %; however it increases to the north, where we find a porosity of around 35 %, mostly having a T_2^* value of 100 ms, indicating the presence of fine sands. The fine sand layer begins at about −10 mAHD and dips to the north to about −70 mAHD. We have identified two specific areas that may warrant further investigation for the purpose of groundwater assessment in the Uley South Bridgewater aquifer (marked with red double-headed arrows in Fig. 6.7). The area to the north shows a basement low that may connect the Coffin Bay groundwater lenses to the northwest to those of the Uley South Basin. The area to the west

is a possible flow path for groundwater discharge from both the Quaternary and Tertiary aquifers to the Southern Ocean. The geophysics results suggest both areas may provide a supplementary groundwater resource to that currently assigned to the Basin. Further work is required to substantiate these observations and to determine whether allocations from the aquifer can be adjusted to reflect a refinement and extension of the available resource.

When coupled with techniques such as airborne and surface electromagnetics, surface nuclear magnetic resonance can assist in the non-invasive estimation of hydraulic parameters over a given area. Furthermore, in addition to providing direct evidence of water content and porosity in the subsurface, sNMR also provides an estimate of bound and mobile water fractions and offer comparisons of the permeability for given aquifers in the subsurface. Arguably, the technique presents a cost-effective supplement to exploration drilling in areas of environmental sensitivity, and can assist in the development of a targeted borehole drilling campaign with a minimal environmental impact.

References

Abragam A (1961) Principles of nuclear magnetism. Clarendon, Oxford

Ames DP (1967) Magnetic resonance. In: Condon EU, Odishaw H (eds) Handbook of physics. McGraw-Hill, New York

Barnett SR (1978) Eyre Peninsula groundwater survey – Uley South Basin progress report no. 5 – water balance and safe yield. Department for Water Resources, Adelaide

Bloch F (1946) Nuclear induction. Phys Rev 70:460–473

Bransden BH, Joachain CJ (1994) Introduction to quantum mechanics. Longman Scientific & Technical, London

Brodie RC (2010) Holistic inversion of airborne electromagnetic data. PhD thesis, Australian National University, Canberra

Clarke DS, Berens V, Dennis KJ (2003) Uley South – Coffin Bay observation well network review. Department of Water, Land and Biodiversity Conservation, Adelaide

Coates GR, Xiao L, Prammer MG (2001) NMR logging principles and applications. Halliburton Energy Services, Houston

Davis AC, Cahill K, Hatch M, Munday T (2012) Aquifer characterisation in the Uley South Basin, South Australia, using NMR: final Report. CSIRO Water for a Healthy Country National Research Flagship, Perth

Dunn K-J, Bergman DJ, LaTorraca GA (2002) Nuclear magnetic resonance: petrophysical and logging applications. Pergamon Press, Oxford

Evans S (1997) Estimating long term recharge to thin, unconfined carbonate aquifers using conventional and environmental isotope techniques: Eyre Peninsula, South Australia. MSc thesis, Flinders University, South Australia

Evans S (2002) Southern basins prescribed wells areas groundwater monitoring status report 2002. Department of Water, Land and Biodiversity Conservation, South Australia, Adelaide

Evans S, Watkins N, Li C, Kuyper N, Weir Y, McLean A (2009) Southern Basins PWA Status Report. Eyre Peninsula NRM Board

Fitterman DV, Deszcz-Pan M (1998) Helicopter EM mapping of saltwater intrusion in Everglades National Park. Fla Explor Geophys 29:240–243

Fitzpatrick A, Cahill K, Munday T, Berens V (2009) Informing the hydrogeology of Coffin Bay, South Australia, through the constrained inversion of tempest AEM Data. CSIRO Water for a Healthy Country National Research Flagship, Perth

Government of South Australia (2001) Understanding the Sourthern Basins Prescribed Wells Area. Department of Water Resources, Adelaide

Guillen A, Legchenko A (2002) Application of linear programming techniques to the inversion of proton magnetic resonance measurements for water prospecting from the surface. J Appl Geophys 50:149–162

Harrington N, Evans S, Zulfic D (2006) Uley basin groundwater modelling project, vol 1, Project overview and conceptual model development. Department of Water, Land and Biodiversity Conservation, Adelaide

Hertrich M (2008) Imaging of groundwater with nuclear magnetic resonance. Prog Nucl Magn Reson Spectrosc 53:227–248

James-Smith JM, Brown KG (2002) Groundwater flow model of the Quaternary Limestone aquifer in the Uley South lens, Eyre Peninsula, South Australia. Department for Water Resources, Adelaide

Johns RK (1961) Geology and mineral resources of southern Eyre Peninsula: Bulletin 037. Geological Survey of South Australia, Adeliade

Kirkegaard C, Sonnenborg TO, Auken E, Jørgensen F (2011) Salinity distribution in heterogeneous coastal aquifers mapped by airborne electromagnetics. Vadose Zone J 10:125–135

Knight R, Grunewald E, Irons T, Dlubac K, Song Y, Bachman HN, Grau B, Walsh D, Abraham JD, Cannia J (2012) Field experiment provides ground truth for surface nuclear magnetic resonance measurement. Geophys Res Lett 39:L03304

Legchenko AV, Shushakov OA (1998) Inversion of surface NMR data. Geophysics 63:75–84

Legchenko A, Valla P (2002) A review of the basic principles for proton magnetic resonance sounding measurements. J Appl Geophys 50:3–19

Legchenko A, Baltassat JM, Beauce A, Bernard J (2002) Nuclear magneric resonance as a geophysical tool for hydrogeologists. J Appl Geophys 50:21–46

Martin R, Clarke D (2000) Prescribed groundwater resources of Eyre Peninsula. MESA J 18:25–27

Morton WM, Steel TM (1966) Eyre Peninsula groundwater study - Uley South Basin - Progress Report 1 - Aquifer evaluation. Department of Mines, Adelaide

Morton W, Steel TM (1968) Eyre Peninsula groundwater, Uley South area. Hydrogeological studies summary and conclusions report – EWS Department. Department of Mines, Adelaide

Morton WM, Steel TM (1970) Evaluation of aquifers in the Uley South groundwater basin, southern Eyre Peninsula. Miner Resour Rev 128:33–48

Mueller-Petke M, Yaramanci U (2010) QT inversion – comprehensive use of the complete surface NMR data set. Geophysics 75:WA199–WA209

Paine J, Minty B (2005) Airborne hydrogeophysics. In: Rubin Y, Hubbard SS (eds) Hydrogeophysics. Springer, Dordrecht, pp 333–357

Painter JAC (1970) Eyre Peninsula groundwater study. Consolidated report no. 2. Summary of available data, June 1970. Department of Mines, Adelaide

Schirov M, Legchenko A, Creer G (1991) A new direct non-invasive groundwater detection technology for Australia. Explor Geophys 22:333–338

Segnit RW (1935) Preliminary report on the Wanilla fresh water basin, Co. Flinders, Eyre Peninsula. Department of Mines, Adelaide

Segnit RW (1942) Final report on the Uley-Wanilla fresh water basin. Department of Primary Industries and Resources, Adelaide

Shepherd RG (1962) Underground water investigations, southern Eyre Peninsula. Presented at the underground water conference of Australia, Adelaide

Shepherd RG (1963) Report on underground water investigations – Sleaford Bay – Coffin Bay Area. Department of Mines, Adelaide

Shepherd RG (1965) Groundwater investigations on Eyre Peninsula 1956–1965 summary report. Department of Primary Industries and Resources, Adelaide
Shepherd RG (1980) Uley south groundwater basin – computer model. Department of Primary Industries and Resources, Adelaide
Sibenaler XP (1976) Eyre Peninsula groundwater survey, Uley South basin, Progress report No 4-Aquifer evaluation. Department of Mines, Adelaide
Siemon B, Christiansen AV, Auken E (2008) A review of helicopter-borne electromagnetic methods for groundwater exploration. Near Surf Geophys 7:629–646
Vouillamoz JM, Sokheng S, Bruyere O, Caron D, Arnout L (2012) Towards a better estimate of storage properties of aquifer with magnetic resonance sounding. J Hydrol 458–459:51–58
Walsh DO (2008) Multi-channel surface NMR instrumentation and software for 1D/2D groundwater investigations. J Appl Geophys 66:140–150
Weichman PB, Lavely EM, Ritzwoller MH (2000) Theory of surface nuclear magnetic resonance with applications to geophysical imaging problems. Phys Rev E 62:1290–1312
Wyman RE (1962) Nuclear magnetism log field test results. Presented at the Society of Petrophysicists & Well Log Analysts. Houston, TX
Zulfic D, Harrington N, Evans S (2007) Uley basin groundwater modelling project, vol 2, Groundwater flow model. Department of Water, Land and Biodiversity Conservation, Adelaide

Chapter 7
Airborne Transient EM Methods and Their Applications for Coastal Groundwater Investigations

C. Schamper, J.B. Pedersen, E. Auken, A.V. Christiansen, B. Vittecoq, J. Deparis, T. Jaouen, F. Lacquement, P. Nehlig, J. Perrin, and P.-A. Reninger

Abstract For more than half a century airborne electromagnetic (AEM) methods have been used worldwide for cost-effective resistivity mapping of areas larger than several hundred km^2. The technical developments and intensive use of these systems, principally in mining exploration during the first decades, led to the development of helicopter transient EM (HTEM) systems. Since the 2000s these systems provide the best lateral and vertical resolution for environmental exploration, and they still keep a good depth of investigation allowing the exploration from the first meters to depths of several hundred meters. This chapter focuses on helicopter borne transient electromagnetic (HTEM) systems, which are well suited for the detection of low resistive targets such as salt water intrusion in coastal zones.

AEM methods are based on the diffusive induction phenomenon. It is a key tool for building realistic hydrogeological models; however it requires an understanding of its limits, and some insight into data processing modeling is necessary. They require careful processing, and removal of cultural EM noise, present in most survey areas, is mandatory in order to get high quality results. Accurate modeling of the data and of the system is also critical. The modeling is most often based on least-square optimization algorithms giving smooth or layered model descriptions of ground.

C. Schamper (✉) • J.B. Pedersen • E. Auken • A.V. Christiansen
HydroGeophysics Group (HGG), Department of Geoscience, Aarhus University, Aarhus, Denmark
e-mail: cyril.schamper@geo.au.dk

B. Vittecoq
Basse Normandie Geological Survey, BRGM, 4 Avenue de Cambridge, 14200 Hérouville-Saint-Clair, France

J. Deparis • F. Lacquement • P. Nehlig • J. Perrin • P.-A. Reninger
Georesources Division, BRGM, 3 Avenue Claude Guillemin, 45060 Orléans, France

T. Jaouen
Mayotte Geological Survey, BRGM, Z.I. de Kawéni, 97600 Mamoudzou, France

C. Wetzelhuetter (ed.), *Groundwater in the Coastal Zones of Asia-Pacific*, Coastal Research Library 7, DOI 10.1007/978-94-007-5648-9_7,

In this chapter we describe the AEM method in detail and we discuss processing and inversion of data. To demonstrate the results from an investigation, we end the chapter with a case study of a SkyTEM survey made in the volcanic island of Mayotte where key geological structures and salt water intrusion were successfully mapped.

7.1 Introduction

Sea water intrusion in the coastal zones is a global problem and prevents the extraction of freshwater for drinking and irrigation. Over-pumping of the aquifers and the future rise of the sea level are of main concern because they change the equilibrium between the fresh and the saline groundwater systems. Conductivities of freshwater, about 0.5 mS/cm (20 Ωm), and of saline water, around 20–50 mS/cm (0.2–0.5 Ωm), are very different, making electromagnetic induction (EMI) methods a unique tool for mapping the fresh/saline water interface.

Airborne electromagnetic (AEM) methods offer the possibility of covering large areas of several hundred km^2 in a short period of time (matter of weeks) and provide information about ground resistivities to depths of several hundred meters. AEM systems are divided into two groups, both of which have been applied to the exploration of coastal zones: the helicopter-borne frequency-domain EM (HFEM) and the helicopter-borne time-domain or transient EM (HTEM) systems. In this chapter we limit ourselves to discuss the use of HTEM systems as they provide a good depth and lateral resolution compared to fixed-wing EM systems (systems operated from an airplane) and HFEM systems.

Because of the early development of the HFEM systems, these were first used for mapping the salinity changes in the top 50–70 m (Buselli and Williamson 1996; Fitterman and Deszcz-Pan 1998; Paine 2003). Later, the development of HTEM systems from the early 2000s allowed the mapping of saline water intrusion down to depths of 150–300 m (Kirkegaard et al. 2011; Teatini et al. 2011; Jørgensen et al. 2012).

AEM is not the only technique used for monitoring fresh/saline water interfaces (*cf.* recent overview study by Werner et al. 2012) and it is not the "Holy Grail". However, it does allow the building of hydrogeological models of coastal zones at a scale and with a precision, which can hardly be obtained by other methods, and the development has been so significant that it was not possible just a decade ago. It is a delicate method, which requires a high level of experience, but if the data are carefully processed and interpreted together with boreholes and other geological/hydrological information, the output can be fantastic and a decisive source of input to the hydrological modeling and the administration of groundwater resources (Thomsen et al. 2004; Møller et al. 2009).

This chapter presents the basics of transient AEM methods by explaining the physics and providing an understanding of how AEM is used to map the fresh/saltwater boundary. It also highlights the limits of the technique and the key points

of the processing and interpretation of AEM. A field example where the SkyTEM HTEM system (Sørensen and Auken 2004; Auken et al. 2009a) was flown on the Mayotte Island in 2009 (Auken et al. 2010a) illustrates the results that can be obtained.

7.2 Introduction to AEM Methods

7.2.1 A Brief Historical Overview

Quite a large number of different AEM systems have been developed since the first system emerged in the 1950s. We will here give a brief overview and refer to Fountain (1998) and Fountain (2008) for a comprehensive chronology of AEM during the second half of the twentieth century and the early 2000s, respectively.

The development of AEM was driven by exploration for minerals with its needs for surveying large areas at a reasonable cost. The first attempts with airborne time-domain/transient EM (TEM) systems in the 1950s were quite successful for base-metal exploration in Canada, and in that decade over ten systems were in use for production. The most successful system resulting from the 1950s was the INduced PUlse Transient (INPUT) system. Canada and the Nordic countries led the development and use of AEM systems, and by the 1970s the methodology was deployed worldwide.

With the decline in exploration for base metals in the 1980s, the use of AEM methods turned from anomaly detection to conductivity mapping, and HFEM systems appeared (*e.g.* DIGHEM and Resolve). These were intensively used as they provide both good lateral and vertical resolution of the near surface (top 50–70 m).

The 1990s see a reappearance of AEM activities in mining exploration, but also an increasing use in environmental investigation. Environmental targets mainly concern near surface (top 300 m) where mining targets can easily be more than 500 m deep. Due to different targets and cost profiles, AEM development started to split into two main directions: the traditional fixed-wing (*i.e.* with a transmitter loop strung around the aircraft and a receiver bird towed behind the aircraft) time domain systems for the mapping of deep conductive targets, and the HFEM systems, which provide a better near-surface resolution.

In the early 2000s development of HTEM systems took off (Allard 2007; Fountain 2008) and since then they have been the focus of most new developments. As any helicopter borne EM system, in particular compared to fixed-wing systems, they offer a better flexibility for obtaining a good signal level with a low flight altitude. This improves both the vertical and the lateral resolution of the ground. With the most recent technical developments HTEM systems are now the most flexible systems since they provide not only good depth of investigation, but also near-surface lateral/vertical resolution competitive with the one from HFEM systems.

Several HTEM systems exist on the commercial market today, *e.g.* VTEM, Aero-TEM, NEWTEM, HoistEM, Heli-GEOTEM and SkyTEM. Most of the systems, such as VTEM (Witherly et al. 2004), have been intensively used for mining targets, whereas the SkyTEM system, developed and steadily improved over the last 10 years, has been specially designed for groundwater mapping and environmental investigations (Sørensen and Auken 2004). Siemon et al. (2009) give an overview of different HFEM and HTEM systems applied to groundwater exploration.

7.2.2 Mapping Aquifers with HTEM Systems

As shown in Fig. 7.1a the response of a mineralization, which is very conductive compared to the host rock, is much larger compared to the response of a freshwater aquifer (Fig. 7.1b). Despite the response is not as large as the response from the mineralization, the response of a saline aquifer is larger and clearly visible compared to a freshwater aquifer (Fig. 7.1b). The figure illustrates that smaller resistivity contrasts encountered in hydrogeological exploration require more careful and accurate measurements compared to mineral exploration because of the much lower signals. Thus, special considerations and corrections, which in many cases are unnecessary for mining targets, are mandatory for hydrogeological targets.

7.3 Physical Response from the Ground

An introduction to TEM methods is given in the following. For a more detailed discussion the reader is referred to Christiansen et al. (2006).

7.3.1 Basics of the Transient EM Method

In the transient EM method the ground is first "energized" by a primary magnetic field generated by a transmitter loop (Fig. 7.2a). The electrical current is maintained until the electric charges in the ground are at a steady state, then the current in the loop is turned off abruptly (top plot of Fig. 7.2b). During this rapid decay of the current (from few to several 100 μs depending on the system) an electromotive force (middle plot of Fig. 7.2b) results in eddy currents whose strength is largest in conductive parts of the ground. This electromagnetic induction phenomenon generates what is called the secondary magnetic field (bottom plot of Fig. 7.2b) which is measured just after the end of the turn-off using an induction coil as receiver. The actual measurement is the time derivative of the magnetic flux passing through the receiver coil, db/dt.

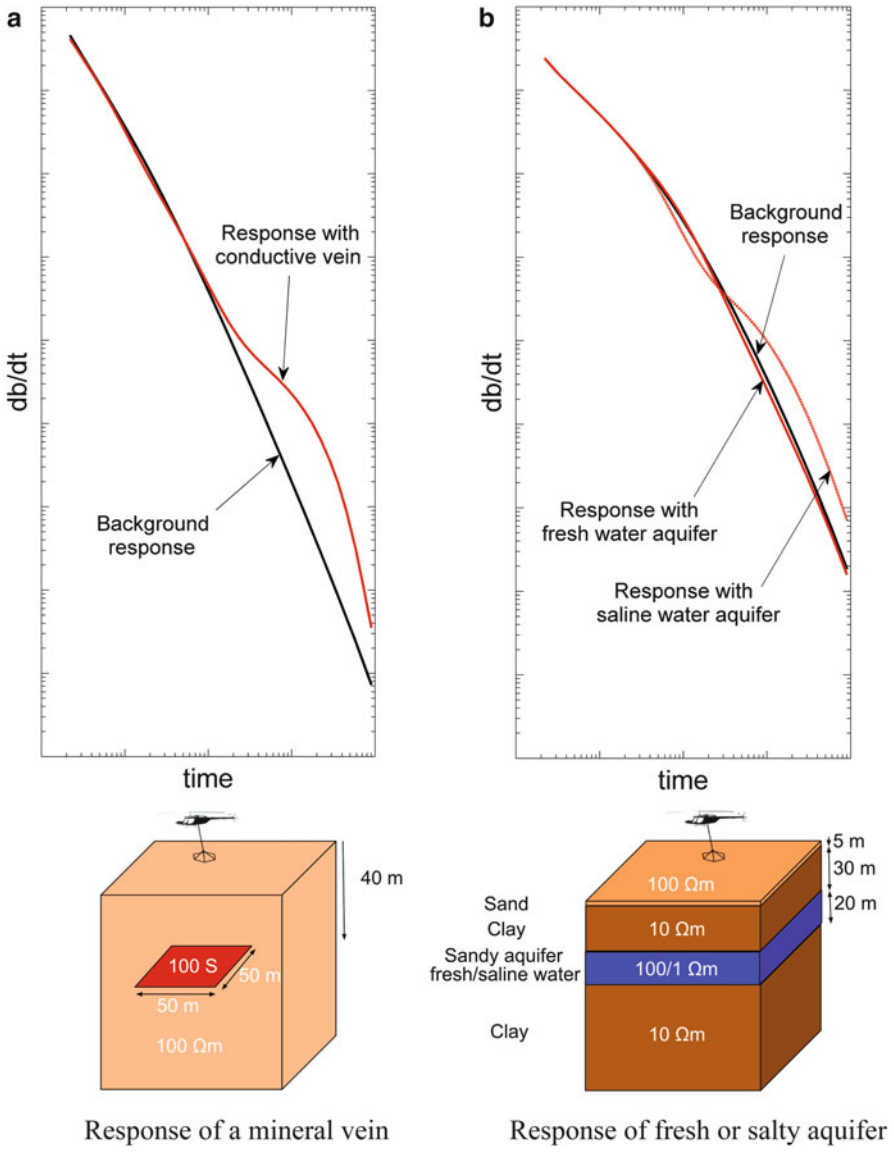

Fig. 7.1 Comparison of the responses of (**a**) a mineralization and (**b**) a hydrological targets. The mineralization is approximated by a horizontal thin sheet while the hydrological model is layered-earth model

Since the decaying secondary magnetic field is vertical in the middle of the transmitter (Tx) loop for plane and parallel layers, the receiver (Rx) induction coil generally measures the vertical component of the magnetic field even if it is slightly shifted from the center of the Tx-loop.

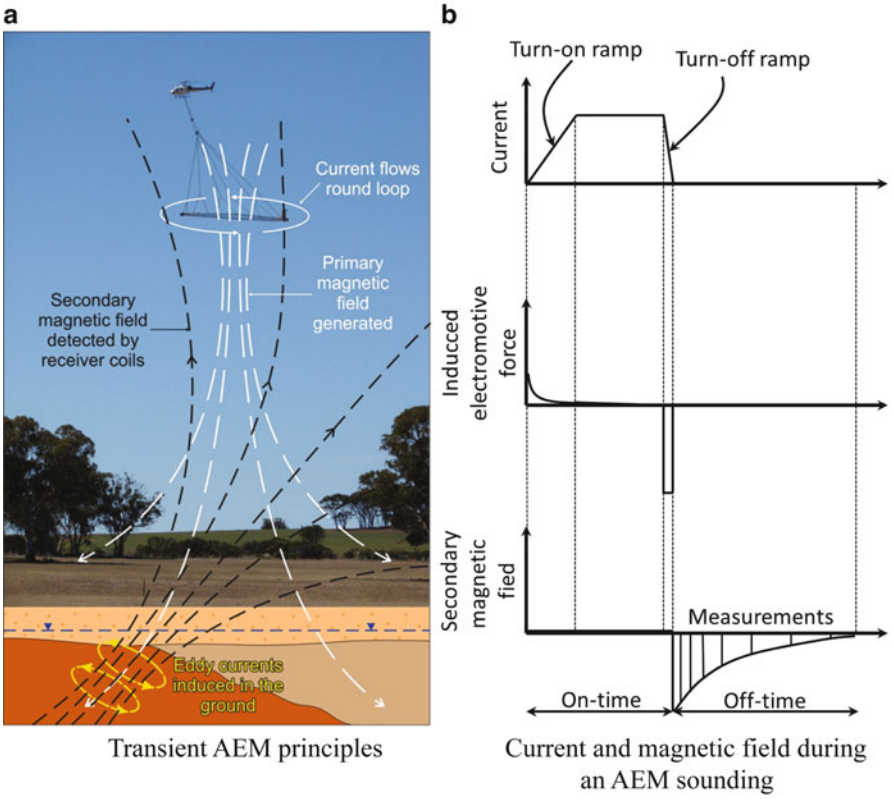

Fig. 7.2 Transient airborne electromagnetic concept: (**a**) currents and electromagnetic fields during the acquisition; (**b**) the corresponding curves of the current and measured electro magnetic field. The different steps of a transient AEM sounding are: (1) A primary magnetic field is generated by the transmitter loop (figure after T. Munday, CSIRO); (2) the current is turned off, which causes generation of eddy currents in the ground; (3) the response from the eddy currents is measured by the receiver coil; (4) the measured secondary field is further interpreted to get the resistivity distribution of the ground

Just after the current in the Tx-loop is shut off, the eddy currents in the ground will be close to the surface, and the measured signal primarily reflects the resistivity of the top layers. At later times the current will run deeper in the ground, and the measured signal contains information about the resistivity of the deeper layers. Measuring the db/dt in the Rx-coil will therefore give information about the resistivity as a function of depth, also called a sounding.

7.3.2 Typical Response from the Ground

The mathematical expression and demonstration of the electromagnetic response from the ground will not be detailed in this chapter. For a deeper insight about the

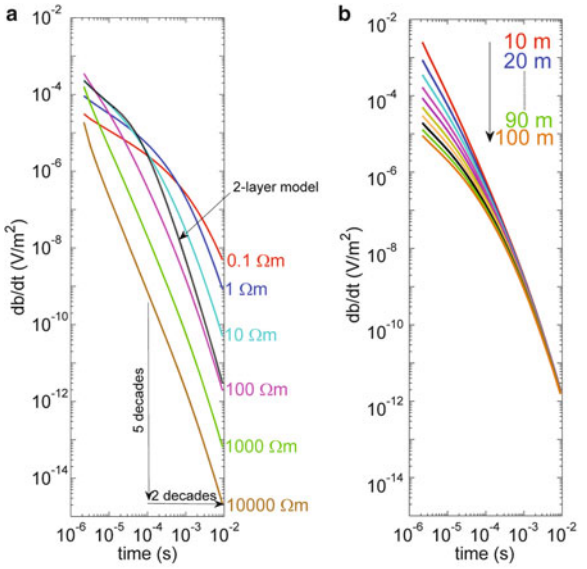

Fig. 7.3 (**a**) db/dt responses for a homogeneous half space with varying resistivities are shown; the *black line* corresponds to the response of a 2-layer model with a top layer of 10 Ωm and 15 m thickness and a second layer of 100 Ωm. (**b**) db/dt responses for a homogeneous half space of 100 Ωm with different flight heights every 10 m from 10 to 100 m

physics the reader is referred to Ward and Hohmann (1988). An approximate expression for the db/dt over a homogeneous ground at late times is given by:

$$\frac{\partial b_z}{\partial t} \approx \frac{-I\rho^{-3/2}\mu_0^{5/2}a^2}{20\pi^{1/2}} t^{-5/2} \tag{7.1}$$

where:

$\partial b_z/\partial t$ is the induced electromotive force from the ground
ρ is the electrical resistivity of the homogeneous ground
μ_0 is the magnetic permeability
I is the injected current
a is the radius of the transmitter loop
t is the time from the beginning of the turn-off ramp (*cf.* Fig. 7.2b)

The decaying secondary field of Eq. 7.1 is shown for different ground resistivities in Fig. 7.3a. As seen the decaying field shows a linear slope of −5/2 in a log-log plot at the latest times. This means that a time period of *e.g.* two decades corresponds to a decrease in amplitude of five decades of the secondary field which is the same as a factor of 100,000. Thus, the signal level is changing greatly from the early to the late times in a TEM sounding.

The amplitude of the secondary field also depends on the ground resistivity, a lower resistivity induces a stronger response (Fig. 7.3a).

The 2-layer response represented by the black line in Fig. 7.3a shows how the secondary field is moving from the response of a 10 Ωm ground at early times (the resistivity of the first layer) to the one of a 100 Ωm ground at late times. This curve cannot be translated directly to a resistivity model as the transition is smooth with both over- and undershoots.

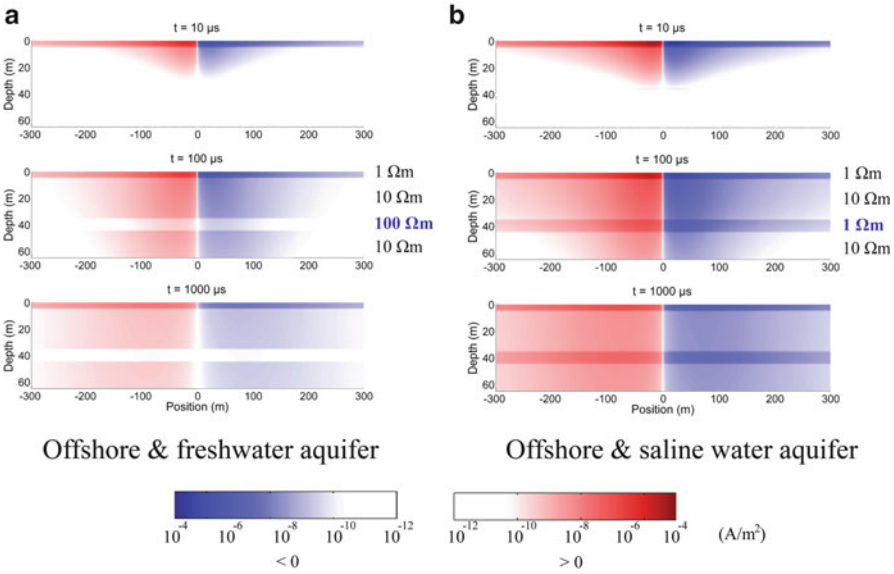

Fig. 7.4 Current density distribution in an offshore area (5 m of sea water) for a four-layer model with either (**a**) a high-resistivity (*e.g.* sand aquifer saturated with freshwater) or (**b**) a low-resistivity (*e.g.* sand aquifer saturated with saline water) layer embedded in conductive marine sediments. The three times are calculated from the beginning of the turn-off of the current in the transmitter loop

To illustrate the behavior on the measured fields when the system is lifted from the ground, Fig. 7.3b shows the effect of the transmitter (and consequently of the receiver) altitude for a homogeneous ground of 100 Ωm. The increase of the altitude induces a decrease of the measured secondary field. This lowering is much more pronounced at the early times, the responses from different altitudes becoming closer and closer at later times.

This observation has a very important impact on the necessity to fly the AEM system as close as possible to the ground. For example, above an open-field area the nominal flight altitude for HTEM frame is normally about 30 m. A too high flight altitude generally results in more noisy data because of the decrease in signal level with altitude and also the resolution of the near surface layers decreases.

7.3.3 Sensitivity of the Method to Ground Resistivity

To understand how the induced eddy currents flow in the earth, we have calculated the current density in the ground at progressively later times after the turn-off of the current in the transmitter loop (Figs. 7.4 and 7.5). The chosen resistivity models are inspired from the geological settings typical for coastal zones. An offshore case with shallow water depths (Fig. 7.4) and an offshore example with a near-surface

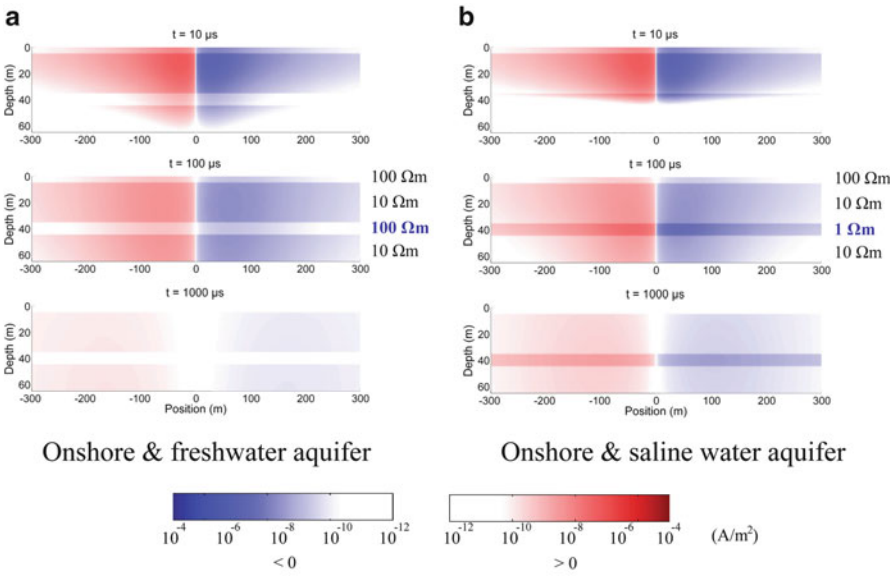

Fig. 7.5 Current density distribution in an onshore area for a four-layer model with either (**a**) a high-resistivity (*e.g.* sand aquifer saturated with freshwater) or (**b**) a low-resistivity (*e.g.* sand aquifer saturated with saline water) layer embedded in conductive marine sediments. The three times are calculated from the beginning of the turn-off of the current in the transmitter loop

sandy layer (Fig. 7.5) are considered. Both models have marine clayey and conductive (10 Ωm) sediments. As shown in Fig. 7.4 the currents are concentrated in the near-surface at 10 µs and go deeper and deeper at later times. This further illustrates the point made earlier that a TEM sounding contains information about the near surface at the early times, while the information about the deep structures is found at late times.

Figure 7.4 also shows that the current flows cylindrically and symmetrically around the vertical axis through the center of the transmitter loop (located at 0 m), which means that a TEM sounding is sensitive to a volume of the ground, which gets gradually larger and larger with time. The volume at very early times is often referred to as the footprint of the system.

Figure 7.4 also allows observing the behaviors of the different layers according to their resistivities. It clearly appears that the currents are more pronounced and last longer in the less resistive layers (especially in the 5 m-depth sea where the currents last a very long time after the turn-off). On the other hand, almost no current exists in the most resistive layers, especially when they are embedded between two conductive layers such as the sandy aquifer saturated with freshwater (100 Ωm) and embedded in marine clayey sediments of 10 Ωm (Fig. 7.4a). The most resistive layers are then less well defined than conductive ones and are more difficult to resolve. In the worst cases such layers are almost "ghosts", and complementary information (*e.g.* other geophysical methods, boreholes) is necessary to

confirm their existence. Contrary, Fig. 7.4b also shows that the aquifer is generating a non-negligible amount of current when saturated with saline water.

Figure 7.5 is the same as Fig. 7.4 except that the top sea water is replaced by a more resistive layer, *e.g.* sand layer. In this onshore case the currents are disappearing quickly in the top 5 m because of the high resistivity. Same differences as for Fig. 7.4 is seen regarding the strength of the aquifer response if this one is saturated by fresh or saline water.

The physics illustrated here make the TEM method well suited to the detection of deep low resistive layers, though the presence of intermediate shallower conductors can "mask" the deeper ones if these first ones are too important.

7.4 Noise and Resolution

7.4.1 Noise

Geophysical measurements are always affected by a degree of uncertainty, since the measurements consist of both the earth response and background electromagnetic noise. The electromagnetic noise is divided into two types, arising from natural sources and from man-made sources.

Natural electromagnetic noise sources come from fluctuations in the Earth's magnetic field due to solar winds. However, the frequencies of the noise are so low, that they do not influence the transient measurement. A more significant noise contribution arises from lightning discharges from thunderstorms occurring all over the globe. Distant thunderstorms give a constant level of noise whereas close by or intermediate thunderstorms result in strong noise bursts referred to as sferics (Macnae et al. 1984). The noise has a random character, though its average amplitude is generally more pronounced during the day than during the night and also during the summer period, as compared to winter.

In populated areas man-made sources likewise contribute to the noise, which is especially the case for the power distribution grid and related electrical installations. The power grid operates at a deterministic harmonic 50 or 60 Hz signal, but there is also a noise contribution with a random character due to transient magnetic fields arising from changes in the grid strain. Additionally, electromagnetic fields from long wave communication equipment can have significant noise contribution because of the strong carrier wave.

7.4.2 Noise and Measurements

A single transient is often more noise than signal and the only way to recover the signal is to repeat the measurement many times and then stack it. By stacking the signal-to-noise (S/N) ratio is increased significantly and consequently an AEM sounding often consists of hundreds to thousands of single transients.

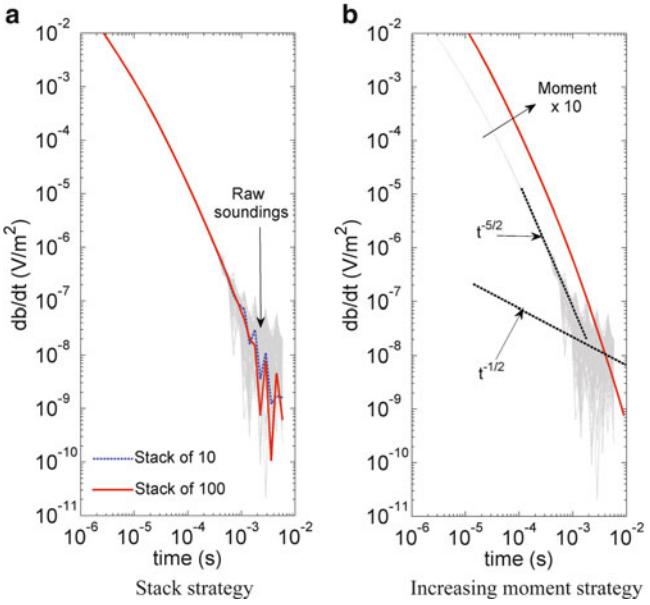

Fig. 7.6 Noise cancellation strategy of a transient AEM sounding (response of a homogeneous ground of 100 Ωm with a flight altitude of 30 m). The raw soundings are shown in *grey* and are repeated in both figures. (**a**) Stack of the raw soundings with 10 and 100, respectively; (**b**) Increase of the transmitter moment by a factor of 10 and illustration of the noise being proportional to $t^{-½}$

The S/N ratio is improved by sampling the transient electromagnetic signal with logarithmically spaced gates. By using the log-gating technique (Munkholm and Auken 1996), the S/N ratio will be proportional to $\sqrt{N}$ for Gaussian distributed noise, where N is the number of single transients. Doubling the number of measurements will consequently improve the signal-to-noise ratio by a factor of 1.41. For coherent noise from *e.g.* long wave radio transmitters, the S/N ratio is proportional to *N*.

The stacking process and the influence on the S/N ratio is illustrated in Fig. 7.6a. The figure shows a stack of ten single transients (the red curve) and a stack of 100 single transients (the blue curve). It is evident that the sounding composed of ten single transients is much more influenced by noise at the latest times compared to the sounding with a stack of 100 transients.

Figure 7.6b illustrates some of the central principles with regard to the noise level for an AEM sounding. The effective noise, *i.e.* the noise after stacking, is typically in the area of 1 nV/m^2, varying between 0.1 and 10 nV/m^2. In Fig. 7.6a the noise level is approximately 10 nV/m^2 at 1 ms. The same sounding curves as in Fig. 7.6a are shown in grey. By using the log-gating technique, the random noise will drop proportionally to $t^{-1/2}$, which corresponds well with the trend of the dark dashed line in Fig. 7.6b.

As mentioned, the signal for the early time measurements is many times larger than the noise level, and the sounding curve has approximately a slope proportional to $t^{-5/2}$ until it reaches the noise level with a slope proportional to $t^{-1/2}$ (Fig. 7.6b). Consequently the transition from a good to a poor S/N ratio happens quickly, and this almost generic slope change can be used in a preliminary automatic filtering to identify and remove data located under the noise level.

To gain more data at later times the S/N ratio can be enhanced either by stacking or increasing the moment of the transmitter. The effect of increasing the moment is shown in Fig. 7.6b as a red line, which shows the level of a sounding with a ten times larger moment (equal to the product of the area of the transmitter loop (A) with the number of wire turns (N) and the intensity of the current (I), NAI). It is clear that the increased moment significantly improves the S/N ratio at late times.

7.4.3 Depth of Investigation

Electromagnetic fields are diffusive, and hence there is no specific depth below which there is absolutely no information on the resistivity structures. However, one can calculate the depth to which the estimated model is most reliable (Christiansen and Auken 2012), which is commonly known as the depth of investigation (DOI). DOI is a useful tool for evaluation of inversion results (methodology used to obtain resistivity model from TEM measurements, *cf.* part 4) and holds valuable information when a geological interpretation is made. The DOI calculation is based on the number of data points and data uncertainty and takes into account the transfer function and the geometry of the AEM system. Consequently, the DOI calculation is purely data driven, and *a priori* information or model constraints are not considered.

To demonstrate the methodology, an example with a SkyTEM system with the last gate at 3 ms is shown in Fig. 7.7. Assuming a simple 3-layer model, the sensitivity function can be plotted versus depth (Fig. 7.7a) and as expected, the sensitivity to the second layer is low (high resistive layer), whereas the sensitivity is high to the first and third layers (low resistive layers).

Figure 7.7b shows the sensitivities summed up from large depth to the surface. This is the total sensitivity at a given depth for all underlying layers. Based on the total sensitivity, a threshold value that indicates the minimum amount of sensitivity needed for information is set. In the shown example a threshold value of 0.8 was used (Christiansen and Auken 2012), giving a DOI of 180 m.

Setting the threshold value is a question of tuning based on experience and comparing different models with different methods. The threshold value used in this example has been tested on many different models and systems and produces trustworthy results in all cases.

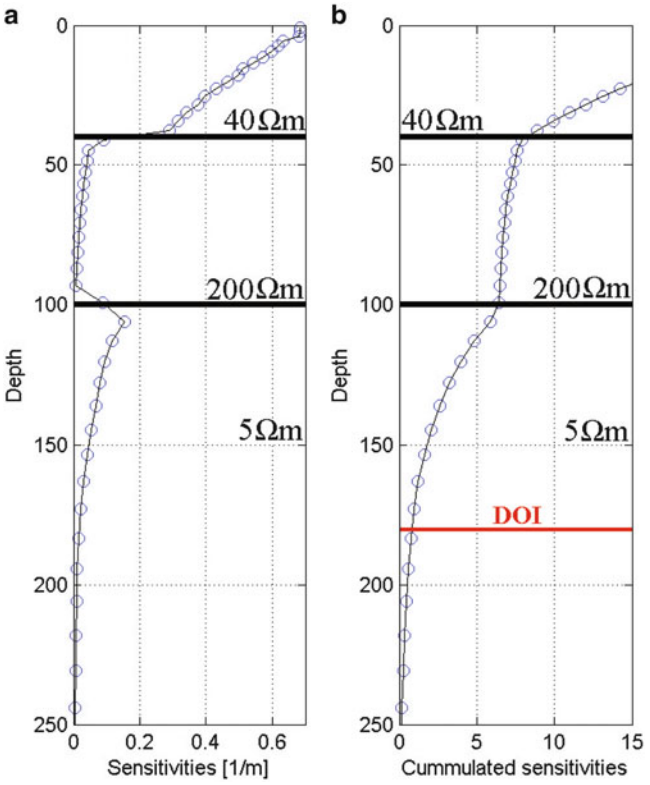

Fig. 7.7 Sensitivities calculated for a re-discretized version of the model indicated by the *black lines*; resistivities of layers are written on the plots: (**a**) the sensitivity function itself; (**b**) the cumulated sensitivities. The *red line* indicates the DOI given by the global threshold value

7.4.4 Model Errors, Equivalence

Models that within the measuring error produce identical responses are called equivalent models. In the ideal case, where there is no noise or measuring errors, a dataset can only be fitted with one model. However, under real field conditions the measurements are always affected by noise, and hence an uncertainty, which reflects the noise level, has to be assigned to the data. In that case a range of models will fit the data equally well within the assigned uncertainty.

The HTEM method is affected by equivalence (Fitterman et al. 1988) only to a limited degree for a low-resistivity layer between two high-resistive layers (low-resistivity equivalence), a high-resistivity layer between two low-resistivity layers (high resistivity equivalence) and layers where the resistive is gradually decreasing (double descending equivalence).

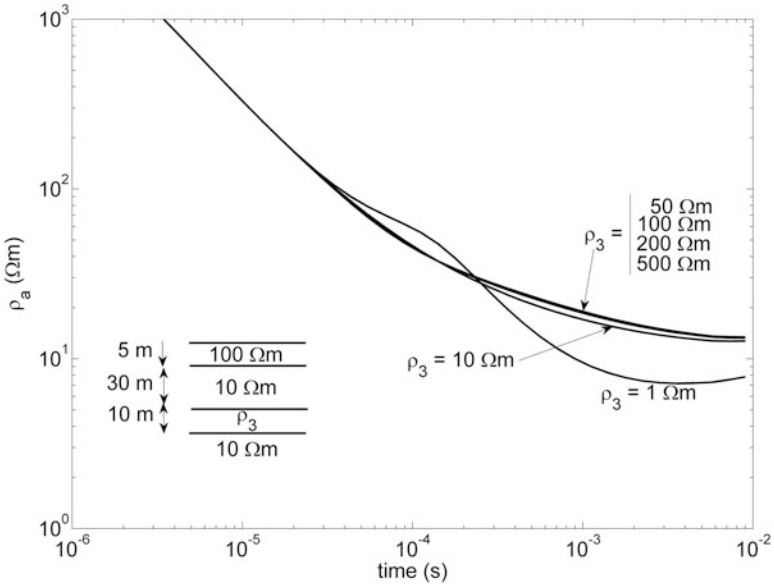

Fig. 7.8 Resistivity equivalence. The resistivity of the third layer is varied from 1 to 500 Ωm. The 4-layer model has a resistive 100 Ωm top layer, a conductive second layer (10 Ωm), a varying third layer (1–500 Ωm) and a 10 Ωm bottom layer. The thickness of layer 1, 2 and 3 are 5, 30 and 10 m, respectively

As discussed earlier the HTEM method has a limited sensitivity towards high resistive layers. This is illustrated in Fig. 7.8, where a suite of responses has been plotted for a 4-layer model with a high-resistive third layer. The first layer in the model has a resistivity of 100 Ωm, and could be a thin near-surface sand layer, whereas the 10 Ωm layers reflect marine clayey sediments in a coastal region. As observed in Fig. 7.8, the response curves of the different models are only slightly separated due to resistivity equivalence, and the curves are only clearly separated when the resistivity of the third layer is either 1 (saline aquifer) or 10 Ωm (in this case the model is reduced to a 2-layer model). This is caused by the fact that the high resistive layer does not produce a significant response, and hence the resistivity of the third layer is poorly determined. On the other hand the thickness of the third layer, if no too small, can be pretty well determined, since the thickness of the second layer and the depth to the fourth layer are well defined due to the high sensitivity of the AEM method to good conductors.

The AEM method is likewise influenced by layer suppression when having two consecutive resistive layers in the model (double ascending model). Again, this is mainly due to the poor sensitivity of the method to a high-resistive layer at the bottom of the model.

As a rule of thumb AEM have difficulties distinguishing layers when their resistivities are higher than 100 Ωm.

7.4.5 Coupling to Man-Made Conductors

Coupling noise is due to induced currents in man-made electrical conductors within the volume in which the transmitted electromagnetic field propagates. The disturbance arises at the same delay time for all decays summed in the stacking process, and hence the coupling effect is deterministic. Unfortunately the effect cannot be accurately removed to ensure a reliable interpretation. Consequently, soundings acquired in the vicinity of cables, power lines, pipelines, rails and metal fences have to be removed before interpretation.

7.4.5.1 Coupling Types

Couplings are categorized into two types; galvanic and capacitive couplings. In general, an oscillating circuit can be used as a general model for describing the disturbance occurring when currents are induced in man-made conductors.

For the galvanic coupling the current has a galvanic return path to the ground as shown in Fig. 7.9a. The disturbance is characterized by an L-R circuit, with the response decreasing exponentially. A galvanic-type coupling could arise from high-voltage power lines, grounded at each pylon. Galvanic couplings are very difficult to identify, since the whole sounding curve is shifted, as seen in Fig. 7.9c. The shift is easily mistaken for that of a low resistive layer at a shallow depth. This kind of coupling, always local, can be identified when looking at a section of several soundings and correlating the positions of the measurements with known man-made installations on a GIS (Geographic Information System) map.

The capacitive-type coupling is characterized by an L-C-R circuit having an inductive return path to the ground (Fig. 7.9b). A capacitive-type coupling could arise from buried polyurethane-isolated cables. The capacitive coupling is easily recognized due to its oscillating character, as seen in Fig. 7.9d.

One can define what is called a safe distance. The safe distance is the minimum distance required between the AEM system and the man-made conductor in order to measure reliable data. By experience this distance should be at least 100 m over a ground with an overall resistivity of 40–60 Ωm. The safe distance increases with the ground resistivity.

7.5 Modeling and Interpretation

7.5.1 Modeling of the AEM System

TEM responses of hydrogeological targets are often much smaller in magnitude than the ones of mining targets where the resistivity contrasts are much larger

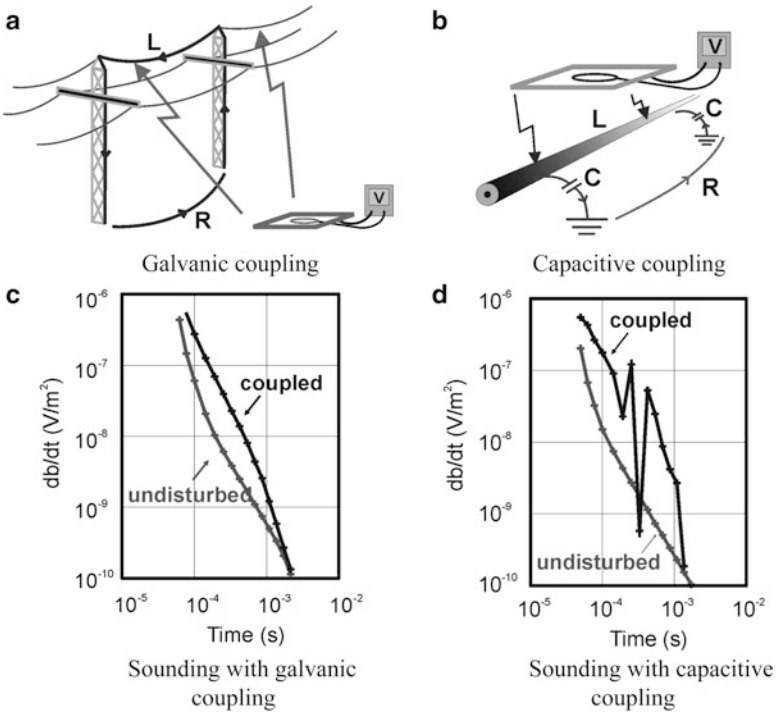

Fig. 7.9 Graphic sketch of the galvanic coupling (**a**) and capacitive coupling (**b**) with the typical imprints in the measured data in (**c**) and (**d**)

(Fig. 7.1). Consequently, a very accurate modeling of the system is necessary to avoid misinterpretation (Christiansen et al. 2011). Such a modeling consists of:

- An accurate modeling of the current waveform, both the turn-on (important for late times) and turn-off ramps (critical for the early times).
- A fine calibration of the system (Foged et al. 2013) to get not only qualitative but quantitative estimation of the ground resistivity structure.
- The modeling of the receiver transfer function, which is expressed as low-pass filters, which have a large impact on the early times.
- Considering the exact geometry of the system, *i.e.* the transmitter frame and the relative position of the receiver coil.
- Correcting for the residual primary field at the very early times <10 μs (Auken et al. 2010b; Schamper et al. 2012).

7.5.2 From TEM Measurement to Ground Resistivity Model

7.5.2.1 Iterative Inversion Procedure in Geophysics

Sounding data cannot be converted to a resistivity model in a single step and therefore non-linear optimization algorithms are used to find a model that fits the

data best. This process is in geophysics often referred to as inversion (Menke 1989; Gubbins 2004).

Any inversion problem can be basically formulated from the start as the resolution of the following equation:

$$\boldsymbol{d}_{obs} = g(\boldsymbol{m}) \tag{7.2}$$

where:

$\boldsymbol{d}_{obs}$ corresponds to the data measured,

$\boldsymbol{m}$ represents the physical parameters of the system to be determined, and

g is the forward modeling operator which gives the synthetic response for a given set of parameters values.

The forward modeling operator g is most often not linear. To solve Eq. 7.2 the usual way is to linearize the problem. Starting from an initial guess $\boldsymbol{m}^{\mathbf{0}}$, the model parameters are updated through successive small steps $\boldsymbol{\delta m}$ which consist in the resolution of the equation:

$$\boldsymbol{d}_{obs} - \boldsymbol{d}_{\boldsymbol{m}^{i-1}} = \boldsymbol{G} \cdot \boldsymbol{\delta m}^{\boldsymbol{i}} \tag{7.3}$$

where:

$\boldsymbol{d}_{\boldsymbol{m}^{i-1}} = g(\boldsymbol{m}^{\boldsymbol{i-1}})$ corresponds to the synthetic data modeled with the parameters values of the previous step $i-1$, and

$\boldsymbol{G}$ contains all partial derivatives of the forward operator regarding each single parameter.

$\boldsymbol{G}$ is also well know as the Jacobian operator which can be replaced by a matrix (also called sensitivity matrix) for small steps $\boldsymbol{\delta m}$. Once the linear system Eq. 7.3 is solved by least square methods, the model parameters $\boldsymbol{m}^{\boldsymbol{i-1}}$ are updated with $\boldsymbol{\delta m}^{\boldsymbol{i}}$ to get $\boldsymbol{m}^{\boldsymbol{i}} = \boldsymbol{m}^{\boldsymbol{i-1}} + \boldsymbol{\delta m}^{\boldsymbol{i}}$, and this process is repeated until the difference $\boldsymbol{d}_{obs} - \boldsymbol{d}_{\boldsymbol{m}^{i}}$, also called data residual or data misfit, is considered as sufficiently small.

As mentioned in Sect. 7.4 of this chapter the data always contain errors, which can come from ambient noise, instrumental precision *etc*. Eq. 7.3 is then solved so that measurements are fitted within the data error $\boldsymbol{e}$:

$$\boldsymbol{d}_{obs} - \boldsymbol{d}_{\boldsymbol{m}^{i-1}} = \boldsymbol{G} \cdot \boldsymbol{\delta m}^{\boldsymbol{i}} + \boldsymbol{e} \tag{7.4}$$

Resolution of Eq. 7.4 in an iterative inversion procedure is not straightforward for the following main reasons:

- The linearization of $\boldsymbol{G}$, even by numerical finite differences, is not necessarily very stable and can lead to unstable algorithms.
- Some elements of $\boldsymbol{G}$ can be very small because of the low impact of certain parameters on the data, which leads to ill-conditioned matrix requiring numerical stabilization (*e.g.* the damping factor in the well-known Marquardt-Levenberg algorithm, *cf.* Marquardt 1963, 1970).

- The evaluation of the error level $\boldsymbol{e}$ can be subjective as it requires the quantification of the impact of all main sources of noise. Such an error level can be estimated from the data stacking process.
- The problem of equivalence as detailed in Sect. 7.4.4. Depending on the starting model $\boldsymbol{m^0}$ and the error level $\boldsymbol{e}$, the inversion procedure can end with different models, which explain the data equally well within the error bar.

The last point reflects the ill-posed problem, which is common to all geophysical methods. To limit this effect, a regularization parameter, also know as Tikhonov parameter α (Tikhonov and Arsenin 1977), is added to Eq. 7.4 to constrain the problem and limit the number of possible solutions:

$$(\boldsymbol{d}_{obs} - \boldsymbol{d}_{\boldsymbol{m}^{i-1}}) + \alpha\left(\boldsymbol{d}_{a\ priori} - \boldsymbol{d}_{\boldsymbol{m}^{i-1}}\right) = \boldsymbol{G} \cdot \boldsymbol{\delta m}^{i} + \boldsymbol{e} \tag{7.5}$$

where:

$\boldsymbol{d}_{a\ priori}$ corresponds to the synthetic data for an *a priori* model from which the estimated model is forced not to be too far, and

α is the regularization parameter, which gives weight to the *a priori* constraint in balance with the data residual $(\boldsymbol{d}_{obs} - \boldsymbol{d}_{\boldsymbol{m}^{i-1}})$.

The weight given to the *a priori* constraint in Eq. 7.5 requires the expertise of the geophysicist and also if possible of the geologist's ability to evaluate the confidence that needs to be set to enforce the inversion procedure. It has to be noted that *a priori* constraint does not have to be applied to all parameters of the model; enforcing only few of them is often sufficient to eliminate most of the "wrong" equivalent models.

7.5.2.2 Number of Dimension of the Ground: 1D, 2D and 3D

The interpretation techniques for airborne TEM methods are computationally intensive because it involves a double Fourier transform. Calculating the TEM response involves calculating a larger frequency spectrum of 50–150 frequencies followed by a transformation from frequency to time domain. This is then followed by a number of convolutions where *e.g.* the transmitter waveform is applied. With the computation power nowadays this is no longer a really serious problem, and TEM data can be interpreted using non-approximate forward solutions and full non-linear inversion at survey scales of thousands of line km.

1D interpretation at each sounding position has been possible in the last two decades (Farquharson and Oldenburg 1993) but only recently it can be done routinely on entire surveys. Today 2D/3D interpretations are available (*e.g.* Yang and Oldenburg 2012; Cox et al. 2012) but the technology is still at its edge. The value of 3D inversion for groundwater targets is not as big as for mining targets as it is often quasi 1D within the footprint of the system. Moreover a helicopter-borne EM system has a sensitivity pattern, which is mainly concentrated just below the transmitter loop making it relatively insensitive to lateral resistivity changes.

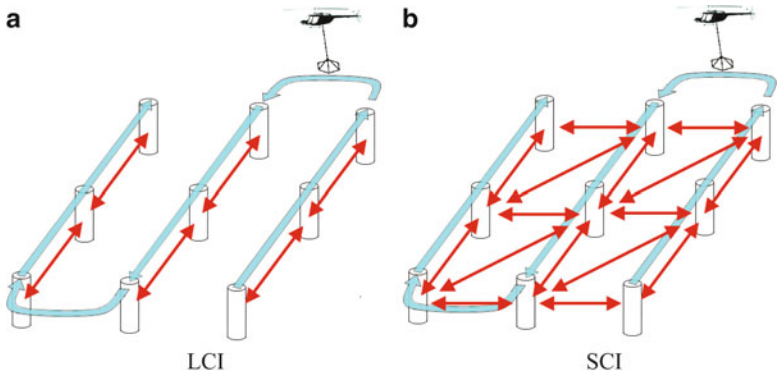

Fig. 7.10 Constrained inversion schemes (figure after Sab 2012): (**a**) Laterally Constrained Inversion (LCI) along each flight line; (**b**) Spatially Constrained Inversion (SCI) where constraints link soundings belonging to different flight lines

Advanced Laterally Constrained Inversion (LCI, Fig. 7.10a) along each flight line (Auken and Christiansen 2004), or Spatially Constrained Inversion (SCI, Fig. 7.10b) over the entire dataset of a survey (Viezzoli et al. 2008) allow getting coherent quasi 2D and 3D distributions of the ground resistivity. In these inversion schemes the resistivities of the layers of surrounding soundings are linked together by lateral constraints, which ensure more continuous and geologically probable models.

When performing an individual or a laterally constrained 1D inversion, two kinds of model discretization can be considered:

- Few-layer/blocky inversion: few layers, generally not exceeding a total of 5, are considered and both resistivities and interfaces are estimated.
- Multi-layer/smooth inversion: a large amount of layers is considered (usually between 10 and 30); only resistivity values are estimated, the interfaces being fixed with thicknesses increasing with depth. The continuity of the vertical resistivity variations is ensured by vertical constraints, hence the name of smooth inversion.

The pros of the two inversion schemes:

- Few-layer: easier estimation of the interfaces' depths, especially in case of sharp resistivity boundaries.
- Multi-layer: can handle the change in the number of geological layers within the same area and generally provides a more complex and coherent ground resistivity model.

The cons:

- Few-layer: artifacts in case of change in the number of geological layers.
- Multi-layer: can smoothen the transitions too much, making the localization of the vertical boundaries approximate and somehow subjective.

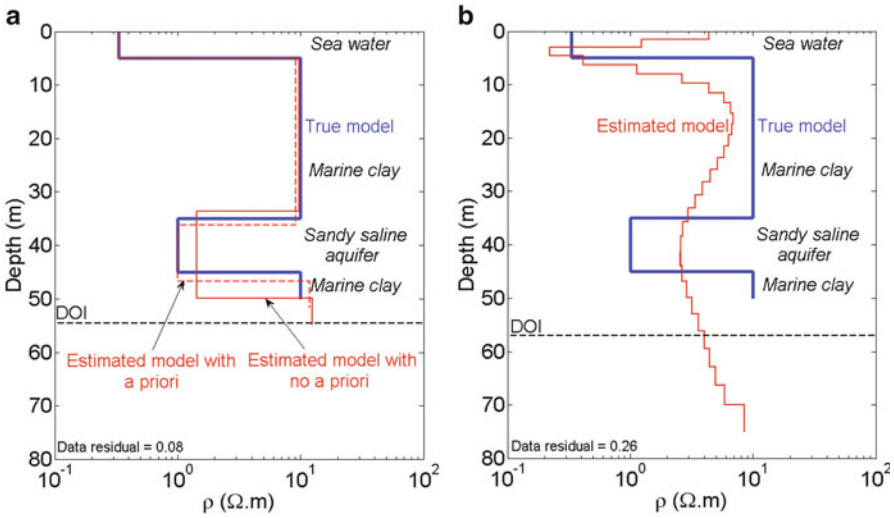

Fig. 7.11 Example of SkyTEM sounding inversion from synthetic data for a saline aquifer in an offshore case: (**a**) few-layer inversion considering four layers, the *a priori* constraint is on the resistivity of the deep conductive layer (saline water aquifer); (**b**) smooth inversion with 30 layers. Data residual indicates how well the model fits the data. A residual below 1 means that data are well fitted within the data standard deviation. The SkyTEM system considered here has a 500 m^2 transmitter loop and two moments with 1 turn/10 A and 4 turns/95 A, the first gate is about 13 μs and the last one around 9 ms

Figure 7.11 shows an example of the few-layer and smooth inversions of a synthetic SkyTEM sounding. The model considered is the offshore case (top 5 m sea layer) with a saline aquifer of 1 Ωm.

As seen in Fig. 7.11a, the estimated model is quite close to the true model. However the estimated thickness of the conductive saline aquifer is larger with a slightly higher resistivity.

Figure 7.11b presents the inversion of the same synthetic model, but considering a smooth/multi-layered inversion scheme. With 30 layers with progressively increasing thicknesses from 1.5 m to a last interface depth of 70 m, the resistivity oscillations due to the different layers are quite well retrieved. Despite the fact that this inversion does not require hypothesis on the number of layers and that it allows variations of the number of layers along a profile, it is hard to determine the boundaries of the layers accurately. Recent mathematical developments allow to get a more focused image of the ground resistivity with sharper boundaries even within an oversampling grid (Portniaguine and Zhdanov 2002; Blaschek et al. 2008).

Figure 7.12 illustrates a field example from data acquired in Antarctica with the SkyTEM system (Auken et al. 2012). The objective here is to better understand the saline aquifer systems, underlying lakes, and glaciers at a close proximity to the sea. The profile shown in Fig. 7.12 crosses one of these hyper-saline lakes. Figure 7.12a corresponds to a few-layer inversion with 4 layers and Fig. 7.12b to a smooth inversion with 29 layers.

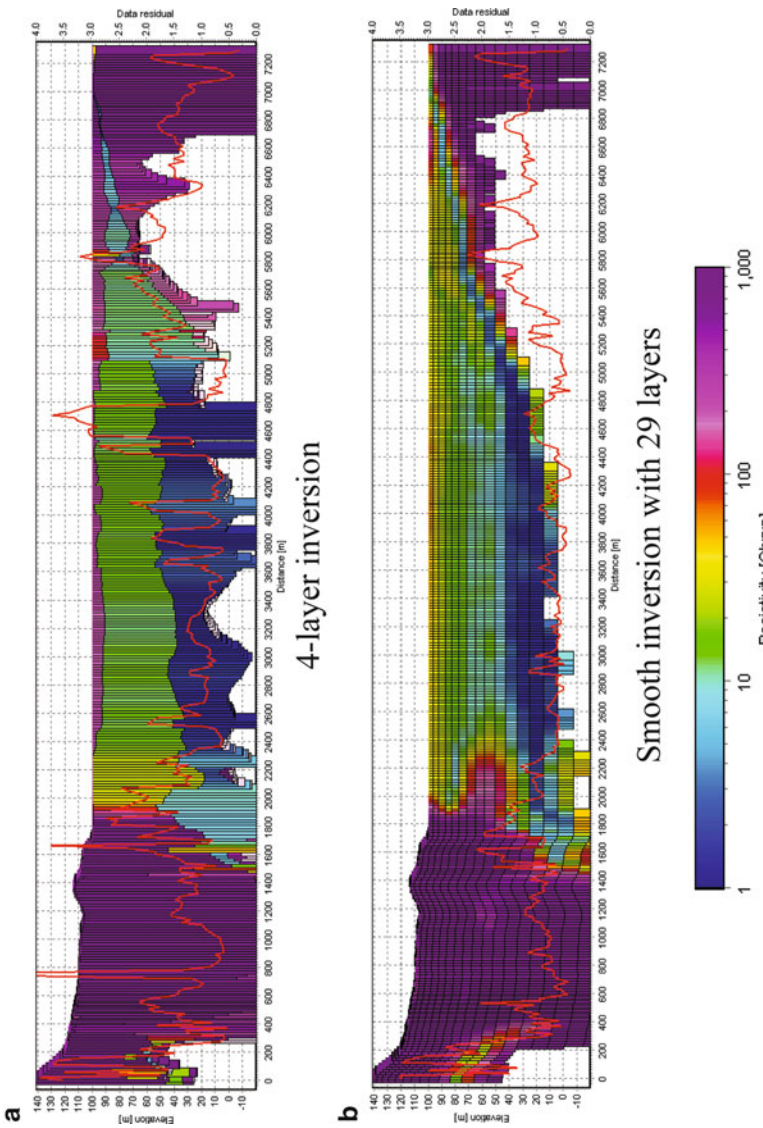

Fig. 7.12 Example of a SkyTEM section with field data from a survey in Antarctica: (**a**) few-layer inversion with four layers; (**b**) smooth inversion with 29 layers. The top thin layer appearing as *purple* color at the center of the section in (**a**) corresponds to the few-meter ice above the lake which appears as conductive values in *green* color. The bottom of the lake (20–30 m deep) is gradually saturated by salt with depth as well as the underlying sediments whose resistivity goes down to 1 Ωm and even below. The two resistive structures on both sides of the section correspond to permafrost. The *red line* indicates the data residual, *i.e.* how well the data are fitted with the estimated resistivity model (a value below 1 means that the data are perfectly explained within the data error)

As seen, the smooth inversion section (Fig. 7.12b) less erratically displays the lateral variations across the section where the number of layers is changing, especially at a position between 1,800 and 3,000 m where a resistive structure can be observed at an elevation of about 60 m. This structure is absent from the few-layer section of Fig. 7.12a.

The data residual, *i.e.* the misfit between the data and the forward response of the resistivity model, is also lower (*i.e.* better) along the profile for the smooth inversion (Fig. 7.12b) compared to the few-layer inversion (Fig. 7.12a), the smooth inversion allowing a better adaptation of the resistivity model along the section.

7.6 Field Case: SkyTEM in Mayotte Island

To demonstrate the powerfulness of the HTEM technique we will present results in the following from a groundwater survey flown at Mayotte Island. This island is a French oversea department and is one of the islands in the Comoro Islands group located between Madagascar and the African continent.

7.6.1 Introduction

The demographic explosion of many tropical volcanic islands requires an urgent investigation of their subsurface in order to provide sustainable solutions to the increasing demand for freshwater. Traditional geological studies and ground-based geophysical measurements are often of limited value due to the generally poorly outcropping geology, difficult access in the terrain and complex geological geometry.

In a similar tropical volcanic island context, the SkyTEM method (Sørensen and Auken 2004) has shown its efficiency on the Santa Cruz Island (d'Ozouville et al. 2008) and on the San Cristobal Island (Pryet et al. 2012) in the Galapagos Archipelago.

In 2010, in order to improve geological and hydrogeological knowledge in Mayotte Island, the BRGM (the French Geological Survey) and the Prefecture of Mayotte decided to fund a research project involving a helicopter-borne 3D resistivity survey. The aim of this case study is to evaluate how the interpretation of a large scale 3D geophysical EM dataset could lead to a detailed geological and hydrogeological characterization in order to identify possible groundwater reservoirs.

7.6.2 The SkyTEM System

The SkyTEM system has been developed for groundwater investigations by the HydroGeophysics Group at Aarhus University, Denmark. During the last decade,

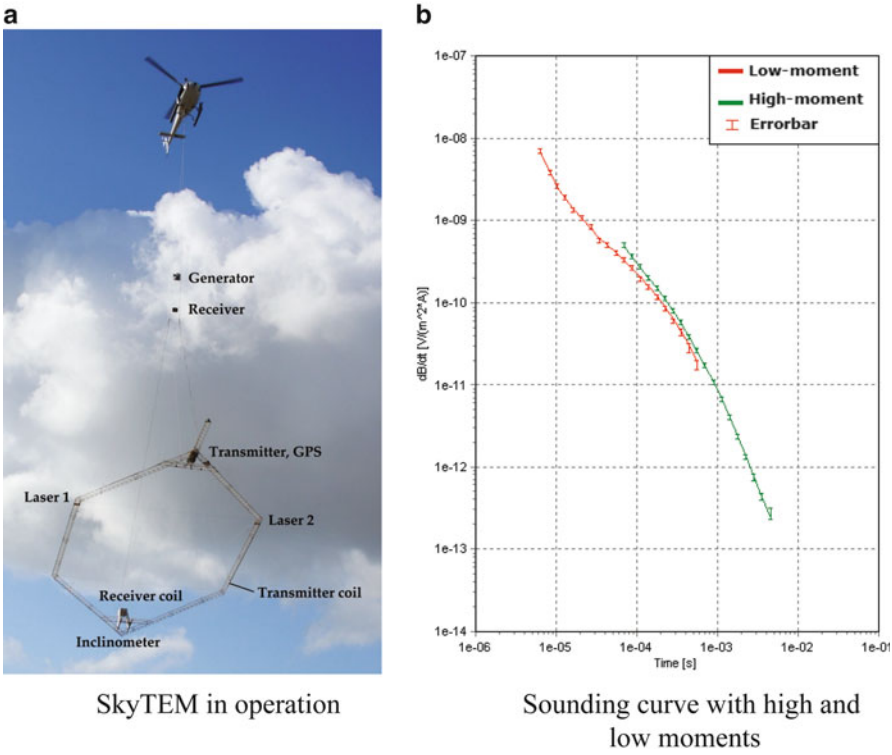

Fig. 7.13 (**a**) The SkyTEM system in operation. The transmitter and receiver coils, power supply, laser altimeters, global positioning system (GPS), electronics and data logger are carried on a hexagonal frame below the helicopter. (**b**) Sounding curve from the Mayotte survey with both low- and high-moment. The two curves are normalized by their respective currents and numbers of wire turns, the reason why they almost match at common gates

the system has been intensively used for groundwater surveys throughout the world. The following is a brief introduction to the SkyTEM system. A more thorough description of the system can be found in Sørensen and Auken (2004).

Figure 7.13a shows the SkyTEM system in operation. The transmitter and receiver coils, power supply, laser altimeters, global positioning system (GPS), electronics and data logger are carried on a hexagonal frame below the helicopter. The transmitter loop used for the Mayotte survey is a 284 m^2 loop, which is mounted on the frame. The receiver coil is placed approximately 1.5 m above the frame. The frame altitude is continuously measured by two lasers attached to the frame, and two inclinometers measure the pitch and roll of the frame. The measured data are automatically averaged, reduced to data subsets (soundings) and stored together with the GPS coordinates, altitude, inclination of the transmitter/receiver coils and the transmitter waveform.

The SkyTEM system is a dual moment system, whereby measurements can be carried out with either one or two transmitter moments. The measurement configuration of the system can thus be customized for each survey depending on the target

geology. Typically, a measurement sequence with both low moment (LM) and high moment (HM) is used for groundwater exploration (Fig. 7.13b). With the LM, a current of 10 A is normally used in a 1-turn wire, which allows a shorter turn-off of the primary current and the interpretation of very early times, hence providing information about the near-surface geological structures. With the HM, a better signal-to-noise ratio is obtained at late times due to the higher moment (here a current of 100 A in a 4-turn wire), thereby providing deeper information. The advantage of having dual moments is thus to provide a very detailed near-surface resolution as well as information about structures down to a depth of several hundred meters. Figure 7.13b shows a sounding curve from the Mayotte survey with both low moment (red curve) and high moment (green curve).

The flight altitude is obviously governed by the flight speed, topography variations, safety concerns *etc*., but for groundwater investigations the nominal flight altitude of the frame is 30–40 m. The goal is to keep the frame as close to the ground as possible in order to achieve a good vertical resolution. In low-land areas with small topography variations the altitude of the frame can be as low as 20 m, but over forested areas the altitude has to be increased in order to maintain the necessary safety distance to the treetops. The operating flight speed is typically 30–80 km/h (8.3–22.2 m/s) depending on the geological target and the desired lateral and vertical resolutions.

7.7 Case Study: Mayotte Island

Mayotte is a French territory located in the northern Mozambique Channel in the Indian Ocean (Fig. 7.14). Mayotte has an area of 374 km^2, and is, like many other tropical volcanic islands, very densely populated (>500 inhabitants/km^2) with a population, which has multiplied by four in less than 30 years. The island, particularly the coastal zones, is now very densely populated, with substantial water needs.

The terrain of the island is undulating, with deep ravines, and ancient volcanic peaks culminating at 660 m. Underground rocks and structures are hidden beneath thick, densely forested and cultivated soils. The island stands 4,400 m above the oceanic floor (Audru et al. 2006) and is the oldest of the four islands constituting the Comoros archipelago (Emerick and Duncan 1982).

Mayotte includes two main islands (Fig. 7.15) called “Grande-Terre” and “Petite-Terre”. The climate is tropical and humid with a dry and a rainy season. The main formations are Miocene and Pliocene basaltic and phonolitic lavas, and pyroclastic ash and block projections (Stieltjes 1988). These formations are deeply weathered and thus overlaid, on about 70 % of the island, by a thick lateritic soil. The lavas of the island are dated from 10.6 ± 0.5 Ma (million years) to a couple of thousand years for very recent phreatomagmatic formations (Nougier et al. 1986; Debeuf 2004).

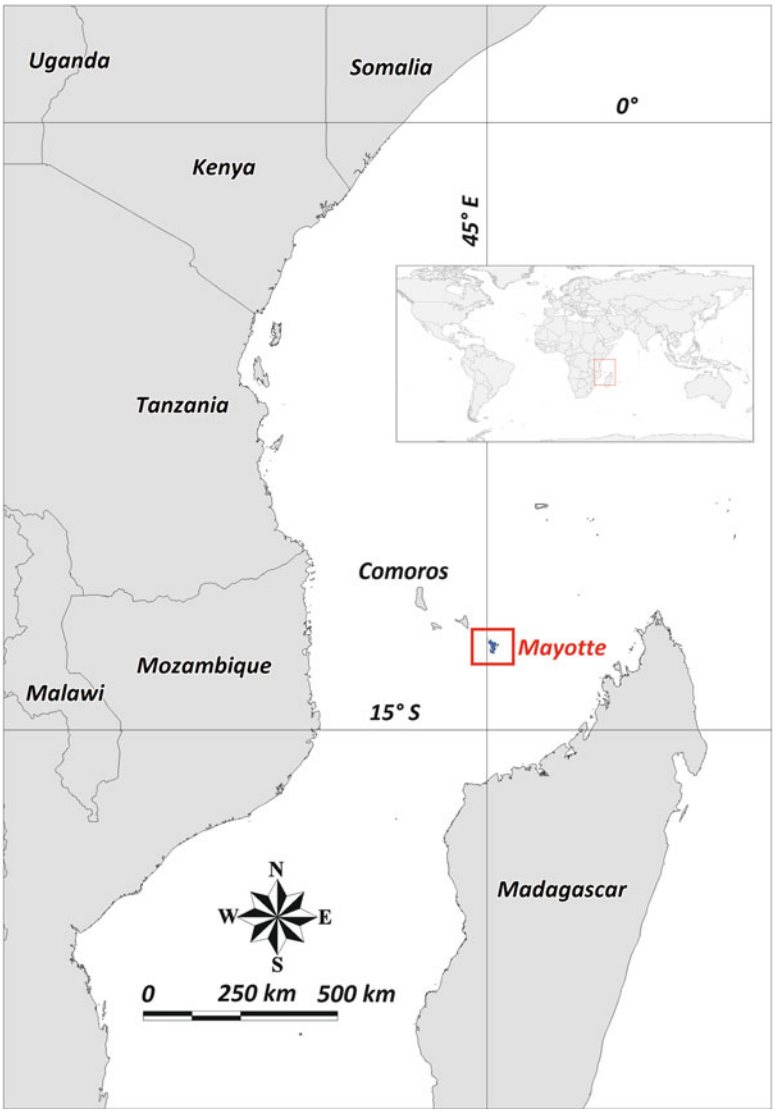

Fig. 7.14 Location of Mayotte Island

7.7.1 Geophysical Data Acquisition

The electromagnetic survey was carried out with a dual-moment Time Domain Electromagnetic system (TEM). This system is specifically designed for hydrogeological surveys with a resolution of the near surface geological layers previously accessible only by means of ground based geophysical techniques.

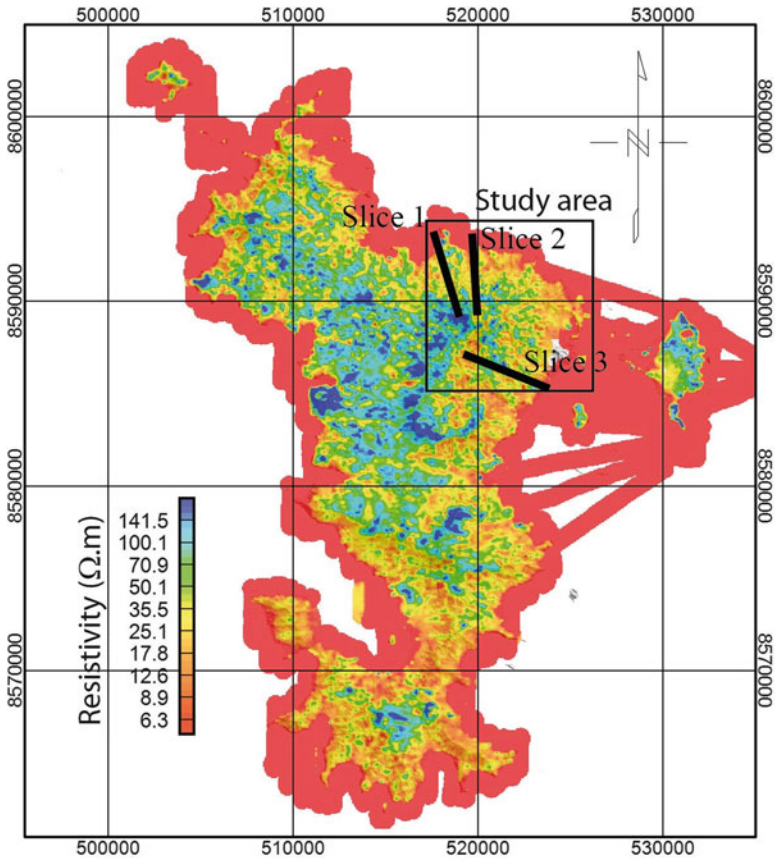

Fig. 7.15 First 5 m resistivity obtained by kriging of the TDEM soundings after smooth inversion

SkyTEM can discriminate between weak conductivity contrasts in the top layers concurrently with those at depth and provides a detailed insight in understanding the internal geological structure of the upper 200 m of the volcanic islands.

The Helicopter borne transient electromagnetic data acquisition was made during 1 month in October 2010. Seventy-two flight hours allowed surveying 2,915 km flight lines, with a 200 or 100 m spacing and a 30–60 m ground clearance. Data corrections for the system being operated in a rough terrain far from horizontal is applied before inverting data with the Spatial Constrained Inversion scheme. Kriging of TDEM soundings was performed with Matlab mGstat toolbox in order to derive 3D resistivity grid. Figure 7.15 is an illustration of the mean resistivity for the first 5 m obtained by smooth inversion.

Good conductivity contrasts between the different rock types allow defining the geometry of the principal geological units in 3D from the surface and down to about 200 m below the surface. Results in the field of water, mineral resources and regolith mapping are very promising and implications concerning water resources are presented below.

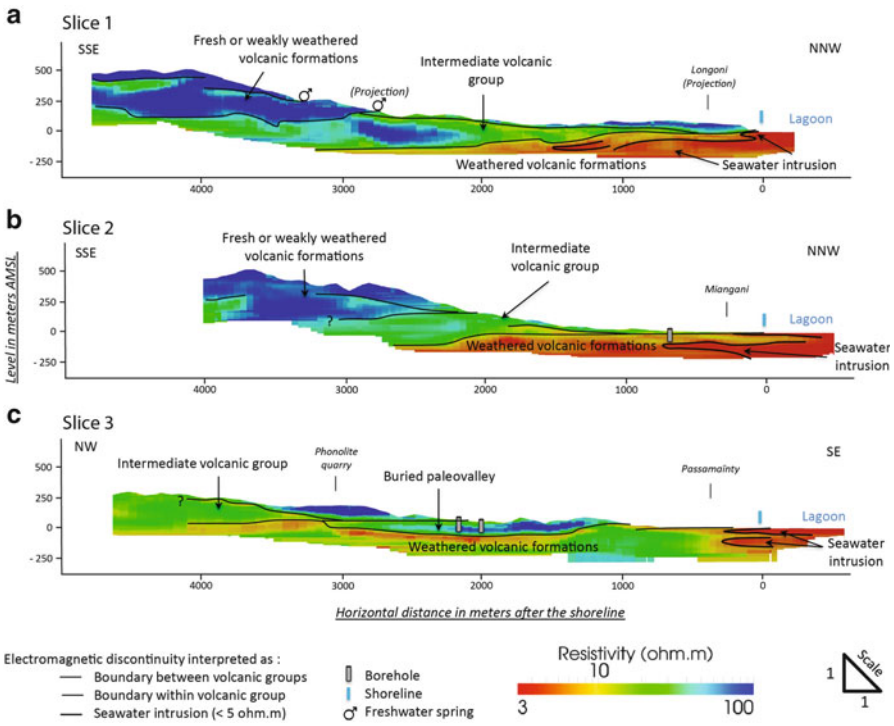

Fig. 7.16 Slices and hydrogeological interpretation derived from 3D resistivity model: (**a**) slice illustrating several stages of the geological construction of the island; (**b**) other slice illustrating several stages of the geological construction of the island; (**c**) slice showing the typical case of a buried paleovalley. The locations of the slices are given in Fig. 7.15

7.7.2 Highlighting Key Geological Structures

Paraview software (Henderson 2007) has been used to visualize the geophysical data and to make resistivity cross sections in the 3D grid (Fig. 7.15). Three cross sections are presented in Fig. 7.16, and their localizations are shown in Fig. 7.15. The lateral extension of these cross sections ranges between 4,500 and 5,500 m and the elevation is ranging from −250 to +550 m. Resistive values are represented in blue and conductive values in red. Figures 7.16a and b show a vertical succession of (from the bottom to the top) low resistivity values (<5 Ωm) from – 250 to 0 m above mean sea level (AMSL), intermediate resistivity values (ranging from 5 to 30 Ωm) up to 100 m AMSL and high resistivity values (>30 Ωm) above. The difference between Fig. 7.16a and b is the shape of the interface between low resistivity and intermediate resistivity values: low resistivity values on slice 2 (Fig. 7.16b) being higher, around 0 m AMSL 2,000 m inland, whereas reaching a maximum elevation of about −100 m on slice 1 (Fig. 7.16a). Figure 7.16c shows low resistivity values only a few hundred meters inland, and with localized resistivity values higher than 30 Ωm

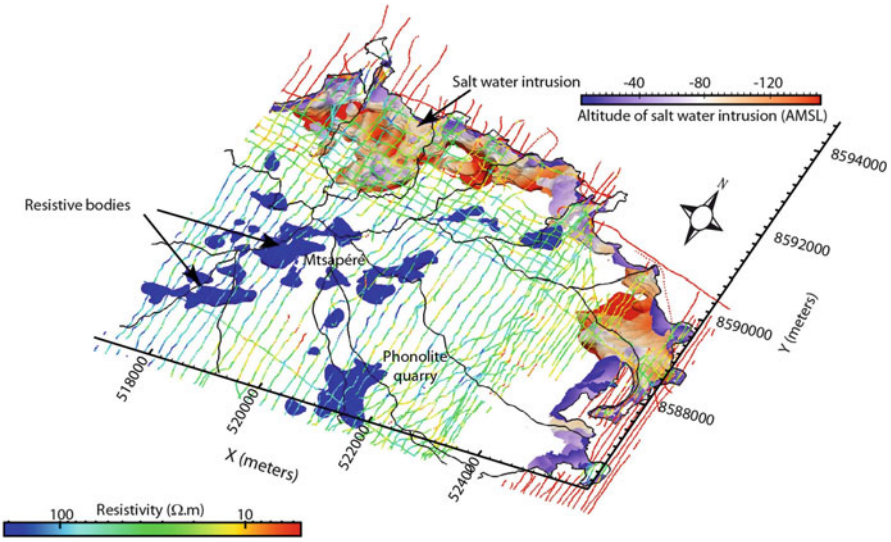

Fig. 7.17 3D hydrogeological interpretation. Altitude of salt water intrusion is given by 5 Ωm isosurface and the resistivity of volcanic bodies is higher than 200 Ωm. Resistivity of the first meters (0–3.5 m) are shown for each sounding

(between 1,200 and 3,500 m, with thickness ranging between 50 and 100 m) overlying intermediate resistivity values.

The cross sections of Fig. 7.16 illustrate four main geological features:

1. Higher resistivity values (>100 Ωm) observed on Fig. 7.16c match with a quarry of Pleistocene phonolic lavas; this is consistent with resistivity ranges found in the literature (Descloitres et al. 1997; Lénat et al. 2000; Albouy et al. 2001; d'Ozouville et al. 2008) similar to unsaturated basalts.
2. Lower resistivity values (<5 Ωm) observed on the three cross sections, correspond to salt-water and volcanic formations invaded by seawater (Lienert 1991; Descloitres et al. 1997; Albouy et al. 2001; d'Ozouville et al. 2008; Pryet et al. 2012).
3. Surveys conducted in the field allow the correlation between resistivity values ranging from 5 to 30 Ωm and weathered lavas.
4. Finally, correlation between geological logs of the two boreholes observed on slice 3 (Fig. 7.16c) and field surveys allow correlating resistivity values ranging from 30 to 100 Ωm with fresh fissured basaltic lavas.

Based on these correlations, a 3D geological model has been produced to map the extension and thickness of the main geological formations. For example, the extension of the top lava flow of the Mtsapéré Mountain is represented by a blue color (resistivity >200 Ωm) in Fig. 7.17. Figure 7.16a and b also illustrate several stages of the geological construction of the island, with younger fresh basaltic lavas overlying a basement constituted by older weathered lavas. Figure 7.16c illustrates the typical case of a buried paleovalley with a basement constituted by weathered

volcanic formations, filled by younger, fresh and fissured lavas. Such features have been observed in several locations of the island (Vittecoq et al. 2011a).

The good conductivity contrasts between the different rock types, allow defining the geometry of the principal geological units in 3D, from the surface down to about 200 m below the surface. Helicopter borne transient electromagnetic data can thus be used to map geological formations and to constrain the hydrogeological model of the island.

7.7.3 Hydrogeological Functioning

Groundwater resources are correlated with the permeability of the rocks, and in volcanic environments permeability is usually considered to be negatively correlated with age formations. Younger lavas have a higher permeability than older ones, which are often strongly weathered (Custodio et al. 1988, 2004; Peterson 1972; Cruz and Silva 2001). The key geological structures also clearly control the hydrogeological functioning. On Fig. 7.16c the two boreholes drilled in fresh and fissured basalts with resistivity values ranging from 30 to 100 Ωm are productive with transmissivities ranging from 6.10^{-4} to 1.10^{-4} m^2/s and a production yield of about 30 m^3/h. The paleovalley structure, revealed by the helicopter borne transient electromagnetic data, controls the groundwater flow: the basement constituted by weathered lavas, resulting from the alteration of an older topographic surface, is acting as an impermeable layer and the groundwater flow is controlled by this impermeable layer at the base and limited laterally by the slopes of the paleovalley. Along profiles of Fig. 7.16a and b, several springs have been observed during a field survey, with seeping and flowing from formations with resistivities also ranging from 30 to more than 100 Ωm. This resistivity range can be considered as representative of aquifer formations for this part of the island. When situated above the sea level, these volcanic formations can correspond to perched aquifers. Furthermore, weathered lavas with resistivity values ranging from 5 to 30 Ωm observed on Fig. 7.16a and b act as semi-permeable layers, their hydrodynamic parameters depending on the intensity and variability of the weathering process.

7.7.4 Seawater Intrusion

Seawater intrusion has a severe impact on the water supply in basaltic volcanic islands (Izuka and Gingerich 2003; Kim et al. 2003; Herrera and Custodio 2008; Auken et al. 2009b; Cruz et al. 2011; Pryet et al. 2012) with intrusion sometimes up to several kilometers inland and thus major quality problems in the water supply. Figure 7.16 illustrates three different shapes of the interface between resistivity values <5 Ωm, interpreted as seawater or groundwater invaded by seawater, and resistivity values ranging from 5 to 30 Ωm, interpreted as weathered volcanic

formations. At most, seawater intrusion penetrates a few hundred meters inland. The position of the seawater-freshwater interface is not uniformly distributed on the three cross-sections due to heterogeneities of the hydrodynamic parameters of the aquifer in the weathered volcanic rocks. These heterogeneities can also be seen on Fig. 7.17. Comparatively to other volcanic islands (Galapagos, Canaries, Jeju Island, Eastern Island...) the penetration of seawater inland is weak, at least in the north-eastern part of the island, due to the low permeability of the weathered lavas constituting the basement of the island. Locally, the permeability of the weathered lavas is slightly higher; especially when alluvium or volcano-detritic sediments are intercalated or overlying. It is in these environments that seawater intrusions penetrate more inland (for instance Fig. 7.16).

7.8 Conclusion – Perspective

The helicopter borne transient electromagnetic survey of the Mayotte Island allowed the mapping of the key geological formations. Their correlation with borehole data and field survey observations allowed improving the knowledge of the hydrogeological functioning of the island.

The 3D resistivity grid analysis also helped to map the extent of seawater intrusions in this coastal zone.

The 3D electromagnetic dataset is now used to plan future water management strategies. For instance the results have been used to determine new borehole locations for possible water extraction (Vittecoq et al. 2011b) by targeting formations with resistivity values ranging from 30 to 200 Ωm, corresponding to paleovalleys or perched aquifers. A campaign of eight drill holes will be performed in 2013. The results of this drilling and logging program will bring new data allowing the refinement of our hypothesis and a better calibration of the geophysical data. Indeed, it will be necessary to correlate a sufficient number of water wells in order to deeper characterize the geological structure and hydrogeological functioning of the entire island.

Acknowledgement This work was carried out with the financial support of the Mayotte Prefecture and Department, the French Ministry of Environment, SIEAM (local water supply authority) and BRGM, the French geological survey.

References

Albouy Y, Andrieux P, Rakotondrasoa G, Ritz M, Descloitres M, Join J-L, Rasolomanana E (2001) Mapping coastal aquifers by joint inversion of DC and TEM soundings – three case histories. Ground Water 39(1):87–97

Allard M (2007) On the origin of the HTEM species. In: Proceedings of exploration: fifth decennial international conference on mineral exploration, Toronto, 2007, pp 355–374

Audru JC, Guennoc P, Thinon I, Abellard O (2006) Bathymay: la structure sous-marine de Mayotte révélée par l'imagerie multifaisceaux. CR Geosci 338(16):1240–1249

Auken E, Christiansen AV (2004) Layered and laterally constrained 2D inversion of resistivity data. Geophysics 69(3):752–761

Auken E, Christiansen AV, Westergaard JA, Kirkegaard C, Foged N, Viezzoli A (2009a) An integrated processing scheme for high-resolution airborne electromagnetic surveys, the SkyTEM system. Explor Geophys 40(2):184–192

Auken E, Violette S, d'Ozouville N, Deffontaines B, Sorensen KI, Viezzoli A, de Marsily G (2009b) An integrated study of the hydrogeology of volcanic islands using helicopter borne transient electromagnetic: application in the Galapagos Archipelago. CR Geosci 34(10–11):899–907

Auken E, Foged N, Roth B, Mikkelsen P (2010a) SkyTEM survey Mayotte 2010, Survey report, Department of Geoscience, Aarhus University

Auken E, Foged N, Sørensen KI (2010b) Approaching 10 microsec (and earlier) with the SkyTEM system. In: ASEG extended abstract, 21st international geophysical conference and exhibition, Sydney, 22–26 Aug 2010

Auken E, Mikucki J, Sørensen KI, Schamper C, Sab G-A, Tulaczyk S (2012) First airborne transient EM survey in Antarctica: mapping of saline ground water system. In: Remote sensing-near surface geoscience extended abstract, 18th European meeting of environmental and engineering geophysics, Paris, 3–5 Sept 2012

Blaschek R, Hördt A, Kemna A (2008) A new sensitivity-controlled focusing regularization scheme for the inversion of induced polarization data based on the minimum gradient support. Geophysics 73(2):F45–F54

Buselli G, Williamson DR (1996) Modeling of broadband airborne electromagnetic responses from saline environments. Geophysics 61(6):1624–1632

Christiansen AV, Auken E (2012) A global measure for depth of investigation. Geophysics 77(4):171–177

Christiansen AV, Auken E, Sørensen KI (2006) The transient electromagnetic method. In: Kirsch R (ed) Groundwater geophysics: a tool for hydrogeology. Springer, Berlin

Christiansen AV, Auken E, Viezzoli A (2011) Quantification of modeling errors in airborne TEM caused by inaccurate system description. Geophysics 76(1):F43–F52

Cox LH, Wilson GA, Zhdanov MS (2012) 3D inversion of airborne electromagnetic data. Geophysics 77(4):WB59–WB69

Cruz JV, Silva MO (2001) Hydrogeologic framework of Pico Island, Azores, Portugal. Hydrogeol J 9(2):177–189

Cruz JV, Coutinho R, Pacheco D, Cymbron R, Antunes P, Freire P, Mendes S (2011) Groundwater salinization in the Azores archipelago (Portugal). Environ Earth Sci 62(6):1273–1285

Custodio E (2004) Hydrogeology of volcanic rocks. In: Kovalevsky VS, Kruseman GP, Rushton GR (eds) Groundwater studies: an international guide for hydrogeological investigations. UNESCO, Paris, pp 395–425

Custodio E, Lopez GL, Amigo E (1988) Simulation par modèle mathématique de l'île volcanique de Ténériffe (Canaries, Espagne). Hydrogéologie 2:153–167

Debeuf D (2004) Etude de l'évolution volcano-structurale et magmatique de Mayotte (Archipel des Comores, Océan Indien), approche structurale, pétrographique géochimique et géochronologique). PhD thesis of The University of La Réunion, 277 p

d'Ozouville N, Auken E, Sorensen KI, Violette S, de Marsily G (2008) Extensive perched aquifer and structural implications revealed by 3D resistivity mapping in a Galapagos volcano. Earth Planet Sci Lett 269(3–4):517–521

Descloitres M, Ritz M, Robineau B, Courteaud M (1997) Electrical structure beneath the eastern collapsed flank of Piton de la Fournaise volcano, Reunion Island: implications for the quest of groundwater. Water Resour Res 33(1):13–19

Emerick CM, Duncan RA (1982) Age progressive volcanism in the ComoroArchipelago, western IndianOcean and implications for Somali plate tectonics. Earth Planet Sci Lett 60(3):415–428

Farquharson CG, Oldenburg DW (1993) Inversion of time-domain electromagnetic data for a horizontally layered Earth. Geophys J Int 114(3):433–442
Fitterman DV, Deszcz-Pan M (1998) Helicopter EM mapping of saltwater intrusion in Everglades National Park, Florida. Explor Geophys 29(2):240–243
Fitterman DV, Meekes JAC, Ritsema IL (1988) Equivalence behavior of three electrical sounding methods as applied to hydrogeological problems. In: EAGE, 50th annual meeting, The Hague, 1988
Foged N, Auken E, Christiansen AV, Sørensen KI (2013) Test site calibration and validation of airborne and ground based TEM-systems. Geophysics 78(2):E95–E106
Fountain D (1998) Airborne electromagnetic systems – 50 years of development. Explor Geophys 29(2):1–11
Fountain D (2008) 60 years of airborne EM – focus on the last decade. In: Proceedings of the 5th international conference on airborne electromagnetics (AEM2008), Haikko Manor, 28–30 May 2008
Gubbins D (2004) Time series analysis and inverse theory for geophysicists. Cambridge University Press, Cambridge/New York, 272 pp
Henderson A (2007) ParaView guide, a parallel visualization application. Kitware Inc., Clifton Park
Herrera C, Custodio E (2008) Conceptual hydrogeological model of volcanic Easter Island (Chile) after chemical and isotopic surveys. Hydrogeol J 16(7):1329–1348
Izuka SK, Gingerich SB (2003) A thick lens of fresh groundwater in the southern Lihue Basin, Kauai, Hawaii, USA. Hydrogeol J 11(2):240–248
Jørgensen F, Scheer W, Thomsen S, Sonnenborg TO, Hinsby K, Wiederhold H, Schamper C, Burschil T, Roth B, Kirsch R, Auken E (2012) Transboundary geophysical mapping of geological elements and salinity distribution critical for the assessment of future sea water intrusion in response to sea level rise. Hydrol Earth Syst Sci 16(7):1845–1862
Kim Y, Lee K-S, Koh D-C, Lee D-H, Lee S-G, Park W-B, Koh G-W, Woo N-C (2003) Hydrogeochemical and isotopic evidence of groundwater salinization in a coastal aquifer: a case study in Jeju volcanic island, Korea. J Hydrol 270(3–4):282–294
Kirkegaard C, Sonnenborg TO, Auken E, Jørgensen F (2011) Salinity distribution in heterogeneous coastal aquifers mapped by airborne electromagnetics. Vadose Zone J 10(1):125–135
Lénat JF, Fitterman D, Jackson DB, Labazuy P (2000) Geoelectrical structure of the central zone of Piton de la Fournaise volcano (Réunion). Bull Volcanol 62(2):75–89
Lienert BR (1991) An electromagnetic study of Maui's last active volcano. Geophysics 56(7):972–982
Macnae JC, Lamontagne Y, West GF (1984) Noise processing techniques for time-domain EM systems. Geophysics 49(7):934–948
Marquardt DW (1963) An algorithm for least-squares estimation of nonlinear parameters. J Soc Ind Appl Math Control 11(2):431–441
Marquardt DW (1970) Generalized inverses, ridge regression, biased linear estimation and nonlinear estimation. J Soc Ind Appl Math Control 12(3):591–612
Menke W (1989) Geophysical data analysis: discrete inversion theory. Academic, San Diego, 260 pp
Møller I, Verner H, Søndergaard VH, Flemming J, Auken E, Christiansen AV (2009) Integrated management and utilization of hydrogeophysical data on a national scale. Near Surf Geophys 7(5–6):647–659
Munkholm MS, Auken E (1996) Electromagnetic noise contamination on transient electromagnetic soundings in culturally disturbed environments. J Environ Eng Geophys 1(2):119–127
Nougier J, Cantagrel JM, Karche JP (1986) The Comores archipelago in the western Indian Ocean: volcanology, geochronology and geodynamic setting. Journal of African Earth Sciences (1983) 5(2):135–144

Paine JG (2003) Determining salinization extent, identifying salinity sources, and estimating chloride mass using surface, borehole, and airborne electromagnetic induction methods. Water Resour Res 39(3):3-1–3-10

Peterson FL (1972) Water development on tropic volcanic islands. Type example: Hawaii. Ground Water 10(5):18–23

Portniaguine O, Zhdanov MS (2002) 3-D magnetic inversion with data compression and image focusing. Geophysics 67(5):1532–1541

Pryet A, d'Ozouville N, Violette S, Deffontaines B, Auken E (2012) Hydrogeological settings of a volcanic island (San Cristóbal, Galapagos) from joint interpretation of airborne electromagnetics and geomorphological observations. Hydrol Earth Syst Sci Discuss 9 (8):9661–9686

Sab G-A (2012) Data processing of an Airborne Electromagnetic survey in Antarctica. Master thesis made at the Hydrogeogphysics Group, Aarhus University, Aarhus

Schamper C, Auken E, Sørensen KI (2012) A new processing system for very early time SkyTEM101 data. In: ASEG, 22nd international geophysical conference and exhibition, Brisbane, 26–29 Feb 2012

Siemon B, Christiansen AV, Auken E (2009) A review of helicopter-borne electromagnetic methods for groundwater exploration. Near Surf Geophys 7(5–6):629–646

Sørensen KI, Auken E (2004) SkyTEM – a new high-resolution helicopter transient electromagnetic system. Explor Geophys 35(3):191–199

Stieltjes L (1988) Hydrogéologie de l'île volcanique océanique de Mayotte (Archipel des Comores, ocean indien occidental). Hydrogéologie 2:135–151

Teatini P, Tosi L, Viezzoli A, Baradello L, Zecchin M, Silvestri S (2011) Understanding the hydrogeology of the Venice Lagoon subsurface with airborne electromagnetics. J Hydrol 411(3–4):342–354

Thomsen R, Søndergaard VH, Sørensen KI (2004) Hydrogeological mapping as a basis for establishing site-specific groundwater protection zones in Denmark. Hydrogeology 12(5):550–562

Tikhonov AN, Arsenin VY (1977) Solution of ill-posed problems. V.H. Winston and Sons, Washington, DC, 258 pp

Viezzoli A, Christiansen AV, Auken E, Sørensen KI (2008) Quasi-3D modeling of airborne TEM data by spatially constrained inversion. Geophysics 73(3):F105–F113

Vittecoq B, Deparis J, Auken E, Nehlig P, Perrin J, Puvilland P, Martelet G (2011a) Buried valleys revealed by helicopter borne transient electromagnetic and hydrogeological implications: example of the volcanic island of Mayotte. In: 2011 GSA annual meeting, Minneapolis, 9–12 Oct 2011

Vittecoq B, Jaouen T, Deparis J (2011b) Programme de recherche et d'exploitation des eaux souterraines de Mayotte – 5ème campagne de forage à Mayotte. Révision des implantations. REPORT/RP-60035-FR, BRGM, Orléans, France

Ward SH, Hohmann GW (1988) Electromagnetic theory for geophysical applications. In: Nabighian MN (ed) Electromagnetic methods in applied geophysics, vol 1. SEG, Tulsa, pp 131–311

Werner AD, Bakkerd M, Posta VEA, Vandenbohede A, Lua C, Ataie-Ashtiania B, Simmonsa CT, Barrye DA (2012) Seawater intrusion processes, investigation and management: recent advances and future challenges. Adv Water Resour 51, 24 pp

Witherly K, Irvine R, Morrison E (2004) The Geotech VTEM time domain helicopter EM system. In: ASEG extended abstracts, 17th international geophysical conference and exhibition, Sydney, 15–19 Aug 2004

Yang D, Oldenburg DW (2012) Three-dimensional inversion of airborne time-domain electromagnetic data with applications to a porphyry deposit. Geophysics 77(2):B23–B34

Chapter 8
Geophysical Investigations of Saltwater Intrusion into the Coastal Groundwater Aquifers of Songkhla City, Southern Thailand

Helmut Duerrast and Jiraporn Srattakal

Abstract Saltwater intrusion into coastal aquifers is an emerging problem for many cities located along coastlines as they are dealing with an increase in the population numbers. The Bo Yang District of Songkhla Province, comprising the City of Songkhla, one of the main provincial capitals in Southern Thailand, is facing a similar problem, although it is already decades old. The city, abound 10 km^2 in area, is bounded to the east by the Gulf of Thailand and to the west by the seasonal saline Lower Songkhla Lake. Geophysical investigations were carried out in order to delineate the saltwater intrusion utilizing widely available equipment. Four seismic refraction and 6 seismic reflection survey lines were acquired, as well as 12 vertical electrical sounding surveys were done mainly in the northern and western part of the city. All methods require several 100 m long straight lines with ground access. In the densely populated city these were mainly found along streets, on football fields, at the beaches, and also on a military airfield. Additionally, data from seven drilling locations provided lithology data, mainly shallow boreholes. Further, for several wells screen depth intervals, chloride and total dissolved solids (TDS) concentrations were known. From all available results three cross sections were drawn, two in EW direction perpendicular to the beaches and one in approximately NS direction crossing the city. In each of the cross sections four main resistivity layers were outlined. A near surface higher resistivity layer can be related to top soil or beach sand. The second later shows medium resistivity values, comprising layers of sand and clay, partially saturated from rainwater infiltration.

H. Duerrast (✉)
Geophysics Research Center, Prince of Songkla University, HatYai, Songkhla 90112, Thailand

Department of Physics, Faculty of Science, Prince of Songkla University, HatYai, Songkhla 90112, Thailand
e-mail: helmut.j@psu.ac.th

J. Srattakal
Department of Physics, Faculty of Science, Prince of Songkla University, HatYai, Songkhla 90112, Thailand

C. Wetzelhuetter (ed.), *Groundwater in the Coastal Zones of Asia-Pacific*, Coastal Research Library 7, DOI 10.1007/978-94-007-5648-9_8,

The related groundwater of this unconfined aquifer has relatively low TDS values. The third layer has resistivity values of about 2–20 Ωm with TDS values of the groundwater of about 2,300–8,200 mg/L. This resistivity layer also comprises different geological layers, sand, clay and gravel layers, likely with brackish to saline water. The fourth resistivity layer shows resistivity values in general around 140 Ωm. For this layer no TDS are available, but the higher resistivity values indicate sand and gravel sediments with minor clay layers and saturated with freshwater. However, no further information is available for this layer. The cross sections further show that the subsurface layers show some topography which is likely to be related to hard rock outcrops, in the south there are granite hills, whereas in the northern part hornfels hills separate the aquifers. For any further groundwater development deeper boreholes into the third resistivity layer might yield the desired freshwater. This process must ensure that during any exploration and exploitations efforts the deeper aquifer is not contaminated by the saltwater intrusion into the second aquifer. However, since some decades a pipeline from a reservoir further south in Songkhla Province is supplying the people in Bo Yang District with tap water.

8.1 Introduction

In many countries around the world coastal zones contain some of the most densely populated areas as they often present the best conditions for livelihood and productivity. However, these regions also face many hydrological hazards; for example, flooding due to cyclones and wave surge, and drinking freshwater scarcity due to problems of saltwater intrusion (e.g. Bhosale 2000). The natural balance between freshwater and saltwater in coastal aquifers can be disturbed by excessive groundwater withdrawal or other activities that can lower the groundwater level significantly. This will reduce the fresh groundwater flow to coastal waters and this then will cause marine saltwater to intrude into coastal aquifers. In many regions groundwater pumping is the primary cause of saltwater intrusion along the coasts; however, the lowering of the water table by drainage canals also can lead to saltwater intrusion.

Saltwater can contaminate a freshwater aquifer through several possible pathways, for example lateral intrusion from the ocean, upward intrusion from deeper, more saline zones of a groundwater system, and downward intrusion from coastal waters. Saltwater can move into an unconfined aquifer from the ocean and into the shallow part of the top confined aquifer from a major bay. The freshwater-saltwater interfaces at the seaward boundary of each of the confined aquifers can also move landward as saltwater is drawn inland from offshore areas (e.g. Barlow 2003).

Saltwater intrusion can reduce the freshwater storage in a coastal aquifer and can result in the abandonment of existing freshwater wells when the concentrations of the dissolved ions are exceeding drinking water standards. The severity of saltwater intrusion can vary among localities and hydrogeological settings. In many regions,

the area contaminated by saltwater is limited to a small parts of the aquifer and has only little effect on wells pumped for groundwater supply (e.g. Barlow 2003).

There are a variety of geophysical techniques that are usually applied in groundwater investigations, but electrical and seismic methods are particularly useful in coastal environments (see Barlow 2003). Electrical methods have been widely used in coastal environments because of their ability to detect an increase in the conductivity of an aquifer that result from increases in pore-water conductivity (Schoen 1996). The electrical conductivity of an aquifer is controlled primarily by the amount of pore space of the aquifer and by the salinity (or TDS) of the water in the pore space. An increase in either the porosity or the concentration of dissolved ions result in an increase of the conductivity of the groundwater. As seawater has a high concentration of dissolved ions, its presence in a coastal aquifer can be inferred from measurements of the spatial distribution of electrical conductivity. Seismic methods cannot detect saltwater, but can be used to delineate the distribution of geologic units within an aquifer that affect the distribution and movement of saltwater (e.g. Ward 1990; Sikandar et al. 2010).

8.2 Study Area

The Kingdom of Thailand has more than 3,200 km of coastline, mainly in the southern part along the northern part of the Malay Peninsula, with the Andaman Sea in the West and the Gulf of Thailand in the East (Fig. 8.1). Major provincial capitals there can be found near shorelines; for example Songkhla, which is located at the Gulf of Thailand side. Songkhla's original name means 'the city of lions' related to two lion-shaped islands located about 1.5–3.5 km from the city. However, in contrast to most other provinces in Thailand, the provincial capital is not the largest city in Songkhla Province. Hat Yai City, around 25 km further south, with a population of about 360,000, is considerably larger. The main regional international airport is located near Hat Yai, as well as the main commercial places can be found in and nearby the city. With the Prince of Songkla University, the main campus of the largest regional university in Southern Thailand is located at the outskirts of Hat Yai, which was founded more than 45 years ago.

The Bo Yang District of Songkhla Province (Fig. 8.2), with a population of more than 76,000 people, comprises the main city area as well as main provincial administration offices, and it is the base for major army and navy units, including a military airfield. It is bounded by the Gulf of Thailand to the east and the Songkhla Lake in the west, which has an opening to the Gulf of Thailand. The salinity of the lower part of the lake, bounded to the east by the Bo Yang District, is seasonally changing from almost freshwater to almost marine water conditions.

Most of the area of Bo Yang District is coastal plain, an area of about 10 km^2. It is enclosed by latitude 7.175–7.230ºN and longitude 100.577–100.623ºE. The shape of the area is a long narrow peninsula along SSE to NNW into the sea. Its elevation is approximately 1–4 m above mean sea level. Two small hills are located

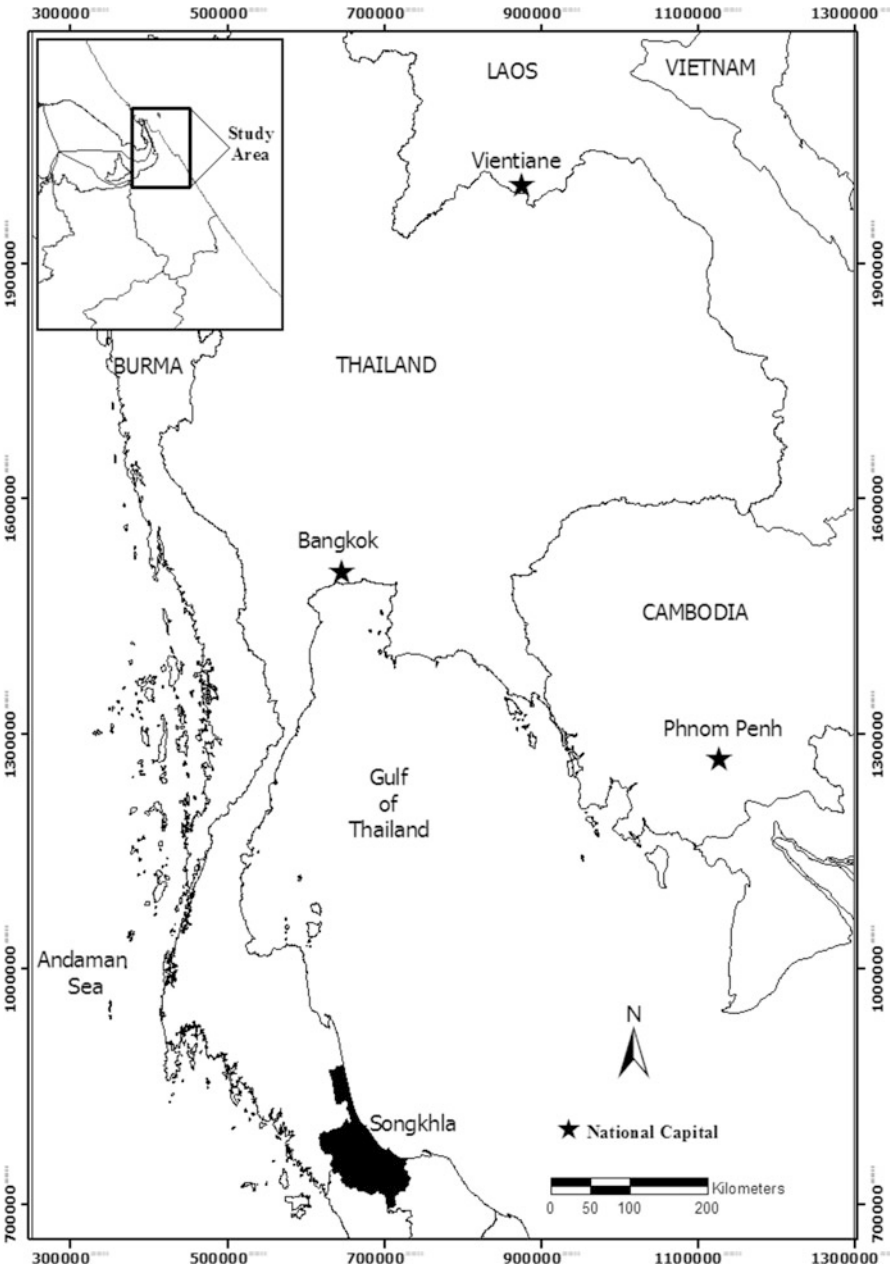

Fig. 8.1 Thailand and the location of the study area

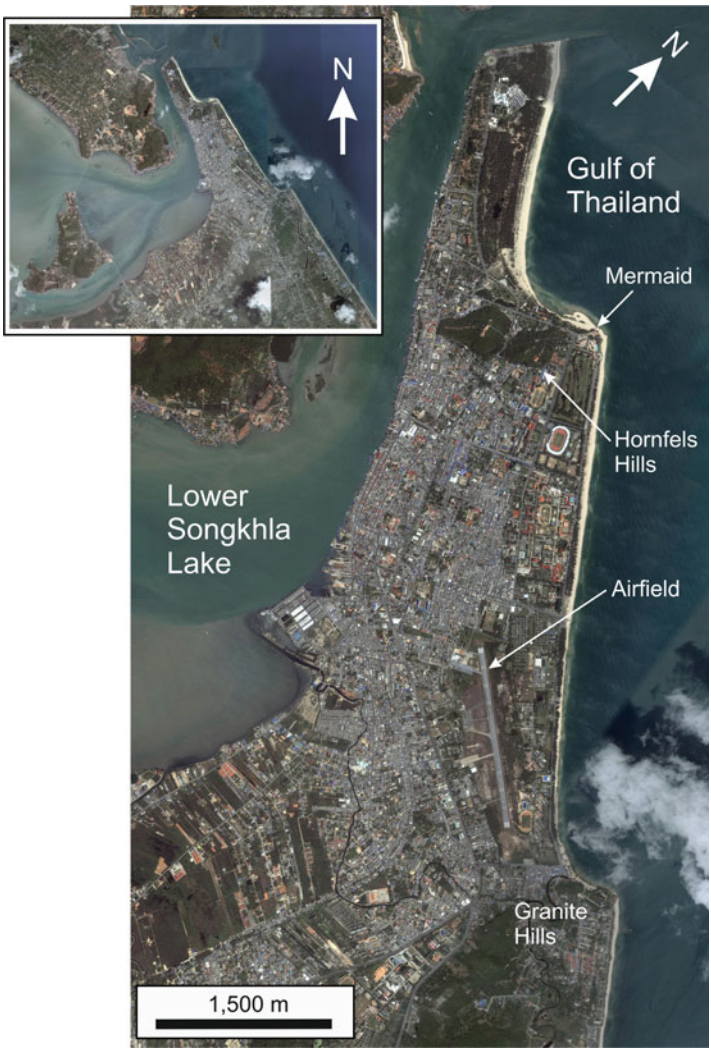

Fig. 8.2 Detailed map of the study area, Bo Yang District, Songkhla Province. Courtesy of GoogleEarth™

in the northern part, Khao Noi and Khao Tang Kuan, with a height from sea level of about 51 and 94 m, respectively. The mountains comprise of dark grey to black very hard hornfels. Outcrops show thin- to medium bedding with slight folding (Ridd 2007). On one of the shallow outcrops found at Samila Beach is the famous mermaid, now a symbol of Songkhla Province. The hornfels occurrence itself is related to contact metamorphisms due to granitic intrusions in and around Songkhla City, for example the hills south of the military airport in Bo Yang District.

Bo Yang District was chosen as the study area for the geophysical investigations; however it can serve as an example for cities with similar problems regarding saltwater intrusion into coastal aquifers.

8.3 Methodology

The study comprises mainly geophysical methods to delineate the subsurface groundwater bearing layers, seismic reflection and refraction methods as well as electrical vertical sounding (VES) method. The equipment for these methods and the related knowledge is widely available in Thailand. Other methods of choice would be electromagnetic ones, but they are not widely available as the ones mentioned above. All methods applied in this study need direct ground access along a straight line, which can be of several 100 m for the VES method. In an urban and densely populated area like Songkhla City these requirements are difficult to fulfill. Therefore, the specific measurements sites were parallel to the beaches, parallel to roads, and at football stadiums (see Fig. 8.3). The airfield in the city also provided a suitable site, with permission from the relevant navy authorities.

The VES method aims to identify the depth of the layers with different resistivity values, which are related to the composition and the fluid content of the sediment (see Table 8.1). Therefore, VES also allows for similar lithology the separation between groundwater layers containing fresh, brackish or saltwater. Saltwater saturated sand has relatively low resistivity values, as the saltwater has relatively high TDS concentrations due to the dissolved Na^+ and Cl^- ions (see Table 8.1). However, saturated clays also can exhibit relatively low resistivity values, due to water trapped between the clay minerals and the presence of a significant negative surface charge (e.g. Patchett 1982).

Seismic P–wave refraction measurements were carried out in order to determine the depths and thicknesses of shallow layers. The additionally gained P–wave velocities of the layers provide constrains of their composition (see Table 8.2). Seismic P–wave reflections surveys were done to delineate deeper layer boundaries, especially between different compositions, where the reflectivity contrast at the boundary is significant. For both seismic surveys following equipment was used, a Geometrics SmartSeis^{TM} S12 Seismograph, 14-Hz geophones (vertical), a roll-along switch, and sledgehammer striking a steel plate as a seismic source.

8.3.1 Seismic Refraction

Four seismic refraction survey lines were acquired in Bo Yang District. Figure 8.4 shows the seismic refraction survey stations of each site. There are Wachiranukul School (SKR01), Mahavajiravudh School (SKR02), Chalathat Road (SKR03), and

Fig. 8.3 Photos of the geophysical fieldwork. (**a**) Mahavajiravudh School (SKR02), (**b**) Airfield, in the back the granite hills (SKV07), (**c**) Chalathat Road (SKR03), (**d**) Northern part at the beach (SKV12), (**e**) Rajamangala University of Technology, Srivijaya (SKL04), (**f**) Samila Beach, in the back the mermaid on hornfels (SKR04)

Samila Beach (SKR04). Table 8.3 shows the seismic refraction data acquisition. SIP Software by a registered trademark of Rimrock Geophysics Inc has been used for data processing of seismic refraction data. An initial model was created based on the traveltime-distance graph. The program determined the velocity of each layer. The depth of each layer beneath each geophone was determined. These depths were

Table 8.1 Resistivity values related to sediments of different composition and fluid content

Resistivity (Ωm)	Possible lithologies and fluids
0.5–2.0	Porous sediments saturated with highly saline water; TDS concentrations of about 20,000 mg/L or greater
2.0–4.5	Probably sediments saturated with saline water with TDS concentrations of about 10,000 mg/L
4.5–10.0	Sandy sediments saturated with brackish water (about 10,000–1,500 mg/L TDS, respectively) or maybe clays
10.0–15.0	Probably sandy sediments rich in clay or possibly sand and gravel deposits saturated with brackish water (about 5,000–1,500 mg/L TDS, respectively)
15.0–30.0	Sand and gravel layers with some clay layers and likely to be saturated with poor to better quality water (1,500–700 mg/L TDS, respectively)
30.0–70.0	Probably sand and gravel sediments with minor clay layers and saturated with freshwater (only a few 100 mg/L TDS)
70.0–100.0	Sand, gravel, no clay, good quality fresh water
>100.0	Coarse sand, gravel, no clay, very good quality fresh water

Modified from Zohdy et al. (1993)

Table 8.2 P–wave velocities in selected earth materials

Material	V_P (m/s)
Air	330–350
Water	1,450–1,530
Soil	100–500
Sand (loose)	200–2,000
Sand (dry, loose)	200–1,000
Sand (water saturated, loose)	1,500–2,000
Sandstone	1,400–4,500
Clay	1,000–2,500
Sand and gravel (wet)	500–1,800
Sand and gravel (dry)	400–1,500
Soil and sand	250–600
Limestone	3,000–4,800
Granites	4,500–5,500

After Schoen (1996)

then interpolated between adjacent geophone positions. The program assumed that each layer encountered was horizontally continuous and that there were no lateral changes in velocity within any layer (Kutrubes et al. 2002).

8.3.2 Seismic Reflection

Six seismic reflection survey lines were acquired in Bo Yang District. Figure 8.4 shows the seismic reflection survey stations of each site. They are Wachiranukul School (SKL01), Mahavajiravudh School (SKL02), Chalathat Road (SKL03),

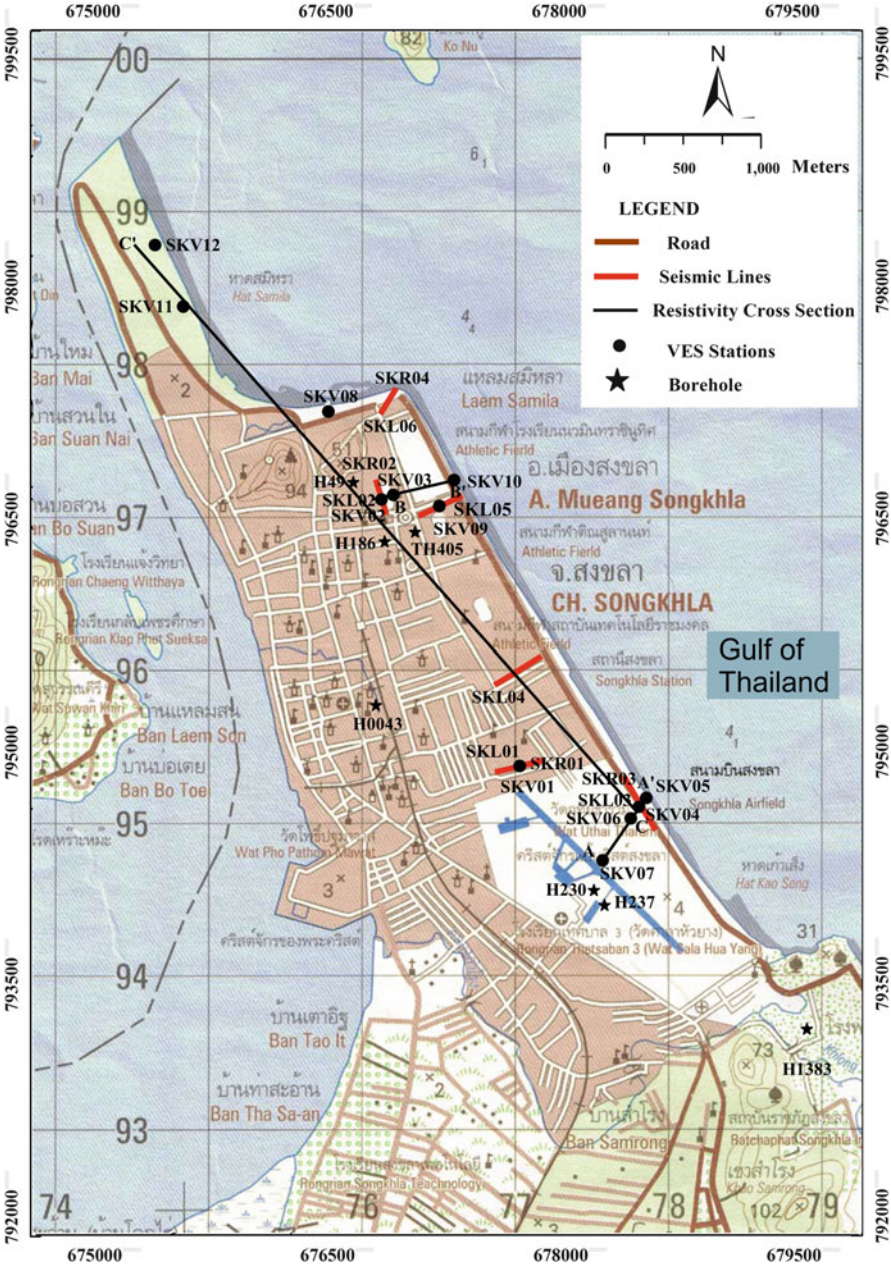

Fig. 8.4 Locations of the geophysical surveys and wells with lithology information. Seismic refraction (SKR), seismic reflection (SKL) and vertical electrical sounding measurements (SKV)

Table 8.3 Seismic refraction data acquisition parameters

Acquisition parameter	SKR01	SKR02	SKR03	SKR04
Shot spacing (m)	18	18	18	12
Geophone spacing (m)	3	3	1.5	1
Shots stacked per shot record	10	10	10	10
Record length (ms)	256	256	512	512
Sampling interval (ms)	0.125	0.125	0.25	0.25
Survey length (m)	40	70	40	25
Line direction	N072E	N015W	N030W	N040E

Table 8.4 Seismic reflection data acquisition parameters

Acquisition parameter	SKL01	SKL02	SKL03	SKL04	SKL05	SKL06
Shot interval (m)	3	3	1.5	1.5	1.5	1
Geophone interval (m)	3	3	1.5	1.5	1.5	1
Optimum offset (m)	27	20.5	15	25	15	10
Shots stacked per shot record	10	10	10	20	15	10
Record length (ms)	256	256	512	512	256	512
Sampling interval (ms)	0.125	0.125	0.25	0.25	0.125	0.25
Shot-receiver configuration	Off-end	Off-end	Off-end	Off-end	Off-end	Off-end
Line direction	N072E	N015W	N030W	N050E	N060E	N040E
Survey length (m)	108	122.5	84	179	174	44

Rajamangala University of Technology Srivijaya (SKL04), Tinsulanonda Stadium (SKL05) and Samila Beach (SKL06). Table 8.4 shows the seismic reflection data acquisition parameters. The first step of the survey was to find the optimum offset in order to obtain the reflected wave, which should be clearly separated from the refracted wave and the airwave arrival time in the record data. A flow chart in Fig. 8.5 shows the main processing steps.

The data were recorded with 16-b precision and 100 dB dynamic ranges. First, the information such as field record number, shot stations, receiver stations, offset and CDP (common depth point) were added. Then trace editing was carried out, with bad traces killing, first arrival muting, and surgical muting. Traces were then sorted into groups, or gathers, with all traces in a given type of gather having a certain common aspect, here the common depth point gather. In the following velocity analysis was done; first, velocity picking provides a first guess approximation of the stacking velocity of the reflections; second, a constant velocity stack (CVS) was used to pick the velocity function, which indicates the best stack section. After filtering amplitudes were enhanced during the scaling process. The normal moveout (NMO) velocity is then estimated and travel times are corrected to remove the influence of offset. Traces in the NMO corrected gather then are summed to obtain a stack trace at the particular common midpoint location.

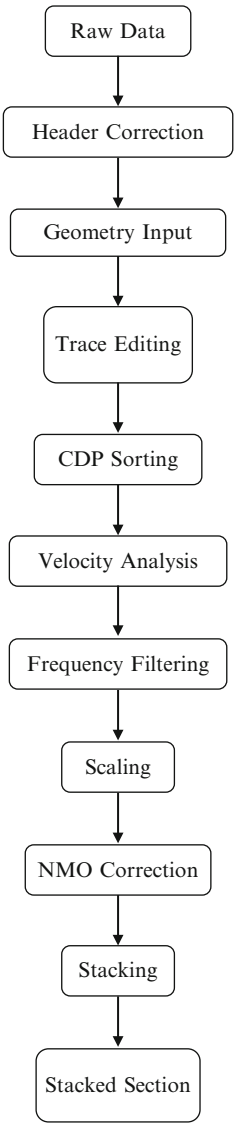

Fig. 8.5 Flowchart of the main seismic data processing steps

8.3.3 Vertical Electrical Sounding Method

In this work, vertical electrical sounding with Schlumberger electrode array was carried out. The apparent resistivity (ρ_a) of the Schlumberger array can be determined from the following equation

$$\rho_a = \frac{\pi(L^2 - l^2)}{2l} \cdot \left(\frac{V}{I}\right) \tag{8.1}$$

where L is half current electrode spacing [m], l is half potential electrode spacing [m] and V/I is reading taking from resistivity meter [ohm]. The VES measurements were conducted at 12 VES stations in Bo Yang District using ABEM Terrameter SAS 1000. All VES stations were measured using the Schlumberger array at half current electrode spacing (AB/2) of 1.5, 2, 3, 4.5, 7, 10, 15, 20, 30, 45, 60, 90, 150, 225, 350 and 500 m. Each survey increased the half potential electrode spacing (MN/2) from 0.5 to 2, 6, 10, 20, 30 and 50 m. The VES data were analyzed by plotting measured apparent resistivity values versus electrode spacing. These apparent resistivity curves were correlated to theoretical model curves in order to determine the subsurface stratigraphy. In this study, the resistivity data were modeled using the IPI2WIN program to obtain a one-dimensional inverse model. The resistivity value of different layers and their corresponding thicknesses were reproduced by a number of iterations until the model parameters of all the sounding curves were resolved with reasonable minimal root mean square errors.

8.3.4 Borehole Data

Some borehole data were available to calibrate the geophysical data interpretation (see Table 8.5, Fig. 8.6). These data came from the Department of Groundwater Resources (DGR), Thailand, and the Provincial Groundwater Office, Songkhla Province. There are seven drilling locations in the study area with available lithology data, but they are mainly shallow boreholes. Further, most of the data are older, up to 40 years, as recently not much drilling has been carried in the study area. Further, for several well screen depth intervals, chloride and TDS concentrations are known (see Table 8.5, Fig. 8.6).

8.4 Results

In most areas a seismic refraction (SKR), seismic reflection (SKL) and a vertical electrical sounding measurement (SKV) were carried. Figure 8.7a–d shows the results from the surveys at Wachiranukul School north of the airfield (Site 1). All three survey lines, SKR1, SKL1, and SKV1 were parallel oriented (see Fig. 8.7d). The first layer with 3 m thickness and almost 600 Ωm resistivity represents a cultural layer (football field) and the top soil. Below is sand with a moderate resistivity and a higher P–wave velocity. The velocity increase at about 9 m depth correlates well with the resistivity decrease to about 8 Ωm, which is likely to be sandy sediments saturated with brackish water or clay layers, or a combination of both. The seismic reflection shows clear reflectors at about 25 and 35 m depth. These are likely clay–sand interfaces. An increase in the resistivity below this layer can be observed (21 Ωm).

Table 8.5 Available well data, with well name, screen interval, chloride (Cl) and (TDS) concentration

Well name	Screen interval (m)	Cl (mg/L)	TDS (mg/L)
H230	3–6		
H49	6–12		
H186	6–12		
H1383	6–12		
H1506[a]	8–12	110	516
TH318[a]	8–16		
TH280[a]	8–22.5	230	670
H1502[a]	12–16		
H1507[a]	12–16		
TH262[a]	12–20, 26–32	42	216
H237	12–42		
H44[a]	15–22.5		
H43	16.5–25.5		
TH405	18–22, 26–28		
TH201[a]	18–26		
TH202[a]	19–27		
H1503[a]	25–28		
TH263[a]	28–32	2,400	4,950
H1504[a]	32–40		
TH281[a]	40–44	1,400	2,330
TH261[a]	40–48	1,100	
TH204[a]	41–45		
TH203[a]	44–50	420	2,560
H1505[a]	48–52	4,800	8,190
H1780[a]	92–106		

See also Fig. 8.6

[a]Wells with no lithology information

The survey data from Mahavajiravudh School (Site 2) exhibit a similar picture than at Site 1 (Fig. 8.8). Here two sounding profiles were carried out (SKV02, SKV03) with different AB/2. The shorter SKV03 misses out the resistivity increase at depth as seen in most of the VES profiles. Therefore a minimum AB/2 of 100 m was recommended for this area. Below high resistivity near surface layers the resistivity decreases to 8.6 Ωm and the increases to 143 Ωm at about 40 m depth. The top of the low resistivity layer (15–19 m) matches not perfectly with an increase in the P–wave velocity from 910 to 1,490 m/s (10–12 m). The low resistivity reflects probably a combination of sandy sediments saturated with brackish water and clay layers.

Four resistivity sounding surveys (SKV04, SKV05, SKV06, and SKV07) as well as a seismic refraction (SKR03) and reflection (SKL03) survey were carried out at Site 3, parallel to the beach and Chalatat Road, and parallel to the airfield (Fig. 8.9). All sounding curves exhibit a similar pattern, with a high (top soil) or very high resistivity (dry beach sand, dry sand layer as drainage for the airfield) near the

Fig. 8.6 Locations of available boreholes (*Yellow* = Cl^- (shown here), TDS value (not shown, see Table 8.5) and screen interval; *Red* = lithology information; *Blue* = only screen interval)

surface. The resistivity decreases down to 4–6 Ωm and then increase again at a depth of about 30–60 m to values of around 150 Ωm. Near the beach this last value is lower (SKV05, Fig. 8.9b). The top of the low resistivity layer corresponds with an increase in the P–wave velocities to 1,200 m/s at around 8 m (to 19 m). A clear seismic reflector at around 30 m correlates well with the increase in resistivity (SKV04, SKV06).

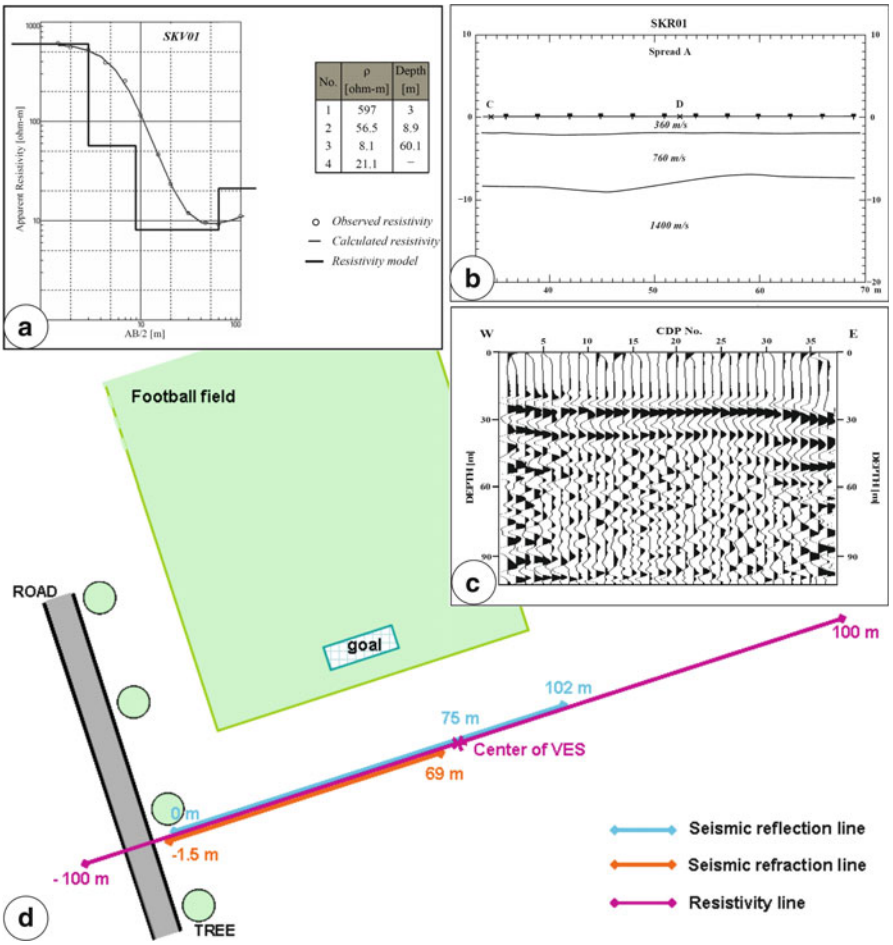

Fig. 8.7 Geophysical results at Wachiranukul School. (**a**) SKV01, (**b**) SKR01, (**c**) SKL01, (**d**) survey overview

8.4.1 Cross Sections

Three cross sections, A–A′, B–B′, and C–C′, are drawn as shown in Figs. 8.10, 8.11 and 8.12 using the available data, with the orientation of the cross sections shown in Fig. 8.4. Cross section A–A′ and B–B′ are oriented perpendicular to the beach towards the Gulf of Thailand in the eastern part of Bo Yang District, whereas C–C′ is crossing the city from NNW to SSE.

In each of the cross sections four main resistivity layers are outlined. A near surface higher resistivity layer can be related to top soil or beach sand. The second layer shows medium resistivity values with about 30–160 Ωm. This resistivity layer comprises layers of sand and clay, partially saturated from rainwater infiltration.

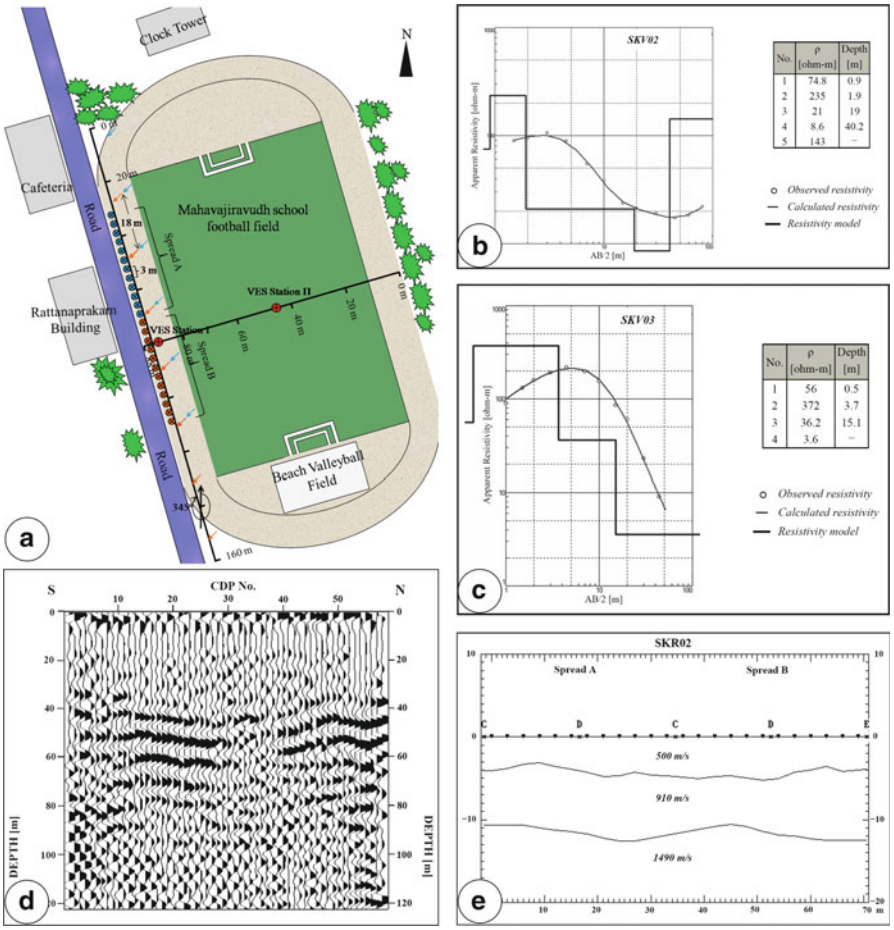

Fig. 8.8 Geophysical results at Mahavajiravudh School. (**a**) Survey overview, (**b**) SKV02, (**c**) SKV03, (**d**) SKL01, (**e**) SKR01

The related groundwater has relatively low TDS values with a few 100 mg/L. A higher number of very shallow wells are utilizing this water from the unconfined aquifer (see Table 8.5). The third layer has resistivity values of about 2–20 Ωm with TDS values of the groundwater of about 2,300–8,200 mg/L (see Table 8.5). In cross section A–A′ well TH281 shows 1,400 m/L chloride concentration and 2,330 mg/L TDS (Fig. 8.10, Table 8.5). This resistivity layer also comprises different geological layers, sand, clay and gravel layers, but the resistivity and TDS data indicate that in the sand and gravel layers the pores are filled with brackish to saline water. Clay itself can have very low resistivity values (Table 8.5). The fourth resistivity layer shows resistivity values of 20–345 Ωm, with several surveys showing data about 140 Ωm. For this layer no TDS are available, although the well H1780 was drilled in 2002. The higher resistivity values indicate that there is no salt or brackish water

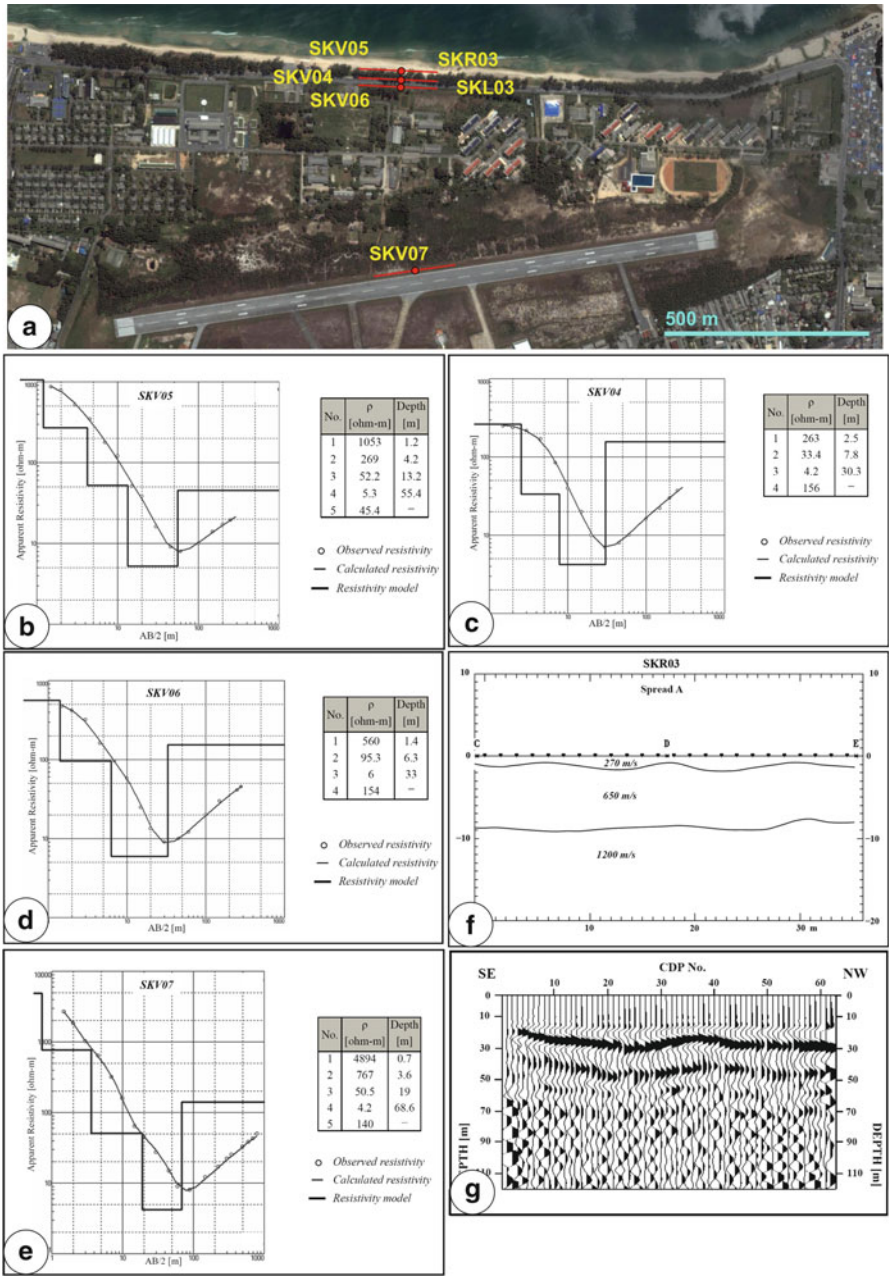

Fig. 8.9 Geophysical results at Chalatat Road. (**a**) Survey overview, (**b**) SKV05, (**c**) SKV04, (**d**) SKV06, (**e**) SKV07, (**f**) SKR03, (**g**) SKL03

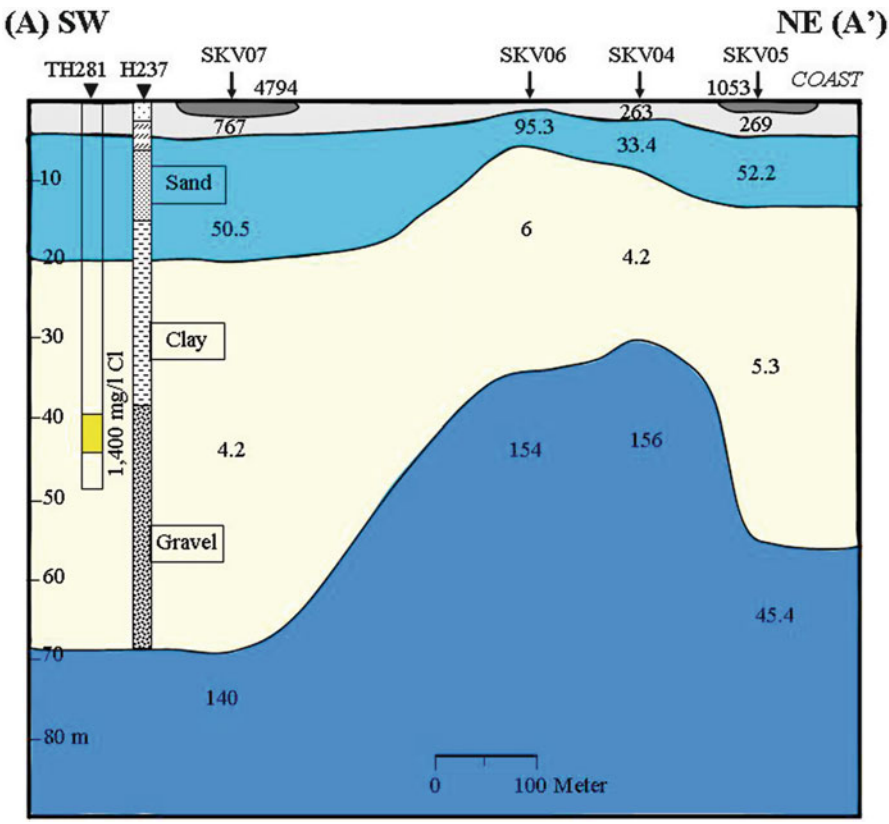

Fig. 8.10 Schematic cross section of the subsurface layers along A–A′

present, although some values indicate poor groundwater. They are more an indication for sand and gravel sediments with minor clay layers and saturated with freshwater. No further information is available here.

Cross section A–A′ shows some morphology of the resistivity layer depth with an increase under SKV04 and SKV06. At cross section B–B′ the thickness of the third resistivity layer is increasing towards the ocean. The longer C–C′ section reveals that the low resistivity layer is separated by the E–W trending hornfels rocks into a northern and southern part. In the northern part the bottom of the salty low resistivity layer is much deeper, about 80 m, than in the southern part, about 30–60 m. The topography in of the resistivity layers in the southern part indicates by section A–A′ and C–C′ might be related to possible deeper hard rock topography of granitic rocks in the south and the hornfels in the north, which is not revealed in this study. As the results have shown here the topography of the subsurface layers have an impact on the saline water intrusion into the coastal aquifers.

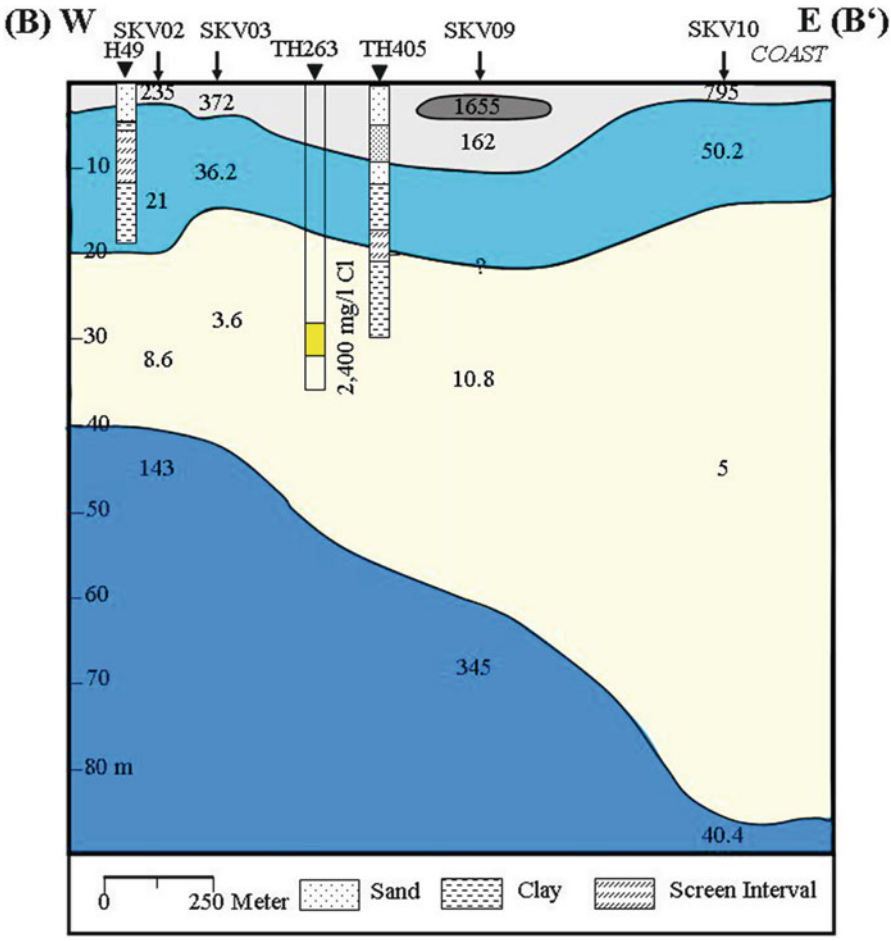

Fig. 8.11 Schematic cross section of the subsurface layers along B–B′

8.5 Conclusion

An extensive geophysical investigation program has been carried out in Songkhla's Bo Yang District in order to delineate saltwater intrusion into the coastal aquifers utilizing mainly widely available methods, seismic refraction and reflection, and vertical electrical sounding method. All methods used in this study require longer (several 100 m) straight lines with ground contact. Even in densely populated areas, like the Yang District, they are possible to find, e.g. football field, and can be utilized for the purpose. The integration of all available data is needed for the interpretation of the geophysical survey results, including surface geology, lithology and screen data from boreholes. Following conclusion can be drawn for the Bo Yang District in Songkhla Province.

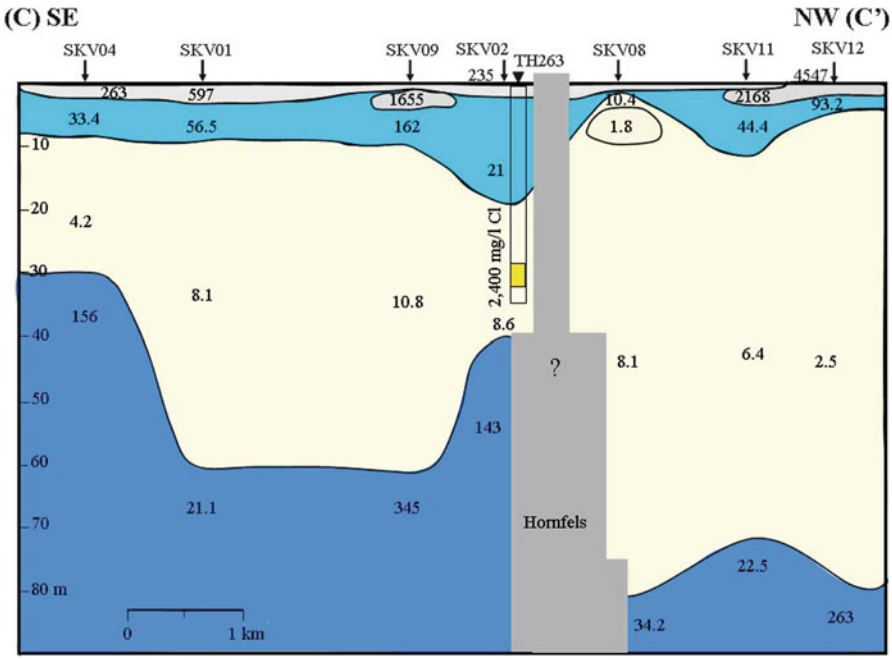

Fig. 8.12 Schematic cross section of the subsurface layers along C–C′

- The subsurface can be divided into three resistivity layers, which represent a combination of sand and gravel aquifers and clay layers. However, the overall resistivity values for each layer together with sparsely available borehole data provide an estimate for aquifer salinity.
  - The first resistivity layer has a depth between 2 and 10 m. It comprises an unconfined aquifer (sand type); the very low velocity near the surface layer indicates top soil or beach sand (dry, loose). The quality of groundwater within the first aquifer was identified to be intermediate to good quality fresh water.
  - The second resistivity layer has a depth between 20 and 50 m (south) to 80 m (north). It comprises a confined aquifer (sand, clay type), which shows intrusion of saline water. The quality of groundwater within the second aquifer was identified to be brackish to saline water.
  - It seems to be likely that the first and second aquifer is separated by a thicker clay layer.
  - The third resistivity layer is below 50–80 m. It is a confined aquifer (sand, clay type). The quality of the groundwater within the third aquifer is likely to be fresh water, however inferred only from the resistivity values.
- For any further groundwater development deeper boreholes into the third resistivity layer might yield the desired freshwater. This process must ensure that

during any exploration and exploitations efforts the deeper aquifer is not contaminated by the saltwater intrusion into the second aquifer. However, no urgency is required as since some decades a pipeline from a reservoir further south in Songkhla Province is supplying the people in Bo Yang District with tap water.

References

Barlow PM (2003) Groundwater in freshwater–saltwater environments of the Atlantic coast. Circular 1262. US Department of Interior, US Geological Survey, Reston. 90 p

Bhosale DD (2000) Simulation of seawater intrusion for Cochin coast (Ernakulam District). M.Tech. dissertation, Centre for Environmental Studies, Department of Civil Engineering, K.L.E. Society's College of Engineering and Technology, Belgaum

Kutrubes D, Zhang J, Hager J (2002) Conventional processing techniques and nonlinear refraction traveltime tomography for imaging bedrock at an Eastern Massachusetts coastal site. GeoTomo LLC, Louisville

Patchett JG (ed) (1982) Shaly sand, reprint volume. Society of Professional Well Log Analysts (SPWLA), Houston

Ridd MF (2007) A geological transverse across peninsular Thailand. J Geol Soc Thail Spec Ed 1:1–48

Schoen J (1996) Physical properties of rocks: fundamentals and principles of petrophysics. Handbook of geophysical exploration, seismic exploration, vol. 18 (series eds Helbig K, Treitel S). Pergamon Press/Elsevier, Oxford

Sikandar P, Bakhsh A, Arshad M, Rana T (2010) The use of vertical electrical sounding resistivity method for the location of low salinity groundwater for irrigation in Chaj and Rachna Doabs. Environ Earth Sci 60:1113–1129

Ward SH (ed) (1990) Geotechnical and environmental geophysics, vols I–III, Investigations in geophysics 5, Society of Exploration Geophysicists, Tulsa

Zohdy A, Martin P, Bisdorf RA (1993) A study of seawater intrusion using direct-current sounding in the southeastern part of the Oxnard plain, California. U.S. Geological Survey, Reston, 139 p

Chapter 9
Three-Dimensional Seawater Intrusion Modelling of Uley South Basin, South Australia

Adrian D. Werner and Le Dung Dang

Abstract Groundwater in the Uley South basin is a vital source of water supply in the Eyre Peninsula, providing approximately 70 % of the region's reticulated water. The groundwater resources are at risk of seawater intrusion given that the aquifer is in direct contact with the sea, and that a general lowering of hydraulic heads has occurred over the past two decades. Seawater intrusion has not been investigated thoroughly in Uley South basin; a similar situation for many of Australia's coastal aquifers. This study develops a three-dimensional seawater intrusion model of Uley South basin using the code MODHMS. The modelling simulates for the first time the current extent of seawater in the aquifer, the temporal salinity variability, and the susceptibility of the aquifer to seawater intrusion, and as such, the model is a significant step forward beyond previous modelling attempts, providing important insights into salinity distributions and salinity mobility. While it is limited by the available information at the time, comparisons with alternative attempts at salinity measurements (e.g. an AEM survey) show a relatively close match between simulated and observed salinities; an encouraging result given well-documented uncertainties in seawater intrusion modelling. Simulations explore the effects of alternative pumping regimes, reduced recharge, and seasonality and other temporal variability effects on seawater intrusion that cannot be assessed using other methods. The impacts of pumping and recharge changes under climate variability are distinguished; both forms of aquifer stress potentially impact on heads and salinities to somewhat similar extents. The ability of the system to recover from long-term pumping is also assessed. At the basin scale, historical changes in the

A.D. Werner (✉) • L.D. Dang
National Centre for Groundwater and Research and Training, Flinders University, GPO Box 2100, Adelaide, SA 5001, Australia

School of the Environment, Flinders University, GPO Box 2100, Adelaide, SA 5001, Australia
e-mail: adrian.werner@flinders.edu.au

C. Wetzelhuetter (ed.), *Groundwater in the Coastal Zones of Asia-Pacific*, Coastal Research Library 7, DOI 10.1007/978-94-007-5648-9_9,

position of the freshwater-seawater interface are mostly localised due to the shape of the aquifer near the coastline (i.e. basement sloping towards the sea). However, the model predicts that some near-coastal piezometers may show increasing salinity trends in the future if current pumping practices continue, and in particular if recharge diminishes under climate change. A comparison between highly dynamic and averaged-stress conditions demonstrates that seasonality is a minor controlling factor in seawater intrusion trends. Aquifer recovery times exceed the periods during which the pumping stresses that induce seawater intrusion are applied. This occurs because cycles of pumping and recovery widen the transition zone between freshwater and seawater, and a large mass of salt remains in the aquifer even after an extensive recovery period.

9.1 Introduction

Seawater intrusion (SWI) is defined as the landward movement of the seawater-freshwater interface (Freeze and Cherry 1979) and is known to be a widespread problem in many coastal aquifers around the world. In Australia, SWI poses a significant threat to freshwater supplies given the density of the population residing in coastal areas. However, assessing the current state of SWI in many of Australia's coastal aquifers remains a challenge (Werner 2010b). A limited number of Australian coastal groundwater systems have been investigated thoroughly (e.g. the Pioneer Valley, the Burnett basin, and the Lower Burdekin basin; Werner and Gallagher 2006; Liu et al. 2006; Narayan et al. 2007; Werner 2010b), highlighting the need for more comprehensive studies assessing Australian occurrences of SWI. The present study is designed as a first attempt at using a numerical model in order to evaluate the vulnerability of SWI in a limestone and sand aquifer in a semi-arid Australian setting; the Uley South basin, South Australia.

The Uley South basin is an important groundwater resource as it provides approximately 70 % of the Eyre Peninsula's reticulated water (Zulfic et al. 2007). Groundwater levels have shown a decreasing trend since the 1970s, in broad terms, with occasional periods of partial recovery. Increasing salinities have been observed in several areas of the wider Eyre Peninsula, leading to public concerns regarding the depletion of this valuable freshwater resource. The risk of SWI in the Uley South basin is presently not well understood. Only rudimentary analyses of SWI in Uley South have been undertaken to date, including steady-state, sharp-interface analyses by Seidel (2008), Ward et al. (2009) and Werner et al. (2011). The application of analytical solutions to estimate the position of the freshwater-seawater interface introduces many simplifications (e.g., steady-state conditions, a sharp freshwater-seawater transition zone, one-dimensional flow, homogeneous and isotropic aquifer properties, and constant recharge). In this study, these simplifications are overcome through the development of a three-dimensional numerical model of transient SWI that simulates a dispersive interface within a heterogeneous aquifer, and including spatially and temporally variable recharge. This research aims to gain an improved

understanding of the current state of SWI in the area, and to provide a prospective view of possible basin behaviour under various potential future conditions (i.e. climate change and groundwater extraction).

9.2 Study Area Description

Uley South is located in the southern Eyre Peninsula, South Australia (Fig. 9.1), and has a temperate climate (i.e. warm, dry summers and cold, wet winters). The average annual rainfall and average pan evaporation are 560 and 1,547 mm/year, respectively. Climate data for this area were obtained at the Big Swamp monitoring station, which is 18 km north-east of Uley South (Ordens et al. 2012).

Uley South is a topographically closed surface drainage basin with an undulating central region, bounded to the south by steep coastal cliffs of up to 140 m AHD (metres Australian Height Datum, where 0 m AHD is approximately mean sea level) and to the west, north and east by low-relief ranges of heights between 50 and 170 m AHD (Werner 2010a). Soils are mainly thin calcareous, sandy and clayey loams, generally less than 3 cm in thickness and absent in areas of outcropping limestone, with widespread sinkholes across the basin (Evans 1997). Surface runoff flows rapidly towards the basin's centre, usually for only a short distance and terminating at sinkholes, which are thought to rapidly recharge the aquifer during rainfall events (Harrington et al. 2006; Ordens et al. 2012). Vegetation in the Uley South basin is dominated by Mallee Scrub (*Eucalyptus diversifolia and E. gracilis*) on sandy hills and Drooping Sheoak Woodland (*Allocasuarina verticillata*) in the areas of calcrete soils (Li 2008). There are also large areas of sparse grassland, and some infestations of woody weeds (Ordens et al. 2012).

The Uley South basin comprises two main aquifers: a quaternary limestone aquifer (QL), known as the Bridgewater Formation, and a tertiary sand aquifer (TS), known as the Wanilla Formation (Zulfic et al. 2007). The QL consists primarily of aeolian sediments, fine sand-sized shell fragments of varying consolidation, and limestone. The QL is known to have a highly variable hydraulic conductivity (K, L/T), varying by several orders of magnitude across the basin. The TS is mainly formed from sands, clays and gravels, being quite silty and carbonaceous at its base with the presence of some lignite lenses (Harrington et al. 2006). These two main aquifers are separated by a tertiary clay aquitard (TC), which comprises mainly clay and silty clay, and is highly variable in its permeability and thickness, to the degree that the QL and TS are connected in places (Morton and Steel 1968; Werner 2010a). Underlying the TS is a weathered basement layer (WB), and basement rock. The basement rock is considered impermeable for the purposes of this study.

Groundwater extraction began in 1976 and expanded in 1999–2000 to consist of 17 production bores, operated solely by the South Australia Water Corporation (SA Water) (Werner 2010a). In recent times, pumping from the QL was approximately 7 GL/year, and this is used predominantly for urban water supply (Ordens et al. 2012).

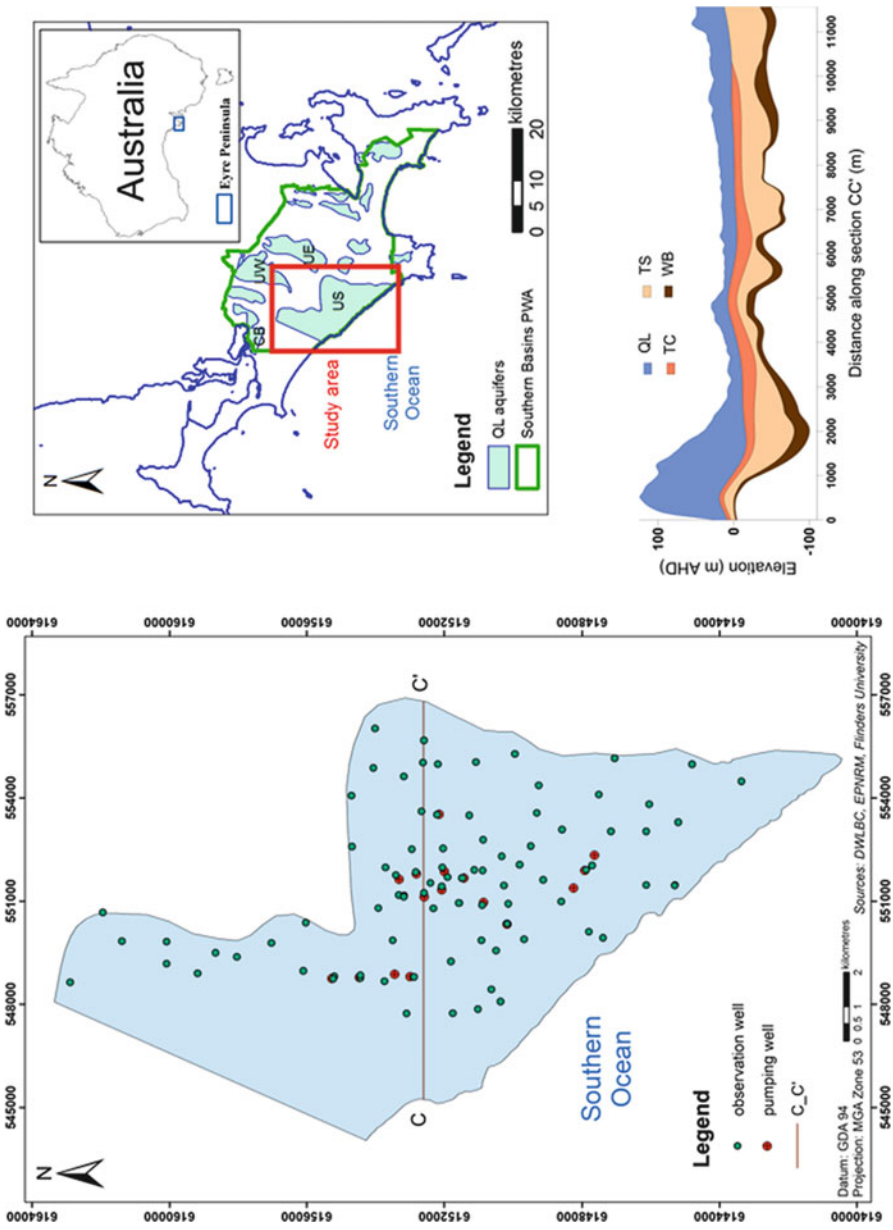

Fig. 9.1 Locality map of the study area and stratigraphic cross-section C–C′

9.3 Methodology

9.3.1 Modelling Software

Prior to the development of the SWI model, a groundwater flow (GWF) model of Uley South was developed using MODFLOW-96 (Harbaugh and McDonald 1996). The GWF model was subsequently converted to a three-dimensional SWI model, which was based on MODHMS (HydroGeoLogic, Inc. 2006). MODHMS is a MODFLOW-based code, which has advantages in the conversion of the GWF model to a SWI model. It is capable of simulating density-dependent flow and solute transport, and is also able to handle unsaturated aquifer conditions, which is an important feature for modelling Uley South, because large areas of the QL are dry, but they nonetheless receive recharge and contribute to the total water balance of the system. Automated calibration of the GWF model was undertaken to refine estimates of the aquifer's flow and storage parameters. This was accomplished using PEST (Doherty 2005). Recharge was obtained using the unsaturated zone model LEACHM-GIS (Hutson et al. 1997). The recharge modelling is summarised by Ward et al. (2008) and Werner (2010a).

9.3.2 Modelling Strategy

The SWI model was developed progressively, starting from the construction of the GWF model, as outlined by the flowchart given in Fig. 9.2. At each stage, comparisons were made between precursor models, e.g., the flow component of the 11-layer MODHMS model was compared to the flow prediction of the 2-layer MODFLOW model, to ensure consistency. While the flowchart in Fig. 9.2 depicts a linear process, the project involved numerous iterations, re-calibration efforts and feedback loops.

9.3.3 Model Set Up

In the GWF model, the top, bottom and thickness of each hydrogeological unit were derived from a combination of bore-log information and airborne electromagnetic survey (AEM) interpretations (Fitzpatrick et al. 2009). The model has 11 layers representing 4 stratigraphical sequences in the area (6 layers for QL, 1 layer for TC, 3 layers for TS and 1 layer for WB). The south-western boundary, where the aquifer is in direct connection with the sea, was a fixed, density-corrected coastal head in the model. The linkage between Uley South basin and adjacent basins is thought to occur through the TS. Therefore, a general head boundary was assigned at various locations in the TS along the northern perimeter to allow water exchanges between

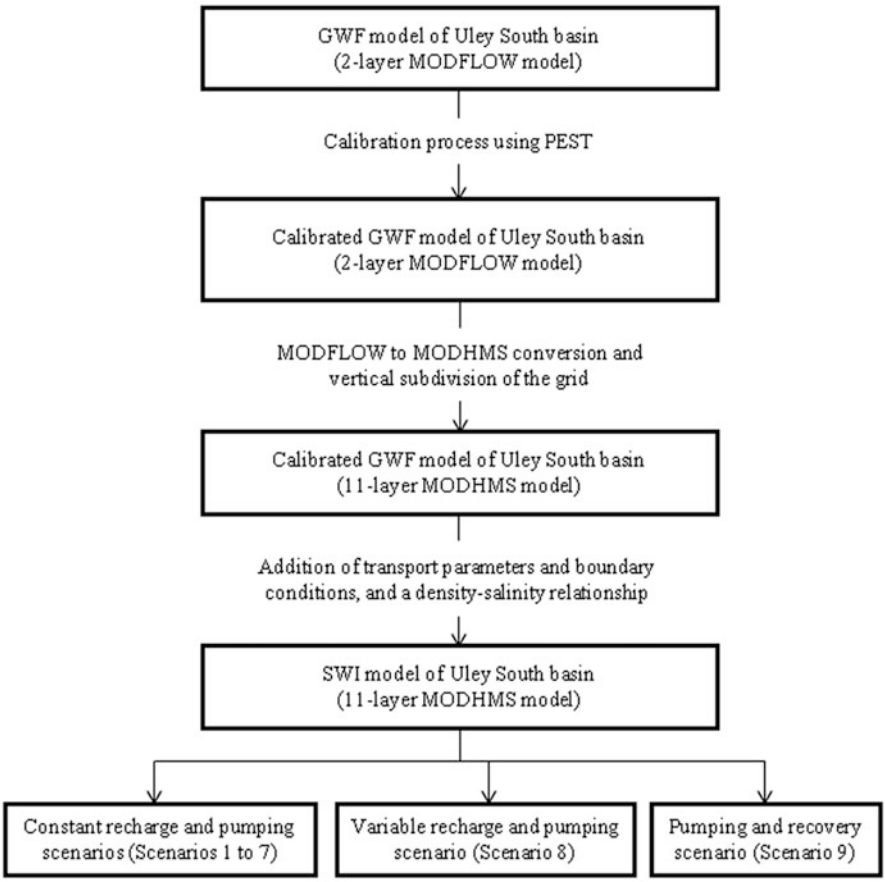

Fig. 9.2 A flowchart of the procedure for developing a SWI model of Uley South basin

basins. Groundwater level contours and the stratigraphy provide indication of the connection between Uley South and northern basins.

The aquifer properties, including K, boundary conductance (T_c), specific yield (S_y) and specific storage (S_s), were derived initially from pump tests, previous models and textbook values, and were then modified through GWF model calibration. Horizontal hydraulic conductivity (K_h) in the QL, TC and TS sequences was calibrated using zones thought to represent areas of geological uniformity. Figure 9.3 shows the zonation and calibrated values. TC values were assigned QL values where TC was thought to be absent. The WB sequence was considered to be of low permeability, and was assigned a spatially invariable K_h value of 0.01 m/day that was shown to be insensitive to calibration efforts due to the lack of relevant head observations. Similar to K_h, vertical hydraulic conductivity (K_v) was calibrated using zones, with a preferred condition of one tenth of K_h. For storage properties, S_y of the QL layer was calibrated as three zones (Fig. 9.3), and S_y and S_s

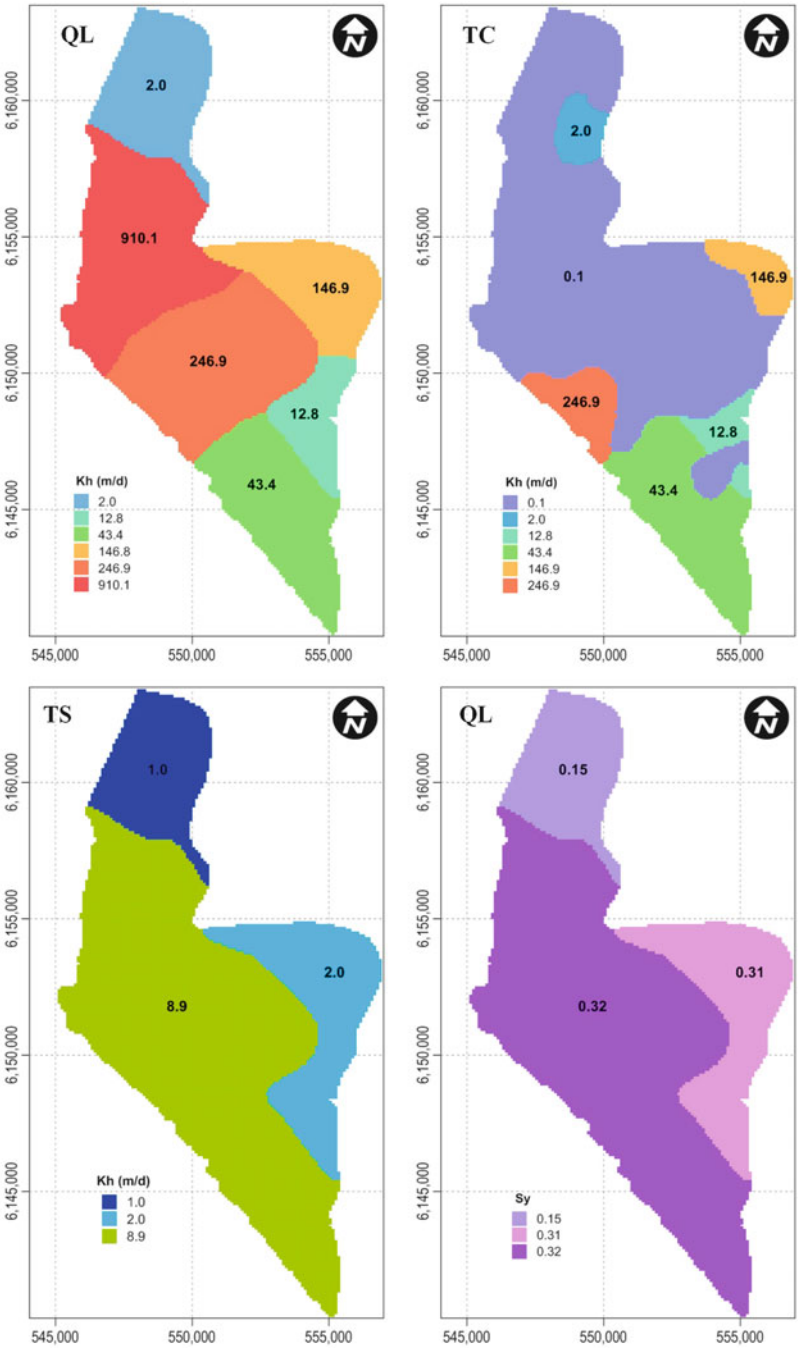

Fig. 9.3 Distribution of aquifer properties in QL, TC and TS layers

Table 9.1 Solute transport parameters, and initial and boundary conditions

Parameter description	Units	Value
Initial relative salt concentration (1 represents seawater)	–	0.0
Coastal boundary salt concentration	–	1.0
Recharge and inland inflow salt concentrations	–	0.0
Longitudinal dispersivity (α_L)	m	1.0
Transverse dispersivity (α_T)	m	0.1
Vertical dispersivity (α_Z)	m	10^{-5}
Molecular diffusion (D_m)	m^2/day	0.0
TS porosity (n)	–	0.30
TC porosity (n)	–	0.42
WB porosity (n)	–	0.30

were calibrated as single values for the entire TS layer, namely 0.14 and 3×10^{-6} m^{-1}, respectively. Additional parameter values required for solute transport are summarised in Table 9.1 and Fig. 9.4. These were textbook values considered typical of the setting.

The SWI model was run under pre-development stresses (i.e. no pumping and pre-development recharge) for 725 years, to establish steady-state conditions that were adopted as the starting conditions for transient simulations (i.e. both historical simulations and scenario testing, unless stated otherwise), as described below (Table 9.2).

9.4 Results and Discussion

The focus of this section is the SWI modelling results and predictions. Only an abbreviated presentation of the calibration is provided here for brevity. The simulated results presented in this section include: (1) Salinities at the end of the simulation period in layers 2 (upper QL), 6 (bottom of QL), 8 (upper TS) and 10 (lower TS); (2) Water level hydrographs at selected piezometers (see Fig. 9.5 for piezometer locations); (3) Salinity hydrographs (salinographs) at selected piezometers. Salinity is expressed in terms of relative salt concentration, such that a value of 1 represents seawater.

9.4.1 GWF Model Calibration

The transient calibration results showed a reasonably good match between the modelled and observed water levels (Fig. 9.6). The following calibration statistics were obtained: root-mean-square error of 0.86 m and scaled-root-mean-square error of 4.2 %. The model was unable to reproduce the water levels of a small number of observation wells, mainly for wells in the northern/inland part of the

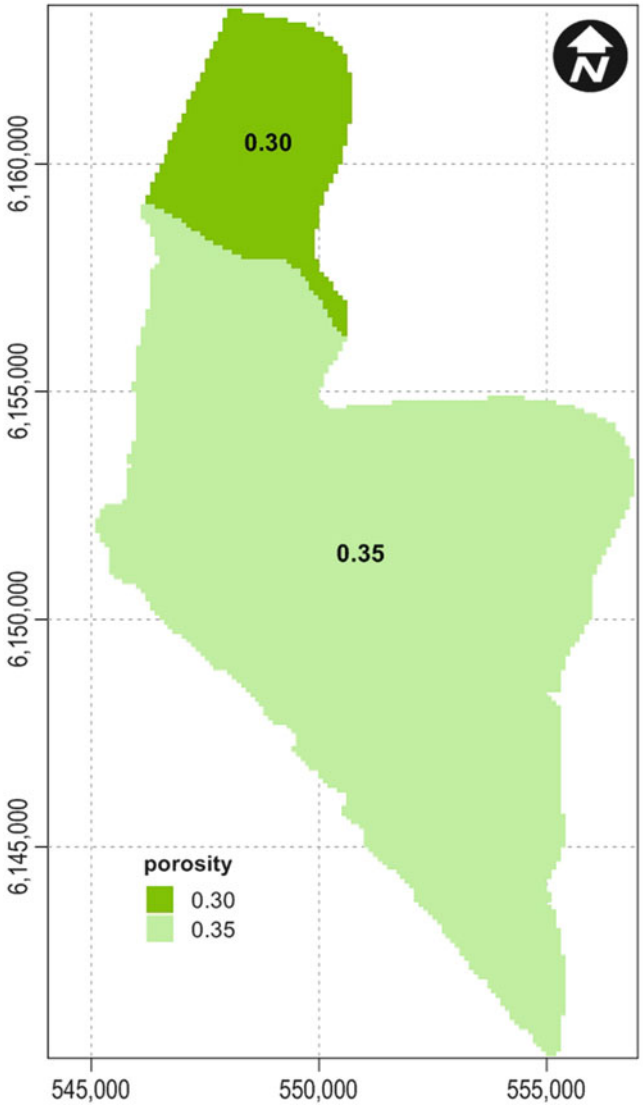

Fig. 9.4 Distribution of porosity in the QL aquifer

basin (i.e. with heads greater than 7 m AHD). The mismatch is probably due to heterogeneities in the northern part of Uley South, which were not represented accurately by the simple parameter zonation of the GWF model (Fig. 9.3). Further modelling efforts using pilot point calibration (Doherty 2005) are ongoing, and are expected to enhance the calibration match in these areas. Given that the model is a reasonable match to field observations in the near-coastal zone (where SWI is most likely to occur), the model's mismatch in the inland zones was considered to be at tolerable levels.

Table 9.2 Scenarios for the SWI model

Scenario	Description	R (GL/year)	R (mm/year)	Pumping times	USPB1-8 Q_p (GL/year)	USPB9-17 Q_p (GL/year)	Total Q_p (GL/year)
1	Natural conditions	13.7	112	Jan-60–Dec-07	0	0	0
2	Low and steady pumping	13.7	112	Jan-60–Dec-07	2.9	0.6	3.5
3	Simplified historical scenario	13.7	112	Jan-60–Oct-76	0	0	0
				Nov-76–Mar-00	5.0	0	5.0
				Apr-00–Dec-07	2.9	3.9	6.8
4	Future scenario: Current practice	13.7	112	Jan-60–Dec-07	2.9	3.9	6.8
5	Future scenario: Increased Extraction	13.7	112	Jan-60–Dec-07	4.5	3.9	8.4
6	Future scenario: Current practice with higher R	14.8	121	Jan-60–Dec-07	2.9	3.9	6.8
7	Future scenario: Current practice with lower R	11.8	97	Jan-60–Dec-07	2.9	3.9	6.8
8	Historical scenario	Recharge varies monthly, averaging 112 mm/year		Jan-60–Oct-76	0		
				Nov-76–Mar-00	Pumping varies monthly		
				Apr-00–Dec-07	Pumping varies monthly		
9	Pumping and recovery	13.7	112	2008–2,155	2.9	3.9	6.8
				2,156–2,303	0	0	0

Note: R and Q_p are recharge and pumping rate, respectively

9.4.2 Simulation of Pre-development Conditions

A long-term simulation of pre-development (no pumping) conditions provided a prediction of the baseline salinity distribution in Uley South (see Fig. 9.7), adopting aquifer stresses representing the period prior to aquifer development; the first such modelling attempt for a South Australian coastal aquifer. The salt distributions from the model are a unique insight into the previously unknown extent of seawater in the aquifer. It is particularly important for the security of pumping wells, because a selection of these is in somewhat close proximity to the model's prediction of the seawater wedge location (compare Figs. 9.5 and 9.7). The peculiar shape of SWI in lower part of the QL (layer 6; Fig. 9.7) is examined in more detail in Fig. 9.8, which illustrates the QL base morphology. The deep channels in the near-shore region provide preferential channels for seawater to encroach inland, leading to the simulated salinity distributions.

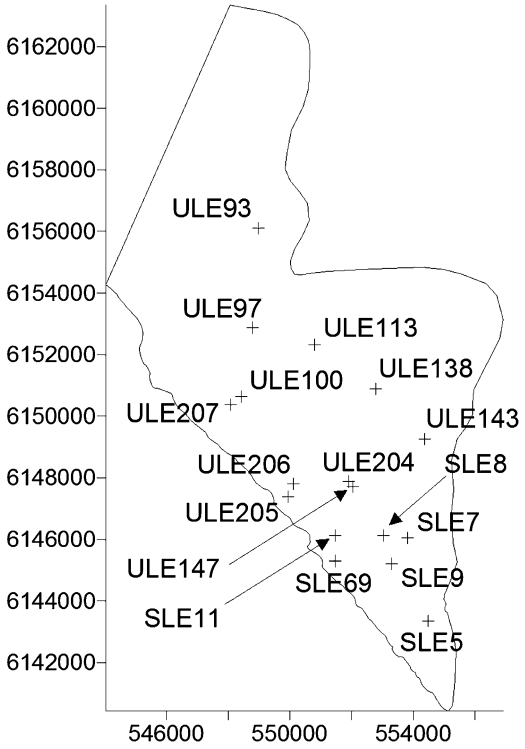

Fig. 9.5 Locations of selected bores

The maximum inland positions of the wedge toe in Fig. 9.7 are largely consistent with first-order sharp-interface estimates by Seidel (2008), who obtained inland toe positions of 400–450 m in the QL, and 2,000 m in the TS (compared to approximately 500 m in the QL and 2,500 m in the TS; Fig. 9.7). Ward et al. (2009) used a similar approach to Seidel (2008), but adopted contemporary stresses, and obtained toe distances of 900 m in the QL (assuming QL is disconnected from TS), and 4,000 m in the TS (assuming the QL and TS act as a single layer).

The simulated zone of saline groundwater in the south-east coastline is also broadly consistent with the zone of saline groundwater reported in the AEM survey by Fitzpatrick et al. (2009), i.e. at location A in Fig. 9.9. Also, two salinity profiles obtained by the South Australian Government are a close match to salinity profiles in the same locations in the SWI model (Fig. 9.10). The reasonable closeness in salinity distributions provides confidence in the model's capacity to simulate the primary physical processes of SWI in Uley South. Notwithstanding the various forms of supportive evidence for the model's predictions, it should be acknowledged that SWI simulation remains a highly uncertain practice, and a model such as the one described here should not be relied on to predict salinities at individual boreholes. The heads and salt distributions from the pre-development simulation were adopted as the initial conditions for various model scenarios.

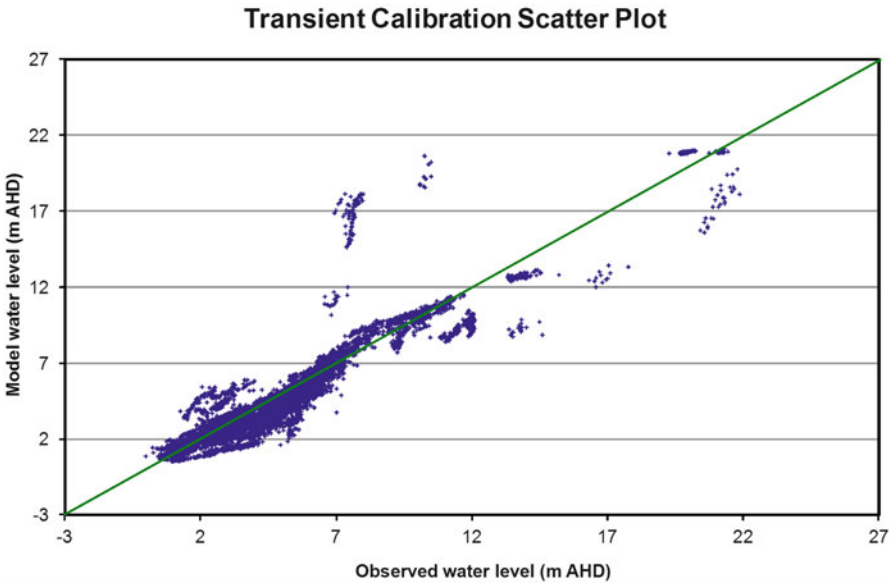

Fig. 9.6 Scatter plot of the match between observed and simulated water levels from the transient calibration of the GWF model

9.4.3 No-Pumping Scenario – Natural SWI

Climate variability has been suggested as a significant contributor to drawdown in Uley South during the period 1960–2007, although only limited attempts to evaluate climate impacts on groundwater decline (i.e. relative to pumping effects) have been undertaken to date. Hence, a no-pumping scenario is considered here, to explore whether the lower rates of recharge during the period 1960–2007, compare to recharge prior to 1960, could have produced significant SWI impacts even in the absence of pumping. The salinity distributions in the base of the QL and TS aquifers are given in Fig. 9.11, which show only small salinity changes by comparing to Fig. 9.7. Clearly, the existence of some amount of seawater in Uley south is a natural condition. Temporal trends from this simulation are given later in this article, and are used as a baseline for comparing to other scenarios adopting the same period (1960–2007), except modified stress conditions.

9.4.4 Historical SWI Scenario

Two forms of the historical stresses in Uley South were adopted in simulations of the period 1960–2007: (a) a highly transient case considering historical seasonality in a monthly temporal resolution (Scenario 8; Table 9.2), and (b) a piecewise,

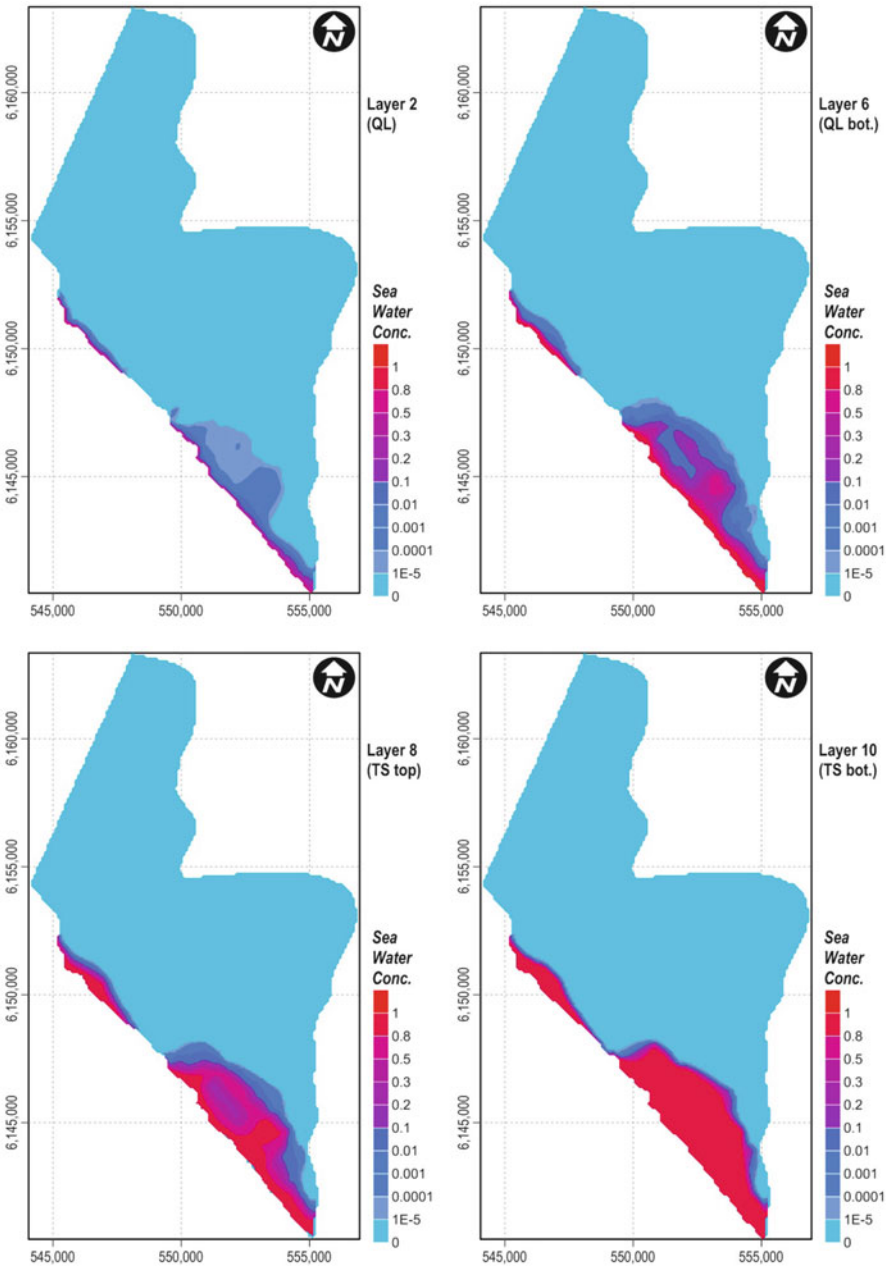

Fig. 9.7 Predicted pre-development salinity distributions

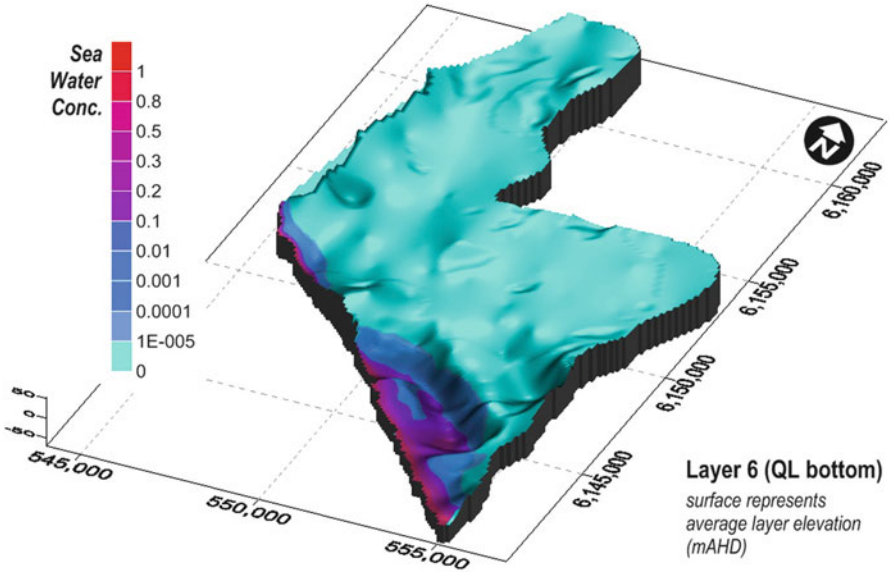

Fig. 9.8 Three-dimensional representation of layer 6 (base of QL) geometry overlain by the layer 6 salinity from the pre-development simulation

time-averaged case in which seasonality was neglected (Scenario 3; Table 9.2). The historical scenario differs from the previous case (i.e. no-pumping scenario) by the addition of historical pumping. The benefits of simplicity in the time-average case brought about significant gains in reduced computer run times, whereas the case adopting seasonality in stresses was considered more physically realistic. The representativeness of the simplified case was evaluated through the inter-comparison, to check whether other scenarios could be run in the more computationally efficient time-averaged form. The comparison also provided insight into the likely intra-annual variability in SWI in Uley South. The salinity contours for the lower part of the QL (i.e. the source aquifer for pumping) are shown in Fig. 9.12. The more north-westerly seawater plume has a larger extent due to the pumping effect, while the more south-westerly plume is of similar extent, except it comprises higher salinity groundwater. It appears that the basement shape restricts SWI in some parts of the aquifer. The long-term effects of seasonality are largely insignificant, given that the two cases shown in Fig. 9.12 are very similar.

Hydrographs (Fig. 9.13) and salinographs (Fig. 9.14) illustrate local variability, associated with the time-averaged and seasonal historical scenarios, with comparison to observed water levels. There is a marked response to the change in pumping rates in 1976 and 2000. In most of the selected piezometers, heads dropped and salinity rose with the increase in pumping rates. There are exceptions in a few wells (e.g. ULE113 and ULE138), in which water levels experienced a recovery phase at the last simulation period. This occurs from the de-centralisation of the extraction in 2000, following the construction of new wells, which allowed decreases in pumping in some existing wells (i.e. USPB1 to USPB8).

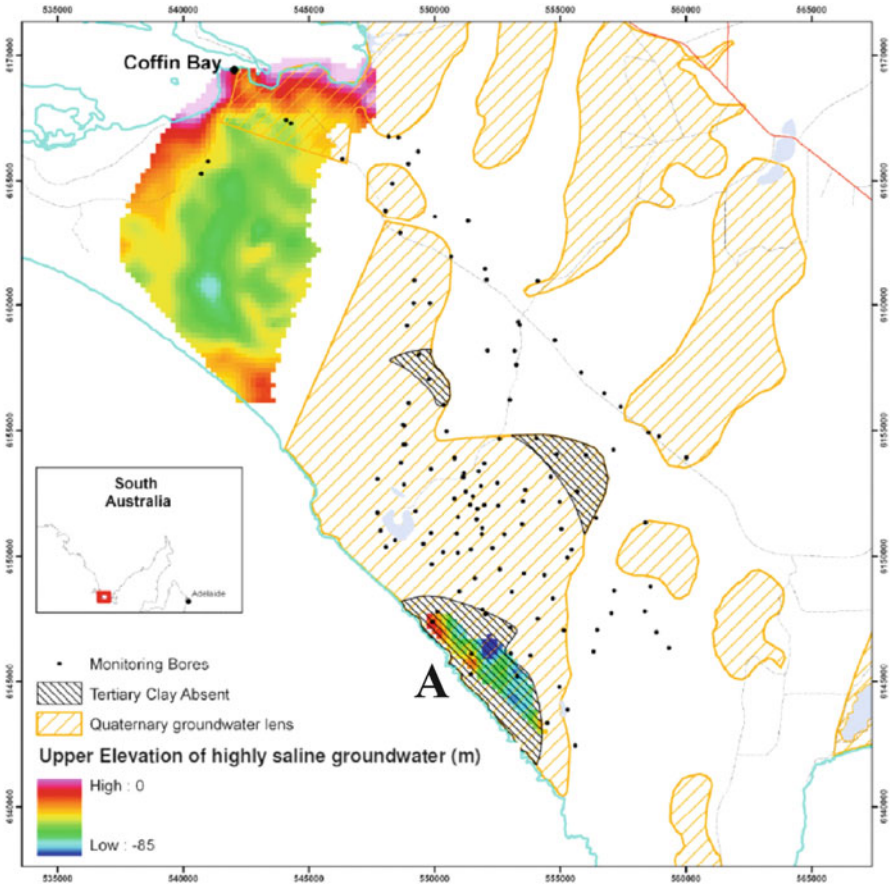

Fig. 9.9 Upper surface of saline groundwater in AEM survey area (taken from Fitzpatrick et al. 2009). Location A highlights the occurrence of highly saline groundwater

The hydrographs and salinographs (Figs. 9.13 and 9.14) of Scenarios 3 and 8 are in general agreement, which suggests that scenarios adopting time-averaged stresses provide a reasonable representation of more complex transient behaviour. Additionally, this emphasises that seasonality does not play an important role in controlling the long-term SWI trends in Uley South, which rather responds to longer-term variability. The comparison to observed water levels in Fig. 9.13 shows, generally, a reasonable match in most cases, particularly considering the high variability in aquifer properties of the system relative to the simple parameterisation. Salinities in most piezometers are below the detection limit of commonly used salinity instruments. Continued monitoring in piezometers in close proximity to the landward extent of the seawater wedge are needed to capture any future SWI trends. A comparison of Figs. 9.1 and 9.12 shows that pumping wells are in close proximity with the predicted edge of the seawater plume in the lower QL domain.

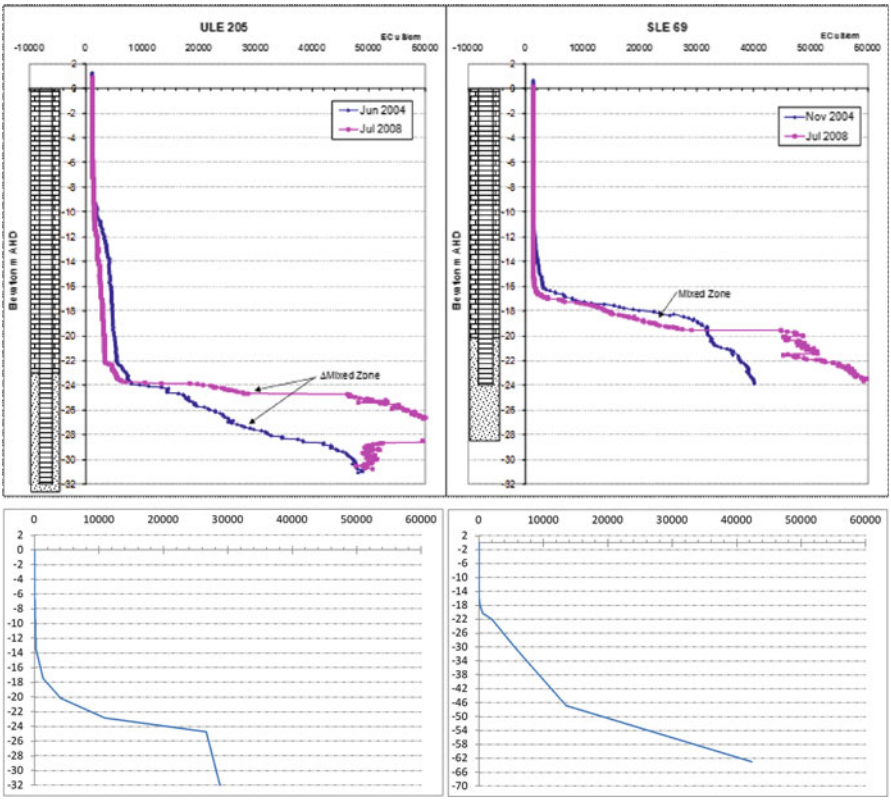

Fig. 9.10 Observed (*upper* two sub-figures) and simulated (*lower* two sub-figures) salinity profiles corresponding to the wells ULE205 (*left graphs*) and SLE69 (*right graphs*). *Horizontal axes* are salinity in μS/cm and *vertical axes* are elevation in m AHD

9.4.5 SWI Scenario Testing – Effects of Pumping and Recharge Changes

Various pumping and recharge scenarios were undertaken, as listed in Table 9.2, to evaluate possible future SWI in Uley South under different stress conditions to the current regime. All scenarios adopt the same pre-development initial condition, to allow comparison with the previous scenarios of no pumping and historical stresses (i.e. during 1960–2007, as described above). The scenario results given in the following focus on the QL base, which is where seawater intrudes the farthest in the QL, which is the source aquifer for water supply. Salinity distributions from Scenarios 4, 5, 6 and 7 are given in Fig. 9.15.

The Fig. 9.15 results show that predicted salinity variations are subtle, at least from a regional perspective, for the four variations of pumping and recharge during the period 1960–2007. Locally, SWI can be observed through salinity changes at

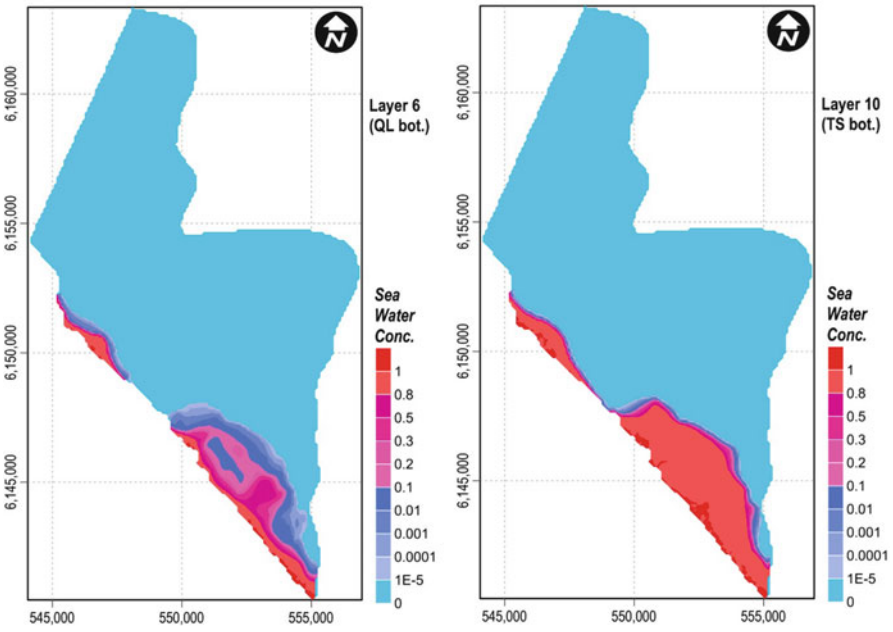

Fig. 9.11 Predicted salinity distributions, for the lower domains of the QL (*left* sub-figure) and TS (*right* sub-figure) aquifer, from a no-pumping, 1960–2007 scenario

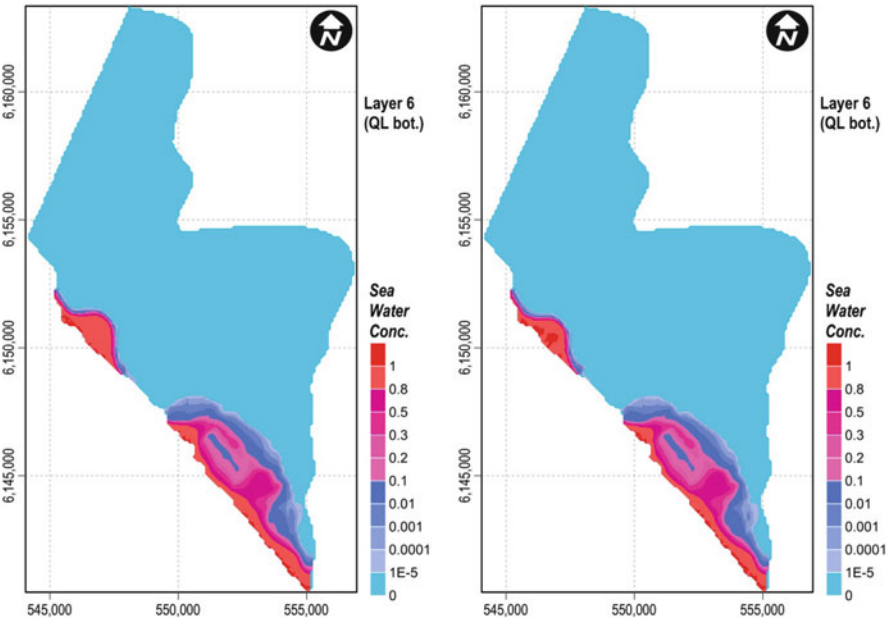

Fig. 9.12 Salinity distributions at the end of the historical simulation (1960–2007) in the lower QL, considering seasonal variability in stresses (Scenario 8; *left* sub-figure) and with time-averaged stresses (Scenario 3; *right* sub-figure), as summarised in Table 9.2

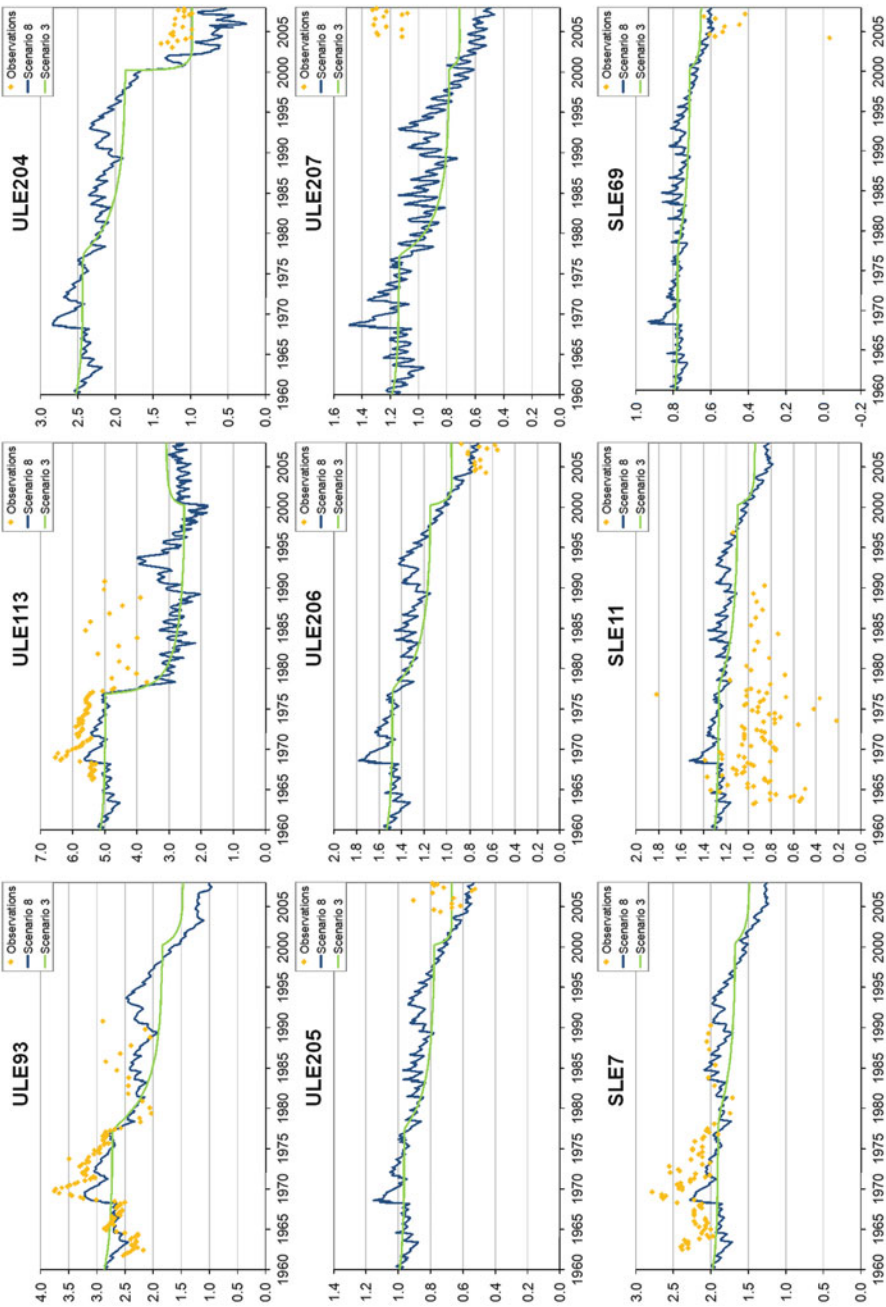

Fig. 9.13 Simulated hydrographs from Scenarios 3 (time-averaged stresses) and 8 (seasonality included), compared to field observations. *Vertical axis* is water level in m AHD

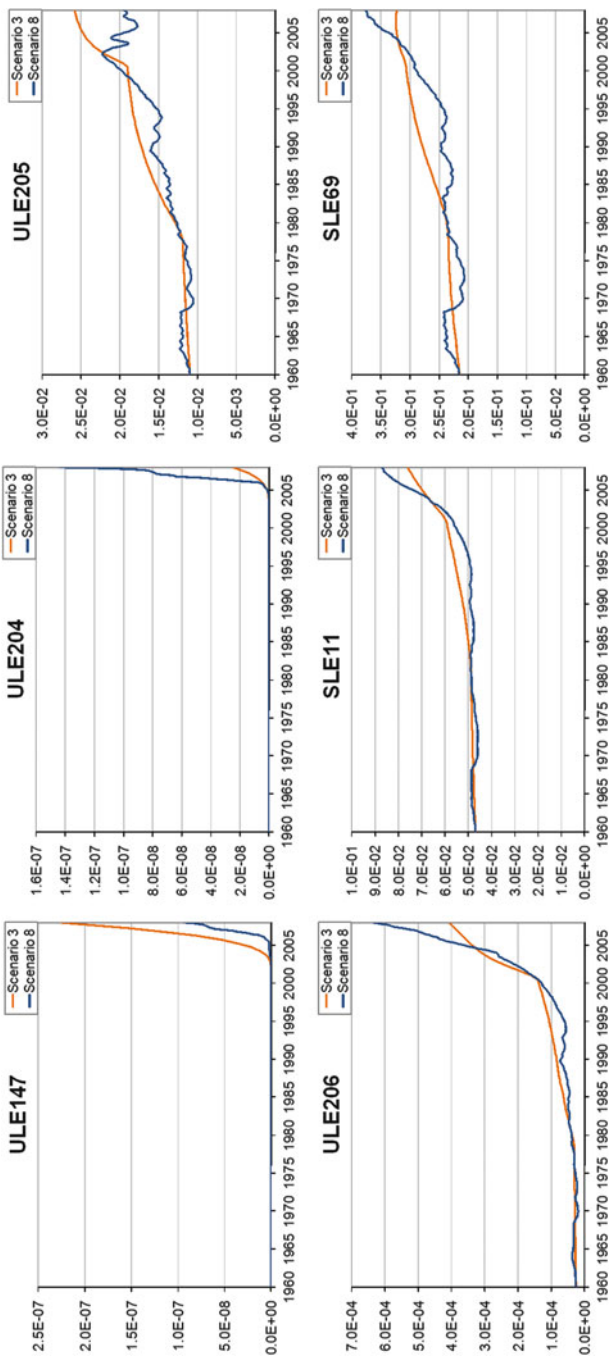

Fig. 9.14 Simulated salinographs from Scenarios 3 (time-averaged stresses) and 8 (seasonality included). *Vertical axis* is relative salt concentration

some piezometers. A selection of hydrographs and salinographs are given in Figs. 9.16 and 9.17 to better elucidate differences between the four scenarios

The water level trends in Fig. 9.16 show that the pumping increase and the recharge reduction produce fairly similar water level responses, in piezometers ULE204 and SLE11, which are near the more south-easterly seawater plume. The head decline in Scenario 5 is between 0.2 m (SLE69) and 2.5 m (ULE113), taking Scenario 1 as the baseline. In terms of salinity, however, there is a slightly higher response in the pumping scenario, likely due to the localised nature of pumping impacts near the coast, compared to the more regional impacts of recharge changes. The salinity responses were very low in most of the bores. For instance, ULE147 and ULE204 (near production bores USPB16 and USPB17) produced salinity levels reaching just 10^{-4} of seawater concentration (approximately 5 μS/cm), which are insignificant. A key observation of the model results is the difference between salinity trends (increasing or variable) and water level trends (stable), at the end of the simulation period. It is worthwhile to note that salinity levels in many piezometers are still rising at the end of the simulations, indicating that the basin has not reached equilibrium in terms of salinity. Interesting salinity trends are apparent, such as fluctuations in ULE205 and a recent decline in SLE11. According to Watson et al. (2010), non-uniform trends are not unusual in simulations that include complex density-dependent flow and dispersive transport processes such as those occurring in the Uley South SWI model.

9.4.6 Uley South SWI Recoverability

The reversibility of SWI in Uley South was analysed using Scenario 9 (Table 9.2), which involved the continuation of current pumping rates for 148 years, followed by a no-pumping period of 148 years. Average recharge for 1960–2007 was applied throughout both pumping and no-pumping phases. The initial conditions were adopted from the end of Scenario 3, approximating the current salinity conditions of the basin. Predicted salinity contours in the lower domains of the QL and TS aquifers, at different times, are given in Figs. 9.18 and 9.19.

Figures 9.18 and 9.19 demonstrate that at the basin scale, the salinity contours do not recover to their pre-pumping state at the end of the simulation (i.e. after 148 years of pumping and 148 years of recovery; Berrio 2010), with the exception of high salinity contours (e.g. in the north-western seawater wedge in the QL aquifer). Even though the extent of the plume at the end of the recovery period was larger than that at the initial stage, the area of highly saline water (relative salinities greater than 0.8) appears to be smaller. That is, the process of intrusion and then recovery produces a dispersed plume, whereby high salinity contours completely recovery to pre-pumping conditions (and more seaward), whereas low salinity contours remain more extensive. Given that only low salinities (relative to seawater) are needed to contaminate wells, it follows that Uley South aquifer requires significantly more time to be able to recover from pumping that induces SWI.

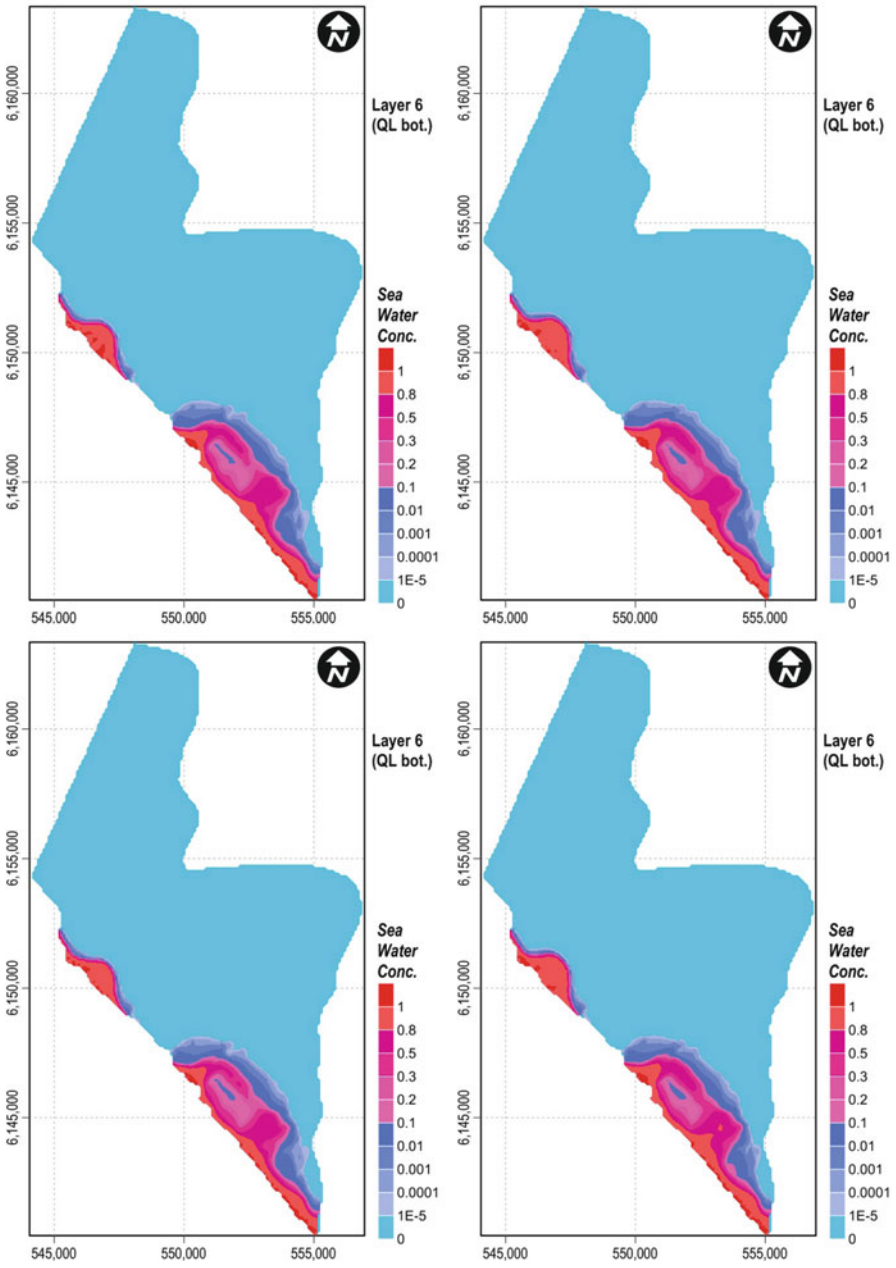

Fig. 9.15 Predicted salinity distributions in the QL base, for Scenario 4 (1960–2007 climate with current pumping; *top-left* sub-figure), Scenario 5 (1960–2007 climate with higher pumping; *top-right* sub-figure), Scenario 6 (1960–2007 higher-recharge climate with current pumping; *bottom-left* sub-figure), Scenario 7 (1960–2007 lower recharge climate with current pumping; *bottom-right* sub-figure)

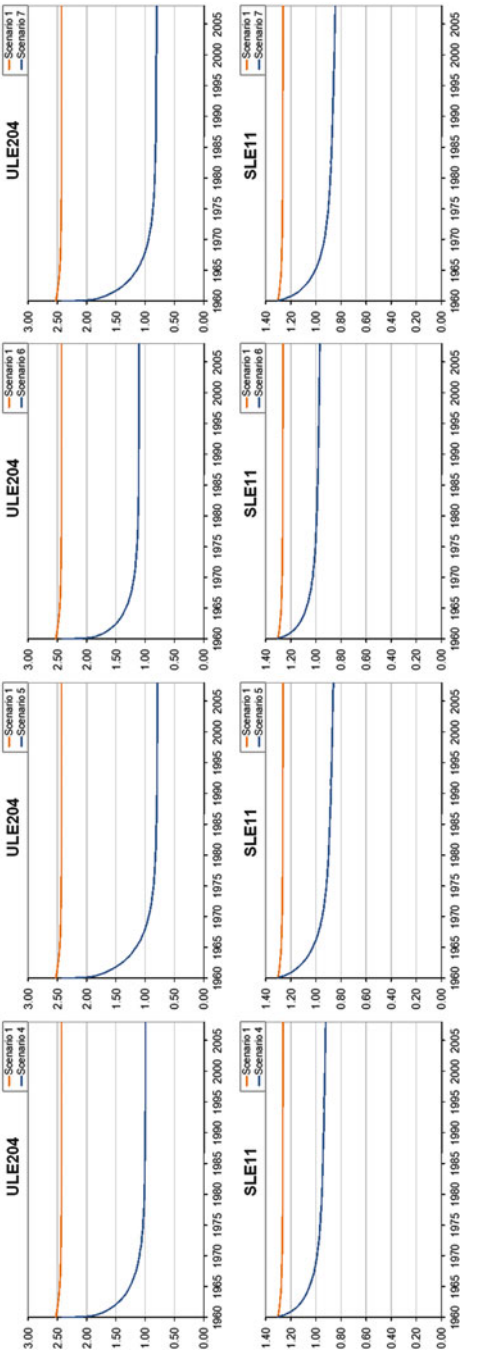

Fig. 9.16 Hydrographs in piezometers ULE204 and SLE11 from Scenarios 4–7. *Vertical axis* is water level in m AHD

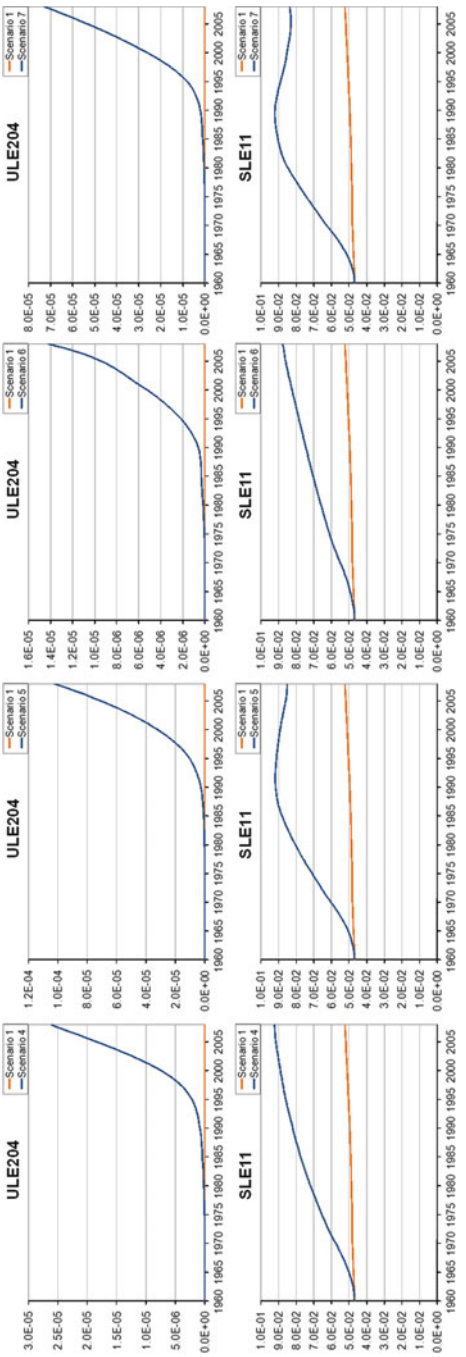

Fig. 9.17 Salinographs in piezometers ULE204 and SLE11 from Scenarios 4–7. *Vertical axis* is relative salinity; note difference in vertical scale

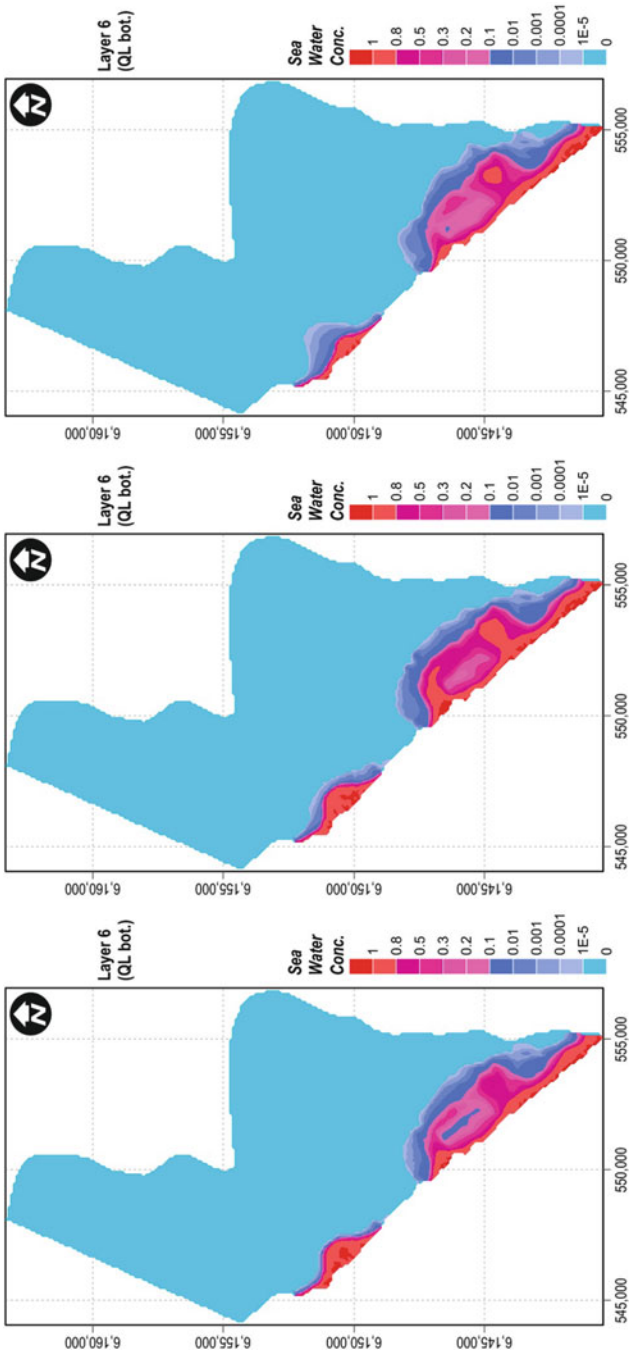

Fig. 9.18 QL salinity distributions from Scenario 9: initial conditions (*left* sub-figure), after 148 years of current pumping (*middle* sub-figure), after an additional 148 years of no pumping (*right* sub-figure). Results from Berrio (2010)

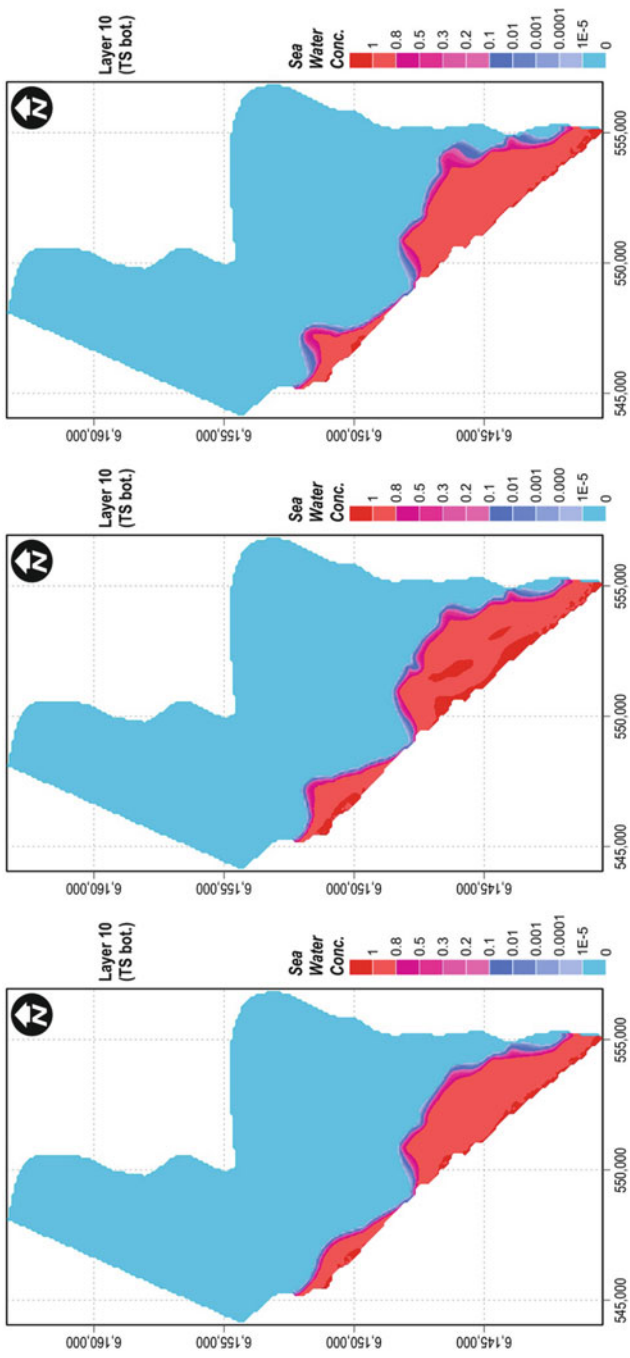

Fig. 9.19 TS Salinity distributions from Scenario 9: initial conditions (*left* sub-figure), after 148 years of current pumping (*middle* sub-figure), after an additional 148 years of no pumping (*right* sub-figure). Results from Berrio (2010)

9.5 Conclusions

Assessment of SWI behaviour in the Uley South basin, South Australia, is assessed using a three-dimensional variable-density numerical model. The model assists in building intuition about SWI in Uley South. Increased pumping and reduced recharge conditions have negative effects on the groundwater system of the area, through lowered water tables and elevated salinities, as one might expect. However, these effects appear to be only small changes from a regional perspective. The SWI response to stress changes varies across the basin, due to the contrast and zonation of hydraulic and storage properties. Simulation results indicate that seasonality in recharge and pumping stresses is not an important factor in controlling SWI in the basin, and that average-stress conditions can be used as reasonable representations of highly transient conditions. A pumping and recovery scenario suggests that the salinization impacts resulting from a given period of pumping require a period for recovery after pumping has ceased that is longer than the pumping period. It follows that repeated SWI and recovery cycles are likely to produce a highly dispersed seawater plume that will be difficult to remediate, and hence SWI should ideally be avoided rather than considering remedial strategies once SWI has occurred.

The observation that heads may stabilise while salinities continue to increase provides important lessons for monitoring and management strategies, which need to evaluate salinities and water level elevations relative to sea level (i.e. rather than water level trends, which can be misleading). Fortunately, the Uley South aquifer has strategic salinity monitoring sites installed at key locations, i.e. between the seawater wedge and pumping wells, and these provide critical monitoring for the future sustainability of the aquifer.

Acknowledgments This research was funded by Flinders University, the South Australian Government, and the National Centre for Groundwater Research and Training (a collaborative initiative of the Australian Research Council and the National Water Commission). The authors wish to acknowledge the invaluable input of industry partners and Flinders University students and staff for their contributions to this research.

References

Berrio JF (2010) A numerical 3D seawater intrusion model of Uley South Basin, Eyre Peninsula, South Australia. Unpublished master's thesis, Flinders University, Adelaide, 52 pp

Doherty J (2005) PEST: model-independent parameter estimation, user manual, 5th edn. Watermark Numerical Computing. Brisbane. Available at: http://www.pesthomepage.org/Download.php, 336 pp

Evans SL (1997) Estimating long-term recharge to thin, unconfined carbonate aquifers using conventional and environmental isotope techniques: Eyre Peninsula, South Australia. Incomplete master's thesis, Flinders University, Adelaide, 176 pp

Fitzpatrick A, Cahill K, Munday T (2009) Informing the hydrogeology of Coffin Bay, South Australia, through the constrained inversion of TEMPEST AEM Data. CSIRO, Adelaide, 159 pp

Freeze RA, Cherry JA (1979) Groundwater. Prentice-Hall, Englewood Cliffs

Harbaugh AW, McDonald MG (1996) User's documentation for MODFLOW-96, an update to the U.S. Geological Survey modular finite-different ground-water flow model. U.S. Geological Survey Open-File Report 96-485. U.S. Geological Survey, Reston, 63 pp

Harrington N, Evans S, Zulfic D (2006) Uley Basin groundwater modelling project. Project overview and conceptual model development, vol 1. Report DWLBC 2006/01. Department of Water, Land and Biodiversity Conservation, Adelaide

Hutson JL, Wagenet RJ, Niederhofer ME (1997) LEACHM: Leaching estimation and chemistry model – a process-based model of water and solute movement, transformations, plant uptake and chemistry reactions in the unsaturated zone. Department of Soil, Crop and Atmospheric Sciences, Research Series No. R97-1, Cornell University, Ithaca, 138 pp

HydroGeoLogic, Inc (2006) MODHMS: a comprehensive MODFLOW-based hydrologic modeling system, Version 3.0. HydroGeoLogic, Inc, Herndon, 811 pp

Li C (2008) Water use by Malle-form *Eucalyptus diversifolia* in a semi-arid and karstic environment. Unpublished honours thesis, Flinders University, Adelaide, 65 pp

Liu F, Anh W, Turner I, Bajracharya K, Huxley WJ, Su N (2006) A finite volume simulation model for saturated-unsaturated flow and application to Gooburrum, Bundaberg, Queensland, Australia. Appl Math Model 30:352–366

Morton WH, Steel TM (1968) Eyre Peninsula groundwater study Uley South Basin, Progress report No. 1 – Aquifer Evaluation. Department of Mines, Report 66/45, Government of South Australia, Adelaide

Narayan KA, Schleeberger C, Bristow KL (2007) Modelling seawater intrusion in the Burdekin Delta Irrigation Area, North Queensland, Australia. Agric Water Manage 89:217–228

Ordens CM, Werner AD, Post VEA, Hutson JL, Simmons CT, Irvine BM (2012) Groundwater recharge to a sedimentary aquifer in the topographically closed Uley South Basin, South Australia. Hydrogeol J 20:61–72

Seidel A (2008) Seawater intrusion on the Southern Eyre Peninsula, South Australia: a first-order assessment. Unpublished honours thesis, Flinders University, Adelaide, 69 pp

Ward JD, Hutson J, Howe B, Fildes S, Werner AD, Ewenz C (2009), A modelling framework for the assessment of recharge processes and climate change: Eyre Peninsula. Report developed through the Eyre Peninsula Groundwater, Allocation and Planning Project, Eyre Peninsula Natural Resources Management Board, 53 pp. http://www.epnrm.sa.gov.au/Portals/4/Water/Recharge%20and%20Climate%20Change%20Final%20Report.pdf

Ward JD, Werner AD, Howe B (2009) Saltwater intrusion in Southern Eyre Peninsula. Report developed through the Eyre Peninsula Groundwater, Allocation and Planning Project, Government of South Australia, Eyre Peninsula Natural Resources Management Board, Eyre Peninsula, 56 pp

Watson TA, Werner AD, Simmons CT (2010) Transience of seawater intrusion in response to sea level rise. Water Resour Res 46:W12533. doi:10.1029/2010WR009564

Werner AD (2010a) A groundwater flow model of Uley South Basin, South Australia. Draft report prepared for the Eyre Peninsula Natural Resource Management Board by Flinders University, Adelaide, 105 pp

Werner AD (2010b) A review of seawater intrusion and its management in Australia. Hydrogeol J 18:281–285

Werner AD, Gallagher MR (2006) Characterisation of sea-water intrusion in the Pioneer Valley, Australia using hydrochemistry and three-dimensional numerical modelling. Hydrogeol J 14:1452–1469

Werner AD, Alcoe DW, Ordens CM, Hutson JL, Ward JD, Simmons CT (2011) Current practice and future challenges in coastal aquifer management: flux-based and trigger-level approaches with application to an Australian case study. Water Resour Manage 25:1831–1853

Zulfic D, Harrington N, Evans S (2007) Uley basin groundwater modelling project. Groundwater flow model, vol 2. Department of Water, Land and Biodiversity Conservation, Report DWLBC 2007/04, Government of South Australia, Adelaide, 128 pp

Chapter 10
Application of a Rapid-Assessment Method for Seawater Intrusion Vulnerability: Willunga Basin, South Australia

Leanne K. Morgan, Adrian D. Werner, Melinda J. Morris, and Michael D. Teubner

Abstract Seawater intrusion (SWI) causes degradation of water quality and loss of water security in coastal aquifers. Although the threat of SWI has been reported in all of the Australian states and the Northern Territory, comprehensive investigations of SWI are relatively uncommon because SWI is a complex process that can be difficult and expensive to characterise. The current study involves the application of a first-order method developed recently by Werner et al. (Ground Water 50(1):48–58, 2012) for rapidly assessing SWI vulnerability. The method improves on previous approaches for the rapid assessment of large-scale SWI vulnerability, because it is theoretically based and requires limited data, although it has not been widely applied. In this study, the Werner et al. (Ground Water 50 (1):48–58, 2012) method is applied to the Willunga Basin, South Australia to explore SWI vulnerability arising from extraction, recharge change and sea-level rise (SLR). The Willunga Basin is a multi-aquifer system comprising the unconfined Quaternary (Qa) aquifer, confined Port Willunga Formation (PWF) aquifer and confined Maslin Sands (MS) aquifer. Groundwater is extracted from the PWF and MS aquifers for irrigated agriculture. In the Qa aquifer, the extent of SWI under current conditions was found to be small and SWI vulnerability, in general, was relatively low. For the PWF, SWI extent was found to be large and SWI is likely to be active due to change in heads since pre-development. Anecdotal evidence from recent drilling in the PWF suggests a seawater wedge at least 2 km from the coast.

L.K. Morgan (✉) • A.D. Werner
National Centre for Groundwater Research and Training, Flinders University, GPO Box 2100, Adelaide, SA 5001, Australia

School of the Environment, Flinders University, GPO Box 2100, Adelaide, SA 5001, Australia
e-mail: leanne.morgan@flinders.edu.au

M.J. Morris
URS Australia Pty Ltd, Level 4, 70 Light Square, Adelaide, SA 5000, Australia

M.D. Teubner
School of the Environment, Flinders University, GPO Box 2100, Adelaide, SA 5001, Australia

C. Wetzelhuetter (ed.), *Groundwater in the Coastal Zones of Asia-Pacific*, Coastal Research Library 7, DOI 10.1007/978-94-007-5648-9_10,

A relatively high vulnerability to future stresses was determined for the PWF, with key SWI drivers being SLR (under head-controlled conditions, which occur when pumping controls aquifer heads) and changes in flows at the inland boundary (as might occur if extraction increases). The MS aquifer was found to be highly vulnerable because it has unstable interface conditions, with active SWI likely. Limitations of the vulnerability indicators method, associated with the sharp-interface and steady-state assumptions, are addressed using numerical modelling to explore transient, dispersive SWI caused by SLR of 0.88 m. Both instantaneous and gradual (linear rise over 90 years) SLR impacts are evaluated for the Qa and PWF aquifers. A maximum change in wedge toe of 50 m occurred within 40 years (for instantaneous SLR) and 100 years (for gradual SLR) in the Qa. In the PWF, change in wedge toe was about 410 and 230 m after 100 years, for instantaneous and gradual SLR, respectively. Steady state had not been reached after 450 years in the PWF. Analysis of SLR in the MS was not possible due to unstable interface conditions. In general, results of this study highlight the need for further detailed investigation of SWI in the PWF and MS aquifers. Establishing the extent of SWI under current conditions is the main priority for both the PWF and MS aquifers. An important element of this involves research into the offshore extent of these aquifers. Further, predictions of SWI in the PWF should consider future extraction and SLR scenarios in the first instance. A field-based investigation of the Willunga aquifer is ongoing, and the current study provides guidance for well installation and for future data collection.

10.1 Introduction

In coastal aquifers, changes in the hydrology of the coastal zone can cause landward movement of seawater, a process referred to as seawater intrusion (SWI). Historically, the occurrence of SWI has been linked to excessive groundwater pumping or groundwater discharge to surface features, and these have led to significant losses in the available freshwater resources in coastal aquifers worldwide (FAO 1997). However, climate change impacts (e.g., sea-level rise (SLR) and reductions in aquifer recharge) can also induce SWI (e.g., Post 2005). Therefore, the vulnerability of coastal aquifers to climate change, increased levels of extraction and SLR should be jointly considered in water management investigations.

In Australia, where over 85 % of the population live within 50 km of the coast (ABS 2004), SWI poses a threat to groundwater resources in all of the states and the Northern Territory (Werner 2010). However, the extent of monitoring and investigations specific to SWI are highly variable across the nation, with detailed SWI investigations having occurred in only a few areas (Werner 2010). A method for rapid first-order assessment of SWI vulnerability is needed to identify current and emerging risk areas, along with the key drivers of SWI in these areas. This information can then be used to prioritise areas requiring more detailed SWI investigations in the future.

SWI is a complex process that involves variable-density flow, solute transport and hydrochemical processes (Werner et al. 2013), which can make SWI assessment relatively difficult and expensive. As a result, the assessment of SWI vulnerability over large scales has been carried out using mainly qualitative methods, such as GALDIT (Lobo-Ferreira et al. 2007) and CVI(SLR) (Ozyurt 2007), which consider only a subset of the factors thought to impact SWI. For example, aquifer fluxes are not accounted for, and SWI vulnerability arising from changes in sea-level, recharge or extraction, are not captured directly, if at all. Also, these methods largely lack a theoretical basis and rather they focus subjectively on a selection of the elements associated with SWI.

Recently, an alternative to the above-mentioned large-scale methods has been developed by Werner et al. (2012). The method is based on the steady-state, sharp-interface equations of Strack (1976), and therefore incorporates the physical mechanics of SWI, albeit under highly idealised conditions. Werner et al. (2012) described the development of a range of simple SWI vulnerability indicator equations for unconfined and confined aquifer systems. The basic premise is that partial derivative equations quantify the propensity for SWI as rates of change in SWI extent for a range of different stresses (e.g., increased extraction, reduced recharge and SLR). Using this approach, SWI vulnerability (defined as the propensity for SWI to occur) can be easily and rapidly quantified. A relatively small number of hydrogeological parameters are required for the method, making it suitable for application within data poor areas. Further, SWI vulnerability to different stresses can be readily compared using this approach, given the simple nature of the underlying equations. Werner et al. (2012) applied the method to a number of coastal aquifer systems, where detailed SWI assessments have been carried out, and found a general agreement between their approach and the vulnerability determinations obtained from more detailed investigations.

The steady-state analysis of Werner et al. (2012) does not provide information on SWI transience (i.e., variability with time), despite that the method is considered an improvement over previous large-scale approaches. Nevertheless, failure to account for SWI transience is arguably a significant limitation, given that the perceived importance of any water resource issue is likely to be a combination of both the magnitude and the immediacy of the event. The lack of temporal insights is a common short-coming of analytical SWI methods (Cheng and Ouazar 1999). Exploration of SWI transience generally necessitates the use of variable-density flow and transport numerical models, which involve a greater degree of complexity and computational effort than analytical approaches. Hence, it is commonplace to undertake cross-sectional 2D numerical modelling to limit the computational effort of transient, dispersive modelling. Watson et al. (2010) and Webb and Howard (2011) used 2D numerical simulations to show that SWI time scales (i.e., the time for new steady-state conditions to be reached following a SLR event) is typically in the order of decades to centuries, at least for idealised hydrogeological conditions. Watson et al. (2010) found that in some cases, an over-shoot in the seawater wedge occurred whereby the final steady-state location was temporarily exceeded during transient simulations, suggesting that steady-state may not be the worst case, as had

previously been thought. These findings highlight the importance of exploring SWI transience as a next step following steady-state SWI assessment (or other first-order analyses), even if a relatively simple and idealised aquifer conceptualisation is used for transient analysis.

In this study, we apply the recently developed method of Werner et al. (2012) for the rapid assessment of SWI that is suitable for use when limited data are available and large areas are to be considered. The method is applied to the Willunga Basin, South Australia, which was selected because it is typical of many Australian coastal aquifer systems at risk of SWI, in that there are currently no SWI-specific monitoring, modelling or management in place. In addition, the Willunga Basin is a multiple aquifer system and, as such, allows demonstration of the method for both unconfined and confined aquifer systems. As an extension to the Werner et al. (2012) method, we examine transient effects, by evaluating the temporal development of SWI under conditions similar to those of the Willunga Basin, as induced by projected SLR.

10.2 Theory

10.2.1 Analytical Approach

The analytic solution for the steady-state location of the freshwater-seawater interface developed by Strack (1976, 1989) is the basis for the method described by Werner et al. (2012), and summarised here. Figure 10.1 illustrates the conceptual model for unconfined and confined aquifers.

The water budget for the problem domain, as shown in Fig. 10.1, is comprised of net recharge (W_{net} [L/T], accounting for infiltration, evapotranspiration and distributed pumping), freshwater discharge to the sea (q_0 [L^2/T]), and lateral flow from aquifers inland of the landward boundary (q_b [L^2/T]). The hydraulic head (h_f [L]) is related to the depth of the interface (z [L]) by the Ghyben-Herzberg relation: $z = h_f/\delta$. Here, δ [-] is the dimensionless density ratio $\delta = (\rho_s - \rho_f)/\rho_f$, and ρ_s (= 1,025 kg/m^3) and ρ_f (= 1,000 kg/m^3) are freshwater and seawater densities, respectively [M/L^3], so that $\delta = 0.025$. The freshwater thickness is h [L], and the base of the aquifer is z_0 [L] below mean sea level. In the confined aquifer, the saturated aquifer thickness in Zone 1 is h_0. Zone 1 is the region inland of the saltwater wedge and Zone 2 is the region between the coast and the inland extent (x_T) of the saltwater wedge. From a conceptual perspective, while the problem domain is theoretically infinite in the landward direction, the cross section is assumed to occur in a coastal fringe of between 1 and 5 km from the coast.

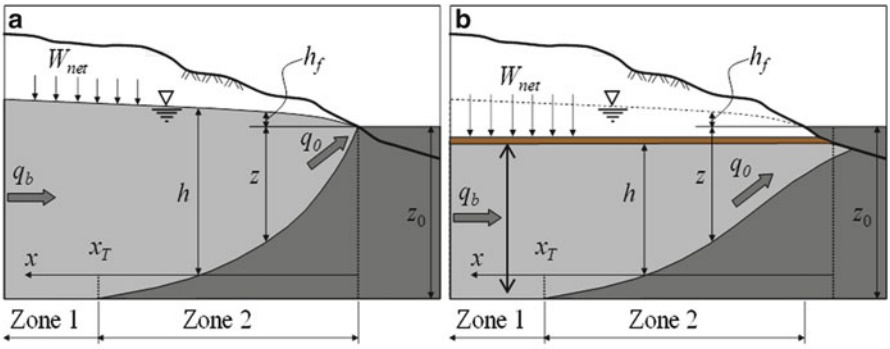

Fig. 10.1 Description of hydrogeological variables for: (**a**) unconfined aquifer and (**b**) confined aquifer settings (adapted from Werner et al. 2012)

10.2.1.1 Unconfined Aquifers

Strack (1976) used the potential method to produce equations for h_f as a function of aquifer parameters and distance from the coast x [L]. In Zone 1 ($x \geq x_T$; Fig. 10.1a):

$$h_f = \sqrt{\frac{2q_0x - W_{net}x^2}{K} + (1+\delta)z_0^2} - z_0 \tag{10.1}$$

In Zone 2 ($x \leq x_T$; Fig. 10.1a):

$$h_f = \sqrt{\left(\frac{\delta}{1+\delta}\right)\frac{2q_0x - W_{net}x^2}{K}} \tag{10.2}$$

Here, K is the hydraulic conductivity [L/T] and other parameters are defined above. Equations (10.1) and (10.2) can be rearranged to allow for the estimation of q_0 for a given h_b at x_b from the coast (i.e., obtained from monitoring well observations), and using estimates of the other aquifer parameters (K, z_0, δ, W_{net}). In Zone 1:

$$q_0 = \frac{K\left((h_b + z_0)^2 - (1+\delta)z_0^2\right) + W_{net}{x_b}^2}{2x_b} \tag{10.3}$$

In Zone 2:

$$q_0 = \left(\frac{1+\delta}{\delta}\right)\frac{K}{2x_b}h_b^2 + \frac{W_{net}x_b}{2} \tag{10.4}$$

Note that the choice of Eqs. (10.3) or (10.4) for estimating q_0 depends on whether the given h_b value occurs within Zone 1 (i.e., head measurement is inland

of the interface) or Zone 2 (i.e. head measurement is above the interface). The location of the wedge toe x_T [L] (see Fig. 10.1) is derived through considering that $h_f = \delta z_0$ at the wedge toe. In situations where recharge (e.g. from rainfall) exceeds the combined outflows from distributed pumping and groundwater evapotranspiration (i.e., $W_{net} > 0$), the wedge toe is obtained from (Cheng and Ouazar 1999):

$$x_T = \frac{q_0}{W_{net}} - \sqrt{\left(\frac{q_0}{W_{net}}\right)^2 - \frac{K\delta(1+\delta)z_0^2}{W_{net}}} \tag{10.5}$$

The conceptualisation of Fig. 10.1a assumes that a no-flow boundary occurs at some inland distance. That is, the lateral inflow is zero ($q_b = 0$) at some distance (x_n) from the coast. By considering the water balance, the value of x_n is given as (Werner et al. 2012):

$$x_n = q_0 / W_{net} \tag{10.6}$$

As the wedge toe approaches x_n, there is progressively less freshwater discharge to oppose the inland movement of the seawater wedge. In other words, the distance x_n serves as a practical limit to the extent of SWI in the aquifer. Conditions causing the wedge toe to reach or exceed x_n (i.e., $x_T \geq x_n$) are more likely to be associated with adverse SWI events. One of the advantages of using analytical equations in assessing problems such as SWI vulnerability is that parameter combinations are identifiable from the relevant equations. For example, Eq. (10.5) can be written in a simplified form, as (Werner et al. 2012):

$$x_T = x_n\left(1 - \sqrt{1 - M}\right) \tag{10.7}$$

Here, M [-] is a useful dimensionless combination of parameters that can be directly related to the SWI conditions, and is defined as (Werner et al. 2012):

$$M = \frac{K\delta(1+\delta)z_0^2}{W_{net}x_n^2} \tag{10.8}$$

Werner et al. (2012) termed M a "mixed convection ratio", because the numerator describes the density-driven processes causing landward migration of the wedge, whilst the denominator represents freshwater advection processes that oppose SWI. If $M \geq 1$, the density-driven processes dominate, creating an unstable SWI situation (i.e., high SWI vulnerability). As such, M is a useful SWI vulnerability measure.

Seawater volume is adopted in this study as an alternative to x_T for quantifying the extent of SWI. The volume of seawater V_{sw} [L^3/L] per metre of coastline is found from the area (in cross section perpendicular to the shoreline) of the saltwater wedge, which is determined by integrating the interface equation (i.e., obtained by

combining Eq. (10.2) and the relationship $z = h_f/\delta$) between the coast ($x = 0$) and the toe ($x = x_T$). For the case $W_{net} > 0$, the following equation is derived (Werner et al. 2012):

$$V_{sw} = n\, z_0 \left(x_T - \frac{x_n}{2} \left(\sqrt{\frac{1}{M}} \arcsin\left(\sqrt{M}\right) - \sqrt{1-M} \right) \right) \tag{10.9}$$

Here, n is porosity [-].

10.2.1.2 Confined Aquifers

As with unconfined aquifers, Strack (1976) used the potential method to produce equations for h_f as a function of aquifer parameters and with distance from the coast in confined aquifers. In Zone 1 ($x \geq x_T$; Fig. 10.1b):

$$h_f = \frac{q_0 x - W_{net} \frac{x^2}{2}}{K h_0} + \delta z_0 - \frac{\delta h_0}{2} \tag{10.10}$$

In Zone 2 ($x \leq x_T$; Fig. 10.1b):

$$h_f = \sqrt{(2 q_0 x - W_{net} x^2) \frac{\delta}{K}} + \delta z_0 - \delta h_0 \tag{10.11}$$

Parameters used here have been defined previously. Equations (10.10) and (10.11) can be re-arranged to allow for the estimation of q_0 from a given h_b (i.e., obtained from monitoring well observations) at x_b from the coast. In Zone 1:

$$q_0 = \frac{K}{2\delta x_b} \left(2\delta h_b h_0 + (\delta h_0)^2 - 2\delta^2 z_0 h_0 \right) + \frac{W_{net} x_b}{2} \tag{10.12}$$

In Zone 2:

$$q_0 = \frac{K}{2\delta\, x_b} (h_b + \delta h_0 - \delta z_0)^2 + \frac{W_{net} x_b}{2} \tag{10.13}$$

The choice of Eqs. (10.12) or (10.13) for estimating q_0 depends on whether the given h_b value occurs within Zone 1 or Zone 2, as previously. x_T can again be derived by considering that $h_f = \delta z_0$ at the wedge toe. We adopt cases where $W_{net} = 0$, because recharge to the Willunga Basin confined aquifers is poorly constrained and likely to be small within the coastal zone given the lithology, and also this is a common first-order assumption (e.g., Custodio 1987). This leads to (Werner et al. 2012):

$$x_T = \frac{\delta K h_0^2}{2 q_0} \tag{10.14}$$

The volume of seawater (per metre of coastline) is found from the area of the saltwater wedge, obtained through integrating the interface equation between $x = 0$ and $x = x_T$, to produce (Werner et al. 2012):

$$V_{sw} = \frac{n\delta K {h_0}^3}{6q_0} \tag{10.15}$$

The confined aquifer conceptualisation used here does not account for continuation of aquifers off-shore and may therefore result in overestimation of the landward position of the interface in confined aquifers. Analytic solutions presented by Bakker (2006) and Kooi and Groen (2001) account for offshore continuation of confined aquifers. However, information on parameters required for the method (e.g., distance the aquifer extends off-shore and the vertical hydraulic conductivity of the semi-confining aquitard) are not available for the Willunga Basin aquifers. Therefore, the approach adopted here assumes that freshwater discharges from the confined aquifer at the coastline, in line with the Werner et al. (2012) approach.

The density corrected freshwater head in a confined aquifer terminating at the coast is:

$$h_{coast} = \delta(z_0 - h_0) \tag{10.16}$$

Equation (10.16) is derived from Eq. (10.13) when $x = 0$. The freshwater head in the aquifer and close to the coast (e.g., from observation wells) needs to be greater than this value for there to be freshwater discharge (i.e., $q_0 > 0$) and to avoid active SWI, i.e., SWI occurring under a hydraulic gradient sloping downwards in the inland direction. It is important to compare aquifer heads with the density corrected head at the coast (obtained from Eq. (10.16)) because Eq. (10.13) provides a positive q_0 value (due to the squared bracketed term) even when the head in the aquifer is less than the head at the coast (i.e., when $h_b < h_{coast}$), and this can lead to erroneous results for q_0, x_T and V_{sw}. If the aquifer continues offshore, the head required for freshwater discharge will be greater than that described by Eq. (10.16).

10.2.1.3 SWI Vulnerability Indicators

The sensitivity of SWI to different stresses has been characterised by Werner et al. (2012) using partial derivative equations. These equations describe the propensity for the wedge toe to change with changes in sea level, recharge or inflows at the inland boundary (as might occur due to increased extraction). Werner and Simmons (2009) found that the impact of SLR in unconfined coastal aquifers is greater in head-controlled systems (where groundwater abstractions or surface water features maintain the head in the aquifer despite SLR) than in flux-controlled systems (where groundwater discharge to the sea remains constant despite SLR). In line with these findings, Werner et al. (2012) developed derivative equations relating to both head-controlled and flux-controlled systems. A number of the partial derivative equations, which will be applied to the Willunga Basin case study, are

Table 10.1 SWI Vulnerability indicator equations

Unconfined aquifers			
Flux-controlled setting		Head-controlled setting	
SLR		SLR	
$\frac{\partial x_T}{\partial z_0} = \frac{x_n M}{z_0\sqrt{1-M}}$	(10.17)	$\frac{\partial x_T}{\partial z_0} = \frac{x_n M}{z_0\sqrt{1-M}} + \frac{x_n M}{\delta z_0}\left(\frac{1-\sqrt{1-M}}{\sqrt{1-M}}\right)$	(10.18)
Change in net recharge		Change in net recharge	
$\frac{\partial x_T}{\partial W_{net}} = -\frac{x_n M}{2W_{net}\sqrt{1-M}}$	(10.19)	$\frac{\partial x_T}{\partial W_{net}} = -\frac{x_n M}{2W_{net}\sqrt{1-M}} + \frac{x_n\left(1-\sqrt{1-M}\right)}{2W_{net}\sqrt{1-M}}$	(10.20)
Change in flux at the inland boundary			
$\frac{\partial x_T}{\partial q_b} = \frac{1}{W_{net}}\left(1 - \frac{1}{\sqrt{1-M}}\right)$	(10.21)		
Confined aquifers			
Flux-controlled setting		Head-controlled setting	
SLR, where $W_{net} = 0$		SLR, where $W_{net} = 0$	
$\frac{\partial x_T}{\partial z_0} = 0$	(10.22)	$\frac{\partial x_T}{\partial z_0} = \frac{\delta(1+\delta)K^2 h_0^3}{2q_0^2 x_f}$	(10.23)
Changes in inflows at the inland boundary, where $W_{net} = 0$			
$\frac{\partial x_T}{\partial q_b} = \frac{\partial x_T}{\partial q_0} = -\frac{\delta K h_0^2}{2q_0^2}$	(10.24)		

Adapted from Werner et al. (2012)

presented in Table 10.1. Derivatives associated with changes in recharge are not presented for the confined aquifers because, as previously mentioned, an assumption of zero net recharge has been made for the Willunga Basin confined aquifers. Werner et al. (2012) provides further details, including assumptions applied in deriving these equations.

10.2.2 Transient Analysis

The transience of SWI arising from SLR was explored using a selection of 2D simulations. The variable-density flow and solute transport code SEAWAT (Version 4; Langevin et al. 2008) was used. Description of the numerical methods and equations used in SEAWAT are given by Guo and Langevin (2002) and Langevin et al. (2008).

10.3 Application to the Willunga Basin

10.3.1 Conceptualisation and Parameterisation of the Willunga Basin

The Willunga Basin is situated south of Adelaide in South Australia, as shown in Fig. 10.2. The Willunga Basin is an important food production region and

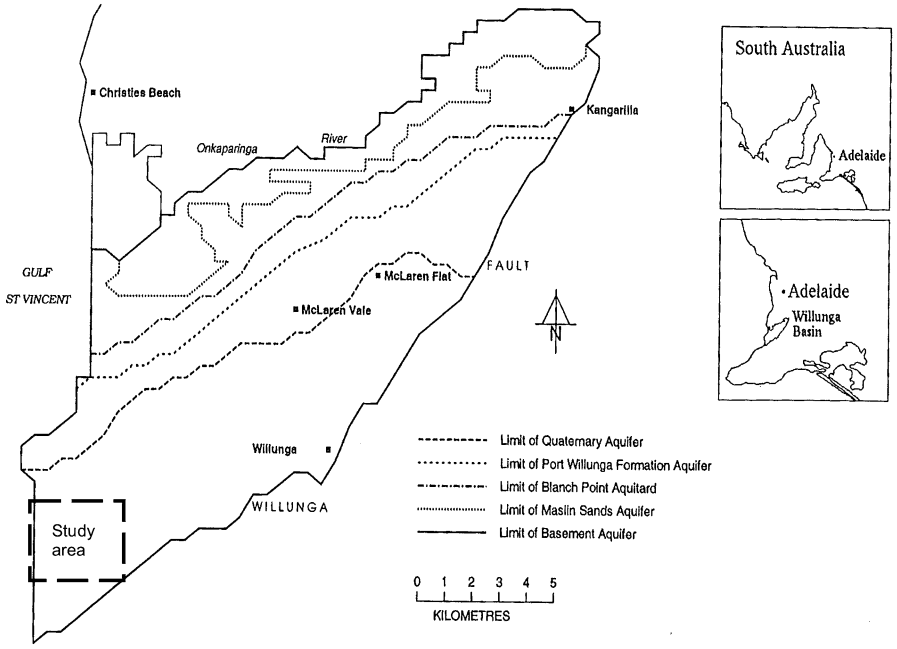

Fig. 10.2 The Willunga Basin location and extent of hydrogeological units (based on Rasser 2001)

groundwater is used to irrigate almonds, grapes and olives. The four main aquifers within the Willunga Basin are the unconfined Quaternary aquifer (Qa) (comprised of sands, gravels and interbedded clays), the confined Port Willunga Formation aquifer (PWF) (loosely consolidated sands and indurated limestone), the confined Maslin Sands aquifer (MS) (very fine to coarse sands) and a fractured basement rock aquifer (FR). The majority of salinities are less than 1,500 mg/L in all four of these aquifers and groundwater is generally considered suitable for irrigation purposes, despite some individual monitoring locations recording significantly higher salinities (Obswell network, https://obswell.pir.sa.gov.au/).

The majority of the metered groundwater extraction is from the PWF aquifer, followed by the MS and FR aquifers. Although groundwater use is regulated under state water allocation planning frameworks, the existing coastal groundwater network is not appropriate for monitoring potential SWI impacts, because observation wells do not penetrate to the base of the aquifers (where any SWI would most likely be observed). However, anecdotal evidence from recent drilling conducted within the Basin's coastal fringe suggests salinity impacts in wells drilled to near the base of the PWF aquifer. Field measured electrical conductivity (EC) during air lifting of two pilot trial aquifer storage and recovery injection wells located at 1,300 and 1,800 m from the coast indicated EC values of around 20 mS/cm (~12,000 mg/L) and 40 mS/cm (~24,000 mg/L), respectively, well outside the average aquifer salinity of 1,500 mg/L. Salinity impacts were not observed during development

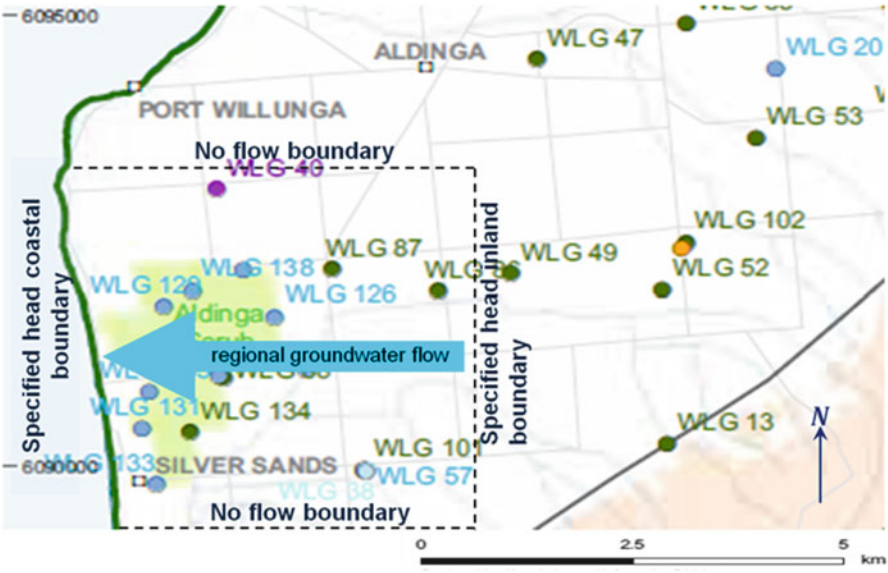

Fig. 10.3 Study area for Willunga Basin conceptualisation, with towns (e.g., Port Willunga) and monitoring boreholes (e.g., WLG47) identified

of two adjacent, shallower wells constructed within the PWF implying a seawater wedge configuration, consistent with SWI and a seawater wedge that is at least 2 km from the coast in the PWF.

The study area selected for the analysis is identified in Figs. 10.2 and 10.3. It covers a distance of approximately 3,500 m of coastline and has an inland boundary approximately 3,500 m from the coast. The aquifers included in the assessment are the Qa, PWF and MS sequences. The FR aquifer was not considered due to lack of water level and aquifer geometry data.

The Willunga Basin parameters required for the Werner et al. (2012) equations were obtained from the following sources: site-specific reports (for net recharge values; Herzceg and Leaney 2002); review of hydrographs using the Obswell network (for heads in the different aquifers); interpretation of lithological logs from the Drillhole Enquiry System (https://des.pir.sa.gov.au/deshome.html) and Obswell (for aquifer geometry); and application of literature values (for hydraulic conductivity and porosity) typical of the study area lithologies. Pump test information was not available for the coastal region of the Willunga Basin. The resulting parameter values are shown in Table 10.2. In estimating W_{net}, it was assumed that all extraction occurs inland of the 3,500 m inland boundary. As such, W_{net} represents rainfall recharge for the Qa aquifer, and W_{net} is zero for the PWF and MS aquifers, as previously mentioned. An estimated pre-development (i.e., pre-pumping) head was also needed for the analysis of the PWF aquifer, and this was based on historical maximum heads.

Table 10.2 Hydrogeological parameters for the Willunga Basin aquifers

Aquifer	K (m/day)	W_{net} (mm/year)	z_0 (m)	h_0 (m)	h_b (m)	x_b (m)	n (-)
Qa (Unconfined)	10	20	20	–	3.0	3,500	0.3
PWF (Confined)	10	0	120	90	1.5 (3.0)[a]	3,500	0.3
MS (Confined)	1	0	225	65	2.0	3,500	0.3

[a]Estimated pre-development head

Table 10.3 Results indicating theoretical SWI extent for the Willunga Basin aquifers

Aquifer	q_0 (m^2/day)	q_0 equation	x_T (m)	M (-)	V_{sw} (m^3/m)
Qa (Unconfined)	0.27	(3)	197	0.08	390
PWF (Confined)	0.03 (0.29)[a]	(13)	31,500 (3,500)[a]	NA	283,500 (31,500)[a]
MS (Confined)	<0.00	(13)	Unstable	NA	Unstable

[a]Calculated pre-development values

10.3.2 Theoretical SWI Extent in the Willunga Basin

The hydrogeological parameters listed in Table 10.2, along with Eqs. (10.3), (10.5), (10.8), (10.9), (10.13), (10.14) and (10.15) were used to estimate discharge to the sea and the theoretical steady-state extent of SWI within each aquifer, as shown in Table 10.3. These results represent the theoretical long-term (i.e., steady-state) condition of the system based on modern-day stresses, unless otherwise stated.

The estimated inland extent of SWI in the Qa aquifer is relatively small, and the low M value suggests that SWI vulnerability is also low. For the PWF aquifer, the theoretical inland distance to the toe is very large (>31 km) under current conditions. This value exceeds the inland limit of the coastal fringe ($x_b = 3{,}500$ m) and is indicative of an extensive seawater wedge. The q_0 calculated using pre-development conditions is almost ten times the value under current conditions. The difference between the current and pre-development values of V_{sw} indicates that a large volume of seawater has entered (or will eventually enter) the PWF since the pre-development period.

The confined MS aquifer was found to have a hydraulic gradient that sloped downwards toward the inland (the head at the coast, calculated using Eq. (10.16), was 4.0 m AHD, while the head in the aquifer was estimated at 2.0 m AHD). This implies that the value of q_0 is negative (no freshwater discharge to the sea, but rather seawater flows inland), which suggests unstable interface conditions. Under these circumstances, the wedge toe is probably moving inland (notwithstanding the limitations of the steady-state analysis and the likely off-shore extension of the confined aquifer), creating the most extensive SWI over long timeframes. It is not possible to calculate x_T or V_{sw} for the MS aquifer due to the theoretically unstable interface condition. However, the location of the interface stability limit (i.e., for $h_b = 4.0$ m AHD) is shown in Fig. 10.4, along with the steady-state interface for the unconfined Qa and confined PWF within the coastal fringe. Given the approximate nature of the analysis, the interface and water table distributions shown in Fig. 10.4 are not intended as accurate representations for the Qa, PWF and MS aquifers.

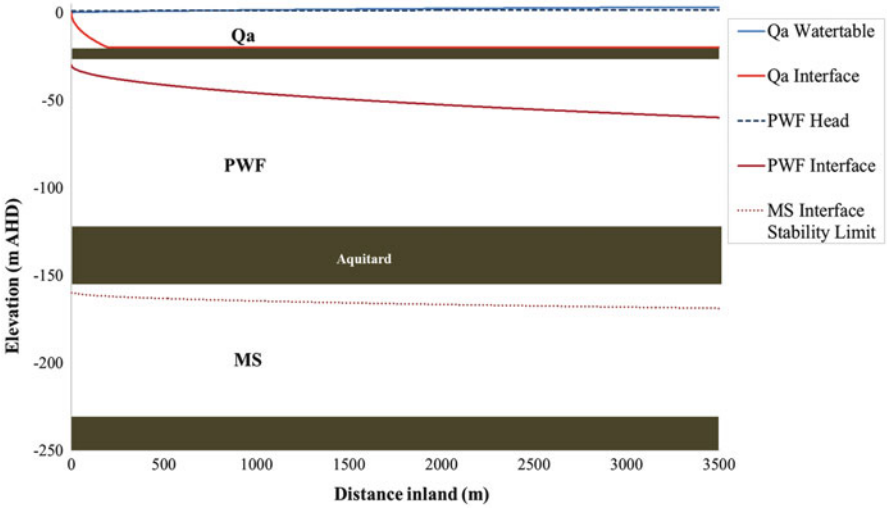

Fig. 10.4 Approximation of the near-coastal water table and interface locations for the Willunga Basin aquifers

Rather, the results provide a rough guide to the likely steady-state extent of seawater in the aquifer, under current-day stresses. In the case that the PWF aquifer (and the MS aquifer) extend significant distances off-shore, the results presented here will tend to over-estimate the inland extent of the interface in these aquifers.

10.3.3 SWI Vulnerability Indicators for the Willunga Basin

SWI vulnerability indicators were calculated using Eqs. (10.17)–(10.24) and parameters in Table 10.2 for the Qa and PWF aquifers. Vulnerability indicators could not be calculated for the MS aquifer as it is theoretically unstable; however, it can be inferred that the already high potential vulnerability of the MS aquifer will increase under increased stresses associated with climate change and pumping. Werner et al. (2012) began a database of aquifers for which SWI vulnerability indicators were calculated and these are presented in Table 10.4, along with results for the Willunga Basin analysis. The addition of more cases to this database allows for an improved relative assessment of SWI vulnerability. In Table 10.4, Cases 1a–1c represent three scenarios associated with the Gaza unconfined aquifer investigation by Moe et al. (2001); specifically 1a represents undisturbed conditions, 1b represents full implementation of a management plan, and 1c is where inland flows have been compromised (inferring increased SWI vulnerability). Cases 2a and 2b represent two locations with differing unconfined hydrogeological settings within the Pioneer Valley aquifer (Werner and Gallagher 2006) whereby the setting for Case 2a was found as having increased susceptibility to SWI. Cases 3a and 3b represent the Nile

Table 10.4 Vulnerability indicators

Case	Aquifer type	Flux-controlled			Head-controlled	
		$\frac{\partial x_T}{\partial z_0}$ (-)	$\frac{\partial x_T}{\partial W_{net}}$ (d)	$\frac{\partial x_T}{\partial q_b}$ (d/m)	$\frac{\partial x_T}{\partial z_0}$ (-)	$\frac{\partial x_T}{\partial W_{net}}$ (d)
1a	Unconfined	12	−3.8E6	−190	26	−1.9E6
1b	Unconfined	9	−5.4E6	−108	12	−2.7E6
1c	Unconfined	15	−8.8E6	−280	29	−4.3E6
2a	Unconfined	67	−2.8E6	−780	570	−1.2E6
2b	Unconfined	14	−5.9E5	−39	21	−2.9E5
3a	Confined	0	n/a	−4.7E4	9,600	n/a
3b	Confined	0	n/a	−1,300	2,700	n/a
4	Unconfined	71	−3.2E6	−460	380	−1.5E6
5	Unconfined	20	−3.7E6	−770	53	−1.8E6
6	Confined	0	n/a	−9.8E5	2.6E5	n/a

After Werner et al. (2012)

Delta and Madras confined aquifer cases, respectively, studied by Sherif and Singh (1999), whereby the Nile Delta (3a) was identified as being more vulnerable to SLR and climate change-induced SWI. Case 4 represents the Uley South limestone unconfined aquifer described by Zulfic et al. (2007) and Werner et al. (2011). Cases 5 and 6 are the Qa and PWF aquifers for the Willunga Basin, respectively.

Vulnerability indicator values in Table 10.4 can be used to rank the vulnerability of different aquifers to the same stress. It can be seen that Case 5 has a relatively low vulnerability to SLR (when compared to Cases 2a and 4) and a relatively low vulnerability to recharge change (when compared to Cases 1b and 1c). However, Case 5 has a relatively high vulnerability to changes in inflows at the inland boundary. Similarly, it can be seen that Case 6 is more vulnerable to changes in inflows at the inland boundary and SLR (for the head-controlled case) than all other cases assessed.

The vulnerability indicators cannot be used to compare sensitivities to different stresses within the same aquifer system because the indicators have different units. Werner et al. (2012) used logarithmic sensitivities in order to make this comparison. Logarithmic sensitivities measure the fractional change in output for a fractional change in a parameter (Kabala 2001). Table 10.5 lists logarithmic sensitivities for Cases 1–6.

There is significant uncertainty regarding the designation of flux-controlled or head-controlled conditions for the Willunga Basin aquifers. However, as the Qa aquifer is not heavily utilised and is responsive to recharge, it is more likely to be flux-controlled. In contrast, the PWF and MS aquifers are heavily utilised for irrigation; therefore aquifer heads are likely to be maintained at a constant value (i.e., head controlled) by pumping despite stress changes arising from SLR or climate change. It can be seen from Table 10.5 that the Qa aquifer (assuming flux-controlled conditions) is more sensitive to fractional changes in SLR than to recharge change or changes in inflows at the inland boundary. For the PWF aquifer (assuming head-controlled conditions) sensitivity to SLR is significantly larger than sensitivity to changes in inflows at the inland boundary.

Table 10.5 Logarithmic sensitivities

Case	Aquifer type	Flux-controlled			Head-controlled	
		$\frac{\partial x_T}{\partial z_0}\frac{z_0}{x_T}$ (-)	$\frac{\partial x_T}{\partial W_{net}}\frac{W_{net}}{x_T}$ (-)	$\frac{\partial x_T}{\partial q_b}\frac{q_b}{x_T}$ (-)	$\frac{\partial x_T}{\partial z_0}\frac{z_0}{x_T}$ (-)	$\frac{\partial x_T}{\partial W_{net}}\frac{W_{net}}{x_T}$ (-)
1a	Unconfined	2.0	−1.0	−0.53	4.4	−0.5
1b	Unconfined	2.0	−1.0	−0.81	2.7	−0.5
1c	Unconfined	2.0	−1.0	−0.70	3.9	−0.5
2a	Unconfined	2.2	−1.1	−0.61	19	−0.5
2b	Unconfined	2.0	−1.0	−0.95	2.9	−0.5
3a	Confined	0	n/a	−1.0	53	n/a
3b	Confined	0	n/a	−1.0	62	n/a
4	Unconfined	2.1	−1.1	−0.82	12	−0.5
5	Unconfined	2.0	−1.0	−0.3	5.4	−0.5
6	Confined	0	n/a	−1.0	980	n/a

After Werner et al. (2012)

In general, the vulnerability indicator and logarithmic sensitivity results suggest that the key drivers of SWI in the Willunga Basin aquifers are changes in flows at the inland boundary (for the Qa and PWF aquifers) and SLR (for head-controlled conditions) in the PWF aquifer. High vulnerability is inferred for the MS aquifer because it was found to have unstable interface conditions.

10.3.4 Transient Analysis

Conceptualisation of the Willunga Basin adopted for numerical modelling of transient SWI was configured as individual representations of the Qa, PWF and MS aquifers in two dimensions, and in cross section perpendicular to the coast, as shown in Fig. 10.5. As head-controlled settings have been shown to result in greater SLR-induced SWI within unconfined and confined aquifers compared to flux-controlled conditions (Werner and Simmons 2009; Werner et al. 2012), all numerical model representations for this study assumed head-controlled conditions. Hence the results represent a worst case and it is assumed that heads are maintained at the same level at 3.5 km from the coast due to pumping.

The model domain was uniformly discretised for transient simulations of both the Qa, PWF and MS aquifers, with 700 vertical columns of 5 m width. The Qa model had 20 horizontal layers of 1 m thickness, the PWF had 36 layers of 2.5 m thickness and the MS had 26 layers of 2.5 m thickness. This grid discretisation is consistent with a Peclet number less than 2, as recommended by Diersch and Kolditz (2002) for the reduction of numerical oscillations. A specified-head boundary condition was applied at the inland boundary. A specified-head and constant-concentration boundary condition was used for the coastal boundary, with a seawater concentration of 35 kg/m^3. For confined aquifers, the coastal boundary head under initial conditions (i.e., pre-SLR) was determined using equation (10.16).

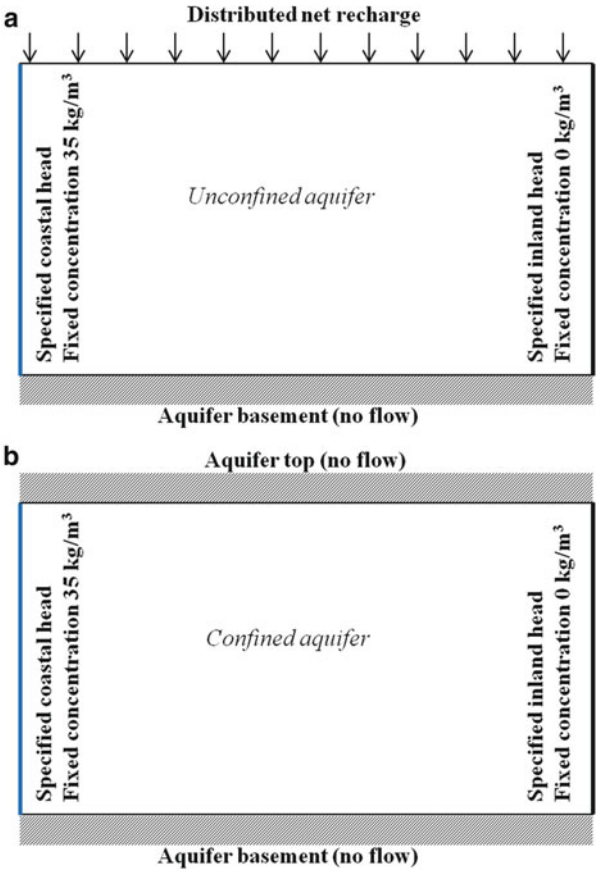

Fig. 10.5 Simplified aquifer conceptualisations for the purposes of numerical modelling of transient SWI: (**a**) Qa aquifer, and (**b**) PWF and MS aquifers

The Strongly Implicit Procedure (SIP) and General Conjugate Gradient (GCG) solvers were selected for flow and transport, respectively. The Hybrid Method of Characteristics (HMOC) solution scheme was selected for the advection term, with a Courant number of 0.75. A Courant number less than or equal to one is generally required to limit numerical dispersion and achieve accurate results (Zheng and Bennett 2002).

The parameter values adopted for the numerical simulations using SEAWAT are shown in Table 10.6. Coastal head values are for initial conditions (i.e., pre-SLR). The assumed pre-development inland head (Table 10.2) was used for the PWF aquifer model so that the wedge toe under initial conditions would occur within the model domain. For the purpose of tracking SWI, the toe was defined as the interception of the 50 % seawater isochlor with the aquifer basement.

For the parameter values in Table 10.6, initial steady-state conditions for the Qa and PWF aquifers were achieved using time marching, until the wedge toe was found to stabilise. Steady state was not achieved for the MS aquifer after 2,000 years (for parameter values in Table 10.6), which is in line with previous findings

Table 10.6 Parameter values adopted for numerical simulations using SEAWAT

Parameter (units)	Label	Qa value	PWF value	MS value
Inland head (m)	h_b	3	3	2
Inland distance (m)	x_b	3,500	3,500	3,500
Coastal head (m)		0	0.75	4
Aquifer base below sea level (m)	z_0	20	110	215
Aquifer thickness (m)	h_0	–	90	65
Recharge (mm/year)	W_{net}	20	0	0
Horizontal hydraulic conductivity (m/day)	K_x	10	10	1
Vertical hydraulic conductivity (m/day)	K_y	10	10	10
Longitudinal dispersivity (m)	α_L	1	1	1
Transverse dispersivity (m)	α_T	0.1	0.1	0.1
Molecular diffusion (m^2/day)	D	$9E^{-5}$	$9E^{-5}$	$9E^{-5}$
Effective porosity (-)	n_e	0.3	0.3	0.3
Specific yield (-)	S_y	0.2	–	–
Specific storage (/m)	S_s	–	$2E^{-5}$	$2E^{-5}$
Seawater density (kg/m^3)	ρ_s	1,025	1,025	1,025
Seawater salinity (kg/m^3)		35	35	35

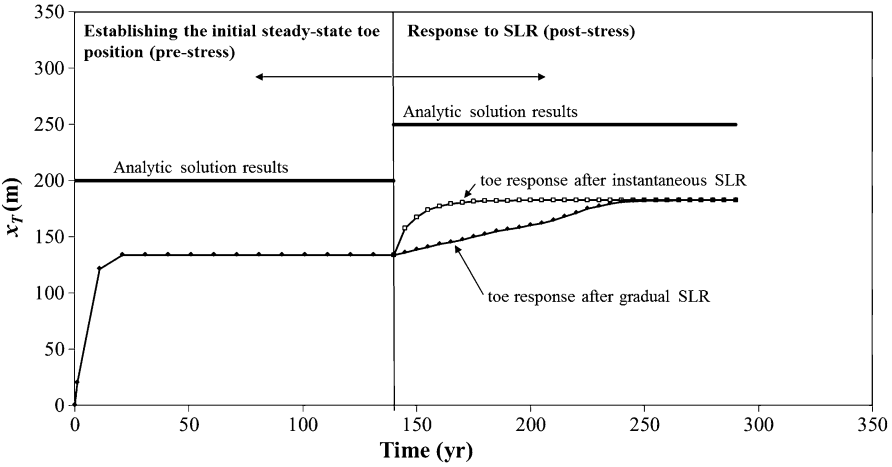

Fig. 10.6 Comparison of toe positions in the Qa aquifer before and after SLR using the analytic, steady-state approach and transient numerical modelling

(i.e., that the interface is unstable). After an initial steady state was reached for the Qa and PWF aquifers, an instantaneous SLR of 0.88 m was applied. This value is consistent with the upper value presented by the IPCC (2007) for the year 2100 and conforms to the value used in previous studies (e.g., Werner and Simmons 2009). The effects of gradual SLR were also considered. This was achieved by applying a linear rise in sea level of 0.88 m over 90 years, consistent with the approach of Webb and Howard (2011). Results for the Qa and PWF aquifers are shown in Figs. 10.6 and 10.7, respectively.

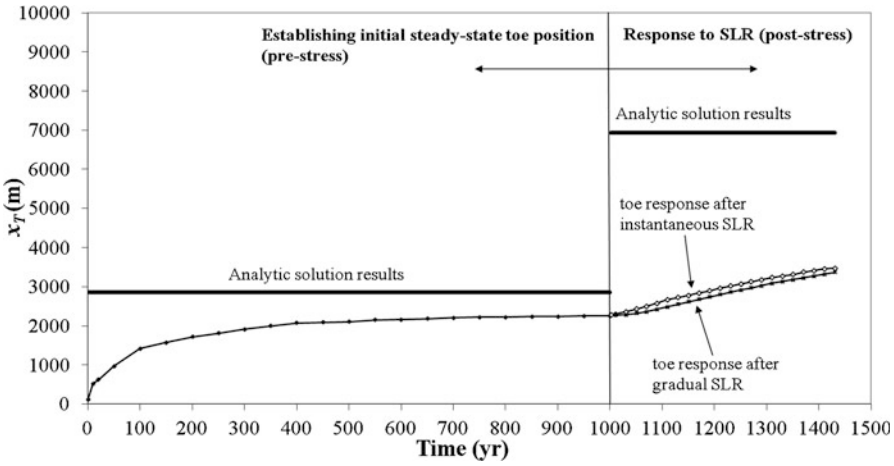

Fig. 10.7 Comparison of toe positions in the PWF aquifer before and after SLR using the analytic, steady-state approach and transient numerical modelling

For both the Qa and PWF aquifers, x_T determined using the numerical model was less than that predicted by the analytical approach. Over-estimation of the toe by the sharp-interface method is expected (e.g., Cooper 1964; Pool and Carrera 2011), because the freshwater-saltwater interface contracts when the seawater circulation cell, caused by the mixing of seawater and groundwater, is considered.

Application of an instantaneous SLR to the unconfined Qa aquifer model resulted in a maximum x_T extent of around 180 m after 40 years (i.e., about a 50 m increase from pre-stress conditions). In contrast, the maximum x_T extent for the gradual SLR case was reached after approximately 100 years.

From the simulation of the PWF aquifer a steady state had not been reached after approximately 450 years in both the instantaneous and gradual SLR cases, at which time the simulation was stopped because the toe was within 50 m of the inland model boundary ($x_b = 3{,}500$ m) for the instantaneous SLR case. This demonstrates that it takes a longer time for interfaces to equilibrate following SLR in the PWF than in the Qa aquifer. This is not surprising given that the PWF is more sensitive than the Qa to SLR (under head-controlled conditions) and the change in the steady-state interface position is much greater, involving larger volumes of seawater entering the aquifer. At 100 years after the commencement of SLR (a period of time relevant to management time frames), x_T had increased by about 410 m for the instantaneous rise and about 230 m for the gradual SLR.

10.4 Conclusions

A method for rapid assessment of SWI vulnerability is needed to pinpoint Australian coastal aquifers at risk of SWI and assist with prioritisation of areas where further detailed SWI investigation may be required. In this regard, the vulnerability

indicators method of Werner et al. (2012) was found to be an improvement over previous methods because it is theoretically based and can be used to identify the key drivers of SWI. Also it can be applied when limited data is available. Within this study, the Werner et al. (2012) method was described through an application to the Willunga Basin, South Australia. In addition, the method was extended using a transient analysis of SLR.

The unconfined Qa aquifer was found to have relatively small SWI extent under current conditions. Comparison with cases considered previously by Werner et al. (2012) indicated that the Qa aquifer had relatively low vulnerability to SLR and recharge change and relatively high vulnerability to changes in flows at the inland boundary (as might occur under increased extraction).

The confined PWF aquifer was found to have large SWI extent under current conditions and there is the potential for a large volume of seawater to have entered (or to eventually enter) the PWF since the pre-development period. As such, active SWI is likely in the PWF aquifer. Like the Qa aquifer, the PWF aquifer was found to have a relatively high vulnerability to changes in flows at the inland boundary. Logarithmic sensitivities indicated that the PWF was most sensitive to fractional changes in SLR, assuming head-controlled conditions. In order to reduce vulnerability to SLR in the PWF aquifer, a management approach that allows heads to rise commensurate with sea-level is required. Further detailed SWI assessment of future extraction and SLR scenarios is warranted for the PWF aquifer.

The MS aquifer was found to have unstable interface conditions, suggesting that the interface is moving inland. As such, the already high vulnerability of the MS aquifer will increase under increased stresses associated with climate change and increased extraction. Further detailed assessment of SWI extent under current conditions is required for the MS aquifer.

Transient analysis of SWI in response to a 0.88 m SLR in the Qa and PWF aquifers demonstrated that instantaneous SLR results in a more rapid SWI response than gradual SLR. For the Qa aquifer, maximum x_T extent was reached after around 40 years for instantaneous SLR and about 100 years for gradual SLR. For the PWF aquifer, a steady state had not been reached after approximately 450 years in both the instantaneous and gradual SLR cases. Instantaneous and gradual SLR results in x_T increases of about 410 and 230 m, respectively, after 100 years.

The Willunga Basin is an important agricultural region and high priority candidate for SWI assessment. At the time of preparation of this report, the existing data set for the Willunga Basin aquifers at the coastal fringe was limited. Therefore the life cycle of the assessment process, from rapid-assessment via application of a first-order analytical approach, to testing of the preliminary assessment outcomes using more complex transient numerical methods, through to extending data sets and developing more realistic numerical representations of coastal aquifer and seawater interactions, can be applied to the Willunga Basin. The results of this study have provided guidance for a planned drilling program within the Willunga Basin which it is hoped will inform future SWI assessment activities.

Acknowledgements This work was partially funded by the National Centre for Groundwater Research and Training, a collaborative initiative of the Australian Research Council and the National Water Commission.

References

Australian Bureau of Statistics (ABS) (2004) Year book of Australia. http://www.abs.gov.au/Ausstats/abs@.nsf/Previousproducts/1301.0Feature%20Article32004. Accessed 10 Apr 2012

Bakker M (2006) Analytic solutions for interface flow in combined confined and semi-confined, coastal aquifers. Adv Water Resour 29:417–425

Cheng AHD, Ouazar D (1999) Analytical solutions. In: Bear J, Cheng AHD, Sorek S, Ouazar D, Herrera I (eds) Seawater intrusion in coastal aquifers – concepts, methods and practices. Kluwer Academic, Dordrecht

Cooper JHH (1964) A hypothesis concerning the dynamic balance of fresh water and salt water in a coastal aquifer, U.S. Geological Survey Water Supply Paper, 1613-C, pp C1–C12

Custodio E (1987) Prediction methods, Chapter 8. In: Bruggerman GA, Custodio E (eds) Studies and reports in hydrology, vol 45, Groundwater problems in coastal areas. UNESCO, Paris

Diersch HJG, Kolditz O (2002) Variable-density flow and transport in porous media: approaches and challenges. Adv Water Resour 25:899–944

FAO (1997) Seawater intrusion in coastal aquifers: guidelines for study, monitoring and control. FAO Water Reports no. 11. Food and Agriculture Organization (FAO) of the United Nations, Rome

Guo W, Langevin C (2002) User's guide to SEAWAT: a computer program for the simulation of three-dimensional variable-density ground-water flow: USGS Techniques of Water Resources Investigations, Book 6, Chapter A7

Herzceg AL, Leaney F (2002) Groundwater replenishment rates to fractured rock and sedimentary aquifers in the McLaren Vale Prescribed Wells Area. Final report to the Onkaparinga Catchment Water Management Board, CSIRO Land and Water, Technical Report 10/02, March 2002

Intergovernmental Panel on Climate Change (IPCC) (2007) Climate change 2007: working group I: the physical science basis. Projections of future changes in climate, http://ipcc.ch/publications_and_data/ar4/wg1/en/spmsspm-projections-of.html. Accessed 29 Apr 2011

Kabala ZJ (2001) Sensitivity analysis of a pumping test on a well with wellbore storage and skin. Adv Water Resour 24:19–35

Kooi K, Groen J (2001) Offshore continuation of coastal groundwater systems; predictions using sharp interface approximations and variable density flow modelling. J Hydrol 246:19–35

Langevin CD, Thorne D, Dausman AM, Sukop MC, Guo W (2008) SEAWAT Version 4: a computer program for simulation of multi-species solute and heat transport: USGS Techniques and Methods, Book 6, Chapter A22

Lobo-Ferreira JP, Chachadi AG, Diamantino C, Henriques MJ (2007) Assessing aquifer vulnerability to seawater intrusion using the GALDIT method: part 1 – application to the Portuguese Monte Gordo aquifer. In: Lobo Ferreira JP, Viera JMP (eds) Water in Celtic countries: quantity, quality and climate variability (Proceedings), IAHS Publication 310. International Association of Hydrological Sciences, Wallingford, pp 161–171

Moe H, Hossain R, Fitzgerald R, Banna M, Mushtaha A, Yaqubi A (2001) Application of 3-dimensional coupled flow and transport model in the Gaza Strip. In: First international conference on saltwater intrusion and coastal aquifers – monitoring, modeling, and management, Essaouira, Morocco, 23–25 Apr 2001

Ozyurt G (2007) Vulnerability of coastal areas to sea level rise: a case study on Goksu Delta, Masters thesis, Department of Civil Engineering, Middle East Technical University, Ankara, Turkey.

Pool M, Carrera J (2011) A correction factor to account for mixing in Ghyben-Herzberg and critical pumping rate approximations of seawater intrusion in coastal aquifers. Water Resour Res 47:W05506. doi:10.1029/2010WR10256

Post V (2005) Fresh and saline groundwater interaction in coastal aquifers: is our technology ready for the problems ahead? Hydrogeol J 13:120–123

Rasser PE (2001) Calibration of numerical models with application to groundwater flow in the Willunga Basin, S.A. Master's thesis, Adelaide University, Adelaide

Sherif MM, Singh VP (1999) Effect of climate change on sea water intrusion in coastal aquifers. Hydrol Process 13(8):1277–1287

Strack ODL (1976) Single-potential solution for regional interface problems in coastal aquifers. Water Resour Res 12:1165–1174

Strack ODL (1989) Groundwater mechanics. Prentice Hall, Englewood Cliffs (out of print, currently published by Strack Consulting Inc)

Watson TA, Werner AD, Simmons CT (2010) Transience of seawater intrusion in response to sea-level rise. Water Resour Res 46:W12533. doi:10.1029/2010WR009564

Webb MD, Howard KWF (2011) Modeling the transient response of saline intrusion to rising sea-levels. Ground Water 49(4):560–569

Werner AD (2010) A review of seawater intrusion and its management in Australia. Hydrogeol J 18:281–285

Werner AD, Gallagher MR (2006) Characterisation of sea-water intrusion in the Pioneer Valley, Australia using hydrochemistry and three-dimensional numerical modelling. Hydrogeol J 14:1452–1469

Werner AD, Simmons CT (2009) Impact of sea-level rise on seawater intrusion in coastal aquifers. Ground Water 47(2):197–204

Werner AD, Alcoe DW, Ordens CM, Hutson JL, Ward JD, Simmons CT (2011) Current practice and future challenges in coastal aquifer management: flux-based and trigger-level approaches with application to an Australian case study. Water Resour Manage 25(7):1831–1853

Werner AD, Ward JD, Morgan LK, Simmons CT, Robinson NI, Teubner MD (2012) Vulnerability indicators of seawater intrusion. Ground Water 50(1):48–58

Werner AD, Bakker M, Post VEA, Vandenbohede A, Lu C, Ataie-Ashtiani B, Simmons CT, Barry DA (2013) Seawater intrusion process, investigation and management: recent advances and future challenges. Adv Water Res 51, http://dx.doi.org/10.1016/j.advwatres.2012.03.004

Zheng C, Bennett GD (2002) Applied contaminant transport modeling, 2nd edn. Wiley Interscience, New York

Zulfic D, Harrington N, Evans S (2007) Uley basin groundwater modelling project. Groundwater flow model, vol 2. Department of Water, Land and Biodiversity Conservation, Report DWLBC 2007/04, Government of South Australia, Adelaide, 128 pp

Part III
Impacts on Groundwater Conditions

Chapter 11
Groundwater Composition and Geochemical Controls in Small Tropical Islands of Malaysia: A Comparative Study

Ahmad Zaharin Aris, Sarva Mangala Praveena, and Noorain Mohd Isa

Abstract Water usage for domestic and irrigation purposes differ greatly from country to country. Roughly, water use per capita increases with the increase of gross national income per capita. As speaking on national incomes, ecotourism activities in tropical countries play an important role in this field. Authorities on finance management focus on small islands as their greater contribution in ecotourism activities. Maintenance of small island ecology especially on groundwater has to be considered otherwise it hinders the growth of ecotourism development when it comes to overexploitation. Kapas Island and Manukan Island in Malaysia are among the islands that are highly developed for the ecotourism. Hence, unintentionally the groundwater in small islands is exposed to natural and manmade interference. A comparative study of these islands was done to clarify the sources of interference in the groundwater aquifer. An attempt to identify the hydrogeochemical processes in these small islands that accompany with current and past intrusion of seawater was made using the analyses on groundwater chemistry, saturation indices and ionic ratios. In addition of the major chemical compositions, analyses gives two different types of water, saturation index also indicates two different processes (saturation and dissolution) happened in the islands. Manukan Island tends to have Na-Cl water type and most of the groundwater samples were in precipitation condition with respect to carbonate minerals. Disparate to Kapas Island, it has Ca-HCO_3 water type and experienced dissolution process in most groundwater samples. The results using ionic ratios were demonstrated to delineate the seawater intrusion process, which includes of Mg/Ca, Na/Cl, Na/K, SO_4/Cl, Cl/HCO_3 and Ca/(HCO_3 + SO_4). Comparison of ions derivation also shows two

A.Z. Aris (✉) • N.M. Isa
Environmental Forensics Research Centre, Faculty of Environmental Studies, Universiti Putra Malaysia, UPM Serdang 43400, Selangor, Malaysia
e-mail: zaharin@upm.edu.my

S.M. Praveena
Department of Environmental and Occupational Health, Faculty of Medicine and Health Sciences, Universiti Putra Malaysia, Serdang 43400, Selangor, Malaysia

C. Wetzelhuetter (ed.), *Groundwater in the Coastal Zones of Asia-Pacific*, Coastal Research Library 7, DOI 10.1007/978-94-007-5648-9_11,

different major groups representing the islands. Other processes that related in this study were the ions exchanges and mineralization.

11.1 Introduction

Small island's special characteristics are varied by geography, physical, climatic, social and stage of economic development. Their characteristics include small physical size, insularity, remoteness and the fact that they are surrounded by large expanses of ocean. Small islands are facing unique challenges due to inherent geographical and demographic constraints above. Many of them are renowned as ocean paradise, especially in Malaysia for its white sandy beaches and major attraction for diverse tropical marine ecosystems, which is one of Malaysia's heritage reserves. Limited populations in most of the small islands enable ecotourism activities to grow. Developments in small islands have come to hit the highest point as small islands serve as an outstanding tourist destinations and bring biggest contributors to national economic growth. Tourism activities, which lead revenue earner in many countries, were predicted to suffer severe disruption as a consequence of adverse impacts expected from fast-growing tourism.

Small islands generally have limited natural resources, many of which already are heavily stressed from unsustainable development activities. Freshwater demands were significantly increased as a result for ecotourism development. Additionally, these small islands have limited water resources options, which aggravated an already tense situation. Due to the absence of surface water, small islands fully reliant on groundwater as the only water resource for domestic uses (Amer 2008; Aris et al. 2007, 2010a; Saxena et al. 2008). Tourism impacts on small islands made more severe to their limited water resources and have resulted in tremendous increased of groundwater extraction as to meet the freshwater demands. Limited natural resources as discussed above are prone to natural disasters and extreme events. As consequence, overexploitation of freshwater by pumping from wells may lead to contamination of groundwater (Praveena and Aris 2010). The contaminated groundwater promotes major concern on human health in many tropical islands, which leads to experiences high incidence of vector and water-borne diseases. Due to these issues, exploring the sources of groundwater contamination is vitally necessary to overcome problems regarding to freshwater supply.

A groundwater aquifer in small islands is balanced by its recharge rate through infiltration from precipitation and surface runoff (Aris et al. 2007, 2010a; Amer 2008; Saxena et al. 2008) and withdrawal rate (Praveena et al. 2012). Freshwater lenses and seawater are separated by different means of density. Due to high density of seawater, it tends to force its way underneath fresh groundwater (Piyadasa 2008; Kresic 2009). Mixing processes in the groundwater aquifer might change its constituent and hydrochemistry of fresh groundwater. The mechanisms involved in mixing processes are chemical reactions such as cation exchange, adsorption of dissolved ions and biological influences (Tijani 1994). Besides, geological properties of a groundwater aquifer may affect mineralization process which contributes to the groundwater composition. In addition, climate as represented by

precipitation (recharge) has been identified as a critical factor influencing groundwater chemistry such as the desalinization process in the aquifer (Gabet et al. 2010; Russak and Sivan 2010).

Specifically, a major threat to coastal aquifer is seawater intrusion (Russak and Sivan 2010; Fleeger 1999; Werner et al. 2009; Aris et al. 2009, 2012; Praveena et al. 2010). Over abstraction of groundwater may cause the movement of seawater, vertical and lateral intrusion (Petalas et al. 2009) into the aquifer and mixes with freshwater. Salinization of groundwater might change the normal groundwater constituents and affect its suitability for drinking purposes and domestic use. Although the severity of threats will vary, it is projected that inundation, flooding, and seawater intrusion will cause salinization to the fresh groundwater aquifer.

Potential chemical reactions undertaken in the groundwater aquifer have been studied thoroughly since freshwater and seawater mixing in the aquifer tends to alter its chemical composition in the system. There are several studies regarding the hydrochemistry in small islands, which explored the saturation index (Aris et al. 2010a), the ionic ratio (Aris et al. 2012), the groundwater status in temporal scale (Russak and Sivan 2010), the water rock interaction (Frape et al. 1984) and the extenuation of saline solutes in the groundwater aquifer (Aris et al. 2010b).

As to retain groundwater quality in small islands, analyses and measurements of groundwater chemistry are necessary. Analyses measurement can reveal some of the important information to overview problems and mechanisms involved in groundwater composition. Studies on tropical small islands become requirement for future especially in rapid ecotourism development islands. This paper aims to explain the evidence of seawater intrusion into shallow aquifers of small tropical islands by looking at its groundwater composition and geochemical controls, especially in Malaysia by selecting Manukan and Kapas Islands.

11.1.1 Site Description

11.1.1.1 Malaysia

Malaysia is located in the heart of Southeastern Asia, representing the peninsula Malaysia and one third of Borneo Island that is separated by the South China Sea. Malaysia comprises 13 states and the federal territories. The Peninsula, Perlis, Kedah, Pulau Pinang, Perak, Selangor, Negeri Sembilan Malacca, Johor, Kelantan, Terengganu and Pahang while Eastern Malaysia comprises the states of Sabah and Sarawak, located on Borneo Island. Around these two halves of Malaysia, there are numerous islands that signify their own unique characteristics. Malaysia is one of the most rapidly developing countries in the east with focus especially on small islands in the field of ecotourism. Manukan Island is located in Sabah (East Malaysia) while Kapas Island is located in Terengganu (West Malaysia).

11.1.1.2 Manukan Island

Manukan Island (Fig. 11.1) with a crescent shaped, (5°57′–5°58′ N and 115°59′–116°01′ E) has an area of 206,000 m^2. Almost 80 % of the area is covered by forest, while the rest 20 % of the low-lying area in the island is developed for tourism activities. Enacted under government's Parks Enactment 1978, the island is well known for its sandy beaches and corals, and being an attraction to visitors and divers. According to Basir et al. (1991), geological of Manukan Island has isolated from the mainland for about one million years ago. The island is underlain by interbedded sandstone and shales of the Middle Miocene Crocker Range Formation. The main aquifer of Manukan Island comprises quaternary carbonates, which originated from coral deposits and is overlain by quarternary coarse sandy alluvium.

11.1.1.3 Kapas Island

Kapas Island as shown in Fig. 11.1 (5°12′–5°14′ N and 103°15′–103°16′ E) with an area about 2,000 m^2 was gazetted as Marine Park to protect and conserve various habitat and aquatic marine life since it is famous for an infinite variety of hard and soft corals, abound with seashells, fish and turtles. Kapas Island is also well known for its sandy white beaches and swaying palms, which are relatively isolated. It is ideal for relaxation and is describe as heaven for visitors. Approximately 90 % of Kapas Island represents hilly area and the rest is a relatively low-lying area. About 8 % of the areas represent secondary forest and only 2 % of the area is sandy coastal area that are actively developed for ecotourism activities regarded its accessible. Kapas Islands is underlying by Permo-Carboniferous metasediments formation and unconformable overlying by conglomerate sequence. Metasediments rocks basically represent the sandstone, mudstone, shale and silt while the conglomerate groups were followed up with sandstone and mudstone (Ali et al. 2001). Kapas Conglomerate is known underlain to other formations thus suggesting that Kapas Conglomerate formation could be from Late Permian to Triassic age or still be of Jurassic-Cretaceous age (Shuib 2003).

These islands experienced a warm and humid climate with annual rainfall range between 1,500 and 2,800 mm, humidity between 80 and 90 % all year-round and temperatures range over from 21 to 32 °C. The climate is typically tropical climate as it influenced by monsoon blows in the middle of November and January. The northeast monsoon blows from November to March, and the southwest monsoon from May to September and usually the periods between the monsoons are marked by heavy rainfall as both islands are situated in the tropical region. At present, Manukan Island and Kapas Island rely on shallow aquifer for its water supply. Dug wells are used for extracting the groundwater from its sandy aquifer. The groundwater pumping activities have been practiced in these islands over years to provide the freshwater supply for the consumers.

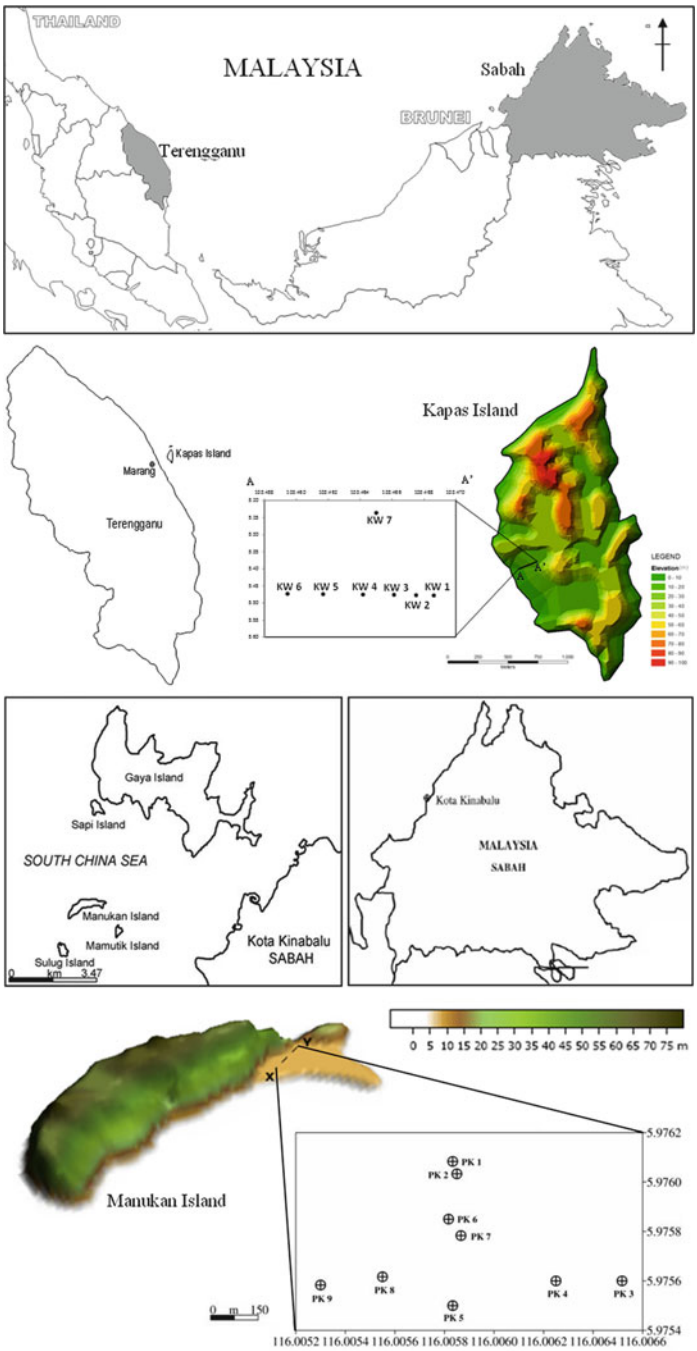

Fig. 11.1 The geographical location of Manukan Island in Sabah and Kapas Island in Terengganu, Malaysia

11.2 Methodology

11.2.1 Sampling and Analyses

Groundwater samples for Manukan Island were collected from March 2006 to January 2007. A total of 162 groundwater samples were obtained during the sampling period from 9 existing wells while a total of 126 samples from Kapas Island were collected bimonthly from 7 constructed boreholes since August 2010 to October 2010. The location of boreholes (monitoring wells) constructed for these islands were located in a low-lying area as to provide important information and implications of the hydrochemical facies of groundwater changes in response to salinization processes in the island's aquifer. Moreover, low-lying areas with dense population are suitable in this research since it has been developed for tourism activities where pumping actions were concerned.

11.2.2 In-Situ Parameters

Field measurements were done immediately to acquire representative value of groundwater ambient conditions. Triplicate data for *in-situ* parameter were taken precisely. The measurement of water samples was carried out to assess *in-situ* parameters such as pH, temperature, electrical conductivity (EC), salinity and total dissolved solids (TDS). Polyethylene bottles soaked in a prepared solution containing 5 % HNO_3 acids and pre-rinsed with deionized water were used to store groundwater samples based on the methods described in APHA (2005). The samples were transported in an ice-filled cooler box and kept refrigerated at 4 °C prior to analysis in the laboratory.

The instruments used were calibrated using specific calibrating solutions before use to analyzed groundwater samples. A mean value was calculated for each parameter, with the standard deviation (SD) being used as an indication of the precision of each parameter measured in triplicate samples. Careful quality controls and accuracy check were undertaken to obtain a reliable analytical dataset by checking the blank samples and triplicate of sub-samples.

11.2.3 Major Ions Analyses

Groundwater constituents were analyzed for sodium (Na), potassium (K), calcium (Ca), magnesium (Mg), bicarbonates (HCO_3), chloride (Cl), and sulfate (SO_4). Water samples collected were filtered through 0.45 μm membrane filter paper (Millipore) and acidified with concentrated HNO_3 to pH < 2 for cation determination. Cl and HCO_3 were respectively analyzed using argentometric ($AgNO_3$) and

titration methods (HCl) at the field, respectively. Sulfate was detected using a spectrophotometer by HACH meter (DR/2040 for Manukan Island and DR/2000 for Kapas Island). The major cations (Na, K, Ca, and Mg) were determined using flame atomic absorption spectrometry (Zeeman Atomic Absorption Spectrophotometer Z-5000, Hitachi, Japan – Perkin Elmer, Massachusetts, USA). Overall, the procedures of analyses adopted in this study were based on the methods described in APHA (2005).

11.2.4 Data Analyses

Impacts of seawater on the chemical composition in fresh groundwater via ionic states and saturation states in fresh groundwater are identified and investigated. Ionic ratios are widely used to assess the impact of seawater on aquifer chemistry using Cl as an indicator to the groundwater chemical constituent and changes with the ionic concentrations given in milliequivalents per liter (meq/L). Additionally, geochemical analyses using PHREEQC were employed to calculate saturation states of groundwater resulting from the freshwater–seawater mixing process occurring in the study area. Saturation Indices (SI) values equal to 0 indicate equilibrium between mineral and the solution while positive SI values shows supersaturation and negative SI values reflect subsaturation (Appelo and Postma 2005). SI value can be expressed in other ways such as to describe the dissolution or precipitation of minerals.

11.3 Results and Discussion

11.3.1 Descriptive Statistics

11.3.1.1 Manukan Island

The overall data of *in-situ* and major ions in these studies is shows in Table 11.1. The pH values varied between 6.59 and 7.97. The groundwater temperatures are generally between 26.3 and 29.4 °C respectively. Significant differences are found in the salinity, EC and TDS values for different islands ($p < 0.01$). Salinity values were in the range of 0–7.1 ppt. EC and TDS values were in the range 0.30–12.26 mS/cm and 204–8,294.16 mg/L respectively. It can be seen that the high values of conductivity observed (EC > 5 mS/cm) are related to seawater intrusion (Aris et al. 2009). It was supported by correlation between Cl and/with the major component of seawater (Na and SO_4) were strong (Cl-Na, $r = 0.656$; Cl-SO_4, $r = 0.757$). It explained that groundwater salinization in Manukan Island was due to seawater intrusion based on the present of elevated Cl concentrations and the strong correlations between those parameters.

Table 11.1 Descriptive analysis of *in-situ* and major ions for Manukan Island and Kapas Island

		Manukan Island (n = 162)				Kapas Island (n = 126)			
	Unit	Mean	SD	Min	Max	Mean	SD	Min	Max
In-situ									
Temp	°C	27.89	0.77	26.30	29.40	30.12	1.48	27.20	35.10
pH		7.27	0.25	6.59	7.97	7.13	0.15	6.68	7.64
EC	mS/cm	4.79	3.14	0.30	12.26	0.59	0.15	0.41	0.91
Sal	ppt	2.72	1.99	0.00	7.10	0.29	0.08	0.20	0.45
TDS	mg/L	4535.51	1733.33	1133.15	8294.16	295.80	77.26	204.00	455.00
Major ions									
Ca	mg/L	390.00	168.16	60.26	866.29	43.40	25.42	9.16	145.20
Mg	mg/L	110.05	64.23	2.92	297.66	5.85	3.38	1.62	14.00
Na	mg/L	1181.37	693.39	103.90	2780.00	20.75	14.19	0.80	58.80
K	mg/L	36.51	20.85	4.44	93.51	1.22	0.88	0.03	3.89
HCO_3	mg/L	327.83	55.09	195.20	524.60	382.21	113.59	241.56	893.04
Cl	mg/L	2118.45	914.98	339.89	4098.73	50.86	33.62	11.49	141.96
SO_4	mg/L	256.05	146.98	25.00	660.00	13.17	7.20	1.00	30.00

11.3.1.2 Kapas Island

The temperature of groundwater ranged from 27.8 to 35.1 °C. The pH values of the analyzed samples varied from 6.70 to 7.60. In general, pH of groundwater samples were slightly acidic to alkaline condition with mean value of 7.12. The electrical conductivity (EC) values varied from 0.41 to 0.91 mS/cm, while salinity values varied from 0.20 to 0.45 ppt respectively. Total Dissolved Solid (TDS) values display a wide range from 204 to 455 mg/L with an average value of 281.90 mg/L. High values of TDS were referred to the high concentration of dissolved ions in groundwater samples, which have significantly correlated with high EC values ($r = 0.999$; $p < 0.01$).

The differences in major ions concentration are shown in Fig. 11.2. The distribution of groundwater samples provides as initial understanding of distinct grouping between these two islands. The orders of ion contents are $Na > Mg > Ca > K$ and $Cl > HCO_3 > SO_4$ for Manukan Island while Kapas Island mostly in trend of $Ca > Na > Mg > K$ and $HCO_3 > Cl > SO_4$ (Fig. 11.2).

The evolutions of groundwater types are graphically presented in Piper plot (Fig. 11.3). Groundwater composition in Manukan Island, were largely dominated by Na-Cl while only 9 % of Ca-Cl water type was encountered. Comparatively, Kapas Island demonstrated a Ca-HCO_3 water type, comprises of carbonates aquifer, which originated from coral deposited (Isa and Aris 2012). Large proportions of Na-Cl water type indicate seawater influence to the aquifer. The mixing process between two types of water was obviously explained by the ions exchange process.

11.3.2 Saturation Indices

Data for SI values is shown in Table 11.2 and Fig. 11.4. pH of groundwater in Manukan Island influenced the saturation states of calcite and aragonite. There were

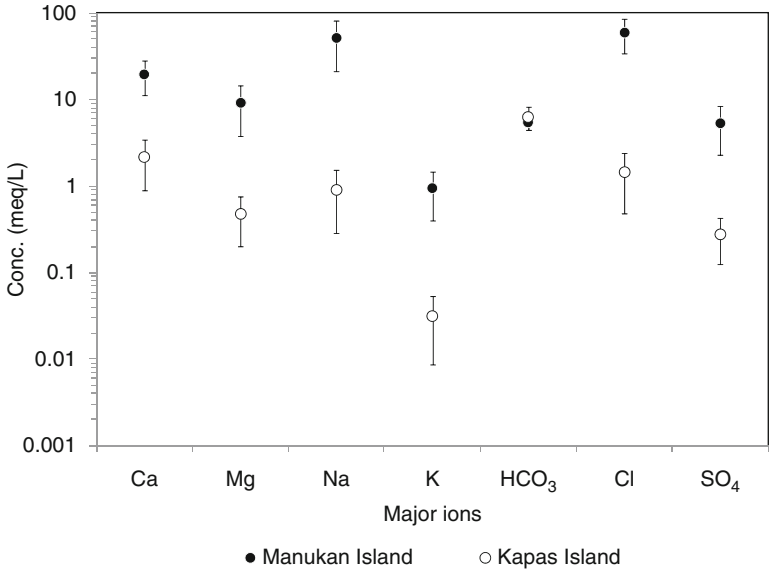

Fig. 11.2 Major ions concentration for Manukan Island and Kapas Island

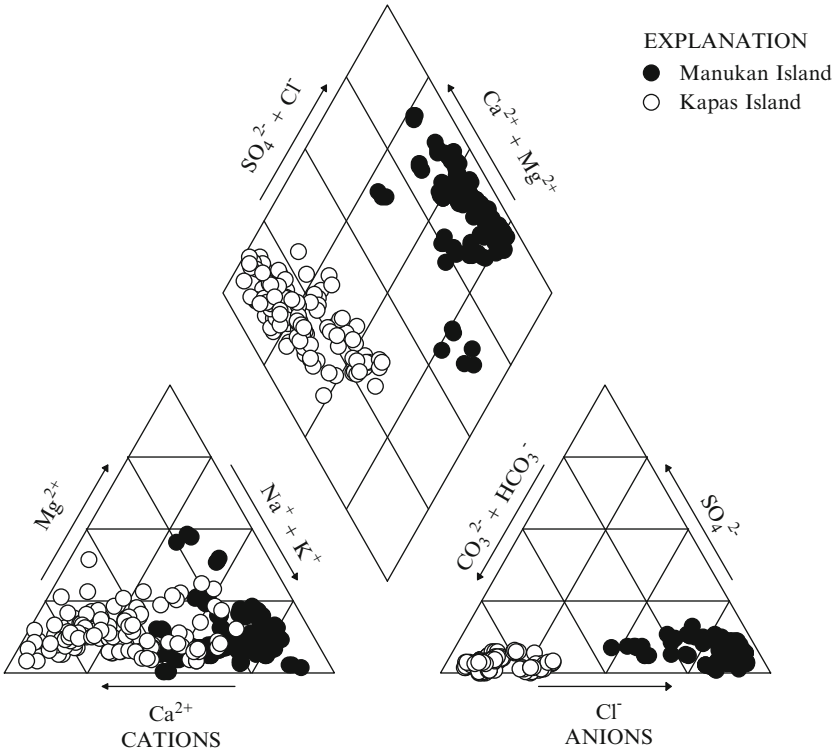

Fig. 11.3 Overall Piper plot of groundwater samples collected from Manukan Island and from Kapas Island

Table 11.2 SI of calcite, aragonite and dolomite for Manukan Island and Kapas Island

	Manukan Island (n = 162)				Kapas Island (n = 126)			
	Mean	SD	Min	Max	Mean	SD	Min	Max
Calcite	0.65	0.26	0.06	1.23	−0.05	0.25	−0.78	0.85
Aragonite	0.51	0.26	−0.08	1.09	−0.19	0.25	−0.92	0.71
Dolomite	1.10	0.50	0.03	2.35	−0.56	0.40	−1.25	0.62

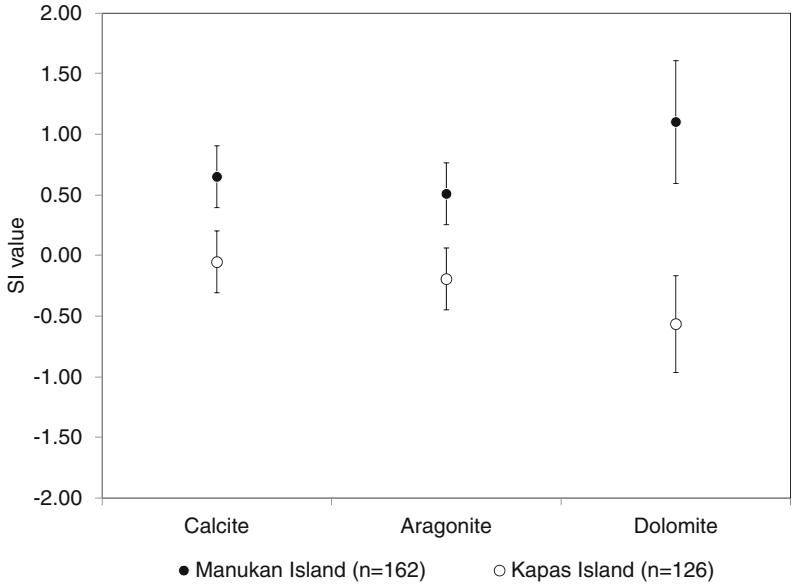

Fig. 11.4 Mean SI value for calcite, aragonite and dolomite of the groundwater in Manukan and Kapas Island

positive correlations ($p < 0.01$, Fig. 11.5) between pH and SI values of calcite, aragonite and dolomite suggesting that precipitation of those mineral species was due to the increasing alkalinity of groundwater (increasing pH). Hence, it indicates seawater that intruding into the aquifer was not the direct factor that contributes minerals precipitation, but might be possibly contributed by the increasing alkalinity of groundwater due to its high pH.

SI values for groundwater in Kapas Island aquifer were mostly in dissolution states (Fig. 11.5). It is conceivable for Kapas Island groundwater samples; therefore, observation of correlation showed significant different between pH with Ca and pH with Mg with r values $= -0.278$ and -0.282, $p < 0.01$ respectively, which play a role as one of the dissolution factor. The explanations on precipitation states were due to CO_2 in a close system, have neutralized the OH^- ions and increased H^+ ions in the aquifer as explained in Eq. 11.1;

$$CO_2 + H_2O + CaCO_3 \rightarrow Ca^{2+} + 2HCO_3^- \tag{11.1}$$

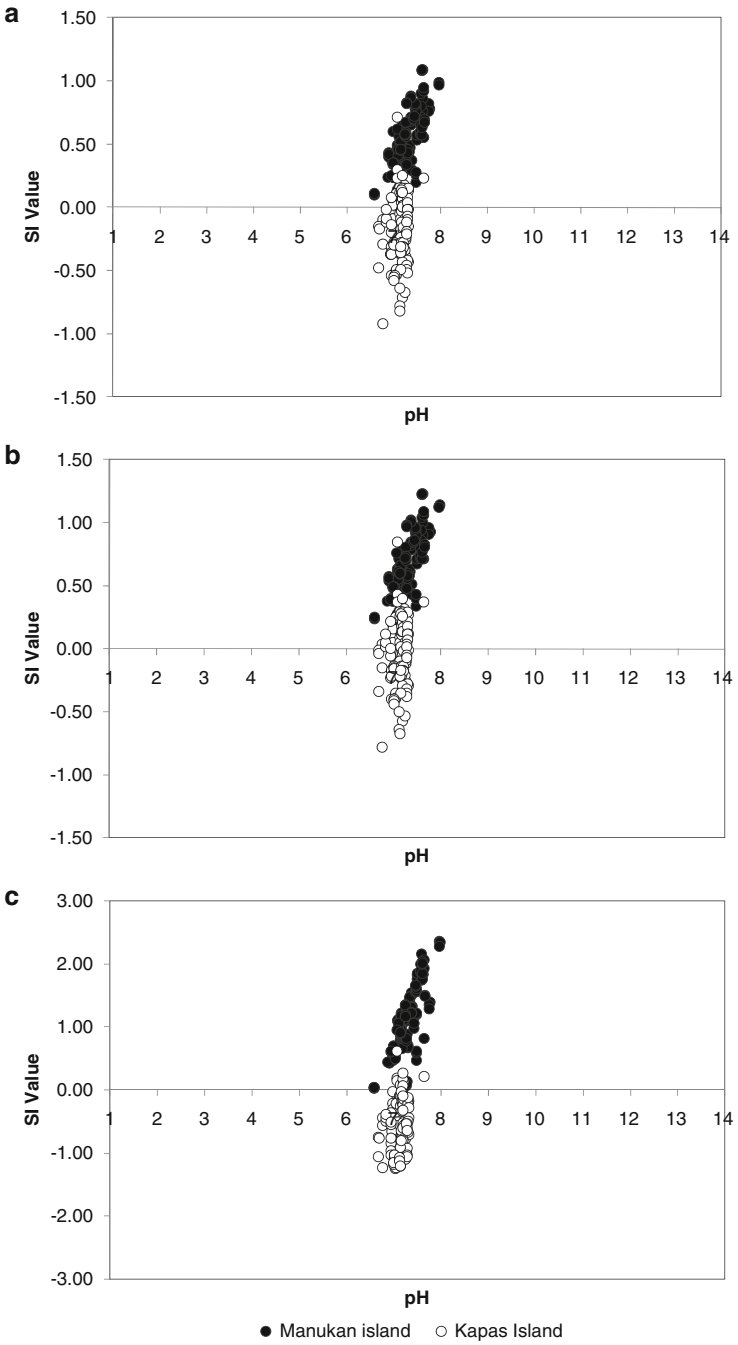

Fig. 11.5 Plot of SI for selected mineral species [(**a**) aragonite, (**b**) calcite and (**c**) dolomite] versus pH of the groundwater

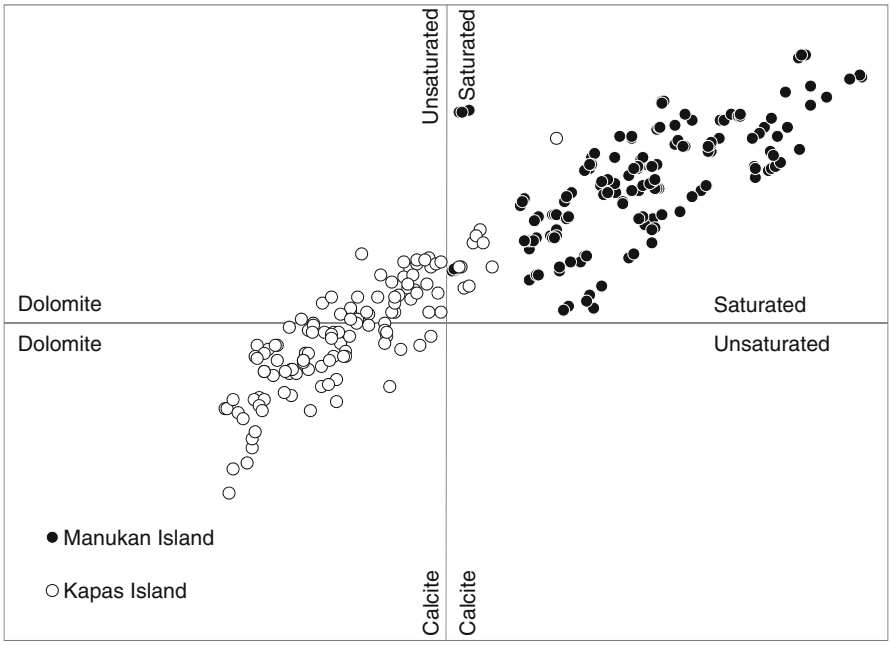

Fig. 11.6 Saturation indices plot for calcite and dolomite

Reaction of CO_2 in the close aquifer system results in the formation of carbonic acid, subsequently dissociates to produce H^+ and HCO_3^- ions (Tijani 1994).

The SI values in Fig. 11.6 shows the distribution of groundwater samples in saturation states for Manukan Island and dissolution states for Kapas Island. The plot of SI in Fig. 11.6 demonstrates dolomite SI values are higher than calcite SI values for Manukan Island and vice versa for Kapas Island. The groundwater samples distribution showed strong and positive correlation with $r = 0.675$; $p < 0.01$ (Manukan Island) and $r = 0.855$; $p < 0.01$ (Kapas Island). Incongruent solutions are solution processes, in which one mineral dissolves, while another mineral inevitably precipitates. In Manukan Island, dolomite and calcite were under saturated condition after an equilibrium state has attained. With an addition from seawater component, the Ca and Mg concentrations in groundwater are increased, which in turn inevitably causes super-saturation with respect to calcite and dolomite and thus precipitation of these minerals. Minerals in Kapas Island were under unsaturated condition where increase of Ca and Mg in the aquifer via the processes of mineralization that usually take place over years to attain equilibrium state (Merkel and Planer-Friedrich 2008).

Table 11.3 Ionic ratio for groundwater

	Manukan Island (n = 162)				Kapas Island (n = 126)			
	Mean	SD	Min	Max	Mean	SD	Min	Max
Mg/Ca	0.61	0.54	0.01	2.63	0.28	0.22	0.05	1.33
Na/Cl	1.03	1.19	0.10	11.28	0.65	0.25	0.06	1.22
Na/K	63.34	40.97	10.65	325.53	53.54	81.10	1.55	561.52
SO_4/Cl	0.09	0.04	0.01	0.24	0.26	0.16	0.01	0.64
Cl/HCO_3	11.59	5.35	1.72	23.12	0.23	0.13	0.07	0.54
Ca/(HCO_3 + SO_4)	1.92	0.96	0.39	5.86	14.54	12.08	2.63	108.49

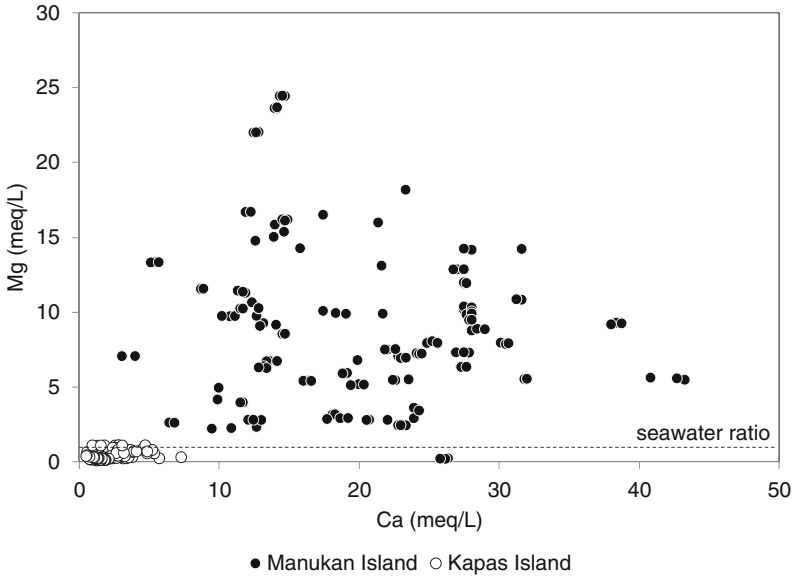

Fig. 11.7 Ionic ratio of Mg/Ca concentration in meq/L for both islands

11.3.3 Ionic Changes

Ionic changes are widely applied to delineate the processes contributing to the increasing salinity due to the influence of seawater on aquifer chemistry in the study area (Lee and Song 2007). As the study area surrounded by a marine environment, the ratios in Table 11.3 were used to distinguish the factor responsible for the evolution of groundwater chemistry.

Ratio of Mg/Ca that exceeds 1.00 indicates dolomitization process may take place due to the present of seawater in the aquifer (Pulido-Leboeuf 2004). Based on this study, Manukan Island has the higher ratio (0.61) than Kapas Island (0.28) which explained the interruption of seawater component (Fig. 11.7). It has supported by the calculation of Na/Cl ratio (Manukan Island = 1.03;

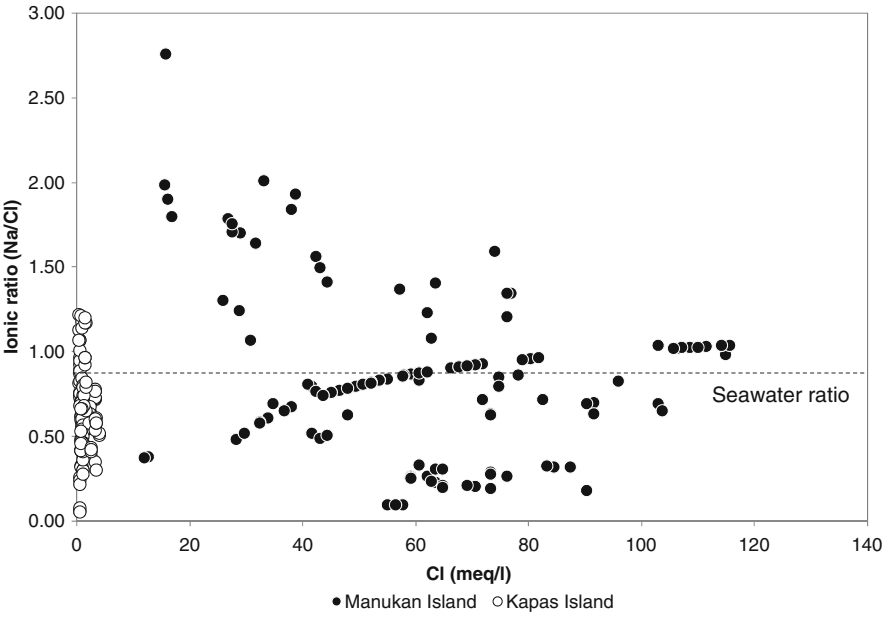

Fig. 11.8 Ionic ratio of Na/Cl vs. Cl concentration in meq/L

Kapas Island = 0.65), which were compared with the seawater ratio from the previous study (Na/Cl of seawater = 0.67; Aris et al. 2010b; Fig. 11.8). Exceed values of Na/Cl describe seawater disturbance. Furthermore, the correlationship between Mg and Ca is specifically responsible for dissolution of minerals where Kapas Island ($r = 0.538$; $p < 0.01$) is moderately correlated compared to Manukan Island ($r = 0.054$; $p > 0.05$).

The effects of groundwater salinization from both islands were analyzed using Cl/HCO_3 ratios (Aris et al. 2012). Linear relationship indicates the mixing of seawater and fresh groundwater in the study areas. Figure 11.9 shows the distribution of groundwater samples in Manukan Island and Kapas Island where ratios less than or equal to 0.5 indicates unaffected groundwater, 0.5–6.6 for slightly and moderately affected, and 6.6 and above for strongly affected (Aris et al. 2012). About 83 % of Manukan Island samples were strongly affected by seawater. This result implied that the fresh groundwater was contaminated by seawater. Comparatively, Kapas Island groundwater samples (76 %) lie in area of slightly/moderately affected.

Salinization process in Kapas Island described as slightly affected (Fig. 11.9) which explained by other processes such as ion exchanges and mineralization. From this study, about 95 % of Na/Cl ratios were lies <1, this is due to ionic exchange process that acts as a dominant process controlling the groundwater constituents. Moreover, calculation of Ca/Mg in Kapas Island revealed that the dissolution of minerals was one of the prime processes involved in attaining the present chemical makeup of the groundwater (Isa and Aris 2012). The ratio

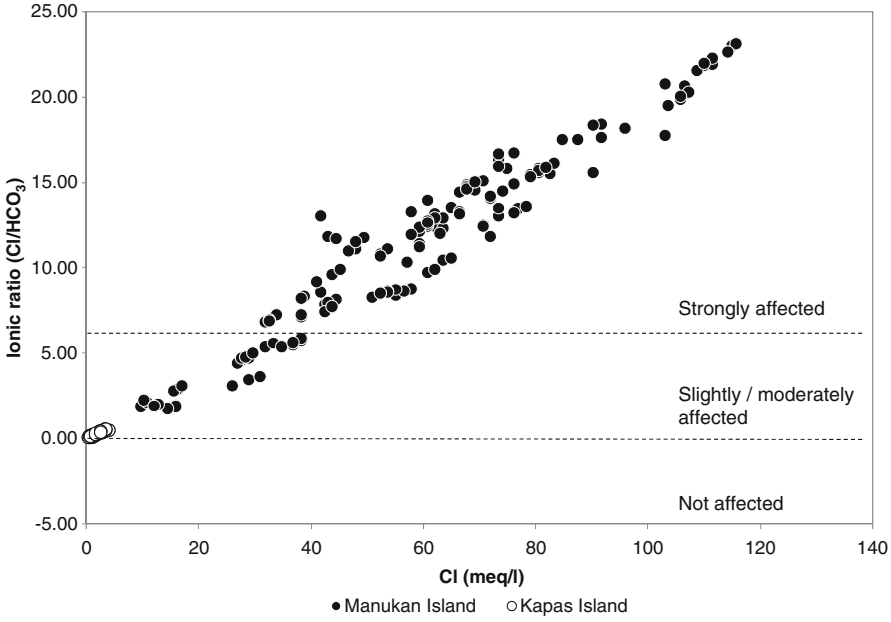

Fig. 11.9 Ionic ratio of Cl/HCO_3 vs. Cl concentration in meq/L

indicated the dissolution process of dolomite (8.7 % of groundwater samples >1) and the effect of silicate minerals, which suggested calcite dissolution in the study area (88 % of groundwater samples >2).

The variation in the ionic ratio of SO_4/Cl is evaluated with respect to the distribution of Cl concentrations (Fig. 11.10). It was found that more than 70 % of Manukan Island samples and 15 % of Kapas Island samples fall below the seawater ratio value (0.10) which indicates of seawater contamination The positive and strong correlation were attained in this study indicates an increase of SO_4 and Cl from seawater component (Manukan Island, $r = 0.757$; $p < 0.01$).

11.4 Conclusion

In order to identify the hydrogeochemical processes that determine the salinization of the groundwater, major ions along with in-situ parameters were measured. Groundwater chemistry characteristics of Manukan Island indicated the occurrence of seawater intrusion by hydrochemical data. The results indicated mixing of seawater and fresh groundwater simultaneously with other processes. Groundwater samples were under saturation states and were grouped closely to seawater type reflected to seawater disturbance. Ion derivation of Mg/Ca (0.61) and Na/Cl (1.03) explained the interruption of seawater component. In addition, ratio of Cl/HCO_3 shows the groundwater

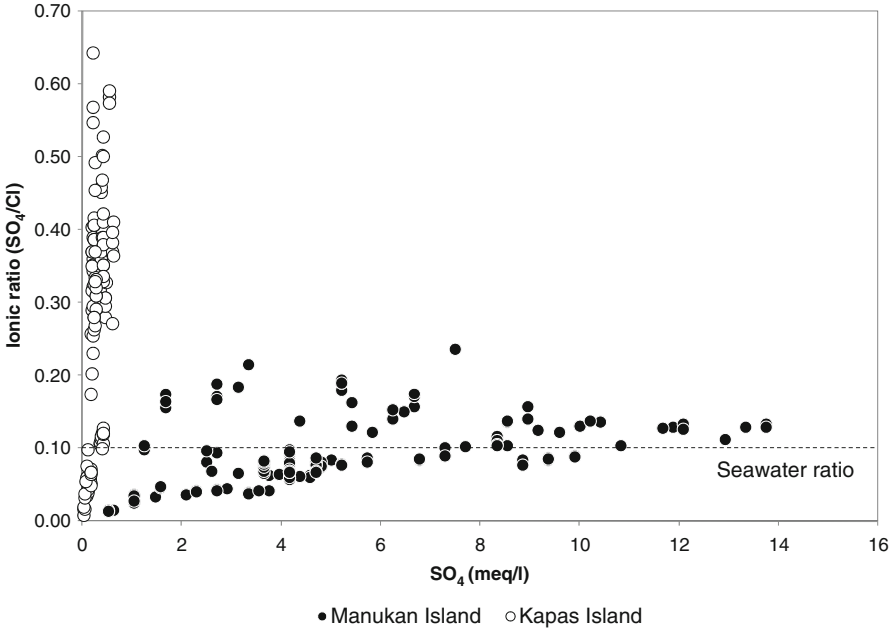

Fig. 11.10 Ionic ratio of SO_4/Cl vs. Cl concentration in meq/L

samples were strongly affected by seawater with values >6.6. SO_4/Cl ratio explained the seawater contamination with >70 % of groundwater samples were under seawater ratio. Despite of Kapas Island is not experiencing seawater intrusion so far but it is facing other processes such as ions exchanges and mineralization. Based on SI values, 76 % of groundwater samples in Kapas Island experienced dissolution process and the ratio of groundwater samples of Cl/HCO_3, Na/Cl and SO_4/Cl have not exceeded the seawater ratio. As conclusion, the hydrochemistry of these small islands revealed the original sources of salinization in the aquifer system which is useful for island management and further investigation.

References

Ali CA, Mohamed KR, Abdullah I (2001) Geologi Pemuliharaan dan Cadangan Taman Geologi Bagi Pulau-Pulau di Perairan Terengganu. In: Komoo I, Tjia HD, Leman MS (eds) Warisan Geologi Malaysia-Pemetaan Geowarisan dan Pencirian Geotapak. Institut Alam Sekitar dan Pembangunan (LESTARI), Selangor

Amer KM (2008) Groundwater resources sustainability in Qatar: problems and perspectives. In: Bhattacharya P, Ramanathan A, Mukherjee AB, Bundschuh J, Chandrasekharam D, Keshari AK (eds) Groundwater for sustainable development, problems, perspectives and challenges. Taylor & Francis, London, pp 25–37

APHA (2005) Standard methods for the examination of water and wastewater, 21st edn. American Water Works Association, Water Environment Federation, Washington, DC

Appelo CAJ, Postma D (2005) Geochemistry, groundwater and pollution, 2nd edn. Balkema, Rotterdam

Aris AZ, Abdullah MH, Kim KW (2007) Hydrochemistry of groundwater in Manukan Island, Sabah. Malays J Anal Sci 2:407–413

Aris AZ, Abdullah MH, Kim KW, Praveena SM (2009) Hydrochemical changes in a small tropical island's aquifer: Manukan Island, Sabah, Malaysia. Environ Geol 56:1721–1732

Aris AZ, Abdullah MH, Praveena SM, Yusoff MK, Juahir H (2010a) Extenuation of saline solutes in shallow aquifer of a small tropical island: a case study of Manukan Island, North Borneo. EnvironAsia 3(Special Issue):84–92

Aris AZ, Praveena SM, Abdullah MH (2010b) Saturation states of carbonate minerals in a freshwater-seawater mixing zone of small tropical island's aquifer. Chin J Geochem 29 (3):278–286

Aris AZ, Praveena SM, Abdullah MH (2012) The influence of seawater on the chemical composition of groundwater in a small island: the example of Manukan island, East Malaysia. J Coast Res 28(1):64–75

Basir J, Sanudin T, Tating FF (1991) Late eocene planktonic foraminifera from the Crocker Formation, Pun Batu, Sabah. War Geol 14(4):1–15

Fleeger GM (1999) The geology of Pennsylvania's groundwater, vol 3, Educational series. Pennsylvania Geological Survey, Harrisburg

Frape SK, Fritz P, McNutt RH (1984) Water-rock interaction and chemistry of groundwaters from the Canadian Shield. Geochim Cosmochim Acta 48(8):1617–1627

Gabet EJ, Wolff-Boenisch D, Langner H, Burbank DW, Putkonen J (2010) Geomorphic and climate controls on chemical weathering in the High Himalayas of Nepal. Geomorphology 122:205–210

Isa NM, Aris AZ (2012) Preliminary assessment of the hydrogeochemistry of Kapas Island, Terengganu. Sains Malays 41(1):23–32

Kresic N (2009) Groundwater resources: sustainability, management and restoration. McGraw Hill, New York

Lee JY, Song SH (2007) Groundwater chemistry and ionic ratios in a western coastal aquifer of Buan, Korea: implication for seawater intrusion. Geosci J 11(3):259–270

Merkel BJ, Planer-Friedrich B (2008) Groundwater geochemistry. Springer, Berlin (in German)

Petalas C, Pisinaras V, Gemitzi A, Tsihrintzis VA, Ouzounis K (2009) Current conditions of saltwater intrusion in the coastal Rhodope aquifer system, northeastern Greece. Desalination 237:22–41

Piyadasa RUK (2008) Interactions between saline and fresh water in coastal region of northwestern Sri Lanka. In: Bhattacharya P, Ramanathan A, Mukherjee AB, Bundschuh J, Chandrasekharam D, Keshari AK (eds) Groundwater for sustainable development: problem, perspectives and challenges. Taylor & Francis, London

Praveena SM, Aris AZ (2010) Groundwater resources assessment using numerical model: a case study in low-lying coastal area. Int J Environ Sci Technol 7(1):135–146

Praveena SM, Abdullah MH, Aris AZ (2010) Modelling for equitable groundwater management. Int J Environ Res 4(3):415–426

Praveena SM, Abdullah MH, Bidin K, Aris AZ (2012) Sustainable groundwater management on the small island of Manukan, Malaysia. Environ Earth Sci 66(3):719–728

Pulido-Leboeuf P (2004) Seawater intrusion and associated processes in a small coastal complex aquifer (Castell de Ferro, Spain). Appl Geochem 19(10):1517–1527

Russak A, Sivan O (2010) Hydrogeochemical tool to identify salinization or freshening of coastal aquifers determined from combined field work, experiments and modelling. Environ Sci Technol 44:4096–4102

Saxena VK, Mondal NC, Singh VS (2008) Assessment of groundwater resources by using a simple hydrogeochemical tool in coastal aquifers of Krishna delta, India. In: Bhattacharya P, Ramanathan A, Mukherjee AB, Bundschuh J, Chandrasekharam D, Keshari AK (eds)

Groundwater for sustainable development, problems, perspectives and challenges. Taylor & Francis, London, pp 3–11
Shuib MK (2003) Transpression in the strata of Pulau Kapas, Terengganu. Geol Soc Malays Bull 46:299–306
Tijani MN (1994) Hydrogeochemical assessment of groundwater in Moro area, Kwara state, Nigeria. Environ Geol 24:194–202
Werner AD, Jakovovic D, Simmons CT (2009) Experimental observations of saltwater up-coning. J Hydrol 373:230–241

Chapter 12
Atoll Groundwater Resources at Risk: Combining Field Observations and Model Simulations of Saline Intrusion Following Storm-Generated Sea Flooding

James P. Terry, Ting Fong May Chui, and Anthony Falkland

Abstract The restricted nature of naturally-occurring freshwater resources on atolls is one of the greatest impediments to human settlement on these small, dispersed and remote islands. Any anthropogenic or environmental pressures that deleteriously affect the quantity or quality of atoll water resources are therefore a matter of concern. This chapter focuses on such issues. It first presents an overview of the principal characteristics of atoll fresh groundwater aquifers, which exist in the form of thin lenses within the Holocene sands and gravels that comprise the sedimentary substrate of low-lying atoll islets. Factors that influence the vulnerability of these freshwater lenses are then considered. The chapter continues by summarising the findings of recent studies that investigated the effects of storm-wave washover across atoll islets on freshwater lens profiles, and the subsequent patterns of recovery over time. Both field and modelling approaches are used. Combined results suggest that following groundwater salinisation by seawater intrusion, at least a year is required for full aquifer recovery. Of particular interest, it is found that in spite of a strong saline plume forming at relatively shallow depths, a thin horizon of freshwater sometimes remains preserved deeper within the aquifer profile for several months after the initial disturbance. In the Pacific basin, shifting geographical patterns in severe tropical storm events related to climatic variability and change are a threat to the continuing viability of atoll fresh groundwater resources and the human populations dependent upon them.

J.P. Terry (✉)
Department of Geography, National University of Singapore, AS2, 1 Arts Link, Kent Ridge, Singapore, Singapore 117570
e-mail: geojpt@nus.edu.sg

T.F.M. Chui
Department of Civil Engineering, The University of Hong Kong, Room 6-18A, Haking Wong Building, Pokfulam, Hong Kong

A. Falkland
Island Hydrology Services, Canberra, ACT, Australia

C. Wetzelhuetter (ed.), *Groundwater in the Coastal Zones of Asia-Pacific*, Coastal Research Library 7, DOI 10.1007/978-94-007-5648-9_12,

12.1 Introduction

The atoll islets of the Pacific Ocean are some of the most difficult environments for permanent settlement on Earth. The limited land areas of atoll islets and their low elevation above sea level, their infertile and porous soils, natural rainfall variability, small groundwater resources, and periodic cyclones and drought, all pose significant impediments. This paper focuses on arguably the most severe environmental constraint of all for human habitation – the lack of freshwater. Its aims are threefold. The first aim is to offer an introductory overview of the nature and characteristics of the only significant freshwater resources on atolls: shallow groundwater aquifers that exist in the form of thin freshwater lenses. The second aim is to highlight the influences on vulnerability and principal threats to atoll groundwater resources, which involve a range of both natural and anthropogenic pressures. The third and final aim is to provide a synopsis of recent atoll groundwater investigations by the authors. These encompass both field observations on Pukapuka Atoll in the Northern Cook Islands and mathematical modelling studies. The work examines in particular saline intrusion caused to atoll freshwater lenses by wave-washover events driven by tropical cyclones. Effects on groundwater salinity profiles are illustrated, followed by an account of subsequent recovery over time, where this occurs. The results of these separate studies have recently been reported elsewhere (Terry and Falkland 2010; Chui and Terry 2012), but the key findings are drawn together here in order that a coherent picture can emerge regarding the continuing long-term viability of atoll groundwater resources. The outlook is discussed in the face of possibly changing geographical patterns in severe tropical storm events related to current climate variability and longer term climate change.

12.1.1 Harsh Environments, Hardy People

The remote atoll islets that are dispersed widely throughout the warm waters of Pacific tropical belt can be appreciated as amongst the world's most impressive landforms (Nunn 2010). These living rings of coral reef are entirely zoogeomorphic constructions, sometimes stretching for hundreds of kilometres in length to encircle shallow central lagoons. Their existence is owed to successive generations of hermatypic coral colonies, continually growing upward to keep pace with sea level over many millennia while the extinct volcanoes on which they are anchored slowly subside and become deeply submerged beneath the ocean surface (Darwin 1842). Most of the world's atoll islets are found in a broad sweep between the tropical latitudes of the Pacific Ocean, across the territories of Micronesia and Polynesia (mainly Federated States of Micronesia, The Marshall Islands, Kiribati, Tuvalu, Tokelau, Cook Islands and French Polynesia).

Commonly seen dotting the surface of these Pleistocene-age carbonate platforms are low-lying islets[1] that are known as *motu* by the indigenous Polynesian peoples of the Pacific. These islets probably began forming in the late-Holocene period, when global eustatic sea levels dropped to their present levels from slightly higher levels about 3,000 years ago. Islets are therefore formed of Holocene and recent deposits of calcareous sands and gravels that are produced by wave action on the atoll reefs and wash up to accumulate above the reach of high tide. Individual islets that are separated by surge channels may occasionally be small and elliptical in shape, but often they are narrow and elongate features that follow along the top of the reef for hundreds of meters to many kilometres (Fig. 12.1). The surge channels allow the free circulation of ocean water with the enclosed marine lagoon.

The natural environment of atoll islets is deceptively attractive. To the outsider, at first glance atolls appear exotic and tranquil, enjoying benevolent climates and bestowed with idyllic settings of white sandy shores that are fringed by coconut palms and washed by clear tropical seas teeming with marine life. Yet, in spite of the undeniable physical beauty of atolls, life on these remote islets is precarious and unforgiving (Terry and Thaman 2008). There is little land available for cultivation, and soils formed on the coralline sands are impoverished in nutrients. Only a limited terrestrial biodiversity can therefore be supported (Thaman 2008). Excessive porosity also means that the infertile soils are not able to retain sufficient moisture for many crops. Agricultural productivity is seriously constrained to the extent that eking out a sustainable living is extremely difficult. Nevertheless, it is true to say that Pacific Islanders inhabiting atoll islets are hardy and resourceful people. It is certainly astonishing to consider that they have endured for thousands of years on their isolated and harsh island homes in the face of these major environmental challenges.

12.1.2 The Nature of Atoll Groundwater Resources

A fundamental requirement for any human settlement on Pacific Islands is a supply of freshwater (Depledge and Terry, in press). In consequence, it is the restricted nature of freshwater resources on Pacific atoll islets that is arguably the greatest hindrance for permanent human habitation upon them. Since the permeable coral sands and gravels that form the substrate of the islets are readily infiltrated, rainfall and throughfall under vegetation canopies quickly disappears underground. Surface

[1] Some ambiguity arises with regard to the term 'island' in the context of atolls. To avoid confusion, here 'atoll' is reserved for the entire atoll configuration (i.e. coral reefs dotted with low sandy islands and encircling a central lagoon), whereas 'islet' is used to describe only the low-lying land above sea level. Islets may occur as either a few or more numerous individual small islands on top of the reef and may lie tens of kilometres apart on opposite sides of the lagoon. In some cases, the islets may be nearly continuous around the lagoon's perimeter, while in others they may only occur on parts of the perimeter.

Fig. 12.1 *Upper*: Aerial view of part of Majuro Atoll showing the oceanside reef, the inhabited area, and lagoon (Photo courtesy of R. Thaman). *Lower*: Hand-dug well, Pukapuka Atoll

freshwater bodies such as ponds, streams and lakes that are found on larger volcanic islands in the Pacific are therefore almost entirely absent on atolls. Additionally, the high permeability and small surface areas of islets mean that runoff collection is limited to rainwater harvesting from artificial catchments and constructed surface storages such as rainwater tanks which have relatively small capacities (Falkland 2002).

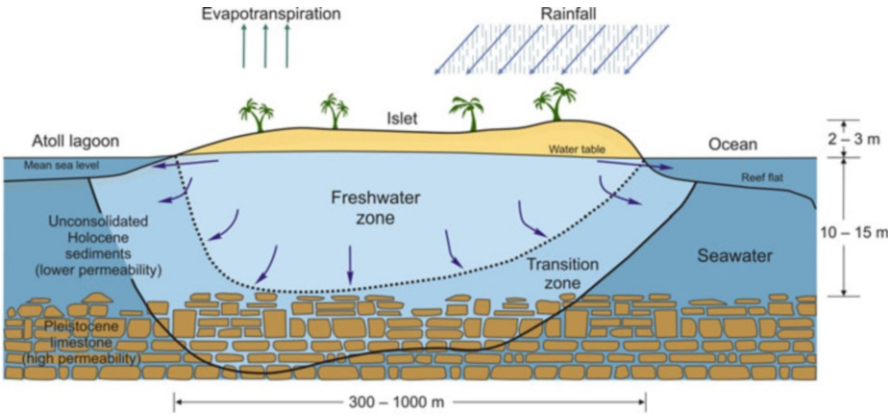

Fig. 12.2 Illustration of a freshwater lens within the substrate of an individual atoll islet (adapted from White and Falkland 2010). Cautionary note: the diagram is highly exaggerated in the *vertical* scale (relative to the *horizontal* scale). This gives an impression of a thick fresh groundwater profile, which is not common on coral islets

Consequently, the only natural potable freshwater resource on atoll islets occurs in the form of thin 'lenses' of fresh groundwater that occur beneath the surface of the larger islets (i.e. those wider than about 300–400 m). Many atoll dwellers are entirely dependent upon these freshwater lenses (FWLs) for drinking water and domestic uses and therefore strive to use available water as efficiently as possible (Nakada et al. 2012). Water is often drawn from simple hand-dug wells (Fig. 12.1) that reach the groundwater table at shallow depths. The close dependency of islanders on these meagre resources means that any short-term intrusion or gradual longer term deterioration in the quality of freshwater lenses can have serious consequences for the continuing viability of atoll settlement.

The stratigraphy of atoll islets is unique. Their fabric comprises unconsolidated coral sands normally approaching 10 to 15 m in thickness, overlying lithified and partly karstified reef limestone. Typical of atoll islets, the surface elevation of the loose sediments normally rise to just 2 to 3 m above mean sea level. Freshwater lenses are able to develop by rainwater infiltration into, and temporary retention within, the carbonate formation. Consequently, FWLs exist as unconfined aquifers that are contained mainly within the Holocene carbonate sands and gravels occasionally, in the case of thick freshwater lenses, within the Pleistocene reef limestone (Fig. 12.2). Owing to this configuration, atoll aquifers are described as 'dual aquifer' systems in hydrogeological terms (Ayers and Vacher 1986), in particular since the surficial sands are characterised by relatively lower permeability compared to the older reef limestone below.

Once the percolating rainwater recharges the aquifer, the groundwater moves gradually downwards and outwards through the permeable substrate. The groundwater mainly moves in a vertical direction and mixes with saline water at the base of the FWL. Near the coastal margin of the islet, some groundwater discharges to the

sea. In the longer term, the total loss of groundwater through mixing and outflow at the margins is balanced with the recharge from rainfall on the islet (see below).

The average saturated hydraulic conductivity of the Holocene carbonate sands and gravels is estimated to be approximately 10 m/day according to observations on a number of atoll islets, for instance on Tarawa and Kiritimati atolls in Kiribati and South Keeling atoll in the Cocos (Keeling) Islands where conductivities have been measured using borehole falling head tests (Falkland 1994; Falkland and Woodroffe 1997; Woodroffe and Falkland 1997; White et al. 2007b). In contrast, the saturated hydraulic conductivity of Pleistocene limestone beneath is considerably greater, typically greater than 1,000 m/day (Oberdorfer et al. 1990) owing to karstification and diagenetic change during past episodes of emergence above sea level (Underwood et al. 1992).

The base of the FWL is not a sharp interface between freshwater and seawater, but rather a broad transitional zone of brackish water, where salinity gradually increases over several metres as the freshwater lens grades into seawater. On many small coral islets, the transition zone may actually be thicker than the freshwater zone above (Falkland 1994). Within the transition zone, both dispersion and outflow occurs mostly in a vertical rather than a horizontal direction (Underwood et al. 1992). Figure 12.2 illustrates a typical cross section through a small coral islet. One observation is the frequently asymmetrical feature of the FWL shape, with the thickest section often displaced towards the lagoon rather than the ocean side of the islet (Falkland 1994). In some cases, where the prevailing wind and wave direction is from the lagoon side, the FWL can be thicker on the ocean side of the islet.

Owing to density differences between freshwater and seawater, FWLs occur above denser seawater (Fig. 12.2). As such, the small average height of the groundwater table (upper surface of a FWL) above sea level varies between islets according to ground elevation, geology, nature of the sediments, and the shape and width of individual coral islets. Over a diurnal tidal cycle, the position of the water table moves up and down in response to the tidal signal but with a reduced amplitude and a lag typically varying between one and three hours. The efficiency of tidal propagation through the coral substrate varies between about 5 and 50 %, primarily depending on the grain–size of the sediments. Ponding of the groundwater at the surface can occur during excessively wet periods in areas where the FWL is close to the land surface, especially during high tides. Over the longer term and for average conditions, the classical Ghyben-Herzberg theory (Badon-Ghyben 1888; Herzberg 1901), which is based on a sharp interface between freshwater and seawater, states that the thickness of the FWL is directly related to the elevation of the water table above sea level; thus for every unit height of freshwater rising above mean sea level, there are approximately 40 equal units of freshwater below sea level. However, due to freshwater and seawater mixing at the base of the FWL causing a transition zone to form, the 1:40 ratio is not an appropriate method of determining the base of the FWL. The ratio may be used as a guide to estimate the mid-point of the transition zone (Falkland 1994). Accurate determination of the thickness and extent of a FWL is best provided through drilling and water sampling from

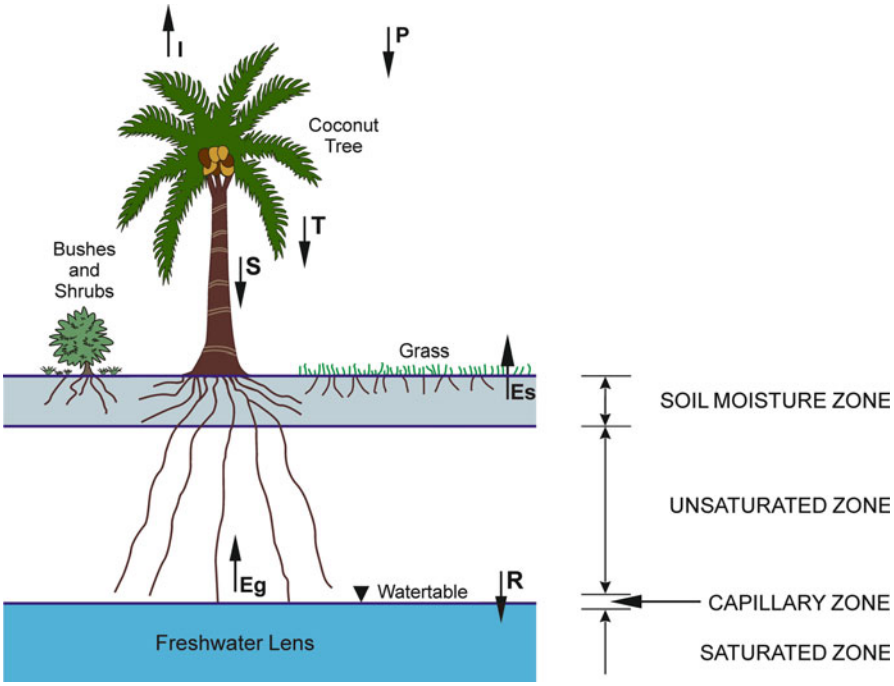

Fig. 12.3 Conceptual water balance model, under a vegetation canopy, illustrating the components that determine the amount of atoll freshwater lens recharge (Adapted from Falkland and Brunel (1993))

monitoring boreholes, although surface electrical resistivity and electromagnetic measurements techniques also provide reasonably good estimates (Anthony 1992).

Overall, the location, volume and quality of FWLs is determined by the size and shape of individual islets, the permeability and porosity characteristics of the soils and substrate, recharge through rainfall infiltration, the type and distribution of vegetation (Anthony 1992; Falkland 1994; White et al. 2002, 2007b; Bailey et al. 2009). For illustration, on Majuro Atoll in the Marshall Islands, the most extensive and best developed FWL has been measured in the west of the atoll at Laura where the area of the FWL approaches 0.9 km^2 (Hamlin and Anthony 1987).

The location, volume and quality of a FWL influences the type and distribution of atoll islet vegetation, as well as the location of village wells and taro pits used for cultivation. Some deep-rooted species among the native vegetation on atoll islets, particularly coconut trees, have evolved to use the shallow groundwater directly to supply most of their water demand (Falkland and Brunel 1993). These species are known as phreatophytes. Recharge to a FWL is equal to the precipitation, which occurs mainly as rainfall, minus evapotranspiration losses as shown in Fig. 12.3. The groundwater recharge model in Fig. 12.3 shows how the magnitude of recharge (R) in a given time period depends on the rainfall (P) and three evapotranspiration (ET) components (I, Es and Eg). The first ET component, I, is the rainfall that is

intercepted by vegetation and which is subsequently evaporated. The remaining rainfall falling on trees becomes either throughfall (T) or stemflow (S). The second ET component (Es) is the evapotranspiration from the soil zone by shallow rooted grasses and plants and the shallow roots of trees. The third ET component (Eg) is the transpiration occurring directly from the FWL through the deep roots of coconut and other trees (phreatophytes). Coconut trees (*Cocos nucifera*) are known to transpire large quantities directly from the water table. Measurements by White et al. (2002) on mature coconut trees at Bonriki islet on Tarawa Atoll in Kiribati indicate that a single tree may transpire between 60 and 150 L of groundwater daily with a mean of about 120 L per day. The same study estimated that groundwater recharge (102 mm) was only 17 % of rainfall (603 mm) over a 6-month monitoring period when the rainfall was significantly below average. The average annual rainfall for Tarawa is approximately 2,000 mm and it has since been estimated that the long-term recharge for Bonriki islet is approximately 980 mm or nearly 50 % of rainfall (White et al. 2007b). On Majuro Atoll in the Marshall Islands, the annual evapotranspiration loss at Laura has been estimated by Hamlin and Anthony (1987) to be about 50 % of rainfall. Average annual rainfall is approximately 3,300 mm, so recharge of the freshwater lens at Laura can be estimated at roughly 1,650 mm per year. However, the exploitable groundwater resources (or sustainable groundwater yield) may be as low as 20 % of the mean annual recharge to the lenses (Anthony 1991).

A relatively common feature of atoll islet geomorphology that is important to mention is the low-lying depressions that often occur in the central area of larger islets (Rankey 2011). If the base of these interior topographic depressions reaches the water table, they become freshwater swamps that are effectively ‘windows’ onto the FWL. This makes them valuable sites for local people to cultivate staple food crops, especially the common taro (*Colocasia esculenta*), giant taro (*Alocasia macrorrhiza*) and giant swamp taro (*Cyrtosperma chamissonis*) (Thaman 2008; Fig. 12.4). Throughout the Pacific atolls, low-elevation depressions on islets containing freshwater swamps that are used for growing food are therefore known as ‘taro pits’ (Manner 2011).

12.1.3 Atoll Groundwater Vulnerability to Physical and Human Disturbance

Freshwater lenses on atoll islets are uniquely fragile types of aquifers, yet their existence is essential for maintaining the natural flora and fauna of atoll ecosystems and for sustaining human settlement. Unfortunately, the fragility of FWLs render them highly vulnerable to a range of human and natural disturbances (White et al. 2007a). Relatively large settlements on some atolls may cause water demand to exceed the local resources. On Tarawa Atoll in Kiribati, the small islet of Betio with an area of just 0.8 km^2 lies in the south west of the atoll. Inward migration from

Fig. 12.4 Cultivation of giant swamp taro (*Cyrtosperma chamissonis*) in a taro pit on Butaritari Atoll, Kiribati (Photo courtesy of R. Thaman)

outlying islands over recent decades and steady population growth means that Betio now has a population density in the region of 15,000 people per km^2. As a result, the local FWL lens is insufficient to meet demands (Depledge and Terry, in press), so water must be piped from larger aquifers on Bonriki and Buota, although these islets lie more than 30 km away in the south east of Tarawa (White et al. 2002). Similarly, tiny Ebeye islet (0.36 km^2) on Kwajalein Atoll in the Marshall Islands has a population density exceeding 40,000 people per km^2. Such horrendous overcrowding poses major challenges for public health, food security and water supply, which are under severe stress (Weir and Virani 2011).

Anthropogenic degradation of atoll FWLs can occur in a number of forms. At the base of a lens, saline intrusion may be caused by excessive groundwater pumping with inappropriate extraction methods (Diaz Arenas and Falkland 1991). Conventional groundwater extraction technology uses vertical bores or wells, but if these are over-pumped, upconing of seawater into the base of the lens can result. Nowadays, shallow horizontal infiltration galleries are recommended as a more appropriate extraction method, whereby freshwater can be 'skimmed' from the FWL surface, leading to greater yet sustainable yields compared to older vertical bore or well installations. Other types of FWL contamination can result from faecal contamination owing to a lack of adequate sanitation and effluent disposal, leading to levels of faecal coliform bacteria in groundwater (especially *Escherichia coli*) exceeding WHO guidelines for safe human consumption (Dillon 1997), while the use of crop pesticides and fertilizers must be carefully controlled to avoid groundwater contamination.

The continuing viability of atoll FWLs also faces further perils from episodic natural climatic perturbations and (human-induced) threats associated with climatic and environmental change on longer timescales. Undeniably, any erosion of the physical substance of coral islets will also lead to a concomitant reduction in the size of the FWL contained within. For those atolls that lie in the tropical cyclone belts, such erosion may occur during the occasional passage of these intense weather systems, where considerable shoreline readjustment may be produced by powerful wave action. Regarding coral islet water balance, the dynamics of hydrological recharge means that FWLs are especially sensitive to disturbances in regular climatic patterns. For example, conditions of moisture deficit may occur during dry seasons that deliver less rainfall than normal. Accentuated dry spells may similarly result from shifts in the usual precipitation patterns across the Pacific, particularly driven by El Niño and La Niña events (White et al. 1999, 2007b; van der Velde et al. 2006). During extended droughts, 'negative' lens recharge occurs, reflecting that rainfall is insufficient to match evapotranspiration losses and hence acts to diminish the FWL volume (Falkland 2002) beyond that occurring due to mixing with underlying seawater and outflow from the lens perimeter (White et al. 1999). A depleted FWL may take over a year and a half to recover according to work by Bailey et al. (2009).

Wave overtopping of low coral islets by high waves and accompanying storm surge during cyclones is a further menace. During heavy storms, large waves coupled with strong winds may affect both the ocean and lagoon shores of atolls. The accompanying storm surge is the temporary sea-level rise experienced during cyclones, produced by the combination of low atmospheric pressure near a storm centre and forceful winds pushing seawater up against a shoreline (Terry 2007). The closer a cyclone track moves towards a coastline, the more probable it is for high waves to roll across the reef flat and inundate atoll islets. Even when the path of a cyclone does not directly traverse an atoll, if the timing of the closest proximity coincides with high tide and wind direction is onshore (Fig. 12.5), then seawater rushing up against a coastline allows wind-driven waves to partially or totally submerge the low-lying islets. Subsequent seawater infiltration into the ground causes salinisation of the aquifer.

12.2 Groundwater Observations in the Northern Cook Islands (A Case Study of Storm-Induced Salinisation and Recovery)

12.2.1 Introduction

In order to demonstrate the effects on atoll islet FWLs of sea flooding caused by storm waves and storm-surge washover, the goal of this section is to describe the impacts on the groundwater of Pukapuka Atoll in the Northern Cook Islands following Tropical Cyclone Percy in February–March 2005. Although the storm did not actually make landfall on the atoll, it passed close by and was the strongest

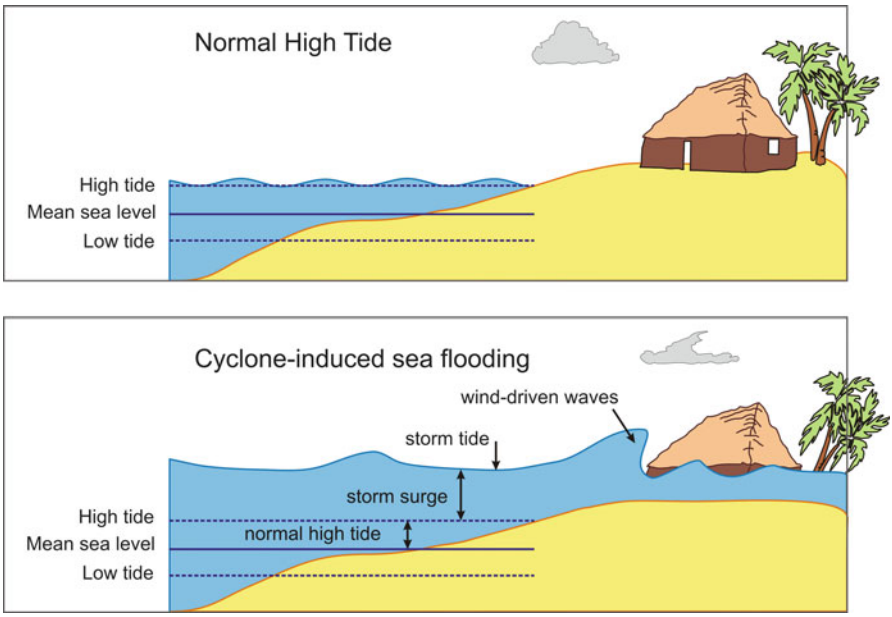

Fig. 12.5 Sea flooding of an atoll islet caused by the combination of wind-driven waves and storm surge at the time of high tide (Adapted from the Australian Bureau of Meteorology (BoM 2005))

storm to affect Pukapuka in recent decades. FWL salinity increases were measured shortly after the cyclone struck and the subsequent timescale of the lens recovery was monitored.

Pukapuka Atoll (10.85°S, 165.83°W) is a remote atoll in the Northern Cooks group (Fig. 12.6) lying more than 1,000 km northwest of Rarotonga, the capital of the Cook Islands. Pukapuka's reef platform is triangular in plan and upon it lie three small coral islets named Wale, Motu Ko and Motu Kotawa, with one islet at each apex of the triangular reef outline. The total land area of Pukapuka totals just 3.8 km^2, although the atoll supports a population of about 640 people, most of which lives in three villages on Wale. The islets comprise Holocene-age sands and gravels, the thickness of which ranges from 7 to 12 m, although the topography rises to only 2 m or so above sea level. The location experiences a diurnal microtidal environment, with mean and spring tidal ranges of only 0.31 and 0.37 m respectively (NOAA 2008). Freshwater for consumption is obtained from rainwater tanks and a limited number of shallow wells that access the water table, while giant swamp taro (*Cyrtosperma chamissonis*) is grown as the main subsistence starch crop in the freshwater swamps occupying the low-lying topographic depressions towards the centre of all three islets. A tropical marine climate prevails, with an annual rainfall averaging 2,845 mm, of which 63 % falls in the 6-month wetter season between October and March. In these same months, 9–10 tropical cyclones normally form over the warm waters of the west and central tropical South Pacific Ocean, but of these only 4–6 cyclones per decade enter Cook Islands waters.

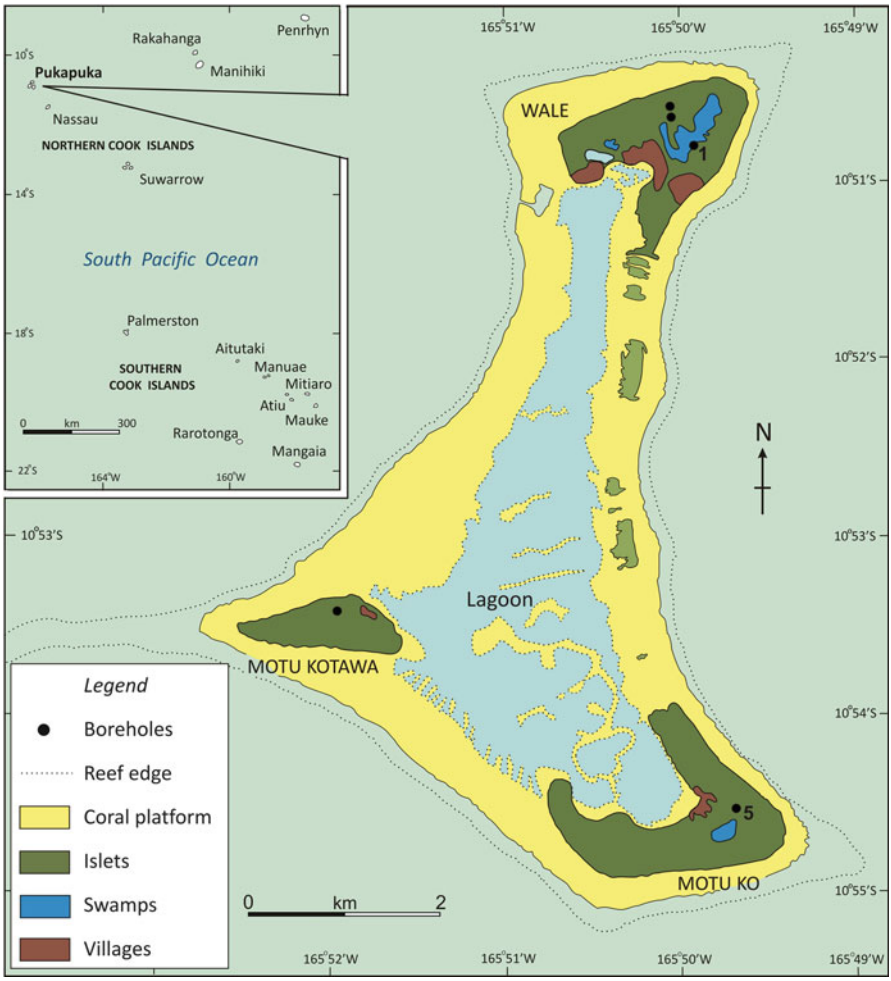

Fig. 12.6 Location and geography of Pukapuka Atoll, showing also sites of groundwater monitoring boreholes on the three islets

12.2.2 Baseline Freshwater Lens Characteristics

As part of groundwater resources assessments carried out on Pukapuka in February 2004, funded by the Cook Islands government, surveys of groundwater level and salinity in wells, ponds and swamps, and electromagnetic (EM) surveys were conducted. Full details are given in Falkland (2005). The maximum amplitude of the groundwater signal influenced by tides is approximately 0.09 m. The tidal efficiency TE (groundwater-to-sea-level amplitude ratio) is therefore approximately 0.30, which is a moderately high value indicating the relatively high permeability of the coral sediments. The assessment also included the installation

Table 12.1 Baseline FWL characteristics in two locations on Pukapuka Atoll prior to cyclone disturbance in January 2005

Borehole No.	Islet	Depth[a] to Pleistocene-Holocene unconformity (m)	Av. depth[a] to top of FWL (m)	Av. depth[a] to base of FWL (m)	Estimated FWL thickness (m)
Borehole 1	Wale	10.1	1.85	7.0	6.1
Borehole 5	Motu Ko	7.2	1.95	12.1	10.1

[a]Measured as the depth below ground level.

of five multi-level monitoring boreholes on the FWLs (Fig. 12.6). Boreholes were 89 mm in diameter, drilled to depths of 10–22 m, and installed with 8 mm nylon monitoring tubes to different depths. The base of each tube was fitted with a glass filter to prevent ingress of sand and the top of each tube was fitted with a snap coupling for attaching a portable electric pump to extract samples for salinity (electrical conductivity) measurements. Boreholes were backfilled with gravel and bentonite layers to form hydraulically-isolated zones around the end of each tube. No permanent casing was fitted inside the boreholes. Each borehole was fitted with a 50 mm PVC pipe to below the water table and protected with a cast-iron cover set flush with the ground surface.

A programme of groundwater salinity measurements then commenced, carried out by locally trained personnel initially at approximately monthly intervals to define the FWL salinity conditions and thickness. Measurements established the average depth to water table and base of the FWLs at each location, allowing estimation of FWL thickness on the three islets (Table 12.1). Electrical conductivity (EC) equal to 2,500 μS/cm was used to define the base of the FWLs. This EC value is chosen as the lower boundary of the FWL because on Pacific atolls such water is routinely used for non-potable domestic purposes, and 2,500 μS/cm is suggested as the upper limit for human use (equivalent to approximately 1,375 mg/L total soluble salts) (George et al. 1996). Thus, maximum FWL thickness was estimated to be 5.2 m, 2.6 m and 10.1 m thick on Wale, Motu Kotawa and Motu Ko islets, respectively, at the approximate centre of each lens.

12.2.3 Cyclone-Induced Impacts on Groundwater and Subsequent Recovery

For the Cook Islands, 2005 was an unprecedented year as 6 cyclones affected various parts of archipelago. Of these storms, TC Percy tracked nearest to Pukapuka (Fig. 12.7) resulting in sea flooding of the islets. The storm attained category-5 intensity (most severe category) on the standard Saffir-Simpson scale, with central pressure falling to 925 hPa around 06:00 on 27 February. At 21:00 the same day the

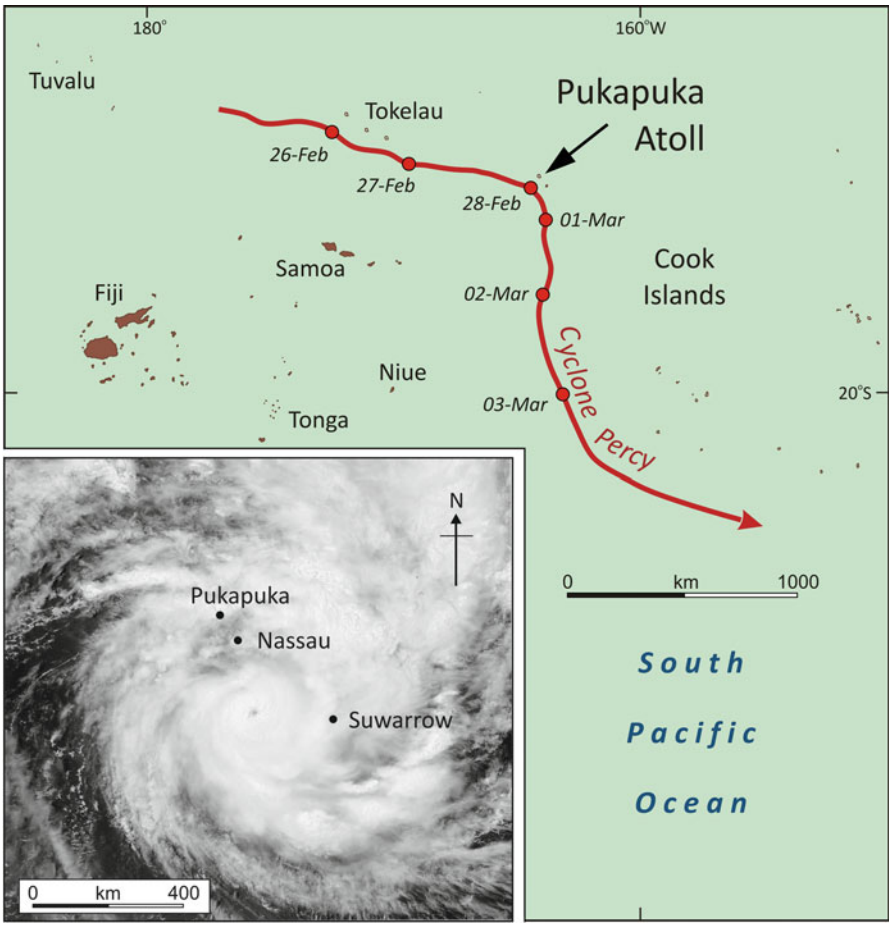

Fig. 12.7 Track of Tropical Cyclone Percy through Tokelau and the Cook Islands during February–March 2005; *red circles* show the position of the cyclone eye at midnight GMT. *Inset map* shows the visible satellite image at 00:40 on 1 March 2005 GMT, after Percy passed close to Pukapuka and Nassau a few hours earlier (Satellite base image courtesy of NASA)

eye passed within 15–30 km to the south of Pukapuka, with maximum sustained 10-min winds of 90 knots (167 km/h) and gusts up to 120 knots (222 km/h) recorded on the atoll (NIWA 2005). Besides wind damage, high waves swept partially across all the low-lying islets causing seawater intrusion into the taro swamps and the few open wells. An urgent shipment of drinking water was organised by the Red Cross from American Samoa.

Subsequent to the sea flooding and wave washover of the islets caused by TC Percy in March 2005, groundwater salinity profiles were determined from borehole EC readings on eight occasions between May 2005 and May 2007. This dataset is

unique as it is the only known atoll groundwater monitoring programme that provides post-disturbance assessment of saline intrusion and subsequent recovery. Figure 12.8 compares the baseline conditions of the FWLs (Jan-05 profiles, blue lines) the post-cyclone saline impacts (red lines, May-05) and subsequent slow groundwater recovery resulting from rainfall infiltration at the thickest part of the FWL on two of the islets: Wale and Motu Ko. The following patterns can be observed from the salinity (EC) profiles.

Baseline conditions prior to disturbance showed that Pukapuka Atoll had moderately thick fresh groundwater resources on each of its three islets. The thickest FWLs existed on Wale (5 m maximum) and Motu Ko (11 m maximum). Measurements at the water table (FWL surface) show groundwater was fresh (EC approximately 1,000 μS/cm). Two months after the cyclone in May 2005, water table salinity had notably increased, especially on Motu Ko (10,050 μS/cm). Over the following months, water table salinity partially recovered. By late January-March 2006, after 1 year of recovery, the water table had improved to pre-disturbance conditions, i.e. below 1,000 μS/cm.

Deeper within the profile of the thickest FWL on Motu Ko, an interesting recovery pattern was observed. The response to saline intrusion on this islet was stratification of the FWL, in particular the appearance of a salinity profile 'inversion' at depth. The inversion was the result of two identifiable features. First, the seawater intrusion produced a well-defined and persistent saline plume within the lens. The salinity profile for May 2005 shows this saline plume (15,450 μS/cm) at about 6 m below the surface. Second, deeper still at about 12 m, a thin horizon of freshwater (1,600 μS/cm) remained unaffected, lying sandwiched beneath the saline plume and the base of the lens. The substrate at this depth is limestone that is heavily fractured, so no geologic explanation can be proposed for the trapped freshwater layer. From the time of the initial sea flooding and for the next six months until September 2006, the saline plume remained in place and gradually decreased in salinity. Over the same period, the sandwiched freshwater horizon beneath the saline plume maintained salinity levels below 1,800 μS/cm (i.e. within usable limits), before gradually mixing and dispersing within the aquifer thereafter.

Overall, the FWL recovery time on Pukapuka was a function of both the sea flooding event and the amount of groundwater recharge over subsequent months. The storm occurred near the end of the cyclone season (March), immediately before the commencement of the dry season that lasts normally from April to September. It is likely that if the saline intrusion had occurred earlier in the wet season, the FWLs may have experienced faster recovery due to rainwater recharge in November and December 2004 (205 and 198 mm monthly rainfall, respectively) helping to flush away of some of the salt in the groundwater. Within the FWL on Motu Ko, the persistence of the trapped freshwater horizon was probably aided by Pukapuka's micro-tidal range of just 0.31 cm (NOAA 2008), because tidally-driven vertical mixing would have been a relatively inefficient mechanism for dispersal. Accessing this thin and fragile fresh horizon would be a difficult challenge, owing to the threat of seawater upconing into the base of the FWL.

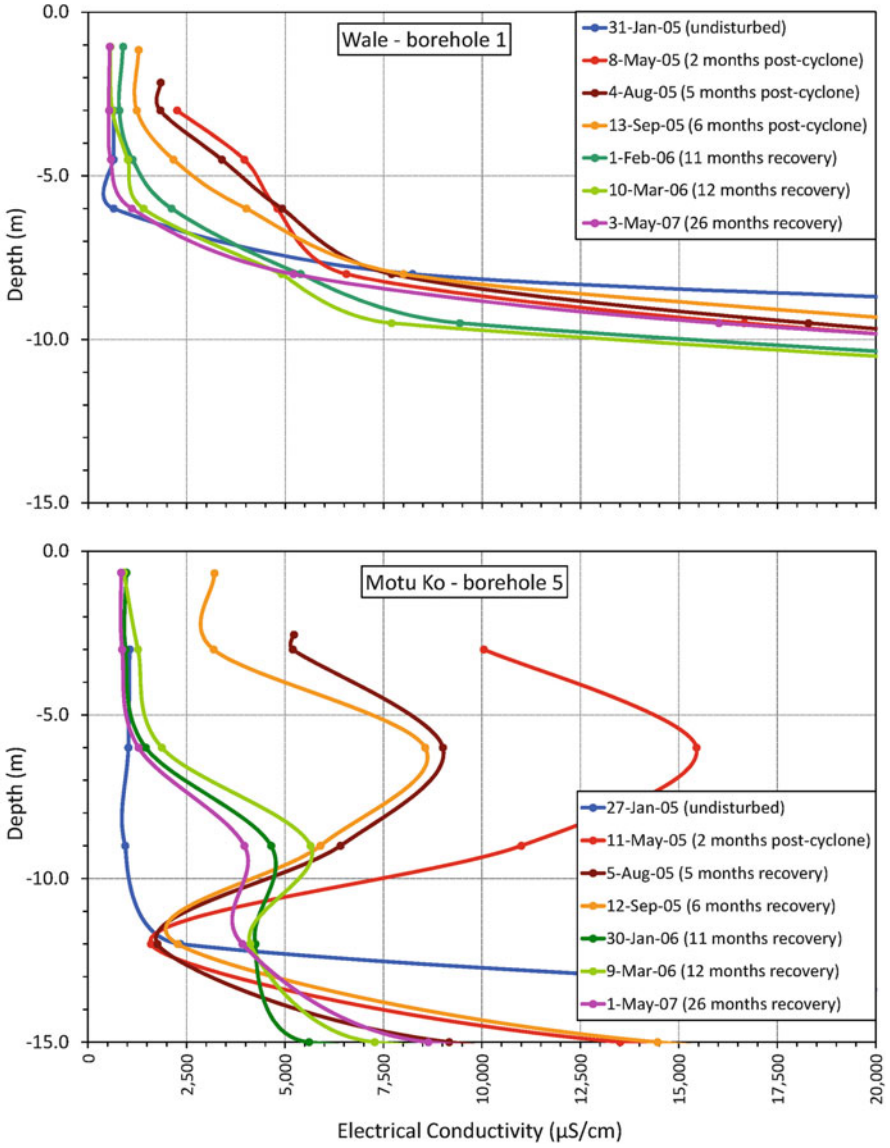

Fig. 12.8 Salinity profiles over time in FWLs, measured from two boreholes on Wale (*top*) and Motu Ko (*bottom*) islets. The Jan-05 profiles (*blue lines*) represent average baseline groundwater conditions prior to cyclone disturbance. The saline intrusion on top of the FWL during TC Percy is clear from the May-05 profiles (*red lines*). Subsequent salinity profiles show the slow recovery of the FWLs until the most recent data in May 2007. Notes: (1) For clarity, only the top part of the FWLs profiles are shown (to 15 m depth). (2) The upper limit of the x-axes (20,000 µS/cm) is approximately 40 % seawater salinity. (3) On the y-axes, 'depth' means 'depth below ground surface'

12.2.4 Modelling Approaches

As in other branches of hydrology, numerical modelling is a valuable technique that complements the findings of field investigations, or can be employed along with appropriate field data in order to facilitate better understanding of atoll groundwater resources. Modelling can assist with both appreciating different properties of atoll FWLs and quantifying the responses to real or anticipated changes in natural and human influences. A number of comprehensive studies have investigated many different scenarios and undoubtedly made important contributions about atoll groundwater sensitivity to different environmental parameters (see, for example, Oberdorfer and Buddemeier 1988; Oberdorfer et al. 1990; Underwood et al. 1992; Griggs and Peterson 1993; Peterson and Gingerich 1995; Singh and Gupta 1999; World Bank 2000; Bailey et al. 2009). This section starts with a brief overview of previous modelling studies on atoll groundwater resources. In line with the theme of this chapter, it then presents a summary of the key findings from a recent investigation (Chui and Terry 2012) that models the impacts of storm-driven wave washover on atoll FWLs.

12.2.5 Overview of Previous Modelling Studies on Atoll Groundwater Resources

The work of Oberdorfer and Buddemeier (1988) was one of the first attempts to use a numerical model to predict the effects of climate change on groundwater in a small atoll islet. They found that for Enjebi islet on Enewetak Atoll in the Marshall Islands, the total freshwater inventory is a monotonic but nonlinear function of recharge. Regarding sea-level rise (SLR), they postulated that it actually improves groundwater availability by increasing the 'useful volume', i.e. the amount of freshwater in the upper portion of the lens above the high-permeability zone. Later, a major economic assessment by the World Bank (2000) on managing and adapting to environmental change in Pacific Island economies dedicated a section to island water resources. Within this, a numerical model was used to examine the impacts of a range of climate change and SLR scenarios on the Bonriki islet FWL, which is the main groundwater supply source for Tarawa Atoll in Kiribati. Water balance modelling suggested that by the year 2050, a 10 % decline in rainfall would result in a 14 % reduction in groundwater recharge, whereas a 7 % rainfall increase would give a 5.5 % increase in recharge (Table 12.2). It was also noted that although evapotranspiration increases as climate warms, its effects on groundwater recharge are less significant than projected changes in annual rainfall. In terms of SLR, the World Bank report concluded that a 0.4 m rise would have little consequence on the Bonriki FWL and would even slightly raise its volume. This is due to the fact that the average level of the freshwater lens, which is influenced by mean

Table 12.2 Modelled responses of the Bonriki islet FWL on Tarawa Atoll in Kiribati, after various projected climate change and sea-level rise scenarios

Climate change scenario	Percentage change in groundwater thickness modelled
Current[a] sea level, 7 % increase in rainfall	+5.5
Current sea level, 10 % reduction in rainfall	−14.0
0.2 m SLR, current rainfall	−0.9
0.4 m SLR, current rainfall	+2.0
0.4 m SLR, 10 % reduction in rainfall	−12.0
0.4 m SLR, current rainfall, reduced island width	−29.0
0.4 m SLR, 7 % increase in rainfall, reduced island width	−19.0
0.4 m SLR, 10 % reduction in rainfall, reduced island width	−38.0

Data from World Bank (2000)
[a]2000 values

sea level, would rise slightly into less permeable Holocene sediments from the highly permeable underlying Pleistocene limestone. However, possible reduction in islet width associated with inundation is a further consideration, as this would diminish lens thickness even without precipitation decrease.

More recently, Bailey et al. (2009) evaluated the sensitivity of atoll FWLs to several climatic and geologic variables. Their work noted that lens thickness is most sensitive to the hydraulic conductivity of the uppermost Holocene aquifer and the depth of the Holocene–Pleistocene unconformity. The temporal variations of the lens thickness, on the other hand, are sensitive to fluctuations in the recharge rate.

Other modelling studies have focused attention on understanding the transition zone below FWLs and the propagation of tidal influences through them. In a simulation of the FWL within Enjebi islet on Enewetak Atoll, Oberdorfer et al. (1990) determined that tidally-induced flow predominates over density-driven flow and creates an extensive mixing zone of brackish water. Underwood et al. (1992) similarly established that mixing within a FWL is mostly due to the oscillating vertical flow caused by tidal fluctuations and depends to a lesser extent on transverse dispersion. The dispersive mixing is controlled by the combined effects of tidal range, vertical longitudinal dispersivity and vertical permeability.

Numerical modelling also has a crucial role in the development of groundwater management strategies. For example, Griggs and Peterson (1993) simulated groundwater flow in the Laura area of Majuro Atoll in the Marshall Islands and reached the conclusion that multiple pumping centres, instead of individual ones, are more efficient in extracting groundwater. Likewise, Singh and Gupta (1999) were able to arrive at a safe groundwater pumping scheme using a modelling approach for the Lakshadweep Islands in the Arabian Sea. They established that a pumping rate up to 13 m^3 per day was sustainable for wells more than 400 m apart and where the water table was at least 0.15 m above MSL.

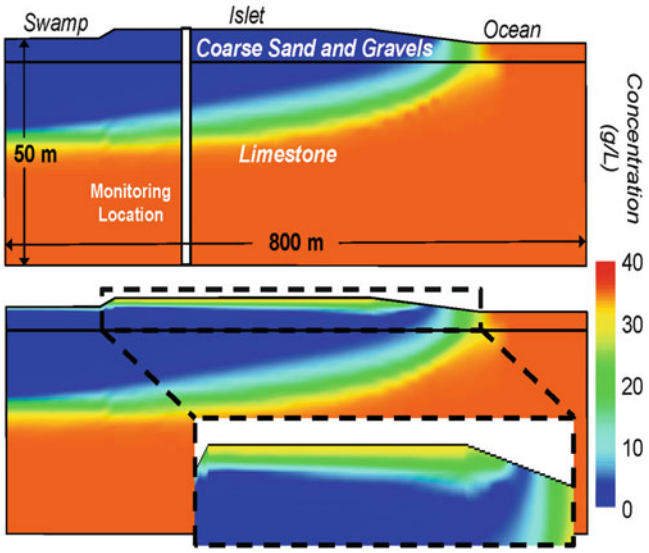

Fig. 12.9 Salinity distributions in the FWL for undisturbed conditions (*top*) and immediately after wave washover (*bottom*). Note: for clarity half of the atoll islet is shown, from the middle of the islet to the ocean side, with an assumed symmetry about the left side of the diagram towards the atoll lagoon

12.2.6 Effects of Storm-Wave Washover on Freshwater Lenses

In recent work, Chui and Terry (2012) examined the saline intrusion as well as the subsequent recovery of a FWL, following wave-washover of an atoll during an intense tropical storm. The initial part of the study involved modelling a coral islet in the tropical Pacific Ocean with specified size, substrate composition, rainfall and infiltration characteristics. Simulation of average long-term conditions thus obtained a FWL typically observed in atolls, as shown in the top image in Fig. 12.9. The study then subjected the FWL to saline intrusion caused by the storm-wave washover, and examined the immediate response, longer term behaviour and subsequent recovery of the aquifer. During the storm-generated washover, seawater quickly infiltrated into the unsaturated zone of the coarse sands and gravels, and caused a salinity increase in the top part of the FWL as seen in the bottom image in Fig. 12.9. After the washover event, the observed saline plume first migrated downwards through the overlying coral sand and gravel sediments, but then exited the FWL to the ocean laterally through the more permeable limestone at the base of and below the FWL. Figure 12.10 illustrates the evolution of the salinity profile at selected time intervals at the simulated 'monitoring' location marked in Fig. 12.9. Interestingly, the profile reveals the existence of a layer of relatively fresher water sandwiched between the saline plume above and seawater below, 2 months and 1 year into the recovery period.

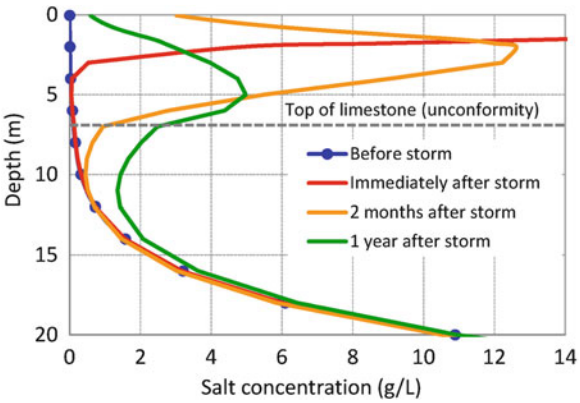

Fig. 12.10 Salinity profiles before and after the storm at the monitoring location marked in Fig. 12.9

This behaviour closely mirrors the field observations reported by Terry and Falkland (2010) on Pukapuka Atoll in the Northern Cook Islands after Cyclone Percy in 2005, as described in Sect. 12.2.3. Model sensitivity analyses also indicated, as expected, that a saline plume takes longer to disperse (i.e. extended recovery time for a salinised FWL) for an atoll with a drier climate.

A notable attribute of Chui & Terry's model is the incorporation of a central low-lying depression (i.e. a freshwater swamp under undisturbed conditions), which is a topographic feature typical of some larger atoll islets. Seawater accumulates in the swamp during marine inundation of the islet and remains there for a number of days after the event. Seawater also accumulates on the surface of the FWL surrounding the swamp, owing to the high infiltration rate through the coral sediments in the unsaturated zone. This affects the deeper part of the FWL and prolongs the later stage of freshwater lens recovery. One suggested mitigation measure in such circumstances is to pump out stagnating seawater from the swampy depression if possible. This would need to be done with caution and at low pump rate so as not to induce further seawater intrusion from below.

12.3 Conclusions and Outlook

A source of clean, potable freshwater is a prerequisite for human existence on small islands in the Pacific (Depledge and Terry, in press; White et al. 2008). From the synopsis presented in this chapter of published research over recent decades, it is clear that the limited fresh groundwater resources found on coral atolls are both uniquely fragile and at risk of disturbance from a range of natural and human-induced pressures. Amongst these threats are over-extraction and pollution associated with growing urban populations, drought and salinisation related to climatic variability and episodic extreme storm events. The last of these has been the subject of recent investigation by the authors. Post-cyclone field measurements on Pukapuka Atoll in the northern Cook Islands over the period 2005–2007 indicated that at least a year is necessary for a freshwater lens to recover completely

from seawater intrusion due to storm-wave washover. Since it is believed that the Pukapuka study is the only documented account of cyclone-induced atoll groundwater salinisation and subsequent recovery, it is suggested that further work of a similar empirical nature should be a matter of priority on affected atolls, in order to improve our understanding of the processes involved. Analysis using a modelling approach has also proved valuable. Simulations show how seawater that accumulates in the low-lying topographic depressions in the interior of some atoll islets during wave washover may prolong the recovery time of a salinised freshwater lens.

In the scientific literature on climate change, discussion continues on the relationships between observed rising sea-surface temperatures and geographical patterns of tropical cyclogenesis and storm intensities, especially in the South Pacific context (Terry and Gienko 2010; Walsh 2004). Although much uncertainty remains, it is nonetheless the case that occasional anomalous episodes and El Niño events have been identified as responsible for generating more cyclones east of 180° longitude (Chu 2004; Terry and Etienne 2010). Additional supporting evidence is provided in the comprehensive review by de Scally (2008) of historical cyclones over the period 1820–2006 in the Cook Islands, where a clear signal of increased cyclonic activity is apparent during El Niño events (even weak ones), compared with La Niñas or neutral ENSO conditions. Such findings imply that possible future climatic swings towards a more sustained El Niño-like state in the South Pacific (Walsh et al. 2012) may portend a heightened level of storminess for the Polynesian atolls of Tuvalu, Tokelau, the Cook Islands and French Polynesia, i.e. atolls which lie in the vicinity and east of the 180° meridian.

Connected with this, there are fears that projected sea-level rise associated with carbon dioxide emissions and global warming might lead to irreversible physical erosion of atoll fabric. The startling scenario of many low-lying atoll islets possibly 'vanishing' later this century as a direct consequence of eustatic sea-level rise is an image that has already captured media attention in recent years and fuelled worldwide public concern about the plight of mounting numbers of Pacific Island 'environmental refugees'. Although many individual atoll islets in reality demonstrate geomorphic resilience to sea-level rise over decadal timescales (Webb and Kench 2010), anticipated higher sea levels will nevertheless enhance the potential for marine inundation of islets during tropical storms, especially if the strongest cyclones also become more intense in future (Elsner et al. 2008). If such scenarios are realised over the coming decades (whatever the timescales may be), then it is not unreasonable to postulate that the attendant risk of atoll groundwater salinisation resulting from storm-wave washover will similarly increase (Terry and Chui 2012). Sound management of atoll water resources is therefore an imperative that cannot be ignored, if continued and sustainable human habitation of atoll islets is to be ensured.

Acknowledgments The authors wish to acknowledge the efforts of the Pukapuka Island Secretary and the staff of the Pukapuka Island Administration for obtaining the groundwater data during the period of monitoring. Mrs Li Kheng Lee, cartographer at the Geography Dept. of the National University of Singapore is thanked for drafting Figs. 12.2, 12.3 and 12.6.

References

Anthony SS (1991) Case study 7: Majuro Atoll. In: Falkland A (ed) Hydrology and water resources of small islands: a practical guide. UNESCO, Paris, pp 368–374

Anthony SS (1992) Electromagnetic methods for mapping freshwater lenses on Micronesian atoll islands. J Hydrol 137:99–111

Ayers JF, Vacher HL (1986) Hydrogeology of an atoll island: a conceptual model from detailed study of a Micronesian example. Ground Water 24:185–198

Badon-Ghijben (Ghyben) W (1888) Nota in verband met de voorgenomen putboring nabij Amsterdam. (Notes on the probable results of the proposed well drilling near Amsterdam.) Tijdschrift van het Kononklijk Instituut van Ingenieurs, The Hague, vol 9. pp 8–22

Bailey RT, Jenson JW, Olsen AE (2009) Numerical modeling of atoll island hydrogeology. Ground Water 47:184–196

BoM (2005) Storm surge preparedness and safety. Australian Bureau of Meteorology, Melbourne. http://www.bom.gov.au/cyclone/about/stormsurge.shtml/. Accessed Apr 2012

Chu P-S (2004) ENSO and tropical cyclone activity. In: Murnane RJ, Liu K-B (eds) Hurricanes and typhoons: past, present and future. Columbia University Press, New York, pp 297–332

Chui TFM, Terry JP (2012) Modeling freshwater lens damage and recovery on atoll islands after storm-wave washover. Ground Water 50:412–420

Darwin CR (1842) The structure and distribution of coral reefs. Smith, Elder & Co, London, 214 pp

de Scally FA (2008) Historical tropical cyclone activity and impacts in the Cook Islands. Pac Sci 62:443–459

Depledge D, Terry JP (in press) Water. In: Rapaport M (ed) The Pacific Islands: environment and society, 2nd ed. University of Hawai'i Press, Honolulu. For more information, please see: http://www.uhpress.hawaii.edu/p-8734-9780824835866.aspx

Diaz Arenas A, Falkland A (1991) Characteristics of small islands. In: Falkland A (ed) Hydrology and water resources of small islands: a practical guide. UNESCO, Paris, pp 1–9

Dillon P (1997) Groundwater pollution by sanitation on tropical islands. Technical documents in hydrology no.6, IHP-V, UNESCO, Paris, 31 pp

Elsner JB, Kossin JP, Jagger TH (2008) The increasing intensity of the strongest tropical cyclones. Nature 455:92–95

Falkland A (1994) Climate, hydrology and water resources of the Cocos (Keeling) Islands. Atoll Res Bull 400:52 pp

Falkland A (2002) Tropical island hydrology and water resources: current knowledge and future needs. In: Hydrology and water management in the humid tropics. Technical Documents in Hydrology No.52, UNESCO International Hydrology Programme-V, Paris, pp 237–298

Falkland A (2005) Pukapuka, Cook Islands, Report on Water Investigations, February 2004 – February 2005. Ecowise Environmental report No. EHYD 2005/46, prepared on behalf of GHD Pty Ltd for the Australian International Development Assistance Agency and the Cook Islands Government, March 2005

Falkland A, Brunel JP (1993) Review of hydrology and water resources of the humid tropical islands. In: Bonell M, Hufschmidt MM, Gladwell JS (eds) Hydrology and water management in the humid tropics. Cambridge University Press/IAHS, Cambridge, pp 135–163

Falkland A, Woodroffe CD (1997) Geology and hydrogeology of Tarawa and Christmas Island, Kiribati. In: Vacher HL, Quinn TM (eds) Geology and hydrogeology of carbonate islands, vol 54, Developments in sedimentology. Elsevier, Amsterdam, pp 577–610

George R, Weaver D, Terry J (1996) Environmental water quality – a guide to sampling and measurement. Department of Agriculture, Perth, 38 pp

Griggs JE, Peterson FL (1993) Ground-water flow dynamics and development strategies at the atoll scale. Ground Water 31:209–220

Hamlin SN, Anthony SS (1987) Groundwater resources of the Laura area, Majuro Atoll, Marshall Islands. US Geological Survey, Water Resources Investigations Report no. 87-4047, 69 pp

Herzberg A (1901) Die Wasserversorgung einiger Nordseebäder (The water supply on parts of the North Sea coast). Ztg Gasbeleucht Wasserversorg München 44:815–819; 45:842–844
Manner HI (2011) (revised) Farm and forestry production and marketing profile for Giant Swamp Taro (*Cyrtosperma chamissonis*). In: Elevitch CR (ed) Specialty crops for Pacific Island agroforestry. Permanent Agriculture Resources (PAR), Holualoa, 18 pp. http://agroforestry.net/scps. Accessed November 2011
Nakada S, Umezawa Y, Taniguchi M, Yamano H (2012) Groundwater dynamics of Fongafale Islet, Funafuti Atoll, Tuvalu. Ground Water 50(4):639–644. doi:10.1111/j.1745-6584.2011.00874.x
NIWA (2005) The Island Climate Update 56, May 2005, National Institute for Water and Atmospheric Research, Wellington, 6 pp
NOAA (2008) Tidal station location and ranges. National Oceanic and Atmospheric Administration. http://co-ops.nos.noaa.gov/tides06/tab2wc3.html. Accessed Oct 2008
Nunn PD (2010) Pacific atolls: a world apart. In: Migon P (ed) Geomorphological landscapes of the world. Springer, New York, pp 349–356
Oberdorfer JA, Buddemeier RW (1988) Climate change on reef island resources. In: Proceedings of sixth international coral reef symposium, Townsville, 1998, vol 3, pp 523–527
Oberdorfer JA, Hogan PJ, Buddemeier RW (1990) Atoll island hydrogeology: flow and freshwater occurrence in a tidally dominated system. J Hydrol 120:327–340
Peterson FL, Gingerich SB (1995) Modeling atoll groundwater systems. In: El-Kadi AI (ed) Groundwater models for resource analysis and management. CRC Press, Boca Raton, pp 275–292
Rankey EC (2011) Nature and stability of atoll island shorelines: Gilbert Island chain, Kiribati, equatorial Pacific. Sedimentology 58:1831–1859
Singh VS, Gupta CP (1999) Feasibility of groundwater withdrawal in a coral island. Hydrol Sci J 4:173–182
Terry JP (2007) Tropical cyclones, climatology and impacts in the South Pacific. Springer, New York, 210 pp
Terry JP, Chui TFM (2012) Evaluating the fate of freshwater lenses on atoll islands after eustatic sea-level rise and cyclone-driven inundation: a modelling approach. Glob Planet Chang 88–89:76–84
Terry JP, Etienne S (2010) Tempestuous times in the South Pacific Islands. Science 328 (5977):428–429
Terry JP, Falkland AC (2010) Responses of atoll freshwater lenses to storm-surge overwash in the Northern Cook Islands. Hydrogeol J 18:749–759
Terry JP, Gienko G (2010) Climatological aspects of South Pacific tropical cyclones, based on analysis of the RSMC-Nadi (Fiji) regional archive. Clim Res 42:223–233
Terry JP, Thaman RR (2008) Physical geography of Majuro and the Marshall Islands. In: Terry JP, Thomas FR (eds) The Marshall Islands: environment, history and society in the atolls. Faculty of Islands and Oceans, The University of the South Pacific, Suva, pp 1–22
Thaman RR (2008) The ecosystems and flora of Majuro Atoll. In: Terry JP, Thomas FR (eds) The Marshall Islands: environment, history and society in the atolls. The University of the South Pacific, Suva, pp 23–68
Underwood MR, Peterson FL, Voss CL (1992) Groundwater lens dynamics of atoll islands. Water Resour Res 28:2889–2902
van der Velde M, Javaux M, Vanclooster M, Clothier BE (2006) El Niño-Southern Oscillation determines the salinity of the freshwater lens under a coral atoll in the Pacific Ocean. Geophys Res Lett 33:L21403.1–L21403.5
Walsh KJE (2004) Tropical cyclones and climate change: unresolved issues. Clim Res 27:77–83
Walsh KJE, McInnes KL, McBride JL (2012) Climate change impacts on tropical cyclones and extreme sea levels in the South Pacific – a regional assessment. Glob Planet Change 80–81:149–164
Webb AP, Kench PS (2010) The dynamic response of reef islands to sea-level rise: evidence from multi-decadal analysis of island change in the Central Pacific. Glob Planet Change 72:234–246

Weir T, Virani Z (2011) Three linked risks for development in the Pacific Islands: climate change, disasters and conflict. Clim Dev 3:193–208

White I, Falkland T (2010) Management of freshwater lenses on small Pacific islands. Hydrogeol J 18:227–246

White I, Falkland A, Scott D (1999) Droughts in small coral islands: case study, South Tarawa, Kiribati. Technical documents in hydrology no. 26, IHP-V, UNESCO, Paris, 55 pp

White I, Falkland A, Etuati B, Metai E, Metutera T (2002) Recharge of fresh groundwater lenses: field study, Tarawa Atoll, Kiribati. In: Hydrology and water management in the humid tropics. Technical Documents in Hydrology No. 52, UNESCO International Hydrology Programme-V, Paris, pp. 299–332

White I, Falkland A, Perez P, Dray A, Metutera T, Metai E, Overmars M (2007a) Challenges in freshwater management in low coral atolls. J Clean Prod 15:1522–1528

White I, Falkland A, Metutera T, Metai E, Overmars M, Perez P, Dray A (2007b) Climatic and human influences on groundwater in low atolls. Vadose Zone J 6:581–590

White I, Falkland A, Metutera T, Katatia M, Abete-Reema T, Overmars M, Perez P, Dray A (2008) Safe water for people in low, small island Pacific nations: the rural–urban dilemma. Development 51:282–287

Woodroffe CD, Falkland A (1997) Geology and hydrogeology of the Cocos (Keeling) Islands. In: Vacher HL, Quinn TM (eds) Geology and hydrogeology of carbonate islands, vol 54, Developments in sedimentology. Elsevier, Amsterdam, pp 885–908

World Bank (2000) Cities, seas, and storms: managing change in Pacific Island economies. Vol IV Adapting to climate change. Papua New Guinea and Pacific Islands Country Unit, The World Bank, Washington, DC, 135pp

Chapter 13
Seawater Intrusion Assessment and Mitigation in the Coastal Aquifer of Wadi Ham

Mohsen Sherif, Mohamed Almulla, and Ampar Shetty

Abstract The United Arab Emirates (UAE) typifies an arid environment with limited freshwater resources and harsh climatic conditions. Rainfall is scarce, random and can be regarded as an integral element of the water resources at UAE. Groundwater resources, although non-renewable, contribute by more than 50 % of the total water demand in the country. Due to the excessive pumping of groundwater to meet the agriculture demands, groundwater levels have declined in the coastal aquifer of Wadi Ham and the quality of the water has deteriorated due to the seawater intrusion problem.

In this study, MODFLOW and MT3D are employed to simulate the groundwater flow and assess the seawater intrusion problem in Wadi Ham and possible mitigation measures. The flow model was calibrated and validated through comparisons with two independent sets of data collected over periods of 5 and 11 years, respectively. The results of the transport model were calibrated against available groundwater concentrations at some locations. The developed model is then used to study the effects of pumping and artificial recharge on seawater intrusion. Results indicated that reducing the pumping from Khalba well field will retard the seawater intrusion in the southeastern part of the aquifer. Applying artificial recharge through a surface basin of 100 $\times$ 100 m at a rate of 1 m/day will cause equi-concentration contour line 10,000 mg/l to retreat about 1.25 km towards the coast within a period of 12 years.

M. Sherif (✉) • A. Shetty
Civil and Environmental Engineering Department, College of Engineering, UAE University, P.O. Box: 15551, Al Ain, United Arab Emirates
e-mail: msherif@uaeu.ac.ae

M. Almulla
Water Resources Division, Ministry of Environment and Water, P.O. Box: 15096, Dubai, United Arab Emirates

C. Wetzelhuetter (ed.), *Groundwater in the Coastal Zones of Asia-Pacific*, Coastal Research Library 7, DOI 10.1007/978-94-007-5648-9_13,

13.1 Introduction

Groundwater resources constitute an important element of the water budget in many countries. This is typically true in arid and semi-arid regions, where rainfall is limited and surface water bodies, such as lakes and rivers, are absent. In many regions, groundwater represents the only source of freshwater and hence all development activities are entirely dependent on its availability with the required quantities and qualities for the intended uses. Groundwater flow in coastal aquifers cannot be considered separately from transport of dissolved salts (Post and Abarca 2010).

All coastal aquifers around the globe are subjected to the seawater intrusion problem. However, the degree of intrusion differs from one aquifer to another depending on natural and manmade conditions. Natural conditions, such as the aquifer geometry and hydrogeologic parameters, are difficult to control but manmade conditions, such as pumping and recharge activities, might be managed to mitigate the seawater intrusion problem.

Steady state analytical solutions of seawater intrusion problems can be obtained for idealized homogenous aquifers. The Ghyben-Herzberg relation provides a rough estimate for the interface and has been questioned by many researchers. The interface between the freshwater body and saline water body can also be obtained numerically by solving the two non-linear governing equations for hydraulic heads of freshwater and saline water (Bear 1979). This approach provides a fairly accurate solution for undisturbed coastal aquifers with a narrow transition zone, mild water surface and/or piezometric gradients and low flow velocities. In such aquifers, mechanical mixing and advection processes are relatively small and the diffusion process dominates the solute transport.

A more representative approach is the dispersion zone approach which accounts for a mixing zone between freshwater and saline water bodies. In the mixing zone, the fluid flow is governed by the hydraulic gradient, while the transport of salt ions is dominated by hydrodynamic dispersion processes and also the density effects in the vertical direction (Huyacorn et al. 1987; Sherif et al. 1988).

Management of coastal aquifers under the conditions of climate changes and possible rise in the seawater levels requires a comprehensive understanding of the processes that affect the degree and rate of the seawater intrusion problem. Due to the complexity of the problem associated with high uncertainties of many of the parameters, it is not always possible to accurately predict the sharp interface or the transition zone between the freshwater and saline water bodies. This is mostly attributed to the randomness and uncertainty of rainfall, lateral inflow through boundaries and pumping and recharge events.

To control saline intrusion, a seaward hydraulic gradient should be maintained and a proportion of the fresh-water should be allowed to flow into the sea. Risks of saline intrusion clearly limit the extent to which a coastal aquifer can be developed for water supply. The management of a coastal aquifer is actually concerned with deciding an acceptable ultimate landward extent of the saline water and calculating the appropriate discharge of freshwater necessary to keep it in that position.

Groundwater systems are generally heterogeneous and anisotropic and not all hydraulic and transport parameters can be properly assessed. However, it is generally possible to determine proper groundwater pumping scenarios that would help to mitigate the seawater intrusion problem under a given set of constrains. In other words, unless the investigated aquifer constitutes an ideal system in which all parameters, boundary conditions and recharge and discharge events are fully identified and controlled, the results of the numerical models would be qualitative. This means that the time scale of the problem may not always be accurate.

Due to the complexity of the problem, powerful numerical models were developed to simulate 3D variable density and solute or energy transport, e.g., SUTRA (Voss and Provost 2002), FEFLOW (Diersch 2006) and SEAWAT (Langevin et al. 2007). A number of 2D and 3D variable density benchmarks that are used to test software were also presented (Voss et al. 2010). Sherif and Hamza (2001), among others, used numerical techniques to demonstrate that pumping of brackish water from the seaside boundary would reduce the seawater intrusion. They also concluded that distance from the seaside boundary and the depth of pumping below the mean seawater level will affect the retardation rate. Among the various analytical studies to simulate the seawater intrusion, Kacimov et al. (2009) provided an assessment for the effect of different parameters on the movement and control of the sharp interface between the freshwater and saline water bodies in coastal aquifers using analytical methods and on the dispersion zone using numerical methods.

In this study, the seawater intrusion phenomenon in the coastal aquifer of Wadi Ham is simulated and the effects of different scenarios of groundwater pumping are evaluated. To that end, MODFLOW is employed to simulate the groundwater flow in the aquifer. The calibration and verification of the flow model were performed before using MT3D to simulate the seawater intrusion, assess its current level and discuss the impacts of several pumping scenarios. The results contribute to a better understanding of groundwater management in Wadi Ham aquifer and other similar coastal aquifers located in arid regions.

13.2 Physical Setting of Wadi Ham

Wadi Ham catchment is located in the north-eastern part of the UAE along Kalbha and Fujairah coast (Fig. 13.1). The catchment lies between the city of Fujairah on the Gulf of Oman to the east and the town of Masafi located on the divide of the Masafi mountain chain. The total catchment area of Wadi Ham is 192 km^2. The upper part of the catchment is characterized by narrow valleys, with distinct channels in the alluvial fill, and steep flanks along the surrounding peaks. The lower eastern part of the catchment widens and forms a large fan until it reaches the Gulf of Oman. The catchment is characterized by its arid conditions and for most of the year there is no flow in the channels. However, occasional intense rainfall events can generate short-duration flash floods. Average annual rainfall in the

Fig. 13.1 Location map of the study area including the wells in Wadi Ham

catchment is around 150 mm/year, with a range between 20 and 506 mm/year (Sherif et al. 2009, 2011). The review of rainfall records in the study area over the last 10 years has shown that the average annual rainfall dropped to less than 80 mm.

Within the catchment area, the ground surface elevation varies from 60 above mean sea level (amsl) to about 950 amsl at the mountain peaks. The land use consists of arid region indigenous vegetation, irrigated farm lands and housing areas. Groundwater is used in the irrigation of cultivated areas along the Wadi streams and also in the vicinity of the coast line. Due to the current developments, the water demands for both domestic use and agriculture needs increased while the available groundwater has decreased and its quantity has deteriorated. The seawater intrusion in the coastal aquifer of Wadi Ham constitutes a major constraint against the sustainable development in the region.

Sherif et al. (2006a) employed 2D resistivity imaging methods to assess groundwater quality and identify the dispersion (mixing) zone, where the groundwater salinity/resistivity varies gradually, in the coastal aquifer of Wadi Ham. They demonstrated that the quality of the groundwater in the study area varies from slightly brackish water in the northwestern and northeastern parts of the area to

saline water in the coastal zone. Empirical relationships between water resistivity, earth resistivity and TDS were developed. Fresh water in the Wadi Ham area has a chloride ion concentration of 224 ppm and a specific conductivity (SC) of 0.98 mS/cm. Saline water in the aquifer of Wadi Ham, on the other hand, has chloride levels of 15,000–30,374 ppm and an SC of 20–79 mS/cm (Sherif et al. 2006a). This 100-fold difference in SC can produce a similar difference in the conductivity of geologic materials saturated with fresh or saline water. The relationship between earth resistivity and TDS, together with inverted 2D true resistivity-depth sections were used to identify the average TDS at any point and at any depth along the 2D resistivity profiles. Therefore, it was possible to classify the groundwater as fresh, brackish, or saline. They concluded that the thickness of the freshwater zone is varying from less than 1 m near the shoreline to about 20 m at distance 3 km from the shore line.

13.3 Geological and Hydrogeological Settings of Wadi Ham

Wadi Ham (Fig. 13.1) is dominated in its upper part by the Masafi Mountains and by alluvial plains in its lower part. The lower plains of Wadi Ham is composed of recent Pleistocene Wadi gravels. This layer is underlain by the consolidated rocks of the Semail formation (Ophiolite sequence) with a mantle of fractured zones at some locations. The Wadi gravels are poorly sorted sub-rounded to sub-angular. The degree of consolidation varies from recent un-cemented sandy gravel to the older well cemented and consolidated gravels. Clastics size ranges from silt grade to boulder sized material with a very high sand content. The gravels are typically composed of basic igneous clasts with other clasts of very well cemented sandstone and conglomerates (Sir Williams Halcrow and Partners Consulting Engineers 1969).

The location of available lithological information of existing bore is presented in Fig. 13.1. The aquifer bottom and ground surface contours were developed as shown in Fig. 13.2a and b, respectively. Several subsurface cross sections along different directions were constructed. Examples of these cross sections are shown in Fig. 13.3a–c. The thickness of Wadi gravel varies from 15 to 100 m (from inland to coast). The minimum thickness is found in the area of well number BHF-19 close to the mountain series (Fig. 13.3a). The maximum thickness is observed in the area of well number BHF-14 which is very close to the coast of Oman Gulf (Fig. 13.3b). The cross-sectional depth of Wadi gravels and sand along the Wadi course varies from 24 to 99 m (Fig. 13.3a–c). Its thickness decreases with increasing the distance from the shoreline, for example within a distance of 3 km it varies from 24 (BHF-7) to 73 m (BHF-12). This is attributed to the regional dipping of Ophiolite series towards the Wadi channel. It should be noted, however, that the gabbro and diorite of the Samail Ophiolite are encountered beneath the Wadi gravels. The gabbro/diorite is likely to be confined in some places by the cemented units. The depth to the ophiolite layer varies from 15 to 100 m.

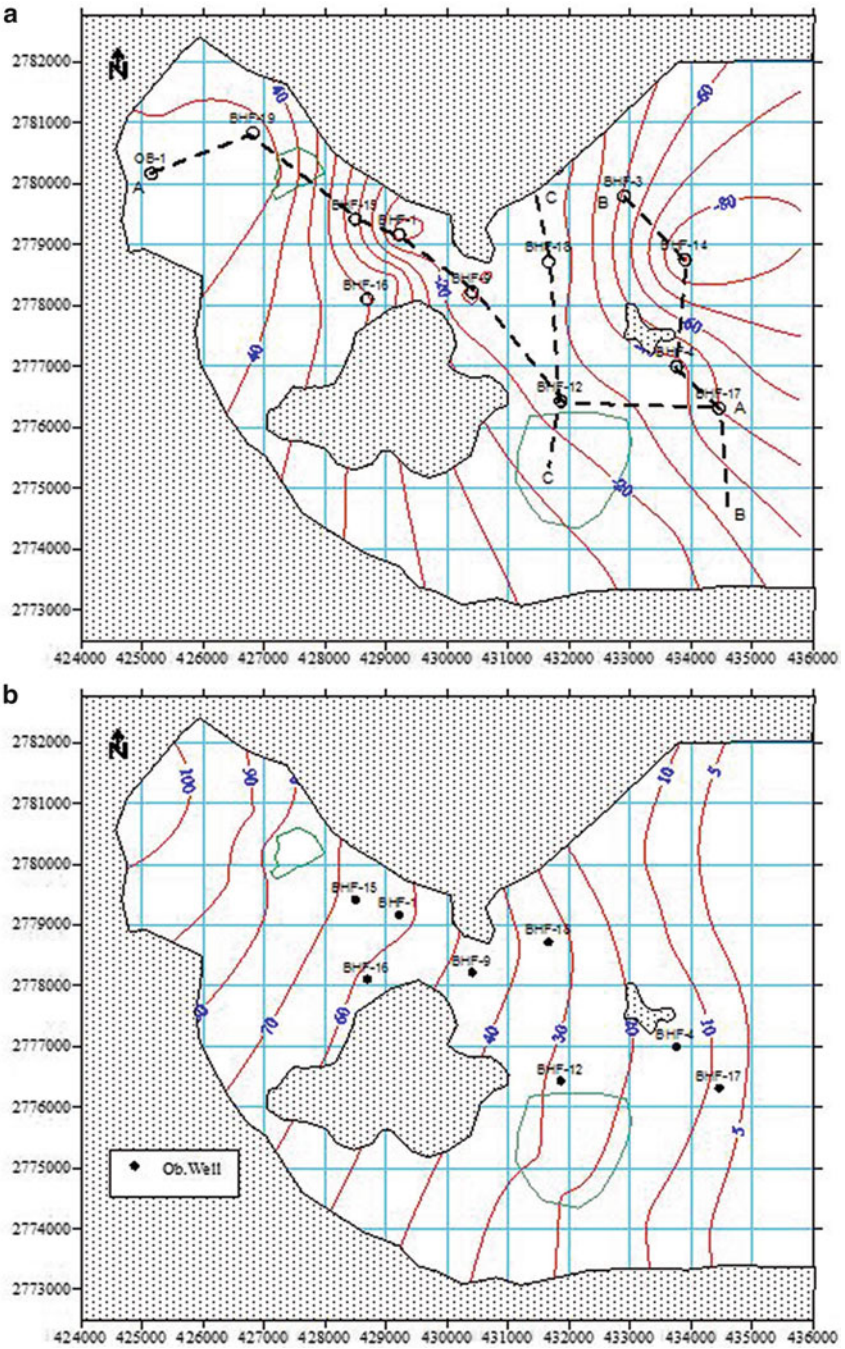

Fig. 13.2 Contour maps of: (**a**) aquifer bottom and location of the geological sections and (**b**) ground surface elevation with reference to msl

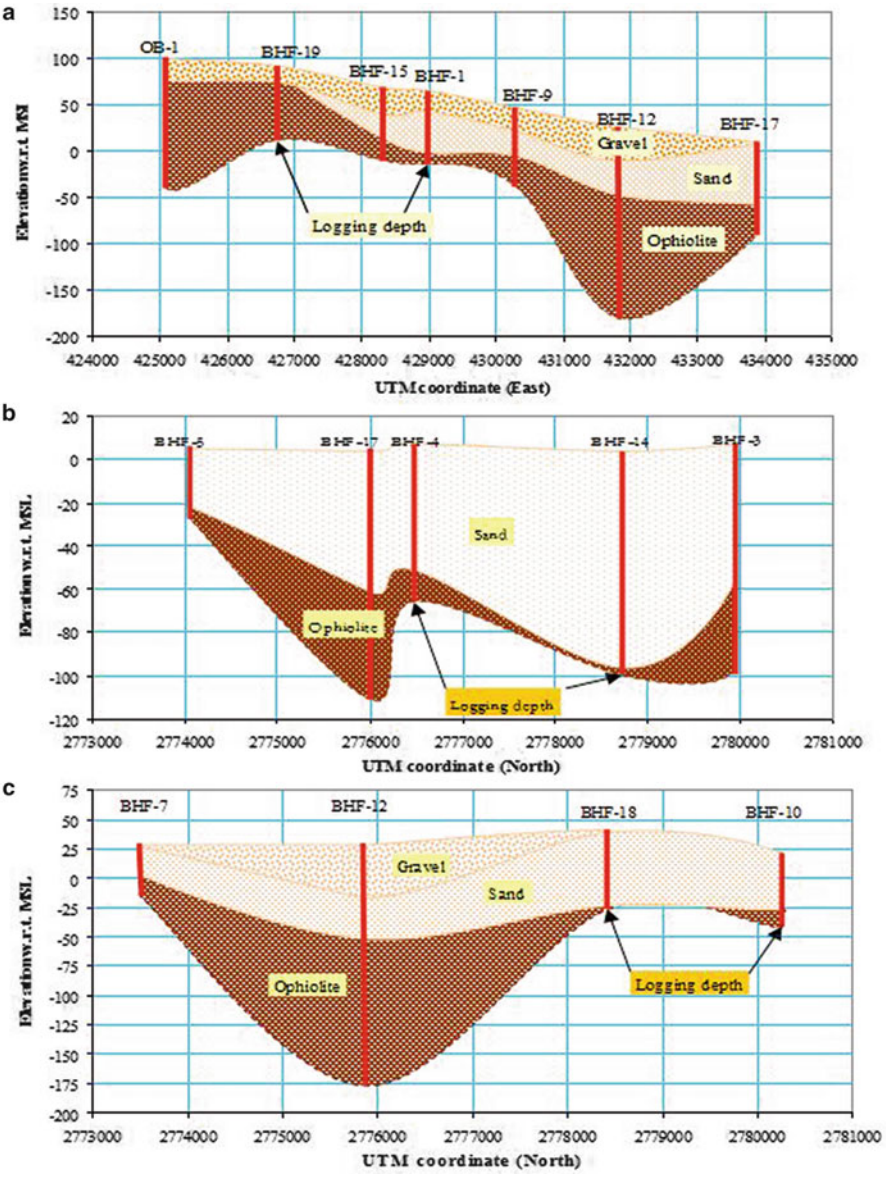

Fig. 13.3 Geological cross sections in Wadi Ham as outlined in Fig. 13.2

Based on interpretation of the above data, two aquifers can be identified; namely the Quaternary aquifer which is composed of Wadi gravels and constitutes the main aquifer and the fractured Ophiolite which is of low groundwater potentiality. The gravel layer is highly permeable and tends to be unconsolidated at the ground surface. The degree of consolidation varies with depth from recent uncemented sandy

gravel to the older well cemented consolidated gravel. According to Electrowatt (1981) this gravel layer could be subdivided into recent gravels, being slightly silty sand gravel with some cobbles; young gravels, which are silty sandy gravels with many cobbles and boulders; and old gravels, which are silty sandy gravels with many cobbles and boulders which are weathered and cemented.

Values of the hydraulic conductivity of the unconsolidated gravels tend to be high, typically from 6 to 17 m/day and in the range 0.086–0.86 m/day for the cemented lower layers (Electrowatt 1981; ENTEC 1996). The primary porosity of unconsolidated gravels is very high when compared to the cemented gravels. The storage coefficients typically range from 0.1 to 0.3 (Electrowatt 1981; ESCWA 1997). The width of the Wadi is about 2.0 km, the saturated thickness various between 10 and 40 m and the transmissivity varies between 100 and 200 m^2/day. Towards the shore line, the saturated thickness varies between 50 and 100 m and the transmissivity value ranges between 1,000 and 10,000 m^2/day. The hydraulic conductivity ranges from 2 to 250 m/day (IWACO 1986).

A number of short duration pumping tests performed by IWACO (1986) were analyzed by using Cooper & Jacob and Theis methods. Available data and results of the pumping tests are given in Table 13.1. The results show that the transmissivity varies from 4.13 to 11,700 m^2/day by Cooper and Jacob method and from 3.83 to 9,120 m^2/day by Theis method. Using Theis method, the hydraulic conductivity ranges from 4.73 to 203 m/day, whereas for the case of Cooper and Jacob method, hydraulic conductivity values vary from 3.16 to 745 m/day. Another pumping test was conducted on well number HAM-OB1 in the month of December 2003 for 75 min. Drawdown curves were analyzed by using Cooper and Jacob method and Theis method. The estimated of transmissivity and hydraulic conductivity was very low as compared to the values obtained from the other wells.

13.4 Groundwater Modeling in Wadi Ham Aquifer

13.4.1 Model Geometry and Boundary Conditions

The study domain of Wadi Ham aquifer comprises an area of 117.81 km^2 with a length of 11.9 km east to west and 9.9 km north to south (Fujairah to Kalbha). The study area and the aquifer boundaries were delineated by digitizing the remote sensing image of Wadi Ham as shown in Fig. 13.4. The model domain includes the Gulf of Oman and the ophiolite sequence rock out crops. The ophiolite outcrops are separated as inactive or no flow area. The area of separated outcrop is about 6.56 km^2. The area occupied by the Gulf of Oman in the model domain was considered as a constant head boundary cells with a specified seawater level (0.0 m) throughout the simulation period. The model area of lower plains of Wadi Ham is composed of Recent Pleistocene Wadi gravels. This layer is underlain by the consolidated rocks of the Semail formation (Ophiolitic sequence).

Table 13.1 Estimated aquifer parameters

	UTM coordinate		Transmissivity (m^2/day)	Transmissivity (m^2/day)		Hydraulic conductivity (m/day)		
Borehole	Northing	Easting	IWACO	C&J method	Theis method	Theis method	C&J Method	Storativity
BHF-1	2,779,163	429,211	30	101	148	7.76	11.4	0.00161
BHF-4A	2,776,995	433,773	8,630	11,700	9,120	203	259	2.01×10^{-15}
BHF-12	2,776,432	431,865	1,340	947	789	15.5	18.6	0.00239
BHF-3A	2,779,800	432,900	3,450	6,246	744	14	118	6.21×10^{-8}
BHF-5	2,773,400	432,950	4,347	8,940	1,260	105	745	1.33×10^{-20}
BHF-10	2,780,250	431,800	1,230	480	258	6.79	12.6	0.00197
BHF-11	2,781,000	430,450	386	101	151	4.73	3.16	0.00666
BHF-13	2,774,900	427,800	8.5	4.13	3.83	25.6	27.5	0.0101
BHF-14	2,778,750	433,900	2,882	4,750	3,630	39.4	51.6	3.03×10^{-7}
HAM-OB1	2,780,166	427,151	–	0.49	0.51	0.0058	0.0056	0.00128

Fig. 13.4 Study domain and boundary conditions

Based on the available geological information, the top layer is gravel and sand and the bottom layer is of ophiolite. The bottom layer of ophiolite is impermeable in nature and hence, a one layer model of Wadi gravel and sand is considered. Contour lines of the aquifer bottom and ground surface are shown in Fig. 13.2a and b, respectively. The DEM (digital elevation model) of the SRTM (Shuttle Radar Topography Mission) in a resolution of 3 arc sec was used for the identification of the top boundary of the model domain. The base of the whole aquifer system was built by an interpolation of isolines and cross-sections. Aquifers' parameters are identified through comprehensive geophysical and hydrogeological surveys that were conducted in the eastern coast of UAE.

The study domain is divided into a mesh of 11,781 square cells. However, the net area of the aquifer is only 64.94 km^2 and was covered by 6,494 active cells. Rainfall daily data was collected from the nearby Farfar gauge station and was assigned to all active cells in the modeled area. Evapotranspiration losses vary linearly with the depth of water table below the ground surface until the extinction depth. An evapotranspiration rate of 0.014 m/day and an extinction depth of 2 m were considered.

Monthly groundwater levels for 16 observation wells in Wadi Ham area were collected over a period of 16 years. This data showed significant variation in groundwater levels in response to pumping and recharge events. Maximum groundwater levels were observed in the year 1996 in which the highest precipitation was recorded. Initial head values were obtained through steady state simulation and from available data of groundwater levels within the study domain when the aquifer was not heavily exploited in the early 1980s (Sherif et al. 2006b). Two well fields (Fig. 13.4) in the study area were in operation for the domestic and agricultural water supply. The first one is Sharah well field, 2 km downstream of Wadi Ham with a total pumping of about 1 million m^3/year since 1988. Out of the nine wells, in this field, five wells were dried up in the year 2003. Discharges from the remaining four wells were drastically reduced during the period from 1988 to 2005. The Kalbha well field including 60 wells is the second field which has been in operation since 1995. The total pumping from this field is about 6 million m^3/year.

13.4.2 Calibration and Verification of the Flow Model

MODFLOW was calibrated over a 5-year period from January 1989 to December 1993. The steady state groundwater levels obtained for December 1988 of all observation wells were considered as initial head values. The model calibration was performed through varying two parameters namely; hydraulic conductivity and specific yield. Abstractions and inflows across the boundaries were simulated by a number of scenarios. Recharge due to rainfall was also adjusted to ensure that the calculated heads at observation wells are reasonably matching field measurements. A recharge factor of 20 % was considered in the active cells of the model.

Measured groundwater levels in observation wells were matched with the corresponding simulated groundwater levels. Time series graphs of simulated versus observed groundwater levels were developed for several observation wells. A temporal agreement between model results and observed groundwater levels considering abstractions and rainfall events was achieved. However, limited discrepancies in the peak values in some of observation wells were observed. Such discrepancies might be attributed to the fact that observed groundwater levels are taken once every month and not necessarily on the same day in every month. Figure 13.5a shows a comparison between all temporal and spatial records of water levels in all observation wells during the calibration period with the corresponding simulated groundwater levels. The figure indicates that the results are consistent with the observed groundwater levels. The calibrated values of specific yield and hydraulic conductivity were used in model verification.

The model verification was carried out over a duration of eleven years starting from January 1994 to March 2005. Similar to the calibration period, rainfall data for this period was assigned to all active cells as recharge over the whole model area with recharge factor of 0.2. The pumping rate from Shaara well field at the beginning of the verification period was 3,150 m^3/day. This rate was gradually

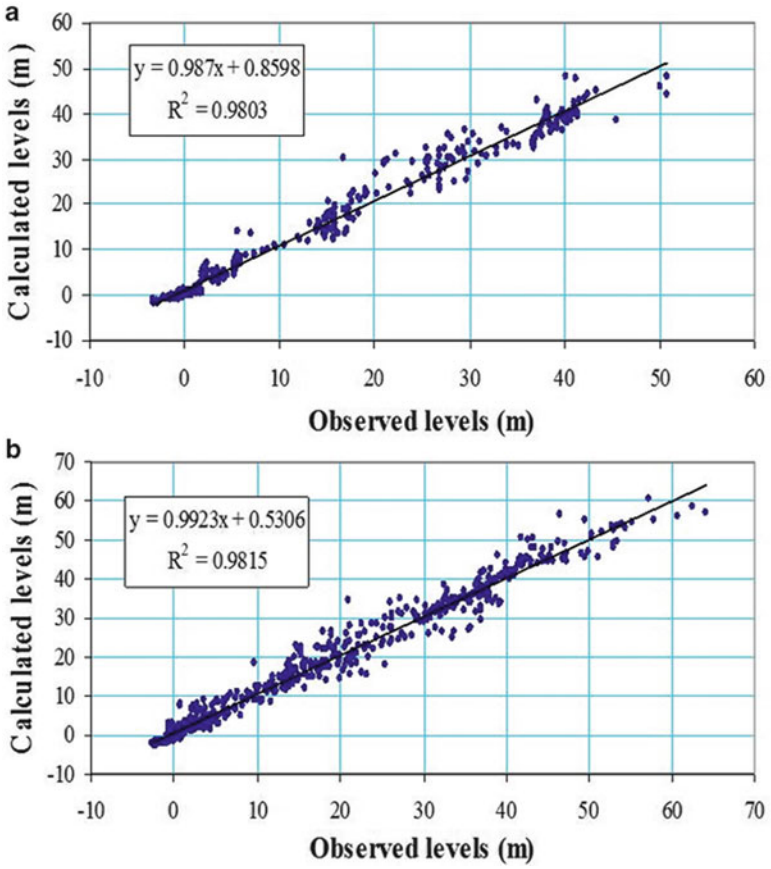

Fig. 13.5 Comparison between observed and simulated groundwater levels; (**a**) calibration period and (**b**) verification period

decreased to 1,700 m^3/day by the end of the verification period. The well field at Kalbha experienced a significant pumping increase from 4,000 to 20,000 m^3/day during the same period.

The calibrated distributions of specific yield and hydraulic conductivity were used in the validation exercise with the new pumping rates and rainfall records. Other input parameters were kept unchanged. The simulated hydrographs over the verification period were compared with observed field hydrographs for the same observation wells that were used in the calibration process. A good agreement between simulated hydrographs and the corresponding observed hydrographs was achieved. Similar to the calibration period, peak values of the simulated groundwater levels in some observation wells were slightly shifted from the peak values of the observed levels. The observed groundwater levels versus simulated levels for all observation wells at different times are presented in Fig. 13.5b. Good agreement between observed and simulated values was observed. The model was therefore considered validated.

Table 13.2 Calibrated parameters for the transport model

Parameter	Value
Retardation factor	1.0
Longitudinal dispersivity α_L	20 m
Transverse dispersivity α_T	2 m
Vertical dispersivity α_v	0.2 m
Molecular diffusion coefficient	0.1

13.4.3 The Transport Model

A transport model was developed to study the impact of pumping and recharge events on seawater intrusion in Wadi Ham aquifer. MT3D was used to simulate the groundwater concentration in space over the calibration and verification periods. The retardation factor, defined as the ratio of average linear velocity of groundwater to the motion of the contaminant to deviate from groundwater motion, was taken as 1.0. In other words, the solute was considered to move with the same velocity of the groundwater. The molecular diffusion coefficient was set equal to 0.1. The value of the longitudinal dispersivity was varied between 80 and 10 m while the ratios between the longitudinal and lateral dispersivities and was longitudinal and vertical dispersivities were set as 0.1 and 0.01.

Cells representing the Gulf of Oman in the study domain were considered to have a constant concentration with a salinity of 35,000 mg/l. The evapotranspiration concentration boundary condition was not considered because the extinction depth was assumed 2 m and the evapotranspiration from the water table was found negligible. A longitudinal dispersivity of 20 m provided the best match with the available measured groundwater concentrations and was, hence, considered as representative for the medium. A summary of the calibrated transport parameters is presented in Table 13.2.

The simulated concentration distribution in the study domain at the end of calibration period (January 1994) is presented in Fig. 13.6a. The spatial distribution of the simulated salinity levels at the end of verification period (March 2005) is presented in Fig. 13.6b. The comparison between Fig. 13.6a and b indicates that there is a change in the concentration distribution in the coastal area especially in the south-eastern area where Kalbha well field is located.

Two pockets of fresh water bodies are located around well BHF-4A. The fresh water pocket zone around well number BHF-4A enlarged over the verification period. In other words, the fresh water moves towards west and southwest of well BHF-4 due to pumping from Kalbha well field. The over exploitation of groundwater at Kalbha well field has created hydraulic gradient towards the well field. Figure 13.6c shows the spatial distribution of the concentration level 10,000 mg/l at different simulation times and over the verification period. It indicates a landward movement of SWI except during the year 1996 which was a wet year with a relatively heavy rainfall (510 mm). This indicates that the groundwater salinity is sensitive to the recharge from rainfall events. The ingression trend was remarkable in the area where the well field is located.

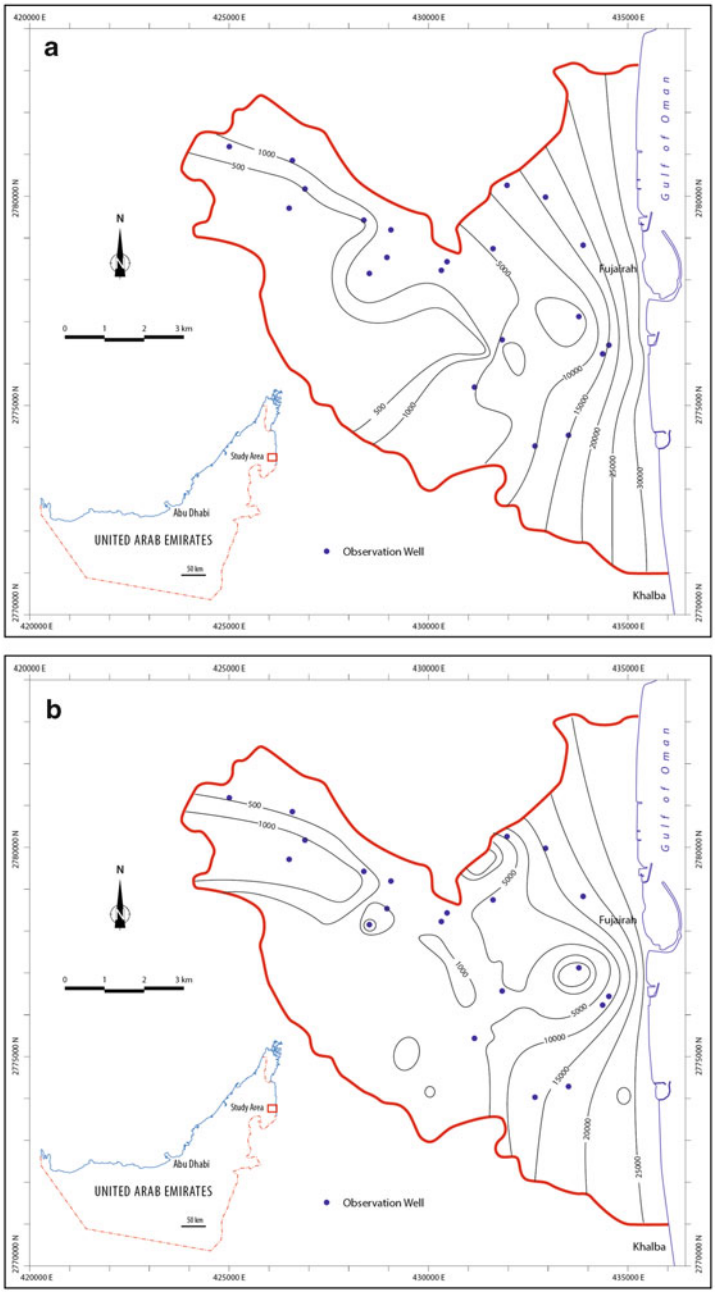

Fig. 13.6 Simulated equiconcentration lines; (**a**) January 1994, (**b**) March 2005 and (**c**) Equi-concentration line 10,000 at different simulation times

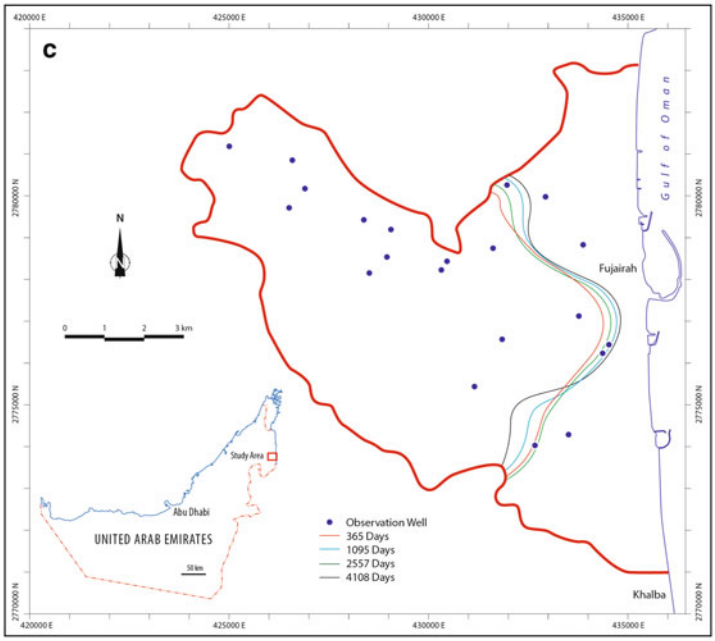

Fig. 13.6 (continued)

North of the well field, and over the same simulation period, there is a different trend for the concentration distribution where the contour lines are retarded towards the coast. This may also be attributed to the presence of the Wadi Ham dam and the frequent recharge from the water storage in the ponding area of the dam. The equi-concentration lines of 25,000 and 30,000 mg/l did not exhibit significant movement over the simulation period as they are very close to the shore line. As expected, lower equi-concentration lines are generally more sensitive to recharge and discharge events. High equi-concentration lines are mostly dominated by the seaside constant boundary condition.

13.5 Pumping Management to Reduce Seawater Intrusion

The developed model was used to simulate the impacts of groundwater abstraction on seawater intrusion in Wadi Ham aquifer. Three scenarios were simulated; in the first scenario all the pumping wells in the study area were assumed to be terminated. In the second scenario, the pumping from Kalbha well field only was ceased. In third scenario the pumping from Kalbha well field was doubled. The simulated groundwater levels in the first scenario were compared with those obtained under the current pumping conditions. Figure 13.7a–c provide a comparison between measured and simulated water levels in three observation wells under scenario one. The figures reveal that without the current pumping groundwater levels would

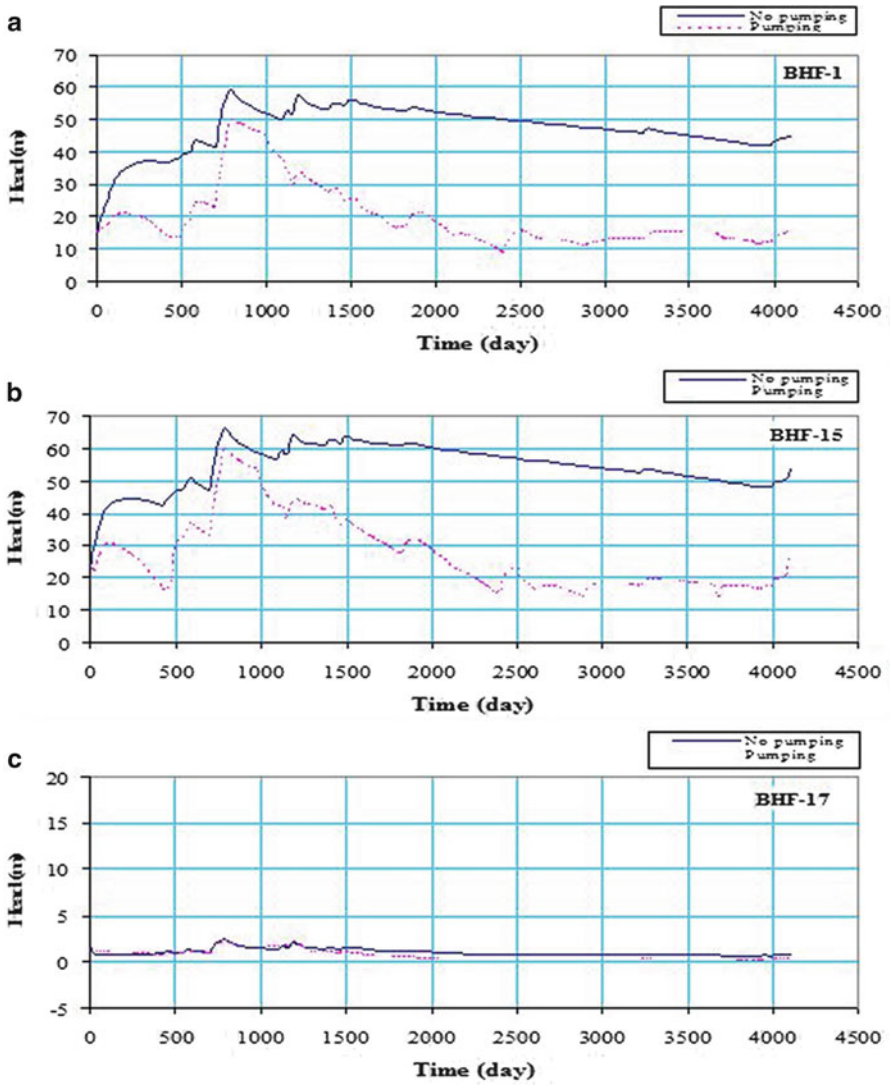

Fig. 13.7 Comparison between groundwater levels with and without pumping under scenario one

have been at much higher levels. The impact of pumping is more visible during low recharge periods when the groundwater levels are relatively low. The minimum effect of pumping was found during the rainy periods. Water levels at BHF-1 and BHF-15 would have been 30.0 m above the present levels if there was no groundwater pumping. Groundwater levels in observation well BHF-17 (Fig. 13.7c) was not affected by the termination of pumping. The groundwater level in BHF-17 was mostly constant and did not change with time. This may be due to the proximity of this well to the coast line of the Gulf of Oman. In other words, the water table in the

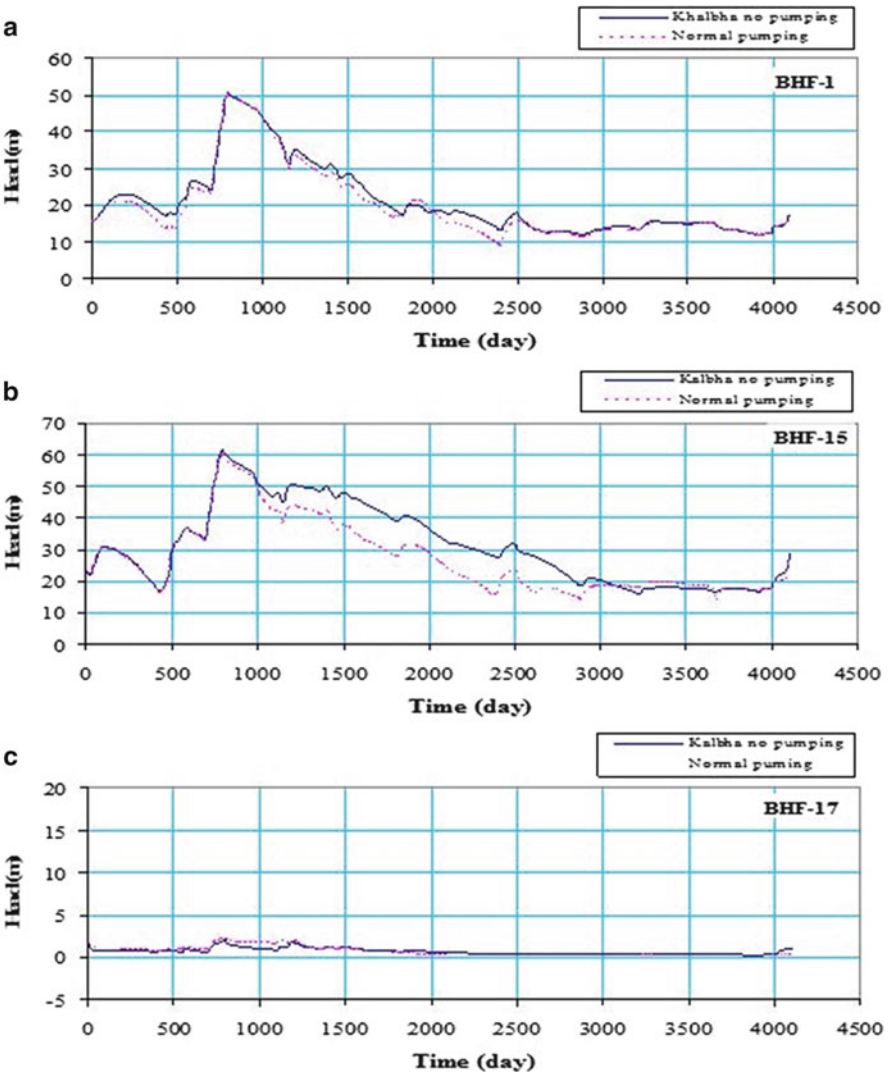

Fig. 13.8 Comparison between groundwater levels with and without pumping under scenario two

coastal zone is controlled by the water level in the Gulf of Oman and not to be the pumping activities. Considering the location of this observation wells (shown in Figs. 13.1 and 13.3), it is evident that a higher recovery of groundwater levels occurs inland and away from the coastal zone.

The out flux of the groundwater to the sea was also higher when the pumping was terminated. The decrease of groundwater outflow to the sea during the simulation period was attributed to the increase of groundwater abstraction as well as the decrease of recharge from rainfall events due to the scarcity of rainfall during the last 10 years (Sherif et al. 2011).

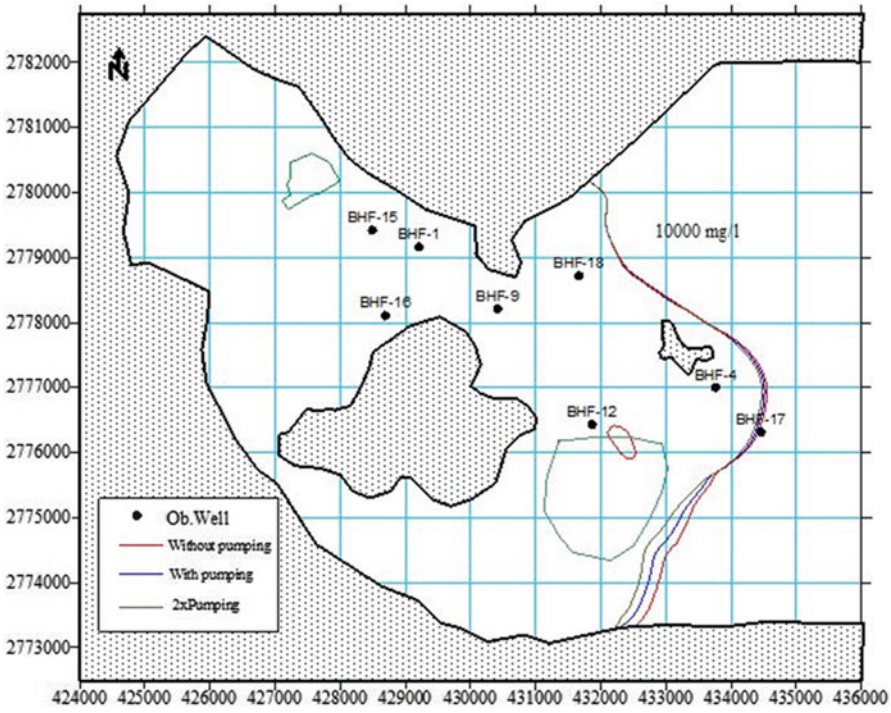

Fig. 13.9 Equiconcentration line 10,000 under different pumping conditions after 1 year of simulation

In order to evaluate the effect of pumping from Kalbha well field only pumping from this field was terminated in the second scenario. The simulation was conducted for the same period as for scenario one to assess the changes in groundwater levels and subsurface inflow and outflow through the constant head boundaries of the study domain. The resulted groundwater hydrographs under normal pumping conditions are compared with those obtained assuming zero pumping from Kalbha well field and presented in Fig. 13.8a–c. The groundwater levels in the observation wells that are away from the pumping field were not very much affected by pumping. This is attributed to the fact that these wells lies on the other side of the impervious ophiolite outcrop. Results of this scenario reveal that pumping from the Kalbha well field contributed to the seawater intrusion in the southeastern coastal zone of Wadi Ham. This is also consistent with decline in the water table below mean sea level especially at well number BHF-12.

In the third scenario, the pumping from Kalbha well field was doubled to meet the expected increase in water demands during the coming two decades. A significant decline in the groundwater levels in the vicinity of the Kalbha well field was observed. Figure 13.9 provides a comparison between the equi-concentration lines 10,000 mg/l that resulted under the current pumping, scenario one and scenario three. After 1 year of simulation time, seawater intrusion increased slightly at the southeastern area when the pumping was doubled as shown in Fig. 13.9a. No sign of an increase in the groundwater salinity level was observed in other areas during the

same period of simulation. However, after 10 years of simulation, there is a considerable inland movement for the concentration contour 10,000 mg/l near Khalba well field. This indicates that, the long term pumping from the Khalba well field has a significant effect on the groundwater quality in the aquifer system.

13.6 Effects of the Wadi Ham Dam and Artificial Recharge

The Wadi Ham dam was constructed to retain surface water runoff after rainfall events, enhance groundwater recharge, and prevent other possible hazardous impacts from flash floods. A water pond was created upstream of the dam, as shown in Fig. 13.4. In this exercise MODFLOW was used to assess groundwater recharge during the eleven-year verification period from January 1994 to March 2005. Different simulation scenarios were performed. The groundwater recharge was assessed under the conditions of no dam (no recharge from the ponding area) and with the presence of the dam.

The results revealed that the total groundwater recharge during the validation period due to rainfall and water storage in the pond was 17,495,862 m^3. If no water storage in the pond area is assumed the total recharge from rainfall would have been 13,969,180 m^3. Therefore, groundwater recharge from the ponding area; and due to the construction of the dam, has increased by about 20 %. In other words, the recharge from the water pond represents about 25 % of the distributed recharge within the catchment area from the rainfall events. Figure 13.10 presents a comparison between the cumulative recharge curves for both cases (i.e. with and without recharge from the water pond).

Figure 13.11a and b provide examples of the groundwater flow vectors during dry and wet periods, respectively. During dry period, the effect of the dam on the

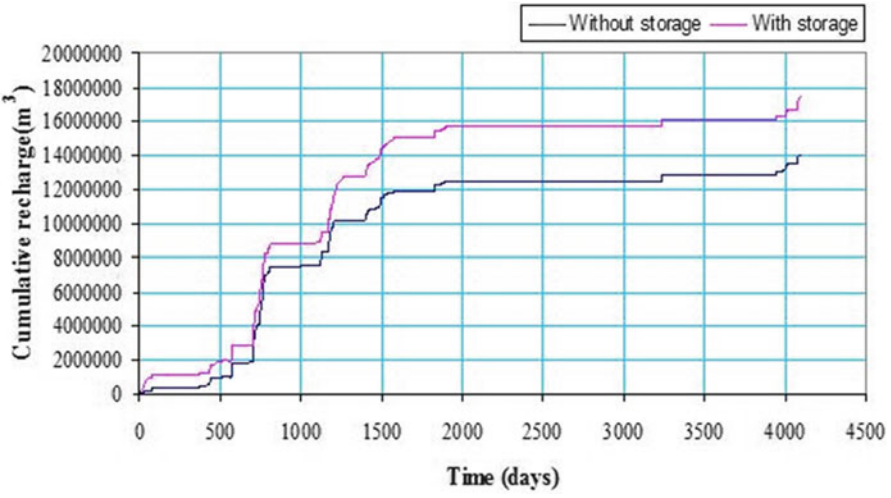

Fig. 13.10 Cumulative recharge with and without water storage in the dam of Wadi Ham

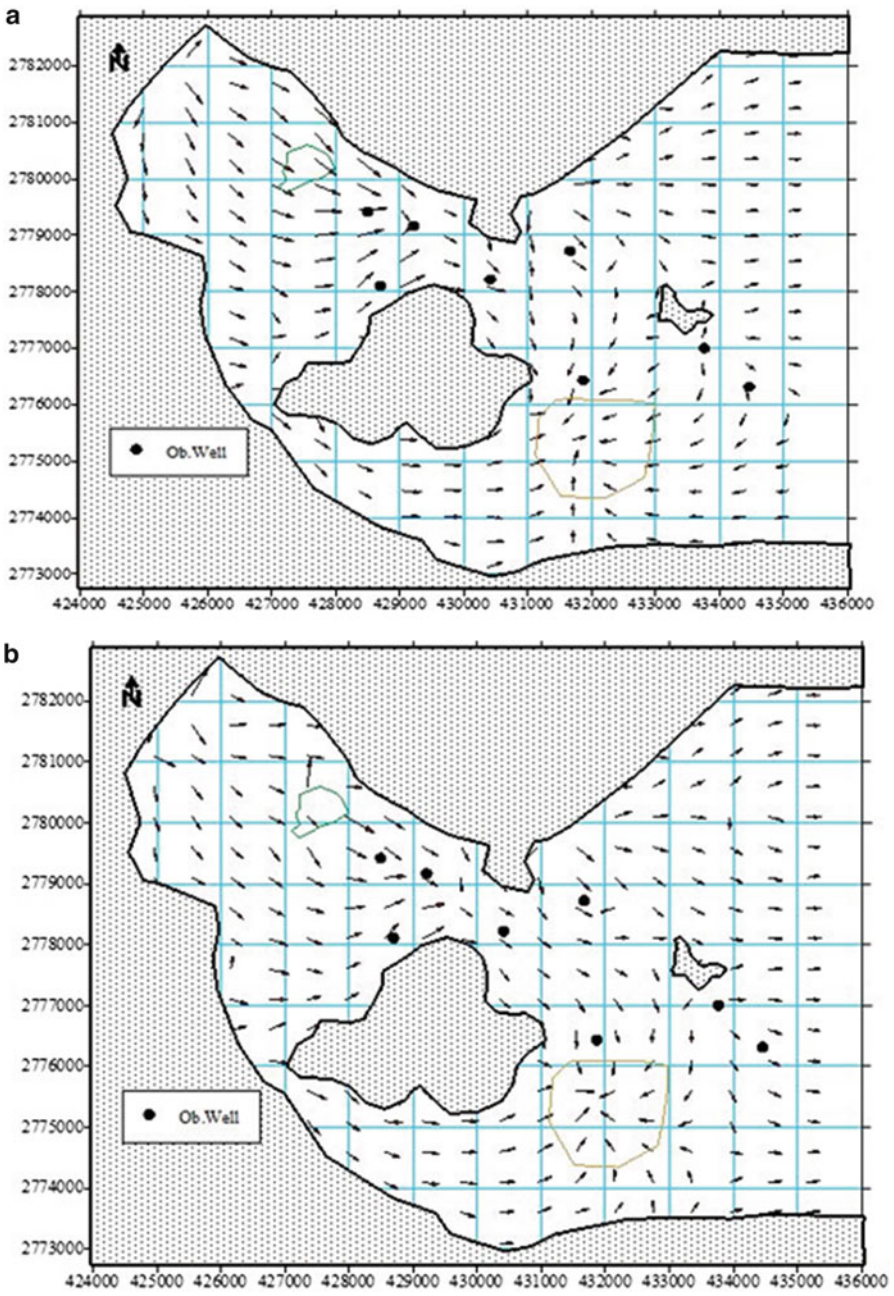

Fig. 13.11 Velocity vectors under: (**a**) dry conditions and (**b**) wet conditions

Fig. 13.12 Location of experimental pond in Wadi Ham

velocity vectors in the vicinity of the ponding area is not visible. Also, the seawater intrudes the aquifer from the southeastern part of the sea boundary. To the contrary, during wet periods, the flow field in the vicinity of the ponding area is modified and the groundwater velocity vectors are directed towards the sea boundary and hence the intrusion is reduced. However, because of the frequent and long dry periods and seldom and short wet periods, the seawater problem has severely affected the Wadi Ham aquifer.

An artificial pond of 20.0 × 20.0 m was constructed closer to the Gulf of Oman (Fig. 13.12). Four field experiments of recharge using this pond were conducted. The first experiment was conducted for a duration of 48 days from October 4, 2004 to November 21, 2004. The average recharge rate in this experiment was 307 m^3/day for 20 days. The second experiment started on January 4, 2005 till January 13, 2005 with a recharge rate of 336 m^3/day. The third experiment took place on May 9, 2005 for a duration of 16 days and the recharge rate was 300 m^3/day. The fourth and final experiment took place on December 7, 2005 for a duration of 18 days. The recharge rate in this final experiment was kept at 288 m^3/day.

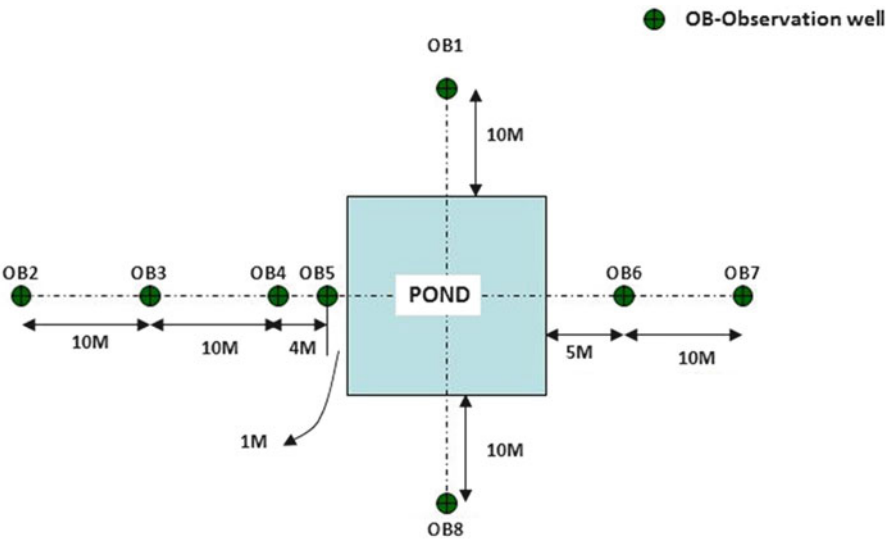

Fig. 13.13 Location of observation wells around the pond

Eight observation wells were constructed around the pond as illustrated in Fig. 13.13. Data of groundwater levels from these eight observation wells were collected during the four recharge experiments. Calibration and validation of the developed model to recharge events were performed by matching observed groundwater levels collected from the eight observation wells with the corresponding simulated groundwater levels in both space and time. The recharge due to rainfall was adjusted to 20 % of the total rainfall. A good match was observed and the maximum deviation between observed and simulated heads was about 0.2 m. It was also noted that during the third experiment, the increase in groundwater levels was low as compared to the water levels of other experiments with lower recharge rate. This might be attributed to the fact that the initial groundwater level before the start of the third experiment which was approximately about 0.5 m higher than those of the other experiments. The results of the transport model did not reveal any significant changes in the equi-concentration lines as the recharge rates and durations were not enough to combat the seawater intrusion process.

13.7 Hypothetical Recharge Scenarios

The calibrated flow model developed for the study area was used to assess the effect of different scenarios of surface water recharge on seawater intrusion and salinity distribution in the groundwater system. A recharge pond with size of 100 by 100 m

was assumed at the same location of the physical recharge pond presented in Fig. 13.13. The first scenario presents the case of no recharge. In the second scenario a recharge of 0.5 m/day (5,000 m^3/day) was simulated while in the third scenario, the recharge was increased to 1.0 m/day (10,000 m^3/day).

The effects on groundwater levels were clear at the wells that are located relatively close to the recharge pond including BHF-4, BHF-12, BHF-17A, BHF-17R and BHF-18. On the other hand the a slight effect on the groundwater levels was observed at the wells that are located away from the recharge area including BHF-1, BHF-9, BHF-15 and BHF-16.

The equiconcentration line 10,000 mg/l was considered to study the impacts of the three scenarios of recharge on seawater intrusion. A remarkable variation in the salinity level was observed during the period of simulation under the different scenarios. Depending of the recharge rate, the artificial recharge will reduce the groundwater salinity in the region between the pond and the shoreline. The water quality was significantly improved after 10 years of simulation. Equiconcentration line 10,000 mg/l shifted by about of about 1.25 km towards coast after about 12 years of recharge at a rate of 1.0 m/day. In general, increasing the recharge rate contributes to the improvement of the groundwater quality but only in the area located between the recharge pond and the coast line. A set of recharge ponds parallel to the coast line might be needed to enhance the groundwater quality in the entire aquifer.

13.8 Conclusions

The Quaternary aquifer of Wadi Ham, UAE, is naturally replenished by the rainfall as well as from the water storage in the ponding area. The construction of the dam increased the groundwater recharge by 20 %. Nevertheless, historical groundwater measurements indicate a significant variation in the response to recharge events and groundwater abstractions. Groundwater levels in all observation wells in Wadi Ham continue to decline and its quality continues to deteriorate. The quality of the groundwater in the study areas varies based on the distance from the shoreline and the depth below the seawater level. MODFLOW was calibrated and validated to simulate the groundwater flow and MT3D was used to simulate the groundwater concentration in space and time. A recharge pond of 20.0 $\times$ 20.0 m was established to identify the infiltration rates and assess the effects of recharge on groundwater levels and seawater intrusion. The numerical simulations included hypothetical cases with artificial recharge of 5,000 and 10,000 m^3/day. Maintaining the current pumping practices and applying a recharge of 10,000 m^3/day would cause a tangible local reduction in the seawater intrusion on the long term. However, a set of recharge ponds that are aliened parallel to the shoreline are needed to fully restore the groundwater quality in the Wadi Ham aquifer.

References

Bear J (1979) Hydraulics of groundwater. McGraw-Hill, New York

Diersch HJ (2006) FEFLOW manual. WASY GmbH, Berlin. 190 pp. www.wasy.de

Economics and Social Commission for Western Asia (ESCWA) (1997) Mathematical of the Wadi Ham aquifer, Fujierah coastal plain, UAE. Advisory services to the Ministry of Agriculture and Fisheries, Dubai

Electrowatt Engineering Services Ltd (1981) Wadi Ham Dam and groundwater recharge facilities, vol I, Design. Ministry of Agriculture and Fisheries, Dubai

Entec Europe Limited (ENTEC) (1996) Survey on groundwater recharge and flow in Wadi Ham, vol 1. Ministry of Agriculture and Fisheries, Dubai

Halcrow, Sir Williams and Partners Consulting Engineers (1969) Water resources of trucial states. Internal report. Ministry of Agriculture and Fisheries, Dubai

Huyacorn PS, Andersen PF, Mercer JW, White HO Jr (1987) Saltwater intrusion in aquifers: development and testing of a three-dimensional finite element model. Water Resour Res 23:293–312

IWACO (1986) Ground water study. Drilling of deep water wells at various locations in the UAE. Internal report, Ministry of Environment & Water, Dubai

Kacimov AR, Sherif MM, Perret JS, Al-Mushikhi A (2009) Control of sea-water intrusion by salt-water pumping: coast of Oman. Hydrogeol J 17(3):541–558

Langevin CD, Thorne DT, Dausman AM, Sukop MC, Guo W (2007) SEAWAT version 4: a computer program for simulation of multi-species solute and heat transport. U.S. Geological Survey techniques and methods book, vol. 6, chap. A22, 39. USGS, Reston

Post V, Abarca E (2010) Preface: saltwater and freshwater interactions in coastal aquifers". Hydrogeol J 18:1–4

Sherif MM, Hamza KI (2001) Mitigation of seawater intrusion by pumping brackish water. Transp Porous Media 43:29–44

Sherif MM, Singh VP, Amer AM (1988) A two dimensional finite element model for dispersion (2D-FED) in coastal aquifers. J Hydrol 103:11–36

Sherif MM, El MA, Garamoon H, Kacimov A, Akram S, Ebraheem A, Shetty A (2006a) Geoelectrical and hydrogeochemical studies for delineating seawater intrusion in the outlet of Wadi Ham, UAE. Environ Geol 49:536–551

Sherif MM, Kacimov A, Akram SF, Shetty AV (2006b) Artificial recharge of groundwater: field experiment. JCCP-UAEU symposium on sustainable environment and water resources in GCC Countries, Abu Dhabi, UAE, 28–30 January 2006

Sherif MM, Akram S, Shetty A (2009) Characterization and analysis of rainfall in the Northern Wadis of the United Arab Emirates. J Hydrol Eng, ASCE 14(6):445–454. doi:10.1061/_ASCE_HE.1943-5584.0000015

Sherif MM, Mohamed M, Shetty A, Almulla M (2011) Rainfall-runoff modeling of three Wadis in the northern area of UAE. J Hydrol Eng, ASCE 16(1):10–20. doi:10.1061/(ASCE) HE.1943-5584.0000280

Voss CI, Provost AM (2002) SUTRA, a model for saturated-unsaturated variable density ground-water flow with energy or solute transport. U.S. Geological Survey Open-File Report 02–4231, 250 p

Voss CI, Simmons CT, Robinson NI (2010) Three-dimensional benchmark for variable-density flow and transport simulation: matching semi-analytic modes for steady unstable convection in an inclined porous box. Hydrol J 18:5–23

Chapter 14
Seawater Intrusion Under Current Sea-Level Rise: Processes Accompanying Coastline Transgression

Tariq Laattoe, Adrian D. Werner, and Craig T. Simmons

Abstract The freshwater resources of coastal aquifers are vulnerable to seawater intrusion (SWI) caused by the current rising trends in sea levels, amongst other factors. Recent studies have examined the extents, rates and timescales associated with SWI induced by expected levels of sea-level rise (SLR), but have neglected the effects of transgression (i.e. inland migration of the shoreline in response to SLR). In this chapter, variable-density numerical modelling is used to examine the implications of transgression for a range of SWI scenarios based on simplified coastal aquifer settings. Vertical intrusion during transgressions can involve density-driven convective processes, causing substantially larger amounts of seawater to enter the aquifer and creating more extensive intrusion than that of horizontal SWI occurring in the absence of transgression. Interestingly, cases of transgression where no vertical mixing occurs involve reduced landward migration of the wedge toe, relative to otherwise similar situations without transgression. The rates and extents of SWI caused by transgression and associated vertical mixing appear to be almost non-responsive to the choice of landward boundary condition, contradictory to the findings of SLR-SWI studies that neglect transgression. The findings of this study suggest that modelling analyses that neglect the effects of transgression in SLR-SWI investigations may underestimate significantly the rates and extent of SWI.

14.1 Introduction

The freshwater resources of coastal aquifers are vulnerable to salinization from seawater intrusion (SWI; the landward migration of the freshwater-seawater interface) in response to rising sea levels (Werner et al. 2012a). Recent studies have

T. Laattoe (✉) • A.D. Werner • C.T. Simmons
National Centre for Groundwater Research and Training, and School of the Environment, Flinders University, GPO Box 2100, Adelaide, SA 5001, Australia
e-mail: tariq.laattoe@flinders.edu.au

C. Wetzelhuetter (ed.), *Groundwater in the Coastal Zones of Asia-Pacific*, Coastal Research Library 7, DOI 10.1007/978-94-007-5648-9_14,

examined the extents, rates and timescales of SWI caused by sea-level rise (SLR), albeit for simplified coastal boundary conditions. For example, Werner and Simmons (2009) present a generalised assessment of the shift in steady-state position of the seawater wedge toe (i.e. the intersection of the interface with the aquifer basement) due to an increase in sea level. They used a sharp-interface approximation and simplified aquifer geometries to show that the choice of landward boundary condition (constant-head or constant-flux conditions) was an important factor in SLR-induced SWI. SWI from SLR was found to occur over tens of metres for flux-controlled systems, and hundreds of metres to several kilometres for head-controlled systems. The analysis of Werner and Simmons (2009) was extended by Werner et al. (2012b), who adopted a similar sharp-interface approach to produce SWI vulnerability indicators for climate change and SLR stresses, and for various hydrogeological conditions. They demonstrated that while SWI vulnerability to SLR impacts was highest for head-controlled systems, flux-controlled systems had the highest SWI vulnerability to recharge changes (e.g. arising under climate change).

Recent dispersive modelling of SWI in response to SLR by Watson et al. (2010), Webb and Howard (2011), and Chang et al. (2011) explored transient time-scales and processes. Watson et al. (2010) considered an instant SLR of 1 m on a vertical coastal boundary, and observed temporal asymmetry between cases of SWI and seawater retreat. Representative SWI response times of decades to centuries were obtained for typical unconfined aquifer conditions, and a temporary "overshoot" in the toe position was observed whereby the final steady-state toe position was exceeded during transient SWI events. Watson et al. (2010) applied primarily fixed-flux inland boundary conditions, whereas Webb and Howard (2011) considered fixed-head conditions and hence the two studies are complementary. Webb and Howard (2011) focused on disequilibrium (i.e. the difference between the transient and steady-state interface positions) in evaluating gradual SLR. They concluded that the seawater wedge may take several centuries to stabilize following cessation of SLR, for systems with high effective porosities and high ratios of hydraulic conductivity to recharge. Chang et al. (2011) added to previous transient SWI studies by considering confined aquifers, and their conclusions matched the concurrent analysis by Werner et al. (2012b), i.e. that SWI arising from SLR was negligible in confined aquifers subject to constant flux conditions, notwithstanding a temporary overshoot that was similar to that described previously by Watson et al. (2010).

Generalised investigations of SWI caused by SLR, as mentioned above, neglect the effects of transgression, i.e. the inland migration of the shoreline resulting from SLR. Shoreline transgression is expected to produce vertical salinization where the advancing seawater overlies the freshwater portion of the aquifer. Freshwater losses in Israeli coastal aquifers due to transgression under modern SLR were approximated by Melloul and Collin (2006), using a simple steady-state approach. The impacts of transgression on SWI were thought to be significant relative to pumping impacts for the case of a 50 cm SLR and a topographical slope of 0.001. However, the simplified nature of their analysis precluded a comparison of top-down salinization relative to lateral SWI, which are likely to be interdependent.

Examples of top-down salinization include studies of tsunami-related inundation, such as the physical modelling by Illangasekare et al. (2006), who demonstrated the importance of complex free convection processes in the salinization of tsunami-impacted Sri Lankan aquifers.

Previous transgressions and regressions of the coastline have shaped the salinity conditions of many of the world's coastal aquifers, in particular confined aquifers that extend offshore (e.g. Groen et al. 2000). The salinization processes accompanying transgression at geological time-scales were assessed by Kooi et al. (2000), who simulated free convective fingering occurring under unstable density situations. Kooi et al. (2000) adopted slower rates of SLR ($\leq$1 mm/year) compared to modern values (2–20 mm/year), which in combination with other parameters produced dispersive transport that was dominated by molecular diffusion. Salt transport in moderately-to-highly permeable aquifers subjected to modern rates of SLR, as examined in this study, is likely to involve dispersive processes dominated more so by mechanical dispersion. Nonetheless, the study by Kooi et al. (2000) provides key findings for the current investigation, and their methodology forms the basis of the approach applied here, as described in the following section.

The current study uses numerical modelling experiments to explore transient transgression impacts on SWI in a selection of simplified coastal aquifer situations and considering a modern rate of SLR (i.e. 10 mm/year). The results are an extension to the analysis of Kooi et al. (2000), who evaluated a single topographical slope, geological timeframes and relatively fine-grained sediments. We test the distance-lag function of Kooi et al. (2000) for predicting whether free convection will occur during SLR, using a wider range of conditions. The interplay between vertical salinization and lateral SWI are also examined. The transgression simulations described in the following aim to bridge the gap between instantaneous SWI events, such as those described by Illangasekare et al. (2006), and the geological timeframes assessed by Kooi et al. (2000).

14.2 Methodology

The methodology of this investigation followed that of Kooi et al. (2000), who also used numerical modelling in two-dimensional cross section as the basis for their analysis. The current study adopted FEFLOW (Diersch 2005), which is a finite-element, variable-density flow and transport simulator, and has been tested against a range of benchmark problems covering various mixed-convective situations. The Galerkin-FEM finite-element scheme was applied with no up-winding. The Oberbeck-Boussinesq approximation was employed, thereby neglecting all fluid density dependencies except for the buoyancy term in the Darcy equation (Diersch 2005). The reader is directed to the code's User Manual (Diersch 2005) for more information on the solver techniques and other mathematical aspects of the code.

SLR-induced SWI was simulated for situations involving lateral SWI and, under certain circumstances, vertical mixing in the form of free convection driven by an

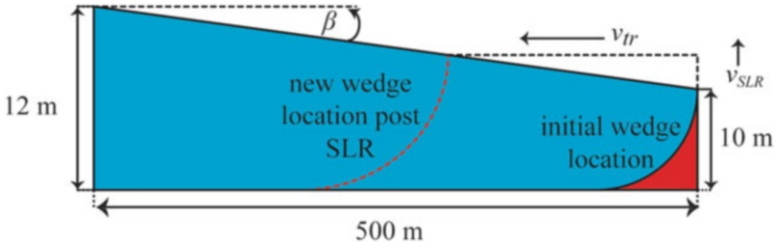

Fig. 14.1 The SLR-SWI model set-up, with a land slope (tan β) of 0.004. The *left* boundary is the landward extent of the model, and the *red* area represents seawater in the aquifer under the initial steady-state conditions. The rate of SLR is v_{SLR} [L/T] and the rate of shoreline transgression is v_{tr} [L/T]

inverted density condition. The timescales of interest in modern SLR scenarios (<100 years) are generally too small for molecular diffusion to drive seawater movement significant distances into the aquifer, relative to the speed of free convection processes for seawater overlying freshwater (see Xie et al. (2011) for guidance on free versus forced convective rates of solute transport). Figure 14.1 depicts the situation, comprising a fully saturated (i.e. watertable at the land surface), shallow aquifer.

The simulated aquifer was shallow (10 m thick at the coastal boundary) primarily to limit model run-times, and to allow for a reasonably small nodal spacing (0.5 m horizontally, 0.1–0.3 m vertically, and 40,000 quadrilateral elements in total). Grid refinement (vertical spacing of 0.1 m) was applied to the top 1 m of the model domain, where the transgressing coastline induced steep solute concentration gradients. Small time-steps (<5 days) were needed to obtain stable predictions (time-step control was automated using the forward Adams-Bashforth/backward trapezoid approach; Diersch 2005). Courant numbers (C_r) for horizontal and vertical directions ($C_r = v\Delta t/\Delta L$, where v [L/T] is velocity, Δt [T] is the time-step, and ΔL [L] is the nodal spacing) were less than the recommended upper limit of unity, at all times.

A single simulation using a finer mesh (160,000 elements) was undertaken, producing free convective finger sizes and frequencies that were largely consistent with the coarser resolution model. The mesh resolution was ultimately constrained by the need for reasonable model run-times, which were in the order of several days for each simulation using the 40,000-element mesh. The mesh Peclet number (P_e), which should ideally be less than 2 (Voss and Souza 1987), varied with the grid resolution (ΔL) and mechanical dispersion parameters (i.e. longitudinal and transverse dispersivities: α_L and α_T [L]) according to $\Delta L/\alpha_L$ or $\Delta L/\alpha_T$, depending on flow direction. P_e values ranging between 0.01 ($\Delta L = 0.05$ m, $\alpha_L = 5$ m) to 5 ($\Delta L = 0.5$ m, $\alpha_T = 0.1$ m) were obtained for the simulation series, and hence some degree of numerical error was expected. Indeed, minor numerical oscillations were observed (most notably in the transgression simulations), but these did not

impact significantly on the predictions. The chaotic nature of free convection imposed further limitation to the analysis presented here, which was deterministic and therefore did not evaluate the range of plausible free convective fingering patterns (Xie et al. 2012). Nonetheless, the results were considered a reasonable first-order approximation of the relevant mixed-convective processes, and the approach was adequate for demonstrating the relative importance of transgression on SWI rates and extents.

Lateral SWI was quantified as the rate of movement of the wedge toe, which was defined by the 5 % isochlor. Vertical and horizontal salt fluxes across model boundaries were also evaluated. The conditions for the onset of free convection during SLR were assessed by Kooi et al. (2000), who presented the following equation for assessing the distance-lag between the transgressing shoreline and the subsurface seawater front:

$$\Gamma = \frac{n\mu v_{SLR}}{k\rho_s g \tan^2\beta} \tag{14.1}$$

Here, n is porosity [-], μ is fluid viscosity [M/L/T], v_{SLR} is the rate of SLR [L/T], k is intrinsic permeability [L^2], ρ_s is seawater density [M/L^3], g is gravitational acceleration [L/T^2], and $\tan\beta$ is topographical slope [-]. A Γ value of one is expected to produce a scenario where the wedge and coastline migrate landward simultaneously at equivalent rates. If Γ is significantly greater than one, transgression advances faster than the lateral movement of the wedge, and the resulting inverted density situation can generate free convection instabilities in the form of saltwater fingers, producing top-down salinization.

The numerical experiments of Kooi et al. (2000) involved similar situations to scenarios III and IV of the current study; as described in Fig. 14.2. They examined rates of SLR up to 1 mm/year, using a single topographical slope of 0.001. The values D^*, n, α_L, α_T, μ, ρ_s and ρ_f adopted by Kooi et al. (2000) were also used here (see Table 14.1 for variable explanations and values). We selected $K_a = 1.0$ m/day to represent a sandy aquifer, whereas Kooi et al. (2000) used $K_a = 0.1$ m/day (typical of silty sand). Kooi et al. (2000) considered head-controlled aquifer systems.

Four different SLR scenarios were examined (Scenarios I to IV), as shown in Fig. 14.2. Initial salinity and head distributions reflected the steady-state pre-SLR conditions, obtained through long-term (1,500 years) transient simulations. Both fixed-head and fixed-flux conditions were trialled for the inland boundary. The seaward boundary was a specified head (i.e. density-corrected sea level) and specified concentration boundary, while the land surface was represented using a transitional boundary condition of no flow inland of the transgressing shoreline, and specified head and concentration for the inundated area, which increased with SLR. Table 14.1 lists parameter values and ranges adopted in sensitivity analyses. In total, 64 scenarios were evaluated.

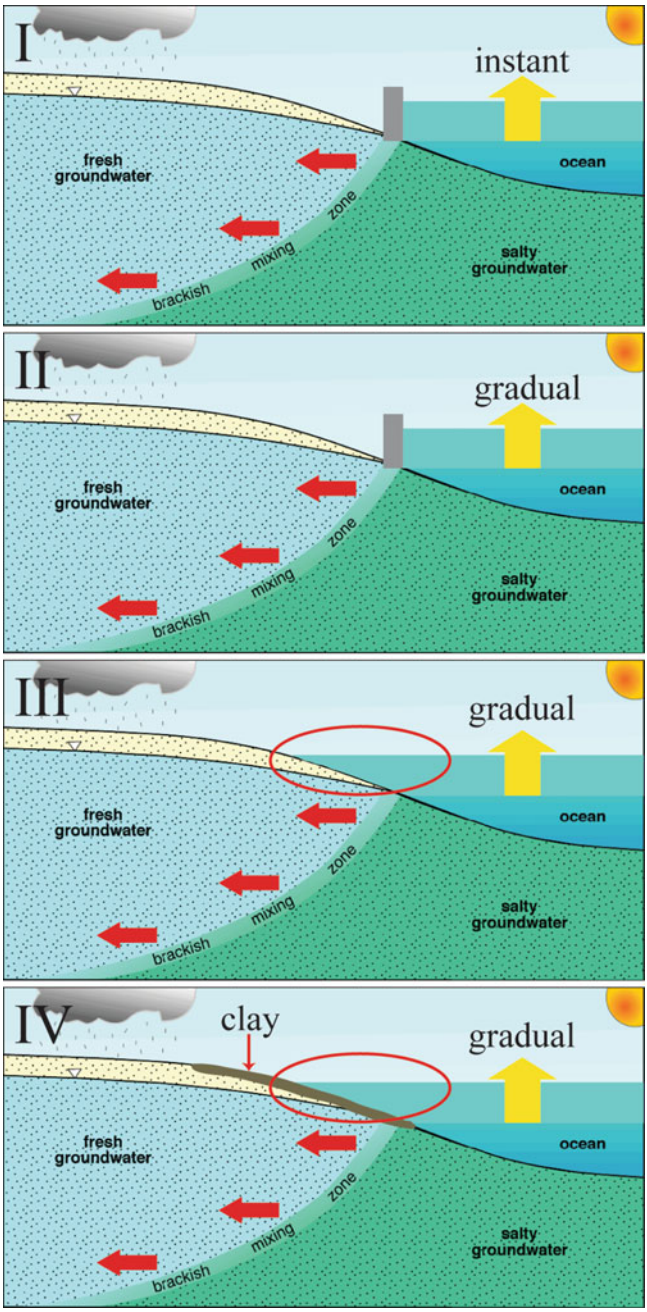

Fig. 14.2 Four SLR scenarios: (I) Instantaneous SLR with no transgression, (II) Gradual SLR with no transgression, (III) Gradual SLR with transgression, (IV) Gradual SLR with transgression and a low permeability layer. *Red ellipse* indicates models where transgression effects are accounted for

Table 14.1 Model parameters and parameter ranges adopted in sensitivity analyses

Parameter	Value or range
Porosity (n)	0.3
Molecular diffusion (D^*)	10^{-9} m^2/s
Longitudinal dispersivity (α_L)	0.001, 0.01, 0.1 m
Dispersivity ratios (α_L: α_T)	1, 10, 1,000
Fluid dynamic viscosity (μ)	10^{-3} kg/m/s
Gravitational acceleration (g)	9.8 m/s^2
Aquifer hydraulic conductivity (K_a)	1 m/day
Clay hydraulic conductivity (K_c)	0.0001 m/day
Freshwater salt concentration (C_f)	0 mg/L
Seawater salt concentration (C_s)	35,000 mg/L
Freshwater density (ρ_f)	1,000 kg/m^3
Seawater density (ρ_s)	1,025 kg/m^3
Rate of SLR (v_{SLR})	10 mm/year, 1.0 m instantly
Topographical slope (tanβ)	0.001, 0.002, 0.003, 0.004
Aquifer thickness at the sea (d)	10 m
Length of aquifer (L)	500 m
Inland boundary condition	Specified head, specified flux
Initial conditions	Pre-SLR steady state

14.3 Results

14.3.1 SLR-SWI Under a Steep-Sloped Land Surface

Figure 14.3 depicts salinity distributions associated with four SLR scenarios (I to IV; Fig. 14.2). The landward boundary was specified head. Scenarios III and IV involved a topographical slope of 0.004 and the parameters are otherwise listed in Table 14.1. Figure 14.4 presents transient SWI trends, as defined by the movement of the wedge toe (5 % isochlor), for the four scenarios. The value of Γ for this scenario is 0.59 which implies faster rates of horizontal intrusion than coastal transgression.

Figures 14.3 and 14.4 show that the SWI rates and extents vary markedly across the different scenarios. SWI in scenario II (gradual SLR, no transgression) lags that of scenario I (instantaneous SLR, no transgression), as expected. SWI in scenario III (transgression with vertical salinization) produces the most extensive horizontal intrusion. The wedge toe remains ahead of the shoreline for scenario III (Fig. 14.4) for the first 55 years of simulation. As expected from the low value of Γ, SWI occurs primarily through forced-convective processes, evidenced by the lack of dense salinity fingers in Fig. 14.3. In scenario IV, the lack of vertical salinization caused by the low-K layer, combined with the hydraulic pressure loading created by transgression, inhibited SWI relative to all other situations, leaving a large storage of freshwater in the submarine aquifer at the cessation of the simulation (Fig. 14.3), notwithstanding some vertical salinization in the upper aquifer caused by dispersion. This result is consistent with the observations by Groen et al. (2000) and Kooi et al. (2000) of

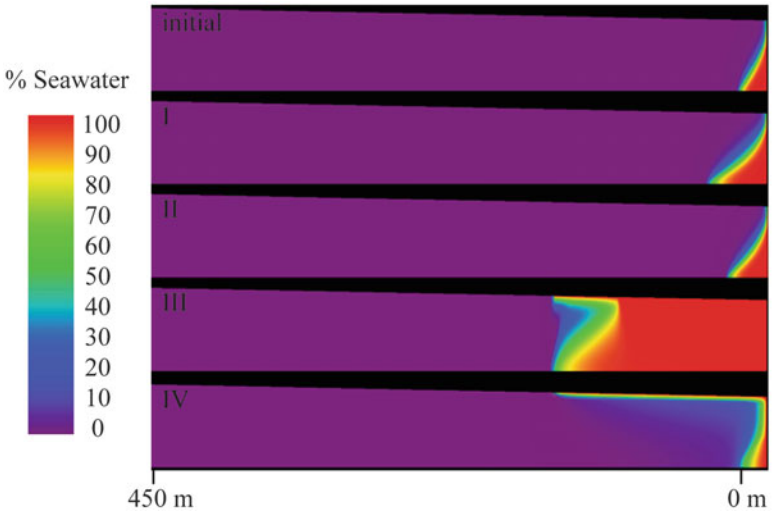

Fig. 14.3 Salinity distributions for SLR cases: ("initial") initial conditions, (I) Scenario I: 60 years after an instantaneous SLR of 1 m (no transgression), (II) Scenario II: 60 years of gradual SLR (10 mm/year; no transgression), (III) Scenario III: 60 years of gradual SLR (10 mm/year) and transgression on a 0.004 slope, (IV) Scenario IV: The same as scenario III, except with a low permeability surface layer. Each sub-figure has a vertical dimension of 10 m at the coast

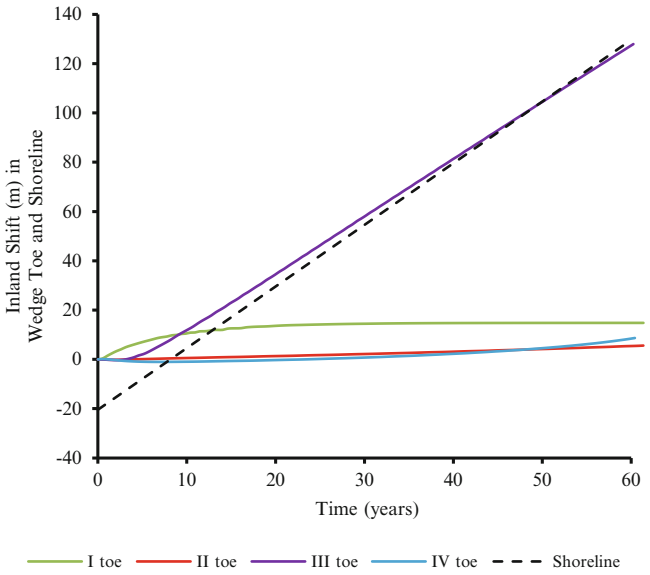

Fig. 14.4 Toe movements for SLR scenarios I–IV. The origin is taken as the initial wedge toe location, and hence the shoreline starts at a negative position (i.e. about 20 m seaward of the initial toe)

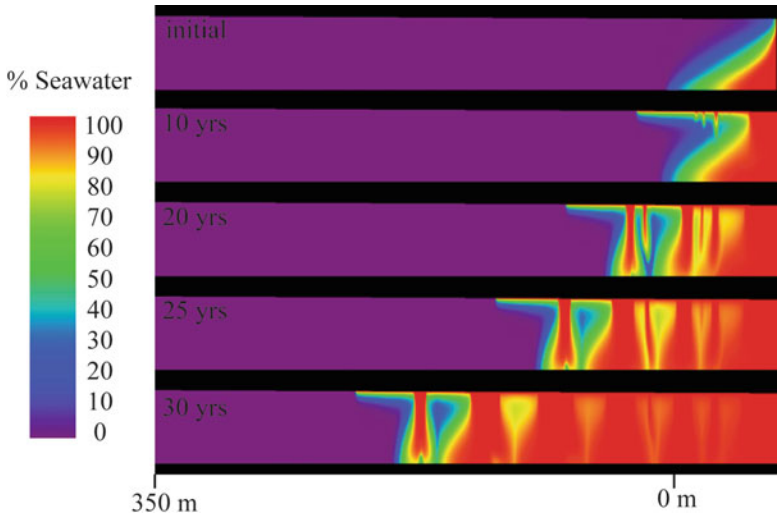

Fig. 14.5 The first 30 years of scenario III with a topographical slope of 0.001. The origin is again taken as the initial wedge toe location

trapped freshwater in offshore aquifers caused by transgression, albeit they considered geological time scales.

14.3.2 SLR-SWI Under a Shallow-Sloped Land Surface

The topographical slope was reduced to 0.001 and the other parameters from the example above were retained, producing $\Gamma = 11.4$, which is indicative of a transgression situation involving free convection processes. The rapid inland migration of the coastline resulted in denser seawater overtopping fresh groundwater. Free convective fingering processes failed to trigger until the coastline advanced a significant distance inland of the top of the saltwater wedge, thereby creating density-inverted conditions. Salinity distributions during the first 30 years of the simulation are presented in Fig. 14.5, and the advance of the toe is given in Fig. 14.6.

The first finger-shaped instabilities formed during the eighth year of the transgression event, but early unstable plumes merged with the underlying wedge, as illustrated by the absence of well-established fingers after 10 years in Fig. 14.5. After this time, new salinity fingers reached the aquifer basement ahead of the salt wedge, approximately every 5 years. This is illustrated by the time-series of salinity distributions in Fig. 14.5, and by the periodicity in the wedge toe trend in Fig. 14.6. Figure 14.6 shows that the wedge toe trailed the coastline, although after 10 years, it maintained the same pace as the transgressing shoreline. This occurred because new toe positions were created when density-driven salt fingers reached the basement.

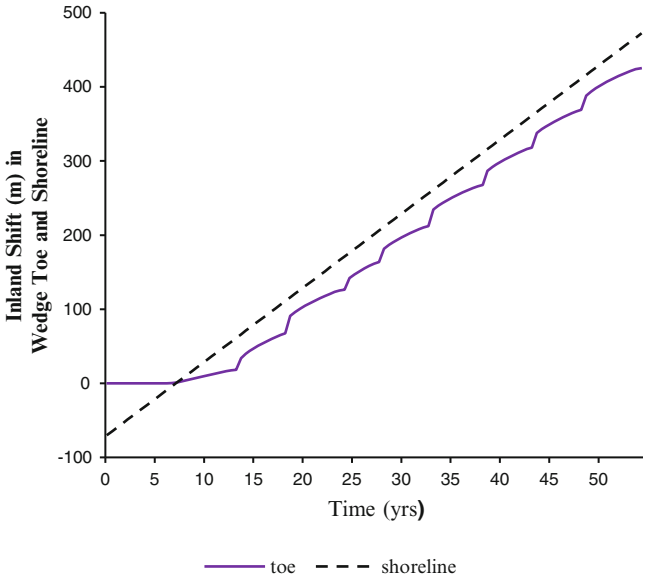

Fig. 14.6 Toe movements for scenario III with a topographic slope of 0.001

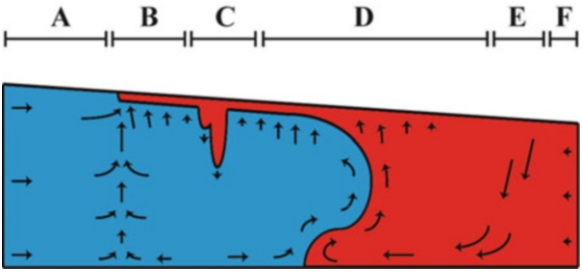

Fig. 14.7 The flow field created during transgression showing the initiation of the first unstable salinity finger. The following zonation was apparent: (A) flow created by regional gradient, (B) strong upward flow at the leading edge of coastal transgression, (C) weaker upward flow, allowing finger formation, (D) strong upward flow field created by the transition zone, (E) strong downward flow responsible for the majority of salt input, (F) horizontal flow that gradually weakens

A schematic of the flow field associated with this scenario is show in Fig. 14.7. As each finger began its descent, a new region of upward flow was created at either side of the finger, inhibiting finger formation from adjacent areas. New fingers formed as the distance between a descending finger and the migrating coastline became sufficiently large so that upward flow between them weakened allowing downward density forces to create new unstable fingers. A region of downward saltwater flow (Fig. 14.7: region E) developed behind the wedge and this was the primary source of salt input into the aquifer (rather than inflows through the right boundary), in particular prior to the formation of the first saltwater finger.

The two land slopes of 0.001 and 0.004 produced significantly different modes of SWI under a scenario III transgression simulation. Nonetheless, the wedge toe largely kept pace in both cases, albeit they differ in whether the toe advances ahead of the shoreline, or vice versa. Hence, it appears that SWI will largely keep pace with transgressing shorelines under the simulated conditions described above, i.e. in shallow aquifers that are moderately permeable, regardless of whether free convection is initiated or not. The main difference between scenario III cases was whether SWI occurred from top-down or laterally from the sea.

14.3.3 Applicability of Γ (Lag Index) to Different Slopes

The numerical experiments of Kooi et al. (2000), involving homogeneous, sandy aquifers and a slope of 0.001, indicated that free convection occurs under the condition $\Gamma \geq 6.51$. For cases of $\Gamma \leq 5.89$, SWI was entirely the result of horizontal plume movements. Hence, the situations assessed by Kooi et al. (2000) depart from the prediction of free convection processes from Eq. (14.1) by a factor of about 6.5. We hypothesise that this is due to the small diffusive forces in Kooi et al.'s (2000) simulations, which lead to time-lags in the generation of free convective process. That is, equation (1) fails to consider the time required for boundary layer development prior to free convective fingering.

In order to test the applicability of Eq. (14.1) under modern SLR conditions, the topographical slope was changed to 0.003 while the other Table 14.1 parameters were retained, producing $\Gamma = 1.05$. The rates of shoreline transgression and wedge movements in this simulation were expected to be almost the same, with shoreline progression slightly exceeding wedge movements. The predicted salinity distributions are given in Fig. 14.8, and toe movements are shown in Fig. 14.9.

Vertical SWI by free convection occurs above the transition zone, but mixes with the wedge before reaching the aquifer basement, at least for most of the scenario, as shown in Fig. 14.8. However, as the transgression moves inland, to areas where the aquifer is deeper, the shoreline gradually outpaces the inland movement of the wedge. After about 80 years, there is a free convection event that causes the toe to move forward suddenly (Fig. 14.9). These results suggest, at least in general terms, that Kooi et al.'s (2000) lag index is a reasonably robust indicator of free convection processes during shoreline transgression, under the modern rates SLR and other aquifer parameters assessed here. That is, as Γ approaches one, free convection processes occur, but only as minor contributions to the landward advance of SWI. The deepening of the aquifer as the shoreline moves inland likely contributes to the widening gap between the seawater wedge and the transgressing shoreline that is observed in Fig. 14.9 prior to 80 years, at which time a significant free convection event occurs. Kooi et al. (2000) adopted rectangular aquifers, and hence the deepening of the aquifer was not considered, and in that case, free convection processes are inhibited because the wedge more readily kept pace with the shoreline. The slower rates of SLR used by Kooi et al.

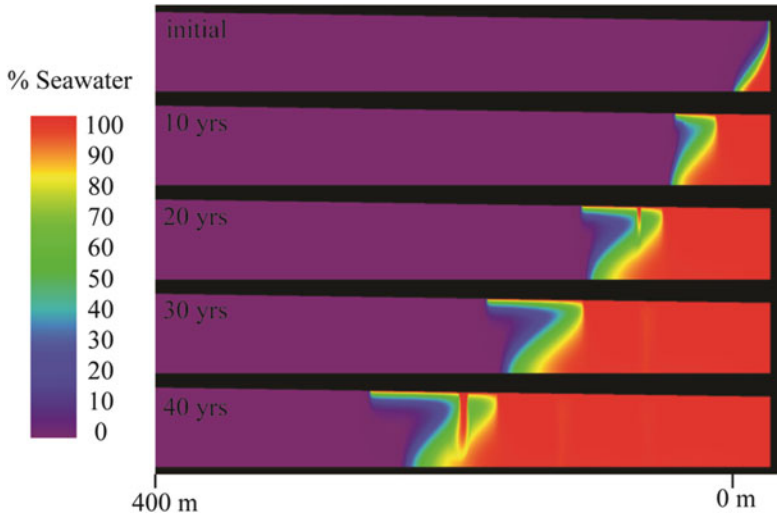

Fig. 14.8 The first 40 years of scenario III with a topographical slope of 0.003

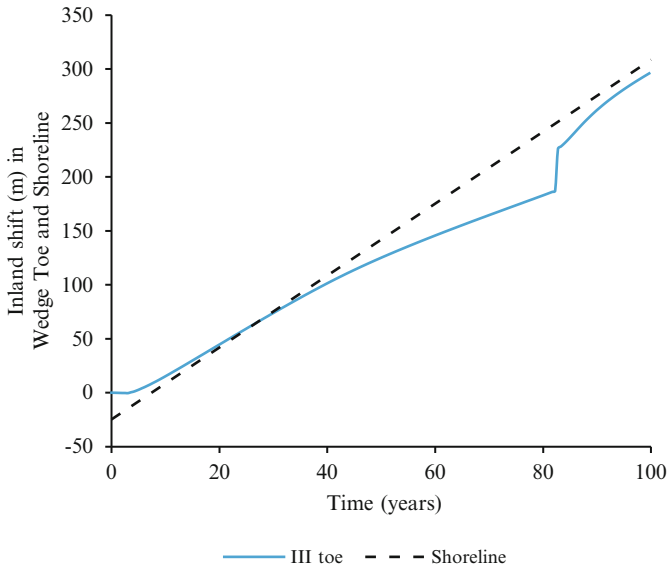

Fig. 14.9 Toe movements for scenario III with a topographic slope of 0.003

(2000) are another likely source of discrepancy between Eq. (14.1) predictions of free convection and the results presented here. The initial lag-time prior to wedge movements, evident in Fig. 14.9, demonstrates a non-linear response in the wedge toe that probably enhances instabilities under faster transgressions. Modification of Eq. (14.1) to account for factors additional to those considered by Kooi et al. (2000) is beyond of the current scope.

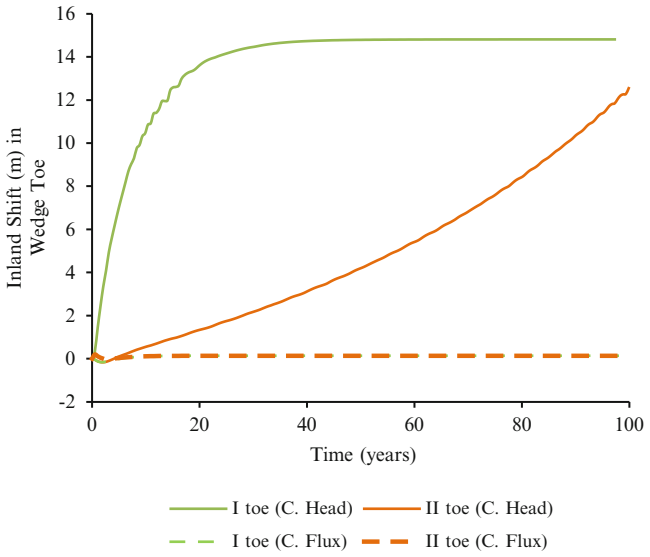

Fig. 14.10 A comparison of wedge toe movements in flux-controlled (C. Flux) and head-controlled (C. Head) systems for SLR scenarios I and II

14.3.4 Assessment of Landward Boundary Condition Controls

Werner and Simmons (2009) showed that choice of head- or flux-controlled landward boundary conditions significantly affects SLR-SWI. Their analyses neglected coastal transgression and therefore correspond with scenarios I and II. Figure 14.10 shows toe positions during model runs for scenarios I and II, and considering two different landward boundary conditions of constant head and constant flux. The flux entering the model at the landward boundary from the pre-SLR steady-state simulations was adopted in the constant flux cases. The results concur with the findings of Werner and Simmons (2009). That is, little change was observed in the toe location after 100 years for flux-controlled systems, whereas the head-controlled situation involved more substantial SWI.

The comparison of inland boundary conditions was repeated using simulations of scenario III (i.e. including coastal transgression), as illustrated in Fig. 14.11. Only minor differences between the flux- and head-controlled movements in the wedge were observed. Minor differences were similarly obtained in scenario III simulations using alternative parameter values that fell within the ranges given in Table 14.1 (results not shown).

The net fluxes of fluid across the right boundary are shown in Fig. 14.12, which demonstrates important differences between SLR scenarios. Prior to SLR, there is net discharge to the sea through the right boundary (i.e. a negative boundary flux). In the absence of transgression (i.e. scenario II), the pressure increase at the coast due to SLR caused a reduction in discharge to the sea, for the case of a specified

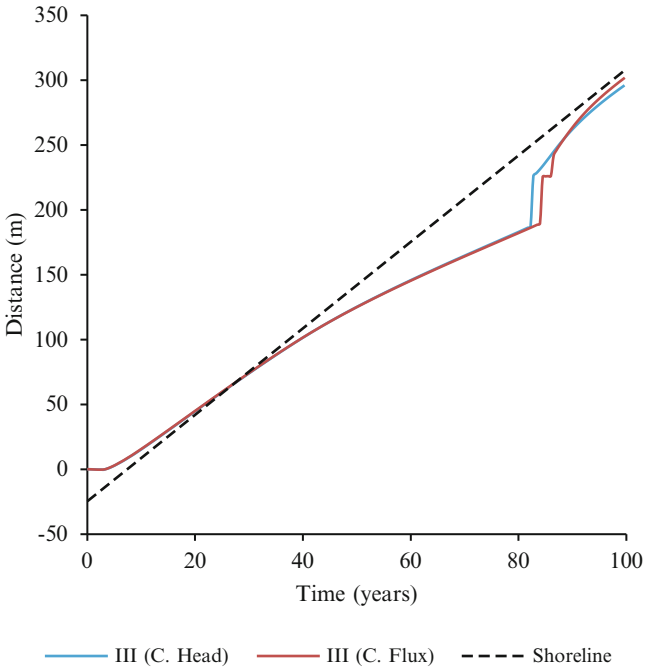

Fig. 14.11 A comparison of wedge toe movements in flux-controlled (C. Flux) and head-controlled (C. Head) systems, for scenario III with a topographic slope of 0.003

Fig. 14.12 A comparison of net fluid flux across the right boundary. Fluxes are given for scenarios II and III, using specified head (C. Head) and specified flux (C. Flux) boundary conditions, and a topographical slope of 0.003. A negative flux represents discharge to the sea

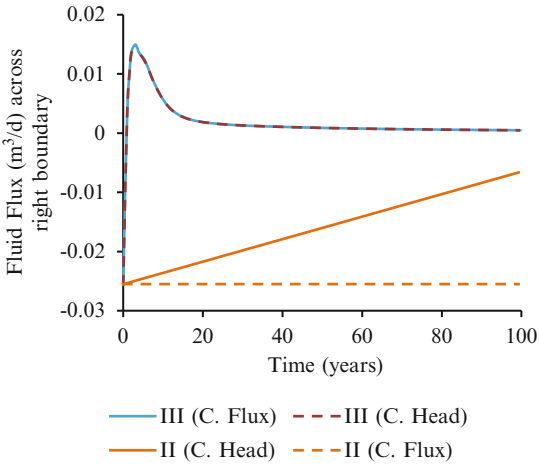

inland head, as expected (Werner and Simmons 2009). Unsurprisingly, the corresponding simulation involving a specific flux landward boundary produces virtually no variation in seaward flux. Under the influence of the transgressing shoreline (scenario III), the net discharge through the right boundary reverses in

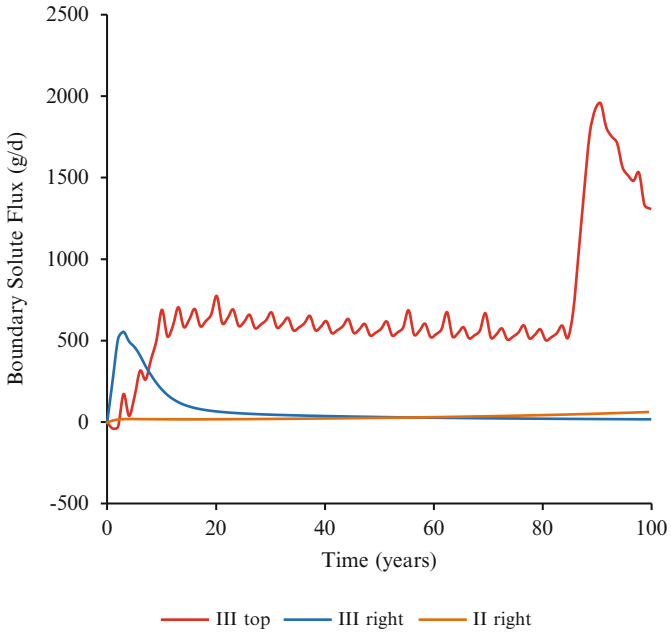

Fig. 14.13 Fluxes through the top and right boundaries from scenarios II and III (specified head inland boundary)

direction soon after the start of the simulation, and the boundary provides net inflow to the aquifer. This occurs because the discharge of freshwater is diverted to the transgressing shoreline, rather than the right boundary, allowing seawater to enter the freshwater aquifer almost unimpeded (i.e. without the mitigating effect of freshwater discharge) and driven by density forces. As the coastal aquifer fills with almost stagnant seawater, seawater inflows through the right boundary abate due to the reduction in concentration (and density) gradients. Eventually, the inflows and outflows from the aquifer during scenario III are almost entirely through the inundated land surface boundary. The influence of the inland boundary conditions (i.e. specified flux or specified head) has little bearing on the right boundary flow trends, in the simulation involving transgression (Fig. 14.12).

14.3.5 Salinization Rates and Volumes

The rates of solute flux through the right and land surface boundaries, and the total salt mass in the aquifer were considered important factors in assessing SWI within the various scenarios. Figure 14.13 presents solute mass fluxes for scenario II and III scenarios involving a specified-head inland boundary and a topographical slope of 0.003. This case is characterised by $\Gamma = 1.05$, as previously, and hence free

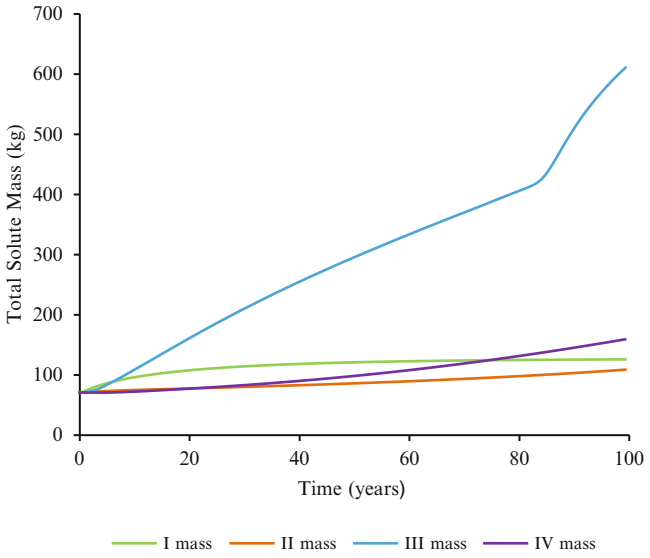

Fig. 14.14 Trends in total solute mass under a head-controlled inland boundary conditions and a topographical slope of 0.003

convective fingering is only a small element of the vertical salinization processes for the majority of the simulation. The late-time free convection event in this case, as shown in Figs. 14.9 and 14.11, allows for the influence of free convection on salt mass loads to the aquifer to be assessed and compared to salt mass fluxes that occur in the absence of free convection (i.e. prior to 80 years).

In Figure 14.13, the oscillations in the scenario III flux through the top boundary arise from the periodic increases in the length of inundated land (i.e. due to the node-by-node advance in the shoreline) during transgression. The large increase in solute input at the 80-year mark coincides with the development of a large free convective finger, which draws large amounts of salt flux through the top boundary prior to reaching the aquifer base, where it merges with the main saltwater wedge. It is clear from these results that free convective processes can create significant increases in salt mass fluxes during transgression, relative to the salt masses caused by the combined effects of advection and dispersion.

Figure 14.14 illustrates changes in salt mass in the aquifer for all four scenarios, again adopting a land surface slope of 0.003. As expected, scenario III involves the largest aquifer salt masses, and the inflexion in the scenario III curve highlights the importance of free convection in aquifer salinization. The vertical dispersive salinization of the aquifer in scenario IV (Fig. 14.3) adds significant volumes of salt to the system relative to the cases with no transgression, as demonstrated by the increasing trend in the scenario IV line in Fig. 14.14.

The vertical descent speeds of free convective fingers, which formed landward of the wedge toe, were obtained by tracking the time required for the 5 % isochlor at the tip of a finger to fall 3.0 m, i.e. between the 12th and 22nd node below the surface.

The average descent speed across various scenario III simulations ranged between 0.01 and 0.02 m/day. These are substantially slower rates of descent compared to those obtained by Xie et al. (2011), who obtained speeds 5–10 times faster; the difference is attributed to the upward flow opposing finger descent in the scenarios examined here. The maximum rate of horizontal SWI was taken as the speed of landward advance of the wedge toe, taken prior to free convection processes in models involving transgression. Toe speeds were between 0.005 and 0.009 m/day across the various scenario III (transgression) simulations, which produced by far the fastest rates of landward wedge movements. It is clear that even under circumstances conducive to rapid SWI, vertical rates of plume movement caused by free convective fingering exceed the rates of landward movements in the wedge.

14.4 Discussion

Scenario III simulations indicate that rates of shoreline transgression are similar to time-averaged rates of SWI, in shallow, permeable, homogeneous unconfined aquifers, regardless of the land slope. This occurs because vertical salinization processes occur in shallow-sloped settings, creating periodic landward advances in the wedge toe, whereas in steep settings, horizontal SWI is sufficient to keep pace with the landward transgression of the shoreline. The apparent insensitivity of SWI to the choice of inland boundary condition, observed in transgression (scenario III) simulations, occurs because rates of seawater wedge movements are controlled by the head and concentration boundary conditions at the surface, representing the advancing shoreline.

Significant differences between the results of Kooi et al. (2000) and the current study were obtained. The value of Kooi et al.'s (2000) lag index for obtaining free convection in transgression simulations was some 6.5 times higher than in the current analysis. The value of Γ that distinguished free convection salinization from primary horizontal salinization was roughly in the order of unity, as was the value purported by Kooi et al. (2000) prior to their numerical experimentation. It is likely that saline boundary layers, which are necessary precursors to free convection, evolved more rapidly in the current study compared to Kooi et al.'s (2000) scenarios given the differences in transgression rates, hydraulic conductivities and dispersive processes, and this led to a greater propensity for free convection to occur under otherwise comparable conditions to Kooi et al. (2000).

14.5 Conclusions

The transient transgression impact on SWI under a modern rate of SLR (i.e. 10 mm/year) was explored by extending the variable-density numerical modelling analysis of Kooi et al. (2000). The interplay between vertical salinization and lateral SWI

was simulated and the temporal behaviour of the wedge toe, fluid and salt fluxes across all boundaries, and the total mass of salt in the domain were predicted. A number of important observations were made from the numerical experiments regarding effects of transgression on SLR-SWI. These are listed as follows:

1. Vertical salinization by free convective fingering in shallow, unconfined coastal aquifers subjected to transgression have wedge toe migration rates that are 1 and 2 orders of magnitude greater than cases where vertical salinization is excluded.
2. The lag index parameter Γ, provides more accurate predictions of free convection events under transgression scenarios with larger values of hydraulic conductivity and faster rates of SLR.
3. Where vertical SWI by density-driven free convection occurs, it can lead to the formation of a new wedge interface and cause significant increases in salt mass fluxes during rapid transgression scenarios in shallow-sloped, unconfined coastal aquifers.
4. Rates of SLR-SWI are equivalent in both head- and flux-controlled unconfined aquifer systems when shoreline transgression effects are included in the model.

It is noteworthy that scenarios presented in this study comprise of idealized coastal aquifers subjected to rapid transgression rates commensurate with modern values. In general, further research on the effect of transgression on SLR-SWI is warranted, as the body of literature on this topic is somewhat scant relative to the potential impacts of SLR and land surface overtopping. The role of heterogeneity, which can modify significantly rates of vertical transport under free convective processes, on rates of salinization need to be examined further.

Acknowledgments This work was funded by the National Centre for Groundwater Research and Training, a collaborative initiative of the Australian Research Council and the National Water Commission

References

Chang SW, Clement TP, Simpson MJ, Lee KK (2011) Does sea-level rise have an impact on seawater intrusion? Adv Water Resour 34:1283–1291

Diersch HJG (2005) FEFLOW user's manual. WASY, Berlin, 208 pp

Groen J, Velstra J, Meesters AGCA (2000) Salinization processes in paleowaters in coastal sediments of Suriname: evidence from d 37Cl analysis and diffusion modelling. J Hydrol 234:1–20

Illangasekare T, Tyler SW, Clement TP et al (2006) Impacts of the 2004 tsunami on groundwater resources in Sri Lanka. Water Resour Res 42:W05201. doi:10.1029/2006WR004876

Kooi H, Groen J, Leijnse A (2000) Modes of seawater intrusion during transgressions. Water Resour Res 36:3581–3589

Melloul A, Collin M (2006) Hydrogeological changes in coastal aquifers due to sea-level rise. Ocean Coast Manage 49:281–297

Voss CI, Souza WR (1987) Variable-density flow and solute transport simulation of regional aquifers containing a narrow fresh water-saltwater transition zone. Water Resour Res 23:1851–1866

Watson TA, Werner AD, Simmons CT (2010) Transience of seawater intrusion in response to sea-level rise. Water Resour Res 46:W12533. doi:10.1029/2010WR009564

Webb MD, Howard WF (2011) Modeling the transient response of saline intrusion to rising sea-levels. Ground Water 49:560–569

Werner AD, Simmons CT (2009) Impact of sea-level rise on sea water intrusion in coastal aquifers. Ground Water 47(2):197–204. doi:10.1111/j.1745-6584.2008.00535.x

Werner AD, Bakker M, Post VEA, Vandenbohede A, Lu C, Ataie-Ashtiani B, Simmons CT, Barry DA (2012a) Seawater intrusion processes, investigation and management: recent advances and future challenges. Adv Water Resour http://dx.doi.org/10.1016/j.advwatres.2012.03.004 (in press)

Werner AD, Ward JD, Morgan LK, Simmons CT, Robinson NI, Teubner MD (2012b) Vulnerability indicators of sea water intrusion. Ground Water 50(1):48–58

Xie Y, Simmons CT, Werner AD (2011) Speed of free convective fingering in porous media. Water Resour Res 47:W11501. doi:10.1029/2011WR010555

Xie Y, Simmons CT, Werner AD, Diersch HJ (2012) Prediction and uncertainty of free convection phenomena in porous media. Water Resour Res 48:W02535. doi:10.1029/2011WR011346

Part IV
The Way Forward: Solutions and Outlook for Groundwater Management

Chapter 15
Integrated Groundwater Use and Management in Vulnerable Coastal Zones of Asia-Pacific

Karen G. Villholth

Abstract Groundwater in coastal zones around the globe is a critical asset in securing water, food and general development for millions of people. Particularly, in the Asia-Pacific region, such resources are significantly depended on in rural as well as urban areas for a wide range of uses, often as the only water source, which is exemplified by small island states. Present and future stresses on these significant, but often vulnerable systems, from human development, urbanization, climate change, and extreme events call for better understanding and awareness of these resources, their protection and best management approaches. The present chapter deals with the current level of knowledge of coastal groundwater systems in continental and island settings in the Asia-Pacific, their uses, vulnerabilities and hazards from various sources. The objective of the paper is to propose through an integrated framework approach how sustainable and resilient groundwater management can be promoted and enhanced. The work is partially based on the case of the tsunami in eastern Sri Lanka and the immense challenges but also opportunities it entailed for local and higher level groundwater management.

15.1 Introduction

Groundwater in coastal zones is a life-sustaining freshwater resource for hundreds of millions of people living in the Asia-Pacific region. There are no estimates of the percentage of the Asian coastal population that is dependent on groundwater, but it may well be more than half. Many small island developing states (SIDS) in the Pacific Ocean as well as states like the Maldives in the Indian Ocean are particularly dependent on groundwater, often as the only locally available natural freshwater source. With high dependence comes great vulnerability of these populations

K.G. Villholth (✉)
IWMI, International Water Management Institute, Pretoria, South Africa
e-mail: K.Villholth@cgiar.org

C. Wetzelhuetter (ed.), *Groundwater in the Coastal Zones of Asia-Pacific*,
Coastal Research Library 7, DOI 10.1007/978-94-007-5648-9_15,

should groundwater resources deplete or degrade for whatever reasons, be it over-abstraction, pollution, climate change or, as progressively seen, a combination of these impacts.

This chapter gives a broad overview of the groundwater resources, and human interactions with it, in the Asia-Pacific region, with specific focus on the coastal areas. Which are the contemporary concerns and problem areas, how are they being addressed, and which further options need to be considered. Ensuring sustainable development, utilization, protection, and management of groundwater is not a straightforward task, but with increasing pressures on the resource from human and climatic forces and associated threats of irreversible degradation, it is also increasingly recognized as a necessary priority in water resources management as well as development planning. It will become clear to the reader that groundwater is not just a source of water supply for human consumption and development aspirations, but equally importantly it is an integrated part of the environment, an integral component and regulator of the hydrological system, and a protector against as well as recipient of intruding contaminants and climatic change impacts.

15.2 Groundwater Occurrence, Characteristics and Uses in Asia-Pacific

Groundwater in the Asia-Pacific region is found in various geological settings, varying from alluvial, sedimentary environments like the large river basins, deltas and flood plains of the major Indus, Ganges and Mekong Rivers to the interior hard rock areas of peninsular India and the primarily Quaternary volcanic regions in the Pacific island states (Figs. 15.1 and 15.2).[1] Local coastal aquifers reflect these overall geological regions though often they are also impacted by recent marine influences, often giving rise to sedimentary basins of relatively smaller extent as exemplified along the eastern coast of peninsular India. Recent sedimentary aquifers also occur in the vast deltas of the Yellow River and Yangtze River in China and the Mekong River in Vietnam.

Groundwater is used extensively in India, Pakistan, Bangladesh, China and Japan (Fig. 15.3). In India, Pakistan and Bangladesh, use is primarily for irrigated agriculture, while in Japan, domestic and industrial uses predominate (Fig. 15.4). In China, use is concentrated in the North China Plains, where groundwater is the main resource for all uses, increasingly supplemented by water transferred from the Yangtze River in the south (Liu et al. 2008). In these areas, groundwater abstraction rates exceed recharge rates (Sun et al. 2009) indicating unsustainable use. However, this is not reflected in Fig. 15.3 due to the national scale aggregation. In general, the use and dependence on groundwater is skewed towards the dryer and more populous regions of Asia, such as Pakistan, peninsular India, Bangladesh and Northern

[1] Note that Fig. 15.1 does not cover the central parts of the Pacific Ocean region though many small islands occur here. This is because most islands are too small to show at the scale used and partly because of lack of data on groundwater conditions.

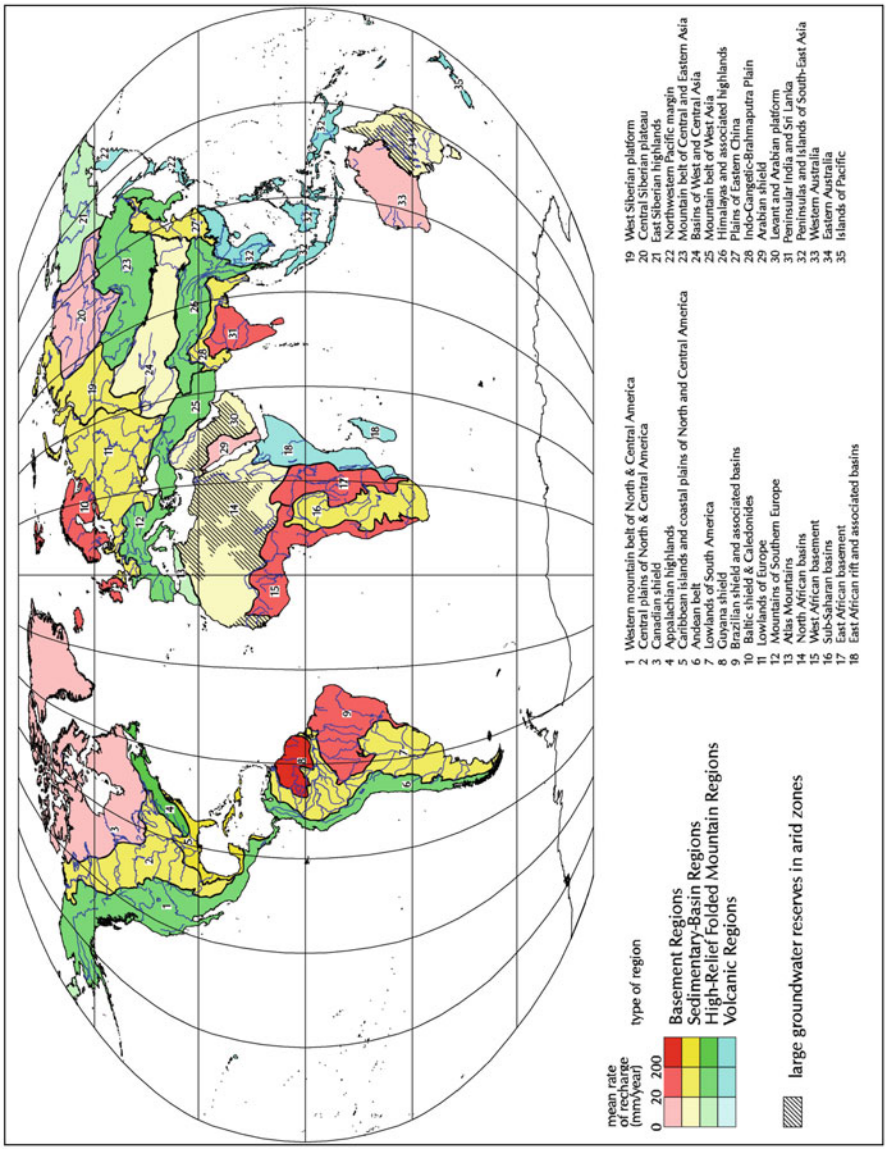

Fig. 15.1 Major groundwater regions of the world (Vrba and van der Gun 2004)

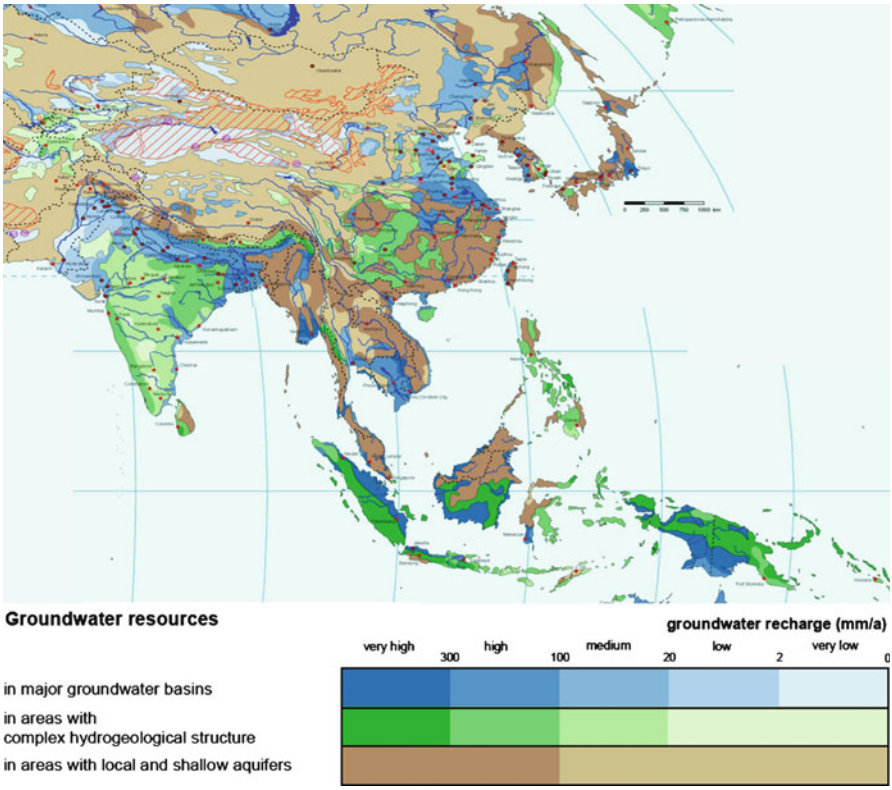

Fig. 15.2 Groundwater resources in Asia-Pacific (WHYMAP 2008)

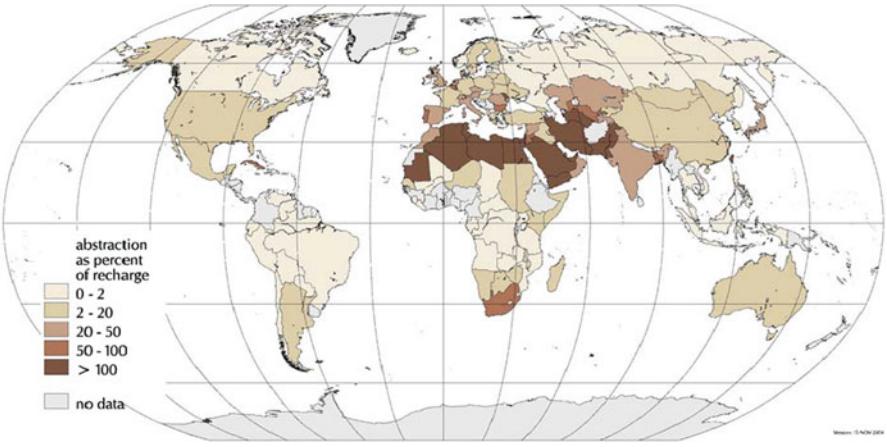

Fig. 15.3 Groundwater abstraction rate as a percentage of mean recharge rate (Vrba and van der Gun 2004)

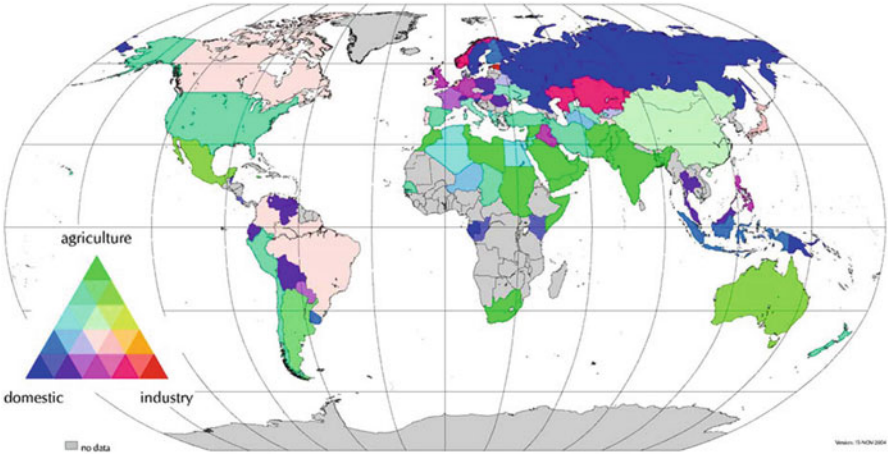

Fig. 15.4 Groundwater abstraction by water use sectors (proportions) (Vrba and van der Gun 2004)

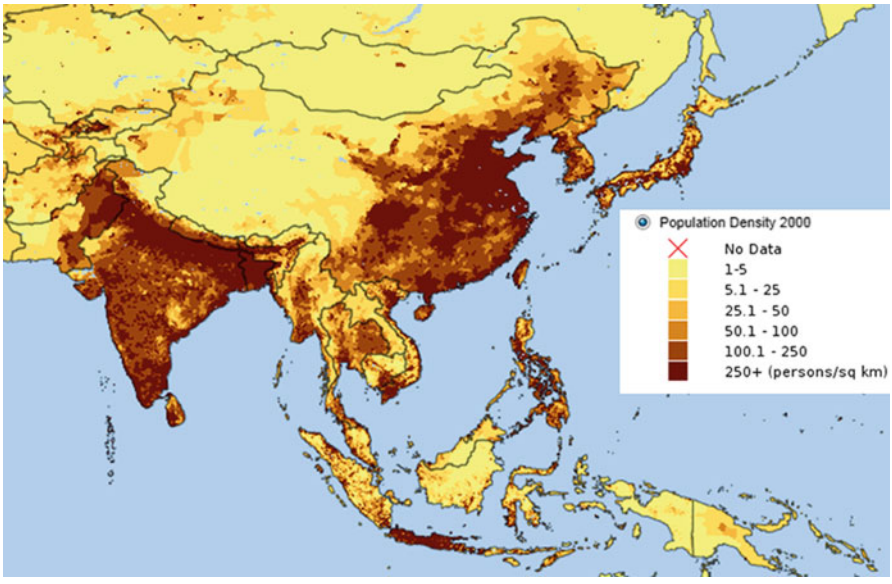

Fig. 15.5 Population density of the Asia-Pacific region (CIESIN 2012)

China (Figs. 15.5 and 15.6). This reflects the need to meet the demand in these regions as well as the general reliability of groundwater for dry season agriculture and domestic water supply. In the Pacific region, rainfall is generally more abundant (Fig. 15.6), giving rise to less groundwater dependence though it still serves as a significant source for domestic water supply, especially on smaller islands as well as for industry in e.g. the Philippines and Malaysia (Fig. 15.4).

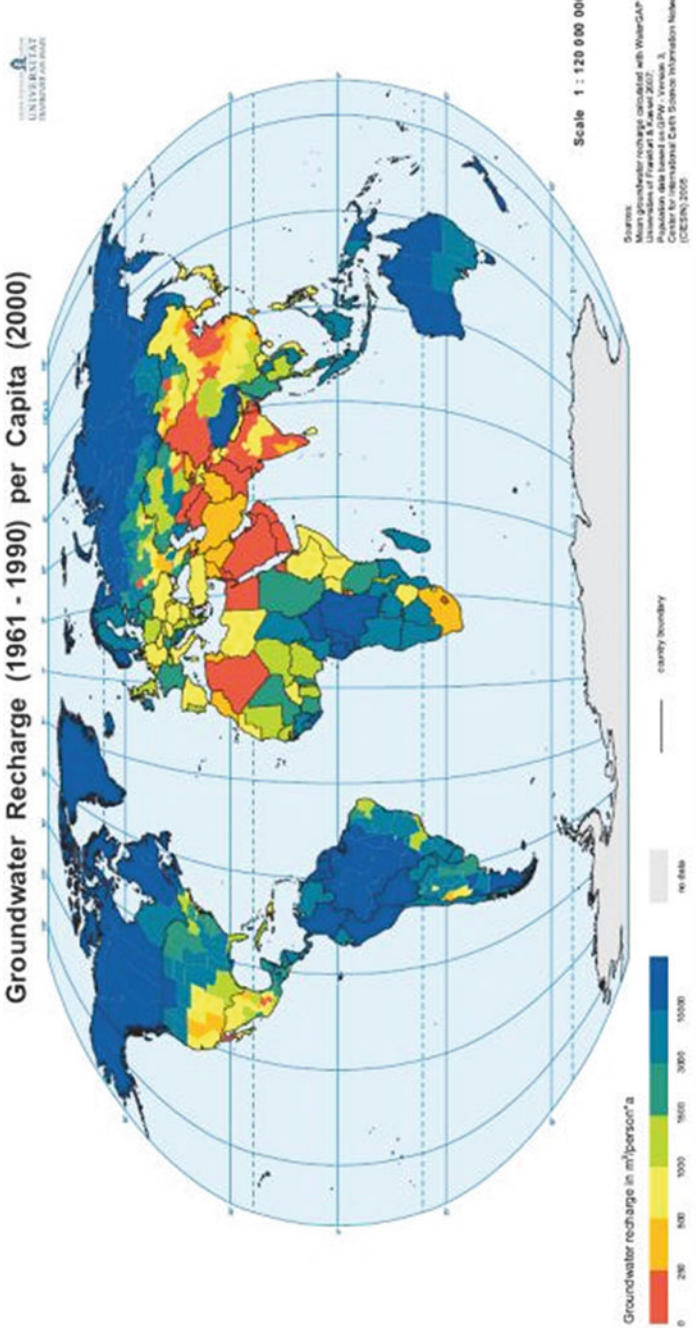

Fig. 15.6 Groundwater recharge (1961–1990) per capita (2000) (University Frankfurt am Main and CIESIN (http://www.whymap.org/whymap/EN/Downloads/Additional_global_maps/gw_recharge_pdf.pdf?__blob=publicationFile&v=3))

15.3 Natural Groundwater Quality

Pristine groundwater is generally of good quality for human use. However, poor groundwater quality due to inherent hydrogeological conditions and hydrogeochemical processes may limit certain groundwater uses or impair the access points. Such is the case when e.g. excessive content of iron, arsenic or fluoride is present in the water. These contaminants beset groundwater use to varying degree throughout parts of the Asia-Pacific region. While iron is mostly a nuisance in terms of giving bad taste to the water and causing staining and blockage of screens, pumps, pipes, and reticulation systems, as seen in many parts of India (CGWB 2010), arsenic and fluoride are hazardous to human health in concentrations naturally encountered (Fendorf et al. 2010; Aayoob and Gupta 2006). Arsenic is a problem of the deltaic sedimentary regions of the Ganges River in Bangladesh, the Red River in Vietnam and less so of the Mekong River in Vietnam (Fig. 15.7), while the fluoride problems are associated with the volcanic formations in the Pacific region and the hard rock areas of southern Peninsular India, Sri Lanka, and central and western China (Fig. 15.8). Arsenic typically originates from inland mountainous geological material transported by rivers and sedimented in river deltas where hydrogeochemical environments and processes favor the subsequent release into the groundwater resources and associated water supplies (Fendorf et al. 2010).

Excessive salt content is another critical water quality parameter of groundwater, restricting its suitability for almost all purposes. Causes of salinity, however, are multifarious, such as from irrigated areas with poor drainage, connate water from previous geological times, or seawater intrusion (SWI) along the coasts (van Weert et al. 2009). It is seen from Fig. 15.9 that salinity is a widespread problem in groundwater in the Asia-Pacific region for various reasons.

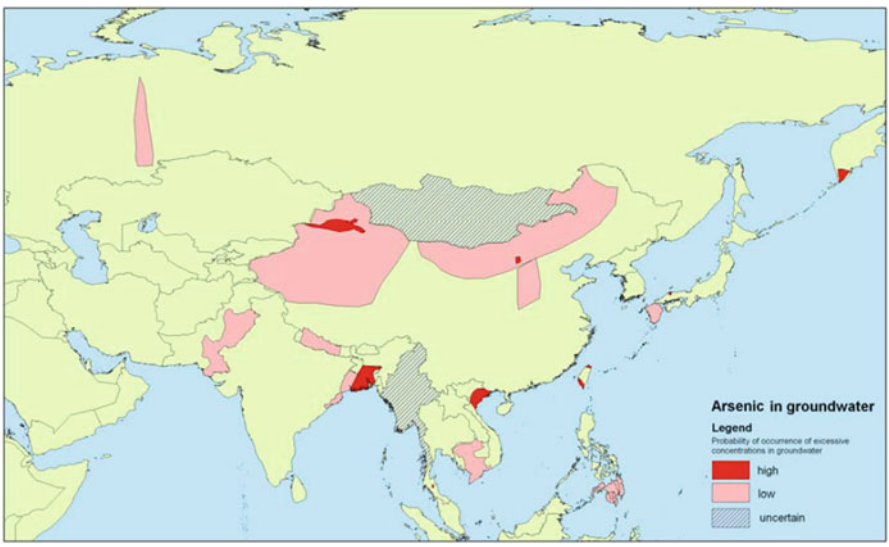

Fig. 15.7 Arsenic in groundwater in Asia (Brunt et al. 2004a)

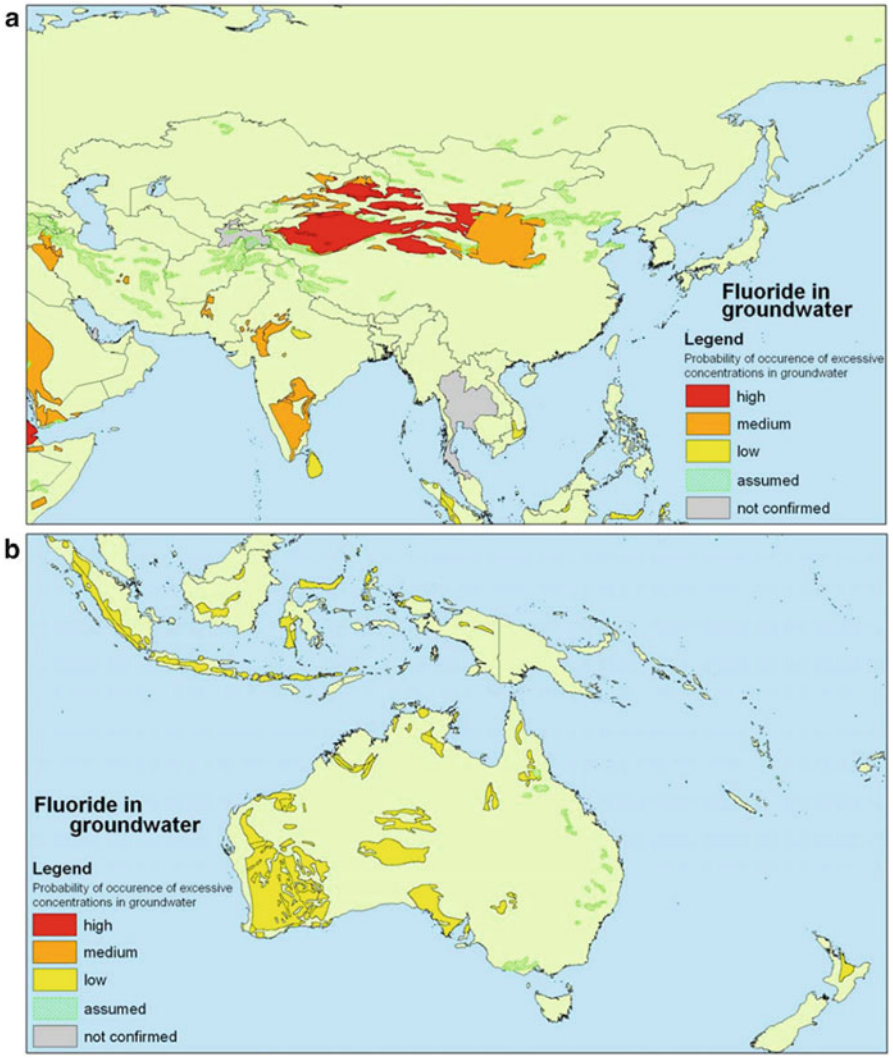

Fig. 15.8 Fluoride in groundwater in Asia (**a**) and Oceania (**b**) (Brunt et al. 2004b)

15.4 Groundwater Vulnerabilities and Challenges in Coastal Areas

Management of groundwater, and water in general, presents added challenges in coastal areas. This is because this zone is the nexus and confluence zone between the upstream/inland areas and the sea, both giving rise to threats and risks in terms of e.g. flooding and contamination. Also, the coastal areas are the most densely populated in the world, including many urban centers and cities (Small and Nicholls 2003). It is estimated that in Asia, 40 % of the population

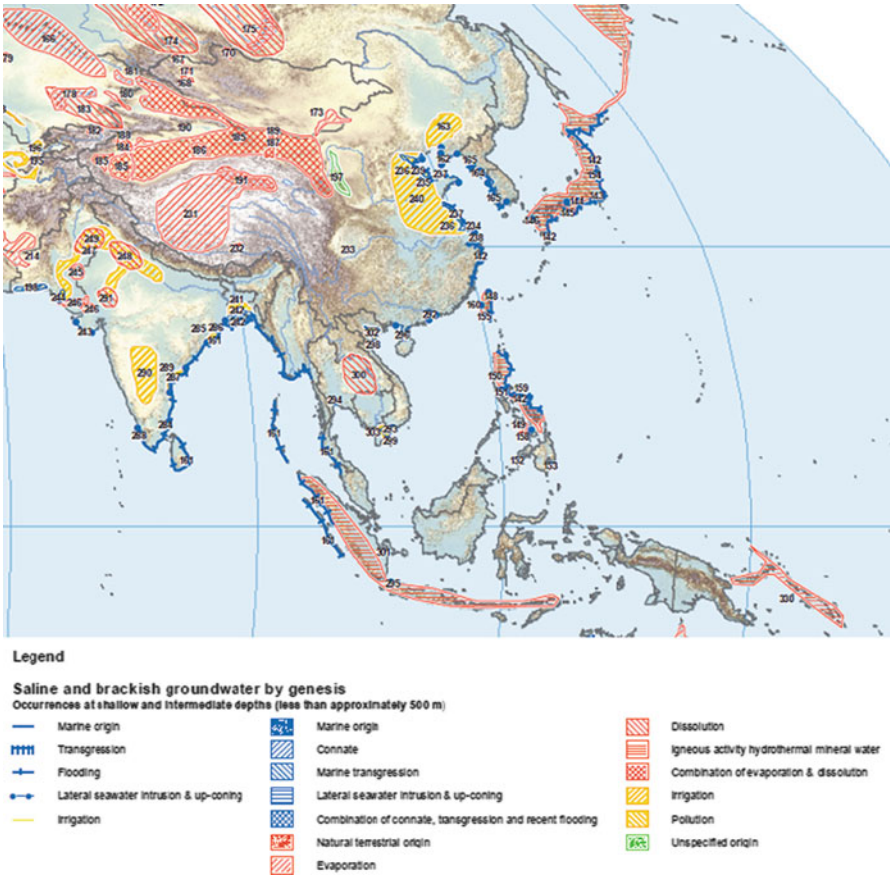

Fig. 15.9 Groundwater salinity in Asia-Pacific (van Weert et al. 2009)

lives within a distance of 100 km from the coast (Hinrichsen 2007). As an example from Sri Lanka, 25 % of its population lives in coastal areas, 62 % of industrial units and more than 70 % of tourist infrastructure are located on its coastal areas (Athulathmudali et al. 2011). The coastal zone accounts for about 43 % of the nation's GDP, so impacts on coastal settlements translate into substantial impacts on the nation's economy (Athulathmudali et al. 2011).

Groundwater in coastal areas is particularly vulnerable to degradation from various sources in the coastal zone. Groundwater salinity in coastal areas is generally associated with marine proximity and recent or prehistoric seawater influences. Occurrences in flood plains and delta areas can be highly complex, determined by present day interactions between seawater, groundwater and surface water, depositional history and prehistoric global sea-level changes or land subsidence as exemplified by the Red River flood plain in Vietnam (Tran et al. 2012). Same global prehistoric sea-level changes may have influenced other delta regions in Asia (indeed worldwide), providing more general and conceptual tools to

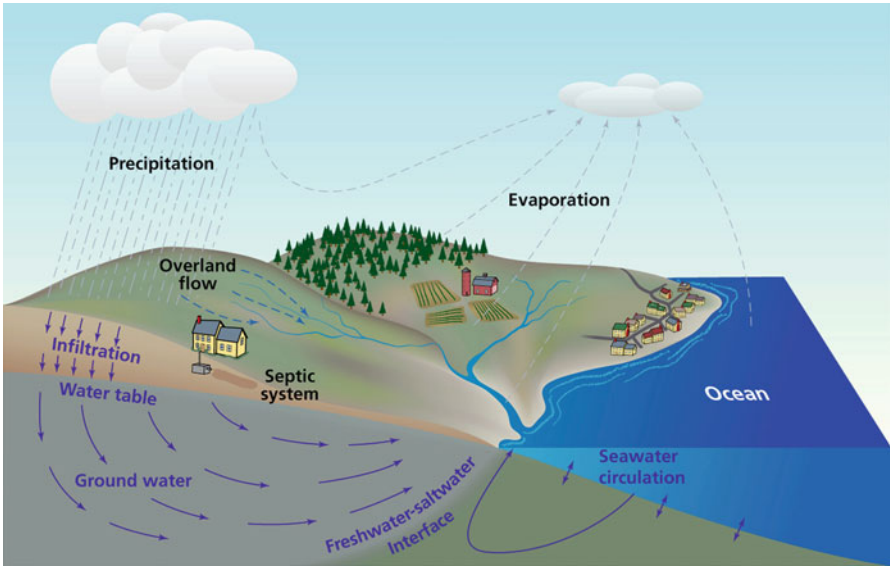

Fig. 15.10 Saltwater-freshwater interaction and submarine groundwater discharge in the coastal margin (from Mulligan and Charette 2009)

understanding coastal salinity phenomena. Due to permeability differences in sedimentary sequences and basic saltwater redistribution processes over time, due to advective, diffusive and density-contrast driven transport, saltwater can be encountered overlying freshwater aquifers (Tran et al. 2012), which is counterintuitive to the conventional model of saltwater intrusion where a saltwater wedge is driven under the upper freshwater zone (Ferguson and Gleeson 2012) (Fig. 15.10). Similar reverse salinity effects were found in coastal areas of Orissa (Singh et al. 2011). Short-term contemporary or historic seawater transgressions, or inundations, from tsunamis and cyclones, may also severely affect groundwater salinity in the shorter and longer term as evidenced in Sri Lanka (Villholth and Neupane 2011) and Orissa, India (Sukhija and Rao 2011). Such cases serve to demonstrate the complex nature of coastal salinity and the need for proper understanding of the influencing processes in order to manage such systems (Custodio 2004).

Naturally, in unaffected situations, there will be a quasi-stationary balance between ingressing seawater and freshwater entailing presence of saltwater at depth (Fig. 15.10). Seawater intrusion (SWI) occurs as a disturbance of this balance when due to excessive pumping or lowering of the hydraulic potential and gradient in the coastal zone, the saltwater moves further inland. SWI is difficult to detect on a larger scale and is most often detected locally through entry of saltwater into pumping wells, through other hydrogeochemical and isotopic analysis of groundwater (Delinom et al. 2009; Onodera et al. 2009; Hiroshiro et al. 2006), and through geophysical methods (Bear et al. 1999). However, these incidences are confounded by the pumping itself, which causes upconing of the saltwater from below and

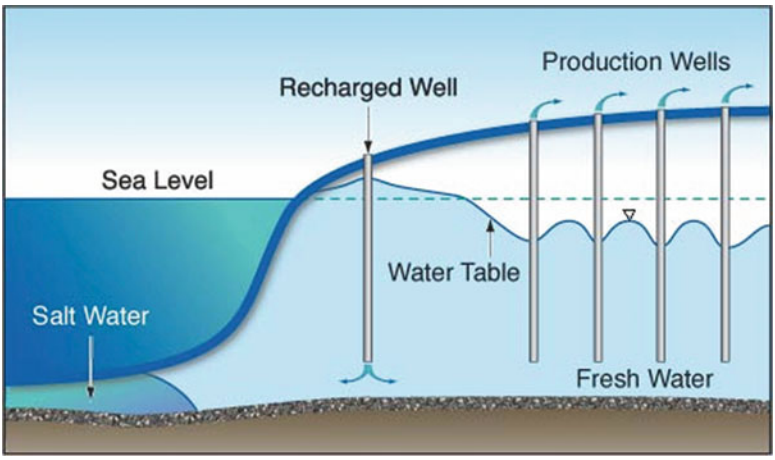

Fig. 15.11 Using artificial recharge to mitigate seawater intrusion

which may be an accelerated process relative to the saltwater ingress. SWI normally is a relatively slow process, occurring over decades, and depending on the conditions, e.g. the permeability of the formations, it will be a reversible or partly irreversible process (Bruggeman and Custodio 1987).

Controlling the saltwater-freshwater balance is of paramount importance for sustainable freshwater access and availability in coastal regions. Normally an approach that combines a flux-based consideration and trigger-level management is applied. In this, estimates of upper limits of groundwater abstraction, and associated pumping guidelines, are constrained by local monitoring of aquifer salinities (Werner et al. 2011). Counteracting or mitigating against SWI typically involves methods of optimizing pumping strategies, demand management (reducing pumping rates through conservation and more efficient use of water), hydraulic barriers (injecting freshwater in critical zones, e.g. from excess river flow, storm water, or recycled water, Fig. 15.11), or substituting groundwater with other sources (like surface water or desalinated water). Such integrated approaches, including modeling approaches, to evaluate effects of various management schemes, and monitoring schemes including warning wells to evaluate effectiveness of management strategies, are presently applied in cases like Australia (Werner et al. 2011), while many cases of SWI in Asia are relatively hampered by lack of human and technical capacities, in countries like India (Rejani et al. 2008; Shanmugam et al. 2007), China (Shanzhong et al. 2007), Thailand (Das Gupta et al. 1987; Onodera et al. 2009), and Indonesia (Delinom et al. 2009; Onodera et al. 2009). SWI was observed in China's coastal aquifers as early as the 1960s. At present, impacts cover an area of more than 580 km^2 in the coastal area of Laizhou Bay in the northeast of the country and are continuing to extend. There is a wide transition zone of 1.5–6.0 km, in which both the simple mixing of local freshwater and seawater and the cation exchange can be recognized (Xue et al. 1993). In Japan, the use of subsurface physical barriers has been proposed to prevent or retard SWI

on the Okinawa-jima Island (Sugio et al. 1987). Other innovative methods to increase fresh groundwater resources are trialed in Singapore where newly acclaimed land is generating subsurface freshwater storage in artificial aquifers (Bo 2002).

SWI into freshwater aquifers is influenced by factors such as tidal fluctuations, long-term climate and sea-level changes, fractures in coastal rock formations and seasonal (due to landuse change) and permanent changes in evaporation and recharge rates (e.g. due to urbanization and less pervious surfaces). Pumping seawater into shrimp ponds can also lead to salinization of groundwater in coastal areas, compromising its use for domestic purposes (Beveridge 2007).

Like the sea may contaminate fresh groundwater under conditions of reduced or reversed hydraulic gradients in the coastal areas, groundwater may reversely contaminate the coastal waters, if contaminated with e.g. nutrients, nuclear waste constituents, and microorganic pollutants. The process of submarine groundwater discharge (SGD) occurs as a natural phenomenon, parallel and conjunctively with the land to seaward discharge of surface water (Fig. 15.10). Though the SGD flow rates generally are lower than surface water discharge, the chemical loadings from SGD may be comparable or exceed that of surface water inputs, due to higher dissolved solids concentrations in groundwater and larger accumulative discharge zones (Mulligan and Charette 2009; Taniguchi et al. 2002). Though a relative new research area, which started in the late 1990s (Taniguchi et al. 2002), emerging results in Asia show that SGD may critically impact geochemical cycling, contamination, end environmental conditions, especially in estuaries and embayments (Taniguchi et al. 2005). Work is ongoing in Australia, Japan, Korea, New Zealand, Philippines, Taiwan, and Thailand (Taniguchi et al. 2002, 2005). Umezawa et al. (2002) showed that nitrogen contamination in coastal coral reefs in islands southwest of the Ryukyu Islands, Japan, may be attributed to SGD and inland agricultural development. Better understanding of SGD may come from a classification or typology of aquifers and hydrogeological, geomorphological, and human factors (Taniguchi et al. 2002).

In addition to the more slow-onset SWI hazards, coastal areas in Asia are particularly vulnerable to event-based hazards, like tsunamis, cyclonic storms, and hurricanes. Exemplifying this, the hotspot areas for tsunamis are shown in Fig. 15.12. Low-lying environments are generally the most vulnerable to both the slow and fast-onset hazards. In this category fall the Asian delta regions of the Ganges, the Red River and the Mekong River as well as the SIDS, and particularly the low-lying atoll countries, like Tokelau Kiribati, and Marshall Islands in the Pacific and the Maldives archipelago state in the Indian Ocean.

While the SIDS represent a diversity in terrestrial, freshwater and marine ecosystems covering little land surface and huge ocean space, they all represent a group of countries faced with high population growth rates and demographic change, like urban drift (South et al. 2004). This entails increased pressure on limited freshwater resources, which is exacerbated by climate change and more generally global change (South et al. 2004). Populations in these environments are relying on local water resources, most often limited freshwater aquifers (occurring as freshwater ‘lenses’, floating on top of saline groundwater) that are both

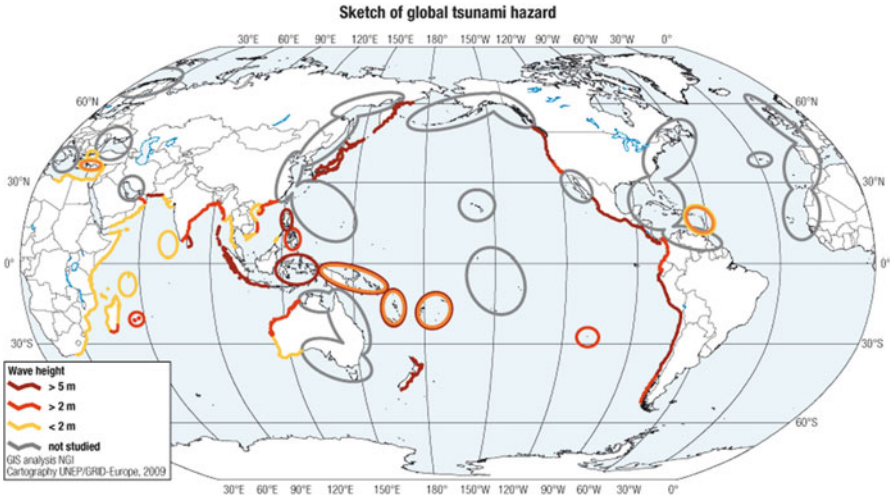

Fig. 15.12 Global map of tsunami hazard (UNISDR 2009)

vulnerable and under great pressure from bacteriological pollution and intensified land and water use. In addition, due to their limited extent, these systems are vulnerable to seasonal and longer-term rainfall and climate variability. As an example, in the Tarawa atoll in Kiribati, it was found that a reduction of 25 % in rainfall caused a 64 % reduction in the freshwater lens thickness (normally about 30 m thick) if pumping rates were maintained (South et al. 2004). Other sources of water in these environments are rainwater harvesting and desalination, but generally speaking, these communities are hard pressed for meeting their water demands and managing their water resources sustainably. Water management programs and technological solutions that promote capture and storage, conservation, and sustainable use of groundwater is integral to meeting local water needs for both domestic and commercial use in SIDS (UNDESA 2010).

Climate change is likely to aggravate already high vulnerabilities of coastal zones of Asia. With respect to groundwater, impacts relate primarily to increased risk of SWI as a result of projected sea-level rises and to coastal flooding events as a consequence of increased frequency and intensity of e.g. tropical cyclonic storms (World Bank 2005; South et al. 2004). Such events potentially contaminate groundwater with salts, but also other harmful chemicals by inundating land and enhancing infiltration rates. In addition, contamination risks relate to release of waste products and chemicals from otherwise protected deposits and storages due to the physical impact of the waves (Bird and Grossman 2011).

Indirect impacts of climate change come from increased groundwater pumping to offset higher temperatures, e.g. for cooling and irrigation. As with tsunami risk, cyclone hazard areas to a high degree coincide with coastal zones already prone to groundwater degradation (like delta areas and SIDS), enabling the identification of areas that need increased attention and efforts in terms of groundwater management in the future (Fig. 15.13).

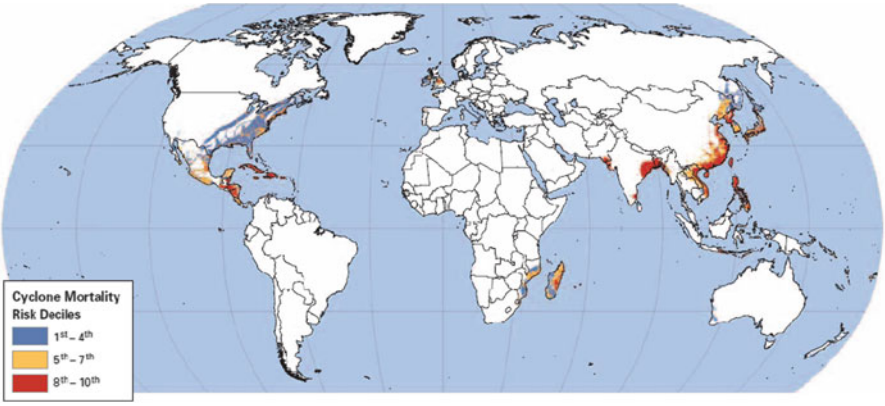

Fig. 15.13 Global distribution of cyclone mortality risk (World Bank 2005)

The relative impact of climate change compared to the anthropogenic effects of population growth and increased water demand on groundwater resources is debated (Ferguson and Gleeson 2012). Simulation results using numerical methods and simplifying assumptions preliminarily indicate that human impacts from pumping will be overriding and that climate change impacts (specifically from SWI associated with sea-level rise) will be secondary, except in low-lying areas, where hydraulic gradients are low. Hence, at least for the shorter term, focus on proper water management should not be compromised by undue attention to adapting to sea-level rise (Ferguson and Gleeson 2012). However, the low-lying areas remain particularly vulnerable due to dual hazards of sea-level rise (and SWI), and flooding hazards.

Interestingly enough, the global impact of groundwater mining (extraction of groundwater above its replenishment), is now significant in terms of contribution to global sea-level rise. This is because accumulated groundwater volumes pumped ultimately is reflected in larger discharges to the oceans. Konikow (2011) estimates the magnitude of groundwater depletion to equivalent to 0.40 mm sea-level rise annually at present, which is directly comparable to estimates of sea-level rise of 3.1 mm/year from other sources, most notably melting of ice storages and thermal expansion of seawater (Konikow 2011). Projecting impacts of climate change and human water demand using global circulation models, this contribution of groundwater depletion to global sea-level rise is estimated to increase to 0.82 mm/year by the year 2050 (Wada et al. 2012), assuming that groundwater exploitation will not be limited by exhaustion or inaccessibility of the resource.

15.4.1 Metropolitan Areas

To the particularly vulnerable areas (low-lying areas and SIDS) can be added the coastal megacities of Asia, which due to their population densities and extensive

water demand pose special risks to groundwater resources. Major coastal cities in Asia relying heavily on groundwater include: Tokyo, Osaka (Japan), Seoul (South Korea), Shanghai, Tianjin (China), Chennai (India), Bangkok (Thailand), Jakarta (Indonesia), Manila (Philippines), and Ho Chi Minh, Hanoi (Vietnam), many of them counting more than 5 million inhabitants. Some of these metropolises are also located in low-lying delta or floodplain areas downstream of major rivers, e.g. Bangkok (Chao Phraya River), Shanghai (Yangtze River), Hanoi (Red River) and hence prone to flooding from river overflow or local cloud bursts.

Groundwater has been developed on a larger scale in these cities since less than a generation, with earliest development dating back to the 1950s and 1960s in Japan. While huge development gains and human welfare can be ascribed to the use and development of groundwater, most cities now demonstrate significant problems related to unsustainable use of the resource (Delinom et al. 2009; Onodera et al. 2009; Nguyen Thi et al. 2008; Das Gupta and Babel 2005; Nguyen and Helm 1995; Braddbaart and Braadbart 1997). Problems, which may be emerging already after a decade of intensive use (Nguyen and Helm 1995), are very alike and relate to an interaction of processes related to both overexploitation and degradation of the resource. Very notable, with intensive exploitation, in magnitudes of several hundred thousand to more than a million cubic meters per day, groundwater levels decline (Das Gupta and Babel 2005). Declines, of up to 2–3 m/year, result in increasing pumping depths and associated cost increases as well as signs of groundwater quality degradation. The latter is often associated with a mix of SWI, induced recharge and downward leaching of surface-derived contaminants, and release of inherent salts and chemicals (Onodera et al. 2009). The relative importance of the SWI and the downward leaching of contaminants are generally not known. However, there will be an increased risk of coastal loading of the leached chemicals (e.g. nitrate) with SGD if the aquifer system is recovered hydraulically (Onodera et al. 2009). Also, interference from intruding paleo-saltwater complicates the analysis of SWI in these settings (Delinom et al. 2009; Hiroshiro et al. 2006; Das Gupta and Babel 2005).

Subsidence of the land surface is another common accompanying phenomenon in these coastal areas, due to a partial collapse of the aquifer matrix formation upon water evacuation. This is especially pronounced in the delta regions where the subsurface is dominated by unconsolidated sediments with significant amounts of clays that are more prone to inelastic compression (Domenico and Schwartz 1998). Land subsidence is an irreversible process and it can in extreme cases, where the land surface drops by up to 10–20 cm per year (Delinom et al. 2009; Das Gupta and Babel 2005), cause major problems for urban infrastructure (roads, pipelines) and built environment. Especially in low-lying areas, the subsidence may disturb drainage patterns and systems and even increase flooding risk (IGES 2007; Das Gupta and Babel 2005; Nguyen and Helm 1995). Often there is a clear relationship between the areas impacted by subsidence and areas of typical drawdown cones in piezometric head (Nguyen and Helm 1995).

Cities, depending on size and dependence on groundwater, typically follow a similar trajectory as populations grow and cities expand, where the negative impacts

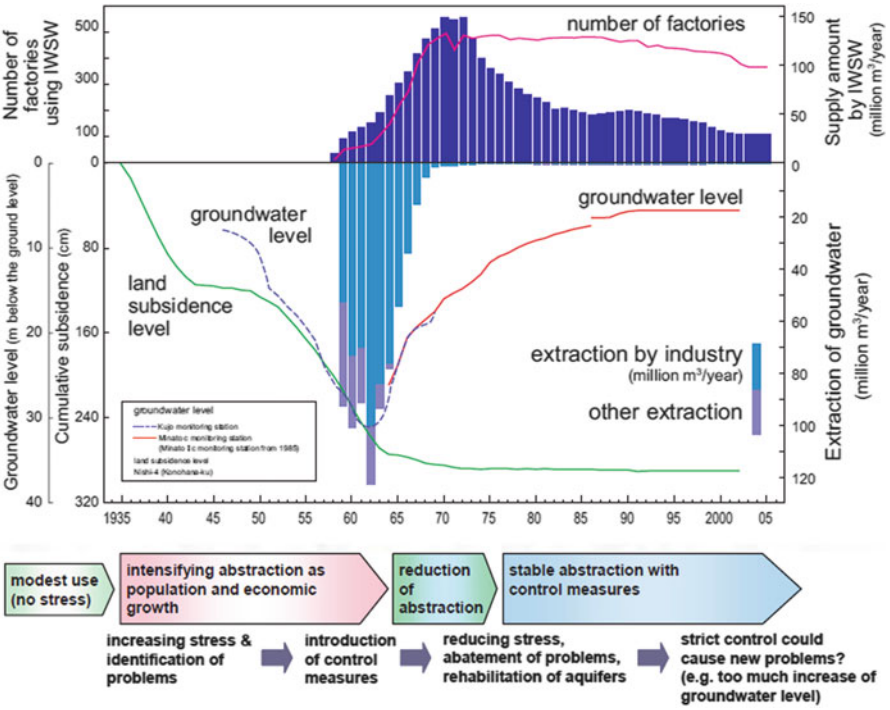

Fig. 15.14 Generalized pattern of urban groundwater use and impacts (case from Osaka) (from IGES 2007)

of groundwater exploitation slowly become evident and partially overshadow positive outcomes (IGES 2007) (Fig. 15.14). In cases like Tokyo and Osaka, where use of groundwater started relatively early, the groundwater pumping has been reduced following significant policy measures from the 1960s and 1970s, mainly through successful substitution of groundwater with surface water for urban supply, reducing water rights for industries, and giving financial incentives (subsidies, favorable taxes, and cheap loans) to industries to implement technologies to conserve water (IGES 2007). In most other Asian cities, groundwater depletion presently presents major challenges. Also, while the depletion and land subsidence problems have been arrested in the Japanese metropolis, they are still confronted with lingering groundwater quality issues (IGES 2007).

In Bangkok, partial and temporary mitigation of the problems were attained through the reduction in groundwater use by phasing out pumping for public water supply, restricting pumping in critical areas of subsidence, and levying charges for groundwater use, which was previously free, and enforcing these in the early 1980s (Das Gupta and Babel 2005). However, with sustained urban development and water demand and insufficient development of alternative water resources, lack of continued enforcement, and too low abstraction fees, the problem of subsidence and depletion resumed (Das Gupta and Babel 2005).

Similar struggles of attempting to control groundwater use in Bandung, Indonesia have been well reported by Braddbaart and Braadbart (1997), pointing at institutional incapacities and conflicting or insufficient incentives for policymakers (having to balance economic development with environmental protection), groundwater users (industries viewing groundwater charges and pumping costs to be marginal), as well as revenue agencies (having to maximize revenues from pumping, while also enforcing the reduction of groundwater pumping) as fundamental to the problem. Enforcement of registration of wells and payment of tariffs and the difficulty of installing and maintaining water meters in industries, which abstract the majority of groundwater, to enable implementation of volume-based tariffs and quotas were critical issues. Finally, revenues collected were not reintroduced into environmental management, hampering further progress.

These cases serve to demonstrate that:

1. Groundwater development at these intensive scales requires early and pro-active management
2. Several strategies need to be implemented simultaneously in order to effectively remediate the situation. These measures include substituting supply from groundwater with surface water, desalinated water or other source, augmenting groundwater recharge through managed schemes using various sources (storm water, flood water, reclaimed water, rainwater), controlling new well development, moving most water-intensive industries out of the cities, promoting water-saving technologies, charging volumetrically for groundwater use
3. Measures need to be enforced continuously
4. Revenues from tariff collection should be returned to groundwater management
5. Institutions need to attain capacity to assess problems through integrated analysis, as well as authority, manpower and incentives to enforce regulations
6. Groundwater-directed measures should be combined by better urban planning in terms of zoning of development, waste and wastewater management and greening of cities
7. Groundwater monitoring and modeling can significantly increase understanding of processes and impacts of potential or actual remediation interventions. However, they are not on their own measures that will improve the management

Besides these principally local measures, there is a need to incorporate urban water management within wider basin-scale and coastal zone management approaches to ensure optimal protection and use of the water resources and related ecosystems.

15.4.2 Suburban and Rural Areas

While huge population concentrations occur in Asian megacities and metropolitan areas, the majority of the region's coastal population still lives in rural and suburban areas (ISEAS 2009; Small and Nicholls 2003). In these areas, populations are often

characterized by poor people with livelihoods based on natural resources, such as fisheries and agriculture, subject to environmental conditions and traditional cultures. Lowland areas, with water access from wetlands, lagoons, floodplains, rivers, and shallow groundwater govern best options. In these areas, groundwater issues pertain to water availability and security, in terms of accessibility, reliability, and adequate quality, and uses are mostly small-scale and dispersed, either from private wells or smaller reticulated systems and for domestic uses and smaller productive uses.

Overdraft of groundwater may be sporadic in these settings and not well documented. However, mostly associated with intense smallholder agriculture and groundwater irrigation, cases of overdraft are reported from the Mekong delta of Vietnam for rice and cash crops (Johnston et al. 2012) and on the west coast of Sri Lanka for vegetable cultivation (Jayasekera et al. 2010). While groundwater use for irrigation is a prominent feature in more inland areas and along alluvial river plains of India, Bangladesh, Pakistan and Northern China (Mukherji et al. 2009), and of high potential for further development in lowland plains and some upland areas of Thailand, Myanmar, Laos, and Cambodia (Johnston et al. 2012) it is more sporadic in the coastal areas, due to other livelihood options, surface water irrigation options and practices, and limitations in soil and groundwater quality. Where soils and groundwater conditions are favorable, it is likely that irrigation in coastal areas using groundwater is presently increasing, partly offsetting shortages and unreliability of surface water.

15.4.2.1 The Case of the 2004 Tsunami

The vulnerability of coastal rural populations dependent on groundwater was brought to the fore when the 2004 Indian Ocean tsunami hit countries like Indonesia, Sri Lanka, India, and Thailand. With huge populations cut off from their traditional water supplies due to physical destruction of wells and salinization of groundwater, the life-sustaining significance of groundwater on the one hand, and the fragility of the systems and the resource on the other, became obvious. Alone in Sri Lanka, it was estimated that in the range of 2.5 million people were cut off from their water source (Villholth et al. 2010). Luckily, the immediate health threatening condition was counteracted through efficient emergency response (Villholth et al. 2010), and the longer-term salinity impact were naturally remediated through rainfall flushing the shallow and quite permeable aquifers within one and a half years after the event, obviating further water supply relief support (Villholth et al. 2011). However, due to uninformed approaches, unwarranted efforts and resources were dedicated to attempting to clean the wells by manually and mechanically pumping the wells in the first months after the event, though these procedures often were counterproductive (Villholth et al. 2010, 2011). Based on field level findings and numerical, field and laboratory experiments, better understanding of the tsunami effect on groundwater and best remedial strategies were developed (Vithanage et al. 2009, 2011;

Goswami et al. 2007). A set of guidelines for the cleaning of wells in the aftermath of a saltwater flooding event in similar settings were subsequently adopted and endorsed by WHO (2011).

Ironically enough, while salinity caused the immediate hindrance to groundwater use and received significant attention in tsunami rehabilitation and research (Illangasekare et al. 2006), the major and chronic pollution source in the affected coastal areas, aggravated by the tsunami, was often from bacteriological contamination originating from poor sanitation, waste and wastewater treatment facilities (van der Linden 2011; Sukhija 2011). Widespread in these coastal areas, domestic wastewater enters directly or via largely unmaintained septic tanks into the groundwater, public canals or drainage systems and eventually reaches rivers and other water bodies (ISEAS 2009). On-site sanitation causes easy groundwater contamination in shallow coastal aquifers. Furthermore, these problems are not restricted to rural areas. More than 20 % of household water supplies in Asian cities violate national health standards (King 2003) pointing to the general lack of proper sanitation structures.

Similarly, SWI intrusion is often quoted as the critical factor in coastal groundwater systems, especially considering climate change scenarios (van der Gun 2012). However, heavy groundwater abstraction and intensive land use more often entails groundwater pollution that is more prominent and critical, like nitrate pollution in intensively cultivated coastal areas with shallow aquifers where populations are equally dependent on the same resource for drinking water (Jayasekera et al. 2010). Numerical evidence suggests that while over-pumping of groundwater in such systems may lead to SWI (Vithanage et al. 2010), the likelihood of facing other pollution problems ahead of this is great. Studies from urban groundwater studies seem to suggest similar findings. So, while the tsunami increased the attention to coastal-specific groundwater issues and links between disasters and groundwater vulnerability, it also highlighted the concurrence with conventional and often more recalcitrant groundwater contamination problems.

15.5 Integrated Solutions

Challenges of sustainable groundwater management in coastal zones of Asia-Pacific relate to both human and naturally induced risks. These risks, which in addition are interrelated and tend to exacerbate each other, need to be integrated into overall strategies for protection of the resource and the benefits derived from it. Most vulnerable are the delta and low-lying coastal areas of the Asia-Pacific, the SIDS, and the megacities dependent on groundwater. Furthermore, groundwater management cannot be performed in isolation, but needs to include aspects of integrated water resources management, coastal zone management, climate change adaptation, and disaster risk management. Just as coastal groundwater may be severely impacted by natural disasters as evidenced in the 2004 Asian tsunami and the 2011 Tohoku tsunami in northeastern Japan (Bird and Grossman 2011),

isolated and well-protected aquifers may serve as emergency water supplies during and after disasters (Vrba and Verhagen 2011). Setting up contingency plans based on proper delineation and characterization of aquifers and installation of reserved emergency wells may prove life-saving and cost-effective in risk-prone areas.

Various initiatives presently exist that address groundwater research and management in coastal Asian regions, each with some particular aim and focus. The Asia-Pacific Coastal Aquifer Management Meetings (APCAMM) is a joint initiative by FAO, ESCAP, IAHS, IAH, IUCN, and others to bring experts and managers together to discuss and share knowledge and experience within coastal groundwater management. Two meetings have been held in 2009 and 2011 covering broad aspects of challenges faced, with focus on SWI (APCAMM 2009). Another initiative focuses on SGD in southeast Asia (Taniguchi et al. 2005), which also involves scientists and managers from both developed and emerging economies in Asia and abroad. Institute for Global Environmental Strategies (IGES) has been nominated the Asia-Pacific Regional Knowledge Hub for Groundwater Management. Over the years, IGES has collaborated with many partners throughout the region to map and assess groundwater problems and management approaches, successes and failures, especially focusing on groundwater in urban and metropolitan areas (IGES 2007). For the South Pacific region, the South Pacific Applied Geoscience Commission (SOPAC) is working actively to support capacity development and technological improvements to groundwater development, use and management as well as disaster risk management. Finally, global initiatives have particular efforts ongoing in the Asia-Pacific region, such as the Groundwater for Emergency Situations Project (GWES) under UNESCO IHE 6th phase (Vrba and Salamat 2007; Vrba and Verhagen 2006) and the Internationally Shared Aquifer Resources Management Project (ISARM), which is a UNESCO and IAH led multi-agency effort aimed at improving the understanding of issues related to the management of transboundary aquifers.

Under the latter, 11 transboundary aquifers in the southeast Asian region have been identified, four of them located in coastal regions (Fig. 15.15 and Table 15.1). It is clear that many issues related to groundwater need transboundary efforts despite some impacts being of a more local nature. The challenges are simply often similar and could benefit from sharing experiences and approaches across borders. Some of the larger contiguous transboundary aquifers and especially the deeper ones need more coherent and collaborative approaches as these resources may serve for future very strategic shared resources. Finally, for lower delta regions, any development of both surface water and groundwater upstream can significantly impact these resources. For the SIDS, that do not share fresh groundwater resources, issues of global change and sea-level rise are transboundary in nature and need an integrated, shared approach (South et al. 2004). Hence, collaboration on identifying and applying best technology and management practices in a transboundary context becomes ever more important in addressing pressing groundwater issues in the future.

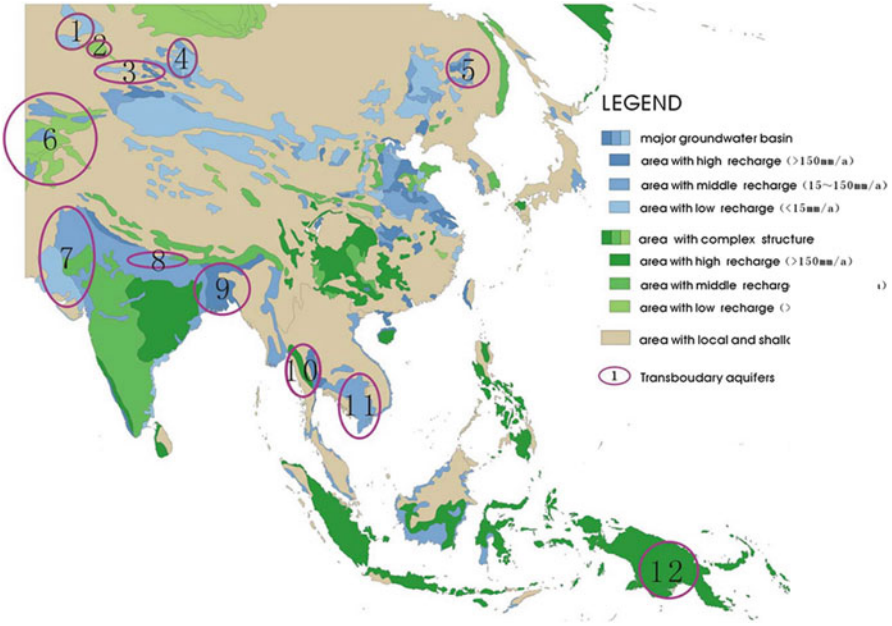

Fig. 15.15 Map of identified transboundary aquifers in Asia-Pacific (Zaisheng et al. 2006)

Table 15.1 Identified transboundary aquifers in Asia-Pacific

No.	Name of transboundary aquifer system	Countries sharing transboundary aquifer	Type of aquifer system[a]	Extension, km^2
1	Ertix River Plain	Russia, Kazakhstan	1	120,000
2	West Altai	Russia, Kazakhstan	1, 2	40,000
3	Ili River plain	China, Kazakhstan	1	53,000
4	Yenisei upstream	Russia, Mongolia	1, 2	60,000
5	Heilongjiang River plain	China, Russia	1	100,000
6	Central Asia	Kazakhstan, Kyrgyzstan, Uzbekistan, Tajikistan, Turkmenistan, Afghanistan	1, 2	660,000
7	India River plain	India, Pakistan	1	560,000
8	Southern of Himalayas	Nepal, India	1	65,000
9	Ganges River plain	Bangladesh, India	1	300,000
10	South Burma	Burma, Thailand	2	53,000
11	Mekong River plain	Thailand, Laos, Cambodia, Vietnam	1	220,000
12	Mekong River plain	Indonesia, Papua New Guinea	2	870,000

From Zaisheng et al. (2006)
[a]1, Porous; 2, Fissured/fractured

15.6 Conclusions

While understanding of groundwater resources in the coastal Asia-Pacific region may be limited in terms of quality and quality and current usage, there is no doubt that groundwater plays an overriding role in supplying freshwater, supporting livelihoods in rural areas and urban centers as well as sustaining important ecosystems. The level of development, the potential for further development, as well as the already registered positive and negative impacts vary greatly across the region.

The most vulnerable areas are the delta and low-lying coastal zones of the Asia-Pacific, the SIDS, and the megacities dependent on groundwater. As seen for the case of the megacities, however a general phenomenon, the common trajectory of groundwater development reveals a double time lag in terms of addressing problems. First, the groundwater is becoming impacted by the development of the resource and the land resources, which takes time to become manifest in groundwater monitoring and other associated parameters. This time lag is due to the physical laggardness of groundwater, the relatively slow flow processes, and the invisible nature of the resource. Secondly, there is a time lag from the time the problem is observed and recognized till it is reacted upon through proper management interventions. This double time lag phenomenon means that groundwater problems often require decades to reverse and hopefully solve. Conversely, it demonstrates the argument for taking a proactive, preventive, precautionary, and adaptive approach in groundwater management.

Bringing the benefits of groundwater to the forefront and the risks associated with loss of same is paramount for increasing the attention and awareness needed to safeguard these precious resources in the vulnerable coastal zones of Asia-Pacific.

References

Aayoob S, Gupta AK (2006) Fluoride in drinking water: a review on the status and stress effects. Crit Rev Environ Sci Technol 36(6):433–487. doi:10.1080/10643380600678112

Asia-Pacific Coastal Aquifer Management Meeting (APCAMM) (2009) Mapping for synergy in the twenty-first century. Proceedings of the 1st Asia-Pacific coastal aquifer management meeting, Bangkok, 9–10 Dec 2009, 25 pp

Athulathmudali S, Balasuriya A, Fernando K (2011) An exploratory study on adapting to climate change in coastal areas of Sri Lanka. Norwegian University of Science and Technology (NTNU), Trondheim. Globalization Research Programme, Faculty of Humanities. 40 p (NTNU Working Paper 02/2011)

Bear J, Cheng A, Sorek S, Ouazar D, Herrera I (1999) Seawater intrusion in coastal aquifers: concepts, methods, and practices. Kluwer, Dordrecht, 625 pp. ISBN 0-7923-5573-3

Beveridge MCM (2007) Cage aquaculture – an overview (chapter 2). In: Beveridge MCM (ed) Cage aquaculture, 3rd edn. Blackwell, Oxford

Bird WA, Grossman E (2011) Chemical aftermath: contamination and cleanup following the Tohoku earthquake and tsunami. Environ Health Perspect 119(7):290–301. doi:10.1289/ehp.119-a290

Bo MW (2002) Fresh groundwater resources from artificial aquifers. In: Guo JJ (ed) Advances in hydraulics and water engineering, volumes I & II: proceedings of the 13th IAHR–APD Congress, Singapore, 6–8 August 2002. World Scientific, pp 631–636. doi:10.1142/9789812776969_0114

Braddbaart O, Braadbart F (1997) Policing the urban pumping race: industrial groundwater overexploitation in Indonesia. World Dev 25(2):199–210

Bruggeman GA, Custodio E (eds) (1987) Studies and reports in hydrology: groundwater problems in coastal areas. UNESC, Paris, 596 pp. ISBN 9231024159

Brunt R, Vasak L, Griffioen J (2004a) Arsenic in groundwater: probability of occurrence of excessive concentration on global scale. IGRAC report nr. SP 2004-1. IGRAC, Utrecht, 9 pp

Brunt R, Vasak L, Griffioen J (2004b) Fluoride in groundwater: probability of occurrence of excessive concentration on global scale. IGRAC Report nr. SP 2004-2. IGRAC, Utrecht, 12 pp

CIESIN (2012) Gridded Population of the World. Center for International Earth Science Information Network (CIESIN) http://sedac.ciesin.columbia.edu/gpw/. Accessed 9 May 2012

Central Groundwater Board (CGWB) (2010) Ground water quality in shallow aquifers of India. Ministry of Water Resources, Govt. of India, New Delhi, 107 pp

Custodio E (2004) Myths about seawater intrusion in coastal aquifers. In: Araguás L et al (eds) Groundwater and saline intrusion: selected papers from the 18th SWIM, Cartagena, Spain. Instituto Geológico y Minero de España, Madrid, pp 599–608. ISBN 84-7840-588-7

Das Gupta A, Babel MS (2005) Challenges for sustainable management of groundwater use in Bangkok, Thailand. Int J Water Resour Dev 21(3):453–464. doi:10.1080/07900620500036570

Das Gupta A, Paudyal GN, Seneviratne AR (1987) Optimum groundwater pumping pattern from a confined aquifer. In: Awadalla S and Noor IM (eds) Groundwater and the environment: proceedings of the international groundwater conference. University Kebangsaan Malaysia, Bangi, pp G60–G68

Delinom RM, Assegaf A, Abidin HZ, Taniguchi M, Suherman D, Lubis RF, Yulianto E (2009) The contribution of human activities to subsurface environment degradation in Greater Jakarta Area, Indonesia. Sci Total Environ 407:3129–3141. doi:10.1016/j.scitotenv.2008.10.003

Domenico PA, Schwartz FW (1998) Physical and chemical hydrogeology, 2nd edn. John Wiley & Sons, New York

Fendorf S, Michael HA, van Geen A (2010) Spatial and temporal variations of groundwater arsenic in South and Southeast Asia. Science 328(28):1123–1127. doi:10.1126/science.1172974

Ferguson G, Gleeson T (2012) Vulnerability of coastal aquifers to groundwater use and climate change. Nat Clim Change 2:342–345

Goswami R, Villholth KG, Vithanage M, Clement TP, Sakaki T, Illangasekare T, Jensen KH (2007) Variable density transport during well rehabilitation after a tsunami-induced saltwater contamination event. Paper presented at the ModelCARE conference, Copenhagen, 10–13 Sept 2007

Hinrichsen D (2007) Ocean planet in decline. Available: [online] http://www.peopleandplanet.net/?lid=26188&topic=44&section=35. Accessed 31 July 2012

Hiroshiro Y, Jinno K, Berndtsson R (2006) Hydrogeochemical properties of a salinity-affected coastal aquifer in western Japan. Hydrol Proc 20(6):1425–1435. doi:10.1002/hyp. 6099

Illangasekare T, Tyler SW, Clement TP, Villholth KG, Perera APGRL, Obeysekera J, Gunatilaka A, Panabokke CR, Hyndman DW, Cunningham KJ, Kaluarachchi JJ, Yeh WW-G, Van Genuchten M-R, Jensen KH (2006) Impacts of the 2004 tsunami on groundwater resources in Sri Lanka. Water Resour Res 42(5):W05201. doi:10.1029/2006WR004876

Institute for Global Environmental Strategies (IGES) (2007) Sustainable groundwater management in Asian cities. IGES, Kanagawa, 157 pp. ISBN 4-88788-039-9

Institute of Southeast Asian Studies (ISEAS) (2009) Urbanisation in Southeast Asian countries. ISEAS, Singapore, 78 pp

Jayasekera DL, Kaluarachchi JJ, Villholth KG (2010) Groundwater stress and vulnerability in rural coastal aquifers under competing demands: a case study from Sri Lanka. Environ Monit Assess 176(1–4):13–30. doi:10.1007/s10661-010-1563-8

Johnston R, Hoanh CT, Lacombe G, Lefroy R, Pavelic P, Fry C (2012) Managing water in rainfed agriculture in the Greater Mekong subregion. Final report. International Water Management Institute (IWMI), Colombo; Swedish International Development Cooperation Agency (Sida), Stockholm

King C (2003) Urban groundwater systems in Asia. UNU/IAS Working Paper No. 101, 27 pp

Konikow LF (2011) Contribution of global groundwater depletion since 1900 to sea-level rise. Geophys Res Lett 38:L17401. doi:10.1029/2011GL048604

Liu J, Zheng CM, Zheng L, Lei YP (2008) Ground water sustainability: methodology and application to the North China Plain. Ground Water 46(6):897–909. doi:10.1111/j.1745-6584.2008.00486.x

Mukherji A, Villholth KG, Sharma BR, Wang J (eds) (2009) Groundwater governance in the Indo-Gangetic and Yellow River Basins: realities and challenges, vol 15, IAH – selected papers on hydrogeology. CRC Press, Boca Raton, 325 pp. ISBN 978-0-415-46580-9

Mulligan AE, Charette MA (2009) Groundwater flow to the coastal ocean. In: John HS, Karl KT, Steve AT (eds) Encyclopedia of ocean sciences. Academic, Oxford, pp 88–97

Nguyen Thi H, Dang Tran T, Ito N (2008) Rapid declining of groundwater level in Hanoi. In: Proceedings of 36th IAH congress, Toyama, Oct 2008

Nguyen TQ, Helm DC (1995) Land subsidence due to groundwater withdrawal in Hanoi, Vietnam. In: Land subsidence: proceedings of the fifth international symposium on land subsidence, The Hague, Oct 1995. IAHS Publ. no. 234, pp 55–60

Onodera S-I, Saito M, Sawano M, Hosono T, Taniguchi M, Shimada J, Umezawa Y, Lubis RF, Buapeng S, Delinom R (2009) Erratum to "effects of intensive urbanization on the intrusion of shallow groundwater into deep groundwater: examples from Bangkok and Jakarta". Sci Total Environ 407:3209–3217. doi:10.1016/j.scitotenv.2009.01.049

Rejani R, Jha MK, Panda SN, Mull R (2008) Simulation modeling for efficient groundwater management in Balasore Coastal Basin, India. Water Resour Manage 22:23–50. doi:10.1007/s11269-006-9142-z

Shanmugam P, Neelamani S, Ahn Y-H, Philip L, Hong G-H (2007) Assessment of the levels of coastal marine pollution of Chennai city, Southern India. Water Resour Manage 21:1187–1206. doi:10.1007/s11269-006-9075-6

Shanzhong Q, Zulu Z, Zhaopei Z, Qiaoyu G, Yan Z (2007) Saltwater intrusion in the Laizhou Gulf, Shandong Province, China: causes and its impact on coastal areas. AMBIO J Hum Environ 36 (4):361–362. doi:10.1579/0044-7447(2007) 36[361:SIITLG]2.0.CO;2

Singh SB, Veeraiah B, Dhar RL, Prakash BA, Rani MT (2011) Deep resistivity sounding studies for probing deep fresh aquifers in the coastal area of Orissa, India. Hydrogeol J 19:355–366. doi:10.1007/s10040-010-0697-7

Small C, Nicholls RJ (2003) A global analysis of human settlement in coastal zones. J Coast Res 19:584–599

South GR, Skelton PS, Veitayaki J, Resture A, Carpenter C, Pratt C, Lawedrau A (2004) The global international waters assessment for the Pacific Islands: aspects of transboundary, water shortage, and coastal fisheries issues. Ambio 33(1):98–106

Sugio S, Nakada K, Urish DW (1987) Subsurface seawater intrusion barrier analysis. J Hydraul Eng 113(6):767–779. doi:10.1061/(ASCE)0733-9429(1987) 113:6(767)

Sukhija B (2011) Tsunamis: risk assessment and management of groundwater resources. In: Vrba J, Verhagen BT (eds) Groundwater for emergency situations – a methodological guide, vol 3, IHP-VII series on groundwater. UNESCO, Paris, pp 158–166

Sukhija B, Rao BSRN (2011) Impact of the October 1999 super cyclone on the groundwater system and identification of groundwater resources for providing safe drinking water in coastal Orissa, India. In: Vrba J, Verhagen BT (eds) Groundwater for emergency situations – a methodological guide, vol 3, IHP-VII series on groundwater. UNESCO, Paris, pp 258–272

Sun R, Jin M, Giordano M, Villholth K (2009) Urban and rural groundwater use in Zhengzhou, China: challenges in joint management. Hydrogeol J 17(6):1495–1506

Taniguchi M, Burnett WC, Cable JE, Turner JV (2002) Investigation of submarine groundwater discharge. Hydrol Process 16:2115–2129. doi:10.1002/hyp. 1145

Taniguchi M, Burnett WC, Dulaiova H, Siringan F, Foronda JM, Wattayakorn G, Rungsupa S, Kontar EA, Shirshov PP, McManus L (2005) Groundwater discharge as an important land-sea pathway in Southeast Asia. Final Report for APN Project 2004-16NSY, 64 pp

Tran LT, Larsen F, Pham NQ, Christiansen AV, Tran N, Vu HU, Tran LV, Hoang HV, Hinsby K (2012) Origin and extent of fresh groundwater, salty paleowaters and recent saltwater intrusions in Red River flood plain aquifers, Vietnam. Hydrogeol J. doi:10.1007/s10040-012-0874-y

Umezawa Y, Miyajima T, Kayanne H, Koike I (2002) Significance of groundwater nitrogen discharge into coral reefs at Ishigaki Island, southwest of Japan. Coral Reefs 21:346–356. doi:10.1007/s00338-002-0254-5

United Nations Department of Economic and Social Affairs (UNDESA) (2010) Trends in sustainable development: small island developing states. Division for Sustainable Development, UNDESA, New York, 35 pp. ISBN 978-92-1-104610-6

United Nations International Strategy for Disaster Reduction (UNISDR) (2009) Risk and poverty in a changing climate – invest today for a safer tomorrow. 2009 Global assessment report on disaster risk reduction. United Nations, Geneva, 210 pp. ISBN 978-92-1-132028-2

van der Gun J (2012) Groundwater and global change: trends, opportunities and challenges. Side publication series: 01.4th UNESCO World Water Development Report. UNESCO, Paris, 38 pp

van der Linden W (2011) The effect of the 2004 tsunami on groundwater in the Maldives islands. In: Vrba J, Verhagen BT (eds) Groundwater for emergency situations – a methodological guide, vol 3, IHP-VII series on groundwater. UNESCO, Paris, pp 285–295

van Weert F, van der Gun J, Reckman J (2009) Global overview of saline groundwater occurrence and genesis. IGRAC Report nr. GP 2009, IGRAC, Utrecht. 1.104 pp

Villholth KG, Neupane B (2011) Tsunamis as long-term hazards to coastal groundwater resources and associated water supplies. In: Mokhtari M (ed) Tsunami – a growing disaster. InTech, Rijeka, Croatia. pp 87–104. ISBN 978-953-307-431-3

Villholth KG, Jeyakumar P, Amerasinghe PH, Manamperi ASP, Vithanage M, Goswami RR, Panabokke CR (2010) Tsunami impacts and rehabilitation of groundwater supply: lessons learned from eastern Sri Lanka. In: Jha MK (ed) Natural and anthropogenic disasters: vulnerability, preparedness and mitigation. Capital Publishing Company, New Delhi/Springer, Dordrecht, pp 82–99. ISBN 978-90-481-2497-8

Villholth KG, Jeyakumar P, Amerasinghe PH, Manamperi ASP, Vithanage M, Goswami RR, Panabokke CR (2011) Tsunami impacts and rehabilitation of groundwater supply: lessons learned from eastern Sri Lanka. In: Vrba J, Verhagen BT (eds) Groundwater for emergency situations – a methodological guide, vol 3, IHP-VII series on groundwater. UNESCO, Paris, pp 296–308

Vithanage M, Villholth KG, Mahatantila K, Engesgaard P, Jensen KH (2009) Effect of well cleaning and pumping on groundwater quality of a tsunami-affected coastal aquifer in eastern Sri Lanka. Water Resour Res 45:W07501. doi:10.1029/2008WR007509

Vithanage M, Villholth KG, Engesgaard P, Jensen KH (2010) Vulnerability analysis of the coastal sandy aquifers in the east coast of Sri Lanka with recharge change consideration. Open Hydrol J 4:173183

Vithanage M, Engesgaard P, Villholth KG, Jensen KH (2011) The effect of 2004 tsunami on a coastal aquifer in Sri Lanka. Ground Water. doi:10.1111/j.1745-6584.2011.00893.x

Vrba J, Salamat AR (2007) Groundwater for emergency situations. In: Proceedings of an international workshop, Tehran, 29–31 Oct 2006. UNESCO-IHP VI, Series on groundwater, vol 5. UNESCO, Paris, 128 pp.

Vrba J, van der Gun J (2004) The world's groundwater resources. Contribution to Chapter 4 of WWDR-2 (Draft). IGRAC Report Nr IP 2004-1. IGRAC, Utrecht, 10 pp

Vrba J, Verhagen BTh (2006) Groundwater for emergency situations: a framework document. UNESCO-IHP VI, Series on groundwater, vol 12. UNESCO, Paris, 94 pp

Vrba J, Verhagen BT (eds) (2011) Groundwater for emergency situations – a methodological guide. UNESCO, vol 3, IHP-VII Series on Groundwater. UNESCO, Paris, 316 pp

Wada Y, van Beek LPH, Weiland FCS, Chao BF, Wu Y-H, Bierkens MFP (2012) Past and future contribution of global groundwater depletion to sea-level rise. Geophys Res Lett 39:L09402. doi:10.1029/2012GL051230

Werner AD, Alcoe DW, Ordens CM, Hutson JL, Ward JD, Simmons CT (2011) Current practice and future challenges in coastal aquifer management: flux-based and trigger-level approaches with application to an Australian case study. Water Resour Manage 25:1831–1853. doi:10.1007/s11269-011-9777-2

WHYMAP (2008) World-wide Hydrogeological Mapping and Assessment Programme. http://www.whymap.org/. Accessed 9 May 2012

World Bank (2005) Natural disaster hotspots – a global risk analysis. World Bank, Washington, DC, 132 pp. ISBN 0-8213-5930-4

World Health Organization (WHO) (2011) Cleaning wells after seawater flooding. Technical notes on drinking-water, sanitation and hygiene in emergencies, No. 15. WHO, Geneva. http://www.who.int/water_sanitation_health/publications/2011/tn15_cleaning_wells_en.pdf. Accessed 6 Aug 2012

Xue Y, Wu J, Liu P, Wang J, Jiang Q, Shi H (1993) Sea-water intrusion in the coastal area of Laizhou Bay, China: 1. Distribution of sea-water intrusion and its hydrochemical characteristics. Ground Water 31:532–537. doi:10.1111/j.1745-6584.1993.tb00584.x

Zaisheng H, Hao W, Rui C (2006) Transboundary aquifers in Asia with special emphasis to China. Paper prepared for ISARM, UNESCO Office Beijing, 43 pp

Chapter 16
Coastal Groundwater and Its Supporting Role in the Development of Gunungsewu Geopark, Java, Indonesia

Sari Bahagiarti Kusumayudha

Abstract Gunungsewu is the largest tropical karst terrain in Southeast Asia. It is about 800 km^2 across, and made up of around 45,000 cones and domes. It is part of Central Java, and lies within Yogyakarta and east Java provinces. Now the area is being developed as a national geopark and so facilities fresh water sources must be adequate. In fact, Gunungsewu is always subject to water shortages, especially in the dry season. The aquifer at Gunungsewu is predominantly a reef limestone, with conduit flow and a subterranean drainage system that discharges to the Indian Ocean through coastal springs. The occurrence of these springs is usually associated with unique hydrogeological phenomena and beautiful landscapes. Because of the very rough topography and steep cliffs, and the difficulty of access, fractal geometry analyses were used to explore the existence of groundwater discharges in the coastal area. The analyses show a good correlation between the fractal dimension value of coastal shoreline and the existence of springs. Shoreline segments with a fractal dimension (D) higher than 1.30 have potential for the existence of coastal springs, whereas when the fractal dimension is less than that, there are no springs. Baron is the biggest verified coastal spring in the Gunungsewu Area, with an average flow rate of 9,000 l/s, and the physical and chemical qualities of its water are within the drinking water standards. This indicates that the coastal springs in the Gunungsewu Area have the potential to support the development of a geopark, as additional fresh water sources, as well as being geosites or geoheritage locations.

S.B. Kusumayudha (✉)
Geology Department, Faculty of Mineral Technology, UPN "Veteran" Yogyakarta, Indonesia
e-mail: saribk@gmail.com

C. Wetzelhuetter (ed.), *Groundwater in the Coastal Zones of Asia-Pacific*,
Coastal Research Library 7, DOI 10.1007/978-94-007-5648-9_16,

16.1 Introduction

Gunungsewu is the largest tropical karst terrain in Southeast Asia. It is about 800 km^2 in extent, and comprises around 45,000 hills displaying specific morphology, i.e. the existence of dolines, uvalas, poljes, and caves (Kusumayudha 2005). The area is currently being developed as a national geopark, with integrated preservation of significant examples of geological heritage in a strategy for sustainable, regional socio-economic and cultural development, and safeguarding the environment (UNESCO 2010).

In order to set the Gunungsewu Area up as a national geopark, the facilities must be adequate, including the availability of fresh water sources. For a long time, however, Gunungsewu has been well known as an area that was subject to water shortages, especially in the dry season. This deficiency occurs particularly in the middle of the area. The basic problem is where to obtain water locally, in order to avoid importing it. Imports will be inefficient and costly.

In the southern parts of Gunungsewu there are plenty of groundwater discharges from subsurface rivers, channels, and conduits to the sea, referred to in general as "coastal springs". The occurrence of coastal springs is generally associated with a variety of unique hydrogeological phenomena and beautiful landscapes. At present, the water from these springs is not used optimally to fulfill the fresh water supply needs, and this is especially true in relation to support of the development of a geopark. While the resource seems to be adequate with respect to quantity and quality, more information is needed on the potential available. The springs need to be explored and identified.

16.1.1 Location

The physiographic map produced by Van Bemmelen (1949) can be used as a base. It shows that the study area is in the Southern Mountains of East Java, although it belongs administratively to the territories of Yogyakarta Special Province, and the provinces of Central Java and East Java, including the regencies of Gunung Kidul, Wonogiri, and Pacitan (Fig. 16.1). Geographically it lies between latitudes 6° 10′ and 6° 30′, and longitudes 99° 35′ and 100° 00′. The area can be reached easily by four-wheel drive vehicle from Yogyakarta City, and the towns of Wonogiri and Pacitan. It is about 25 km south east of Yogyakarta.

16.1.2 Objectives

The objective of this study is to explore and analyse the existence of coastal springs in the Gunungsewu Area, in order to obtain information on both their hydrogeological characters and their potential to contribute to the development of the area as a national geopark.

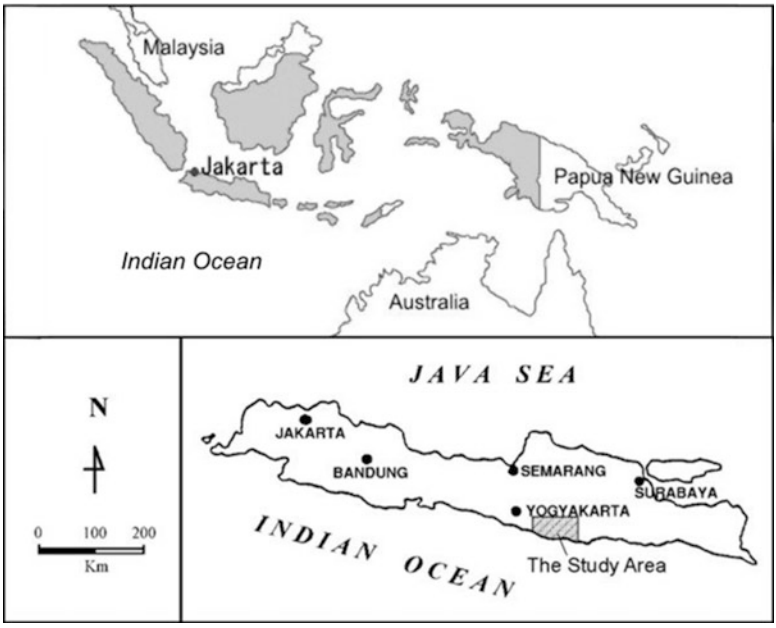

Fig. 16.1 Location of the study area [Derived from Van Bemmelen (1949)]

16.2 Method of Study

The approach applied in this study is an analytical method using primary and secondary data. The primary data were derived from field surveying and mapping, while the secondary data were collected from pre-existing studies. Flow rate measurement and water sampling were carried out at Baron Spring for physical and chemical water quality testing.

Kusumayudha (2009) applied fractal analysis to explore and identify the occurrence of coastal springs in the Gunungsewu Area. In order to do this, aerial photographs at 1:30,000 scale were used to trace and reprint the shoreline pattern of the study area. The curve of the shoreline was then divided into segments about 2 km long and the fractal dimension of the curve of each segment was determined using the box counting method.

Fractal terminology is used to determine non-euclidean objects, which have non-integer dimensions (Mandelbrot 1983). In essence, a simple (original) shape grows more complex as it is repeated in miniature around the edges of the original shape (Xie 1993). A fractal object usually shows a unique shape that is infinite, swirling and complex. In this study, the curve of shoreline is assumed to be fractal.

Some characteristics of fractals are self-similarity, self-affinity, self-inverse, and self-squaring (Peitgen et al. 1992). A fractal scaling system is specified by a non-integer number called fractal dimension (Mandelbrot 1983), which can be used

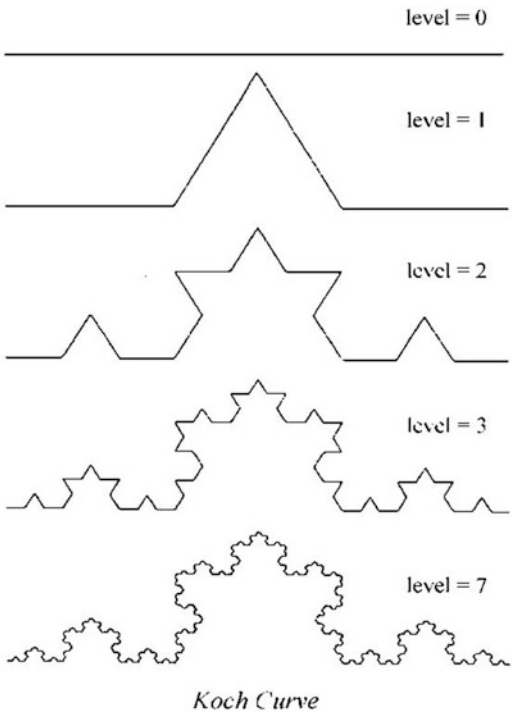

Fig. 16.2 Koch curve, a model of similarity fractal (Mandelbrot 1983)

to quantify the degree of fractal irregularity (Sukmono 1996). Fractal objects themselves are classified into some types, i.e. self similar fractal (Fig. 16.2), self affine fractal, self inverse fractal, self squaring fractal, and complex fractal. The dimensions of self similar, self affine, self squaring, and self inverse fractals can be determined by a similarity method, but the dimension of a complex fractal will need to be computed by other methods which are applicable for statistical fractal, e.g. objects that statistically show fractal configuration.

There are several methods by which a fractal dimension can be determined. These include similarity, cantor dust, ball covering, sandbox, and box counting (Mandelbrot 1983). Kusumayudha (2009) used box-counting. The fractal dimension (D) is determined by drawing grids with known side length (r) over the fractal object and applying Tricot's equation (1996):

$$D = \lim_{r \to 0} \frac{\log Nr(F)}{-\log r} \tag{16.1}$$

Where $Nr(F)$ is the number of boxes that cover the fractal set (F), and r is the length of the box side.

16.3 Geology

According to Van Bemmelen (1949), the Southern Mountains of East Java consist of three physiographic sub-zones, the Baturagung Range, the Panggung Massive, and the Plopoh Range in the north; the Wonosari Plateau in the central area; and the Gunungsewu Sub-zone in the south. The area displays a unique karst topography, with about 45,000 cones and domes, closed basins, caves, shafts, and sinkholes. In all, it is about 800 km^2 across (Kusumayudha 2005). The general disposition of features in the area can be seen from satellite image in Fig. 16.3.

The geology of the Gunungsewu Area consists mainly of Tertiary volcanic rocks and karstic limestone. The formations exposed are predominantly carbonate rocks, including the Oyo, the Wonosari, and the Kepek formations. This group is underlain by a unit of volcanic deposits of the Semilir, Nglanggran, and Besole formations. In some parts, the Sambipitu Formation is found as another bedrock unit of the Gunungsewu Limestone (Kusumayudha 2005). The geology of the area is shown in the map in Fig. 16.4.

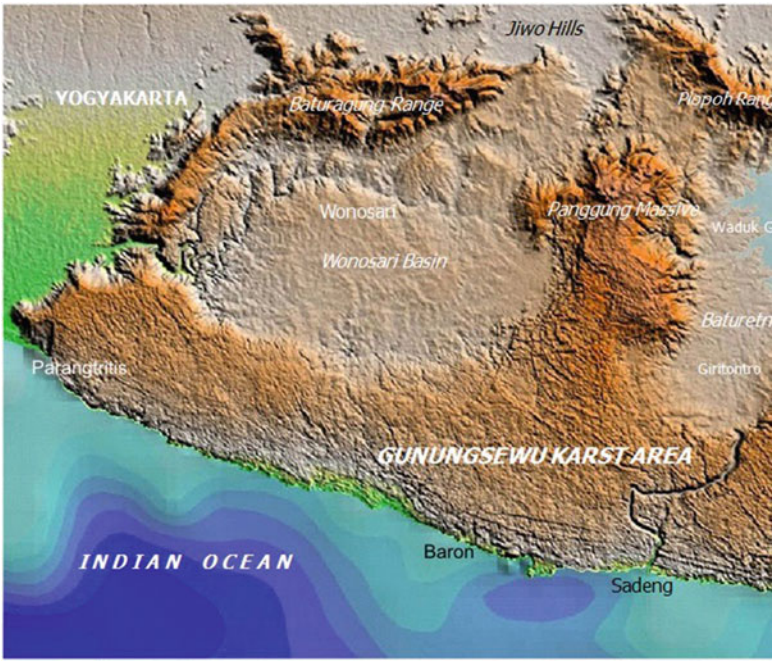

Fig. 16.3 Satellite image of the Gunungsewu Area (Pacitan Regency data 2011)

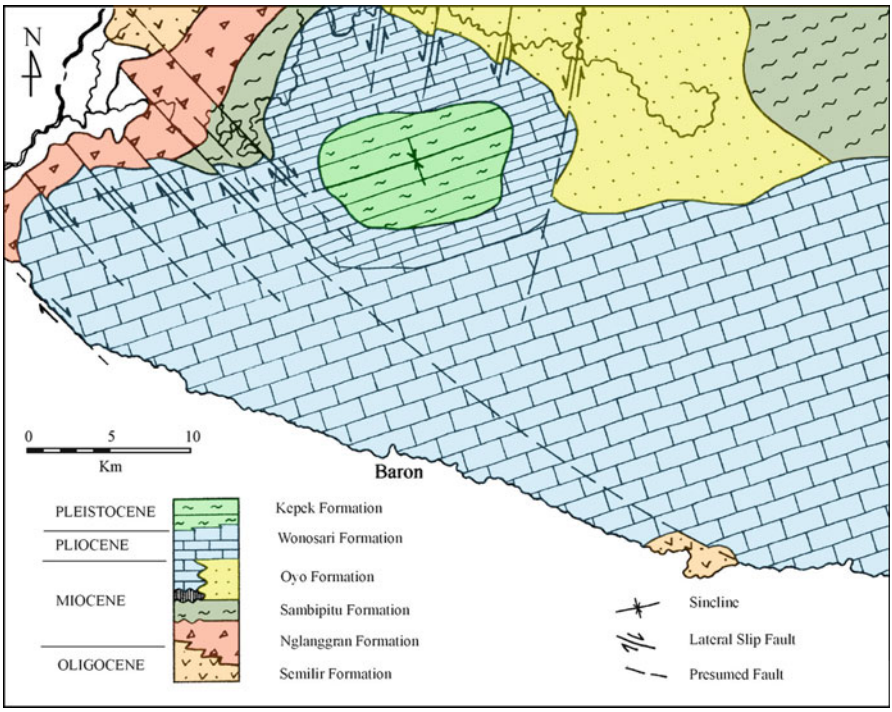

Fig. 16.4 Geological map of the Gunungsewu Area (Kusumayudha 2005)

16.3.1 Stratigraphy

The rock formations in the Gunungsewu Area, taken in standard geological order from the oldest to the youngest, are:

Semilir Formation
Sedimentary rocks deposited in a deep sea environment and comprising andesitic tuffs, sandstones, tuffaceous sandstones, lapilli, agglomerates, claystone, siltstone, shale, and andesitic to basaltic breccia. The formation is of Oligocene to early Miocene age (Kusumayudha 2005).

Nglanggran/Besole Formation
This formation overlies the Semilir Formation conformably, but with an interfingered relationship in some places.

The Nglanggran Formation consists predominantly of andesitic to basaltic breccias, lava deposits, agglomerates, poly-mixed breccias, sandstones, and tuffaceous sandstones. Limestone blocks can be found as exotic fragments in the volcanic breccias at times. The formation was deposited during Mid-Oligocene to middle Miocene (Kusumayudha 2005).

Sambipitu Formation
This marine sedimentary sequence overlies the Nlanggran Formation conformably but with an interfingering relationship. It consists of marl, mudstone, interbedded calcareous sandstones, and tuffaceous sandstones, and is of middle Miocene age (Kusumayudha 2005).

Taken together, these formations – the Semilir, Nglanggran and Sambipitu formation – comprise the basement of the carbonate sequence in Gunungsewu.

Oyo Formation
The Oyo Formation comprises bedded and sandy limestones, calcarenites, marl, marly sandstones, and marly-tuffaceous sandstones. The stratigraphic relationship between the Oyo and Sambipitu formations is conformable in some places but interfingered in others. The Oyo Formation is middle Miocene to Mid-Pleistocene in age (Kusumayudha 2005).

Wonosari Formation
The Wonosari Formation consists of bedded and massive limestones, and reefs. It has two distinct characters – i.e. karstic and chalky (caliche). The karstic limestone is typically cavernous, while the chalky limestone is characterized by its intergranular porosity. This formation is of middle Miocene to Pliocene age (Kusumayudha 2005).

Kepek Formation
The major components of the Kepek Formation are claystone, sandy marl, calcarenite and bedded limestone. They were deposited in an isolated, shallow marine, environment during the upper Pliocene to Pleistocene (Kusumayudha 2005).

Terra Rossa and Merapi Deposits
The youngest lithology in the Gunungsewu area is Terra Rossa, although there are also deposits from Merapi Volcano and of alluvium. The latter consists of clay, silt, sands, granules, gravels and cobbles, as well as flora remnants. On the other hand, the Merapi deposits comprise fine-grained pyroclastics such as sands, volcanic ash and dust.

16.3.2 Geological Structures and History

The Southern Mountains, which are the principal feature of the area, were uplifted and subject to folding. The axis of the syncline in the center the mountains trends northeast (N75°E – N255°E). Topographically, this area comprises a plain known as the Wonosari Plateau. In the south, the Gunungsewu Sub-zone incorporates a homocline dipping about 5–15° southward. There is also a fissure system, present as joints, cracks and faults, with major orientations northwest-southeast and northeast-southwest (Kusumayudha 2005).

The geological history of Gunungsewu began the Oligocene, and was initiated by volcanism that produced the basement rocks of the Semilir and Nglanggran

formations. The tectonic environment of the area was a magmatic arc, with subduction of the Indo-Australian plate beneath the Eurasian plate during the Tertiary (Suyoto 1994). The volcanism was followed by the deposition of carbonate rocks of the Sambipitu, Oyo, Wonosari and Kepek formations respectively, in the period from the middle Miocene to the Pliocene. The process continued with the uplifting and folding that brought the carbonates to exposure. Subsequent interaction of the carbonate rocks under the influence of exogenic processes in tropical conditions, led to the formation of the karst topography.

Surface processes occurred during the Quaternary. The influence of volcanism from the northern side of Gunungsewu led to the development of the Terra Rossa deposits, found the dolines, uvalas and poljes of the karst basins.

16.4 Hydrogeology

The Gunungsewu Area is a representative of a specific, karst hydrogeologic system that is unique as it is composed predominantly of reef limestone. Physically the limestone tends to show karstification and calcification, and both limestone types can function as good aquifers (Kusumayudha 2004). The difference in the physical characteristics of the two types is in their porosity modes. Secondary conduit systems occur in the karstic limestone, whilst an intergranular system exists in the chalky limestone (caliche). The occurrence of the caliche or chalky limestone is usually localised, and so it tends to form perched aquifers (Kusumayudha et al. 1999).

Sir Murdoch MacDonald & Partners (1979) using dye tracers to verify that some subterranean rivers in the Gunungsewu Area discharge to the sea through the Baron coastal spring – see also Kusumayudha (2005). The results of a reconstruction based on a gravity anomaly map (Kusumayudha and Santoso 1998) and the geological structure pattern suggest that a subterranean drainage system, with a main river and tributary channels, is present. This river system discharges to the Indian Ocean through coastal springs, as shown in the hydrogeological model in Fig. 16.5. The subsurface flow pattern and networks in the Gunungsewu are thought most likely to be controlled by fracture structures (Kusumayudha et al. 1999; Kusumayudha 2005).

16.4.1 Existence of Coastal Springs and Fractal Geometry

More than 36 springs are known along the coastal area and surroundings of Gunungsewu, between Ngrenean Beach in the west and Sadeng Beach in the east. Apart from Ngobaran and Baron springs, the flow rates decrease significantly, in general, in the dry season. The rate of flow at Ngobaran Spring is about 200–500 l/s, while Baron Spring flows at around 9,000 l/s. The flow rates of the other springs are typically only 50 l/s or less (Kusumayudha 2009).

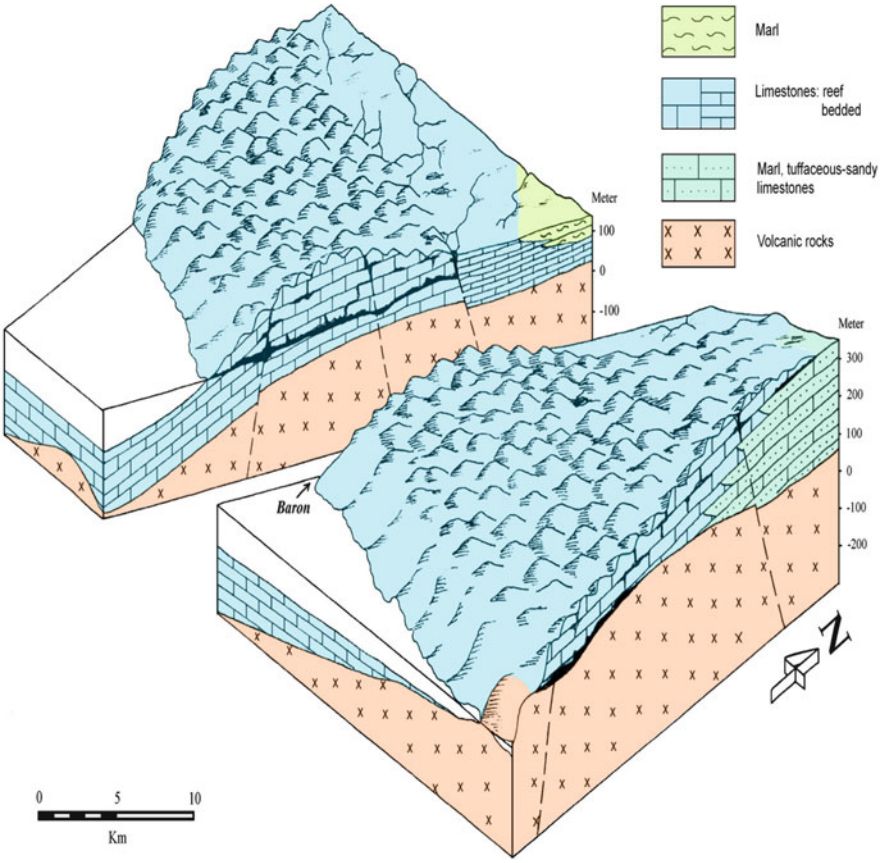

Fig. 16.5 Block diagram showing the conceptual hydrogeological model of Gunungsewu Area (derived from Kusumayudha 2005)

Some coastal areas are difficult to reach because of the very rough topography and steep cliffs. A suitable method is required in order to try to determine the possibility of the existence of more springs. In the Gunungsewu Area, fractal geometry analysis was applied (Kusumayudha 2009). This method can be used to quantify the shape of the shoreline in the coastal part of the karstic zone. The results of the analysis showed that the fractal dimension of the shoreline ranges from 1.230 ± 0.01 to 1.665 ± 0.01 (Kusumayudha 2009).

There is an apparent correlation between the fractal dimension value of the shoreline of a coast and the existence of springs. Shoreline segments with fractal dimensions (D) higher than 1.30 have relatively greater potential for the existence of coastal springs, whereas springs are absent in the segments with fractal dimensions less than 1.30 (Kusumayudha 2009).

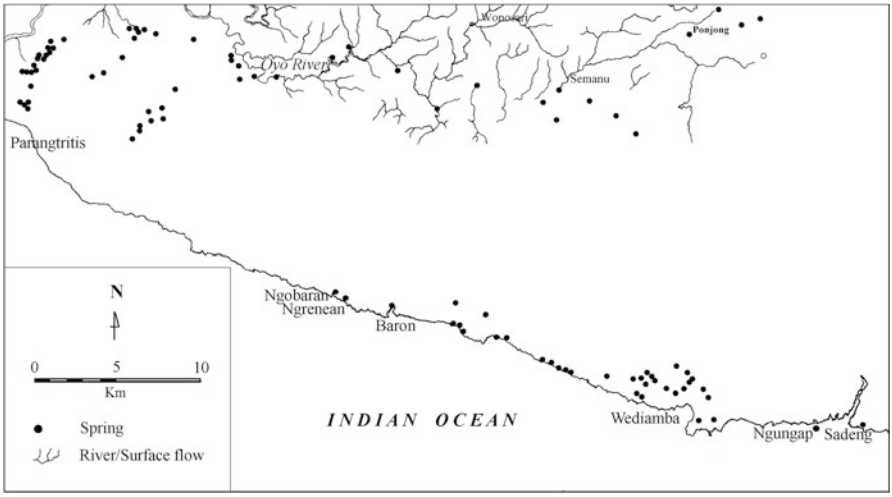

Fig. 16.6 Location of springs identified in Gunungsewu Area (Adapted and revised from Kusumayudha 2005)

Fig. 16.7 Groundwater outlet at Baron Beach in the dry season, the average rate of flow is 9,000 l/s (August 2010) (The photograph was taken in September 2010)

Figure 16.6 shows the locations of springs in the Gunungsewu Area. Figure 16.7 shows the situation at Baron Spring in the dry season. The fractal dimensions of the shoreline are set out in Table 16.1.

16.4.2 Characteristics and Conceptual Model

Baron is the largest verified coastal spring in the Gunungsewu Area. It rises from the karstic limestone of the Wonosari Formation, which is underlain by volcanic

Table 16.1 Fractal dimensions of the shorelines and the existence of coastal springs (Kusumayudha 2009)

Segment	Location	Fractal dimension (D)	Spring	Flow rate (l/s)	Remarks
1	Teluk Becici	1.230 ± 0.01	Absent		Verified
2	Teluk Pule – Gebangkara	1.284 ± 0.01	Absent		Verified
3	Teluk Nunggah – Karangtelu	1.445 ± 0.01	Unknown	?	Presumed
4	Pantai Gesing	1.251 ± 0.01	Absent		verified
5	Ngobaran – Ngrenean	1.382 ± 0.01	Present	200	Verified
6	Teluk Baron – western coast	± 0.01	Present	300	Verified
7	Kukup – Spanjang – Drini	1.239 ± 0.01	Absent		Verified
8	Watulawang	1.315 ± 0.01	Unknown	?	Presumed
9	Watulawang – Wediamba	1.308 ± 0.01	Present	1–30 (episodic)	Verified
10	Wediamba – western coast	1.365 ± 0.01	Unknown	?	Presumed
11	Eastern coast of Wediamba	1.355 ± 0.01	Unknown	?	Presumed
12	Ngungap – Sadeng	1.630 ± 0.01	Present	>5,000	Verified
13	Eastern coast of Sadeng – Tanjung Dadapan	1.448 ± 0.01	Present	5–50 (episodic)	Verified
14	Slili	1.324 ± 0.01	Present	50–200	Verified
15	Sundak	1.317 ± 0.01	Present	50–200	Verified
16	Baron Beach	1.665 ± 0.01	Present	9,000	Verified

? – no measurement

rocks of the Semilir and Nglanggran formations. The spring's water source is an underground conduit flowing from northern and central parts of the area. Data from field surveys show that there are many caves and shafts in the northern part of the area that are connected with subsurface flows. These include the Bribin, Seropan and Suci caves. The subsurface flows are generally derived from rivers that flow over the surface but sink into the sub-surface zone to become underground rivers. The latter then merge to form a "main flow", discharging to the south (the Indian Ocean) via coastal springs. A conceptual hydrogeological model of Baron Spring, based on logging data from ten boreholes, can be drawn on the basis of the geological and hydrogeological data, as shown in Fig. 16.8.

Measurement records covering the period 1998–2009 using current meter and static water level recorder show that the average flow of Baron Spring is 9,000 l/s. The maximum discharge at the peak of the rainy season reaches 20,000 l/s, while the minimum flow in the dry season is about 5,000 l/s. No water is taken from the spring for consumption, yet, but the discharge zone is used for recreation. This is because the water is assumed not to meet the fresh water quality standards, as it is very close to the open sea. In order to obtain information on the water quality from the spring, a sample was taken. Physically the sample is colorless, odorless, and tasteless. The total dissolved solids content (TDS) is 218 mg/l, the electrical conductivity (EC) is 362 μS/cm, and pH 8. Table 16.2 shows the hydrochemistry of the water sample taken from the Baron Spring compared to the groundwater quality elsewhere in the Gunungsewu Area (samples were taken from Cave Suci, Cave Seropan, Cave Bribin, and Cave Ngobaran).

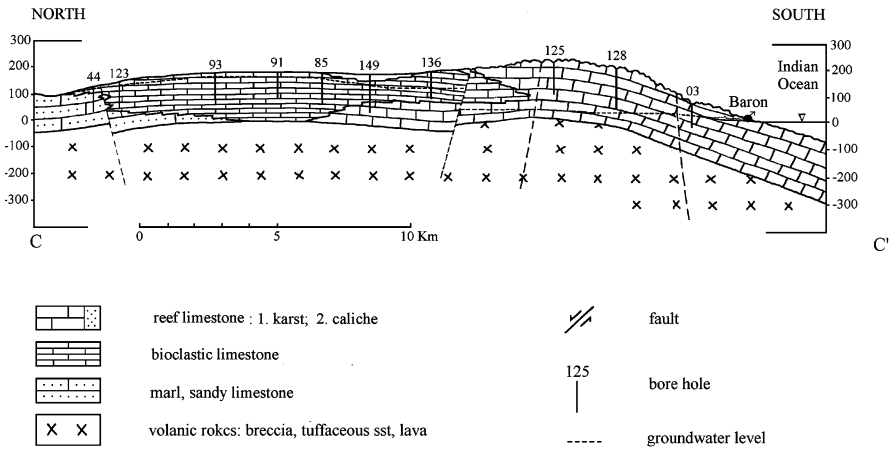

Fig. 16.8 Conceptual hydrogeological model of Baron Spring (Updated and revised from Kusumayudha 2005)

Table 16.2 Groundwater chemistry of the study area compared to that of Baron Spring

	Concentration (mg/l)	
Analyte	Gunungsewu area (Kusumayudha 2005)	Baron coastal spring 2005
Ca	35.00–51.56	34.67
Mg	8.00–20.00	18.31
Na	3.50–12.00	6.51
K	>LoD[a]	>LoD
Fe	>LoD – 0.15	>LoD
Cl	4.00–7.00	5.95
HCO_3	109.00–191.00	177.86
CO_3	>LoD – 6.00	>LoD
SO_4	>LoD – 7.00	0.05
NO_3	1.56–3.00	2.65
PO_4	0.02–0.04	0.02
SiO_2	10.00–15.62	14.26

[a]>LoD indicates that the concentration of the analyte in the sample or samples was below the limit of detection of the analytical methods used

The groundwater from Baron Spring is of calcium-bicarbonate type, and the concentration of all of the chemical compounds determined is reported as being below – i.e., within – that of the drinking water standard.

16.4.3 Support for the Development of the Geopark

Fresh water in Gunungsewu is actually groundwater from subterranean rivers, which discharge to the Indian Ocean via coastal springs arising from the karst hydrogeology. They have a unique interaction with sea water. The big springs are

Fig. 16.9 Scenery on the Ngobaran coast, where there is a coastal spring with a discharge flow rate of 200–500 l/s

influenced and contaminated very little by sea water, but some of the smaller springs seem to be disturbed by the tides. The flow rate from these smaller springs usually decreases in the dry season. The situation at the Baron and Ngobaran springs is different, however, as the water remains fresh throughout the long dry season, and the concentrations of the dissolved chemical species remain below those set in the drinking water standards.

Geomorphologically, the coastal springs in the study area are generally associated with beautiful landforms, which makes them attractive tourism locations. With respect to the development of the area as a geopark, the existence of the coastal springs is a useful contribution as they provide a unique hydrogeological phenomenon as well as beautiful landscapes with interesting views across the open sea (Fig. 16.9). Because of this, they have a role as geosites or geoheritage sites, and will need to be conserved. Apart from this combined tourism and conservation aspect, the springs have the potential to support fresh water demand from the local population and support the development of the geopark. As an example of the potential, the average rate of discharge of fresh water from Baron Spring is 9,000 l/s.

16.5 Conclusions

The coastal springs in the Gunungsewu Area are controlled by a unique hydrogeological (karst) system with conduit flow. The springs are supplied originally from "normal" surface rivers that sink and become subterranean. They discharge to the Indian Ocean. The lithology comprising the karst is limestone of

Wonosari Formation, underlain by volcanic formations consisting of tuffaceous sandstone, breccias, and lava of the Semilir and Nglanggran formations. The largest coastal spring that has been identified is the Baron Spring, which has an average rate of discharge of 9,000 l/s.

According to Kusumayudha (2009), fractal geometric analysis can be applied to explore the occurrence of spring in remote areas. The results of fractal analysis of the type recommended show that the existence of springs can be correlated to the curve of shorelines that have a fractal dimension greater than 1.3.

Analysis of water from the Baron Spring has shown that its physical and chemical characteristics are within the levels prescribed by the drinking water standards. It is assumed that the quality of the water from the Baron Spring is representative of that from other springs in the area.

The existence of coastal springs in the Gunungsewu Area has the potential to contribute in two important roles with respect to the development of the area as a national geopark. They are their potential as additional fresh water sources, and their value geosites or geoheritage sites. The latter arises because the springs are generally associated with unique hydrogeological phenomena and beautiful coastal landscapes.

References

Kusumayudha SB (2004) Introduction to karst hydrogeology. Karst Study Center UPN "Veteran" Yogyakarta. UPN "Veteran" Yogyakarta Publisher, Yogyakarta, 137 p

Kusumayudha SB (2005) Karst hydrogeology and fractal geometry of Gunungsewu area. Adicita Publisher Yogyakarta, 171 p

Kusumayudha SB (2009) Detecting springs in the coastal area of the Gunungsewu karst terrain, Yogyakarta Special Province, Indonesia, using fractal geometry analysis. Science & Technology Bulletin ("Majalah Iptek"). Surabaya Institute of Technology (ITS), Surabaya, pp 169–176

Kusumayudha SB, Santoso A (1998) Underground river of Gunungsewu based on gravity anomaly and the geologic structure patterns. In: Proceedings of the PIT HAGI XXIII, Bandung, pp 66–72

Kusumayudha SB, Zen MT, Notosiswoyo S, Gautama RS (1999) The hydrogeologic system of Gunungsewu. In: Proceedings of the IAGI The 28th annual convention, vol IV, Jakarta, pp 73–84

Mandelbrot BB (1983) The fractal geometry of nature. WH Freeman & Co, New York, 468 pp

Pacitan Regency (2011) Pacitan as a global geopark network. In: Seminar on scialization of Pacitan as Global Geopark Network, Pacitan, 20 July 2012

Sir MacDonald & Partners (1979) Gunung Kidul groundwater project final report. Geohydrology, vol 3A, Department of Public Work Republic of Indonesia, Yogyakarta

Peitgen HO, Jurgen H, Saupe D (1992) Fractals for the classroom: part one introduction to fractals and chaos. Springer, New York, 450 pp

Sukmono S (1996) Fractal analysis on the seismicity of Sumatera active fault. In: Proceedings of the annual meeting, HAGI XX, Bandung, pp 78–83

Suyoto (1994) Stratigraphic sequence of the Gunungsewu carbonates. In: Proceedings of the PIT IAGI XXIII, vol 1, Yogyakarta, pp 19–32
Tricot C (1996) Curves and fractal dimension. Springer, Paris, 323 pp
UNESCO (2010) Guidelines and Criteria for National Geoparks seeking UNESCO's assistance to join the Global Geoparks Network (GGN). UNESCO, Paris, 12 pp
Van Bemmelen RW (1949) The geology of Indonesia, vol IA. Martinus Nijhoff, The Hague, 792 pp
Xie H (1993) Fractals in rock mechanics. A A Balkema, Rotterdam, 453 pp

Chapter 17
Gascoyne River, Western Australia; Alluvial Aquifer, Groundwater Management and Tools

L. Leonhard, K. Burton, and N. Milligan

Abstract The Carnarvon Horticultural Area adjacent to the Gascoyne River, Western Australia has since around 1928 grown to be the major supplier of fresh fruit and vegetables for the Perth region. Horticulture in this area is sustained by a small niche humid climatic zone within an arid environment with an annual rainfall generally less than 200 mm (8 in.). The Gascoyne River alluvial aquifer system is the sole source of "fresh" water for both the Carnarvon Horticultural Area and Carnarvon Township. This alluvial aquifer system comprises the River Bed Sand and an Older Alluvial Aquifer. Significant "fresh" groundwater is present within these alluvial aquifers, where groundwater storage is recharged only during brief restricted periods of river flow. Management of the Gascoyne River alluvial aquifer system has always been essential to ensure that the required quantity and quality of groundwater for both irrigated horticulture and town water can be sustained through extensive periods of no recharge (no flow). Groundwater management techniques have progressed from an early trial and error process referred to as the "Rules of the River" through to groundwater modelling techniques ranging from spreadsheets in the early 1980s to the current MODFLOW 2000. The Western Australian Department of Water has used the outputs of these processes, together with regular measurement of both groundwater level and salinity obtained from a network of observation bores, to ensure sustainability of the water supply to both the reticulated horticultural precinct and Carnarvon Township.

L. Leonhard (✉) • K. Burton
Department of Water, Perth, WA, Australia
e-mail: laz.leonhard@water.wa.gov.au

N. Milligan
Cymod Systems, Perth, WA, Australia

C. Wetzelhuetter (ed.), *Groundwater in the Coastal Zones of Asia-Pacific*,
Coastal Research Library 7, DOI 10.1007/978-94-007-5648-9_17,

17.1 Introduction

The town of Carnarvon is in the mid-west of Western Australia (WA) just south of the Tropic of Capricorn and approximately 950 km (600 miles) north northwest of Perth. The town is located at the mouth of the Gascoyne River adjacent to the Indian Ocean at a latitude of 24°53′02″S and longitude of 113°39′40″E (Fig. 17.1).

The combination of a localised mild humid environment together with the availability of fresh groundwater from the Gascoyne River alluvial aquifer has supported the development of the Carnarvon Horticultural Area (CHA) as an important source of fruit and vegetables for Perth metropolitan area. The major constraining factor on horticultural production is the ephemeral nature of the Gascoyne River, where river flow is required to recharge the alluvial aquifer system. The CHA has continued to be challenged by uncertainties related to maintaining an adequate, dependable and low salinity groundwater supply from an intermittent ephemeral river system.

This chapter summarizes the development of horticulture in Carnarvon area as related to the Gascoyne River alluvial aquifer system. The complexity of this alluvial system has been the basis of numerous studies and groundwater modelling exercises. Most of these studies have endeavoured to quantitatively establish the sustainable volume for groundwater abstraction in order to develop appropriate water use policies to ensure quality and quantity of the resource.

17.2 History

Carnarvon is one of WA's most important horticultural producing areas based on the use of the groundwater from the Gascoyne River alluvial system. There are currently 1,030 ha of land under horticultural production in the CHA. The gross value of the horticultural production in 2008 was $72.8 million for 34,500 t. Bananas are the highest value fruit crop; with an average yield of 43 t/ha (Hill 1993). Other crops producible in the CHA include tomatoes, capsicum, table grapes, oranges, cucumbers, melons, avocado, mandarin and pumpkins.

Horticultural activity in the Carnarvon region began with the planting of the first banana suckers in 1928 (Dodson 2009). Irrigated banana-growing was not on a large scale until after 1933 when the area was sub-divided. The irrigation water for these bananas was obtained from the Gascoyne River alluvial aquifer through unrestricted pumping of fresh groundwater from bores located within the plantation boundaries or from shallow wells located in the riverbed and banks. As the horticultural activities continued to develop and groundwater consumption steadily increased, it was observed that water in the riverbed sand was available for less time after recharge from each river flow. Growers in unfavourable locations adjacent to the river found it necessary to obtain part or all of their water supplies from deeper bores developed in the older alluvium of the Gascoyne River. Increased groundwater production

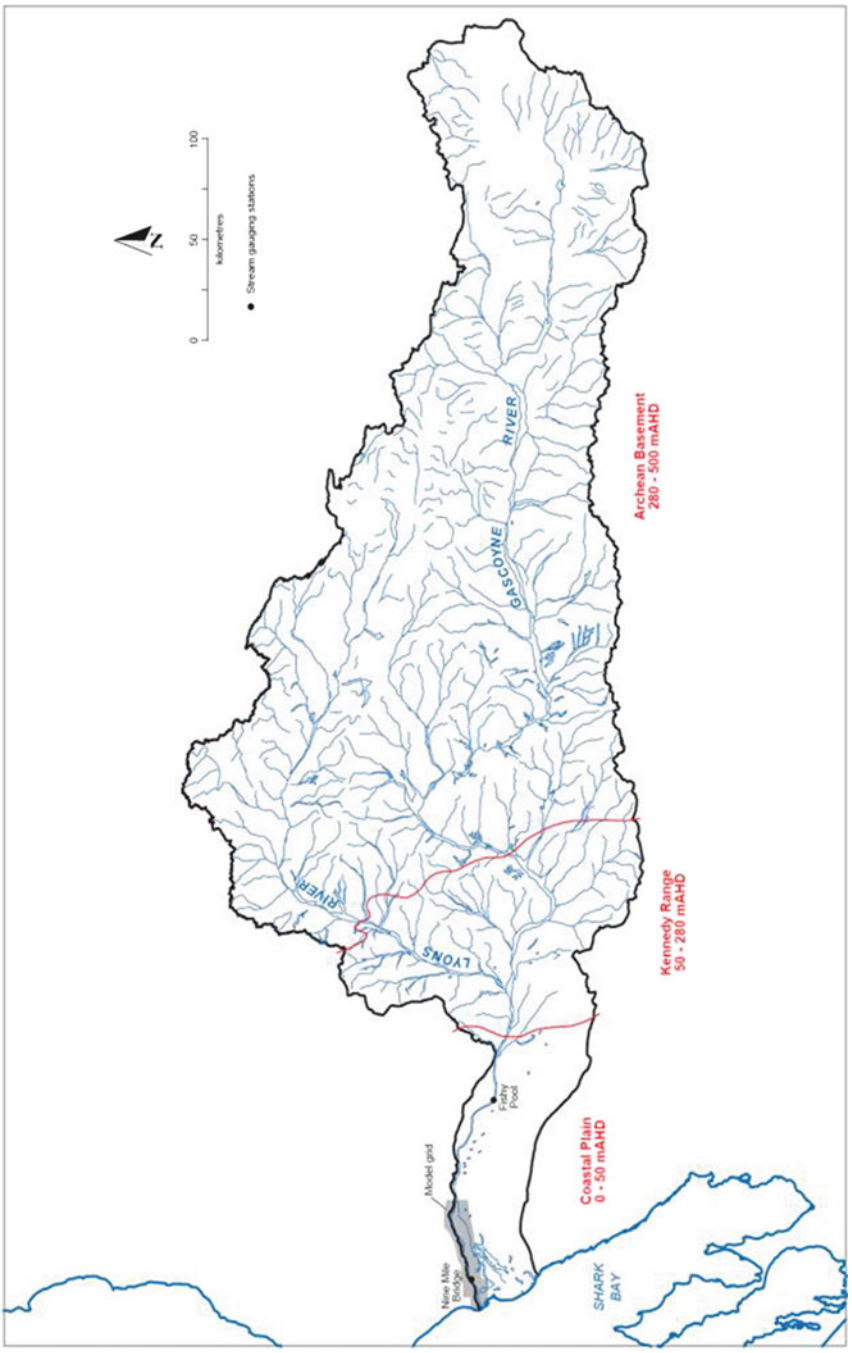

Fig. 17.1 Gascoyne River catchment and Carnarvon groundwater management area

from the deeper alluvium adjacent to the river channel resulted in a lowering of the groundwater levels in many areas. This induced the lateral flow of brackish groundwater from areas further away from the river with subsequent increases in local groundwater salinity (Department of Northern Development 1972).

Drought conditions occurred over the Gascoyne River catchment in the mid 1950s and again in 1959 during an era of local expansion in the Carnarvon Horticultural Area. Excessive extraction from the older alluvium during this period resulted in saline groundwater contamination of some portions of the alluvial aquifer with subsequent abandonment of several plantations. The reduction in groundwater quality was observed to be more severe in wells and bores on the south bank of the Gascoyne River which, with the exception of those immediately adjacent to the river channel, became too saline for irrigation. Many bores furthest from the river on the northern bank were also abandoned for the same reasons (Department of Northern Development 1972).

The original town water supply for Carnarvon was until 1960 obtained from a borefield located on Water Supply Island within the Gascoyne River channel 3 km north of the Carnarvon town site. Here a combination of increased groundwater production for plantations situated on the north bank of the Gascoyne River near the river mouth and groundwater abstraction for town water supply lowered groundwater levels below sea level. This induced the landward movement of a marine saline wedge and subsequent abandonment of plantations situated in the far western area of the CHA and the town water supply bores on Water Supply Island (Department of Northern Development 1972).

Declining groundwater quality during this period resulted in the WA Government assuming management of the CHA groundwater abstraction, gazetting it as a groundwater area in 1959. Government policies implemented included licensing of private bores and restricting groundwater production when groundwater salinity exceeded 1,000 mg/L total dissolved solids (TDS). These policies combined with a succession of favourable river flow years through the 1960s prevented further deterioration of the groundwater resources across the CHA Public Works Department (Public Works Department 1973).

Increasing salinity of the groundwater drawn from the alluvial aquifer beneath Water Supply Island for public water supply forced the gazetting and subsequent development of groundwater resources within the Carnarvon Water Reserve (Fig. 17.2).

As a management tool, the river channel and adjacent bank was divided into 11 groundwater management units referred to as Subareas A through L (excluding I). Subarea A comprises the CHA from Nine Mile Bridge to the river mouth at Carnarvon. Subareas B–L make up the Carnarvon Water Reserve (CWR) located between Rocky Pool and Nine Mile Bridge.

Groundwater within the alluvial aquifer of Subarea A is abstracted for horticulture from privately constructed wells, bores and spear points. To enhance groundwater abstraction from the alluvial aquifer, plantations adjacent to the river have been allowed access to the river channel through “prolongations” or extensions of the property line to the river channel centre point. Not all plantations have access to

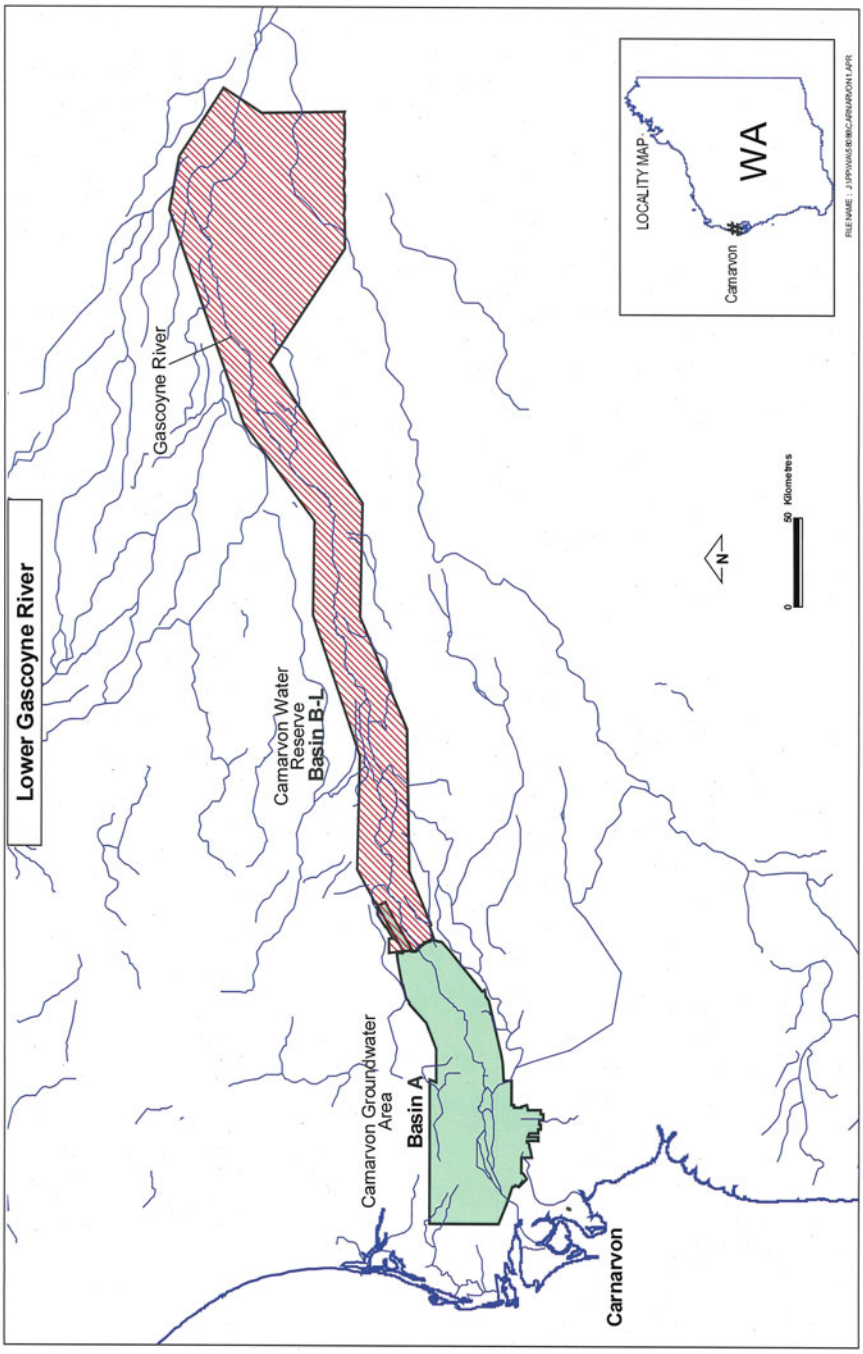

Fig. 17.2 Lower Gascoyne River, groundwater management areas

groundwater from Subarea A due to a number of reasons including not having access to the river through a "prolongation", or being located in an area where the river bed sand is poorly developed across the "prolongation" or the underlying older alluvium contains brackish groundwater.

The CWR has been developed under license by the WA Water Corporation (WC) as the public water source for the Town of Carnarvon and as an additional water source for irrigation of the CHA. The Gascoyne Water Cooperative (GWC) has an agreement with the WC to distribute this water to the CHA.

While bananas are still an important crop, the CHA has diversified, with other fruit and vegetable production including mangoes, stone fruit, melons, avocados, tomatoes, pumpkins and more recently grapes. This horticulture, including bananas, was valued in 2009 at approximately 75 million dollars (Gascoyne Development Commission 2010).

The Gascoyne River groundwater management policy for the CHA has been challenged by an increase in groundwater demand. This demand has been driven by an expansion of the horticultural area under the WA Government's Gascoyne Foolbowl Initiative and the incorporation of new crop varieties resulting in longer growing seasons. Other issues affecting management policy include changes in plantation ownership with loss of local water management knowledge and more extreme rainfall variability affecting the extent and duration of river flow events with subsequent less dependable groundwater recharge.

17.3 Previous Work

To address the CHA water supply demand issues, the WA Government has instigated a number of groundwater investigations and evaluations commencing in 1938 with the drilling of 60 exploration groundwater bores along the river, of which 35 were successful. Another 50 bores, 22 of which were successful, were constructed in 1946 (Dodson 2009).

Following the failure of the river to flow in 1954, the WA Government initiated another drilling program to evaluate groundwater resources across the Gascoyne River flood plain. This program constructed 40 bores, with only one being successful and the rest too saline for horticulture. Both the WA Geological Survey and the WA Water Authority conducted a number of groundwater resource evaluations for the Gascoyne River between 1968 and 1993. Their estimations of groundwater storage were used in early groundwater modelling for aquifer status reporting.

17.4 Physiography and Climate

The Gascoyne River extends in a westerly direction from about 650 km inland of the Indian Ocean and occupies an elongate drainage basin with a catchment area of about 79,000 km^2 (Martin 1990). The river rises below the Wilgoona Hill in the

Robinson Ranges west of the Gibson Desert and flows into the Indian Ocean at Carnarvon. The catchment physiography comprises two distinct areas: an inland etched, granitic plain; and the Carnarvon Basin, which includes the Kennedy Range Plateau and coastal plain (Dodson 2009).

The granite plain, with an average elevation of 400 m above the Australian Height Datum (AHD), is situated east of the Kennedy Range Plateau. This area is characterised by gentle slopes with broad, ill-defined flood ways within wide valleys interspaced with isolated peaks rising to approximately 700 m AHD. Rainfall over the inland granitic plain is the source for surface flow, as the flood plain lacks significant tributaries.

The Gascoyne River flood plain is situated within the coastal plain, which slopes gently to the west from the Kennedy Ranges. Downstream from Rocky Pool, the river bed falls about 0.67 m/km. Mudflats, palaeodrainages and abandoned river channels associated with former Gascoyne River processes are identifiable within the flood plain.

The climate across the Carnarvon region is classified as arid with erratic and unreliable rainfall, hot summers and mild winters. Evaporation in Carnarvon is about 2,600 mm/annum, with most occurring during the summer period November–April. Rainfall across the Gascoyne River catchment averages between 180 and 200 mm (8 in.). River flow is predominately associated with rainfall originating from cyclones and summer thunderstorms related to atmospheric lows that penetrate beyond the Kennedy Ranges some 400 km inland.

17.5 Gascoyne River System and Hydrogeology

The Lower Gascoyne River flows along a well-confined braided channel through quaternary alluvial terraces, resting upon early Tertiary and Mesozoic sediments of the Carnarvon Basin (CyMod 2009). It crosses the Rocky Pool Anticline at Rocky Pool, with the westward portion of the Gascoyne River channel occupying a low-sinuosity channel varying in width from about 75 to 1,200 m (Martin 1990). This anticlinal structure constrains groundwater flow, separating the alluvial aquifer system present downstream of Rocky Pool (latitude 24°45′15″S, longitude 114°08′08″E) from that in the Rock Pool – Fishy Pool area (Rockwater 2001).

The Gascoyne River has a great variation in runoff and duration of river flow, largely the consequence of the size of the catchment combined with erratic and fluctuating climatic conditions that deliver rainfall to the area. Groundwater is stored within the Gascoyne River flood plain sediments to a depth of 60 m below ground level. The key features of the sediments are:

- The Gascoyne River has a relatively stable terrace morphology that tends to maintain the river to the primary channel and overbank areas of ponding.
- The river sediment load varies in particle size from clay to gravel fractions, resulting in an alluvium of mix character. Clay and silt fractions are commonly

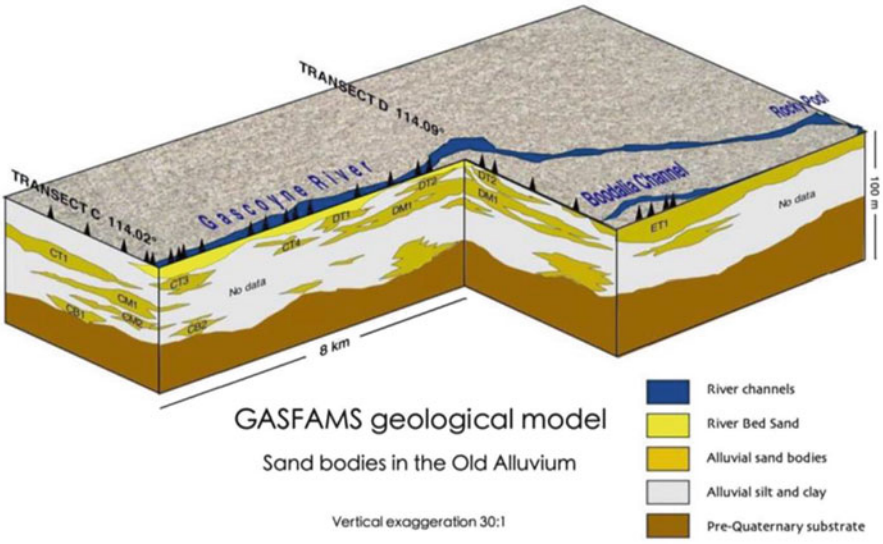

Fig. 17.3 Conceptual cross section of the Gascoyne River alluvial sediments comprising Older Alluvium

deposited in overbank ponding areas, with the heavier sand and gravel fractions forming aggrading channel bed-loads.

- The river sediments occur as an alluvial wedge containing isolated sand sheets and channel-derived sand bodies within a matrix of sandy silt and clay.

The groundwater flow system in the saturated alluvial sediments (alluvial aquifer system) associated with the Gascoyne River is unconfined to semi-confined, heterogeneous and anisotropic (Fig. 17.3). The base of the alluvial aquifer system is formed by the relatively impermeable Cretaceous Toolonga Calcilutite or (the equally impermeable) Tertiary Cardabia Calcarenite (Martin 1990).

The saturated alluvial sediments of the Gascoyne River have been informally defined as Older Alluvium Aquifer (OAA) and River Bed Sand (RBS). The OAA ranges in thickness from approximately 20 m west of Rocky Pool to greater than 50 m near Carnarvon (Dodson 2009). Sediments comprising the OAA consist predominately of alternating and irregular, unconsolidated to semi-lithified, thin beds of poorly sorted sand, gravel and clay with varying sand and silt fractions (Martin 1990). The OAA is a heterogeneous and anisotropic aquifer system which is laterally not continuous having been deposited as channel lag or point-bar river channel sediment. The aquifer is unconfined to semi-confined depending upon its position within the Gascoyne River alluvium profile.

The RBS occupies the entire channel of the Gascoyne River where it occurs as the river bed load that is incised up to 5 m into the underlying OAA. This aquifer is composed predominately of angular to sub-angular quartz sand, with granitic and metasedimentary detritus rock, and angular secondary laterite, calcrete and silcrete

(Dodson 2009). Grain size of the RBS varies from fine sand to cobbles. The thickness of the RBS varies from 1 to 12 m with an average thickness of 3.5 m. The RBS is recharged during river flow events, where saturation of this aquifer occurs soon after commencement of flow. The downward and lateral leakage of groundwater from the RBS recharges the underlying OAA and adjacent older alluvium within the river bank and flood plain. The RBS contains a finite amount of water which, in the vicinity of Carnarvon, is exhausted 6–9 months after a river flow (Allen 1972).

The "fresh" (<1,000 mg/L TDS) groundwater resources are isolated to those alluvial sediments that have good connection to the surface water during river flow. The efficiency of recharge and quality of the groundwater within the OAA is directly controlled by the degree of connection that the aquifer has with the overlying RBS. Estimates of the groundwater storage with salinity less than 1,000 mg/L TDS within and adjacent to the CWR range between 100 and 340 GL (Martin 1990; Allen 1972).

17.6 Management Areas and Policies

Expansion of the irrigated areas in Carnarvon in the 1950s through a period of below normal river flow resulted in the WA Government enacting control measures for the Gascoyne River alluvial aquifer system in 1959 Department of Northern Development (Martin 1990). The initial measures included establishment of the Carnarvon Irrigation District Advisory Committee (CIDAC) consisting of growers and representatives of the WA Public Works Department and Department of Agriculture. This was followed by the division of the Gascoyne River alluvial aquifer system from Rocky Pool to the river mouth into the 11 management Subareas A–L (excluding I), with Subarea A equating to the CHA and B–L comprising the CWR.

Initially only extraction from the RBS was managed but in 1963 special legislation was enacted to extend control to wells and bores on private property through the issue of groundwater licences. Plantations were licensed for 36,000 or 72,000 kL/a depending upon size, with up to 10,000 kL available per month and a cease pumping condition when groundwater salinity exceeding 1,000 mg/L TDS. There are currently 156 groundwater licences in Subarea A (Fig. 17.2), with a total licensed allocation of 8,300 GL/year. Calculations of the sustainable groundwater allocation for both the RBS and OAA within Subarea A vary in accordance with the estimation of aquifer storage, groundwater quality and the statistical analysis of river flow events. Current estimates of the sustainable groundwater resource for Subarea A range between 5.8 and 6.1 ML. This is based upon the alluvial aquifer being able to supply the required volume of groundwater of a quality less than 1,000 mg/L TDS in 8 out of 10 years (CyMod 2009).

Historically, the over-allocation of the groundwater resources was not a problem, as governance based upon local knowledge and experience was sufficient to maintain sustainability of the groundwater resource. Full licence allocation was

never accessible due to cessation of pumping at 1,000 mg/L TDS groundwater salinity. The WC is licensed to abstract 10.4 GL/a of groundwater from the CWR of which 1.8 GL/a is for town water supply. The GWC, through agreement with the WC, distributes reticulated water from the CWR to plantations within the CHA. The location and development of economic bores within the CWR is a limiting factor with only 1 out of 10 drilled bores productive due to the discontinuous and anisotropic nature of the alluvial aquifer system. The GWC is evaluating the groundwater resources north of the Gascoyne River (Brickhouse Borefield) for an additional 4 GL/a (Crute and Nixon 2008).

The Gascoyne River alluvial aquifer is currently under stress. Aquifer stress is due to increased groundwater abstraction with expansion of the CHA, greater duration between river flows considered to be the related to climate change, extension of growing season through the use of more varied crop varieties and changes in plantation ownership with expectations of full use of groundwater allocations.

Management of the Gascoyne River alluvial system utilises a combination of policies developed to take into consideration historical data and stakeholder knowledge. These policies include:

- Metering and limiting abstraction to the determined sustainable yield;
- Imposing a maximum monthly limit on groundwater production during periods of 'no river flow' to protect groundwater supply and quality;
- Maintaining a maximum groundwater salinity threshold of 1,000 mg/L TDS to minimise the risk of lateral movement of saline groundwater from bank storage and the landward movement of the salt water interface at the mouth of the river;
- Allowing 'unrestrictive pumping during river flow events; and
- Limiting water trading due to the variability in the aquifer system.

17.7 Groundwater Management Tools

A number of management methods and tools have been used to regulate groundwater abstraction from the Gascoyne River alluvial aquifer system. Anecdotal information indicates that the earliest method comprised the application of community knowledge together with individual experience of growers to maintain private supplies of groundwater with salinity less than 1,000 mg/L TDS. Groundwater resources were developed in accordance to local knowledge and, historic practice without reference to accurate estimations of aquifer capacity or potential long term impacts.

Aquifer stress following several extended periods of no flow in the 1950s led to the construction of a clay barrier approximately 4 km east of the Bibbawarra Crossing. The clay barrier was constructed above the "cease of flow" flood level with the purpose to enhance groundwater recharge and storage. The structure reduced underflow and subsequent flattening of the upstream hydraulic gradient. A minor improvement in groundwater supply was reported by growers abstracting groundwater immediately upstream of the clay barrier. The barrier was destroyed by the 1957 flood and not replaced.

Major groundwater quality problems through the 1950s cumulating in 1959 lead to the commencement of management of the Gascoyne River by the WA State Government through controls to limit the quantity of groundwater available for abstraction. This quantity became known as the "basic allocation", which was defined as the quantity of water required through the latter part of a "drought" (no flow period) to sustain 1.6 ha of bananas for a single family unit or 3,000 m^3/property/summer months (September–April) + 1,500 m^3/property/winter months (May to August). Pressure from large plantations together with issues regarding groundwater abstraction during "good seasons" resulted in the development of a complex revised groundwater allocation formula in 1962. The revised groundwater allocation limit was defined as the: Basic Allocation + Uniform Increase + Son Allowance + Banana Allowance + Capital Value Allowance, with:

- Basic Allocation
  Quantity of water required to sustain the "Basic Area" of 1.6 ha and determined as 3,000 m^3 per property per 28 days in summer, being September to April, and 1,500 m^3 per property per 28 days in winter, being May to April.
- Uniform Increase
  Seasonal quantity of surplus water evenly allocated to all properties and expressed as a % over the "Basic Allocation".
- Son Allowance
  An allowance equivalent to half of the "Basic Allocation" granted in respect of a 17 year old or married son who continued to work full time on a plantation.
- Banana Allowance
  An allowance of 110 m^3/28 days in summer and 550 m^3/28 days in winter granted to properties with an area of bananas greater than 1.22 ha to assist planting of new areas of bananas as the old area reached the end of its economic productive life of about 3 years.
- Capital Value Allowance
  An allowance which all properties received based on the capital valuation of the property. It encouraged the more industrious growers who would attract a higher allocation by improving facilities such as tanks, pipes, bores and buildings, similar to "Uniform Increase.

Implementation of this formula required the licensing and metering of all bores under the 1914 "Rights in Water and Irrigation Act (RiWI).

The continued degradation of the aquifer through a period of adequate river flows in the 1960s also marked the start of comprehensive hydrogeological studies by the WA Department of Public Works (PWD) and Geological Survey of Western Australia. These studies, together with regular groundwater monitoring, provided the data needed to develop groundwater models for assessing the status of the Gascoyne River alluvial aquifer system and modifying groundwater abstraction policies.

The earliest model developed to assess the status of the Gascoyne River alluvial aquifer system was designed by the WA PWD in 1980 (Ventriss 1980). This system was a distributed parameter numerical model running on a mainframe UNIVAC computer. In the early 1990s the UNIVAC model outputs were incorporated into a

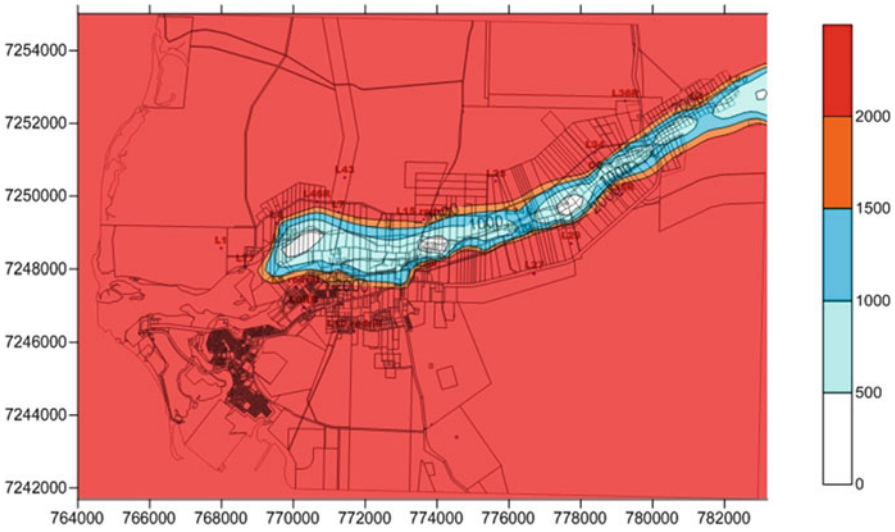

Fig. 17.4 September 2012 Gascoyne River Aquifer Status Reporting groundwater salinity contouring of the Carnarvon Horticultural Area derived from electrical conductivity measurement of both DoW observation and private production bores

spreadsheet tool referred to as CIDAC after the Carnarvon Irrigation District Allocation Committee. CIDAC aquifer status calculations were based upon "full" groundwater storage for the CHA and CWR estimated at 19.4 GL for the RBS and a 0.00 "Depletion Volume" in the semi confined OAA. The model used groundwater level measurements from a selected set of observation bores with pre-calculated 'lookup' tables to provide a rapid and uniform means of relating groundwater level to aquifer storage. CIDAC continues to be utilised to provide a uniform method for the estimation of aquifer status for the Gascoyne River alluvial aquifer system. Reports generated by CIDAC date back to May 1997. Data prior to this date were lost due to corruption of the application. Current aquifer status reporting incorporates groundwater salinity modelling of the CHA (Subarea A).

The CIDAC spreadsheet together with salinity contouring (Fig. 17.4) is supported by regular WA Department of Water (DoW) and Water Corporation (WC) monitoring of groundwater level and salinity from the CHA to Rocky Pool. These data are evaluated to provide a quarterly review of the status of the Gascoyne River alluvial aquifer system that is used by the DoW to manage CHA groundwater allocation and trigger the release of "Low Aquifer Storage Relief Water" from the CWR Southern Gascoyne River Borefield operated by the WC.

The WA Government funded the development of a groundwater model in 2000 that utilised the United States Geological Survey three dimensional, finite difference, modular groundwater flow model (MODFLOW). The groundwater model was referred to as the *Gascoyne River Floodplain Aquifer Model* or GRFAMOD. GRFAMOD was constructed as a numerical model of the Gascoyne River groundwater flow system that simulated transient historical groundwater flow events. This

was accomplished for the for the entire length of the public and private abstraction area of the Gascoyne River from Rocky Pool to the river mouth through division of the area into 100 × 100 m^2 finite difference grids (Dodson 2009). GRFAMOD outputs indicated that the groundwater system was capable of supplying 18 GL/a over 2 years of 'no flow'. The model was not capable of incorporating solute flow and could not predict groundwater quality changes arising from groundwater abstraction over an extended period of 'no flow'. This limitation restricted the use of the model's outputs as management policy required maintaining groundwater quality to less than 1,000 mg/L TDS. A precautionary approach was adopted and the existing 12.4 GL/a allocation limit was maintained (Dodson 2009).

The WA DoW contracted the construction of a new groundwater model in 2009, GASFAMS (**GAS**coyne River **F**loodplain **A**quifers **M**odelling **S**ystem), over the Gascoyne River alluvial system. The DoW's stated objectives for the development of GASFAMS were:

- *Simulate groundwater flow within and between all hydrogeological units in the Gascoyne River floodplain groundwater system.*
- *Establish water budgets for each aquifer.*
- *Evaluate a range of scenarios, including pumping and climate variations to predict the scale of changes in recharge, groundwater potentiometric heads/water levels and groundwater salinity within the Gascoyne River alluvial aquifer system.*
- *Evaluate likely changes in groundwater discharge to ocean environments.*
- *Predict the general drawdown in water levels near other groundwater users, wetlands, and rivers and streams in the project area, and provide seasonal variations in such reductions.*
- *Provide results that will support the determinations of sustainable yields based on impacts on identified groundwater dependent ecosystems (GDEs).*
- *Estimate the likely range and uncertainty of water level changes as a result of pumping and climatic stresses.*

GASFAMS was developed using MODFLOW 2000 and the MT3DMS solute module together with Visual MODFLOW 2009 as the graphic user interface, subsequently updated to MODFLOW 2011. The model coverage runs from east of Rocky Pool to the river mouth and used time sequenced monitoring data from available DoW, WC and private (plantation) bores (Fig. 17.5) (CyMod 2009).

The eastern boundary of the GASFAMS study area coincides with Rocky Pool, where the Cretaceous bedrock crops out to form a flow barrier relative to the Gascoyne River alluvial aquifer system (Fig. 17.6). The Gascoyne River discharges into the Indian Ocean at the western end of the GASFAMS study area with the salt water interface forming a natural boundary for the groundwater model.

The Gascoyne River alluvial aquifer system was portrayed in GASFAMS as 10 layers with Layers 1–3 depicting the RBS and Layers 7–10 describing the OAA. A no-flow boundary was incorporated underlying Layer 10 that represents the Toolonga Calcilutite (CyMod 2009). Both the RBS and OAA comprising Layers 1–10 were constructed with fixed heads utilised in the upper layers (Table 17.1).

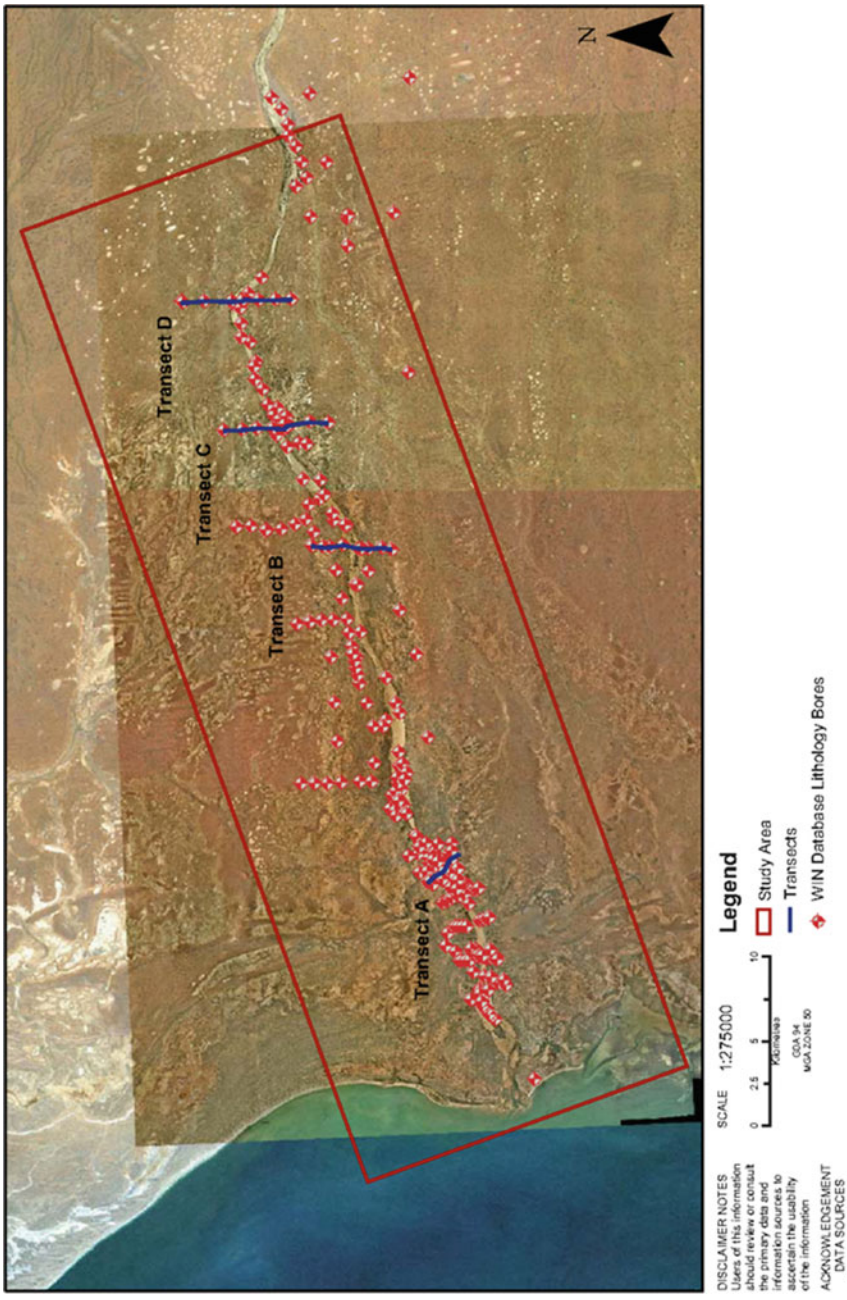

Fig. 17.5 GASFAMS study area coverage with database bores locations

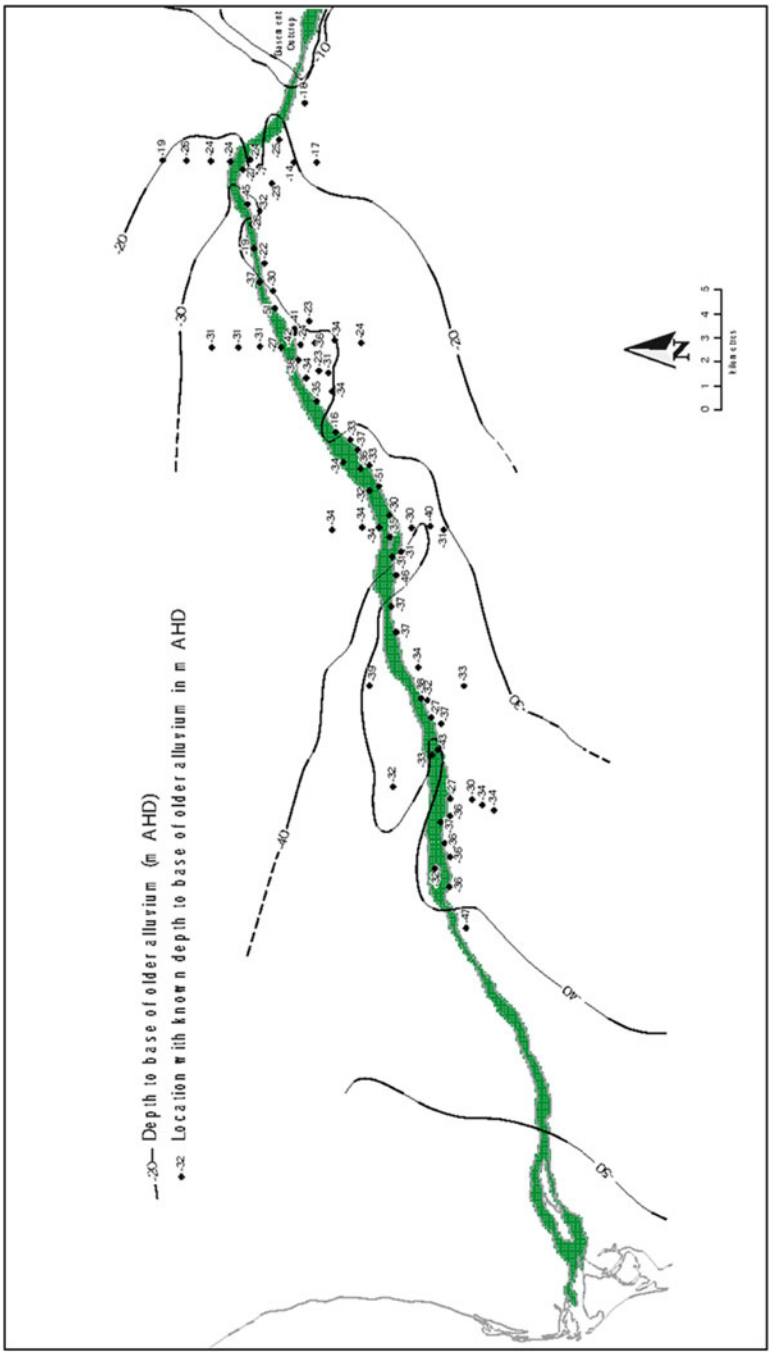

Fig. 17.6 Depth of Cretaceous basement beneath the Gascoyne River Older Alluvial Aquifer (OAA) (Dodson 2009)

Table 17.1 Gascoyne River alluvial aquifer system accepted GASFAMS aquifer characteristics

Unit	Layer	Thickness (m)	Aquifer	Kh (m/day)	Kv (m/day)	Transmissivity (m^2/day)	Specific yield	Storage coefficient
RBS	1,2	4–12	Alluvial	20–812 (164)		78–3,980 (850)	0.29–0.32	
OAA	3–10	3–57	Alluvial	0.8–121 (18)	0.03	5–830 (166)	−0.15	0.0005–0.006 (0.0025)
Toolonga	Base		Aquiclude					

Table 17.2 Climate Scenarios and predicted sustainable allocation

Scenario	Description	Recharge sequence	Allocation components (GL/annum)		
			Area A	Area B–L	Total
1	Base case	Normal 1991–1999	5.8	12.2	18.0
2	No flow	Drought 2000–2008 Salinity A >1,000 mg/L	0.0	18.0	18.0
3	Areas A–L best case	Normal	5.8	>12.2	>18.0
4	Areas A–L best case	Drought 2000–2008 Salinity A >1,000 mg/L	0–5.8	>18	>18.0
5	Brickhouse Borefield 4 GL/a	Normal	5.8	>12.2 + 4	>22.0
6	Brickhouse Borefield 4 GL/a	Drought 2000–2008 Salinity A >1,000 mg/L	0–5.8	>18 + 4	>22.0

The RBS has a higher conductivity and storativity than the underlying OAA, which allows it to be readily saturated during a river – flow event with subsequent recharge of the OAA through vertical leakage. Lateral movement of groundwater within the RBS into bank storage is driven by the difference between the vertical and horizontal conductivity with discharge back into the river as base flow following cessation of river flow. The function of river flow in aquifer recharge was enhanced through using the hydraulic grade line together with the stage height to interpolate the active flow area. This eliminated the need to explicitly account for river bed topography but introduced some error by assuming that the flow height is linear between reference points at Rocky Pool and Nine Mile Bridge. It was noted that the use of a calibrated Mike11 model would have improved the simulation of stage heights estimates.

The use of the Modular Transport in Three Dimensions, Multiple Species (MT3DMS) solute module allowed GASFAMS to be run as a transient model combining the functions of both saturated flow and solute transport. This permitted the development of multiple river flow and abstraction scenarios (Table 17.2) to provide a predictive tool for groundwater management. Scenarios run considered both normal and drought (extended 'no flow' cycles) conditions. A maximum abstraction of 5.6 GL/a (Subarea A) and 22.8 GL/a (Subarea B–L) was indicated

for "drought" conditions if additional abstraction from the Northern Gascoyne River (Brickhouse) Borefield was available.

The GASFAMS numerical model relied upon data contained in the earlier GRFAMOD model. These data were incorporated with a number of improvements the foremost of which comprised the use of:

- A non-uniform rectangular cell grid;
- Ten vertical lays instead of three layers allowing the use of more accurate aquifer parameters based upon the quantitative hydrogeology;
- An improved aquifer recharge process that highlighted the importance of river flow;
- A multi – mode well package to simulate abstraction; and
- MT3DMS to track groundwater salt increase and movement related to aquifer dewatering.

The MT3DMS solute module provided the ability for GASFAMS to simulate the movement of salinity in the RBS and OAA aquifers through the finite difference grid as defined by the horizontal and vertical discretisation in the groundwater flow model. The assignment of the solute boundary conditions was considered analogous to the flow model conditions with the exception that salt concentration or mass flow was specified rather than potentiometric head or groundwater flow (CyMod 2009).

The importance of the solute transport module has been highlighted following a prolonged brackish river flow event through 2010 and 2011. This event resulted in the intrusion of brackish surface water into the RBS affecting the quality and usability of the groundwater resource for irrigation purposes. A new set of scenarios were developed following this event that consider groundwater abstraction relative to the quality of a river flow event (Table 17.3).

17.8 Conclusion

The Gascoyne River alluvial flood plain contains a complex and non-uniform aquifer system comprising both current riverbed sand (RBS) and palaeo-sediments (OAA). The groundwater within the alluvial aquifer supports the CHA where maintenance of water quantity and quality is essential to sustain current markets and growth envisioned under the Gascoyne Foodbowl Initiative Aha! (2010). There are competing water interests across the CHA comprising varying groundwater conditions, crop requirements and commercial values. Local knowledge of the groundwater system is diminishing. It is difficult to maintain excess groundwater storage through normal years to ensure water availability through the periods of no flow. Aquifer monitoring and accurate data assessment is essential to make confident predictions that provide water security to the CHA. The importance of appropriate and defendable management strategies has heightened due to a range of factors including the use of more salt tolerant crops, longer growing seasons and the change from family plantations to agribusinesses. Changes to the CHA have

Table 17.3 GASFAMS scenarios based upon Gascoyne River flow and salinity

Gascoyne river – river flow and salinity scenarios					
Scenario name	**Management actions**	**Model evaluation for effects**	**River flow/channel width stage height (m @ 9 mile bridge)**	**River flow duration (weeks)**	**River flow salinity**
1 Normal/normal with salty flow.	Pumping ceases at 1,000 mg/L TDS	Effect on RBS & OAA, until river ceases to flow	Normal flow height/full channel width	Normal	Normal
2 Normal/normal with salty flow.	Pumping ceases at 1,000 mg/L TDS	Effect on RBS & OAA, until river ceases to flow	Normal flow height/full channel width	Normal	Salty
3 Normal/long with salty flow	Temporarily allowing abstraction in RBS Subareas A & B–L above the 1,000 mg/L to dewater it.	Effect on RBS & OAA, until river ceases to flow	Normal flow height/full channel width	Normal	Normal
4 Normal/long with salty flow	Temporarily allowing abstraction in RBS in Subareas A & B–L only above the 1,000 mg/L to dewater it.	Effect on RBS & OAA, until river ceases to flow	Normal flow height/full channel width	Normal	Salty
5 Normal varying to low/V long with salty flow	Temporarily allowing abstraction in RBS in Subarea A only above the 1,000 mg/L to dewater it.	Effect on RBS & OAA, until river ceases to flow	Low flow height/1/2 channel width	Normal	Normal
6 Normal varying to low/V long with salty flow	Temporarily allowing abstraction in RBS in Subarea A only above the 1,000 mg/L to dewater it.	Effect on RBS & OAA, until river ceases to flow	Low flow height/1/2 channel width	Normal	Salty
7 Normal varying to low/V long with salty flow	Temporarily allowing abstraction in RBS in Subareas A & B–L above the 1,000 mg/L to dewater it.	Effect on RBS & OAA, until river ceases to flow	Very Low flow height/1/4 channel width	Long	Salty
8 Low/V long with salty to v salty	Temporarily allowing abstraction in RBS in Subareas A & B–L above the 1,000 mg/L to dewater it.	Effect on RBS & OAA, until river ceases to flow	Very Low flow height/1/4 channel width	V Long	Salty to V salty

• Flow height	-	V High	>6.5 m	Full channel width/very high
(Channel width)	-	High	4.5–6.5 m	Full channel width/High River
	-	Moderate	2.5–4.5 m	Full channe; width/Normal River
	-	Low	0.5–2.5 m	1/2 channel width/Small River
	-	V Low	<0.5 m	1/4 channel width
• Flow duration	-	V Long	>150 days	V Long River
	-	Long	110–150 days	Long River
	-	Moderate	70–110 days	Normal River
	-	Short	30–70 days	Short River
	-	V Short	<30 days	
• River flow aalinity	-	V High	>1,500 mg/L	V Salty
	-	Moderate	500–1,500	Salty
	-	Low	<500	Normal

L Leonhard/AMaskew 12/06/2012 Mid West Gascoyne Region – GASFAMS Scenarios

increased the pressure on Government to develop innovative and technically supported management policies that can be successfully promoted to business and community. This has lead to continual improvement in the evaluation methodology, such as GASFAMS, use to define management strategies aimed at enhancing the sustainable use of the Gascoyne River alluvial aquifer groundwater resource whilst maximising production from the CHA.

References

Aha! Consulting (2010) In: Workshop notes 23rd and 24th February 2010. Gascoyne Foodbowl Local Consultative Committee, Perth, Mar 2010, pp 1–25

Allen AD (1972) Results of investigation into groundwater resources along the Lower Gascoyne River for Carnarvon irrigation and Town water supplies. Geological Survey of Western Australia Record 1972/9, Perth, p 7

Crute J, Nixon R (2008) Gascoyne river alluvium – Brickhouse Station, Groundwater Modelling for Government of Western Australia (DAFWA and DoW), Global Groundwater, Perth, Feb 2008, p 17

CyMod Systems Pty Ltd. (2009) The development of the Gascoyne River Floodplain Aquifers Modelling System, GASFAMS V1, Western Australia Department of Water, Perth, Sept 2009, pp 1–133

Department of Northern Development (DND) (1972) Carnarvon and Gascoyne groundwater supply scheme, Western Australia. Commonwealth of Australia, Canberra, pp 17–19

Dodson WJ (2009) Groundwater recharge from the Gascoyne River, Western Australia, Hydrogeological record series HG 32. Western Australia Department of Water, Perth, pp 3–128

Gascoyne Development Commission (2010) Gascoyne horticulture investment profile. Government of Western Australia, Perth, pp 2–4

Hill T (1993) Growing bananas in Carnarvon. Information and Media Services, Western Australia Department of Agricultural, Carnarvon, p 5

Martin MW (1990) Groundwater resources of the Older Alluvium, Gascoyne River, Carnarvon. Western Australia, Western Australia Geological Survey Hydrogeology Report, 1990/21, pp 3–20

Public Works Department (1973) Water supply of Carnarvon and the Gascoyne irrigation area, an environmental impact study. Western Australia Public Works Department, Perth, pp 3–4

Rockwater (2001) The separation of fresh groundwater resources along the Gascoyne River by the rocky pool anticline. Western Australia Water Corporation, Perth, pp 7–9

Ventriss HB (1980) Gascoyne River groundwater scheme yield study. Water resources technical report no. 91, Water Resources Section, Public Works Department of Western Australia, Perth, Nov 1980, pp 3–24

Index

C. Wetzelhuetter (ed.), *Groundwater in the Coastal Zones of Asia-Pacific*,
Coastal Research Library 7, DOI 10.1007/978-94-007-5648-9,